

# **HIGH PRECISION STUDIES OF AN INTRAPLATE EARTHQUAKE SEQUENCE IN NORTHEAST BRAZIL**

by

**Mario Koechi Takeya**

M.S., Geophysics, São Paulo University, 1985.

A thesis submitted for the degree of Doctor of Philosophy at the  
University of Edinburgh.

September 1992



## **Abstract**

From May 1987 to April 1988, a 9 station, seismic network was operated near the town of João Câmara (5°33'S, 35°51'W) in Rio Grande do Norte state, Brazil. The network was installed 6 months after the occurrence of a  $m_b = 5.1$  earthquake. This thesis is concerned with the study of microearthquakes recorded by this network, which is in the Precambrian Borborema Province of northeast Brazilian shield.

The study revealed a remarkably well-defined distribution of seismicity associated with a simple fault structure. Hypocentre location was done using the HYPO71 program. The results of the analysis show that the fault is divided into two main segments with the same N37°E strike. The north segment is dipping 76°NW. The south segment is more nearly vertical, dipping about 82°NW and composed of three or more closely spaced almost parallel faults. A small gap and a low seismicity zone were found to separate the north and south segments. No events deeper than 9 km were found in the entire region studied. Examination of the epicentral map and corresponding vertical cross sections also revealed that events are not random but are clustered. Right lateral strike slip with a small normal component was inferred as the fault mechanism from composite fault plane solutions.


Off-fault events distant from the main fault were also observed, their pattern showing a classical example explained by the model of Das & Scholz as a consequence of off-fault shear stress increase after the occurrence of the main earthquake. Magnitude determinations for the events recorded by the telemetric network have been performed by developing a specific earthquake magnitude scale based on the duration of the observed seismic signal. A maximum likelihood estimate of b-value shows no significant variation during the recording period.

Shear wave splitting was observed in the J.Câmara region in all the selected events recorded by the three component station JCAZ. The polarization direction of the first split shear-wave arrival for those events lay in the north-south direction which does not agree with the premise of extensive dilatancy anisotropy for a maximum compressive stress in the east-west direction as inferred by the fault plane solutions.

## Declaration

I declare that the work submitted is entirely the result of my own investigation except where stated otherwise and that the work has not already been submitted in substance for any other degree and is not concurrently submitted for candidature for any other degree.

Mario K. Takeya  .....

Dr. Robert G. Pearce  .....  
(Supervisor)



## **Acknowledgements**

Unfortunately this is the only part of this work where emotion can be expressed. This study really started in January 1987 when I first met Dr. Robert Pearce in the Federal University of Rio Grande do Norte (UFRN) in northeast Brazil. At that time I was still collecting data using a small smoked-paper drum recorder network in João Câmara, and I was taken by surprise when Bob invited me to work with a Geostore based network. From May 1987 until April 1988 I was busy operating the seismic network installed by Bob. From October 1988 I have been in Great Britain doing the present work. Working with Bob has been a tremendous experience, however the first people I would like to thank are my wife Denise and my children Rodrigo and Julia. During all this time they stayed in Brazil, except for one year in France. It is unnecessary to say how difficult has been our personal life due to this thesis.

I would like to thank my research supervisor Dr. Robert Pearce who provided continuous support and enthusiasm in all stages of this work. I know how patient he was by talking slowly and correcting all my spelling and writing. My respect for him has grown not only in the scientific but in the human aspect. Dr. Marcelo Assumpção provided my first lessons in seismology and encouraged me to do this work; I am grateful for his advice, support and for helpful discussion.

I am deeply indebted to Dr. David Booth for his kindness, comments, tolerance, and for providing me guidance and support concerning the shear-wave anisotropy study. My thanks to Dr. Roger Hipkin, Mrs. Helen McKeating, Mr. Graham Dawes and Mr. Terry Turbitt for their warm welcome to Edinburgh. Thanks to Dr. Ian Main for his expert advice through the topic of magnitude calculation. Thanks to Dr. Russ Evans and Mr. Charlie Fyfe for their help in the business of digitizing my data. I would like to express my thanks to Dr. Ian Stimpson for helping Bob and I to install the telemetric network in Brazil and after that for the many useful discussions.

I must thank my Brazilian colleagues from the staff of the UFRN Mr. Joaquim Ferreira, Mr. João da Mata, Mr. Ronaldo Teixeira and Mr. José Moreira for their help and support for this work. Mr. Carlos dos Anjos and Mr. Eduardo Menezes deserve many thanks for the good job done in the field work and particularly because they demonstrated immense patience in the reading of hundreds of smoked-paper seismograms. My thanks to Miss Claudia Sophia for the opportunity of working together in João Câmara and for the endless discussion.

I wish to express my thanks to the geologists of the Brazilian oil company (Petrobrás) in Natal, particularly to Dr. Renato Bertrani and Mr. José Geraldo Gusso for valuable information and discussion. My thanks also to Dr. Carlos Oiti Berbert from the Brazilian Department of Mineral Production (DNPM) for his immense support in the early stage of the field work.

I would like to express my gratitude to the support and hospitality of Mr. José Ribamar, mayor of João Câmara at the time of data collection. My thanks to the priest of João Câmara, Padre Luciano and to many other anonymous people who kindly helped me during my one and half years of field work in that region.

The installation of the João Câmara telemetric network would be impossible without the support from the British Council's office in Recife. The field work for the João Câmara project was funded by the Overseas Development Administration (ODA) and by the Brazilian agency Superintendência do Desenvolvimento do Nordeste (SUDENE) of Recife and Natal. The equipment for the telemetric network was loaned by the NERC Geophysical Equipment Pool. My thanks to these institutions.

My four year studentship was provided by the Brazilian agency Coordenadoria de Aperfeiçoamento do Pessoal de Ensino Superior (CAPES).

## **List of Contents**

Abstract .....	I
Declaration II .....	
Acknowledgements .....	III
List of Contents .....	V
 CHAPTER 1 INTRODUCTION .....	 1
1.1 Objectives .....	1
1.2 Intraplate earthquakes .....	1
1.2.1 Some differences between interplate and intraplate earthquakes .....	2
1.2.2 Stress field and intraplate earthquakes .....	5
1.3 Intraplate earthquakes in Brazil .....	7
1.4 Seismological studies in Brazil.....	8
1.5 Seismicity in Northeastern Brazil.....	9
1.6 The João Câmara region.....	13
 CHAPTER 2 JOÃO CÂMARA EARTHQUAKE ACTIVITY .....	 16
2.1 Evolution of 1986-1990 series from drum recorder data .....	16
2.1.1 Locations of aftershocks .....	21
2.1.2 Location of the two main events .....	26
2.1.3 Historical data.....	29
2.2 Calculation of J.Câmara event magnitudes .....	29
2.3 The 1987-88 telemetric network .....	32
 CHAPTER 3 DATA ANALYSIS .....	 37
3.1 Digitization .....	37
3.2 Phase picking.....	38
3.3 Hypocentre location.....	39
3.4 Half space and two layer models .....	43
3.5 Wadati diagram.....	49
3.6 Magnitudes .....	52
3.7 Coda duration magnitude.....	54
 CHAPTER 4 AFTERSHOCK PATTERN.....	 67
4.1 Seismicity map from the telemetric network data .....	67
4.2 Fault heterogeneities .....	69
4.2.1 Mechanical effects of fault offsets .....	70
4.3 Fault irregularities from epicentre locations .....	73
4.4 Cross section analysis .....	78
4.5 Geometric irregularities in the south part of the fault .....	85
4.5.1 Reanalysis of the drum-recorder data .....	87
4.5.2 Discussion .....	90
4.6 Geometric irregularities in the north part of the fault .....	90
4.6.1 Reanalysis of the drum-recorder data .....	92
4.6.2 Relocation of the mb =5.0 earthquake .....	92
4.6.3 The structure of the north end.....	93
4.7 Conclusions .....	98
 CHAPTER 5 DEPTH DISTRIBUTION OF EVENTS AND OFF-FAULT SEISMICITY.....	 101
5.1 Introduction.....	101

5.2 Depth distribution of the main aftershocks .....	102
5.3 Depth distribution of other aftershocks as a function of magnitude .....	104
5.4 Aftershock and main shock faulting.....	108
5.4.1 The mb =5.1 earthquake.....	108
5.4.2 The mb =5.0 earthquake.....	112
5.5 Off-fault aftershocks.....	113
CHAPTER 6 CLUSTERING IN TIME AND SPACE.....	118
6.1 Introduction.....	118
6.2 Clustering effects in the south segment .....	120
6.2.1 Analysis of the main cluster C4 .....	123
6.2.2 Fault plane solutions in the south segment.....	126
6.3 Clustering effects in the north segment.....	133
6.3.1 Some characteristics of the north segment .....	134
6.3.2 Identification of the clusters in the north segment.....	138
6.3.3 Analysis of the most significant clusters in the north segment .....	140
6.3.4 Clusters and main fault heterogeneities .....	145
6.3.5 Fault plane solutions in the north segment .....	148
6.4 Clustering effects in off-fault segments .....	152
6.5 Note on analysis of clusters .....	157
CHAPTER 7 SHEAR-WAVE ANISOTROPY .....	158
7.1 Introduction.....	158
7.2 Data selection for the shear-wave splitting study .....	160
7.3 Data analysis .....	162
7.3.1 Procedures for the analysis.....	162
7.3.2 Shear-wave polarization and time delay measurements .....	165
7.4 Results and interpretation.....	170
CHAPTER 8 CONCLUSIONS AND SUGGESTIONS FOR FURTHER WORK.....	172
8.1 Summary of findings .....	172
8.2 Relationship with other geophysical studies .....	175
8.3 Suggestions for further work .....	180
APPENDIX A NETWORK STATUS TIMETABLE .....	182
APPENDIX B STATION LOCATIONS, RESPONSE CURVE OF THE SYSTEM AND COMPUTER PROGRAMS .....	185
B.1 Station coordinates.....	185
B.2 Response curve.....	186
B.3 Computer programs .....	188
APPENDIX C LIST OF EARTHQUAKES .....	191
C.1 Earthquakes recorded by the telemetric network .....	191
C.2 Earthquakes recorded by the drum-recorder network .....	216
REFERENCES .....	218
REAR POCKET (2 papers)	

## **CHAPTER 1**

### **INTRODUCTION**

#### **1.1 Objectives**

This work is related to the study of an aftershock sequence that followed the  $m_b = 5.1$  earthquake on 30 November 1986 in northeastern Brazil. This is a classical intraplate area by any definition. The objectives of this work are:

- a) To compute a precise seismicity map of the area;
- b) To study the spatio-temporal pattern of the seismicity in terms of the composition and structural features of the focal area and upon its stress field;
- c) To develop a local magnitude scale;
- d) To verify the presence of any anisotropic structure in the area close to the one three component station.

#### **1.2 Intraplate earthquakes**

For the general purpose of classification, there are two types of tectonic earthquake. Those ones that occur along the boundaries of lithospheric plates are in general known as interplate earthquakes to distinguish them from another class of events that are less numerous, the intraplate earthquakes. About 90% or 95% (depending on the definition) of the world's earthquakes belong to the category of interplate type earthquakes. Most intraplate earthquakes occur in areas of active continental deformation (e.g. Greece, Tibetan Plateau). But a small number occur inside the Earth's stable cratonic regions where earthquake activity is very small. Maybe because intraplate earthquakes are scarce, they have received relatively little attention.

Despite their small number, intraplate earthquakes as large as magnitude 7 have occurred in several populated areas including parts of central and eastern North America, Europe, Australia, Asia, South America and Africa. A classical and very well-known example of a destructive and large intraplate earthquake sequence is that of New Madrid, Missouri, USA, 1811-1812. Other historical examples include

## *Chapter 1*

those of the St. Lawrence Valley, Canada, 1663; Lisbon, Portugal, 1755; South Carolina, USA, 1886; India 1819, 1897, 1905, and 1950 (Richter, 1958). Among more recent and better studied intraplate earthquakes are those of Meckering, Australia 1968; Uzbekistan, USSR, 1976 and 1984 (Pearce, 1987); Guinea, West Africa, 1983 (Langer et al., 1987) and Tennant Creek, Australia, 1988 (Choy & Bowman, 1990).

### **1.2.1 Some differences between interplate and intraplate earthquakes**

In comparing the India, 1897 and California 1906 earthquakes, Richter (1958) concluded that both had comparable magnitude but the former had a larger felt area. Indeed, there is evidence that all the historical intraplate earthquakes cited here were marked by intense ground motion in the epicentral area and by very large areas of damage and perceptibility compared with most shocks of similar magnitude and energy along plate boundaries (Sykes & Sbar, 1973). In studying magnitude relations for eastern North America, Nuttli (1973) concluded that the attenuation of surface waves with periods between about 0.3 and 3 seconds (the main contribution to perception at large distances), is much greater for the western than for the central and eastern United States. He found that differences in attenuation values are sufficient to explain the observation that earthquakes in the eastern United States have a radius of perceptibility as much as 10 times larger than that of earthquakes of the same magnitude in the western part. Thus, although they are not numerous, large intraplate shocks constitute an environmental risk that must be taken into account in the design and siting of critical facilities. Fortunately, most of the historical earthquakes occurred at times when the affected areas were not heavily populated, so that loss of life was not as large as can be expected for future great mid-plate earthquakes. Exceptions to this are the 1755 Portugal earthquake and the 1905 and 1950 Indian earthquakes, which did take a great number of lives (Richter, 1958). The 1755 Lisbon earthquakes are said to have caused canals and lakes to go into visible oscillations as far away as Scotland and Sweden (Bullen & Bolt, 1985). A more detailed description of the effects caused by these earthquakes can be found in Richter (1958).

Another way to describe this same basic difference between intraplate and interplate earthquakes can be found in looking at the work done by those authors who analyzed seismograms from intraplate earthquakes. Mendiguren (1971) analysed the focal mechanism of a moderate size earthquake to derive the stress in the Nazca Plate and found very clear impulsive P wave first motions for the vast majority of stations not close to the nodal plane. In studying the lithospheric stresses and the driving mechanism of plate tectonics, Sykes & Sbar (1973) found

## Chapter 1

that even though intraplate earthquakes are relatively rare, it was possible to obtain a large number of fault plane solutions by successfully analysing the first motion of P-waves for events as small as magnitude  $m_b = 5.0$  using standard short period records. They concluded that the corner frequency of these events is higher than about 1 Hz. Most intraplate earthquakes have a larger short-period magnitude  $m_b$ , than events with the same long period magnitude  $M_s$  along plate boundaries. The enrichment in short-period energy may be caused by greater effective stress that may be present within plates and/or higher Q paths through the upper mantle (Sykes & Sbar, 1973). More recently, Pearce (1987) recognised that anomalously high stress drop favours the observation of simple P-waves on short period seismograms which recorded the 1976 and 1984 Gazli, USSR intraplate earthquake sequence, since this implies short rupture duration which helps to keep direct P and surface reflections discrete and within the short period passband. It is likely therefore that these aftershocks do have anomalously high stress drop. There is a direct connection between all these observations and seismic hazard since man-made structures normally exhibit resonant frequencies between 0.1 and 5 Hz (Phillips & Aki, 1986).

Although some controversy exists in quantifying the differences between intraplate and interplate earthquakes (Xie et al., 1991; Sommerville et al., 1987) the majority of authors (Kanamori & Anderson, 1975; Nuttli, 1983; Scholz et al., 1986) agreed that large intraplate earthquakes consistently have greater seismic moment ( $M_0$ ) per unit fault length than interplate events, the difference being about a factor of five, so their stress drops are accordingly that much higher. Apart from the different methods used by different authors in evaluating the stress drop, the discrepancies found in the value obtained for this parameter could be a consequence of the definition of intraplate earthquake (Scholz et al., 1986). For example, Nuttli (1983) defined three classes of earthquakes: plate margin events, which occur at subduction and spreading margins and along transform faults separating plates; near-boundary events, which occur within a plate but less than 500 km from its margins, and mid-plate events, such which occur at least 500 km from plate margins. Recognizing that any classification is to some extent arbitrary, Scholz et al. (1986) suggested three categories of earthquake on the basis of the slip rate of the faults they occur on. According to this classification an event with slip rate greater than one centimetre per year (cm/yr) will be classified as interplate type whilst those having a slip rate lower than 0.01 cm/yr would be a mid-plate earthquake. A plate boundary-related type would have a slip rate in between those values. This classification agreed with that of Nuttli (1983), but Scholz et al. (1986) noted that

## Chapter 1

the majority of the events called intraplate earthquakes by Kanamori and Anderson (1975) should be classified as plate-boundary related.

In developing scaling relations using empirical  $m_b$ ,  $M_s$  and  $M_0$  for mid-plate earthquakes, Nuttli (1983) concluded that because the corner periods of large mid-plate earthquakes are smaller than those of plate-margin earthquakes, the fault rupture dimensions are smaller than those of plate-margin earthquakes of the same  $M_s$  value. Thus, for example, for  $M_s=8.0$  a mid-plate earthquake has a fault rupture length of approximately 40 km (according to Table 2 of Nuttli, 1983) whereas a more customary world average is approximately 300 to 400 km (Nuttli, 1983). He estimated the  $m_b$  value of the 16 December 1811 New Madrid earthquake to be 7.2, with a moment ( $M_0$ ) of  $4.0 \times 10^{27}$  dyne-cm, rupture length 60 km, average stress drop 100 bars and fault displacement 580 cm. Analysing the same event, Evernden (1975) concluded that it was not a "great" earthquake, based on the rupture length and energy released. This brings back an old discussion about what is the measure of the size of an earthquake. Is it the seismic moment (low frequency ground motion) or rupture area, or is it the value of  $M_s$  and  $m_b$  (high frequency ground motion)? It seems that this is still an open question. Faults that produce intraplate earthquakes cannot be identified readily (Herrmann et al., 1978; Pearce, 1987; Hinze et al., 1988). There are cases in which the surface trace caused by an intraplate earthquake can be observed, showing that Nuttli's scaling relations are valid for intraplate earthquakes in regions other than the east of the USA. For example, Choy & Bowman (1990) found for the three main shocks of January 22, 1988, with  $M_s$  of 6.3, 6.4 and 6.7, that occurred near Tennant Creek, Australia, had stress drops of 58, 136 and 85 bars respectively, and had a surface fault trace of 32 km length divided into three fault zones.

Notable intraplate analogies to the Tennant Creek sequence in which three earthquakes of comparably large magnitude occur in a small interval of time and in a small volume, can be found that suggest that the multiple main shock may be a more significant aspect of intraplate faulting than previously recognized (Choy & Bowman, 1990). The New Madrid sequence of 1811-1812 occurred over a 3-month period. Iseismals of the three largest New Madrid earthquakes (having  $m_b$  greater than 7.0) suggest that the epicentre of each earthquake was northeast of the preceding event and may have occurred on a fault or in a source volume that had not been ruptured by an earlier strong earthquake (Nuttli, 1983). The two Gazli earthquakes of 1976 ( $M_s$  7.1) were separated by only 20 km and occurred 39 days apart. The Gazli earthquakes are inferred to have ruptured along fault planes with substantially different strikes (Kristy et al., 1980; Pearce et al., 1980). The two Nahanni, Canada, earthquakes in 1985 ( $M_s$  6.6 and 6.9) were separated by only 3



## Chapter 1

km and occurred 79 days apart. Choy & Bowman (1990) suggest that in the multiple main shock sequence the spatial and temporal proximity of earthquakes indicate that the earthquakes did not occur independently and that they can be interpreted in terms of the time-dependent rupture model of Das & Scholz (1981a).

### 1.2.2 Stress field and intraplate earthquakes

Another important factor in the study of intraplate earthquakes is related to the driving mechanism of plate tectonics. One of the most direct means of investigating the causes of plate motion is through the state of stress in the lithosphere, since the stress is a response to the distribution and magnitude of forces applied to the plates (Bergman & Solomon, 1980). Intraplate earthquakes have been recognized as an important source of information because their fault plane solutions provide one of the few constraints on the orientations of principal stresses within plates (Mendiguren, 1971; Sykes & Sbar, 1973; Bergman & Solomon, 1980). Sykes & Sbar (1973) investigated the focal mechanism of about 80 intraplate earthquakes and indicated that the interior of many lithospheric plates are characterized by a large horizontal compressive stress, and pointed out that these stresses seem to be related to the driving mechanism of plate tectonics. A variety of possible models have been proposed to explain the driving mechanism of plate motions on the basis of intraplate stress orientation (Sykes & Sbar, 1973; Richardson et al., 1976, Richardson, 1978) but Liu & Kanamori (1980) pointed out that the details of the source processes of intraplate earthquakes are not well understood and a more quantitative understanding of the source processes of these events is important for evaluating these models.

In an attempt to put the intraplate earthquakes into the framework of plate tectonics Fletcher et al. (1978) described seismic intraplate activity as being located along continental extensions of oceanic transform faults. It was difficult for them to devise a mechanism for extending deformation inland from these transforms. A more satisfying explanation (Kristy et al., 1980; Anderson, 1986; Choy & Bowman, 1990) comes from Sykes (1978) in which continental intraplate earthquakes result from reactivation of appropriately oriented preexisting zones of weakness, inherited from the last major orogeny, in the presence of stress fields of sufficient magnitude. These zones of weakness were reactivated during continental rifting; several remained active as zones of alkaline magmatism for as long as 100 m.y. after initial rifting, and many are now the loci for the release of intraplate stresses during earthquakes. Hinze et al. (1988) point out that increasing evidence supports the "zone of weakness model" as the appropriate model for the dominant contemporary tecto-

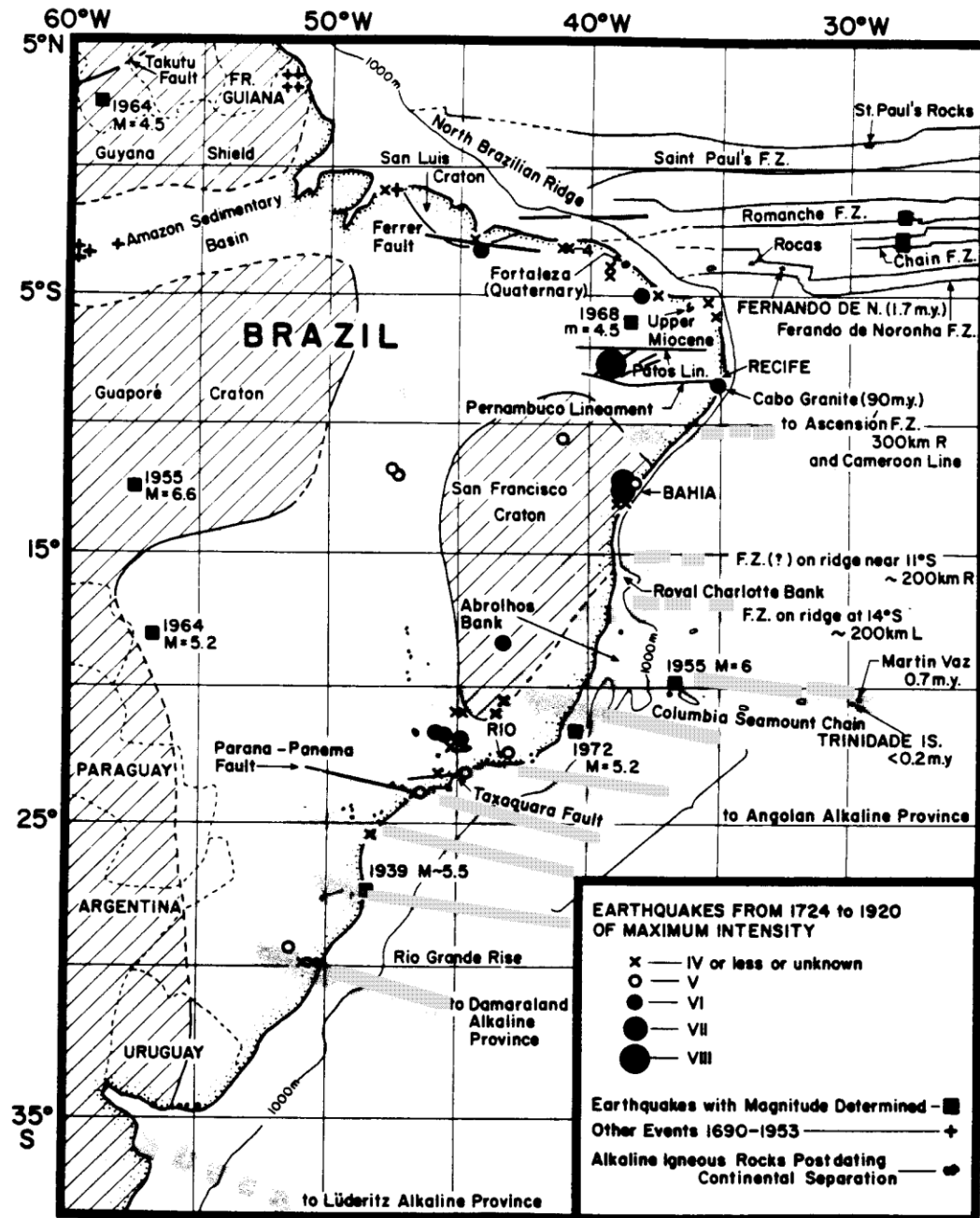


Figure 1.1 Seismicity, igneous rocks postdating continental separation, and fracture zones near the continental margin of Brazil. Earthquake locations are as follows: 1724-1920, felt reports of Branner (1912, 1920) with intensities in the Rossi-Forel scale; felt reports 1690-1953, for the Amazon basin, O'Reilly Sternberg (1955); instrumental locations with magnitude determined (squares), Gutenberg and Richter (1954); Rothé (1969) and reports of U.S. Geological Survey through 1975. Some felt reports (not shown) for western Brazil may be from shocks located farther west in the Andean region. Fracture zones near continental margin (continuous grey lines) are from Francheteau and Le Pichon (1972), Gorini and Bryan (1976), and Kumar et al. (1977). Fracture zones inferred from offsets of mid-Atlantic ridge by appropriate finite rotations are indicated by dashed grey lines. Young igneous rocks are from Almeida (1971), Marsh (1973), Neill (1973), Asmus and Ponte (1973), Baker (1973), and Gorini and Bryan (1976). Tectonic features on land are from de Loczy (1970), Gorini and Bryan (1976), and Kumar et al. (1977). Cratonic areas (hatched) older than 800 m.y. are from Almeida et al. (1973) and Hurley and Rand (1973). (Figure and captions are from Sykes (1978)).

## Chapter 1

nism and the "local basement inhomogeneity model" as the mechanism for minor, low energy release earthquake activity. However, Anderson (1986) points out that these explanations offer no means of estimating the rate of earthquake occurrence.

### 1.3 Intraplate earthquakes in Brazil

Central and eastern South America, and in particular the country of Brazil, are characterized by low midplate seismicity and a low density of seismograph stations. In Brazil, the first seismograph station (RDJ) was installed in 1906 in the city of Rio de Janeiro, in the southeast of the country. Only in 1965 was the second station (NAT) installed in the capital city of the State of Rio Grande do Norte where the data for the present work were collected. The station NAT was part of the WWSSN network and operated until 1975. In 1980 it was transferred to Caicó in the interior of the same State with station code CAI. In 1966 an array type station was installed in Brasilia, the Brazilian capital city. So, until 1970 only three seismograph stations were operating in Brazil. Maybe for this reason, very little comprehensive work was done until that time to study the seismicity of this large intraplate area. An important catalogue of known earthquakes from 1724 up to 1920 was made by Branner (1912, 1920) but this was mostly restricted to the northeast region.

With the implementation of nuclear power stations and some big hydroelectric projects in the early seventies, more seismograph stations were installed in Brazil and more seismicity and tectonic-related studies begin to appear. Most of these works are referenced in the study of Sykes (1978) which, in this respect, can be considered a summary of the investigations done until then on this subject. The map of figure 1.1 from Sykes (1978) gives an idea of the seismicity of Brazil. Epicentres of the western part close to Peru-Brazilian border do not appear in the map because they are plate margin-related earthquakes. The largest recorded shock that occurred in Brazil is the  $m_b = 6.6$  event of 31st January 1955 near Serra do Tombador, State of Mato Grosso, in the Guaporé craton (figure 1.1). This earthquake occurred in a sparsely populated area and there is no report about damage or felt area, but it is known to have been felt at the city of Cuibá, 375 km away from the epicentre.

### 1.4 Seismological studies in Brazil

A more complete and detailed compilation of the seismicity of Brazil was carried by Berrocal et al. (1984). Some epicentres referenced by Sykes (1978) were relocated and some dates in the seismicity map of figure 1.1 were corrected. Although they were able to find a significant number of events previously unknown, the basic pattern shown in figure 1.1 remained unchanged. Detailed descriptions of some of the felt events are given by them. For example, the magnitude 5.5 earthquake of 3rd April 1939 is reported as causing small damage in several localities along the coast of the Santa Catarina State, felt in another three states of Brazil, and in the northeast of Argentina. The  $M_S = 6.0$  earthquake of 28th February 1955 occurred about 360 km off-shore, slightly north of the Vitoria-Trindade ridge, and was felt in the city of Vitoria with intensity **V** (Modified Mercalli Intensity scale, MM). The Mogi-Guaçu, São Paulo, event of 27th January 1922 is particularly important because it happened close to the most populated and industrialized area in Brazil. Macro seismic data for this event indicated a felt area of 250,000 km<sup>2</sup> and its magnitude was estimated as  $m_b = 5.1$ . Berrocal et al. (1984) also made a preliminary correlation between tectonic features and seismicity in Brazil. Seven seismotectonic regions were identified but as noted by the authors the classification is very preliminary due the scarcity of data.

To support the idea that continental intraplate earthquakes tend to be concentrated along preexisting zones of weakness, Sykes (1978) observed that earthquakes in southern Brazil are concentrated in areas characterized by the occurrence of young alkaline rocks. These areas coincide with regions where a large number of fracture zones are found near the continental margin (figure 1.1). The Amazon basin is regarded as a major zone of weakness of pre-Mesozoic age. He noted that the St. Paul's and Romanche fracture zones are located nearly along the strike of this basin. Several historic earthquakes are known within the basin. In order to explain the occurrence of earthquakes far from the trend of an existing fracture zone, or far from continental margins, Sykes suggested that other reactivated zones of weakness could be found in different tectonic settings. Examples of such zones would be major faults in older fold belts that developed in either the Mesozoic or the Cenozoic, suture zones, failed rifts and other tectonic boundaries.

To understand the state of stress within the South American plate, Mendiguren & Richter (1978) were able to find the focal mechanisms of five shocks and for a swarm sequence. They found thrust mechanisms for these shocks and suggested that a dominant regional NW-SE oriented maximum compressive stress would be consistent with all their data. According to them the dominant source of

## Chapter 1

stress in the South American plate would be the ridge push from the Mid Atlantic Ridge, whereas the resistive force at the base of the lithosphere is sufficiently small that it does not exceed the ridge push. However, Assumpção et al. (1985) pointed out that only near the Atlantic coast are the available data compatible with Mendiguren & Richter's hypothesis. Further to the west, the stress field changes and the direction of the maximum compressive stress seems to be aligned N-S. Thus, the stress field in Brazil is certainly not uniform and, in some areas, local sources of stress may predominate over regional fields (Assumpção et al., 1985). Among the events they studied is the  $m_b = 5.5$  event of 5th August 1983 that occurred in the middle of the Amazon sedimentary basin. The epicentral area is covered by about 2 km of sediments and no major tectonic feature has yet been mapped nearby that could be clearly related to the earthquake (Assumpção et al., 1985). The focal depth of this event was well determined by them as in the lower crust at 23 km. This indicates a brittle behaviour at an unusual depth (Ansell et al., 1986). Another event happened in this region on 14th Dec 1963 and was studied by Assumpção & Suarez (1988). They located this event in the upper mantle at a depth of 43 km. Both central Amazon basin events shown reverse faulting mechanism with N-S aligned stress.

### 1.5 Seismicity in Northeastern Brazil

Since the studies of Branner (1912; 1920) it is clear that the Northeastern region is one of the most active seismic areas in Brazil. The earthquake catalogue computed by Berrocal et al. (1984) confirms this picture. Table 1.1 shows a list of the most important historical earthquakes in the region. Most of the seismicity in this area is confined to three zones (figure 1.2):

- the Potiguar basin boundary where the major seismic activity is located, especially since 1968.
- the Recôncavo Baiano area, where at least two events with magnitude 4 occurred at the beginning of the century.
- the eastern Pernambuco zone where a relatively continuous seismic activity is known since the beginning of the century.

According to Torquato & Cordani (1981) the northeast of Brazil where the seismic zone A is found (see figure 1.2) lies in the Precambrian Borborema Province (see figure 1.3) which is part of a much larger unit including the territories of Dahomy, Nigeria and Cameroon in West Africa. Two fundamental types of terrain can be found in the Borborema Province: gneissic (migmatitic-granitic massifs) and

DATE	LOCAL TIME	LOCALITY	STATE	MM INT.	MAG. $m_b$
08.08.1808	08H--	Açu	RN	<b>VI</b>	4.8
14.02.1903	----	Baturité	CE	<b>VI</b>	4.1
15.02.1903	----	Baturité	CE	<b>VI</b>	4.1
16.02.1903	----	Baturité	CE	<b>VI</b>	4.1
22.03.1911	15H--	I.de Itaparica	BA	<b>VII?</b>	---
06.11.1915	15H30M	I.das Fontes	BA	<b>VI</b>	4.0
07.11.1917	20H25M	Rio Fundo	BA	<b>VI-VII</b>	4.3
23.11.1919	01H20M	M.Recôncavo	BA	<b>VII</b>	4.2
14.04.1928	21H59M	Aracati	CE	<b>VI</b>	4.0
31.12.1949	----	Lajes	RN	<b>VI</b>	---
12.01.1968	22H55M	Sa.Macacos	RN	<b>VI</b>	3.9
15.02.1968	10H20M	Sa.Macacos	RN	<b>VI</b>	4.1
23.02.1968	11H23M	Sa.Macacos	RN	<b>VII</b>	4.6
29.01.1970	----	S.C.Capibaribe	PE	<b>VI</b>	---
---.11.1970	----	Alagoinha	PB	<b>VI</b>	---
22.07.1973	18H22M	Parazinho	RN	<b>VI-VII</b>	4.3
15.12.1974	02H14M	S.L.Curu	CE	<b>VI</b>	3.3
18.05.1976	05H30M	Ibicaraí	CE	<b>VI</b>	3.7
25.05.1976	05H30M	Ibicaraí	CE	<b>VI</b>	3.7
25.02.1977	10H40M	Riachuelo	RN	<b>VI-VII</b>	3.6
12.03.1977	04H--	Ibaretama	CE	<b>VI</b>	---
20.11.1980	00H29M	Pacajus	CE	<b>VII</b>	5.2

Table 1.1 Important earthquakes ( $m_b \geq 3.0$  or  $I \geq \text{VI}$  MM) which occurred in Northeast Brazil (after Berrocal et al., 1984).

metavolcanic-metasedimentary mobile belts. The region of Brasiliano folds presents a complex arrangement, in mosaic, including different systems of linear folds mutually separated by elevated parts of the basement, either related to faults or not.

The Borborema Province is divided into sections by a complex fault system, separating the fold systems or cutting through them (Almeida et al. (1981). According to these authors, the faults seem to be very old, deep and reactivated on different occasions, with a different character. For example, the transcurrent character noted on the maps is only the most obvious, having occurred late in the Brasiliano Orogenic Cycle. The general trend of the province's structures is arranged as a fan opening towards the northeast, diagonally to the coast. It suffered deviations and inflexions due to the faulting movements; two of these faults, the lineaments of Pernambuco and Patos or Paraíba, both with a E-W direction (see figure 1.3), stand out in this assemblage due their size (Almeida et al., 1981). Lithospheric shear zones frequently behave as permanent zones of weakness during

## SEISMICITY OF NORTHEAST BRAZIL

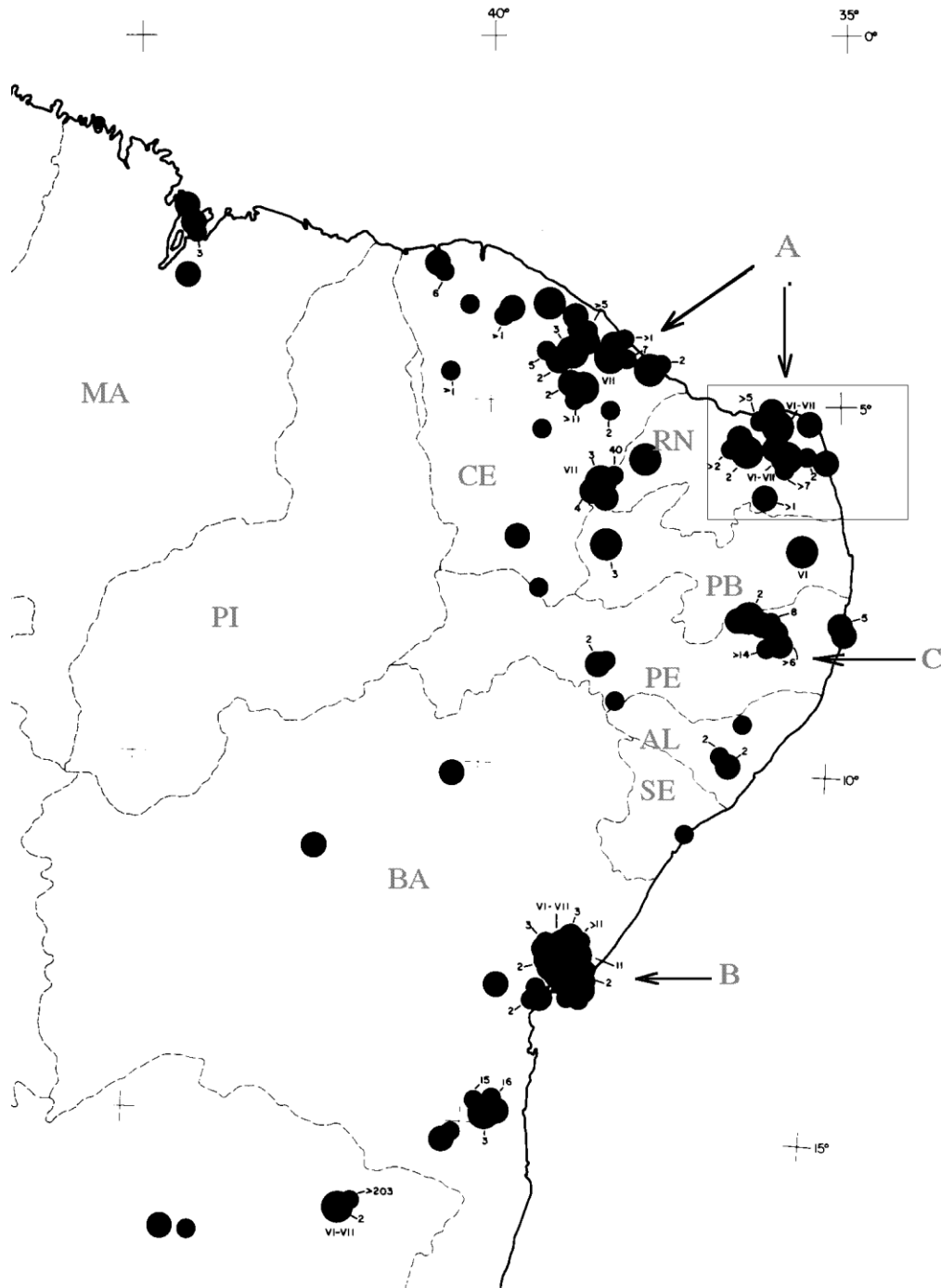


Figure 1.2 Seismicity map showing the major seismic zones of Northeast Brazil: the Potiguar basin (zone A); the Recôncavo Baiano area (zone B); the eastern Pernambuco (zone C). Pecked lines represent the boundaries between states. The box in zone A contains the area of the present study. Filled circles indicate epicentres. Roman numerals indicate intensity values based on the Modified Mercalli Intensity Scale (MM). Arabic numbers indicate the identification numbers of events used in the study. (after Berrocal et al., 1984).

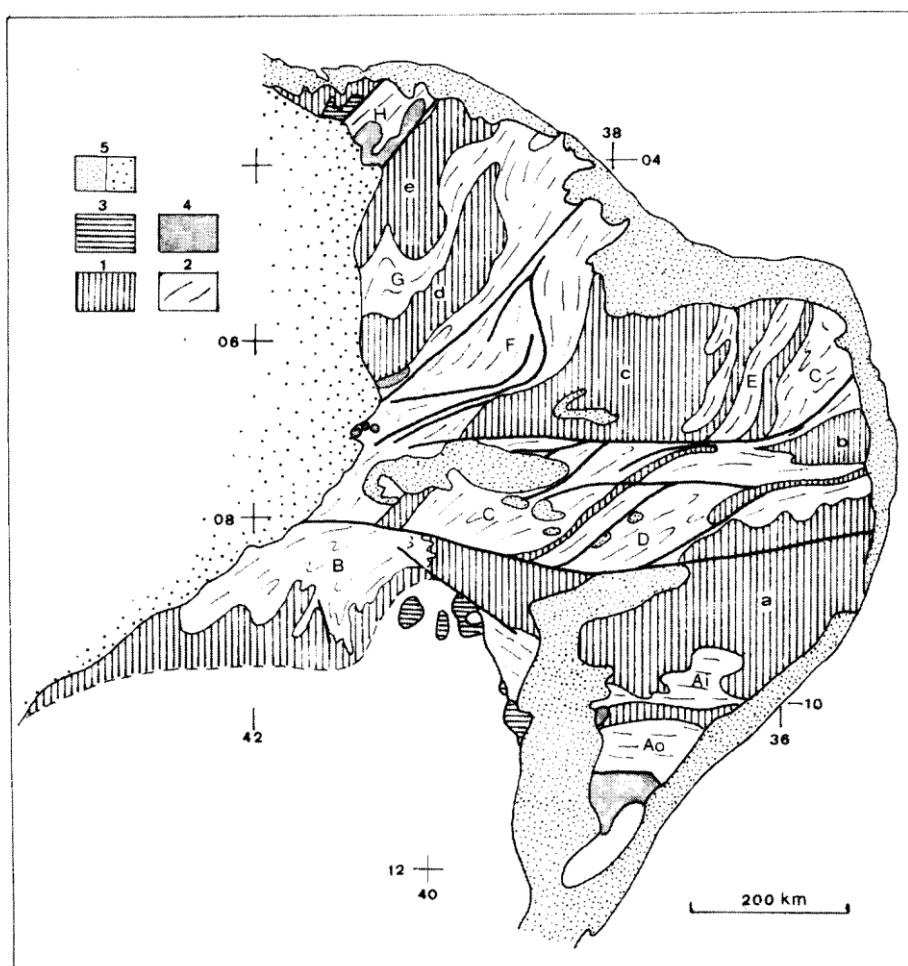


Figure 1.3 Borborema Province. Legend: 1 = Older basement reworked during the Upper Precambrian; 2 = Brasiliano fold belts (E = Seridó belt); 3 = sedimentary covers correlative of the Brasiliano belts; 4 = molasse deposits; 5 = Phanerozoic sedimentary covers. Heavy lines represent major faults. (after Almeida et al., 1981).

the evolution of continents: they are easily reactivated when the crust is submitted to a new tectonic event and the deformation tends to be localized at the vicinity of, or within, ancient faults zones (Sykes, 1978).

In northeast Brazil, seismicity seems to be concentrated more in the northern part of the Precambrian Borborema Province than in the southern part. Excepting in the Recôncavo Baiano area (zone B in figure 1.2), no events greater than magnitude  $m_b = 4.0$  are known to have occurred south of latitude  $6^\circ\text{S}$  (Assumpção et., 1985). In the northern part of Borborema Province, and in



## Chapter 1

particular in zone A of figure 1.2, the structural trend and small faults tend to be oriented in the northeast direction, whereas in the less seismic southern part of the province the structural trend and major faults are preferentially oriented in the east-west direction as seen in figure 1.3 (Almeida, 1981). The largest known earthquake in northeast Brazil ( $m_b = 5.2$ ) occurred on 20th Nov 1980 in the state of Ceará (see figure 1.2) in the northern part of the Borborema Province. Assumpção et al., (1985) inferred an east-west compression from fault mechanism studies for this earthquake. They suggested that a regional east-west compressional stress would be compatible with the structural trend of the region. According to those authors, this regional east-west compression can explain the observed higher level of seismicity in the northern half of the fold belt as a consequence of the favourably oriented structural trend in the northeast direction, and the fewer observed earthquakes in the southern half of the province as a consequence of the unfavourably E-W oriented structures. A few other studies have confirmed this supposition and additionally show that seismicity in northeast Brazil is confined to a shallow depth; no events deeper than 10km were found in the region (Assumpção et al., 1985; Ferreira et al., 1987; Assumpção et al. 1989a).

### 1.6 The João Câmara region

João Câmara lies 70km from the northeast Brazilian coast in the Precambrian Borborema Province. This area lies in the transition between an Archean granite-gneiss massif in the east and a Late Proterozoic biotite-schist mobile belt to the west (see figure 1.4). The transition zone comprises three major north-south trending shear zones and quartz-feldspar paragneiss and basic migmatite lithologies. To the north of the road BR 406 the Precambrian is unconformably overlain by the Cretaceous Açu formation (quartz arenites) and Jandaira Formation (micritic limestones) (I.G.Stimpson, pers. commun., 1987).

On 30th November 1986 a magnitude  $m_b = 5.1$  earthquake occurred near João Câmara. Epicentre determinations and a composite fault mechanism performed from the aftershock sequence suggest an almost vertical, SW-NE oriented fault (see Samambaia fault in figure 1.4) and a right lateral strike-slip mechanism with a small normal component (Ferreira et al., 1987). The east-west compressive stress inferred for this earthquake is compatible with the previous regional stress direction hypothesis of Assumpção et al. (1985). Unfortunately the velocity structure of the Borborema Province, and in particular of the João Câmara region, is largely unknown as a consequence of the almost complete absence of previous geophysical

studies in the region, but good epicentral determination with small arrival time residuals typically less than 0.06 sec with a halfspace model, suggests a very simple velocity structure (Takeya et al., 1989).

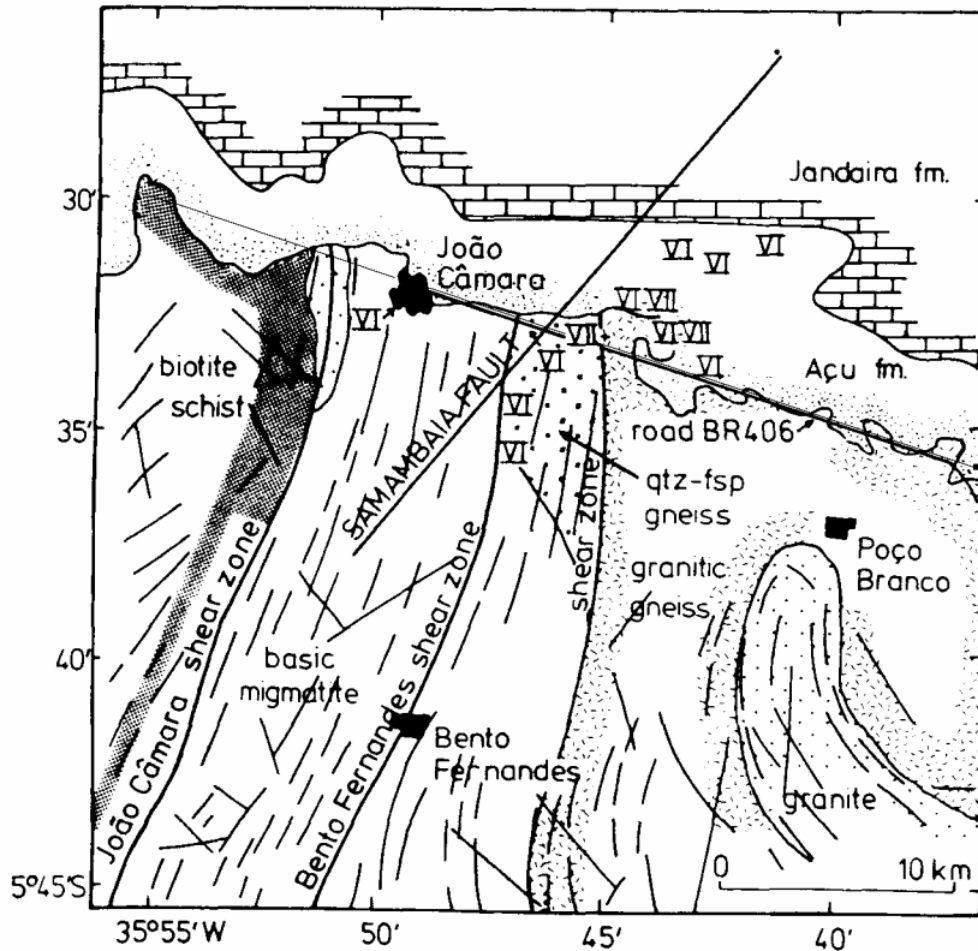


Figure 1.4 Map of the João Câmara area showing the Precambrian shear zones of Bento Fernandes and João Câmara, and the Samambaia fault inferred from the recent seismicity recorded by smoked paper drum recorder. Intensity values (Modified Mercalli) for the 30th November 1986 event of  $m_b = 5.1$  are also shown. Geology from aerial photography, interpretation of DNPM (1974), and field observations of I.G.Stimpson (pers. commun., 1987) (after Takeya et al., 1989).

Some geophysical studies have been performed in the João Câmara area since the occurrence of  $m_b = 5.1$  earthquake. Moreira et al. (1990) computed a Bouguer anomaly map of the area and their residual map shows a positive anomaly approximately aligned with the epicentres of the Samambaia fault, bounded by two negative anomalies probably caused by low density plutons. Padilha et al. (1990) performed observations in the same area using magnetotelluric methods. In a preliminary interpretation they found a small differentiated structure in the upper

## *Chapter 1*

crust of the epicentral region. According to those authors, this structure is characterized by a lower resistivity than the surrounded area, extending from 500m below the surface down to about 3km. Other concentrations of heterogeneities to the west of Poço Branco are referred to by the authors as also probably related to the seismic activity of the region. In 1974 the Brazilian Department of Mineral Production undertook a radar imagery project (DNPM, 1974) for the purpose of geological survey in the Northeast Brazil and the geological map of figure 1.4 was based on the results of that project.

Gallardo (1988) and Gallardo & Perez (1988) carried out neotectonic investigations in the region, based on a geomorphological approach, and attributed the seismicity in the João Câmara area to a consequence of E-W and ENE dextral-extensional fault zones. They found no field evidence to support the existence of the Samambaia fault as proposed by seismological studies. The governmental mapping agency, CPRM, undertook a project in the coastal region of Rio Grande do Norte, enlarging the area previously investigated by Gallardo (1988). They also added outcrop scale structural data (fracture and striation pattern analyses), calculating a number of local stress fields across the region. The structures regarded as the youngest, and related by them to the present-day activity, were explained by NW compression and dextral strike slip movement on E-W and ENE faults, supporting the assumptions of Gallardo (1988). One of the obvious reasons for such a discrepancy in relation to the seismological observations, as for example of Ferreira et al. (1987), is that the inferred stress fields and geomorphological features do not reflect the present-day activity. Many of the outcrops analysed display complex patterns of faults and striae, and the computer methods utilized were not adequate ones for such cases (E.J. de Sá, pers. commun., 1991).

## **CHAPTER 2**

### **JOÃO CÂMARA EARTHQUAKE ACTIVITY**

#### **2.1 Evolution of 1986-1990 series from drum recorder data**

A magnitude 3.0 earthquake on the 5th August 1986 which was strongly felt at the town of João Câmara (hereafter abbreviated to J.Câmara or simply JC), in the state of Rio Grande do Norte, began the longest swarm of earthquakes so far recorded in northeast Brazil. At that time no instruments were available locally to monitor the aftershock sequence. This event was very well recorded by the WWSSN station CAI (Caicó) located 300 km south of the epicentre. Results from a preliminary macroseismic survey made in the days immediately following the earthquake by the staff of the Universidade Federal do Rio Grande do Norte (UFRN) indicated a felt area of about 1,500 km<sup>2</sup>, as shown in figure 2.1. The felt area seems large for an earthquake of this size and two factors may explain this. First, the magnitude of 3.0 for this event was calculated from the seismogram of the station CAI (Ferreira et al., 1987), but Assumpção et al. (1989b) have shown that a correction has to be made when using data from this station. After applying the station correction the magnitude increased to 3.4. Secondly, as stated in section 1.2.1, one of the distinct characteristics of intraplate earthquakes is the large felt area when compared with interplate earthquakes. Assumpção et al. (1980) showed that the following magnitude-felt area relations can be used in Brazil:

$$m_b = 1.63 + 0.60 \times \log(A_f) \quad 2.1$$

$$m_b = 2.29 + 0.55 \times \log(A_{IV}) \quad 2.2$$

where  $A_f$  and  $A_{IV}$  are felt areas limited by isoseismals **II** and **IV** respectively in the Modified Mercalli Intensity Scale. In applying equation 2.1 to this event, the value  $m_b = 3.5$  is obtained, which is in close agreement with the station-corrected magnitude.

## Chapter 2

On 21st August 1986 an event of 4.3  $m_b$  was felt not only at J.Câmara town but at Natal, capital city of the state, 70 km from the epicentre. This earthquake caused intensities up to **VII** MM in the locality of Samambaia, 5 km northeast of J.Câmara. Figure 2.2 shows the felt area. Next day, the first portable seismograph station, a Sprengnether MEQ-800 smoked paper drum recorder, coded

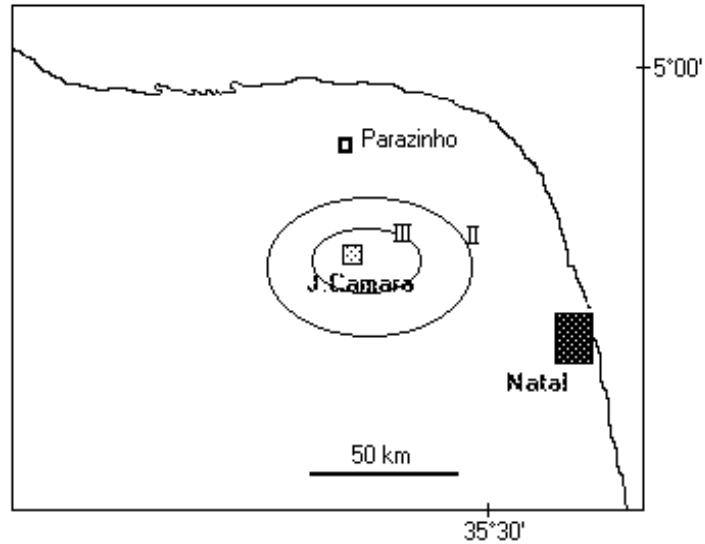


Figure 2.1 Intensity values for the 5th August 1986 event of  $m_b = 3.0$ . This magnitude was later recalculated as 3.4 (see section 2.2). Isoseismal values are based on the Modified Mercalli Intensity Scale.

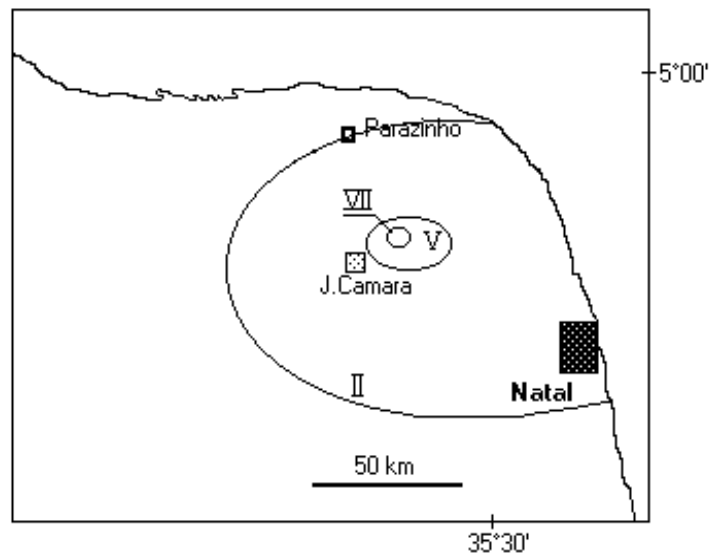


Figure 2.2 Intensity values for the 21st August 1986 event of  $m_b = 4.3$ . This event was felt in Natal, capital city of the Rio Grande do Norte State.

## Chapter 2

JC01, was installed at the farm of Pedra D'gua (5°34'S, 35°51'W). Since then, this station has been recording the seismic activity in the region almost continuously. More than 38,000 events have been recorded by JC01 up to January 1991. Figure 2.3 shows the monthly activity from August 1986 to April 1991. Figure 2.4 (a to e) show the same activity on a daily basis. From those figures it can be seen a decrease in the daily number of events after 22nd August 86 until 2th September 86, when a second burst of activity began with the events on 3rd and 5th September, both with  $m_b = 4.2$ . The third burst of activity started with the main shock ( $m_b = 5.1$ ) on 30th November 1986, continuing with several events of magnitude 4 until February 1987. After then, several other periods of reactivation can be seen, of which the largest is the burst associated with the  $m_b = 5.0$  earthquake on 10th March 1989.

Earthquakes recorded by station JC01

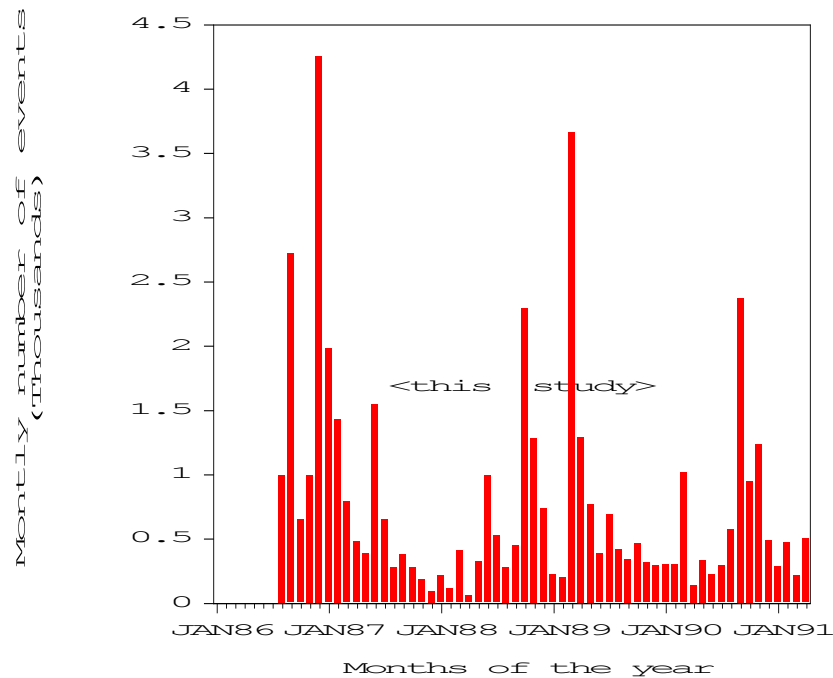
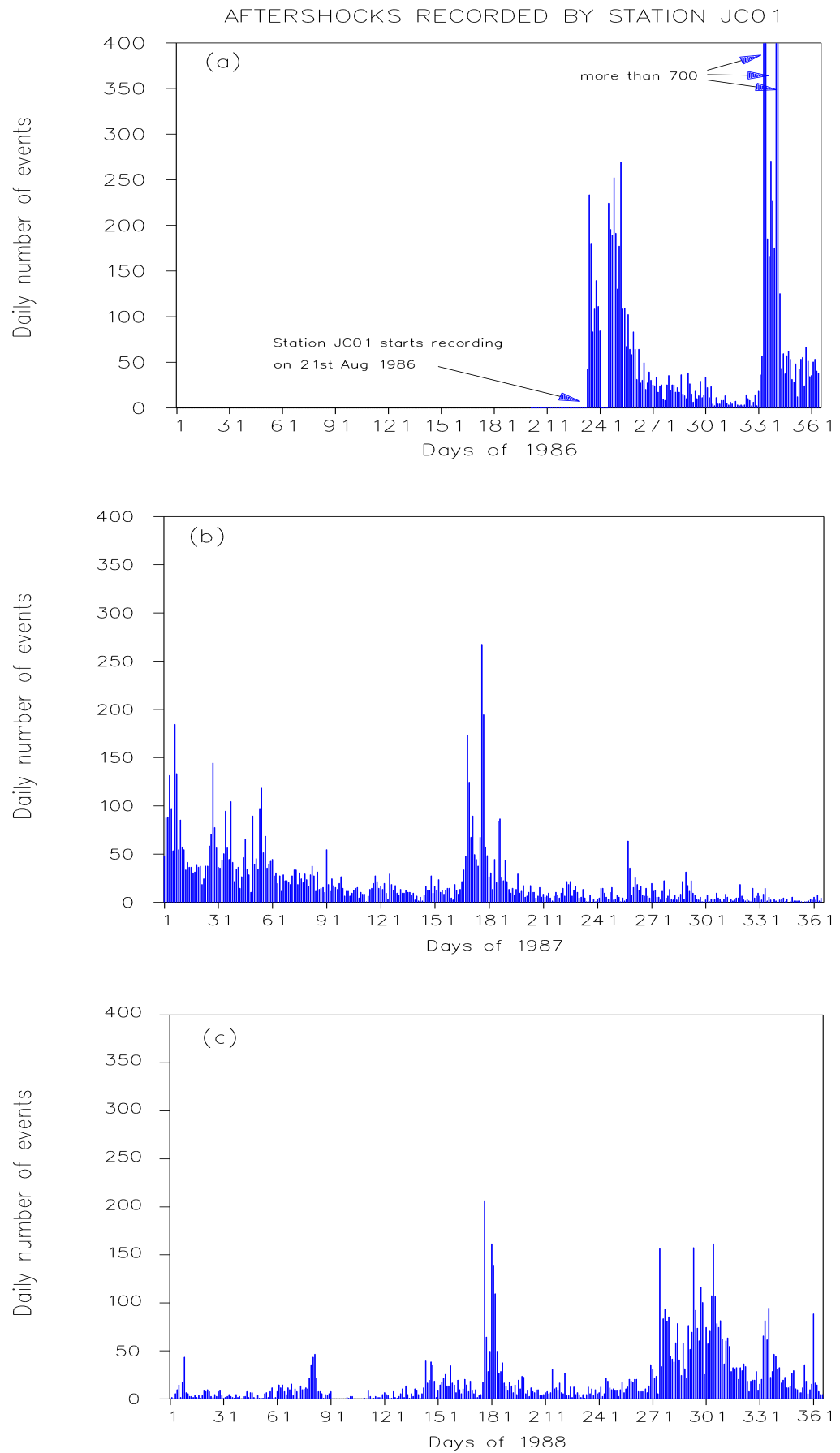


Figure 2.3 Monthly number of earthquakes recorded by station JC01 from 22nd August 86 to 31st March 91.

## Chapter 2



## Chapter 2

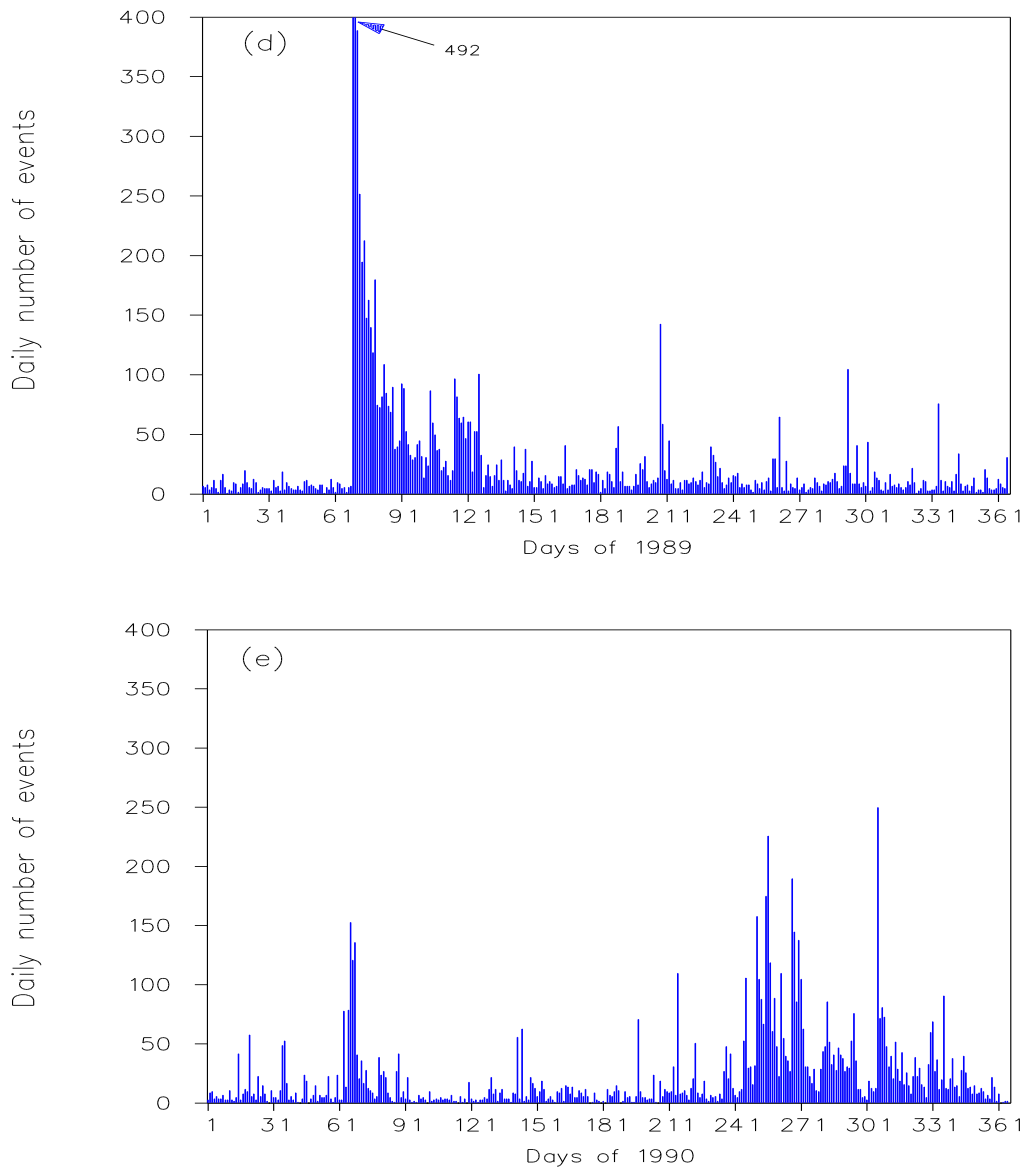


Figure 2.4 Daily histogram of J.Câmara swarm recorded by the smoked paper drum recorder station JC01 between 1986-1990. (a) 1986 (b) 1987 (c) 1988 (d) 1989 (e) 1990. Between 30th Aug 86 and 2nd Sep 86 the station was not recording due to technical problems.

The main shock on 30th November 1986 caused extensive damage to property in and around J.Câmara; some damage also resulted from the earlier events of August and September 1986. Two farmers' houses, distant no more than 2km from the road (indicated as BR406 in figure 2.5), one north and the other south of the road, collapsed and three people were injured at the time of the main shock. Of 4000 houses with varying degrees of damage, 500 were completely rebuilt. Most



## Chapter 2

were rebuilt using a standard design developed by the Brazilian army, comprising timber lattice panels with concrete infill. Many public buildings of brick or stone suffered extensive cracking and, in some cases, including the Church of J.Câmara, partial collapse of walls. A medical centre and two schools were completely rebuilt in reinforced concrete. Serious damage was confined mainly to brick buildings of poorer quality. Cracks and collapse of walls due to failure of mortar or sun-dried bricks was widespread, as was the collapse of tiled roofs. Traditional wooden-framed mud houses suffered superficial cracks at most. Well-constructed concrete buildings, including a new hospital, suffered little damage.

### 2.1.1 Locations of aftershocks

From 24th Aug 1986 several small networks were installed and operated at different periods of time around the epicentral area. All stations deployed were vertical component only, except for one station of the telemetric network. Table 2.1 is a summary describing the equipment and institutions responsible for the temporary seismological works in the region.

In general, the smoked paper recorders were very successful, thanks to the apparently simple velocity structure, good transmission and impulsive S arrivals on almost all seismograms. All these characteristics conspired to ensure good-quality data for the determination of hypocentres, magnitudes and fault plane solutions even when only four stations were operating. However, some of these data remain to be analysed. It is interesting to note that all people questioned during the macroseismic surveys reported tens of events as being audible. Audibility was confirmed by the several teams deploying seismic networks in the area. This observation is an indication that events were rich in high frequency energy and it can be explained by the low attenuation of the basement or by the hypothesis of the presence of high stress in the area. Based on a provisional magnitude scale it was possible to say that events between magnitude 2 and 2.5 were not felt but were audible for the majority of people in the J.Câmara town, sounding like a distant explosion, a quarry blast, or the rumble of distant thunder. Sounds were combined with discernible vibration for events above magnitude 2.5. In localities less than 2km from the epicentre, the loud sound of a magnitude 3.5 event was similar to close thunder and ground vibrations were felt strongly. Richter (1958) relates some cases of sounds accompanying earthquakes in Alaska. In his examples the onset of the sound coincides with P arrival while perceptible vibrations did not begin until the S wave arrived. Because of the short path length it is not possible to say whether this is the case in J.Câmara although technicians and seismologists recording the

## Chapter 2

earthquakes could not detect any appreciable difference in the onsets of the P wave and the sound.

Table 2.1 Summary of the networks deployed to investigate the seismic activity in the J.Câmara area.

Period	N	Seismometer	R	Recorder	Institution
24Aug86 to 30Aug	2 1	S-13 Ranger SS-1	3	MEQ-800	UnB
02Sep86 to 10Sep86	3 1	MKIII-A Ranger SS-1	3 1	Portacorder MEQ-800	IAG
12Sep86 to 10Oct86	3 1	S-13 Ranger SS-1	4	MEQ-800	UnB
04Dec86 to 09Dec86	3 4	S-13 MKIII-A	3 4	MEQ-800 Portacorder	IAG
26Dec86 to 10Apr87-	4	S-13	4	MEQ-800	UFRN
22May87 to 08Apr88*	9	MKIII-A	1	Geostore	CARDIFF /UFRN
20Jul88 to the present	4	MKIII-A	4	MEQ-800	UFRN
11Mar89 to 21Mar89	10	MKIII-A	10	MEQ-800	UFRN

Institutions responsible for the networks: UnB-Universidade Federal de Brasília; IAG-Instituto Astronômico e Geofísico da Universidade de São Paulo; UFRN-Universidade Federal do Rio Grande do Norte; CARDIFF-University College Cardiff. N denotes the number of stations and R the number of recorders. S-13 is from Teledyne Geotech; Ranger SS-1 from Kinometrics; Willmore MKIII-A from Sonosonics; MEQ-800 from Sprengnether and Portacorder is from Teledyne.

\* Refers to the study reported here.

The results of the majority of the studies derived from the several networks referred in Table 2.1 (Velo, 1986; Assumpção, 1986; Lomnitz, 1986; Berrocal et al., 1987; Costa et al., 1989; Oliveira et al., 1989; Sophia & Assumpção, 1989) are in close agreement with the conclusions of Ferreira et al. (1987) and Takeya et al. (1989). Hypocentres were determined by the last authors using the HYPO71 program (Lee & Lahr, 1975) which gave epicentral uncertainties (due mainly to reading errors) generally smaller than about  $\pm 1$  to  $\pm 2$  km. The P to S wave velocity

## Chapter 2

ratio, estimated by the use of a Wadati plot, varied between  $1.73 \pm 0.01$  and  $1.71 \pm 0.01$ . A half-space model with P velocity between 5.9 km/s and 6.2 km/s was used by them. From the event locations it is clear that activity is constrained to a narrow linear zone of length 35 km with a strike of N040°E, and all the located events are shallow (less than 8 km) (Takeya et al., 1989). Despite this fact and the absence of sedimentary cover, no correlation with any surface geological feature has been established. To avoid confusion with other known geological structures in the region, this zone of activity was referred to as the Samambaia fault by Ferreira et al. (1987).

	Strike °	Dip °	Rake °		Azimuth °	Dip °
Fault plane	220	70	201	P axis	81	29
Aux. plane	123	70	-21	T axis	171	0

Table 2.2 Parameters of the fault acquired from the analysis of composite focal plane solutions for selected events from drum recorder data according to the convention of Aki & Richards (1980). From Ferreira et al. (1987)

The composite fault plane solution method has been employed. Results from Ferreira et al. (1987) which are shown in Table 2.2 indicate that the fault mechanism is mainly strike-slip with dextral motion along a N40°E striking fault, with a small component of normal movement. The nodal plane striking SW-NE and dipping about 70°NW coincides with the trend of epicentres and depths. This conclusion has been confirmed for the events with epicentres to the north of the road (Oliveira et al., 1989) but presents some inconsistencies when confronted by solutions for the events to the south of the road (see for example Sophia & Assumpção, 1989) where the situation is not very conclusive.

One interesting feature that arises when putting all these epicentres together is related to their evolution in time and space. Events are not uniformly distributed along the linear zone of the fault but are clustered along certain sections. When including smoked paper drum recorder data analysed by Sophia & Assumpção (1989), Takeya et al. (1989) and Oliveira et al. (1989), the pattern is as in figure 2.5.

For a better description of time evolution the epicentral zone was divided into four sections. The bursts of activity between Aug 86 and Sep 86 took place in section I of the fault but in Oct 86, before the mainshock of 30th Nov 86, some epi-

# João Câmara seismicity map from drum recorder data

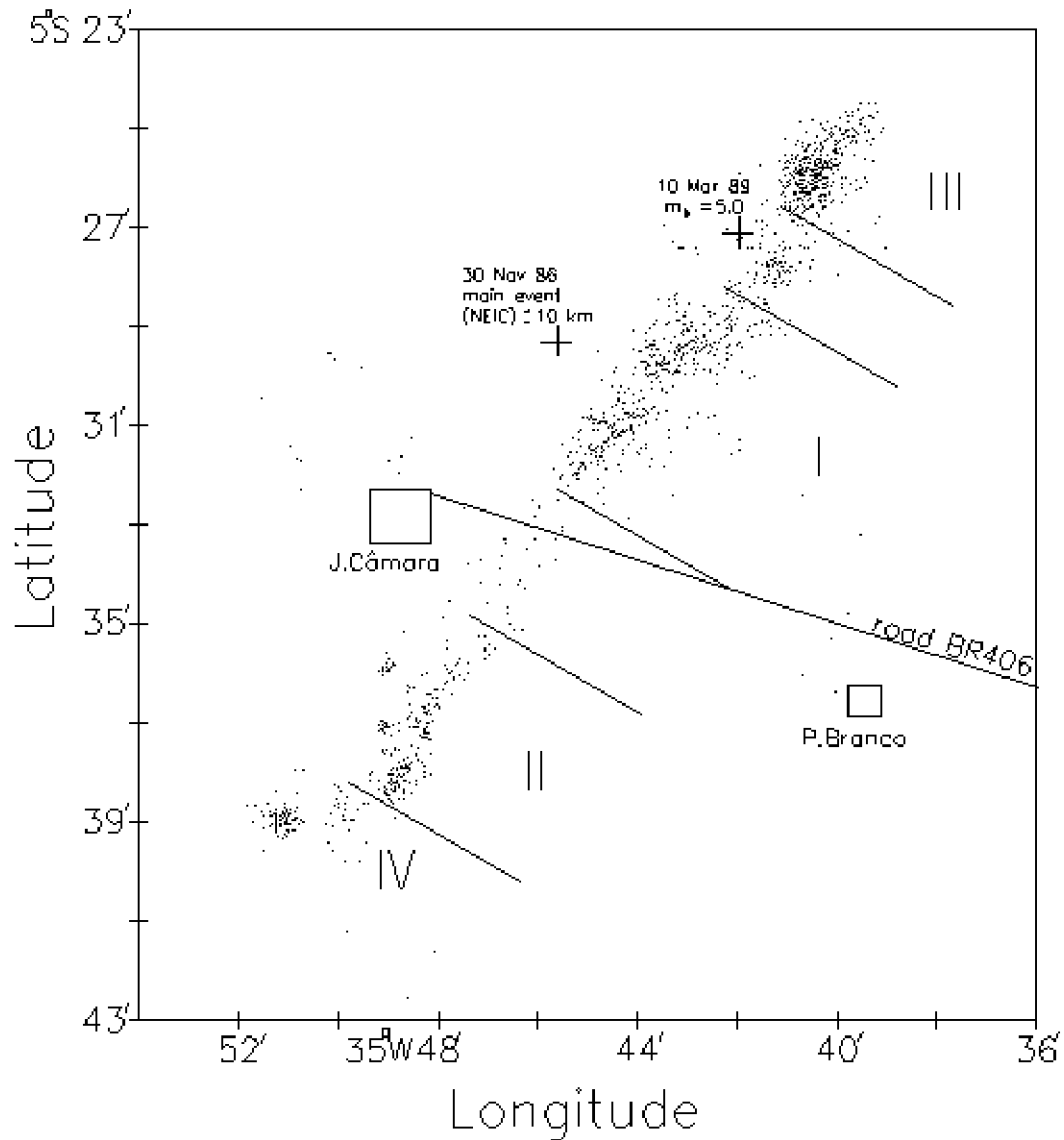


Figure 2.5 Epicentre locations from smoke paper drum recorder data. This map was made from the results of Sophia & Assumpção (1989), Takeya et al. (1989) and Oliveira et al. (1989). It is possible that there is some bias due to the slightly different velocity models and different layouts of the networks used. The fault zone was divided into four provisional sections in order to facilitate the description of its evolution in time. Sections I and II are the more persistent and were defined since the beginning of the activity in 1986. The mainshock of 30th Nov 86 probably occurred between these two sections. Section III was defined in 1988 some months before the second largest shock that happened on 10th Mar 89. Section IV was defined in 1990 with no major shock associate to it.

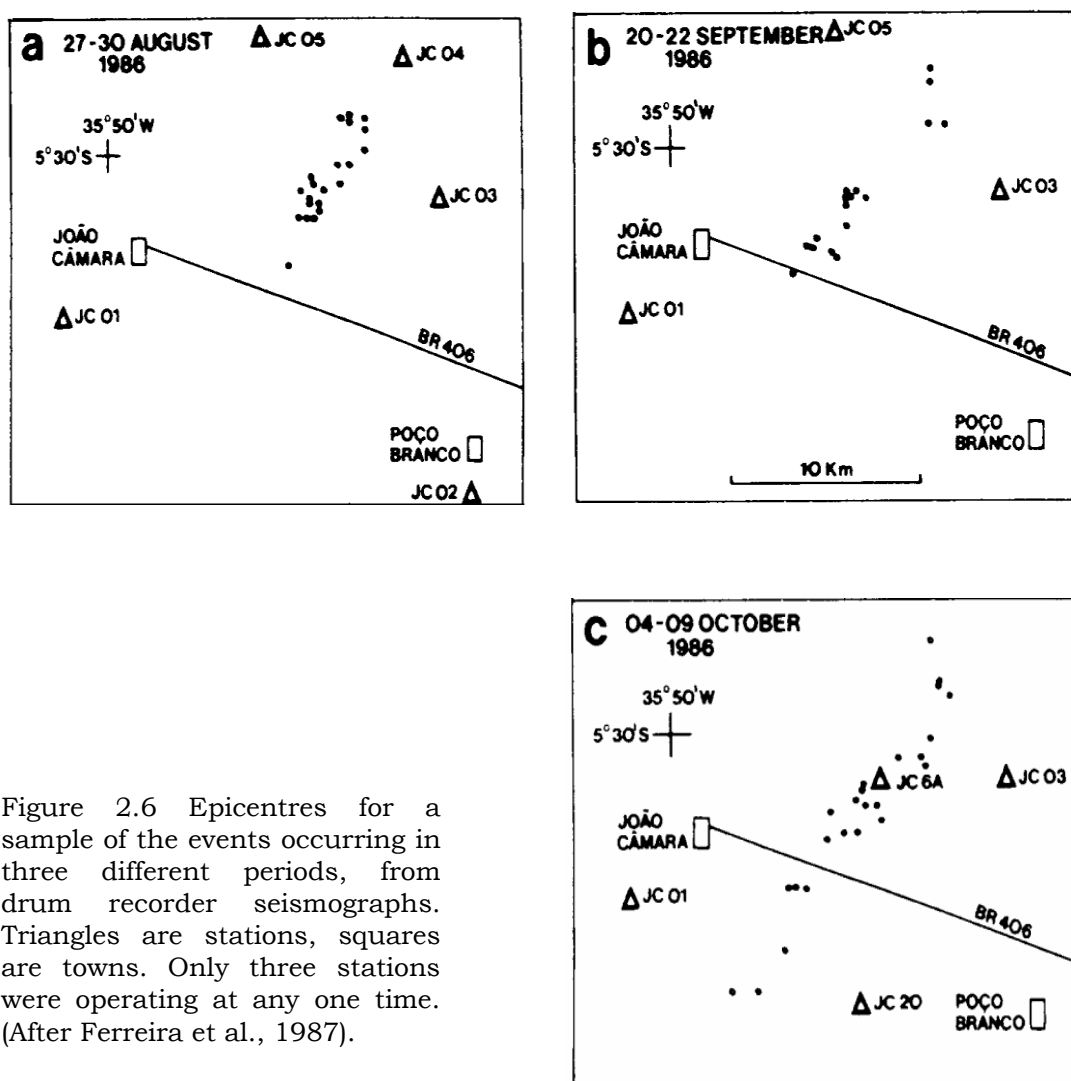


Figure 2.6 Epicentres for a sample of the events occurring in three different periods, from drum recorder seismographs. Triangles are stations, squares are towns. Only three stations were operating at any one time. (After Ferreira et al., 1987).

centres were located in section II as shown in figure 2.5. During this period, activity was restricted to a narrow zone 15 km long. The aftershocks in Jan and Feb 87 that followed the mainshock of 30th Nov 86 were located in sections I and II. Between Aug 88 and Nov 88, events were found mainly in two new locations whilst activity had continued in section I (see figure 2.7). One cluster was detected at the southern edge of section II and another cluster was found in the north part of the fault, defining section III. On 10th March 89 a magnitude 5.0 event happened at the north end of section I (Oliveira et al., 1989). During the following months aftershocks had epicentres in section I or in section III with decreasing activity. In March 90 some earthquakes occurred at a new location at the south of section II, their significance being confirmed by the burst during October 90 which defined section IV. At that time, the length of the active fault was about 35 km. The observations show clearly that section I is the most active section of the Samambaia fault.

## Chapter 2

Figure 2.5 is a plot of the best located events from the available data between Jan 87 and Dec 90. Data useful for location estimates were not collected continuously during that period as can be seen in Table 2.1. Also, not all the accumulated data have been analysed. Nevertheless, figure 2.5 is representative of the data gathered by the drum recorder networks deployed during the 86-90 period. The analysis of the data collected by the telemetric network between May 1987 and Apr 1988 is part of the present study.

### 2.1.2 Location of the two main events

Unfortunately, at the time when the main event occurred on 30th Nov 1986, only station JC01 was working and thus it was not possible to get an accurate location for this event. The National Earthquake Information Centre (NEIC) location of the main event is shown in figure 2.5 though its error is relatively large. Macro seismic observations indicate that the epicentre was near the road, not more than 3 km from it, at the southern border of section I in figure 2.5. Activity prior to this event had defined section II.

The second largest event ( $m_b = 5.0$ ) on 10th Mar 89 was located by a four station smoked paper drum recorder network (Costa et al., 1989) at the opposite boundary of this same section and activity earlier to it defined section II. The ISC location for this second largest shock is  $5^{\circ}81'S$ ,  $35^{\circ}56'W$  but its error relative to the epicentre calculated by the local drum recorder network is large as well. All the events with magnitude greater than 4 occurred in sections I and II. In contrast to the main event, the second largest event had a reasonable coverage by the four station drum recorder network. It was possible to record its sequence of foreshocks and aftershocks.

A magnitude 3.9 event occurred on 1st October 1988 in the very north part of the Samambaia fault. The burst of activity that followed it defined zone III in figure 2.5. This event was located at the south end of zone III and can be regarded as the initiation of the foreshock activity for the second largest event that was located two kilometres southward of it. Although the  $m_b = 5.0$  shock was recorded by the four station network, the sequence of aftershocks that followed it caused an overplot in two of the four records in such way that the arrival time at these stations could not be read. An attempt to relocate this event from a reanalysis of these seismograms will be made later in this work. Based on the time difference between the arrival time in the two remaining stations, in foreshock and aftershock locations,

# Evolution of seismicity from drum recorder data (Aug88-Mar89)

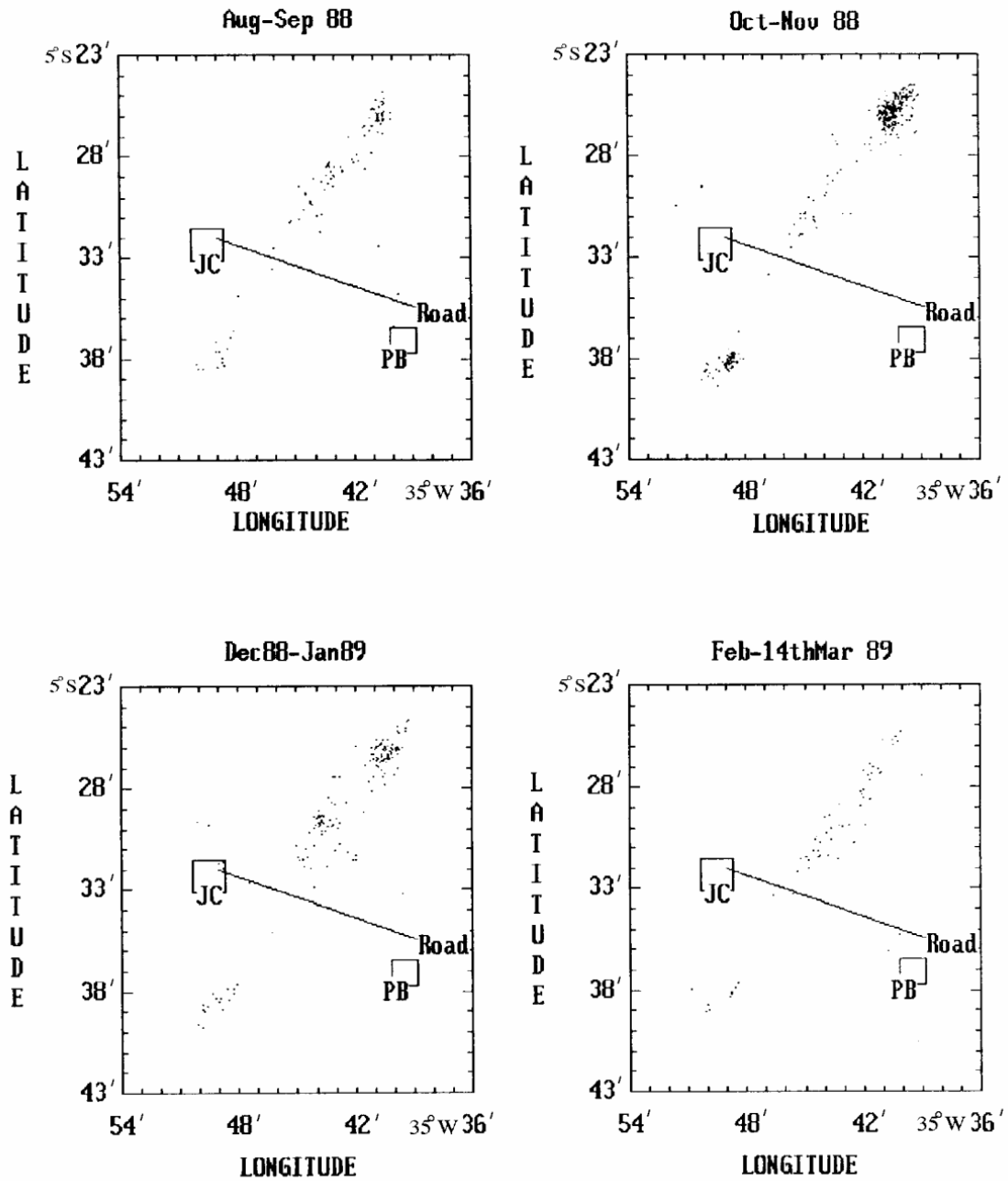


Figure 2.7 Epicentral maps showing the evolution in time of the best located events from the drum recorder data for different periods between August 88 and February 89. Data are from Oliveira et al. (1989).

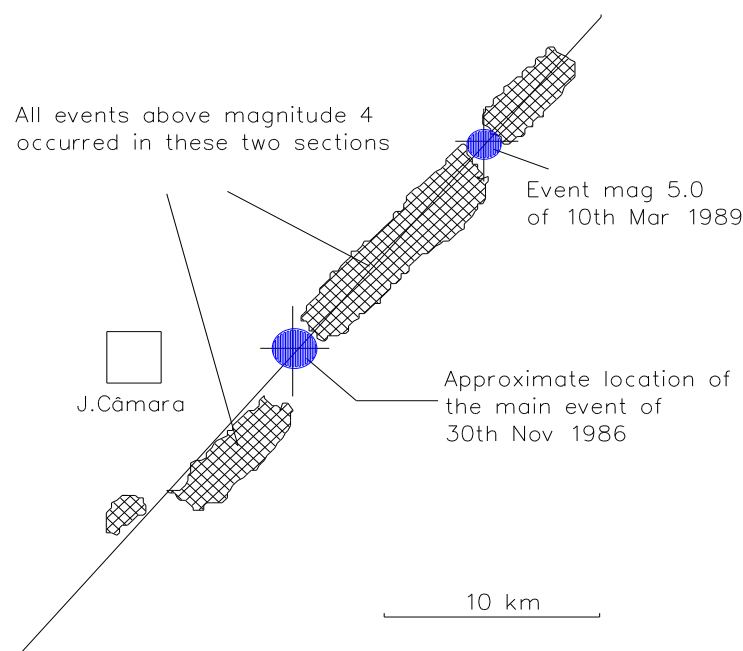


Figure 2.8 Delineation of the Samambaia fault and the location of the two largest events. The location of the main event is based on the macroseismic survey and on the location of foreshock and aftershock activity in the week before and after the main shock. Errors bars indicate assumed S.D. in the location of the two shocks.

and mainly in the macroseismic evidence, Costa et al. (1989) concluded that this event happened in the location indicated in figure 2.5. In assuming the location of these authors as being correct, this means that the magnitude 5.0 event happened in a part of the fault otherwise of relatively low activity. Aftershocks following this event have been located in zones I and III, and very few events were found in the close vicinity of the epicentre. It seems that all the stress which had accumulated in the epicentral area was liberated at once by the slip and this movement caused a local increase in stress at the boundary of the epicentral region, which generated the aftershock sequences found in zone I and III.

Some strong common features arise when the activity behaviour of the two main shocks is compared, and for this reason it is impossible to ignore the possibility that the main shock occurred in the gap between zones I and II. Although this eventuality has been considered improbable in previous work (see for example Takeya et al., 1989), it is now considered to be a realistic possibility and further evidence to support this idea will be found in this study. Figure 2.8 outlines the Samambaia fault and shows the locations of the two main shocks inferred by the works of Ferreira et al. (1987) and Costa et al. (1989) relatively to the clusters of events.



### 2.1.3 Historical data

There is evidence of previous seismicity in the J.Câmara area. In particular, earthquake activity occurred locally in 1983-84 (maximum magnitude 2.2) (Ferreira & Assumpção, 1983; Brazilian Geophysical Society, 1984, 1985; Ferreira et al., 1987). Activity also occurred in 1952 and on previous occasions earlier this century, for which no detailed information is available.

A nearby swarm between July and September 1973 was recorded by the WWSSN station NAT that operated from 1964 to 1975 in the city of Natal located 70 km from J.Câmara. Berrocal et al, (1984) reported a magnitude  $m_b = 4.1$  earthquake on 22nd July 1973 as the major event related to that swarm which occurred in the region of Parazinho located 40 km to the north of J.Câmara (see figure 2.2). This earthquake was felt in Natal and was well documented in the local press.

Another swarm developed during the last week of February 1977 close to the town of Riachuelo, 40 km southward of J.Câmara (Berrocal et al, 1984). Unfortunately no records are available for these events. Although there is no evidence that they are associated with the swarm activity near J.Câmara, it is clear from historical data that people of J.Câmara experienced repeated earthquake activity, by contrast with many communities which appear to have no recollection of felt earthquakes.

### 2.2 Calculation of J.Câmara event magnitudes

All the magnitudes previously referenced for the 1986 series of J.Câmara earthquakes were calculated from the records of Brazilian WWSSN station BDF located in the capital city of Brazil (see figure 2.9) or CAI in the state of Rio Grande do Norte. However, more stations and some corrections are necessary for a better determination of magnitudes and this has been done by Assumpção et al. (1989b). Magnitudes of the major events of the 1986-1987 J.Câmara earthquake swarm were calculated using records from regional and teleseismic stations. Station corrections were determined allowing more homogeneous magnitudes with smaller standard deviations.

For events with epicentres in Brazil but recorded outside, the magnitude calculations were made using the body wave magnitude scale  $m_b$  (Gutenberg and Richter, 1956). The magnitudes for events recorded by Brazilian stations were normally calculated using the regional magnitude scale  $m_R$  (Assumpção, 1983). This magnitude scale was constructed to be consistent with  $m_b$ . In some cases, when the

## Chapter 2

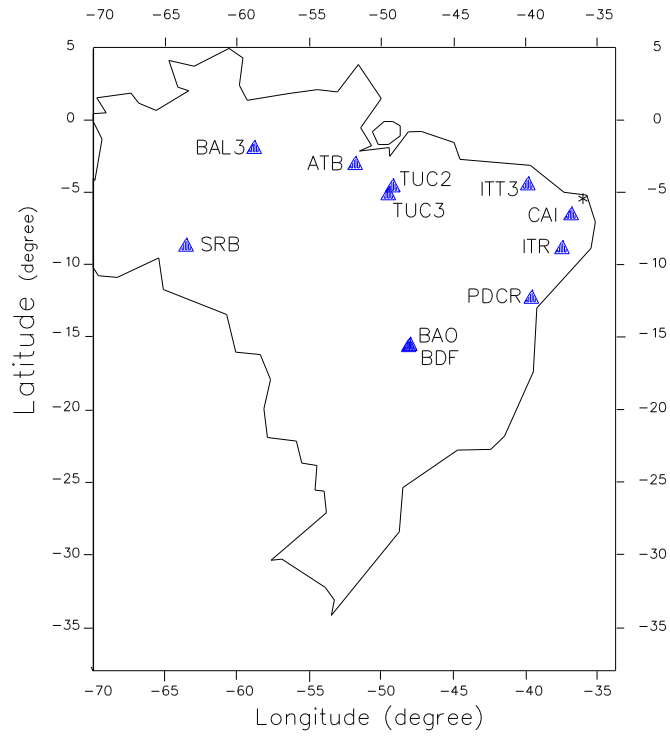


Figure 2.9 Distribution of the Brazilian stations used in magnitude calculations. From Assumpção et al. (1989b).

Table 2.3 Average magnitude residuals and corrections determined for stations. From Assumpção et al. (1989b).

Station	No of events	<u>No correction</u>		<u>With correction</u>	
		Average residual	SD1	Station correction	SD2
ATB	14	0.53	0.04	-0.57	0.03
BAL-3	8	-0.27	0.04	0.29	0.03
BAO	2	-0.04	0.09	-0.14	0.14
BDF	7	0.14	0.05	-0.11	0.04
E1	6	0.16	0.02	-0.17	0.05
E1(Lg)	16	0.27	0.03	-0.22	0.04
CAI	11	-0.25	0.05	0.39	0.04
ITR	23	-0.09	0.04	0.17	0.02
ITT-3	14	-0.31	0.06	0.42	0.04
PDCR	10	-0.28	0.03	0.35	0.03
SRB	9	-0.17	0.06	0.10	0.06
TUC-2	6	0.24	0.04	-0.34	0.05
TUC-3	8	0.13	0.06	-0.16	0.03

SD1 Standard deviation of the mean of the magnitude residuals.

SD2 Standard deviation of the mean of the residuals with station correction (average = 0.0).

## Chapter 2

Date	Time, U.T.	m	S.D.	N
20Aug86	18:00:13	3.82	0.09	6
21Aug86	09:34:40	4.22	0.08	12
23Aug86	20:06:30	3.66	0.15	6
03Sep86	01:16:04	4.06	0.10	4
05Sep86	20:39:29	4.07	0.12	5
09Sep86	20:02:33	3.61	0.10	2
11Sep86	09:05:41	3.6		1
30Nov86	05:19:48	5.03	0.22	19
30Nov86	05:26:10	3.9		1
30Nov86	06:07:35	4.0		1
30Nov86	06:10:20	4.16	0.08	5
30Nov86	06:58:57	3.81		1
30Nov86	07:02:05	4.15	0.17	6
30Nov86	14:01:46	3.76	0.16	4
01Dec86	01:04:49	3.77	0.11	6
02Dec86	09:50:48	3.60	0.11	2
03Dec86	10:06:02	3.55	0.03	2
05Dec86	22:10:08	3.97	0.09	6
06Dec86	09:31:32	3.60	0.02	2
06Dec86	09:51:04	3.77	0.21	2
08Dec86	21:23:42	3.6		1
08Dec86	21:49:03	3.5		1
09Dec86	06:48:44	4.42	0.08	10
24Dec86	07:05:25	3.82	0.16	7
03Jan87	13:31:04	3.6		1
07Jan87	11:08:27	3.69	0.09	5
07Jan87	12:14:16	3.75	0.17	5
28Jan87	16:16:12	3.73	0.10	5
03Feb87	23:51:56	3.84	0.12	7
07Feb87	22:12:38	3.73	0.07	5
28Apr87	04:59:17	3.6		2
29Jun88	13:14:27	3.9		2
10Mar89	04:11:22	5.0		3
10Mar89	10:07:13	3.9		2
10Mar89	21:26:39	3.5		2
06May89	19:55:46	3.6		3

Table 2.4 Events from 1986-87 series extracted from Assumpção et al. (1989b), those of the 1988-90 series from bulletins of the Brazilian Geophysical Society. Magnitude values (m) without standard deviations (S.D.) were calculated without using station corrections. N denotes the number of stations used in the magnitude calculation.

event was small and did not display a clear P wave, magnitudes were estimated using the surface wave  $L_g$ . Twenty seven events with magnitudes ranging between 2.1 to 5.0 were used in the calculation of the station corrections. Amplitude data were read from the available seismograms for the Brazilian stations (figure 2.9) or

## Chapter 2

extracted from Berrocal et al. (1987) for the station ITR. For some teleseismic stations (SPA, DUG and ALQ) readings were made from the station records; for the others, data from USGS and ISC bulletins were used. Initially the average magnitude ( $m$ ) for each event was calculated without any correction. The average magnitude residual for each station gives an initial estimate of the correction. Magnitudes were recalculated using these corrections. Such corrections caused smaller residuals that were used again to improve the previous correction values. This iterative process finishes when the corrections produce zero average residuals for each station. The final station corrections are given in the fifth column of Table 2.3.

Without using station corrections, the magnitudes of 23 J.Câmara earthquakes with magnitudes above 3.5, recorded by two or more stations, had an average standard deviation of 0.33 units of magnitude. This deviation dropped to 0.11 when station corrections were applied. Table 2.4 shows all events with magnitude above 3.5, after applying the corrections of Table 2.3, which occurred in the J.Câmara region between August 1986 and December 1990.

The event of 5th August 1986, whose isoseismal regions are given in figure 2.1, is believed to be the first event in the J.Câmara series of earthquakes. At that time the magnitude of that event was calculated to be 3.0 using the data from the CAI station. Using the station correction of Table 2.3 the calculated magnitude becomes 3.4, as referred to before in section 2.1; this is more reasonable considering the felt area.

### 2.3 The 1987-88 telemetric network

The persistence of activity in the J.Câmara region and concern for its future evolution prompted the installation of a telemetric network by the University College of Cardiff in a joint project with UFRN in May 1987. The network was loaned from the NERC Geophysical Equipment Pool and consisted of nine stations including one three-component station, using Willmore Mark III-A seismometers with peak response at 1 Hz and central analogue FM tape recording on a Racal Geostore. The digital Earth Data 9690 System was used in three outstations (JCAZ, JCUM and JCSC). Their signals were converted to analog by the Line Interface Unit (LIU) before being recorded by the Geostore. The 15/160 inches per second recording speed of the Geostore determined its bandwidth with an upper limit of 32 Hz. At this speed, a tape change had to be made every 3.5 days.

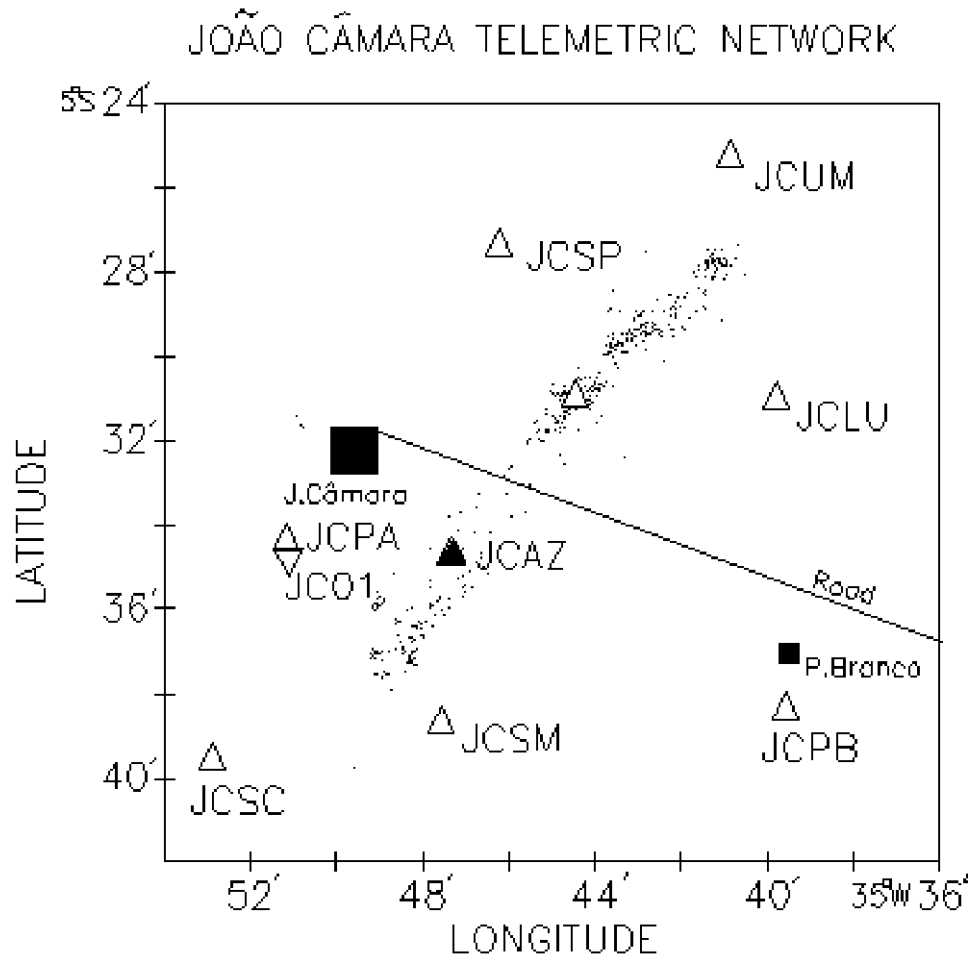


Figure 2.10 J.Câmara telemetric network. Open triangles represent vertical component stations; the filled triangle is a three component station. The inverted triangle represents the drum recorder station JC01. Dots represent epicentres locations made by Sophia & Assumpção, (1989) prior to the installation of the telemetric network and were used to define the geometry of that network. Squares represent towns.

The geometry of the network was based on the previous epicentral locations (Assumpção, 1986; Ferreira, 1987; Sophia & Assumpção, 1989) as shown in figure 2.10. The stations were spaced approximately ten kilometres apart, covering an area of approximately 300 km<sup>2</sup>. The seismometers of the outstations located to the south of the road shown in figure 2.10 were installed directly on the Precambrian outcrops of the region whilst those located on north of the road were placed in soil cover of variable but unknown thickness (20 m on average). Background cultural noise was low in this rural area. The central recording facilities were installed in J. Câmara town. The signal of the outstation JCSC was retransmitted to the laboratory at UFRN providing a real time recording on a smoked paper drum recorder, to allow easier monitoring of the activity. A Store 14 tape replay and an eight channel

## Chapter 2

Mingograf jet pen recorder were available in the laboratory for quality control of the recording system.

In all cases station locations were determined with reference to 1:100,000 maps and from compass bearing. Station location errors were estimated to be  $\pm 50$  m, except for station JCUM whose error was thought to be  $\pm 150$  m due to the difficulties of identifying characteristic features on the map. The station locations are given in Appendix B.1. In August 1992, after completion of data processing, it became possible to recheck all station locations using a hand-held GPS receiver and these locations are also given in Appendix B.1. It is now apparent that the location of JCUM as used in this study is in error by 0.84 km (S.Voss, pers. commun., 1992). No hypocentre were relocated using the new station coordinates. So, it is difficult to say the real effect of this change. However, it is evident that the 0.84 km difference in the location of JCUM is mainly in the direction across the fault strike. So, it is believed that this error would affect the direction of the calculated ray paths, and the error in distance would be insignificant. The topography of the region is almost flat except for isolated hills rising about 70 m from the plain, whose average height is around 150 m.

The João Câmara telemetric network was installed during the period 13th - 29th May 1987 with operational recording commencing on 22nd May, and it was dismantled on 8th April 1988. Thus, the earthquake activity in this area was monitored by this network for a 321 day period. Recorded events were stored on 88 magnetic tapes. Some malfunctions in the Geostore and in the power supply occurred at several times, resulting in a total of about 31 days of lost data (about 10% of the entire period).

The number of lost events and the detection capability of the telemetric network was evaluated by a comparison with the number of events recorded by the drum recorder station JC01 during the same period. This is a crude approximation since station JC01 (figure 2.10) was located in the southern part of the Samambaia fault and is therefore less sensitive to small events with epicentres in the northern part. This approximation is compensated to some extent by the criterion adopted to determine which events recorded by the telemetric network would be useful for further analysis, since only events recorded by at least three stations of the network were counted. In fact, considering only the period when the network was working properly, the comparison shows that the total difference between the number of events recorded by JC01 and the telemetric network is approximately 75, which shows a similar detection capability for station JC01 and the telemetric network.

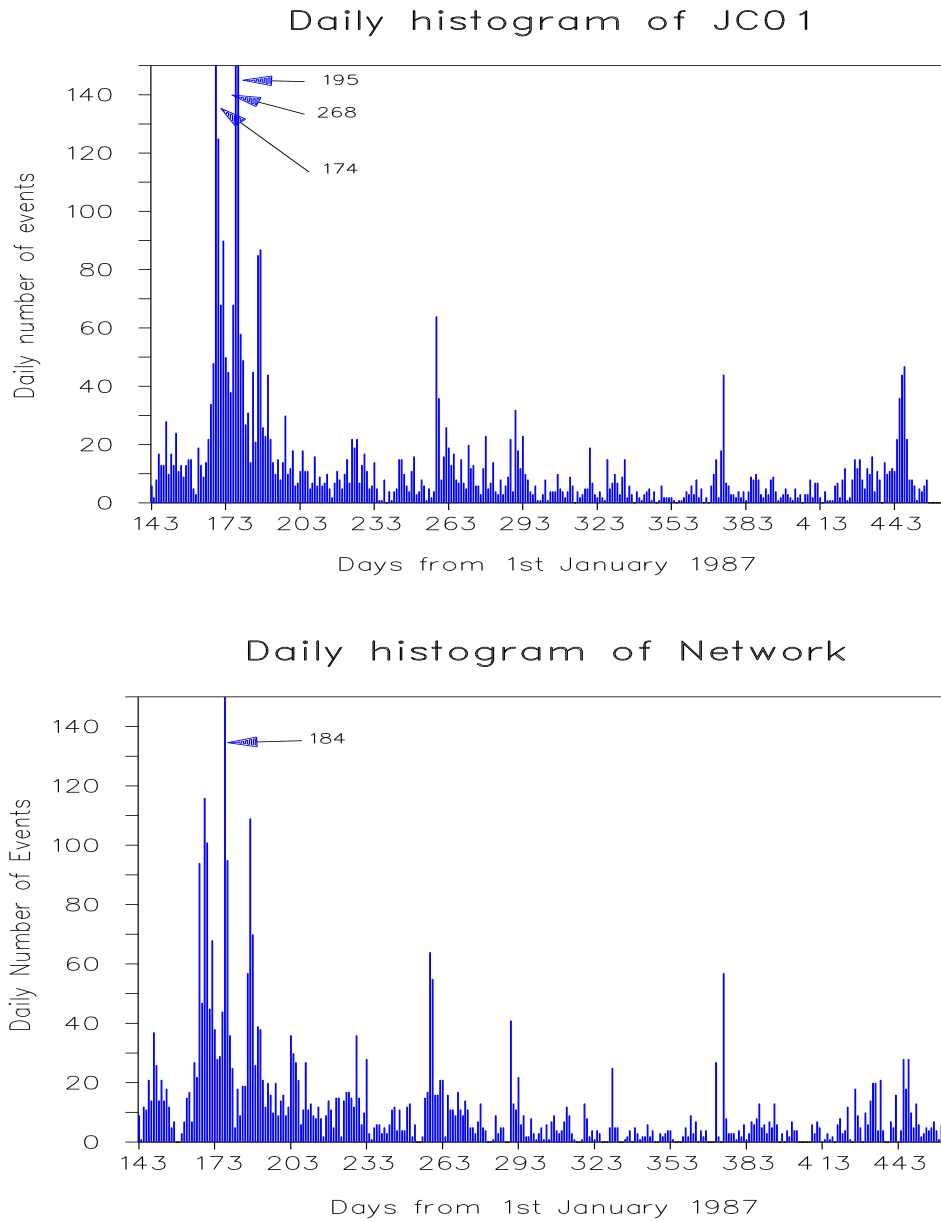


Figure 2.11 Local events recorded during the working period of the J.Câmara telemetered network. The upper histogram shows the number of events per day for the drum recorder station JC01. The histogram in the bottom shows the number of events per day recorded by the telemetric network for the same period. The first day is 23th May 1987 (143 days from 1st Jan 87) and the last day is 07th Apr 1988 (464 days from 1st Jan 87)

Thus, a comparison with station JC01 reveals that during the 31 days in which the telemetric network was not recording, the number of lost events to this study is approximately of 350.

The daily status of the network is shown in Appendix A. Apart from the breaks in recording due to Geostore failure, there were several other periods of

## *Chapter 2*

minor problems with the outstations. During one week from 19th June digital stations JCAZ, JCSC and JCUM were not working due to problems with the Line Interface Unit, and from the installation of the network until 26th August station JCSM was inoperative.

Figure 2.11 shows the daily histograms of station JC01 and of the telemetric network for the same time period. In an overall description from 23th May 87 until 07th April 88, station JC01 recorded 4,175 local events whilst the telemetered network recorded 3,819 events this gives an operational efficiency of 91.4%.



## **CHAPTER 3**

### **DATA ANALYSIS**

#### **3.1 Digitization**

Digitization was performed at the British Geological Survey (BGS) in Edinburgh, using the facilities of the Global Seismology Research Group. A list of picked arrival times of events of interest was necessary for digitization. The contents of all 88 magnetic tapes were played back on ordinary paper using the Store 14 FM tape replay and the 16 channel Mingograf jet pen recorder running at 25 mm/sec. Events of interest were identified and the corresponding arrival times were read from the VELA timecode that was displayed by two of 16 channels on the paper. In this way, an input file of digitization start times was obtained for the digitizing PDP11 microcomputer adding a pre-event time length of 5 sec to the arrival time. The corresponding magnetic tape was placed on the Store 14 connected to the digitizing system and after that, all the procedures were automatic. The computer read the start time and searched for the event in the analog tape. Events were digitized at a rate of 100 samples/second; this compares with the nominal FM Nyquist frequency of 32 Hz. The digitized seismogram files output from the microcomputer were then stored on magnetic tapes. Figure 3.1 shows a sample of digitized seismograms of a small event recorded by all stations.

It was not possible to use the automatic procedure for all the events. Sometimes failures in the electronics of the Geostore time encoder board generated codes impossible to be read by the digitizing system. Normally, problems in the timecode caused the Geostore to stop, but in some cases it continued recording the signal from the outstations even with this kind of malfunction. The time code could not then be interpreted by the digitizing system. In these cases the process of digitization was done manually, using the program MANDIG supplied by the BGS, and the arrival time of each event was estimated by measuring the paper length between the last readable time mark and the onset of the event. 166 events were digitized in this way.

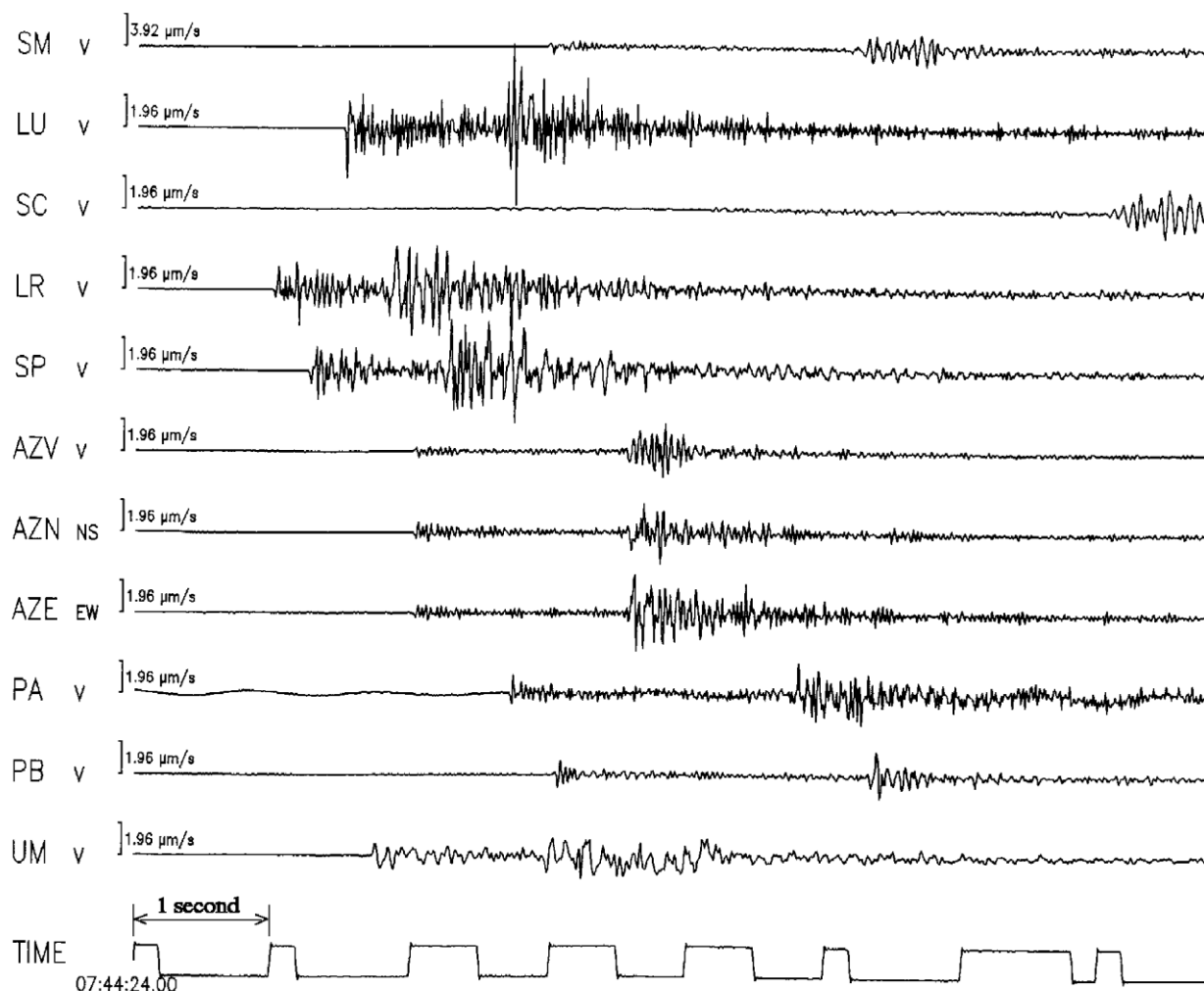


Figure 3.1 An example of digitized seismograms displayed by the BGS's PICK program. This is a small event which occurred on 12th March 1988 recorded by all the stations of the telemetered network. The bottom line shows the VELA time code.

### 3.2 Phase picking

After finishing the digitization process, phase picking programs were employed. Initially, about 1,200 events were analysed using the PICK program from the BGS and a high resolution graphics display. For the rest of the events it was decided to employ the PCEQ software (Valdés, 1989) from the International Association of Seismology and Physics of the Earth's Interior (IASPEI) installed on a IBM compatible PC. For this purpose it was necessary to write a program to convert BGS data format to the PCEQ format.

The P and S arrival times and duration of the event were picked for each event. The reading error for the P onset was estimated to be  $\pm 0.02$  sec. Because the S waves are preceded by other arrivals and this could lead to a misidentified S

## Chapter 3

arrival, the reading error for this phase was estimated to be  $\pm 0.04$  sec. Amplitude measurement facilities were not available in the PICK nor PCEQ programs whose output is in the HYPO71 (Lee & Lahr, 1975) format. Each picked arrival time was assigned a quality from 0 (excellent) to 4 (very poor) as suggested by Lee & Lahr (1975). It was decided to give quality 0 (full weight) to arrival times which had a maximum estimated reading error of  $\pm 0.02$  sec, quality 1 (weight=0.75) for  $\pm 0.04$  sec, quality 2 (weight=0.50) for  $\pm 0.06$  sec, quality 3 (weight=0.25) for  $\pm 0.08$  sec and quality 4 (zero weight) for  $\pm 0.10$  sec. The measurement quality is used by the location program to give a relative weight to each reading and this is an important parameter for the hypocentre determination. Time readings with quality 4 have no weight and are not used to calculate the location of the event. In general the quality assignments for the P onsets were better than for the S onsets and virtually no S onsets were assigned with quality 0. Two other parameters measured were (1) the first motion direction of the P wave arrival, to be used in the focal mechanism determination, and (2) whether this onset exhibits an impulsive or emergent onset.

A total of 3,877 local and regional events were analysed and catalogued in this way (dataset 1). Eleven teleseismic events were digitized but not analysed.

### 3.3 Hypocentre location

A preliminary hypocentre determination was made with all events in dataset 1 (see Table 3.1) using a half space model. This preliminary model had been successfully tested in previous work (Ferreira et al., 1987; Takeya et al., 1989). The velocity model consists of a half-space with a P wave speed of 6.2 km/sec and a constant  $V_p/V_s$  ratio of 1.73. Events were located using the program HYPO71 (Lee & Lahr, 1975). Initial examination of these locations revealed that 3,819 events were within or in the close vicinity of the J.Câmara and Poço Branco region and 58 events were located outside (more than 50 km from J.Câmara) and were classified as regional events. The majority of these regional events (microearthquakes or explosions) were found around the Açú Dam close to the town of Açú, located 150 km to the west of the telemetric network. Regional events are not of direct interest to the present work and they were eliminated from the analysis. For the purpose of this work only the 3,819 events located within a area of 30 km from the centre of the network were considered and they comprise dataset 2. To discard events with possible reading errors or typing mistakes, one first and general criterion was applied; events with RMS in their travel time residual greater than 0.20 seconds were eliminated. After the application of this filter 3,780 events were retained for the J.Câmara and Poço Branco region (dataset 3). 229 events in dataset 3 were

### Chapter 3

identified as belonging to the Poço Branco fault near the town of Poço Branco, 12 km to the east of the Samambaia fault. This activity was not detected until the installation of the telemetric network. The Poço Branco fault was inferred for the first time by the routine quality analysis of the Geostore magnetic tapes and reported by Takeya et al. (1989).

Dataset	Region	N	selection
Dataset 1	J.Câmara+P.Branco+regional	3877	
Dataset 2	J.Câmara+P.Branco	3819	local
Dataset 3	J.Câmara+P.Branco	3780	local+rms<.20

Table 3.1 A summary of the number (N) of events picked and selected for analysis.

A subset of dataset 3 was selected to calibrate the local velocity model. To ensure good quality data and a reasonable coverage by the stations for this process, the events used were restricted to those with fifteen or more phases (total of P and S readings) and with a time residual lower than 0.06 seconds in the preliminary location process. A total of 651 events were found to fulfil those requirements.

Assuming that the  $V_p/V_s$  ratio does not change with depth, laterally or with time, aftershocks were located using HYPO71 for several velocity models and different values for the  $V_p/V_s$  ratio. The aim was to find the best combination of  $V_p$  and  $V_s$  which gave the minimum time residual in the event location process. Initially the calculation was performed by increasing the P wave velocity in steps of 0.10 km/sec starting with  $V_p = 5.6$  km/sec up to  $V_p = 6.5$  km/sec for each value of  $V_p/V_s$ . The corresponding P velocity to S velocity ratio ranged from 1.67 to 1.75. The root mean square error of time residual (RMS) of individual events was obtained from the output of HYPO71 for one particular combination of  $V_p$  and  $V_s$ . Then, the average parameter (AV\_RMS) of these values for the suite of events were calculated for those particular values of  $V_p$  and  $V_s$ . This procedure was repeated for other combinations of  $V_p$  and  $V_s$ . Figure 3.2 shows the best four curves obtained by this process. Each curve shows the variation of AV\_RMS with chosen P wave velocity for one value of  $V_p$  to  $V_s$  ratio. For comparison, one curve with P phase only and another with the S phase only were included. The curves do not represent the best fit; rather each curve has been linearly interpolated between the computed points. A similar procedure was applied to get the average of the standard error of the epi-

## AV\_RMS time residuals for half-space models

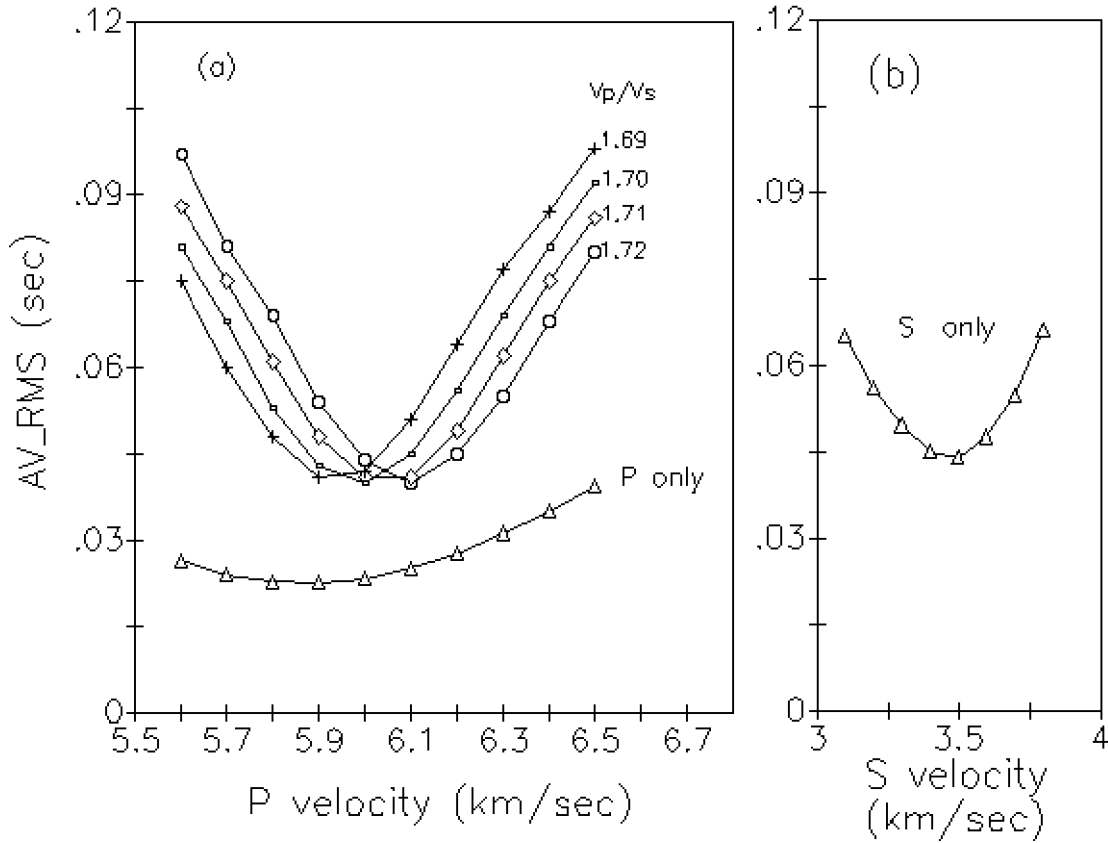


Figure 3.2 (a) Average of the Root Mean Square Errors (AV\_RMS) of time residuals in seconds for different half-space models applied to 651 aftershocks with 15 or more (P plus S) phases. (b) AV\_RMS when using only S readings.

centre location (AV\_ERH) and the average of the standard error of the depth (ERZ), which are both given in kilometres. Figure 3.3 illustrates the corresponding curves for the averages of horizontal distance (AV\_ERH) and depth (AV\_ERZ) standard errors of the hypocentres for the same dataset. For comparison, the curve formed from P only readings is also shown. In all cases the errors in depth are larger than the errors in epicentre.

The time residuals of the P only curve (figure 3.2a) for P wave velocities below 6.2 km/sec are in close agreement to what is expected from the accuracy on the P onset readings and supports the decision to assign quality 0 (or full weight) to the P onset with estimated error less than or equal 0.02 seconds, as discussed in section 3.2. The S only curve (figure 3.2b) shows that the time residuals for the S phase readings are on average twice as larger as for P readings, and this confirms the choice made in assigning a relatively lower quality to the S arrival readings. In limiting the analysis for the minimum time residual in each curve of figures 3.2a

### Chapter 3

and 3.2b, it is possible to attribute the time residuals in the curves with P and S readings to the readings errors in the S arrivals.

The small time residuals obtained when P only readings are used could lead to the wrong conclusion that hypocentres would be better located if S readings were not used. Buland (1976), by performing a series of numerical experiments, shows that the matrix inversion is more stable and the results are more accurate when S readings are included. This can be seen in figure 3.3. The omission of S readings gives large errors in hypocentral locations when compared with models using P and S readings. In comparing the P only curve with curves including P and S readings in both figures, it is noticeable that absence of S reading is more critical in the determination of depth.

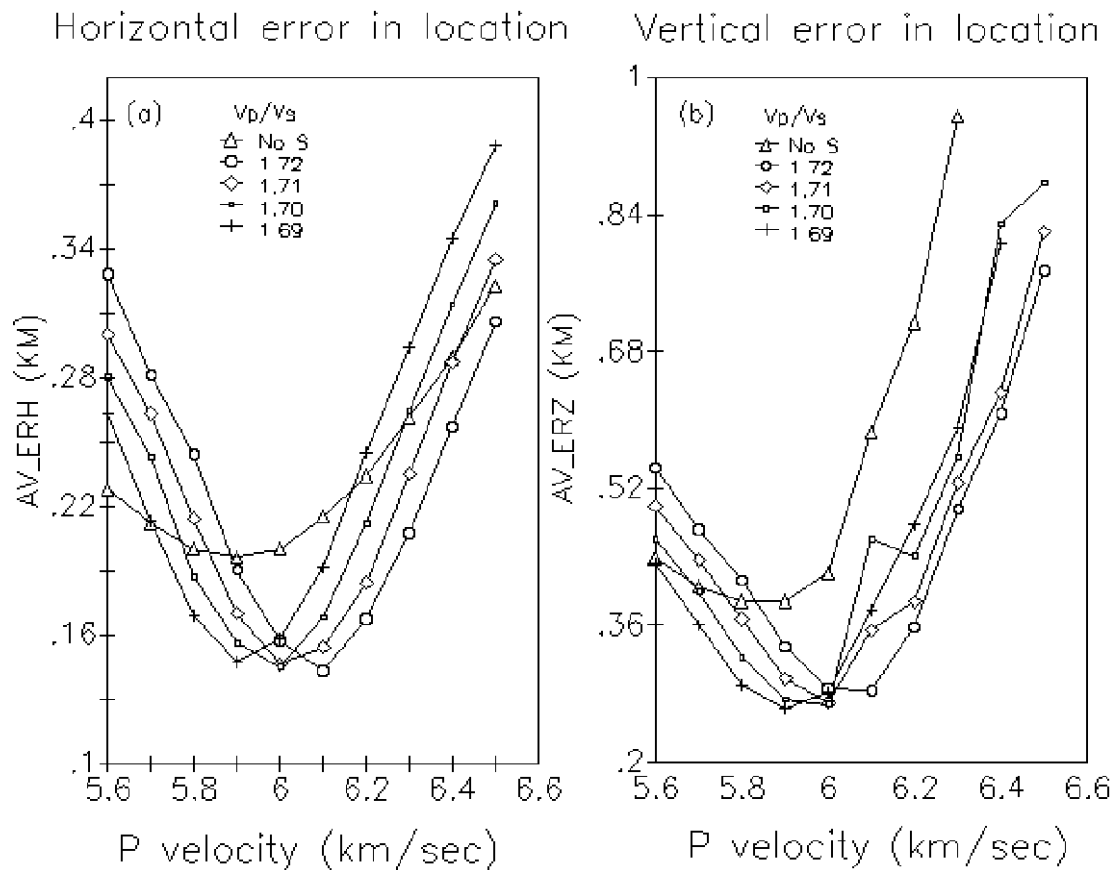


Figure 3.3 Errors in hypocentre locations for the same data used in figure 3.2.(a) Error in horizontal location. (b) Error in depth.

### 3.4 Half space and two layer models

For the purpose of finding the best half space model the same parameters (AV\_RMS, AV\_ERH and AV\_ERZ) were calculated for P wave velocity increasing in smaller steps of 0.01 km/sec for the four best values of  $V_p/V_s$  ratio. Figures 3.4 and 3.5 show the results. The absolute minimum in time residuals is found for velocity 5.98 km/sec and  $V_p/V_s = 1.70$ . There is no significant difference in time residuals in the range of velocities between 5.97 km/sec to 5.99 km/sec for the curve with  $V_p/V_s = 1.70$  or between velocity 6.01 km/sec to 6.06 km/sec for the curve with  $V_p/V_s = 1.71$ .

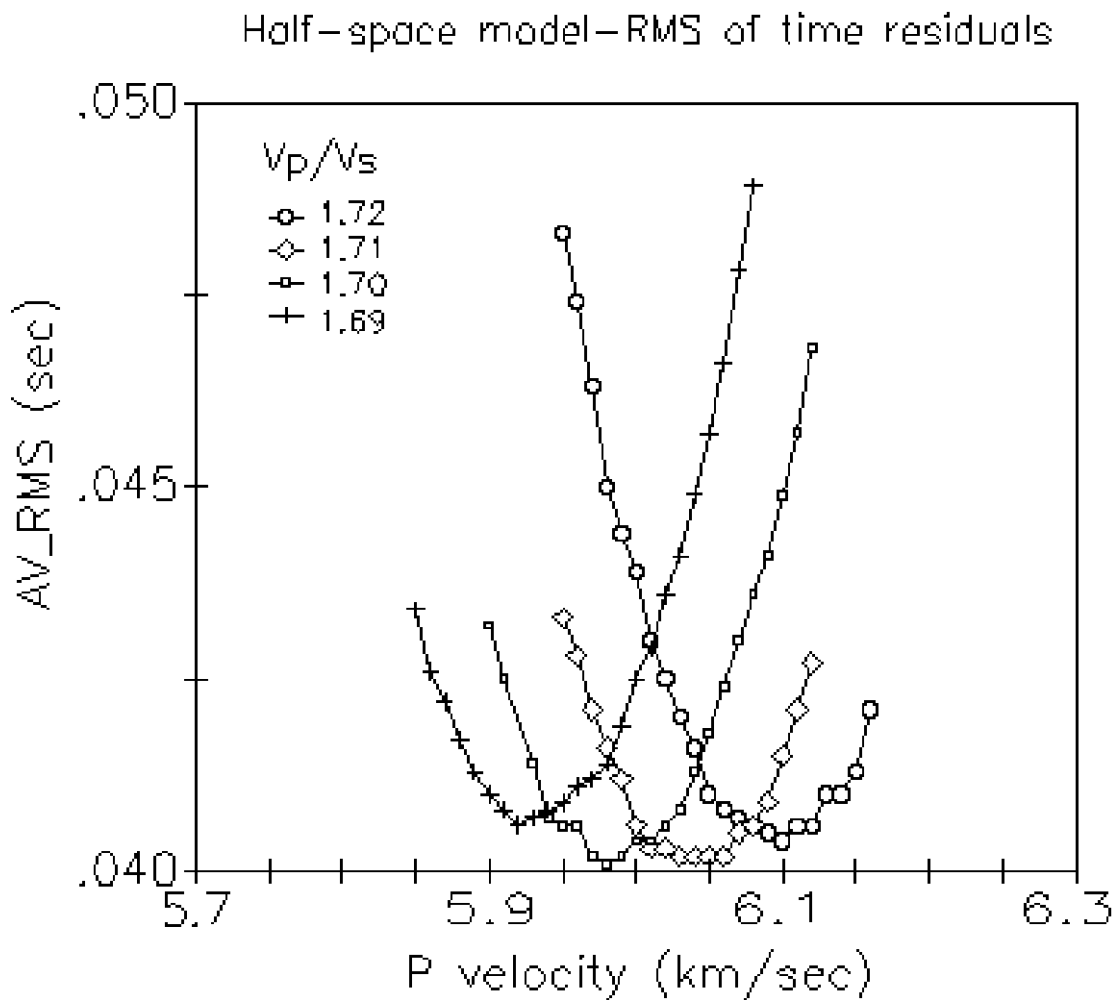


Figure 3.4 Average root-mean square of time residuals (AV\_RMS) for P wave velocity, half space model for a sample of  $V_p/V_s$  values.

## Half-space model

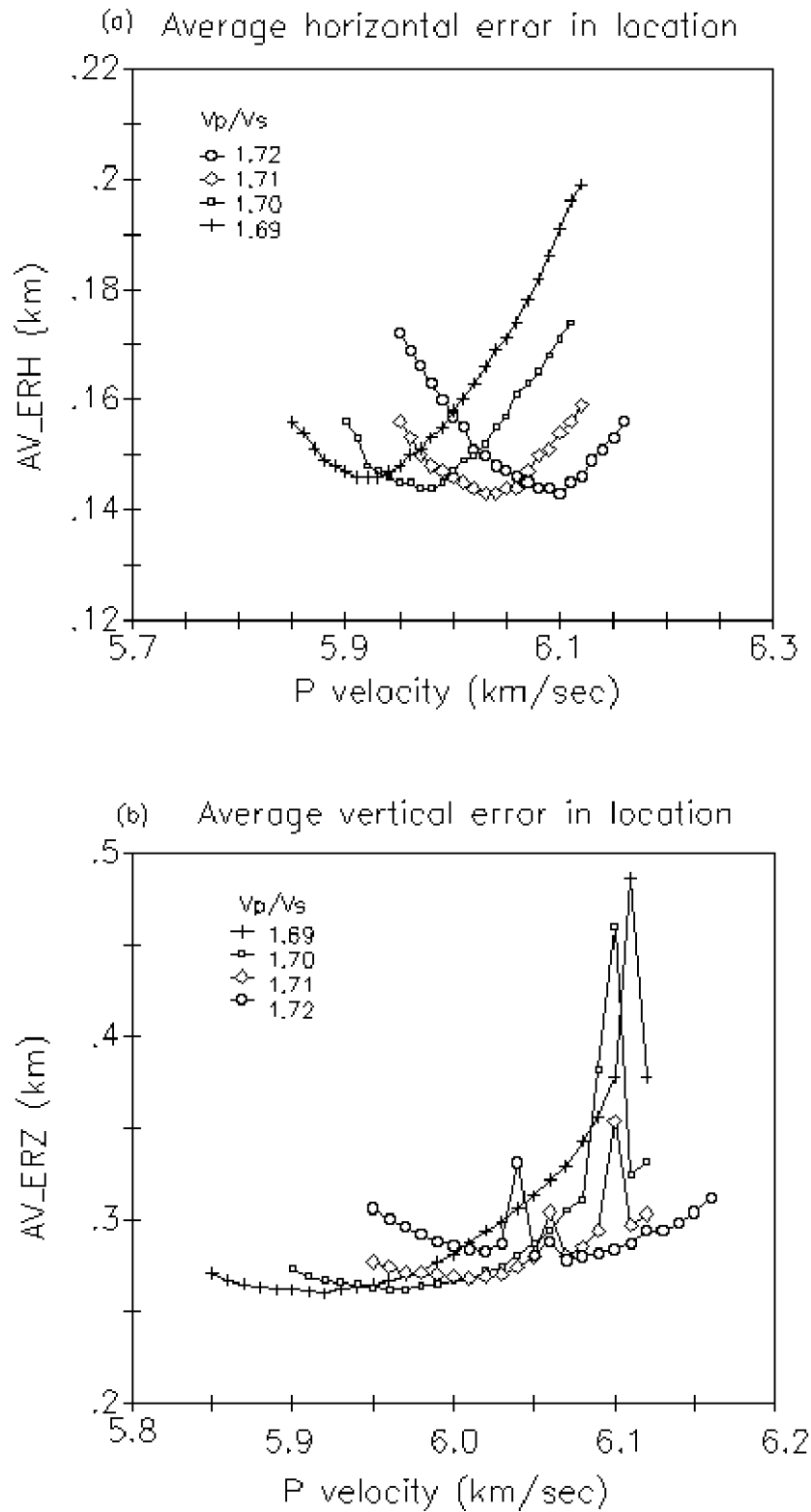


Figure 3.5 Average horizontal error (AV\_ERH) and average vertical error (AV\_ERZ) in location using half space velocity model for the same data as used in figure 3.4.



### Chapter 3

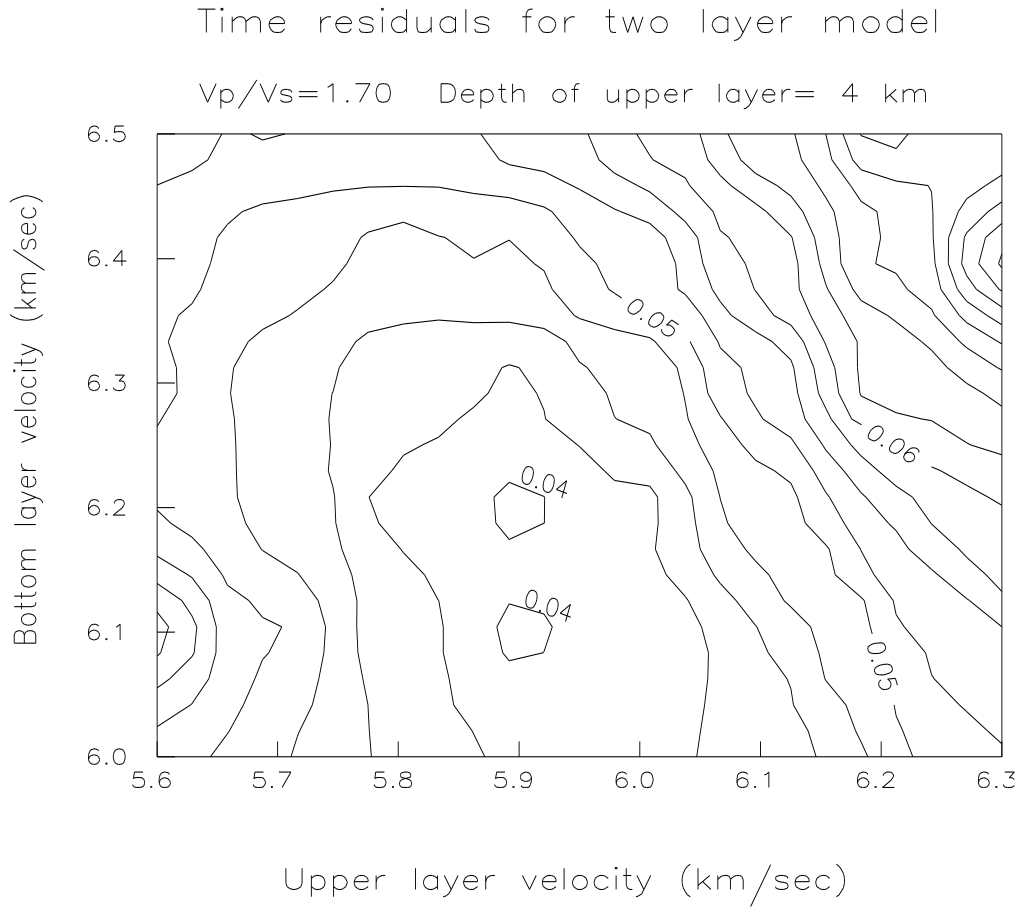


Figure 3.6 Contour map of average time residuals for a layer with a depth of 4 km.  $V_p/V_s$  is 1.70.

In order to assess the results obtained using a half space model, a trial was made with a two layer model. For this purpose, the same approach used for the half space study was employed, with two new parameters added. The velocity of the upper layer ( $V_U$ ) was varied from 5.1 km/sec to 6.2 in steps of 0.1 km/sec and the depth of layer from 1 km to 5 km in 1 km steps. The velocity of the bottom layer or half space ( $V_b$ ) was varied from 6.0 to 6.5 km/sec. The velocity of the half space had to be always larger than the velocity of the layer because no low velocity layer is accepted by HYPO71. The range of  $V_p/V_s$  velocity ratio went from 1.68 to 1.74.

As in the case of the half space model, the two best families of results in the two layer model correspond to  $V_p/V_s$  values 1.70 and 1.71. The absolute minimum in time residual for the two layer model was found for the model with a surface layer 4 km thick and P wave velocity of 5.9 km/sec overlying a half space with a P velocity of 6.1 km/sec. The corresponding P to S velocity ratio was 1.70. Figure 3.6 is the contour map for the average time error residuals found for this model. It can be seen

### Chapter 3

that there is no significant difference in adopting a surface layer between 3 km and 4 km thick. Table 3.2 shows the results for the best half space velocity and for the best two layer velocity model. In comparing the two models it can be seen that no improvement is observed in epicentre locations, but depth determinations are slightly more precise and more stable when the layered model is used. A velocity increment from 5.9 km/sec to 6.1 km/sec in 4 km suggests a low velocity gradient of 0.05 km/sec/km for the region. This is consistent with the previous work done with the half space model. It was decided to make use of the layered model in this study. In applying station residuals as station corrections for relocation using the same dataset, all errors decreased as shown in Table 3.3. Therefore, these station corrections obtained from the selected dataset were used to locate all the remaining events.

Table 3.2 Comparison between the best half-space velocity model and the best two-layer model used to locate 651 selected events.

	$V_u$ km/s	$V_b$ km/s	d km	AV_RMS sec	AV_ERH km	AV_ERZ km
half space:	5.98			$.0401 \pm .0100$	$.144 \pm .057$	$.264 \pm .107$
two layer :	5.90	6.10	4.0	$.0395 \pm .0093$	$.143 \pm .055$	$.243 \pm .086$

$V_u$  and  $V_b$  are the P-wave velocities of the upper and bottom layers, respectively; d denotes the thickness of the upper layer measured from the surface. AV\_RMS is the average root-mean square of time residuals; AV\_ERH and AV\_ERZ are the average of the horizontal and the average of the vertical errors in location respectively.  $V_p/V_s$  is 1.70.

Table 3.3 Velocity model chosen for the event location. Results shown are after applying station corrections.

$V_u$ km/s	$V_b$ km/s	d km	AV_RMS sec	AV_ERH km	AV_ERZ km
5.90	6.10	4.0	$.0362 \pm .0104$	$.129 \pm .052$	$.219 \pm .088$

Symbols are the same as in Table 3.2.

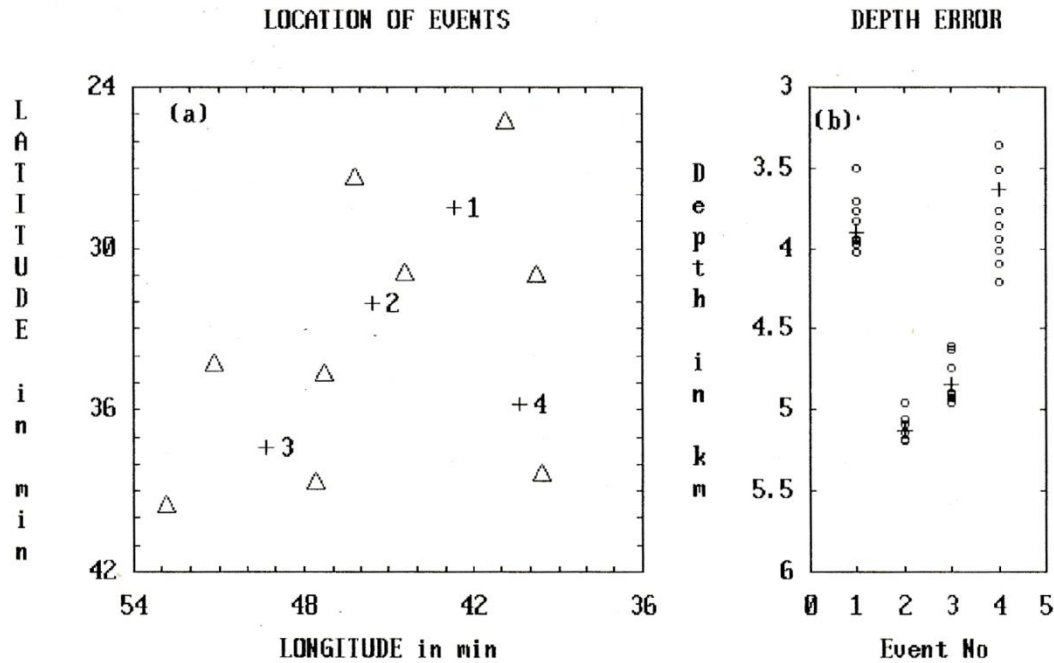


Figure 3.7 The left figure shows the location of the four events used in the location test. Triangles are stations. The figure on the right shows the variations in depth caused by varying velocity models. The plus sign denotes the location obtained with the best model, and circles represent those obtained with other models. Latitude and longitude are in minutes ( $5^{\circ}\text{S}$  and  $35^{\circ}\text{W}$ ).

The results acquired in comparing the two models show that the velocity structure of the region seems to be very simple when compared with other regions, for example California (Lee et al., 1971), the East African Rift (Young et al., 1991) or even Uzbekistan (Hartzell, 1980) which is within a shield region. The average error of the time residuals found in Table 3.2 is an indication that the errors are random because their values are close to the estimated error in the S readings. However, there is no easy way to check the existence of any systematic error that could be introduced, most likely by the mis-alignment of the tape recording (or replaying) heads; this error can be up to 0.05 sec on certain seismic channels (Evans et al., 1987) and so can represent a limiting factor in this study. Another source of systematic error is the uncertainty in the velocity model. In this case it is possible to have a general idea by doing numerical calculations. For this purpose the Samambaia fault was relocated several times using ten different velocity models. The same process was repeated with events located at the centre and in the south of the network, and also one event in the Poço Branco fault was chosen. The results are shown in figures 3.7 and 3.8. The velocity of the upper layer was varied from 5.7 km/sec to 6.1 km/sec in 0.1 km/sec steps and the velocity of the bottom layer from 5.9 km/sec to 6.3 km/sec. The horizontal distance and depth errors were

### Chapter 3

approximately the same but varied in size according to the event location. For events in the north and south of the Samambaia fault the errors found were about 0.4 km. Errors for the event at the centre of the network were only 0.2 km but the event close to Poço Branco gave the largest error of about 0.7 km. Then, in summing statistical and systematic errors it is reasonable to assign an overall error in location of up 0.6 km for events in the Samambaia fault and up 1 km for events in the Poço Branco fault. Relative location errors between events will be less than those values.

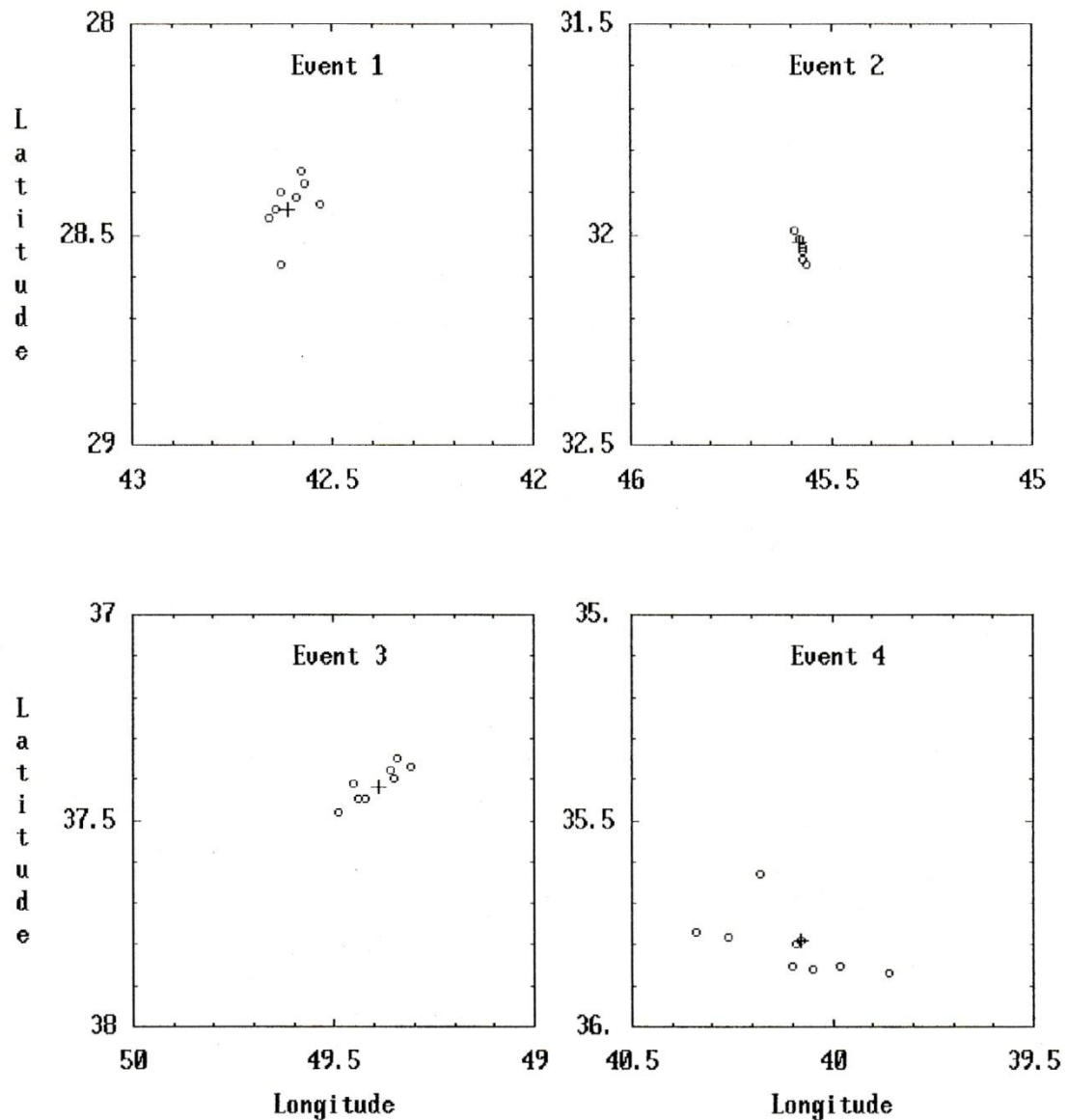


Figure 3.8 Location misfit calculated when varying the two layer velocity model and using four events. The relative locations are shown in figure 3.7a. Symbols have the same meanings as in figure 3.7. Latitude and longitude are in minutes ( $5^{\circ}\text{S}$  and  $35^{\circ}\text{W}$ ).

### 3.5 Wadati diagram

It is well-known that  $V_p/V_s$ , the ratio of the apparent mean P to S velocity, can change both laterally and with depth (Nicholson et al., 1984; Assumpção & Bamford, 1978; Teague et al., 1986). Also, temporal changes of  $V_p/V_s$  have been observed before mainshocks (e.g., Chiu et al., 1984), and this has sometimes been claimed to be a precursory phenomenon for earthquake prediction (Aggarwal et al., 1973). The  $V_p/V_s$  ratio can be obtained very easily by means of the Wadati diagram. In a Wadati diagram, the difference in time of arrival of S and P waves ( $t_s - t_p$ ) on a seismogram is plotted against the arrival time of P waves ( $t_p$ ). Projecting the curve back to zero ( $t_s - t_p$ ) gives the origin time  $t_0$  of the event, and the slope, equal to  $(t_p/t_s - 1)$ , gives  $t_s/t_p$  and hence the  $V_p/V_s$  ratio.

One variation of the Wadati diagram (the modified Wadati diagram) is to make plots for several events with the same origin to get  $(t_s - t_p)$  against  $(t_p - t_0)$ . Wadati's method is valid even if the assumption of constant Poisson's ratio is not satisfied. It is necessary for the geometry of the source-receiver system to be such that the arrival readings correspond to waves that have travelled upwards from the source (Kisslinger & Engdahl, 1973). In addition to giving an estimate of the origin time, the technique is useful because it yields important information about the velocity ratio without requiring the development of travel-time curves or the location of the event. Because the location of events in this study is done using both P and S arrival times it is important to know whether any exceptional variation in the  $V_p/V_s$  value is occurring in a particular location or in a specific period of time. If this happens it will cause a mislocation of hypocentres (Doyle et al., 1982). In addition, a correlation could be made with the corresponding characteristics of the seismicity. In figure 3.9 Wadati diagrams are plotted for two earthquakes. The data points show only a very small scatter about straight lines; this supports the previous estimate of the accuracy of the phase readings. In these two examples only readings with quality 2 or better were used.

Figure 3.10 shows the results of the modified Wadati diagram applied to the 651 selected events. The value  $V_p/V_s = 1.72$  with standard deviation of 0.06, is not significantly different from the value of 1.70 that was found previously using the hypocentre location procedure.

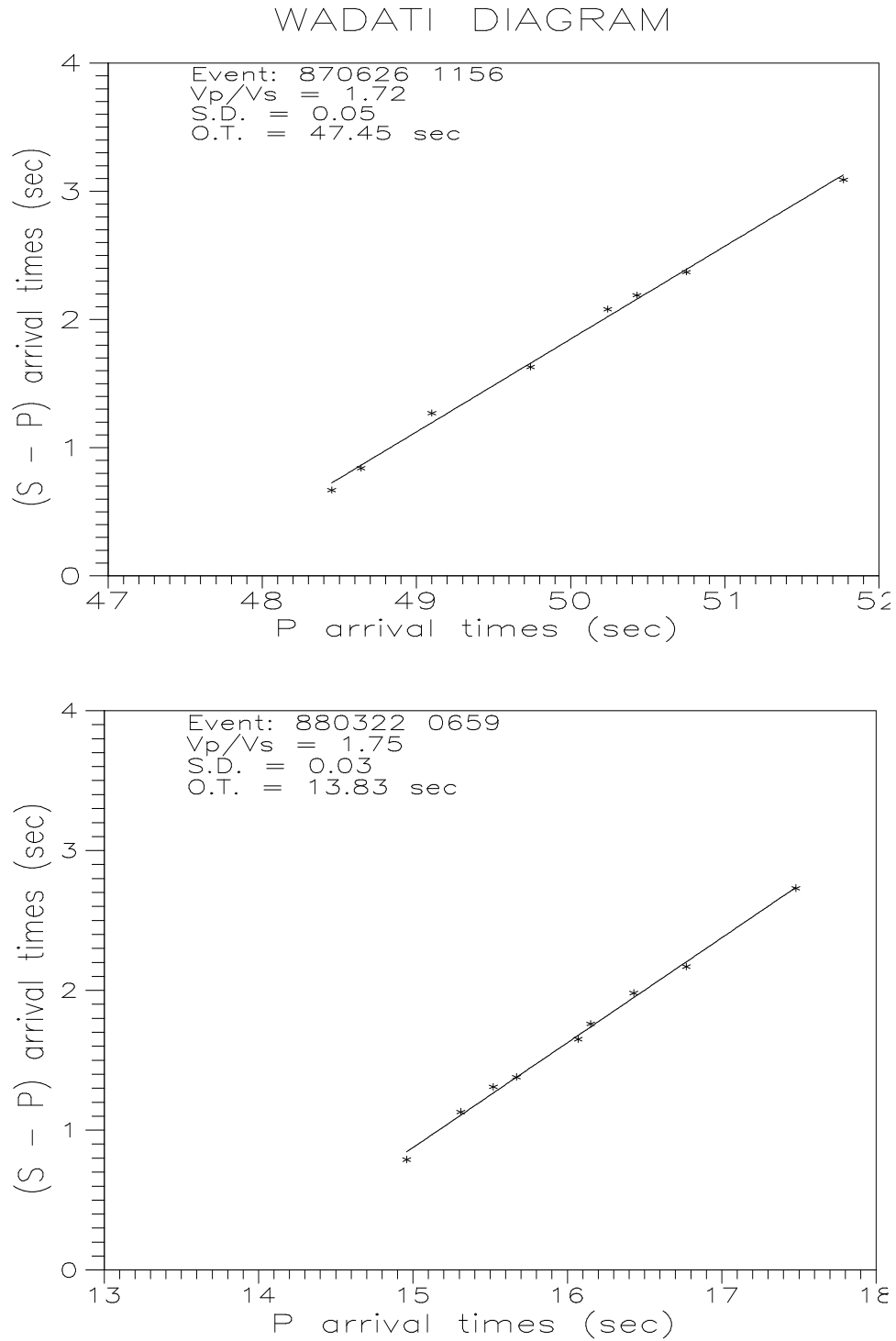


Figure 3.9 Example of Wadati diagram applied to two events in which arrival time readings with quality 2 or better were used. S.D. is the standard deviation and O.T. is origin time inferred from the fit.

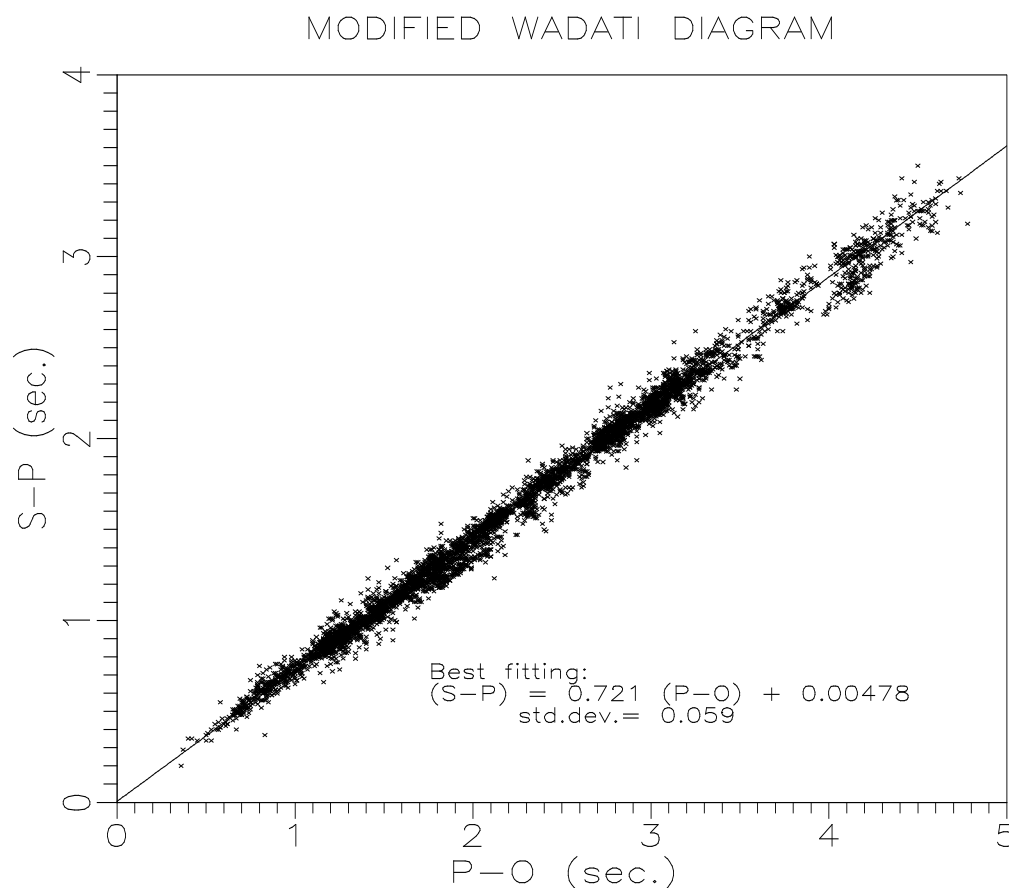


Figure 3.10 Modified Wadati diagram applied to the 651 selected events used to choose the best velocity model. (S-P) denotes S minus P arrival time and (P-O) P arrival time minus origin time.

Although the use of variations in  $V_p/V_s$  as a premonitory parameter for earthquake prediction has failed in several cases (Kisslinger & Engdahl, 1973; McEvilly & Johnson, 1974) an attempt was made with data from the present network. Following Aggarwal et al. (1973), a decrease - typically up to 13% - in the  $V_p/V_s$  ratio prior to a major event could occur, with the time duration of the anomalous decrease in velocity ratio being longer, for increasing magnitude of the event. The bulletin of the Brazilian Geophysical Society (see table 3.4) reports a magnitude 3.0 event on 18th June 87. According to Aggarwal et al. (1973), for an earthquake of this size a decrease in that ratio would be expected during the days 14th and 15th of June. The plot on figure 3.11 shows no variation in the  $V_p/V_s$  ratio during those preceding days. During the whole week for which the data were analysed, the minimum value in  $V_p/V_s$  was 1.66, only 4% less than the average value, but even this result is insignificant because of the large standard deviation in  $V_p/V_s$  over the week.

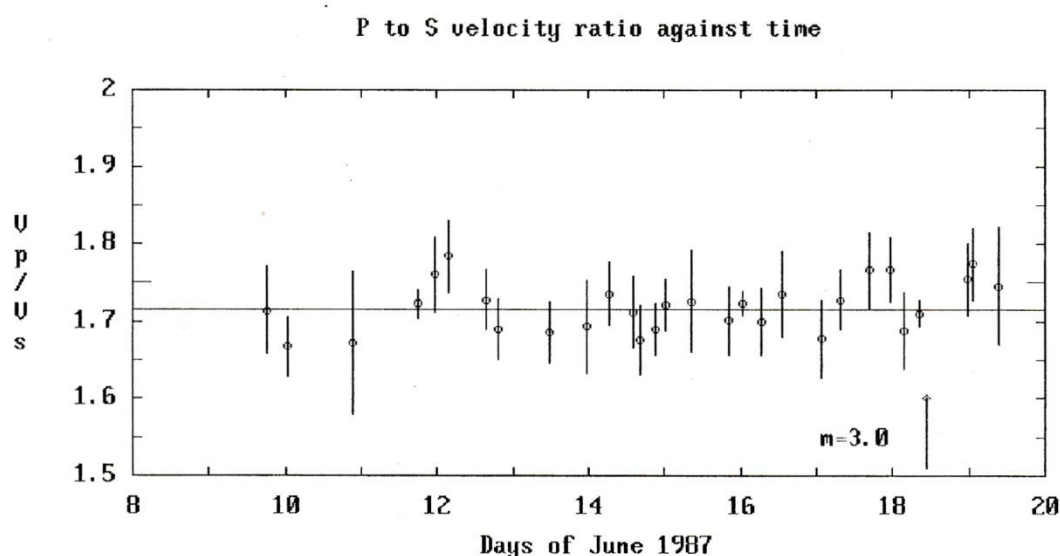


Figure 3.11 Velocity ratio  $V_p/V_s$  against time. Vertical bars indicate the standard deviation of the  $V_p/V_s$  values. The horizontal line represents the average  $V_p/V_s = 1.72$ . The time of the magnitude 3.0 event of 18 June 1987 is indicated at the bottom. No abnormal decrease in  $V_p/V_s$  is observed.

### 3.6 Magnitudes

The concept of magnitude was introduced by Richter in 1935 (Richter, 1958). His intention was to classify Californian earthquakes into simple categories such as small, medium and large. At that time, earthquakes were classified by subjective judgement such as its effects on people or by evaluating the damage to physical structures. In formulating the new concept of magnitude, Richter formed an objective scale based on instrumental data (Richter, 1958). This new scale, known as the local Richter magnitude scale or simply  $M_L$ , is an arbitrary logarithmic scale in which magnitude is related to the maximum amplitude in a seismogram after correction for attenuation with distance.

There are some problems with  $M_L$  such as its requirement for measurement to be performed with a Wood-Anderson torsion seismometer (Eaton et al., 1970). Another problem is that the amplitude attenuation correction used in  $M_L$  is valid only for the south California. In other geologically different regions the  $M_L$  scale could not be valid. To overcome the deficiencies of this scale, other magnitude scales were developed such as the surface wave magnitude  $M_s$  (Gutenberg, 1945) and the body wave magnitude  $m_b$  (Gutenberg & Richter, 1956), which are both used for earthquakes recorded at teleseismic distance.



### Chapter 3

Although it does not correspond directly to any physical quantity, the concept of magnitude is important for two main reasons. Firstly, it is easy to measure and then quickly provides an idea of the 'size' of the earthquake. Secondly, it can be empirically correlated with other physical parameters which are difficult to calculate, such as seismic moment (Brune, 1968), or energy (Gutenberg & Richter, 1956). In addition, the magnitude-frequency relation of Gutenberg & Richter (1954) is well-known:

$$\text{Log } N = a - bm \quad 3.1$$

where  $N$  represents the number of events with magnitude  $m$  or higher, and  $b$  can be calculated by least-squares regression.

Some statistical studies using the  $b$  parameter suggest a relationship with the tectonic characteristics of a region (Båth, 1981). Temporal variations in the  $b$  parameter could be a premonitory signal representing variations in the stress level near the rupture. Although the  $b$  parameter can be evaluated by least-square regression, the presence of even a few large earthquakes influences the resulting  $b$ -value significantly (Bullen & Bolt, 1985). An alternative is to use the method of maximum likelihood to estimate  $b$  because it yields a more robust value when the number of infrequent large earthquakes changes. The maximum likelihood estimate of  $b$  is given by:

$$b = \frac{0.4343}{\langle m \rangle - m_0} \quad 3.2$$

(Aki, 1965), where  $\langle m \rangle$  is the average of magnitudes above magnitude threshold  $m_0$ . In the past, it was necessary to obtain several years of observations to get good statistics for a particular region. Seismologists have overcome this limitation by recording microearthquakes (generally, events lower than magnitude 3.0). Inside the area of interest, a network of high gain instruments is installed. When the magnitude-frequency study is performed, it is possible to calculate the constants  $a$  and  $b$ , predicting results for higher magnitudes. Whilst useful, some studies (Båth, 1981) suggest that the  $b$  coefficient is not the same for all ranges of magnitudes. In order to obtain sufficient observations for a statistical analysis of the magnitude-frequency relationship, it is necessary to obtain reliable magnitude determinations for microearthquakes.

The magnitudes of events recorded at regional distances (less than  $20^\circ$ ) from J.Câmara were calculated using the  $m_R$  scale as referenced in paragraph 2.2. However, in practice this applied only for events above magnitude 3.0 because

### Chapter 3

regional coverage was very poor and  $m_R$  is not suitable for distances smaller than 200 km. A magnitude scale based on the signal duration was used to measure the magnitudes of small events.

#### 3.7 Coda duration magnitude

A method of measuring the magnitude of an earthquake from the total duration of surface waves of the observed seismogram was proposed by Bisztricsany (1958). The duration ( $D$ ) of the observed seismic signal was correlated with magnitude  $M_s$  determined by the conventional method. Tsumura (1967) and Lee et al., (1971) were able to apply this concept to small local earthquakes by extending the duration measurement criterion, where the duration was defined to be from the onset of the P waves until the point where the amplitude of the coda waves falls below an arbitrary value. The coda portion of a local earthquake record is defined as that energy arriving after the passage of all direct body and surface waves (Real & Teng, 1973). For this reason the method is usually referred to as coda duration magnitude or coda length magnitude. The coda duration magnitude relation determined by Tsumura (1967) is used to determine the magnitude of small events in Japan (Adams, 1977). For local and regional observations, the duration of the signal is almost independent of the epicentral distance, depth or fault orientation (Real & Teng, 1973; Suthau & Whitcomb, 1979). So the duration of the signal can be correlated with magnitude, thus providing a practical way to assess the magnitudes of small events recorded by local stations. In general the relationship between magnitude and duration (B  th, 1981) is expressed by:

$$m = c_1 \log(D) + c_2 \Delta + c_3 \quad 3.3$$

where  $D$  is the duration of the signal expressed in seconds,  $\Delta$  is the distance between the station and the epicentre in km. The coefficient  $c_2$  is small, typically 0.003 (Lee et al., 1972), so for local events the simplified formula:

$$m = c_1 \log(D) + c_3 \quad 3.4$$

is used.

In general the duration  $D$  is measured from the onset of the P wave to an arbitrary amplitude threshold that could be the background noise (e.g. Real & Teng, 1973; Herrmann, 1975). For example, Lee et al., (1972) found an amplitude threshold of 1cm to be a convenient definition for the records of events that were

### Chapter 3

displayed on a Geotech film viewer adjusted in a way that 1cm distance on the horizontal component of the projected seimogram corresponds to a time interval of 1 second. This freedom in defining the coda duration introduces an arbitrary element in the magnitude scale. Herrmann (1975) shows that the decay in the envelope of the coda wave amplitude conforms with the power law in time,  $t^{-q}$ , where  $t$  is the duration measured from the onset of the S wave. In this condition, he shows that the coefficient  $c_1$  in equation 3.4 is equal to  $q$  and thus related to the decay in the envelope. This explains the dependency of the constant  $c_1$  on the kind of instrument used and on the geological characteristics of the region as found by Real & Teng (1973). In addition, Herrmann (1975) shows that the constant  $c_3$  is only instrument dependent. This means that different conventions for the choice of the amplitude threshold would only affect the constant  $c_3$ , not the constant  $c_1$ . As an example, suppose that one particular event is recorded by one particular station and the duration is measured by two different criteria, for example  $t_5$  for an amplitude threshold of 5 mm, and  $t_1$  for an amplitude threshold of 1 mm. If the decay in the coda envelope follows the law  $t^{-q}$ , then  $\log(t_1) = \log(t_5) + (\log 5)/q$  and when this is substituted into equation 3.4, the result for this example is that the two magnitudes differ by the constant  $\log 5$  since  $c_1 = q$ . That is, the difference is in the constant  $c_3$ .

Of all events recorded in this study by the telemetric network, only two were recorded by the Brazilian regional network. According to the Bulletin of the Brazilian Geophysical Society (1987) these events are reported as:

Date	Origin time	magnitude
18 JUN 87	16:21:02	3.0
27 JUN 87	05:09:02	3.0

Table 3.4 Aftershocks recorded by the telemetric network and listed in the Bulletin of the Brazilian Geophysical Society (1987)

To calculate the magnitudes of all other events recorded by the J.Câmara telemetered network it was necessary to establish a magnitude scale based on the coda duration. This was a two step task. First, a coda magnitude scale was made for the smoked paper drum recorder station JC01 which was co-located with the telemetric station JCPA. Second, a correlation between magnitudes calculated by JC01 and duration measured by the stations of the telemetric network allowed a local magnitude scale based on the signal duration to be constructed for this study.

### Chapter 3

Because the constants  $c_1$  and  $c_3$  in the equation 3.4 are instrument dependent it is not possible to use the coda magnitude obtained for the smoked-paper drum recorder station JC01 directly.

As stated in section 2.1, the station JC01 has been recording the J.Câmara earthquake activity almost continuously since 22nd August 1986. This makes it possible to correlate the magnitude of events recorded by the Brazilian regional network with the readings of the coda duration for the same events recorded at JC01. The results from Assumpção et al. (1989b) are shown in Table 3.5.

$c_1$	$c_3$	N	S.D.	
$2.05 \pm 0.10$	$-1.61 \pm 0.24$	74	0.18	for $m \geq 1.5$

Table 3.5 Empirical relation between magnitude and duration in station JC01 for the expression  $m = c_1 \log(D) + c_3$ . The duration D was measured from the wave onset until the amplitude of the signal on the seismogram falls below one millimetre. N is the number of events used in the correlation and S.D. is the standard deviation of the fit.

Using 27 events with simultaneous readings at drum recorder station JC01 and the telemetric network, with magnitude greater than or equal to 1.5, it was possible to establish a new magnitude scale for the J.Câmara telemetric network. The magnitudes of those events were calculated by using the readings of the station JC01 and duration magnitude scale of Table 3.5. The same events had their durations read on the network stations. The result of the correlation was:

$$m = 2.01 \log(D) - 1.39 \quad 3.5$$

with S.D.= 0.08 and correlation coefficient  $r = 0.98$ . Figure 3.12 shows the correlation.

The duration (D) of an event recorded by the stations of the telemetric network was defined as the time interval between the P wave onset and the point where the amplitude of the signal dropped to twice the average value of the amplitude of the noise. Thus, the end of the record is fixed at the point where the signal-to-noise ratio is 2. This evaluation was done visually. This criterion for duration readings was adopted because the PCEQ picking program displays the event signals using dynamic gain as the maximum amplitude of the seismogram occupies the entire window on the screen. So, only a relative amplitude judgment could be applied.

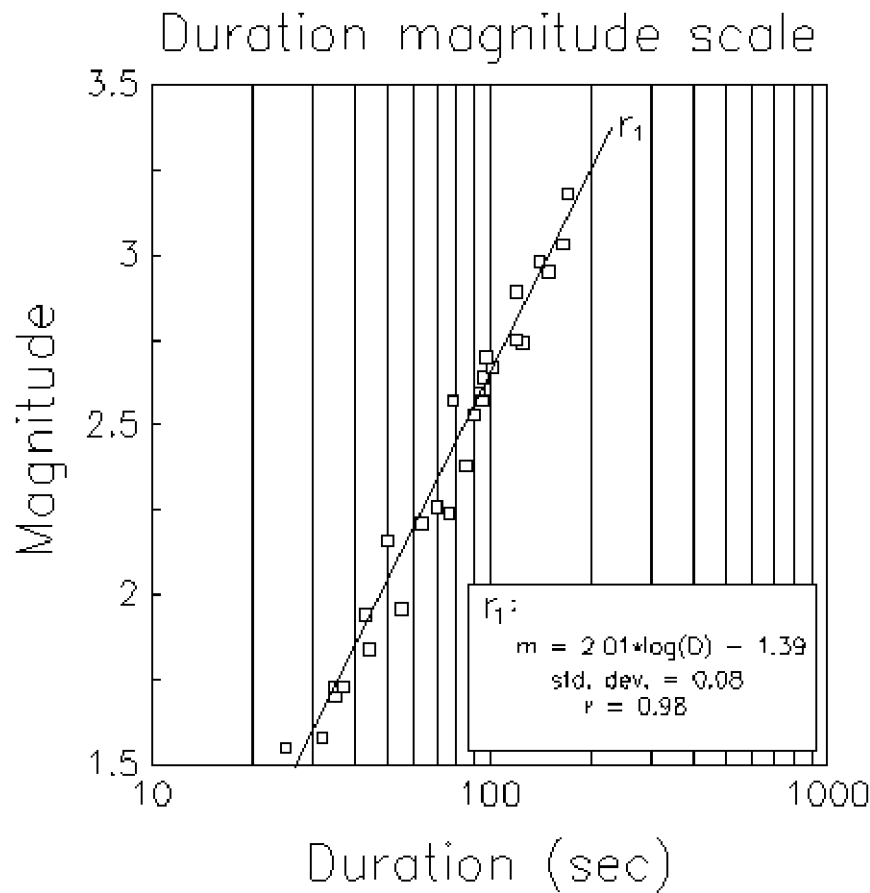


Figure 3.12 Correlation between magnitude calculated using data from smoked-paper drum recorder station JC01 and duration measured by the telemetered network stations. The inset shows the results of the correlation;  $r$  is the correlation coefficient.

The above definition of duration has one disadvantage in relation to the duration measured from the P wave onset to a fixed amplitude threshold such as that adopted by Lee (1972) or Assumpção (1989). The signal duration of earthquakes having the same magnitude may differ as a result of a change in the amplitude of the background noise, since by definition this sets the end of the earthquake signal. Cultural noise or other transient disturbances are relatively unimportant since their probability of simultaneous occurrence in all stations for one earthquake is low.

The long-term variations due to a seasonal change in microseismic activity are of more concern. Real & Teng (1973) studied this problem in southern California and concluded that the effect of variations in background noise on magnitudes

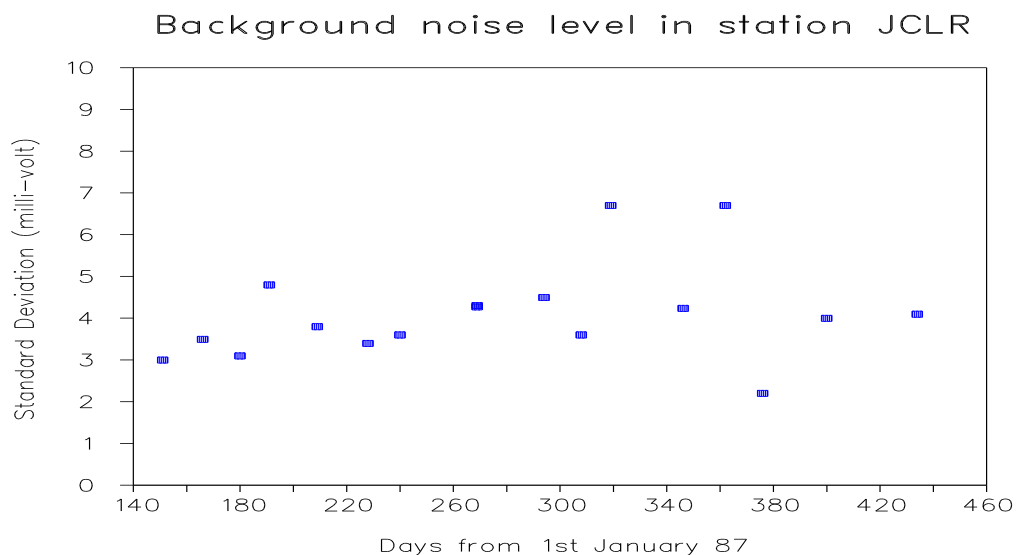


Figure 3.13 Standard deviation of the amplitudes of the background noise measured in the time window of one second for some events recorded by station JCLR. Amplitudes in millivolts.

determined by signal duration is insignificant in that region. However, they point out that it should be recognized that in regions of strong annual climatic change where the background noise variations may be great, it may be necessary to correct the signal duration seasonally. In northeast Brazil and particularly in the Rio Grande do Norte state which lies close to the equator, the climate is recognized to be steady throughout the year and so seasonal corrections in the duration are not necessary. Figure 3.13 shows the standard deviation in the amplitudes of the background noise measured in volts in a time window of one second preceding some events which were recorded by the station JCLR. The signal was filtered with a 0.2 to 2 Hz band before evaluating the standard deviation. The period of time corresponds to the working period of the network and events were randomly chosen. No significant variation in the background noise was detected.

The maximum variation in the standard deviation of background noise in the data of figure 3.13 is about 6 millivolts. This variation is not important as it probably represents some ephemeral local disturbance. The absence of any seasonal variation is more significant. The standard deviation in the data of figure 3.13 is about 2 millivolt. The effect of this variation in the measurement of duration is insignificant, less than ten percent. For example, figure 3.14 shows the seismogram of a small event located about ten kilometres away from station JCLR. The standard deviation of the background noise preceding the P wave onset (measured in the interval between 6 and 7 sec) is 3.6 millivolts and the duration of this event is 5 seconds, measured from the onset of P wave until the point A which is considered to

correspond to the amplitude threshold. Suppose now the background noise preceding the P wave onset for this event is like the region comprising the instants 13 sec and 14 sec in figure 3.14. In that region the standard deviation of the amplitude is 7.2 millivolts, that is, twice the real background noise. In this hypothetical situation, the duration of this event would be 3.4 sec, measured until the point B in figure 3.14. Doubling the amplitude of the background noise has shortened the duration by 31% and the difference in the magnitude calculation using equation 3.5 is 0.3 units. This represents an extreme case, as the average fluctuation in the noise given by the standard deviation over the data of figure 3.13 is only 2 millivolts. Tsumura (1967) concluded that the subjective decision about the end of signal implies an uncertainty of 20% in the duration measurement. Then, this factor is more influential than the variation in the background noise in this study and the uncertainty in the duration magnitude for the events recorded by the J.Câmara network is estimated to be  $\pm 0.2$  units of magnitude.

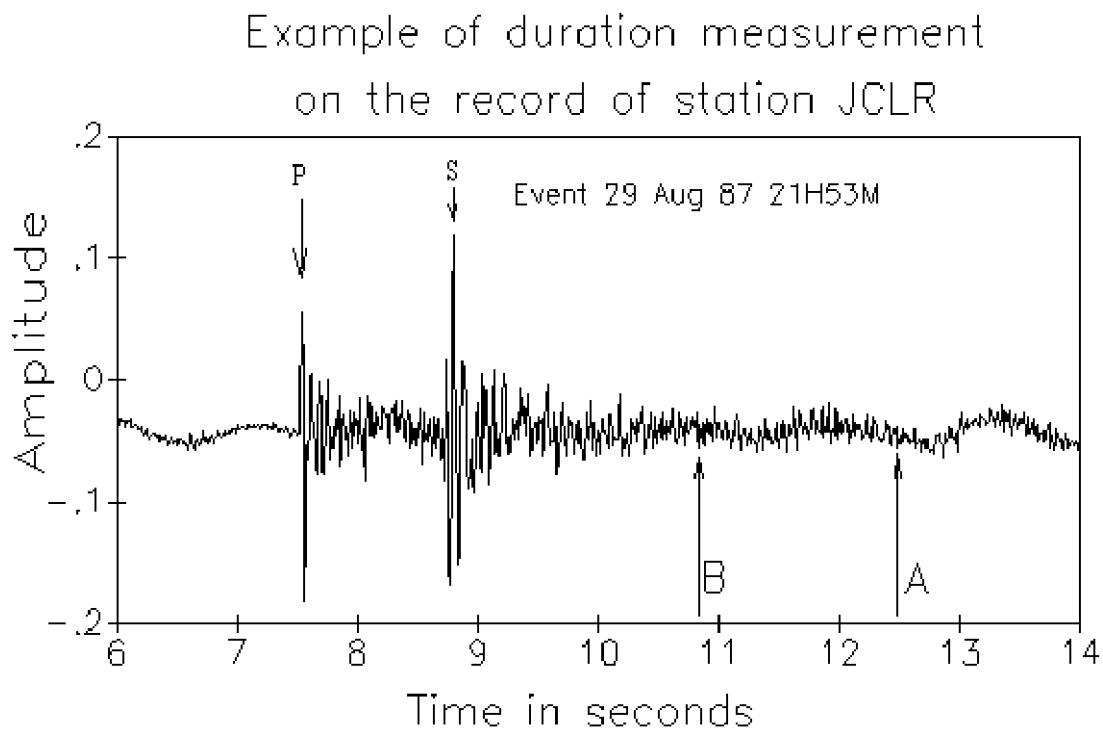


Figure 3.14 Seismogram of a small event recorded by station JCLR. Duration is 5 sec, measured from the onset of P wave to the point A. Amplitude fluctuation of background noise is 3.6 millivolts, measured from the standard deviation of the amplitude signal in the time window of 1 sec, preceding the onset of the P wave. This event was located at about 10 km from the station JCLR. Point B represents a duration of 3.4 sec in a theoretical case in which the noise changes to a signal pattern equal to the oscillations in the time interval between 13 sec and 14 sec.

## Chapter 3

A plot of earthquake magnitude distribution against cumulative number of events ( $N$ ) for all the 3,780 events recorded in the J.Cámara region is shown in figure 3.15a. Ignoring events around magnitude 3.0, the curve seems linear down to magnitude 1.0. For a magnitude threshold equal to 1.1, the  $b$ -value found using the maximum likelihood estimation (equation 3.2) is 0.84. In figure 3.15a, the line represents this  $b$ -value but it is not the best fitting line; it is just a line to make a comparison with the alignment of the points to emphasise the break in linearity. This set of data is not complete, although it should be representative of the recor-

### Cumulative number of events against magnitude

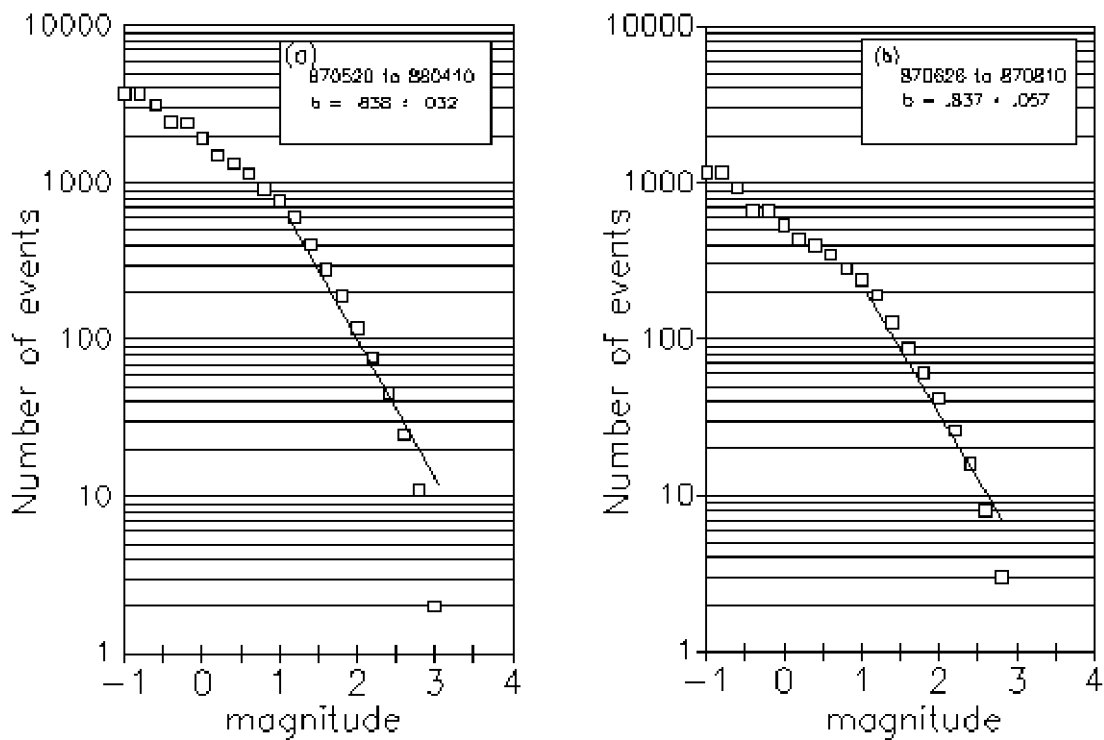


Figure 3.15. (a) Cumulative number ( $N$ ) of events versus magnitude for the period of 20th May 87 and 8th April 88.  
(b) Cumulative number ( $N$ ) of events versus magnitude for the period of 29th June 87 and 10 August 87.

ding period. Appendix A shows a pictorial summary of the operational log of the telemetric network. In total, the network was down about ten percent of the time. To ensure the completeness of data another period was chosen. The period between 26th June 1987 and 10th August 1987 is the longest interval of time during which the telemetric network recorded continuously (discounting a few minutes for tape changes). During this period, at least two stations in the north part and two stations



### Chapter 3

in the south part were working properly to ensure a good coverage of the area. That period is coincident with the most active period of this study as can be seen by the histogram of figure 2.11. The b-value found for this particular period is 0.84 for the same magnitude threshold and coincides with the previous b-value found for the entire period of this study. The cumulative number of events is plotted against magnitude for the period between 26th June and 10th Aug is plotted in figure 3.15b.

A magnitude threshold of 1.1 has been chosen visually, based upon the plots in figure 3.15, and there are some uncertainties concerning this value. For a better estimation of the b-value, an average was made using different magnitude thresholds. Table 3.6 shows some b-values that were calculated using the maximum likelihood method for the two periods mentioned in the last paragraph, and using three different magnitude thresholds. For those values, the weighted average  $b = 0.83$  was found.

b	S.D.	N	$m_0$	Period
.778	.028	761	1.0	20JUN87-10MAY7
.838	.032	680	1.1	20JUN87-10MAY7
.908	.037	603	1.2	20JUN87-10MAY7
.764	.049	239	1.0	26JUN87-10AUG7
.837	.057	218	1.1	26JUN87-10AUG7
.900	.065	192	1.2	26JUN87-10AUG7
Average $b = .83$ S.D.= .02				

Table 3.6 b-values calculated for different periods of time and different magnitude thresholds using the maximum likelihood estimation method. S.D. is the standard deviation; N is the number of events and  $m_0$  is the magnitude threshold.

The magnitude threshold 1.1 or 1.0 was found by examining the plots of figure 3.15 and this means that the list of events with a corresponding coda duration below 17.3 sec or 15.4 sec is supposedly not complete. With this assumption, an extrapolation of the line representing the b-value in figure 3.15a for lower magnitudes, shows that the number of events with a coda length of 10 seconds should be about twice the number of events actually recorded by the network. Such an error is very unlikely. Events of this size (coda length of about 16 sec) with epicentre in the J.Câmara region are still big enough to be registered by any stations in the network even for events with epicentres in the Poço Branco fault located ten kilometres from the centre of the network. In practice, only events with

### Chapter 3

duration below six seconds are not recorded by all the stations. This should represent the real event detection threshold. Accepting the linearity in the magnitude distribution relation of Gutenberg & Richter (1956), the discrepancy in the magnitude threshold should be credited to the non-linearity of the duration magnitude relation. This implies that the departure from the linearity for lower magnitudes found in figures 3.15a and 3.15b is not real but is a consequence of an inappropriate extrapolation of the duration magnitude scale in equation 3.5 for small events.

In theoretical studies made by Aki (1969) and Aki & Chouet (1975) the coda waves are interpreted as the result of backscattering of the body and surface waves on the heterogeneities of the crust and upper mantle. According to those studies, and those of Suteau & Whitcomb (1979), the magnitude versus  $\log(D)$  relationship is not linear. It is characterised by successive lines whose gradients decrease with decreasing magnitude.

This kind of peculiarity in the coda duration magnitude has been observed in several other studies (e.g. Herrmann, 1975; Real & Teng, 1973). Bakun & Lindh (1977) found that magnitude is better represented if two different coda length magnitudes, each one for a particular magnitude range, are used. For  $1.5 < \text{magnitude} < 4.5$  the values  $c_1 = 3.32$  and  $c_3 = -3.59$  were established and for  $0.5 < \text{magnitude} < 1.5$  they found  $c_1 = 0.71$  and  $c_3 = 0.28$ . These results applied for the North California region when using LC-4 seismometer with peak response around 20Hz.

For the J.Câmara region, a similar study was made by Assumpção et al. (1989b) using the station JC01. They assumed linearity in the magnitude distribution relation of Gutenberg & Richter (equation 3.1). The suggested departure point from linearity is around magnitude 1.5. To adjust lower magnitude events according to that relation they propose a coda length magnitude scale with  $c_1 = 1.00$  and  $c_3 = -0.02$  for events lower than magnitude 1.5.

For the purpose of verifying the hypothesis of non-linearity in the coda duration magnitude (equation 3.5) for lower magnitudes, and to make the appropriate correction, a different approach was tried. A plot of amplitudes against duration was created. To avoid complications with attenuation correction, only events located in a small region were used, using a station far from the epicentral region in order to make variations in epicentral distances insignificant. All chosen events lie within a 2km diameter circle close to the station JCAZ. Recording station JCLU was 16 km from the centre of this circle and was considered suitable for this plot. As the attenuation of amplitude with distance is not available for the region, a rough estimate of the distance effect can be obtained from the attenuation curves for

### Chapter 3

the eastern North America obtained by Nuttli (1973) using short period waves. This seems a good approximation because that region such as J.Câmara lies in an intraplate area. For these events (which lie between 15 and 17 km from JCLU), variations in the epicentral distance give a maximum of 20% attenuation on the amplitudes measured at station JCLU. If the station JCAZ (which lies between 2 and 4 km from the epicentres) was chosen, the variations in the hypocentres would account for an attenuation of over 70% in the amplitudes, and a correction in that parameter will be necessary. Other disadvantages arise when a station close to the epicentres is used. There are complications due to near field radiation and if events are close enough to the station, hypocentral distance and not epicentral distance has to be used because the depth of the event becomes significant. It is well-known that depth errors are larger than errors in epicentral location.

For each event the maximum P wave amplitude and corresponding frequency were measured on the seismogram and the amplitude was converted to volts using the response curve in Appendix B.2. The event duration was measured in seconds using the PCEQ picking program (Valdés, 1989) referred to in the IASPEI software, section 3.2. Figure 3.16 shows the results for the station JCLU which was about 16 km from the epicentral area. The alignment of data points suggests a change in the slope between 10 and 20 seconds. The straight line  $r_1$  in figure 3.16 represents the best least squares fit for events with duration above 17.5 sec and the data are reasonably well correlated (correlation coefficient is 0.84). The same is not true for the line  $r_2$  which represents the best fit for events below 17.5 sec in duration (correlation coefficient is 0.60). The duration 17.5 has been used only for practical reasons and was taken from the magnitude threshold used for the calculation of the b-value in the previous paragraph; it does not represent the corner duration in figure 3.16. There is no easy way to improve the data for small shocks. Events with duration below 3 or 4 seconds are not recorded by all stations. Consequently, location errors become larger as the size of the event decreases. In addition, the difficulty in identifying the onset of the P wave could introduce an error in the duration measurement. For stations closer to the epicentral area the seismogram saturates earlier, narrowing the range of useful data for defining the line  $r_1$ , and all the disadvantages described in the previous paragraph for the station JCAZ become relevant.

Although it is not possible to get any reliable correction in the duration magnitude formula by correlating amplitude and duration for small events, two conclusions arise from the plot of figure 3.16. Firstly, despite the relatively high

# Events recorded by station JCLU

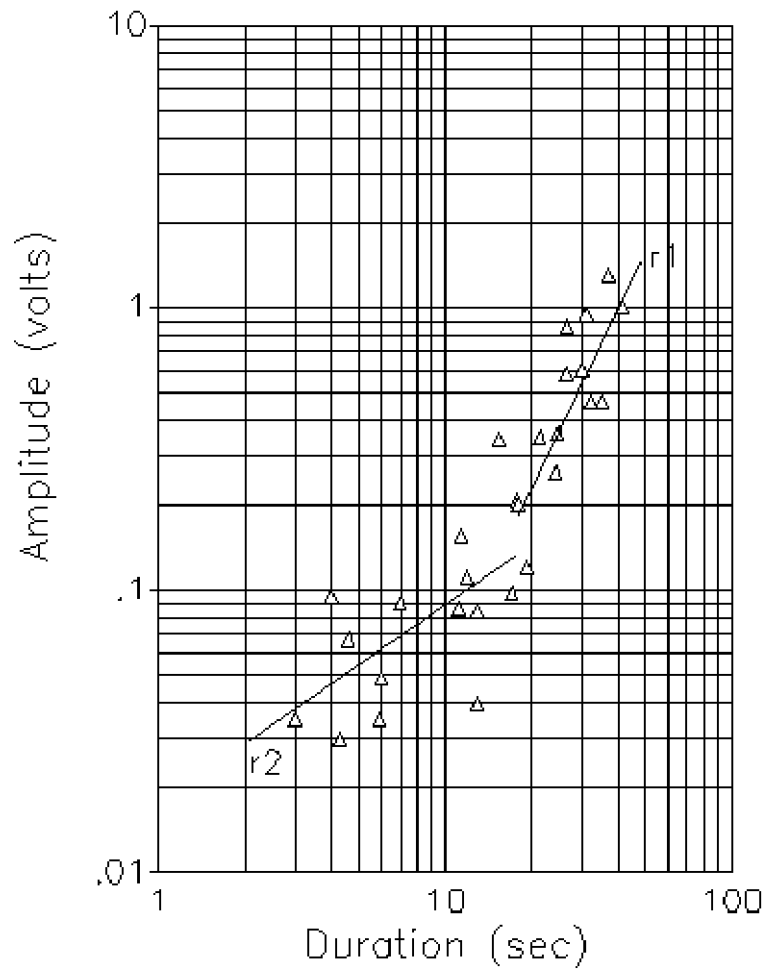


Figure 3.16. Amplitude measured in volts against duration measured in seconds for events recorded by station JCLU. The line  $r_1$  is the best fitting line for events with duration above 17.5 seconds and is represent by the equation  $r_1$  :

$$\log(V) = (2.18 \pm 0.40) \times \log(D) - (3.45 \pm 0.58),$$

where  $V$  is the amplitude and  $D$  is the duration. The correlation coefficient is 0.84 and the standard deviation of the estimate is 0.17. The line  $r_2$  is the best fitting line obtained using events with duration below 17.5 and represented by  $r_2$  :

$$\log(V) = (0.71 \pm 0.27) \times \log(D) - (1.76 \pm 0.25).$$

The correlation coefficient is 0.60 and standard deviation 0.24.

uncertainty in the slope of line  $r_1$  , the value 2.18 is close to the coefficient 2.01 of coda magnitude formula 3.5. Then, the line  $r_1$  would represent this formula. In figure 3.16, the line  $r_1$  seems linear for events above duration 15.5 sec and this means that the coda magnitude given by equation 3.5 would be valid for events with magnitude above 1.0. Secondly, it was possible to show the non-linearity of the

# Cumulative number of events against magnitude (after correction for small magnitudes)

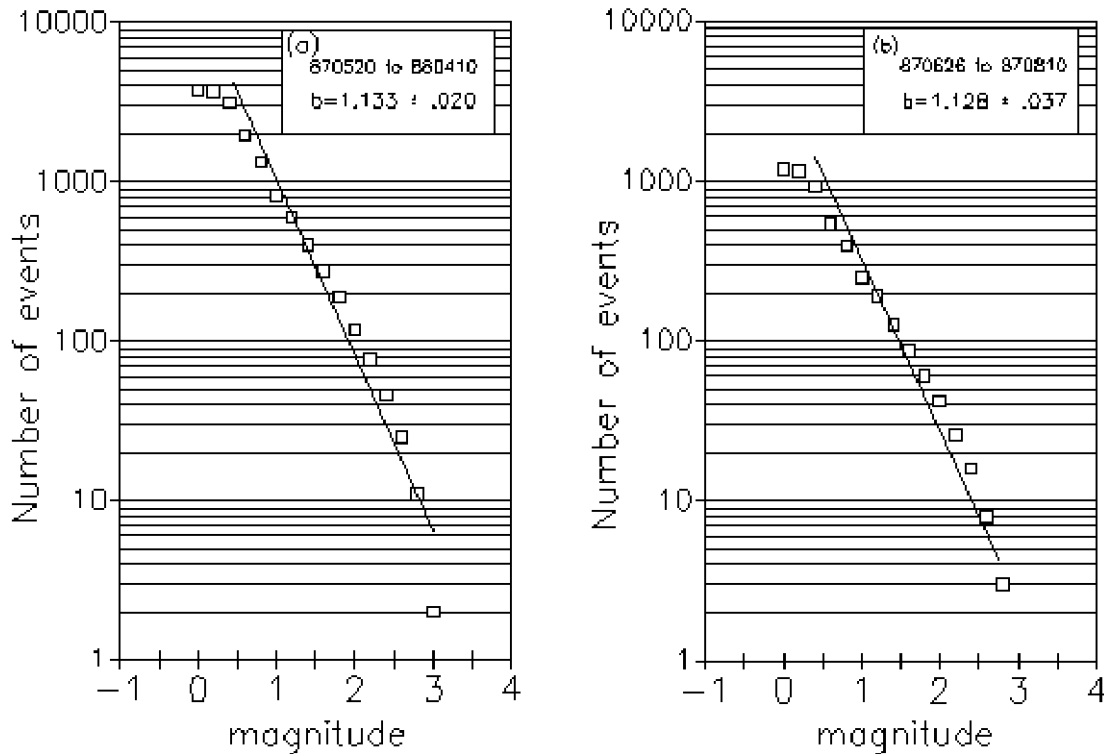


Figure 3.17 b-value using magnitude scale of equation 3.5 for events with duration above 15.5 seconds and  $m = 0.71 \times \log(D) + 0.16$  for smaller events. (a) for events in the entire period, (b) for events in the period between 26 JUN 87 and 10 AUG 87.

coda magnitude 3.5 for events with duration below about 15.5 sec or magnitude 1.0. The slope of line  $r_2$  is clearly lower than that of line  $r_1$ . This means that in reality the magnitudes of small events increase more slowly with the duration than the magnitudes of larger events. This is what would be expected in order to explain the discrepancy in the magnitude threshold of figure 3.15 where no correction was made for small events. To clarify this point, magnitudes were recalculated correcting the magnitude of small events with the suggested coefficient given by  $r_2$ . For events below duration 15.5 seconds, which correspond to magnitude 1.0, the relation

$$m = 0.71 \times \log(D) + 0.16 \quad 3.6$$

was used, and for events above that duration equation 3.5 was employed. The corresponding plot of the cumulative number of events against magnitude for this case is shown in figure 3.17. Comparing this with figure 3.15 some differences can be noted. After applying the magnitude correction, the magnitude threshold is

### *Chapter 3*

around magnitude 0.5, which corresponds to a duration of 3 seconds. This is a more realistic figure for the magnitude threshold. For example, it was not possible to identify the onset of the P wave of any small event with duration below 3 seconds located 16 km from the station JCLU, which should be included in figure 3.16. That is, it was not possible to measure either the duration or the P wave amplitude of those events from the records of station JCLU which was one of the most distant station from the centre of the network. A b-value of 1.13 obtained for the magnitude threshold 0.5 is higher than that obtained previously but is closer to the b-value found by Assumpção et al. (1989b).

Although consistent, the above correction for the magnitude of small events is not reliable because it is based on poorly constrained data as shown in figure 3.16. So, in this study the suggested correction for events of duration below 15.5 sec will be applied because it is closer to reality, but only events with magnitudes above 1.0 will be used to calculate parameters that are magnitude dependent.

## **CHAPTER 4**

### **AFTERSHOCK PATTERN**

This chapter is intended to show how the two main shocks in the J.Câmara series of earthquakes can be correlated with major fault heterogeneities. Because no surface rupture was found following these earthquakes, the assumption of geometric irregularities, which will be explained in section 4.2, has to rely on the aftershock pattern interpreted from the hypocentral maps. Chapter 5 continues the analysis of the main features in the seismicity, and in Chapter 6 the analysis is extended to small scales.

#### **4.1 Seismicity map from the telemetric network data**

Appendix C.1 shows the summary output of the location program HYPO71 (Lee & Lahr, 1975) for all the 3,780 events of dataset 3 which were computed using the two layer model of Table 3.3. Magnitude calculations have also been included. The average RMS of the time residuals for this dataset is 0.04 sec; the average epicentre location error is 0.19 km, and the average depth error is 0.40 km. With the aim of constructing an epicentral map with optimum accuracy and completeness, a subset (named dataset 4) of events from dataset 3 was taken. In dataset 4 every event has a horizontal error (ERH) in location of less than 1 km; no restriction was imposed on the depth error (ERZ). Dataset 4 lists 3,714 events which are marked with an asterisk in Appendix C.1. The average time residual obtained in the epicentral location was 0.04 sec; the horizontal error averaged 0.17 km and the average depth error was 0.38 km. These low values suggest that random errors are small and that the epicentre locations are reliable.

The epicentral map in figure 4.1 was plotted from this dataset. It shows that the general pattern found in the previous location map (figure 2.5) drawn using data from the drum recorder stations, remains basically the same. However, epicentres are now more accurately determined (horizontal error less than 1 km) and it is clear that the aftershocks are clustering in several places. Almost all the events which

occurred during the period between May 87 and April 88 are concentrated on the so-called Samambaia fault. The region of low seismicity around the road is also evident in this dataset; it divides this fault into two segments. The north segment is larger and more homogeneous than the south segment.

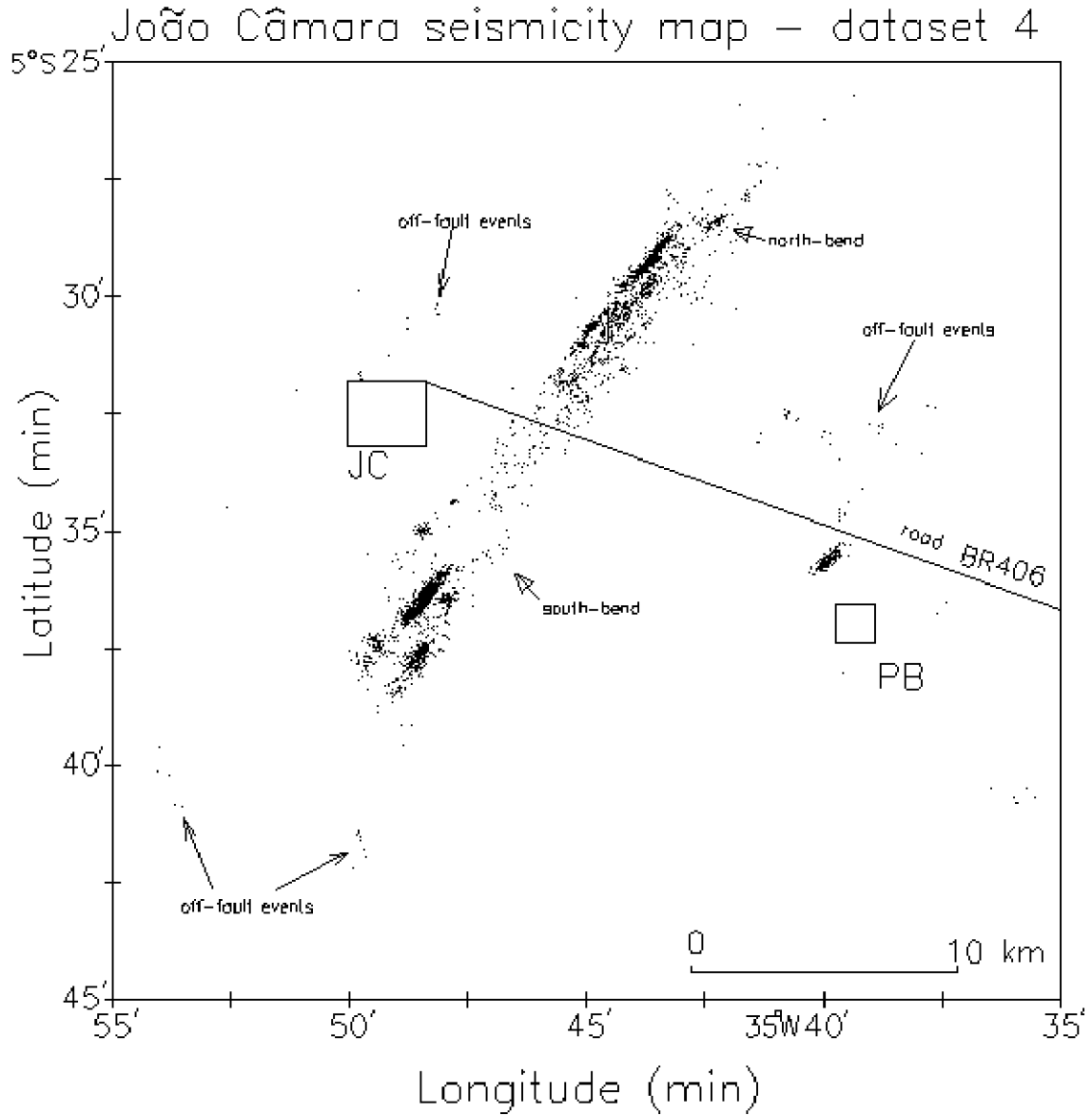


Figure 4.1 Epicentral map of the 3,714 events from dataset 4. Horizontal errors in epicentre location are less than 1 km. (The two intersecting lines of epicentres close to the site of station JCLR are artifacts which will be explained in section 4.4).



### 4.2 Fault heterogeneities

In examining some historical earthquakes, Das & Aki (1977) point out that in many cases the trace of an earthquake fault observed on the surface is not a single continuous line but consists of discontinuous segments. Segall & Pollard (1980) extend these observations and conclude that faults are discontinuous geologic features consisting of numerous discrete segments, commonly arranged as *en echelon* arrays, and they state that discontinuous fault traces occur at all scale lengths. Discontinuities are important in an aftershock study such as this, because according to those authors, geologic and geophysical evidence indicates that they play an important role in the kinematics and dynamics of the faulting process. In general, correlation between fault heterogeneities and earthquake rupture has been conducted on large magnitude earthquakes (e.g. Barka et al., 1988; Schwartz et al., 1989).

It is recognized that the fault rupture process may be characterized by irregular slip motions caused by intermittent locking of fault segments, stress variations, and roughness of the faulting surfaces (Bullen & Bolt, 1985). To describe heterogeneity in a fault plane or between fault planes the terms "barrier" and "asperity" are frequently used. Both terms refer to strong patches of the fault that are resistive to breaking, but they have distinctly different roles in the modelling of the earthquake faulting process (Aki, 1984). The 'barrier' concept was introduced by Das & Aki (1977), who constructed a two-dimensional fault model that contained a nonuniform distribution of strength over the fault plane. They found that a rupture may start at the focus near a strong section of the fault, which they called a barrier, and then propagate over the fault plane. According to them, the rupture and the barrier will interact in the following three different ways, depending on the magnitude of barrier strength relative to tectonic stress:

- 1) If the tectonic stress is relatively high, the barrier is broken as the crack tip passes.
- 2) If the tectonic stress is relatively low, the crack tip proceeds beyond the barrier, leaving behind an unbroken barrier.
- 3) If the tectonic stress is intermediate, the barrier is not broken at the initial passage of the crack tip but eventually breaks because of subsequent increase in dynamic stress.

In this model, the presence of barriers on the fault plane will introduce diverse slip functions and a variety of seismic waveforms. Das & Aki (1977) suggest that an earthquake fault is usually a composite of faults separated by barriers and that unbroken barriers are naturally the sites of stress concentration and the

## Chapter 4

sources of aftershocks. In addition, they stated that if the barriers are completely broken, there may be no aftershocks within the main-shock fault plane.

The term "asperity" seems to have appeared first in Kanamori & Stewart (1978), who used it to describe regions within which earthquakes with relatively high moment release occurred. In their model the stress is heterogeneous before the main shock and becomes homogeneous afterwards. Thus this model represents the main shock as a stress-smoothing process in contrast to the barrier model in which the main shock is considered to be a stress-roughening process (Aki, 1984).

Barriers were broadly classed by Aki (1979) according to whether they are a consequence of fault geometry or of rock properties. The first type, associated with a change in orientation of two active faults, were called geometric barriers and the second type, which incorporate possible changes of fault strength, inhomogeneous barriers. An extension to the concept of geometric barriers was proposed by King & Yielding (1984) who divided these into two types: conservative and non-conservative barriers. In conservative barriers the slip vector is common to both fault planes, whereas in non-conservative barriers the slip vectors are different on the two fault planes that meet at the barrier. Although both types of barrier arrest dynamic rupture, only non-conservative barriers need produce aftershocks, as off-fault deformation is required to accommodate the difference in slip vectors (King & Yielding, 1984). In general, geometric barriers can be represented by fault offsets or bends in a fault.

### 4.2.1 Mechanical effects of fault offsets

In a further development, King (1986) classified the non-conservative barriers into dilatation and fragmentation barriers. The former occur where faults end on open or fluid-filled voids and on a small scale, fracture can terminate in pore space or microcracks. The barriers do not require the slip to taper at the ends of faults, and finite motion can occur without the creation of new structures or the development of large strains in the medium around the fault. Fragmentation barriers occur under conditions of confining pressure such that large voids cannot open. The slip function on the main fault is constrained to be zero at both ends, and although some motion can be accommodated elastically, finite motion must be accommodated by further faulting. The multiple faulting in the long term must be sufficient to accommodate the slip that cannot be accommodated on the main fault. Sibson (1985) called these two kinds of geometric barriers dilational and antidilational jogs, which he defined according to the tendency for increase or reduction respectively of the area of the step region.

## Chapter 4

A different approach and terminology was used by Segall & Pollard (1980) to describe geometric barriers and their properties. They analysed the stress distribution near *en echelon* faults for some cases of right and left stepping cracks in a static two dimensional stress model. As the stresses due to an individual crack decay with distance, they only considered the stress distribution discontinuity between the two closest segments. For a vertical strike-slip fault in which the length is much greater than depth, significant interactions between segments would be expected if they are separated by a distance less than the depth of faulting. In this range, the perturbing stress is greater than the applied stress and it controls the deformation. They showed that, under appropriate conditions, secondary faults can be generated by extension or shear failure mechanism. In the case of extensional failure, fractures cut the pattern and open perpendicular to the minimum compression. For left-stepping *en echelon* cracks the area under tension is small and lies outside the cracks. For right-stepping cracks, a much larger area of tension bridges the cracks. The stress orientation for left-stepping cracks is such that extension fractures forming near crack tips would propagate away from each other whilst for right-stepping cracks the fractures forming near the cracks tips would propagate into the region between the cracks. The conditions for shear failure depend on both principal stresses. For example, figure 4.2b illustrates shear failure conditions for two non-overlapping left step cracks for the case of strike slip right lateral fault under the conditions shown in figure 4.2a. Curved lines are contours of the shear failure condition  $F$  as defined by Segall & Pollard, (1980). Failure can occur when  $F > 1$  and the figure shows that the shear-failure zone is restricted to the neighbourhood of the cracks tips. Contour lines for two right stepping *en echelon* cracks in figure 4.2c show that the zone of potential shear failure in this case extends over a much wider area.

King (1986) stated that fault offsets which are referred as steps by Segall & Pollard (1980) and as fault jog by Sibson (1986) may be regarded as consisting of one or more bends of opposite sign. In fact, in figures 4.2b and c, the region that links the fault offsets can be interpreted as a fault bend. Sibson (1986) used the term dilational and antidilational jog with approximately the same meaning as the right step and left step crack definitions of Segall & Pollard (1980) and the dilatational and fragmentation barrier of King (1986). Scholz (1990) recognised that in recent years a number of workers introduced new classification schemes with terminologies descriptive of both the geometry and the mechanical processes they feel are most closely associated with the feature. Because these systems are usually neither complete nor rigorously defined, none has been accepted universally and so

they have confused the literature further (Scholz, 1990). Thus, throughout the present study the most suitable term will be used according to the circumstances.

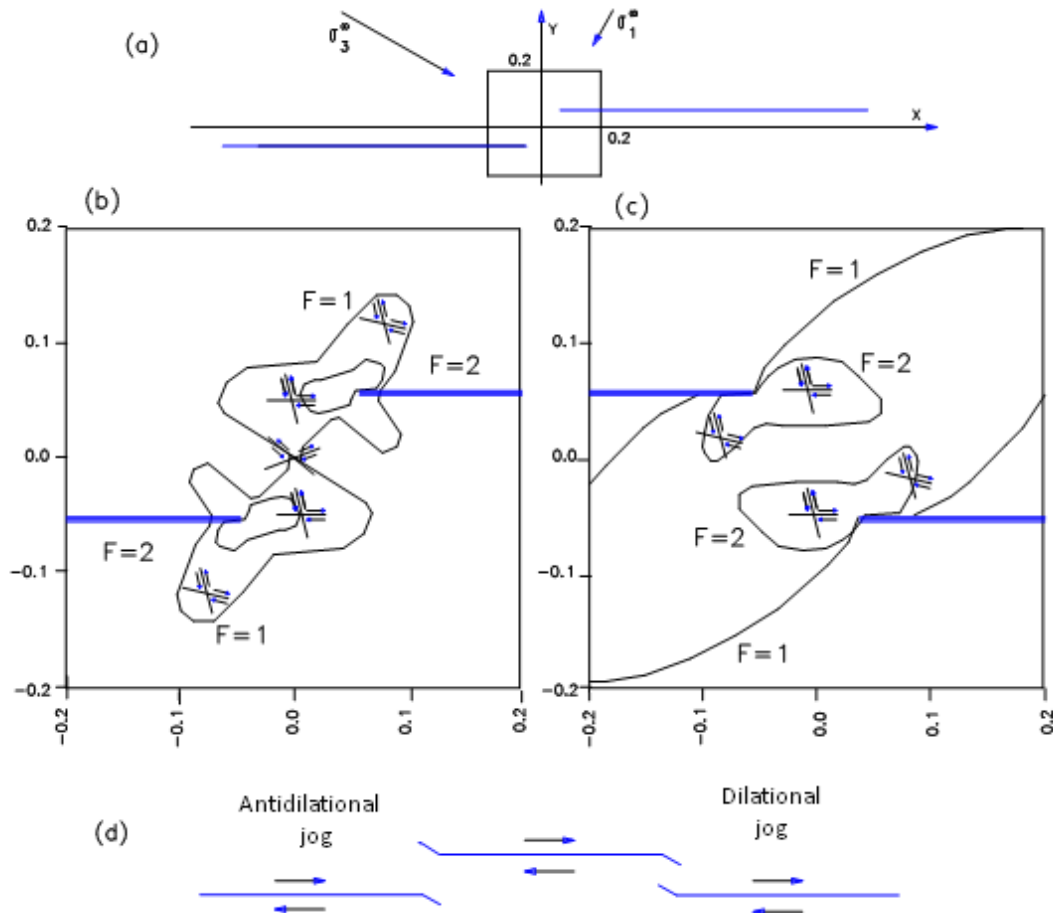


Figure 4.2 Secondary fracturing near *en echelon* discontinuities. (a) Crack geometry, area plotted, and applied stress state. (b) and (c) Contour of shear failure condition  $F$  for left step and right step cracks respectively; Illustrated contours are  $F=1.0$  and  $F=2.0$ ; potential shear fractures are oriented  $30^\circ$  to local maximum compression direction (From Segall & Pollard (1980). (d) Representation and classification of infrastructure into antidilational and dilational jogs with respect to slip sense and far-field principal compressive stresses according to Sibson (1986).

One particular and important feature emphasized by King & Nabelek (1985) is that a bend in a fault requires the appearance of a third direction of faulting (not necessarily a third major fault) and since displacement on the three strike-slip faults must come to zero at the intersection, other deformation must occur to permit fault motion. Thus motion on the main faults will produce subsidiary faulting in a zone

## Chapter 4

around the junction at all scale sizes (King & Nabelek, 1985). They call the deformation area a process zone. Since, the observation of subsidiary faulting must depend on the resolution of the data, sometimes only a third direction of faulting can be distinguished, which is an indication of a process zone or fault bend in that area.

In their analysis, Segall & Pollard (1980) suggest different consequences for left-step and right-step cracks under right lateral shear. For left-stepping segments (or antidualational jog), normal tractions on the overlapped crack ends increase and inhibit sliding; the mean stress increases, and secondary fracturing is restricted and tends not to link the cracks. They suggest that left steps store elastic strain energy and may be sites of large earthquakes. For right stepping segments (or dilational jog), normal tractions decrease and facilitate sliding; the mean compressive stress also decreases and promotes the formation of secondary fractures which tends to link the cracks and allow slip to be transferred through the discontinuity (Segall & Pollard, 1980).

Regarding the effects of a right-step crack, King & Nabelek (1985) and Sibson (1985) report several historical earthquakes in which the rupture propagation has terminated in the vicinity of a right-stepping segment which appears to have acted as a strong barrier, contrary to the expectation of Segall & Pollard (1980). This apparent contradiction is explained by Sibson (1985) by stating that in these cases the dynamic effect was more important than the static effect. The rapid opening of extensional fracture, which would facilitate the slip transfer, is strongly opposed by an induced suctional force in the shear direction increasing effective normal stress and shear resistance on subsidiary shears (Sibson, 1985). In describing their model based on geometric concepts, King & Yielding (1984) state that bend geometry in a fault plays an important role in the earthquake cycle. This suggests that in some cases bends or jogs may control rupture initiation and that the rupture in individual earthquakes is apparently limited to regions between bends in faults.

### 4.3 Fault irregularities from epicentre locations

According to King & Yielding (1984) the initiation and termination of earthquake processes are limited to regions between fault bends. A close look at figure 4.1 reveals at least two lineations, which could be interpreted as geometrical barriers in the form of small bends, one in the north segment of the Samambaia fault and another in the south segment. These will be called the north-bend and south-bend respectively (see figure 4.1). The main shock of 30th Nov 86 was

## Chapter 4

supposed to have occurred close to the south-bend, about 5km from it (Ferreira et al., 1987) and the second larger shock of 10th Mar 89 was preliminarily located in a region to the north of the north-bend, about 3 km from it (Costa, 1989).

### a) The north-bend.

Epicentres of the north segment of the Samambaia fault do lie on a remarkably well-defined plane. However, some off-fault epicentres are found at the north edge of this fault segment, at least. Figure 4.3 shows that region in detail. Dashed line 1 indicates the trend of the main fault and line 2 shows a difference in alignment of some epicentres which characterizes a probable fault bend in that region. Because few aftershocks were found in the region to the north of this bend, it seems that the bend stopped the propagation of aftershocks to the north, which agrees with the role of fault bends in the rupture process described by King & Nabelek (1985). The dashed line 3 points to a line of a few events in a direction approximately normal to line 1. According to King & Nabelek (1985) bends in faults require the creation of a third direction of faulting in order to account for the conservation of the slip vector. In this case, line 3 may represent the third direction of faulting as a result of the fault bend indicated by line 2. Basically, this same third direction of faulting can be found in the epicentral map of Sophia & Assumpção (1989), obtained from smoked paper records, although no interpretation was given by the authors to this feature. It is not clear whether the dashed line 4 in figure 4.3 indicates a different third direction of faulting or whether it represents epicentres which belong to secondary fracturings in the process zone.

### b) The south-bend.

Another possible bend can be identified in the south segment of the Samambaia fault which is showed in detail in figure 4.4. The dashed line 2 indicates the alignment of epicentres which characterize the existence of the bend. The angle between line 1 and line 2 (the bend) is about 17°. Line 3 indicates a poorly defined third direction of faulting. In contrast to the north region, some clear secondary faulting, such as that indicated by line 4, is found in the south region. These features make it difficult to distinguish between fault offsets and secondary fracturings which are a consequence of the mechanical interaction between those fault offsets in the link region. That is, it is more difficult to identify the south bend than the north-bend. Also, it is possible that the south bend could be less well defined due to incompleteness of data from the telemetric network, and so is not easily detectable in the epicentral map of figure 4.4. In any case, it will be assumed

that a fault bend which influences the seismicity exists in the south segment, and in the absence of further evidence, this bend will be represented by the epicentres indicated by line 3.

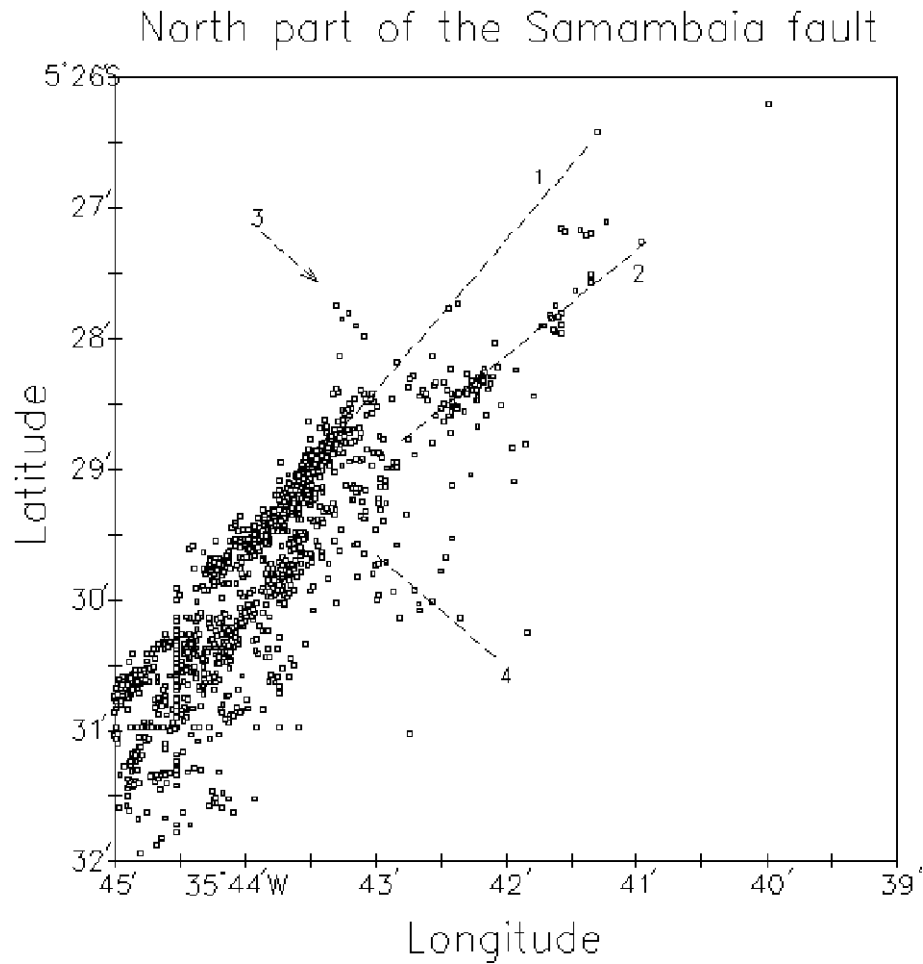


Figure 4.3 The dashed line 1 shows the trend of the north segment of the Samambaia fault. The dashed line 2 shows an off-fault group of events in a plane with a different strike. The intersection of this line with line 1 represents a fault bend. The dashed line 3, points to a third direction of faulting which is not a major fault. Line 4 indicates another possible direction of faulting, in this case not well defined. The linear artifacts in the epicentre location near the left corner at the bottom of the map are explained in section 4.4. Latitude and longitude are in minutes with respect to 5°S and 35°W respectively.

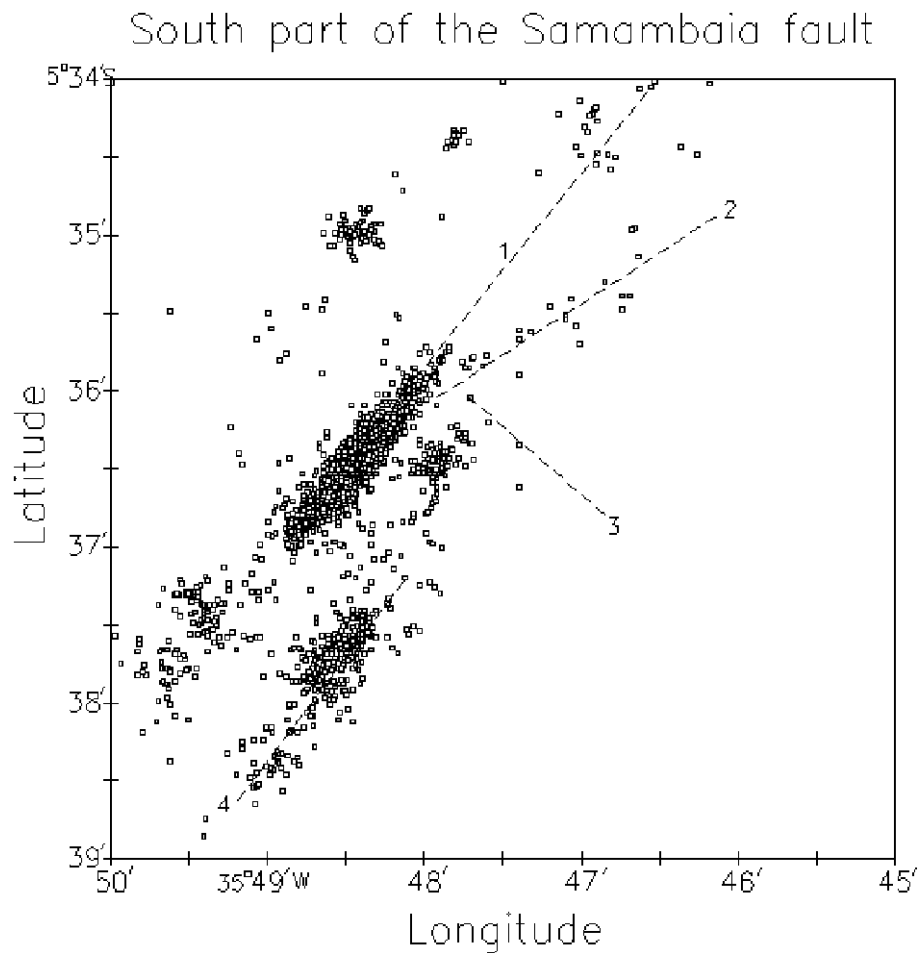


Figure 4.4 Seismicity map of the south section of the Samambaia fault which shows the location of the south bend represented by the change in direction between lines 1 and 2. Dashed lines 1, 2 and 3 have the same meaning as in figure 4.3. Line 4 indicates one of the secondary faults in this region. There is a  $17^\circ$  bend between line 1 and line 2. Longitude and latitude are in minutes following  $35^\circ\text{W}$  and  $5^\circ\text{S}$  respectively.

#### c) The consequences of bends in the Samambaia fault.

It can be seen in figure 4.1 that the region of low seismicity lies immediately to the north of the south-bend, and as discussed in section 2.1.2, the region of low seismicity was considered to be the most probable locus of the main shock. Because only one seismograph station was available at the time of the mainshock, the provisional epicentre was conjectured to be two or three kilometres to the north of the road, as indicated in the sketch of figure 2.8. This provisional epicentre corresponds to the area where the damage to buildings was most severe; that is, it was based on the hypothesis of a correlation between the region which experienced the maximum intensity revealed by the macroseismic data, and the main shock epicentre. However, this area is located in a rural part of J.Câmara where man-made



## Chapter 4

structures are rare and of variable quality, so that the macroseismic survey may not be reliable. Another possibility is that, contrary to expectation, the epicentre of the main shock is not necessarily the region where maximum slip occurs during the mainshock rupture, as shown by several authors in recent years (eg., Doser & Kanamori, 1986; Mendonza & Hartzell, 1988). Since no other clear bends were found in the epicentral map of figure 4.1, then according to the model of King & Nabelek (1985) in which the initiation and termination of the earthquake rupture is limited by the fault bends, the main shock epicentre is relocated to the south, close to the south-bend, as indicated in the sketch of figure 4.5. This is about five kilometres from the original estimate, still in the low seismicity region and still in the vicinity of the area of maximum intensity.

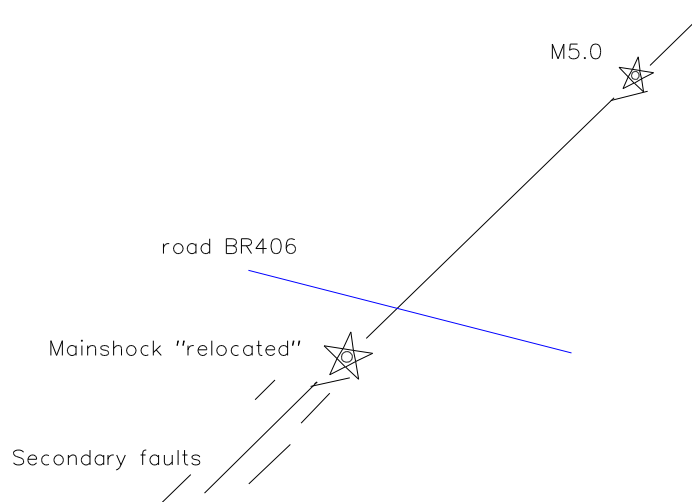


Figure 4.5 Sketch of the Samambaia fault showing the locations of the north and south bends and the two major events according to the model of King (1986).

Assuming that the two bends described above mark the fault ends, it is possible to say that the mainshock initiated in the region of low seismicity close to the south-bend, then propagated to the northeast direction, and terminated at the north-bend of the fault. This process is outlined in figure 4.5 in a preliminary attempt to explain the major features of figure 4.1, but needs other supporting evidence. For this purpose, it will be necessary to analyse the epicentral map in more detail, particularly the projection of the hypocentres onto vertical planes. It will be of particular importance to analyse of the pattern of seismicity related to the second major shock of  $m_b = 5.0$  that occurred in the north part of the fault in 1989. This later sequence is not included in the map of figure 4.1.

## Chapter 4

The directions of the north and south bends are aligned from SW to NE as shown in figures 4.3 and 4.4. The fault mechanism of the Samambaia fault has been reported as a predominantly right lateral strike slip fault with a small normal component (Ferreira et al., 1987). Under such conditions the bends could be described as a dilational jogs or right step cracks. However, from the data in figures 4.3 and 4.4 only one branch of the jog and the bend are evident. This effect could be due to the incompleteness of data. In order to check this hypothesis, it is necessary to analyse data covering a longer period.

### 4.4 Cross section analysis

The epicentral map of figure 4.1 was plotted with selected events in which horizontal errors in location are less than 1.0 km but no restriction was imposed in the precision of the depth. In order to obtain an optimum high quality dataset for the study of hypocentres through the investigation of the distribution of events with depth, and in order to attempt to identify all possible clustering features of the aftershocks, it was decided to make another selection among events in dataset 3. To ensure a more homogeneous high quality dataset, only events with at least eight readings (P plus S), a root mean square time residual (RMS) lower or equal to 0.05 sec, a horizontal error (ERH) lower or equal to 0.3 km, and a depth error (ERZ) lower or equal to 0.5 km were included in dataset 5.

Table 4.1 Statistics of dataset 5 used in the cross sections analysis.

N	MRMS	MERH	MERZ	ARMS	AERH	AERZ
2,746	.05	.3	.5	.03±.01	.14±.06	.24±.10

N is the number of events.

MRMS, MERH and MERZ are the maximum value of rms in the arrival time (s), horizontal and vertical locations (km) respectively, imposed for each event.

ARMS, AERH and AERZ are the average values of the rms in the arrival time (s), horizontal and vertical locations (km) respectively for the N events.

A total of 2,746 events were thereby selected. These events are marked with a cross in Appendix C.1. The average values obtained gave  $0.03 \text{ sec} \pm 0.01$  (1 S.D.) for RMS of time residual,  $0.14 \pm 0.06 \text{ km}$  for ERH and  $0.24 \pm 0.10 \text{ km}$  for ERZ. These are random errors and any systematic error as for example that due to the velocity model, are not considered. The results are summarized in Table 4.1. From these

## Chapter 4

values it is possible to say that the geometrical structure of the clusters can be resolved on a length scale of about 0.5 km. This refers to the precision of the relative hypocentre location of the events and it is an important factor to be considered when trying to discriminate between clusters localized in a small region. This precision is better than that obtained by King et al. (1985) or Eaton et al. (1970), and is comparable to that acquired by Reasenber & Ellsworth (1982) in similar studies. This comparison refers only to the precision in the hypocentre locations, and not with other aspects of the work done by these authors. For example, the dataset collected by Eaton et al., (1970) is among the best studied in seismology because of the unusually large number of continuous observations of the foreshock, mainshock and aftershock sequence of the Parkfield earthquake of 1966, including strong motion records and the deployment of a geodetic network across the fault trace (Bouchon, 1979). In order to study the aftershock sequence in the present work, some procedures adopted by these authors will be followed. Dataset 3 containing all the useful data of the region under study will be used when the completeness of data is important. Dataset 4 contains events which gave reliable epicentre locations (maximum horizontal error of 1 kilometre) but not reliable hypocentres (no restriction on vertical error), so it gives a good overview of the distribution of the epicentres. Dataset 5, although less complete than dataset 3 and 4, comprises events with more reliable epicentre and depth locations - vertical and horizontal errors for these events do not exceed 0.5 km - and they will be used for the study of the depth distribution of the events and to study their clustering characteristics.

Figure 4.6 shows the seismicity map obtained using dataset 5. Comparison with the epicentral map of figure 4.1 shows that the trend of epicentres is better defined in dataset 5. The line AA' represents the average N37°E strike of the Samambaia fault. The vertical cross sections along and perpendicular to the line AA' are shown in figures 4.7a and 4.7b respectively. Although defined by fewer events, off-fault seismicity around Poço Branco and J.Câmara is still significant for this dataset, and the same applies to the other off-fault seismicity that defines the fault bends and secondary faults, which were discussed in the last section.

To facilitate the analysis, the seismicity along the main fault was divided into four sections which are shown by the boxes drawn in figure 4.6. In this division, part of the low seismicity area discussed in sections 4.1 and 4.3 was incorporated in box S because clear secondary faults appear in it. It seems preferable to characterize the south region S as the region where secondary faults occur in contrast to the other segments of the Samambaia fault. A detailed epicentral map and the

projection of hypocentres in boxes N and S onto a vertical plane along the line AA' are shown in figures 4.8 and 4.9 respectively.

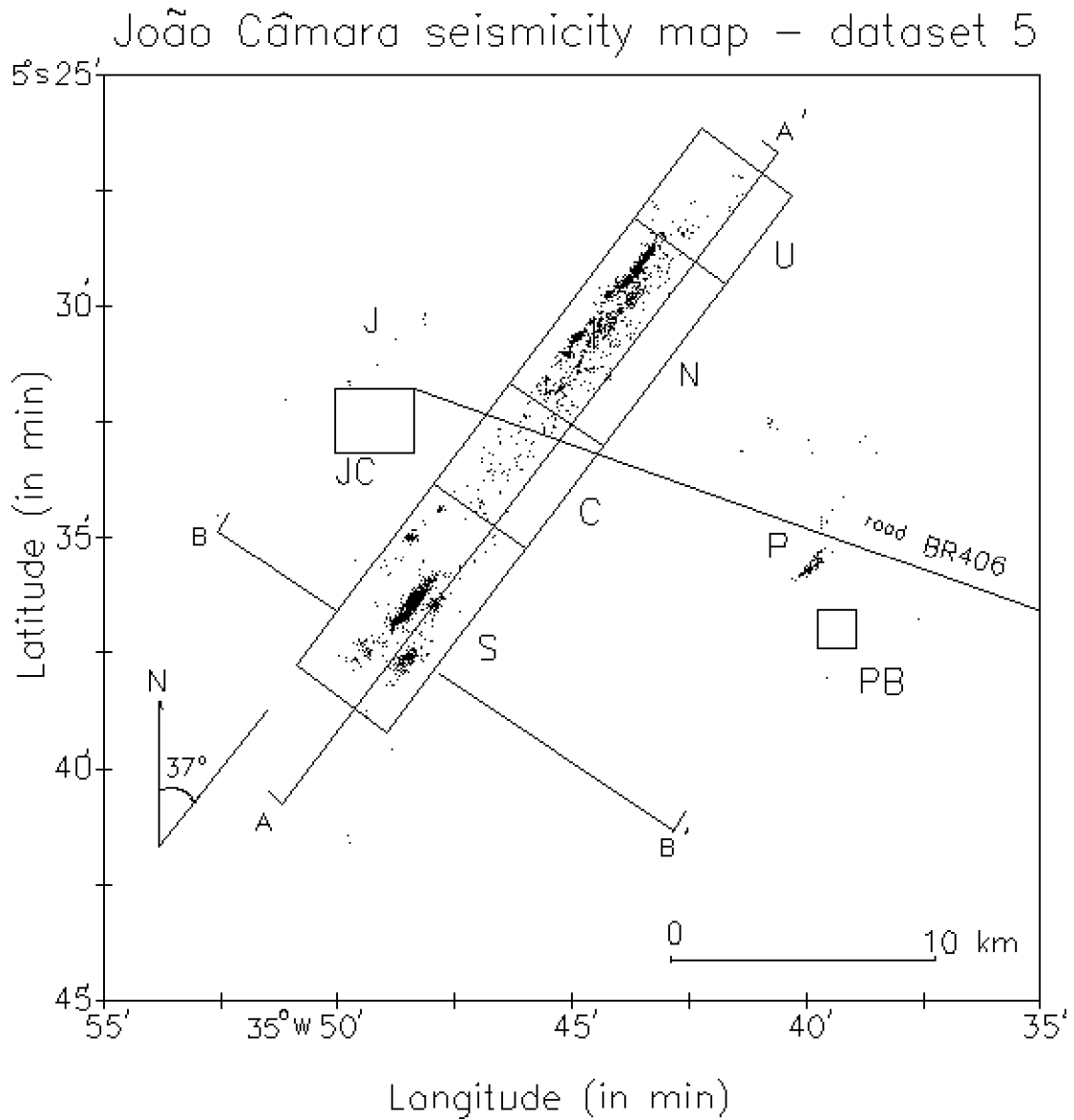
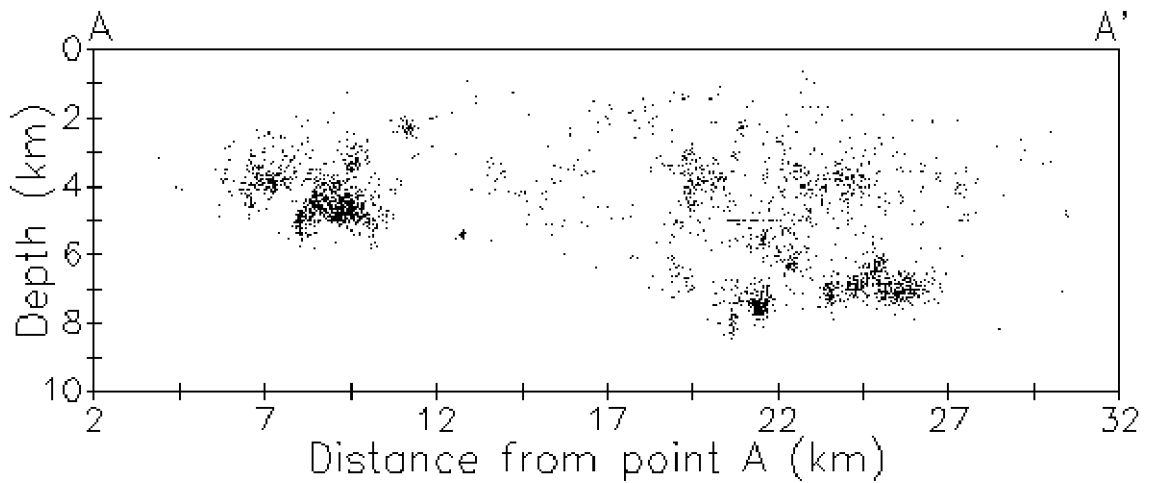


Figure 4.6 Epicentres of 2,746 well located aftershocks (dataset 5) with at least eight phase readings and recorded by the telemetric network. Maximum horizontal error (ERH) is 0.3 km and maximum depth error (ERZ) is 0.5 km. The line AA' represents the N37°E strike of Samambaia fault and line BB' is the line perpendicular to AA'. Unless otherwise stated, these two lines will be the reference lines for the forthcoming vertical cross sections. The Samambaia fault was divided into four sections to facilitates the analysis.

# Cross sections using the best located events

## (a) Longitudinal cross section



## (b) Perpendicular cross section

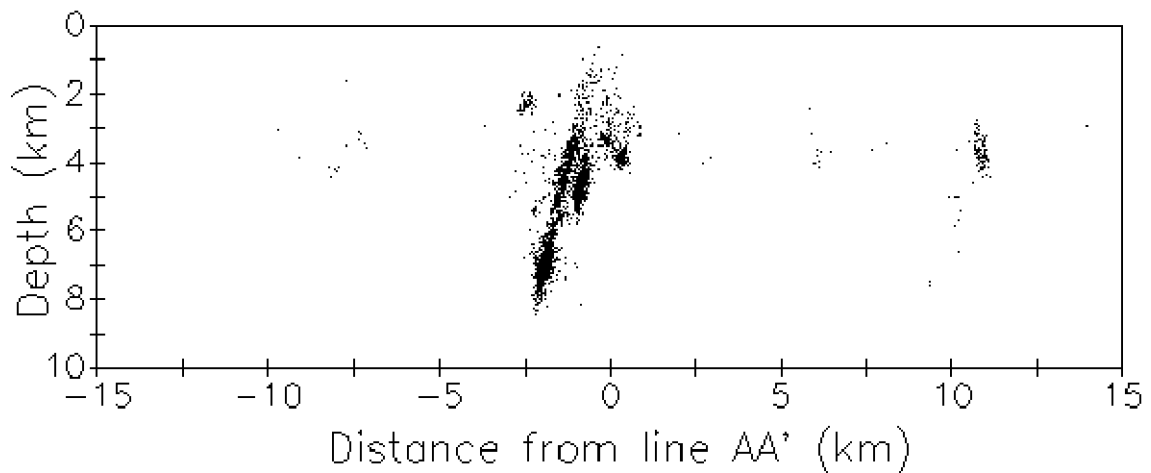


Figure 4.7 (a) Projection of all hypocentres found in dataset 5 on the vertical cross section AA' along the Samambaia fault.(b) Vertical cross section perpendicular to the line AA'. Projections are viewed from A.

Some aftershocks in figure 4.8(b) showing a common depth of 5 km are the result of the initial assignment of 5 km depth made in the location program HYPO71 (Lee & Lahr, 1975). At first sight, this alignment could be interpreted as being caused by events whose depth cannot be precisely determined. A close look at the corresponding epicentral map of figure 4.8a or in of figure 4.3 reveals another alignment of events at longitude 35°44.53'W. This kind of artifact only occurs for some events close to the stations JCAZ or JCLR which are located along the trend of epicentres (see figure 2.10). It is likely that all these aligned events are well located

## Chapter 4

events still having horizontal or vertical error less than 0.5 km but in which the final coordinates and/or depths are heavily constrained by the initial trial assignments of HYPO71. For example, the longitude of station JCLR is  $35^{\circ} 44.43'W$  and according to Lee & Lahr (1975) the location of the nearest station with the addition of 0.1 minutes to both latitude and longitude is used as the initial trial-hypocentre by HYPO71. This explains the alignment of epicentres at longitude  $35^{\circ}44.53'W$  in figure 4.8(a) or in figure 4.3. The trial depth was fixed in 5 km which explains the alignment at this depth in figure 4.8(b). A location test using those aligned events in which the trial hypocentre was forced to another location showed that the alignment of events was removed and that the location of those events became slightly different but no more than 0.5 km from the location given in figure 4.8(a) or figure 4.3.

Projections of hypocentres along the Samambaia fault onto vertical planes perpendicular to the line AA' were divided into four sections and are shown in figure 4.10. These sections correspond to those defined and delineated in figure 4.6. The hypocentres of aftershocks in the north segment (section N) are concentrated in a narrow zone that defines a single fault plane which is dipping  $76^{\circ}$  NW. This cross section perpendicular to the fault, which comprises 1,343 aftershocks, is remarkably simple and linear. These aftershocks are almost all distributed in a zone no more than 500 metres thick (see section N in figure 4.10), which supports the previous assessment of the precision in the location of the events in dataset 5 that is summarised in Table 4.1. The good resolution in the hypocentre determinations outlines at least one small off-fault cluster at a depth of 2 km that possibly belongs to the third direction of faulting marked as line 4 in figure 4.3. Although the cross section perpendicular to the strike reveals a simple plane for the north segment (section N), the cross section along the fault (figure 4.8b) of the same section shows that epicentres are not regularly distributed. They tend to form several clusters which are an indication of small geometric irregularities in the fault plane.

The small number of aftershocks in the region of low seismicity (section C) nevertheless seems sufficient to show that the segment is a continuation of the north segment. At least, in geometrical terms, both planes share the same strike and the same dip. The small number of aftershocks in section C could be interpreted as being caused by an incompletely broken barrier after the main shock rupture. The maximum magnitude observed in the aftershocks of section C, extracted from dataset 5, was a shock of  $m_D = 2.5$ . These characteristics of low seismicity and low magnitude in this section were also observed before and after the main shock by other authors (e.g. Ferreira et al., 1987; Takeya et al., 1989; Sophia & Assumpção, 1989).

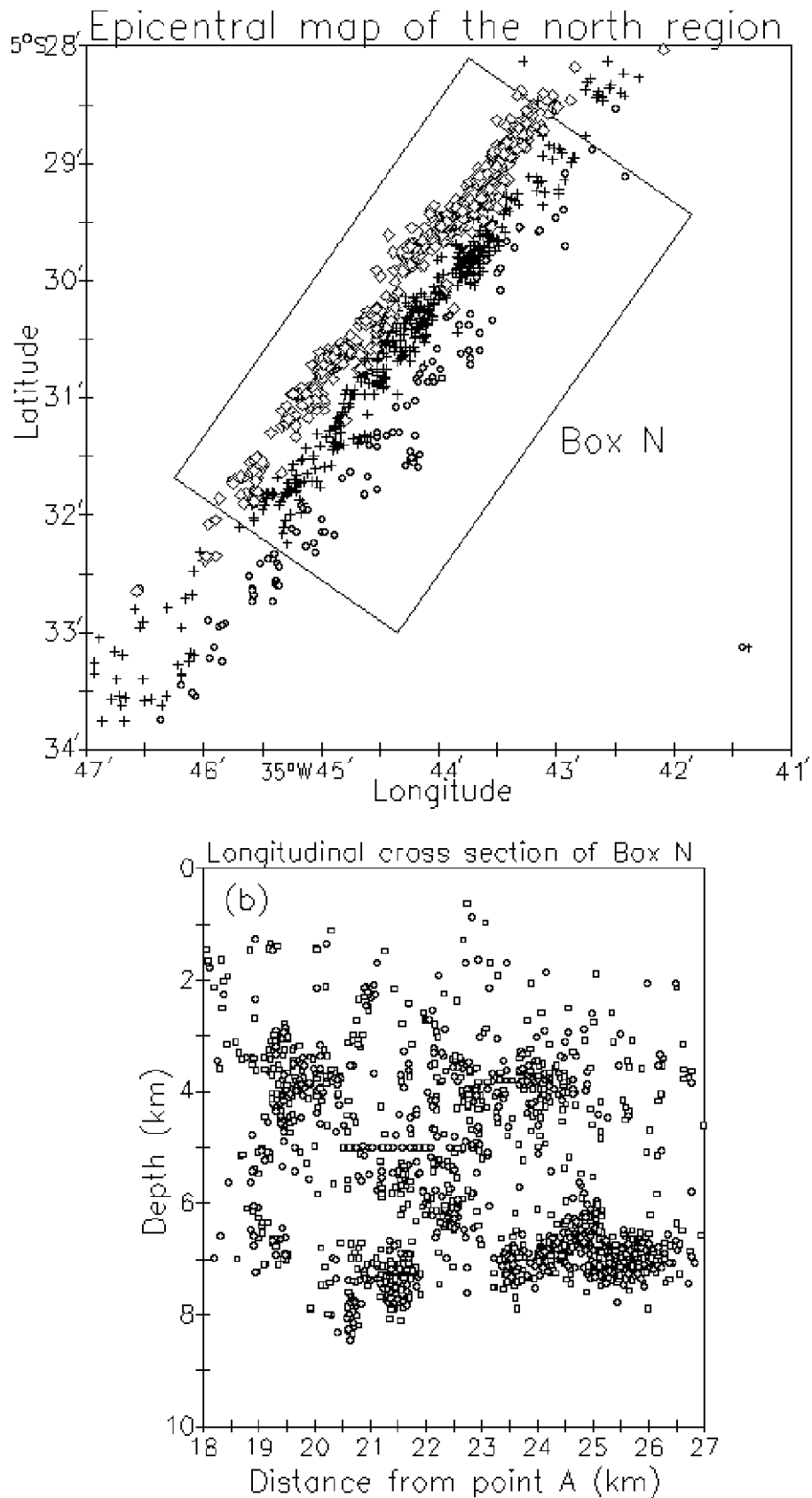


Figure 4.8 (a) Detailed epicentral locations of events in the north segment of the Samambaia fault. Circles, crosses and diamonds represents earthquakes with depth in the range 0 to 3 km, 3 to 6 km and 6 to 9 km respectively. (b) Vertical cross section of events along the fault strike of figure 4.6 and figure 4.8(a) in the box N. The linear artifacts at the depth of 5km are explained in the section 4.4.

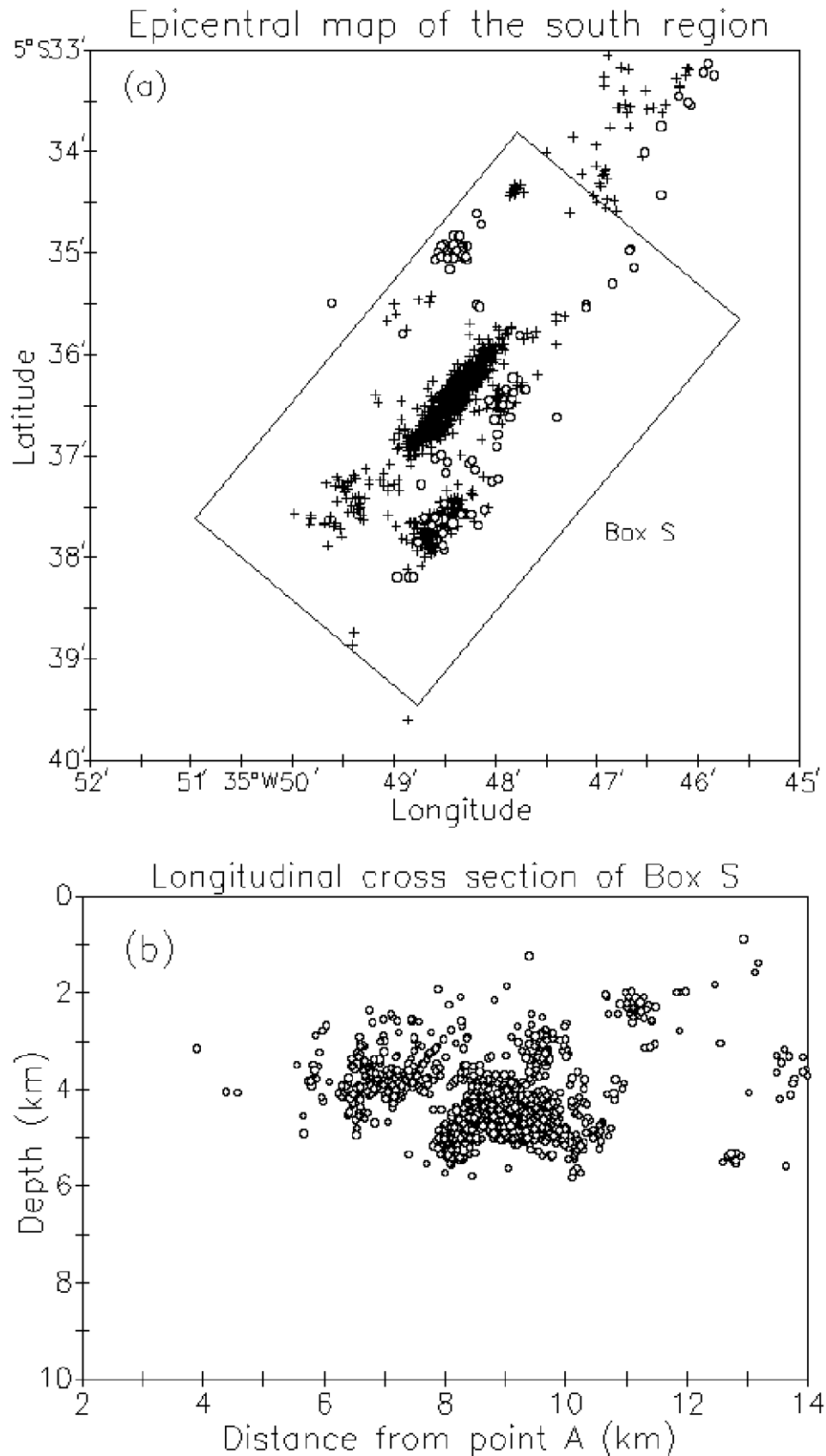


Figure 4.9 (a) Detailed epicentral locations of events in the south segment of the Samambaia fault. Symbols have the same meaning as in figure 4.8 (b) Vertical cross section of events along the fault strike of figure 4.6 and figure 4.9(a) in the box S.



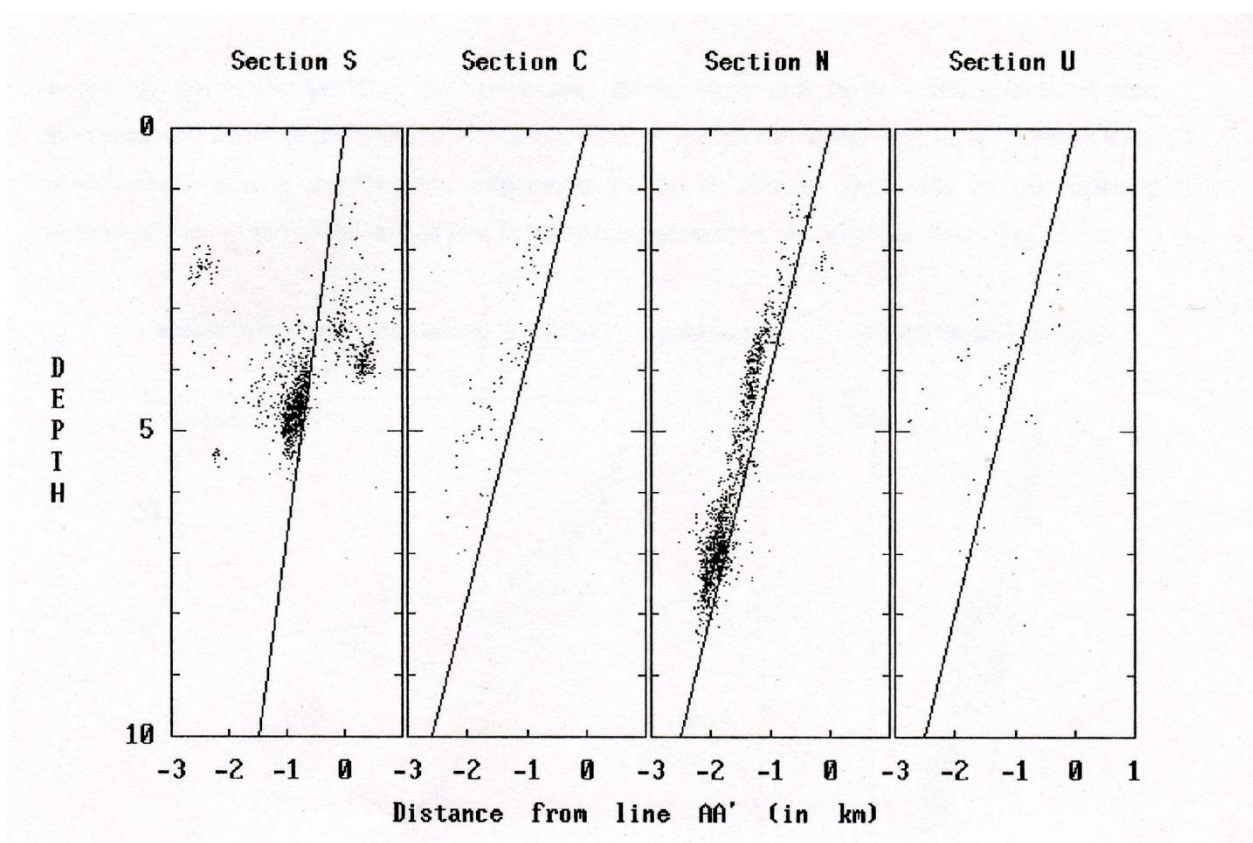


Figure 4.10 Cross section projections of hypocentres of events in the boxes indicated in figure 4.6 onto planes perpendicular to the line AA'. The view is from point A and depths are in kilometres. The dip of the fault plane in section S (south segment), indicated as a solid line is more nearly vertical than the dip of the other sections.

#### 4.5 Geometric irregularities in the south part of the fault

It is clear from figures 4.9 and 4.10 that the south segment (section S) of the Samambaia fault is more complicated than the other segments. The main cluster in this segment defines a fault plane with approximately the same strike but more nearly vertical than the north segment. This plane dips  $81^\circ$  to the northwest. The  $5^\circ$  difference in the dip of the seismicity planes between the low seismicity (section C) and the south (section S) segments characterizes a fault offset and constitutes evidence for the existence of a geometrical barrier in the region between the two segments. Other clusters that are aligned in a different plane to the main cluster in section S can be identified in figure 4.10. This confirms that the seismicity in this section is generated by a series of secondary faults.

A quick analysis of the fault offset characterized by the  $5^\circ$  difference in the dip between the south (section S) and low seismicity (section C) segments show that a barrier of the type known as a fragmentation barrier (King, 1986) or an antidilational jog (Sibson, 1986), is found between these two segments. This is

probably an antidilational jog because, given that the fault mechanism of the Samambaia fault is predominantly right lateral strike slip (Ferreira et al., 1987), this mechanism acting on the two segments tends to reduce the area of the linking region which, according to Sibson (1986) characterizes an antidilational jog.

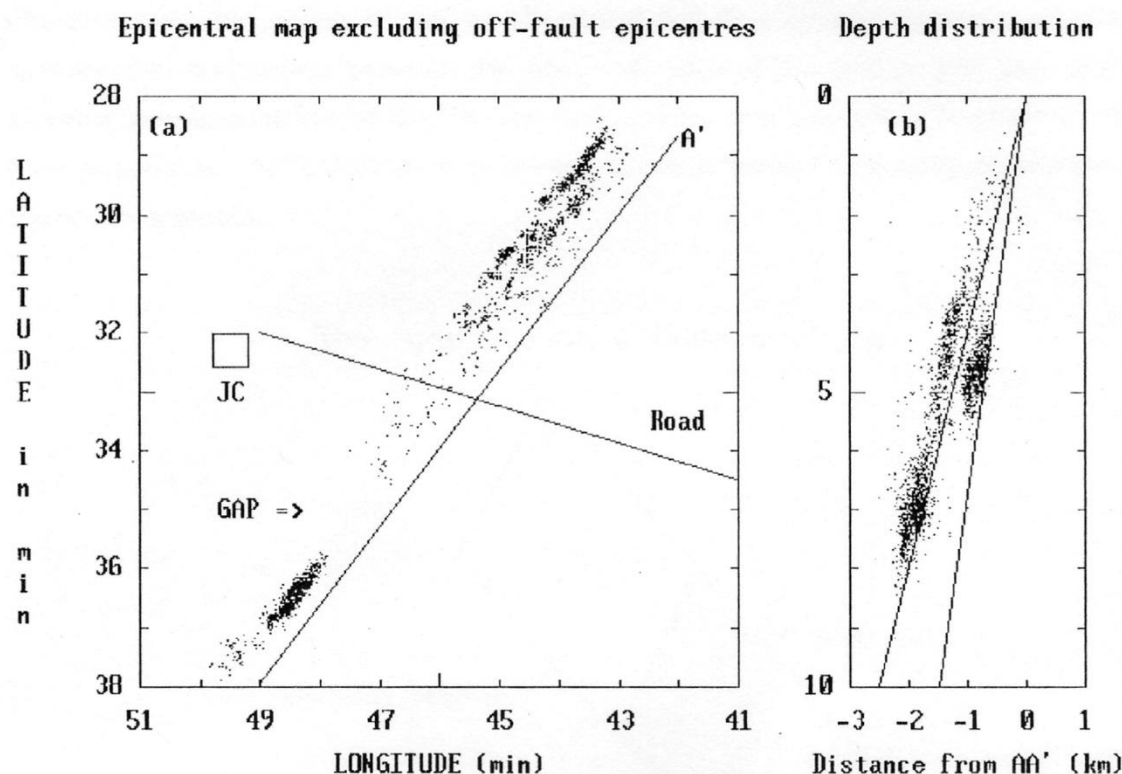


Figure 4.11(a) Epicentres of the main fault only. All supposed off-fault aftershocks were excluded from this view. Only part of the line AA' which represents the strike of the fault plane is shown. (b) Projections of the same aftershock hypocentres onto a vertical plane perpendicular to the line AA'.

It is interesting to note in figure 4.9(a) the small area limited by the longitudes 35°W47.2' and 35°W48.2' and latitudes 5°S35.5' and 5°S37.0'. In this particular area, practically no aftershocks are found and this is the region where the antedilational jog is supposed to be located. When all the aftershocks off the main fault plane are excluded from the epicentral map, the resulting map in figure 4.11(a) shows a distinct gap in the south segment. In the barrier model of Das & Aki (1977), this gap would be interpreted as the region which slipped due to the main shock rupture. This is because if the barrier is completely broken, no slip deficit will be left by the rupture, and as a consequence no aftershocks would occur in the slipped region. This location for the main shock agrees with the location suggested in section 4.3 which was based on the role of fault bends. The vertical cross section perpendicular to the fault strike corresponding to the events shown in figure 4.11(a)

is plotted in figure 4.11(b). This shows more clearly the  $5^\circ$  offset due to the different dip between the south segment and the rest of the main fault. Thus, an antidualational fault jog must be located somewhere in the gap.

In the sketch of figure 4.12 the gap is represented basically as a transition between the low seismicity and the south fault planes. The  $5^\circ$  difference in the dip characterizes this plane as an antidualational jog due to the tendency of areal reduction in the region between the tips. This idea of the gap is just one of the possible representations of the linking region. However, any other hypothesis will have to consider the  $5^\circ$  difference in the dip between the low seismicity segment and the south segment.

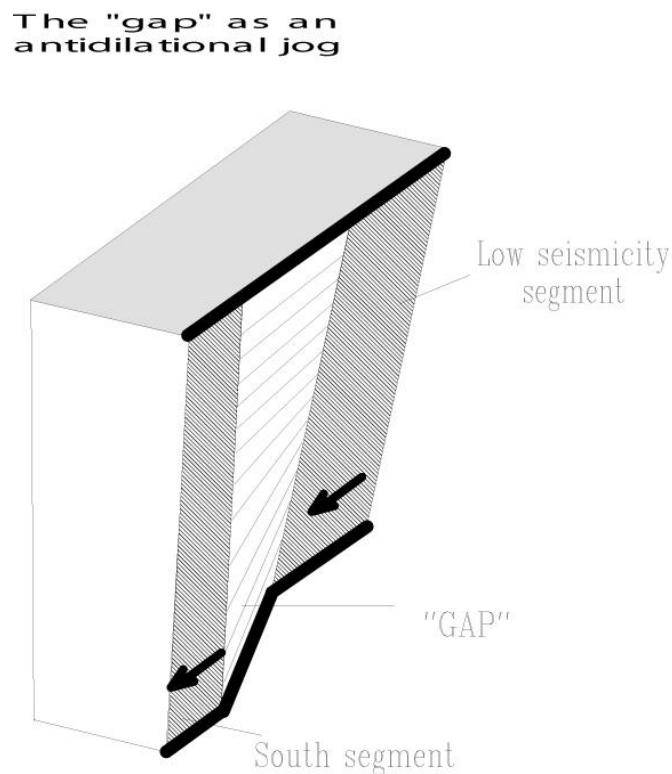


Figure 4.12 Sketch showing the interpretation of the gap as a plane that links the fault tips of the low seismicity and the south segments, inferred from the epicentral map of figure 4.11(a) and (b). This plane forms an antidualational jog and is claimed to be the site of the main shock of  $m_b = 5.1$ .

### 4.5.1 Reanalysis of the drum-recorder data

Due to the limited period of observation by the telemetric network, it is important to check if data recorded in other time periods can substantially modify the analysis made here on the south segment of the Samambaia fault. Examination of the drum recorder data is only of limited value because not all the data were

analysed. Since a maximum of only four stations was used in the drum recorder network, epicentre determinations were obtained that must be considered substandard when compared with the precision of the epicentres calculated by the telemetric network. However, it is believed that the most important periods of reactivation were investigated. To minimize possible bias, epicentres from drum recorder data were recalculated using the velocity model of Table 3.3 used in the present study. Only epicentres calculated with at least six readings, a horizontal error lower than 0.5 km and a vertical error less than 1 km were used.

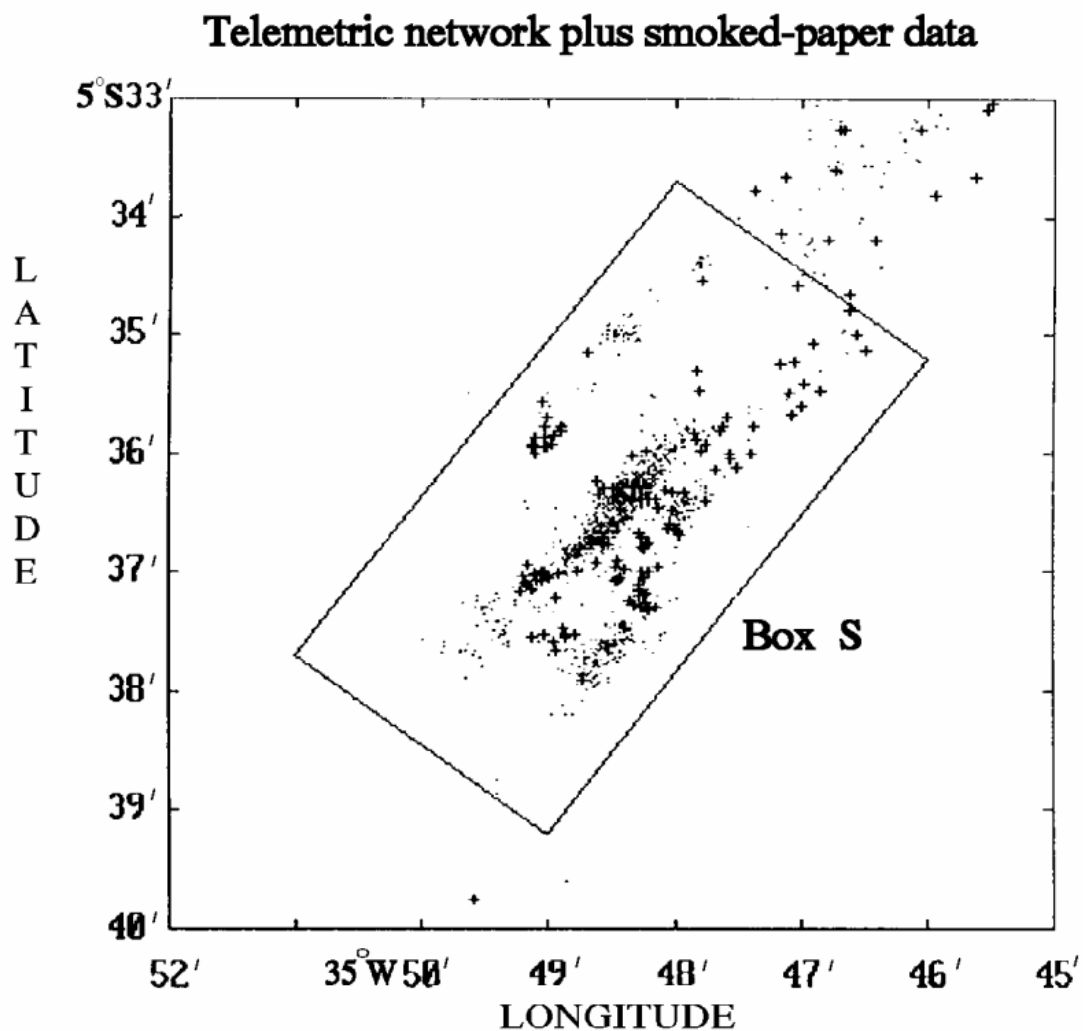


Figure 4.13 Dots represent epicentres determined using the telemetric network data. Crosses represent epicentres from the smoked paper drum recorder network recorded during Jan/Feb 87.

## Chapter 4

An important period of activity started in the south segment before the telemetric network was installed. The period between 7th Jan and 24th Jan 1987 was analysed by Takeya et al, (1989) and the period between 25th Jan and 7th Feb 1987 was analysed by Sophia & Assumpção (1989). The best located events from the smoked paper records of that period are plotted in figure 4.13 and are indicated by crosses to distinguish them from the events recorded by the telemetric network, which are indicated by dots.

In comparing the relative positions of epicentres from the smoked paper data in figure 4.13, it seems possible to explain the seismicity of Jan-Feb 1987 as having taken place in fault planes parallel to the main segment of the south region which was determined by the telemetric network data. These possible fault planes are shown in the sketch of figure 4.14 and marked by the codes D1 and D2. The main segment in this region, inferred from the telemetric network, is marked as M in the same figure.

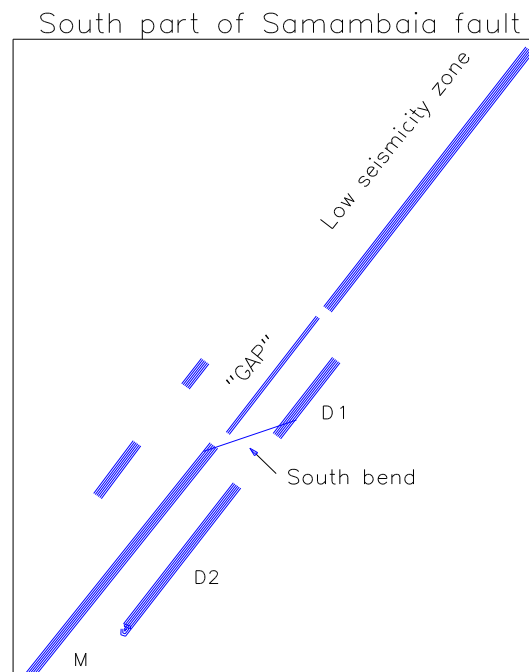


Figure 4.14 Sketch showing the interpretation of the south segment of the Samambaia fault with consideration given to the epicentres from the smoked paper drum recorder data. Segments D1 and D2 were inferred from the drum recorder network, segment M and other segments were inferred from the telemetric network data. The thick dashed line represents an hypothetical fault plane in the gap and the thin line represents the south bend.

### 4.5.2 Discussion

The addition of the fault planes D1 and D2 does not substantially modify the previous ideas about the gap as being the probable locus of the  $m_b=5.1$  earthquake. In supposing that the epicentre of this shock occurred on the fault plane marked by the thick dashed line in figure 4.14, the south bend and the fault plane marked as D1 in the same figure can be interpreted as the result of secondary fracturing which occurred in the vicinity of the linking region of an antidualational jog. As can be seen in figure 4.2b for left stepping cracks, according to Segall & Pollard (1980) there is a tendency for those shear fractures to form ahead of, and parallel to, the segments. In the same way, this model can also provide a possible explanation for the small fault which appears on the opposite side of the gap (see figures 4.4 and 4.14) as secondary fracturing.

In another interpretation, the plane D1 is taken to be the locus of the main shock, in which case D1 must form a dilational jog with the south segment and an antidualational jog with the low seismicity fault segment. This hypothesis justifies the alignment of epicentres that characterizes the south bend (as seen in figure 4.4) as the linking region between the ends of segments D1 and M. The south bend is represented in figure 4.14 by the thin line that links the tips of faults M and D1. The fault segment D2 must be sufficient to account for the additional seismicity to the south which is inferred from the smoked paper data.

### 4.6 Geometric irregularities in the north part of the fault

A small number of events are found in the section U of figure 4.10. This section follows the north segment (section N) and represents the north end of the Samambaia fault (see figure 4.6). The solid line in section U of figure 4.10 represents the projection of the north segment. It can be seen that some events of section U are placed close to that solid line, that is, in the continuation of section N. However, there is one cluster of events to the left and another one to the right side of the solid line. The cluster on the left of the line corresponds to the events in the third direction of faulting, indicated by the line 3 in figure 4.3 at the junction of the latitude  $28.5^\circ$  with the direction of the trend of seismicity. Events to the right of the line characterize the north bend, indicated by line 4 in the same figure.

Those features found in the north part of the fault are not artifacts produced by the limited period of observations or by a model-dependent error. Indeed, the same characteristics are present in the epicentral map of figure 2.10, made with data from smoked-paper records for January 1987 which were analysed by Sophia & Assumpção (1989) using a half space model. In particular, the third direction of

## Chapter 4

faulting shown in figure 4.3 is a small but very well defined feature. Supporting evidence for it can be found in previous work in that area which used data from smoked-paper records (Ferreira et al., 1987 and Takeya & al., 1989). At that time the authors were unable to recognize it, possibly because the precision of the drum recorder data was not sufficient for this purpose.

According to King & Nabelek (1985), the features cited in the last paragraph would be an indication of some heterogeneity at the north end of the north fault segment. However, the most convincing evidence for fault heterogeneity in that region comes from the occurrence of the second major event ( $m_b = 5.0$ ) that is believed to have occurred in section U, no more than 3 km north of the north bend. That is, the description of the seismicity around the north-bend based on data from the telemetric network is not complete. It does not account for the additional complexities in the process that generated the  $m_b$  5.0 event of 10th of March 1989 and its foreshocks and aftershocks, revealed by the analysis of Costa et al. (1989) and summarized in section 2.1.2 Costa et al. (1989), located the epicentre of the  $m_b = 5.0$  earthquake about two kilometres to the north of the north-bend, although the error in the location is large ( $\pm 3$ km). This means that after the main shock rupture that happened on 30th Nov 1987, a slip deficit occurred in the section U after the passage of the main shock rupture, which later initiated the  $m_b = 5.0$  shock on 10th Mar 1989.

Due to the limited period of observation, insufficient data were collected by the telemetric network to delineate the geometry of the fault further north of the north fault segment, that is, in section U defined in figure 4.6. As described in sections 2.1.1 and 2.1.2, most of the seismic activity in this region (section U) was recorded by the four station drum recorder network which was installed on 20th July 1988 (see Table 2.1). A few events in the same region were recorded by previous drum recorder networks. So, any interpretation about the structure of the north edge of the north-segment is only possible if data from the drum recorder network are used. To perform this analysis, the main dataset was that one used in the plot of the epicentral map of figure 2.5 which is a composite of the epicentres found by Sophia & Assumpção (1989), Takeya et al., (1989), Oliveira et al., (1989) and some unpublished locations of events recorded during Dec 1990 (Oliveira, personal communication, 1990). Each author used a slightly different velocity model and the data cover the period between Jan-Feb 1987, Aug-Feb 1989 and Dec 1990. In order to carry out a more precise analysis, those events were relocated using the two layer model used in the calculation of the epicentres of the telemetric network data (see Table 3.3).

### 4.6.1 Reanalysis of the drum-recorder data

A maximum of four drum recorder stations were available at any time, except for a ten-day period from 11th March to 21st March 1989, when the existing drum recorder network was increased to ten stations (see Table 2.1) after the occurrence of the  $m_b = 5.0$  shock on 10th March 1989. More than 300 events were recorded by the ten-station drum recorder network but only thirty events from this period were analysed by Costa et al. (1989). These events were relocated and included in the present study. In addition and as part of this work, phase readings have been made for selected events which have not been analysed before and which occurred during the above ten-day period, in order to improve the reliability of the analysis. So, for the period between 11st to 21st Mar 1989, a total of 195 new aftershocks were analysed. From these, 149 events were selected for the present study and they are listed in Appendix C.2.

A total of 2,359 events from drum recorder smoked paper data covering different periods of time were analysed using the location program HYPO71 (Lee & Lahr, 1975) and the two layer velocity model of Table 3.3. A selection of events were used in order to analyse the seismicity pattern of the north end of the Samambaia fault. Only events to the north of latitude  $5^{\circ}31'S$  with horizontal and vertical errors in location of less than  $\pm 1\text{km}$  and  $\pm 2\text{km}$  respectively, were considered. This process resulted in the selection of 708 events. Exceptions to the selection criteria were the  $m_b = 5.0$  event and two other shocks. The first of these two is a  $m_b = 4.0$  earthquake on 3rd Feb 1987 and the second is a  $m_b = 3.9$  event on 7th Feb 1987. The horizontal and vertical errors in the location of these two shocks were calculated as  $\pm 3\text{km}$  and  $\pm 5\text{km}$  respectively (Takeya et al., 1989). Although having a large error in location, these three events were relocated and included in the selection because few events above magnitude 3.5 were registered by the drum recorder network, and also because it is important to know the location of major shocks relative to the overall seismicity.

### 4.6.2 Relocation of the $m_b = 5.0$ earthquake

As discussed in section 2.1.2, it was difficult to locate the  $m_b = 5.0$  shock of 10th Mar 89. From the four seismograms that recorded it, only two show a clear P wave onset. In the seismograms of the two other stations, the P wave arrival and following phases of the  $m_b = 5.0$  event were overwritten by several aftershocks of that event. However, a close look at these two overwritten records shows that the upper part of the saturated record of the  $m_b = 5.0$  shock can be distinguished from the records originating from other events. From this, it was possible to reconstitute the



## Chapter 4

P wave first motion of the  $m_b = 5.0$  shock from these two seismograms by extending the first peak, which is visible, back to the origin. Assuming an uncertainty of  $\pm 0.2$  sec in the inferred arrival time, a series of calculations, in which the arrival time at these two stations was varied in steps of 0.02 sec up to 0.2 sec, were performed to determine the epicentre. The best estimated location of the  $m_b = 5.0$  event resulting from this process is indicated in Table 4.2.

Table 4.2 Relocation of the  $m_b = 5.0$  earthquake of 10th March 1989.

Date	Time (u.t.)	Lat.	Long.	Depth (km)	ERH (km)	ERZ (km)
870310	04:11:19	5°26.50'S	35°39.78'W	13.4	4	6

u.t. is Universal Time.

ERH is the horizontal error in the epicentre.

ERZ is the vertical error in the depth.

Although the horizontal and vertical standard errors in the determination of the hypocentre of the  $m_b = 5.0$  of 10th Mar 89 earthquake given in Table 4.2 are large, the epicentre determined coincides with the area of maximum intensity experienced during the occurrence of this event (Costa et al., 1989). Thus since the calculated epicentre is consistent with the damage distribution it is concluded that it is approximately correct.

### 4.6.3 The structure of the north end

After an examination of the epicentral map (figure 4.15) of the 708 selected events from the drum recorder data and the corresponding vertical cross sections along (figure 4.17) and perpendicular to (figure 4.16) to the average strike, it is concluded that the northward continuation of the north fault segment does not lie in the same fault plane. It comprises three discrete segments arranged *en echelon* as shown in the inset of figure 4.15. Segment number 1 represents the north fault segment and segments 2 and 3 represent its extension to the north, that is, the fault planes in section U as defined in figure 4.6.

If the right lateral strike slip fault (see table 2.2) is taken to be the basic fault mechanism for these three fault segments, the north segment (segment 1 in figure 4.15) and segment 2 form a right step or dilational fault jog, and segments 2 and 3 form a left step or antidilational jog.

## Epicentres from drum recorders data

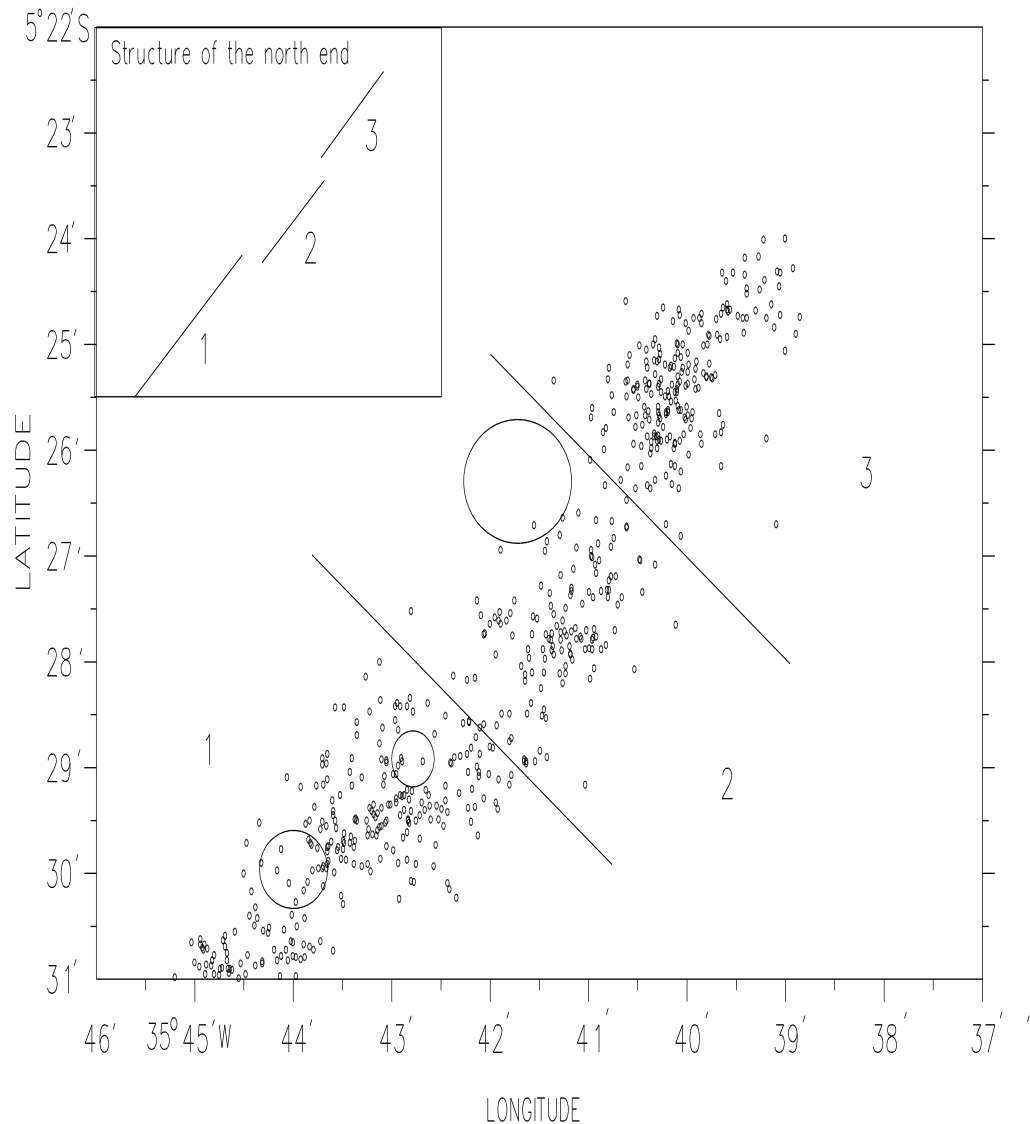


Figure 4.15 Epicentres of the well-located aftershocks from the smoke-paper record data as shown in figure 2.5 plus additional readings made in this study which occurred at the end of the north segment of the Samambaia fault. Epicentres were relocated using the two-layer model of Table 3.3. The large open circle indicates the location of the  $m_b = 5.0$  event. The two other open circles indicate the two aftershocks with magnitude 4.0 and 3.9 respectively, recorded in Feb 1987 (Takeya et al, 1989). The figure inset shows the interpretation of the numbered segments at the tip of the north part of the Samambaia fault.

As can be seen in the projections of hypocentres of each segment onto the vertical plane perpendicular to the strike (figure 4.16), the dilational jog, composed of segments 1 and 2, is not well defined. The majority of events in segment 2 are

shallow and located above a depth of 5 km, which makes it difficult to determine a reliable dip for this fault plane. If it is assumed that the fault plane of segment 2 dips at the same angle as the fault plane of segment 1 (north segment), a fault offset of about 500m can be seen by comparing the two projections. This small offset can be seen in the epicentral map of figure 4.15 and in figure 2.10. Support for the existence of such a dilational jog is given by the third direction of faulting shown by the epicentres in the direction of the dashed line 3 in figure 4.3 that lies close to the junction of the two *en echelon* segments 1 and 2. According to King & Yielding (1984), the third direction of faulting results from the conservation of the slip vector across fault bends. Other evidence comes from the detection of epicentres whose alignment characterizes a bend in the north fault segment. This bend is identified by the dashed line 2 in figure 4.3. The same bend can be seen in the epicentral map

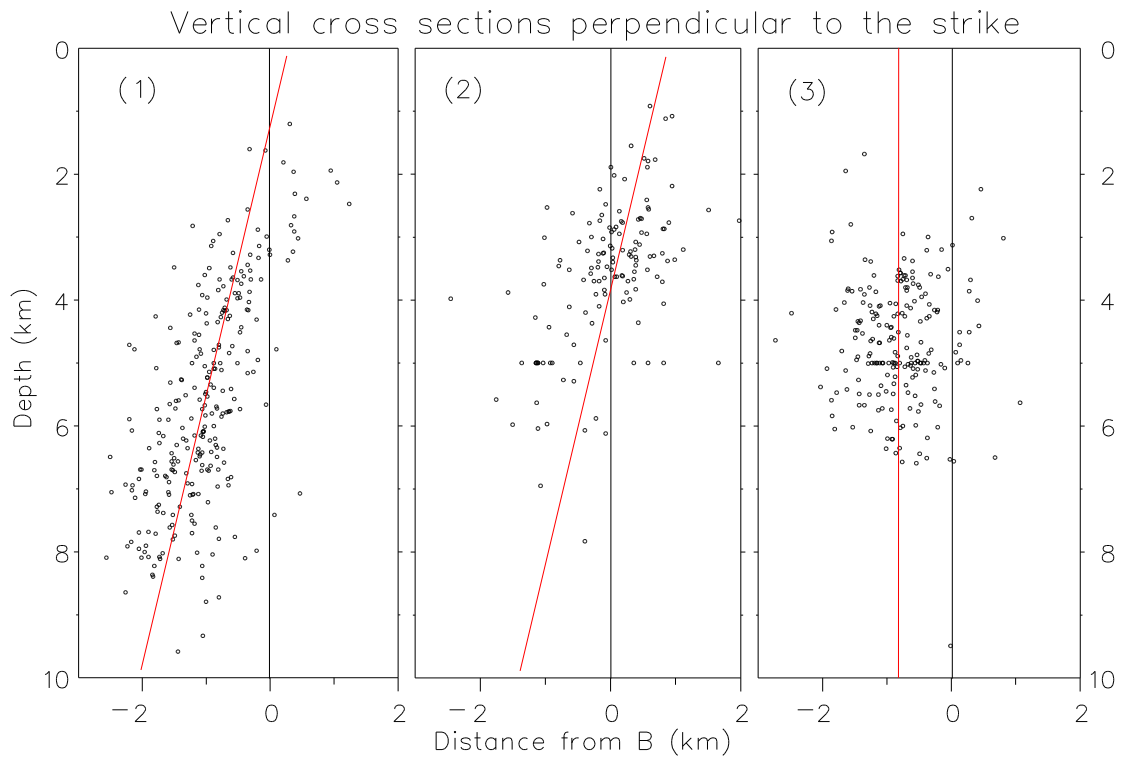


Figure 4.16 Projection of hypocentres onto vertical planes perpendicular to the average fault strike. (1), (2) and (3) are the projections of events in sections 1,2 and 3 respectively, as defined in figure 4.15. Vertical lines were drawn at the point 0 km as a reference line to check fault offset. Diagonal lines indicate the fault dip for each section.

of events which occurred in January 1987, in figure 2.10. This bend was noted by Sophia (1990) but in performing a statistical analysis, she concluded that the data used were not precise enough to discriminate a different fault plane in that region. The epicentres along the fault bend can be interpreted as having been caused by local stress generated by the mechanical interaction between the tips of the cracks 1 and 2 which form a dilational jog. That is, the bend must follow the line that links the two crack tips.

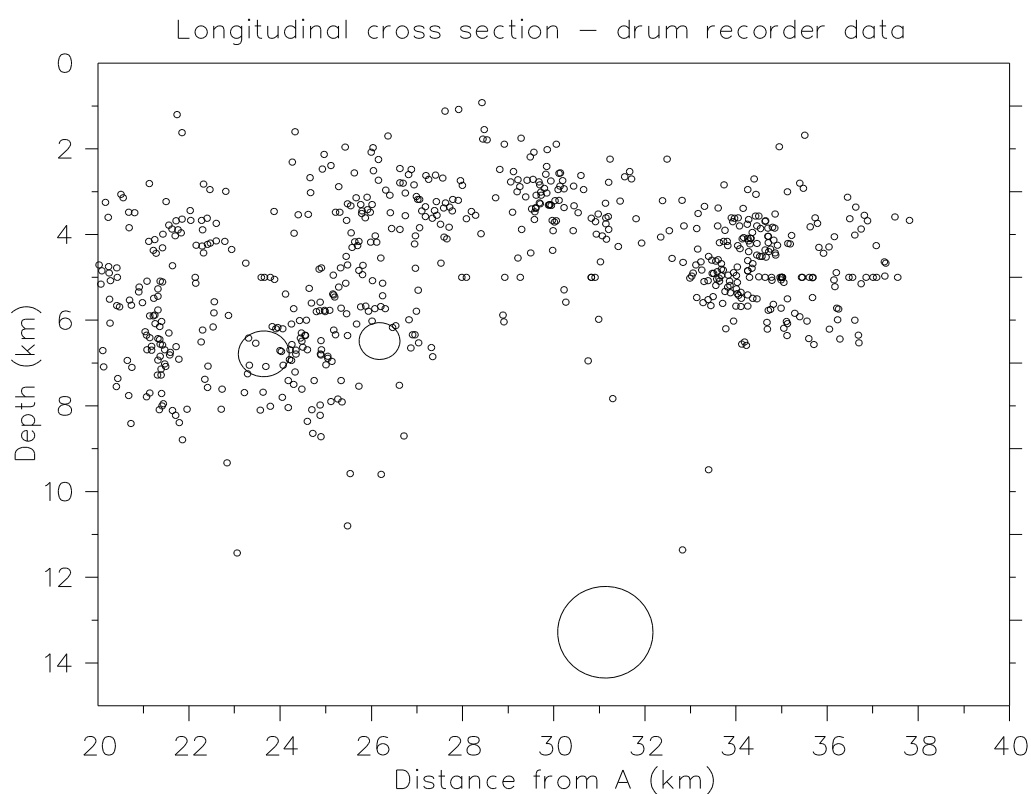


Figure 4.17 Projection of hypocentres onto the vertical plane along the average fault strike. The projection is referred to the events in figure 4.15 from the drum recorder data.

The fault offset between the segments 2 and 3 is better defined than the offset between segments 1 and 2, as can be seen in the sections of figure 4.16 or in the epicentral map of figure 4.15. These two segments form an antidilational jog or left stepping crack. According to the study of Segall & Pollard (1980), in that case secondary fracturing is more restricted and tends not to link the cracks. They suggest that left stepping cracks, for a right lateral strike-slip fault, can store strain

## Chapter 4

energy and may be sites of large earthquakes. It seems that those characteristics are present in the linking region because a relatively small number of events are found there. In addition, the earthquake of 10th Mar 1989 ( $m_b = 5.0$ ) was located close to the left step (see figure 4.15), which agrees with the hypothesis of Segall & Pollard (1980).

In the projection of hypocentres from the drum recorder data onto a vertical plane along the fault (figure 4.17), major events are represented by larger circles. The  $m_b = 3.9$  event is located at the edge of the north segment, close to the dilational jog, in a cluster of aftershocks. On the other hand, the  $m_b = 5.0$  event is found in a region of low seismicity and no other event is found around it. As can be seen in table 4.2, the errors in the location of this event are large. It has been said that the calculated epicentre is supported by the macroseismic data. However, no constraints were found for the depth of the hypocentre except that the depth of 13.4 km calculated from the drum recorder data seems excessive. In fact, it is possible to infer some limit on the depth of that shock by comparing the hypocentre locations of the events in the north segment (segment 1 in figure 4.15) calculated from the drum recorder network with those calculated from the telemetric network. It can be seen from figure 4.17 that some events from the smoked paper data are found at depths between 9km and 12km. In section 5.3 it will be shown that the depth of the seismogenic layer in the same region is limited to 9km, because no event deeper than that was found using data from the telemetric network, which are more precise than the drum recorder data. Thus, the depths greater than 9km calculated from the drum recorder data are probably too large, and therefore it is feasible that the depth of the  $m_b = 5.0$  event of 10th Mar 1989 given in Table 4.2 is also too large.

The record of seismicity shows that events in segment 2 are rare. For example, during all the recording period of the telemetric network, from June 1987 to Mar 1988, fewer than fifty events occurred in that region as can be seen in section U of figure 4.6. Activity in segment 3, started in August 1988, intensified during October 1988 with decreasing activity in the following months. During February and March, until the occurrence of the  $m_b = 5.0$  earthquake of 10th Mar 1989, activity in segment 3 was insignificant, indicating a period of quiescence in the vicinity of the following main shock of 10th March. This sequence is shown in figure 2.7. In terms of stress, it seems that the stress released by successive aftershocks in the segment 1 (north segment), left a slip deficit in the region of segments 2 and 3 (see figure 4.15) which was responsible for the occurrence of the  $m_b = 5.0$  earthquake.

### 4.7 Conclusions

Following the arguments made in the previous sections, it is concluded that the  $m_b = 5.1$  earthquake of 30th Nov 1987 and  $m_b = 5.0$  earthquake of 10th Mar 1989 occurred close to major geometric irregularities in the Samambaia fault. These irregularities were identified as the north and south bends.

Since it is assumed that the main shock released stress in the region of the gap (shown in figure 4.11a), no slip deficit is expected there to generate aftershocks. Assuming that the main event rupture propagated from the gap, it can be understood that the process of rupture left behind unbroken barriers responsible for the aftershock pattern of figure 4.11a. In fact, the north segment (section N in figure 4.6), and the south segment (section S) of the fault (near the road), were described in section 2.1.2 as being the locus of all foreshocks and the locus of all aftershocks with magnitude above 4.0. Thus the slip deficit in these regions must be accommodated by those aftershocks, the background seismicity and foreshocks.

Regarding the number of aftershocks, the low seismicity segment (section C of figure 4.6) can be interpreted as a transition between the gap, where no aftershocks were recorded, and the north segment (section N), where the aftershock activity was more intense and more persistent. For this reason, section C has been identified as the low seismicity segment, which is interpreted as being caused by a barrier incompletely broken by the main shock. In order to explain the difference in the seismic activity between this segment and the north segment, it may be that there is a geometric irregularity located at the interface between the two segments which could be a small dilational jog. This hypothetical jog would be sufficient to arrest but not to stop the main shock rupture to the north and could explain the difference in the seismicity between the two segments.

The pattern of aftershocks in the north segment as seen in figure 4.3 suggests that the main shock rupture stopped exactly at the north bend. This bend has been associated with a dilational jog. Sibson (1985) reports several strike-slip earthquake ruptures which stopped in the vicinity of dilational jogs which, according to him, appear to have acted as kinetic barriers opposing rupture propagation. Probably, a slip deficit or moment-release deficit occurred in section U of figure 4.6. This section U was supposed to be limited in the south by the dilational jog and by an antidilational jog at the north. This description of section U is questionable because it is based mainly on the data from drum recorders, and these have low resolution when compared with data from the telemetric network. In any case, the region must have been maintained at a higher mean stress than the main fault segment, since unlike the main fault segment, it generated a  $m_b = 5.0$  earthquake.

## João Câmara seismicity zone

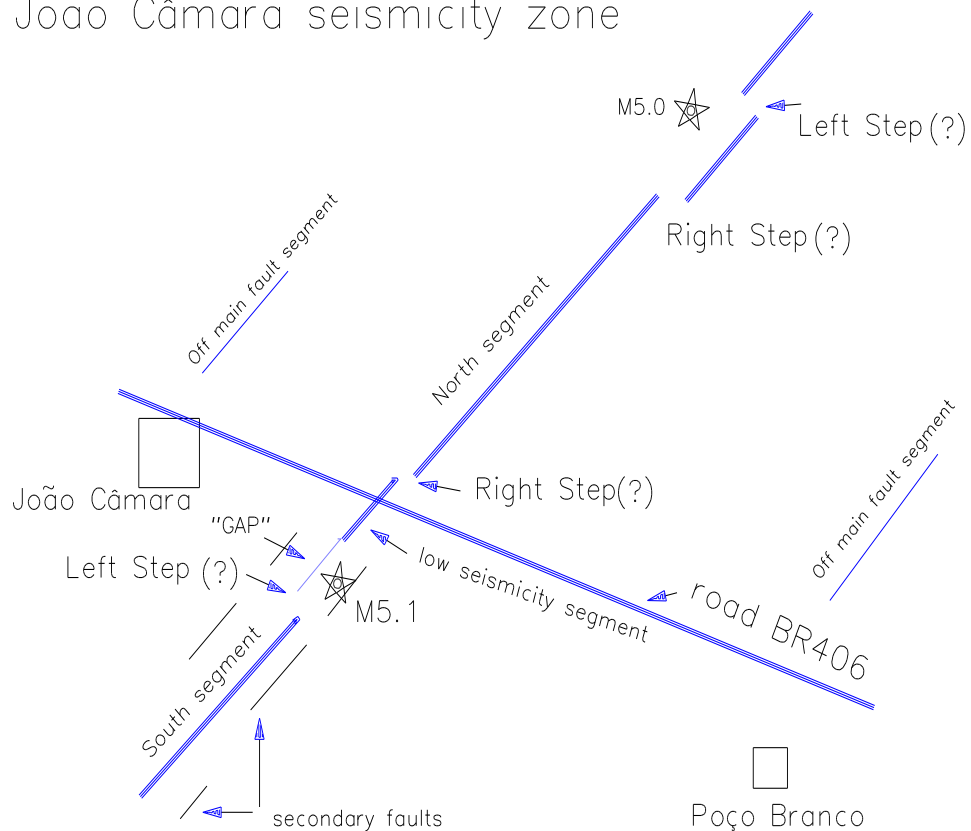


Figure 4.18 Sketch showing the main geometrical features of the João Câmara active fault system interpreted from the aftershock location. Features marked by question marks refers to tentative interpretation which are not well defined as other features.

Figure 4.18 summarizes the ideas in this section. The rupture process has been described as being initiated close to the south-bend shown by line 2 in figure 4.4; that is, in the gap as shown in figure 4.18. In order to justify the absence of any major shock to the south of section S of figure 4.6, it is assumed that the termination of the rupture process in this section was associated with the redistribution of the slip deficit among several secondary faults and fragmentation barriers, which are characteristic of the south segment as can be seen in the detailed epicentral map of figure 4.4. According to King (1986) the fragmentation process cannot continue indefinitely without the creation of an infinite fault area. Thus at some scale an opening must occur and the fragmentation process must be associated with many small dilational barriers. To support this interpretation, it must be observed that up to March 91 no event with magnitude above 3.0 was found south of this region, although during this period many other small clusters of events were detected by the drum recorder network as shown in figure 2.5. Another

## *Chapter 4*

possible interpretation which does not exclude the previous one, is that the slip deficit is absorbed by rocks or fault material with different properties (inhomogeneous barriers). There is some support for this assumption in the difference in depth of the seismogenic layer between the north and the south segments.



## **CHAPTER 5**

### **DEPTH DISTRIBUTION OF EVENTS AND OFF-FAULT SEISMICITY**

#### **5.1 Introduction**

Crustal earthquakes are generally thought to be the result of brittle failure of rock. Brace and Byerlee (1966) first suggested that the primary cause of earthquakes is frictional sliding (stick-slip motion) on pre-existing fault surfaces although the fracturing of intact rock on a small scale may be involved in the generating process. Based on laboratory experiments, Brace and Byerlee (1970) further suggested that earthquakes in California are generally confined to shallow depths of less than 10 to 20 km because stick-slip motion gives way to aseismic creep as temperatures increase to between 300° and 500°C at an approximate depth of 15 km. They also pointed out that their observations do not support a reduction in strength with increasing depth as a significant factor to explain the absence of seismicity in the lower crust. This strong temperature dependence on the cutoff depths for microseismicity was also emphasized by other authors (e.g., Meissner & Strehlau, 1982; Sibson, 1982; Chen & Molnar, 1983) who studied a number of these seismic-aseismic transitions in a variety of regions and tectonic environments, including intraplate and intracontinental regions of the world. The basic explanation is that the absence of seismicity in the crust below a particular depth in a given region is due to the increased ductility with increasing temperature. For example, Sibson (1982) found a correspondence between the brittle-ductile transition and the maximum depth of earthquakes using a two level model of rheology in which the upper part is dominated by frictional faulting that obeys Byerlee's friction law in a typical quartz/diabase crust and the lower part is dominated by a high temperature quasi-plastic deformation law. The intersection of these two laws was taken to mark the brittle-ductile transition in the earth and the suggested maximum temperature allowable for earthquake occurrence in the crust is  $350^{\circ}\pm 100^{\circ}\text{C}$ .

Accurate hypocentre locations have revealed the occurrence of seismicity in the uppermost mantle beneath the aseismic lower crust. In fact, Chen & Molnar

## Chapter 5

(1983) have noted several cases of earthquake occurrence in the uppermost mantle in regions not associated with active subduction. Based on a review of available data on focal depths, they concluded that a seismically active uppermost mantle occurs in regions of recent continental convergence (e.g. Tibetan Plateau). In the cases they studied, the lower crust is aseismic but they point out that it is also possible for the entire crust to be seismically active in regions with average crustal thickness and sufficiently low heat flow such that the limiting temperature of  $350^{\circ}\pm 100^{\circ}\text{C}$  is not exceeded. Seismicity in the uppermost mantle is explained by Chen & Molnar (1983) as an indication of a difference in mechanical properties of crustal and mantle forming materials at similar temperatures and pressures. Based on laboratory results, olivine appears to be stronger than quartz or diabase between the temperatures of  $300^{\circ}$  and  $1000^{\circ}\text{C}$ . Thus they suggested an abrupt change in the composition of material near the Moho, assuming a primarily olivine composition for the upper mantle. So, at a given temperature, mantle materials have higher strength than crustal materials. They estimate that the limiting temperature for earthquake occurrence in the mantle is approximately  $600^{\circ}$  to  $800^{\circ}\text{C}$ .

Another important aspect of the depth distribution of earthquakes is that major earthquakes tend to nucleate at the base of the seismogenic layer (Meissner & Strehlau, 1982). Sibson (1984) pointed out that for stress levels approaching failure through the frictional regime, the largest concentration of shear strain energy (varying as the square of shear resistance) is to be expected around the base of the seismogenic zone and so is the most likely origin of large earthquakes. A different explanation was made by Das & Scholz (1983), using a dynamic crack model in which frictional strength and stress-drop increase with depth. They found that ruptures which nucleate in the low stress-drop (shallow) regions of the model are prevented from propagating. Only those that initiate within the high stress-drop regions can propagate over the entire seismogenic layer.

### 5.2 Depth distribution of the main aftershocks

No major local event was recorded by the telemetric network during the operative period. The maximum magnitude observed was a  $m_b = 3.1$  event. In order to check whether this and other events of similar magnitude display characteristics found in moderate to large earthquakes as described in section 5.1, all events with magnitude above  $m_b = 2.9$  were selected from dataset 3. These are shown in Table 5.1. The magnitude  $m_b = 3.1$  event recorded on 18th June 1987 is located to the south of the road in the section S of figure 4.6 and is identified as event B in Table 5.1. Generally, good precision was obtained in the hypocentre locations of the

## Chapter 5

aftershocks in Table 5.1, even in the absence of S readings due to the saturation of the seismometer.

Table 5.1 List of events with magnitude above 2.9 which occurred in the J.Câmara region recorded by the telemetric network.

Date	hr:min	Lat.	Long.	Depth	Mag.	RMS	ERH	ERZ	Ev.
870618	03:02	S5°36.56'	W35°48.61'	5.33	2.98	.02	.2	.3	A
870618	16:21	S5°36.72'	W35°48.68'	4.76	3.10	.02	.2	.4	B
870622	10:31	S5°28.87'	W35°43.42'	7.02	2.98	.03	.3	.2	E
870627	05:09	S5°36.07'	W35°48.11'	4.87	2.93	.02	.1	.2	C
870709	19:15	S5°35.76'	W35°48.03'	5.00	2.98	.05	.4	.6	D
880109	00:51	S5°29.67'	W35°43.96'	7.52	3.07	.01	.1	.2	F
880128	11:05	S5°30.97'	W35°45.19'	8.33	2.97	.01	.1	.2	G

Depth, horizontal (ERH) and vertical (ERZ) location errors are given in kilometres. Ev denotes events. Events A, B, C and D occurred in the south part and events E, F and G occurred in the north part of the Samambaia fault.

Events above magnitude 2.9 found in Table 5.1 are represented by larger circles in figure 5.1. These events can be seen to have a tendency to nucleate at the bottom of the clusters. Das & Scholz (1983) and Sibson (1984) observed that large earthquakes invariably nucleate at the base of the seismogenic layer and that small earthquakes can nucleate over a broad depth range within the seismogenic layer. Large earthquakes in this case are understood to be those greater than magnitude 5.5, because their rupture can propagate through the entire depth range of the seismogenic layer (Sibson, 1984). Earthquakes with magnitudes between 2.9 and 3.2, as shown in figure 5.1, are not large in any classification. If they can be considered small events, then it is surprising that events in this magnitude range are not randomly distributed in depth as suggested by Das & Scholz (1983) but are concentrated at the bottom of the clusters, which suggests that they are concentrated at the base of the seismogenic layer. So, although the rupture dimension of these events must be a fraction of the thickness of the seismogenic layer, the pattern of the aftershocks shows that they do not propagate into the deeper, high-strength regions.

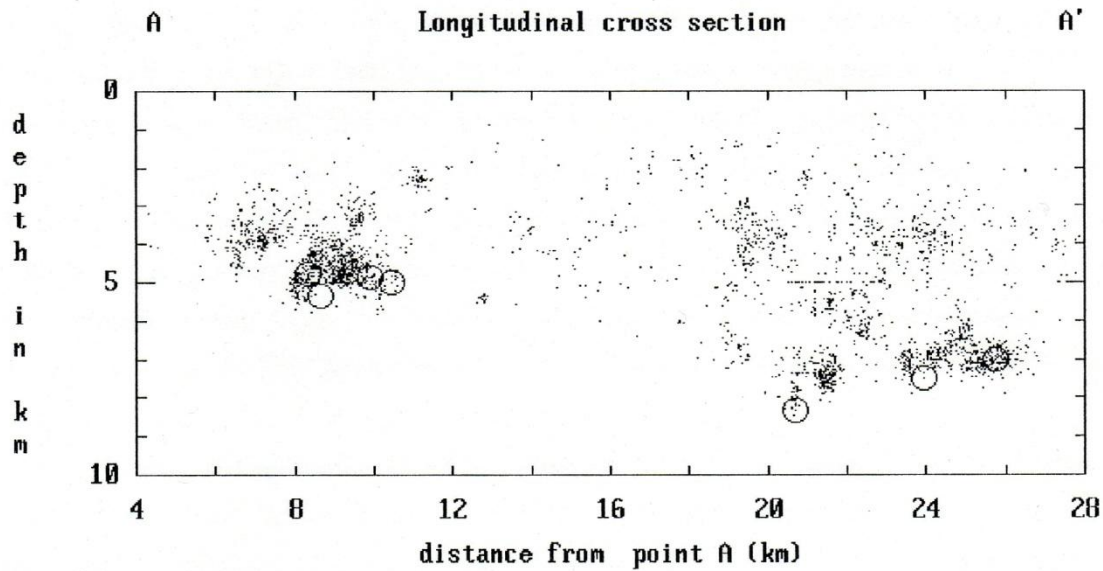


Figure 5.1 Projections of hypocentres evaluated from dataset 5 onto vertical plane along the fault strike. Larger circles indicate events above  $m_D = 2.9$  as shown in Table 5.1. The linear artifacts at the depth of 5 km are explained in the section 4.4.

### 5.3 Depth distribution of other aftershocks as a function of magnitude

One common and noticeable feature in all the vertical cross sections plotted in Chapter 4 using data from the telemetric network, is that no events are found at a depth greater than 9 km. This feature agrees with previous hypocentre determinations performed by Ferreira et al., (1987) and Takeya et al., (1989), and conforms with the idea of an aseismic lower crust (Meissner & Strehlau, 1982; Sibson, 1982) beneath the brittle-ductile transition, which in this case appears to be located at a depth of 10 km. However, events in the south segment (zone S) are shallower (maximum depth is 6 km) suggesting a brittle-ductile transition at a shallow depth, or alternatively, a higher strength material (inhomogeneous barrier) below 6 km. Another general feature of these longitudinal cross sections is that they confirm the distribution of aftershocks in some patches which are not necessarily in the same fault plane. These clusters, according to Das & Aki (1977), occur in unbroken barriers after the occurrence of the main shock, which naturally become the sites of stress concentrations which generate the aftershocks. A study of these clusters will be made in Chapter 6.

## Chapter 5

The number of aftershocks larger than various magnitude thresholds as a function of focal depth for the entire dataset 3 and its components parts are shown in figures 5.2 and 5.3. The Poço Branco fault and the south segment of the Samambaia fault show different characteristics, when compared with the north of the Samambaia fault. The histograms for these regions present a single peak in each curve. On the other hand, the histogram for the north segment shows that events are concentrated at two different depths as can be seen by the two peaks in the family of histograms of figure 5.3(a). In the case of the south segment of the Samambaia fault, it is tempting to attribute this characteristic as due to the existence of a ductile zone below 6 km, where slip is accounted for by a creep process.

In the histogram for the south segment, shown in figure 5.3(b) all the peaks are concentrated around 4 km depth. Only the curve corresponding to the magnitude threshold of 2.9 (not shown) has a different maximum, corresponding to the depth of 5 km, that is, the base of the seismogenic layer in this region. On the other hand the histogram for the north segment shown in figure 5.3 reveals a crude correlation between magnitude and depth. For example, the peak of the histogram representing aftershocks with magnitude threshold 0.0 is around 6 km and the peak corresponding to magnitude threshold 1.5 is around 7 km. In addition, the three events above magnitude  $m_b = 2.9$  which happened in this segment, indicated in table 5.1, were located at depths of between 7 km and 8.5 km. This correlation between magnitude and depth for the north segment is additional evidence in support of the results of Das & Scholz (1983) concerning the tendency of larger events to nucleate at the base of the seismogenic layer. In this case this tendency is exhibited even for small events (figure 5.3). However, this correlation only applies to the second family of peaks which corresponds to deeper events in the histogram of the north segment. No correlation between magnitude and depth is found, when the hypocentral depths of the first family of peaks are considered.

Concerning the depth distribution of events in the north segment it must be observed in the histogram of figure 5.3 that in each curve, the number of events for the first peak is smaller than that corresponding to the second peak. With the exception of the curve corresponding to magnitude threshold 1.5, the number of shallow events was underestimated in each curve. This happened because about 80% of the events excluded from dataset 3 did not satisfy the criterion imposed for the error in depth determination. Since it is very well known that depths of shallow earthquakes are notoriously difficult to constrain tightly (Chen & Molnar, 1983) it is not surprising that most of the events excluded are the shallow ones.

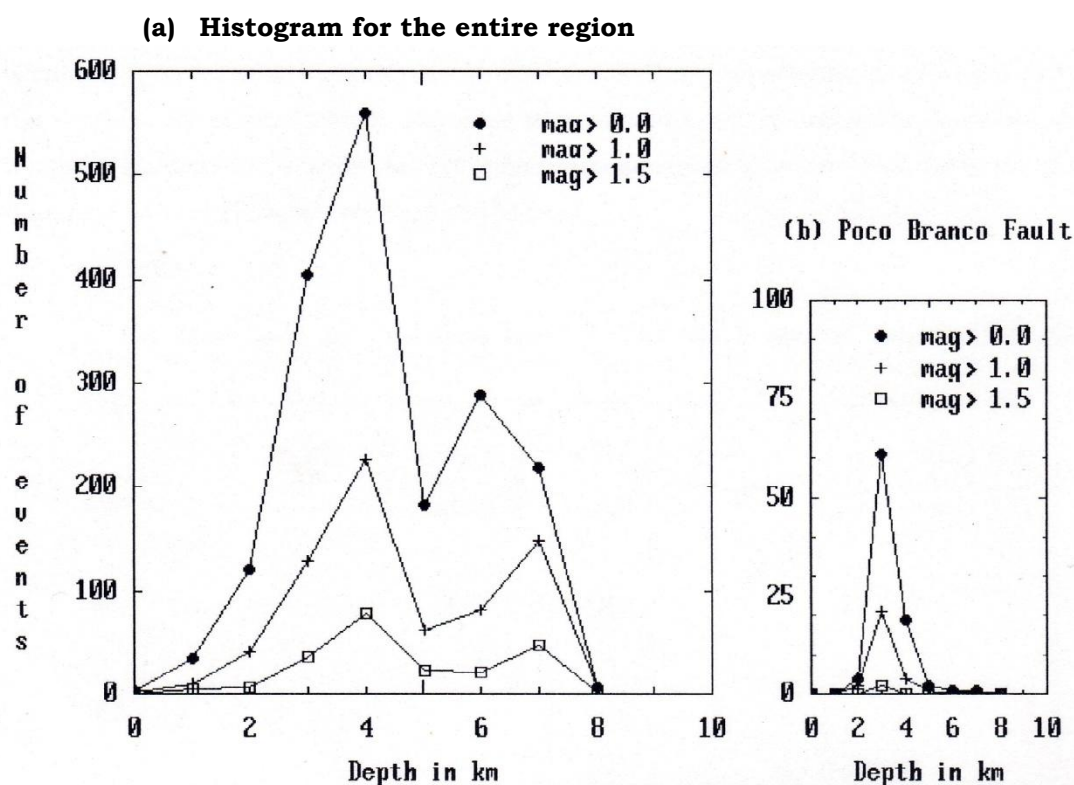


Figure 5.2. Histogram of the number of aftershocks larger than various magnitude thresholds, against focal depth (a) for the entire region and (b) for the Poco Branco fault.

The histogram for the north segment of the Samambaia fault in figure 5.3(a) reveals a minimum centred at 5 km that separates peaks at 3 to 4 km and at 6 to 7 km. This feature is very similar to that found by Eaton et al., (1970) for the aftershocks of 1966 Parkfield-Cholame, California, earthquake.

The minimum that appears in the corresponding histogram of the 1966 Parkfield earthquakes (figure 19 of Eaton et al., 1970), is centred near the 6 to 7 km interval and separates peaks at 2 to 4 km and at 8 to 10 km. Different interpretations were given to this minimum. The similarities between the histogram for the north segment of the Samambaia fault and the histogram of Eaton et al. (1970), suggest that some of these interpretations may be valid for the Samambaia fault, and therefore will be discussed in detail. Eaton et al. (1970), gives two suggestions. The first is that the minimum may result from some depth-controlled characteristic of rocks composing the upper crust. For the second, they observed that the strong concentration of aftershocks in a few patches on the fault plane suggested that the peaks on the frequency-versus-depth histograms may result from geometrical features of the fault plane or from non-depth dependent variations in properties of rocks in contact across the slip surfaces. Thus, one of the suggestions

## Chapter 5

given by Eaton et al., (1970) is to attribute the observed clustering in depth to geometrical irregularities in the fault. This hypothesis is assumed in the case of the Samambaia fault. Because the resolution of the telemetric network data is good, an attempt to infer geometrical heterogeneities from the distributions of the clusters will be made in the next chapter.

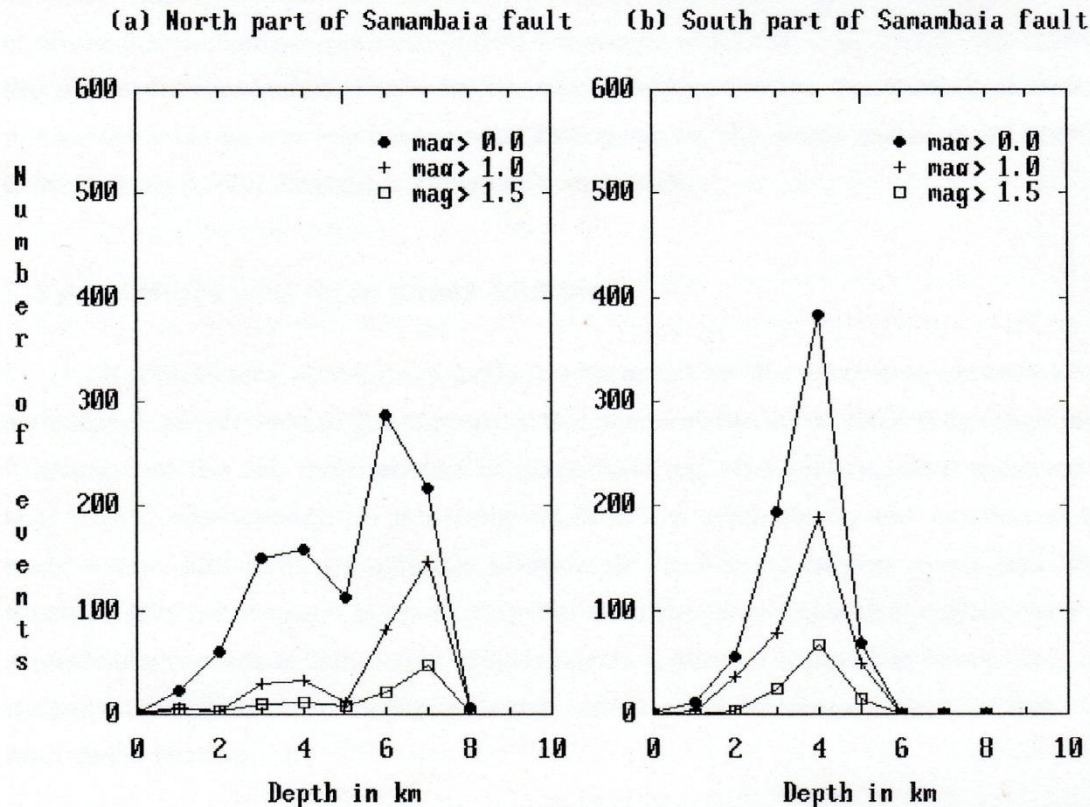


Figure 5.3. Histogram of the number of aftershocks larger than various magnitude thresholds against focal depth (a) for the north and (b) the south part of the Samambaia fault.

Another interpretation of the Parkfield histograms was given by Ribicki (1973). He explains the two strong concentrations of aftershocks at different depths by the presence of a surface layer which extends to a depth of 2 km and whose modulus of rigidity is much lower than that of rocks situated below in which a nearly vertical main fault plane has been formed. Ribicki (1973) performed numerical calculations supposing that a single crack was generated as a consequence of the principal rupturing, and supposing that the upper edge of the main fault plane at Parkfield starts at a depth of 3 km and its lower edge ends at 9 km. He found that the resulting shear stress has higher values in the region

surrounding the upper and lower edges of the fault, where the histogram of Eaton et al., (1970) shows the concentration of aftershocks, and lower values for the shear stress inside the crack.

Regarding the Samambaia fault, it is interesting to note that the best velocity model found in section 3.4 is a half-space below a 4 km deep surface layer with lower P velocity. However, to be consistent with the aftershock concentration at the depth of between 3 and 4 km as shown in figure 5.3(a) and to be consistent with the Ribicki's model, the interface between the layers would have to be located at a depth of about 2 km. Another problem is that the model of Ribicki (1973) can only explain the depth distribution of events for the north segment of the Samambaia fault and not for the fault as a whole because the histogram for the south segment, as distinct from Eaton's (1970) diagrams, shows only one peak.

### 5.4 Aftershock and main shock faulting

If aftershocks above magnitude 2.9 recorded by the telemetric network show a tendency to nucleate at the bottom of the seismogenic layer, then it is reasonable to think that the two main shocks of magnitude  $m_b = 5.1$  and  $m_b = 5.0$  occurred at that depth, even though no instrumental data are available for the location of the main event, and even though the location of the second largest event has large errors. If this assumption is made, together with the hypothesis that regions with no aftershocks represent completely broken barriers, then it is possible to correlate the magnitude of those two shocks with the size of aseismic areas estimated from the aftershock pattern.

#### 5.4.1 The $m_b = 5.1$ earthquake

More recently, with the increasing number of authors studying strong motion data, a new interpretation for the 1966 Parkfield earthquake has been suggested. Mendoza & Hartzell (1988) compared the observed distribution of aftershock hypocentres following some moderate to large earthquakes with the corresponding pattern of coseismic displacement estimated from an inversion of the strong-motion and teleseismic records. They found that, for all the earthquakes studied, the aftershocks occurred mostly outside the areas of maximum slip estimated for the main shock and they point out that the results are consistent with the interpretation that aftershock activity occurs in regions of concentrated stress following primary faulting during the main shock. This is a surprising result that had been previously observed in some few isolated studies only (e.g. Doser & Kanamori, 1986; Hartzell & Heaton, 1986) maybe because for this kind of comparison it is necessary to have not



## Chapter 5

only an estimation of the slip function but also accurate hypocentre locations. In theoretical terms, these results were forecasted by Das & Aki (1977) who, in discussing the consequences of the fault model as a plane with barriers, points out that unbroken barriers are naturally the sites of stress concentration and the sources of aftershocks, and that if barriers are completely broken, there may be no aftershocks within the main-shock fault plane.

In the case of the 1966 Parkfield earthquake, Mendoza & Hartzell (1988) superimposed, on the slip model obtained by Liu (1983), the well-located aftershock hypocentres of Eaton et al., (1970). They concluded that although several aftershocks plot within the areas of major slip, the activity appears to form clusters near the edges of or outside those areas. Thus, the minimum in the histogram of Eaton et al. (1970), can be interpreted as indicating the depth around which the areas of major slip are found.

Unfortunately, for the J.Câmara earthquake sequence there are no data to calculate the slip distribution model for the main shock, with which to compare the location of the aseismic region in the main fault. So, an attempt was made to compare the shape and size of the aseismic region estimated from the distribution of aftershocks with the magnitude of the main shock, supposing that the aseismic region would represent the area which was ruptured by it. To get the size of the aseismic area it is necessary to project the hypocentres onto a vertical cross section along the fault strike as shown in figure 5.4. In this projection, boundaries were drawn between regions with no aftershocks - supposed to be the slipped areas due to the main shock - and the region with aftershocks which according to the model of Das & Aki (1977) may represent unbroken barriers. In what follows, a correlation will be discussed between the size of the aseismic region with the magnitude  $m_b = 5.1$  of the main event considering the standard error of  $\pm 0.2$  in the magnitude determination.

A crude evaluation of the size of the region with aftershocks in figure 5.4 gives an estimated area of  $70 \text{ km}^2$ . Let us suppose that the aftershock area corresponds to the slipped fault plane during the main shock. The slip or the cumulative seismic moment for aftershocks is usually negligible compared to that of the main shock (Eaton et al., 1970). According to Nuttli (1983), a magnitude around  $m_b = 5.7$  would be expected for an intraplate earthquake of this size, which is significantly different from the  $m_b = 5.1$  calculated for the main shock. The second hypothesis is to equate the size of the aseismic region to the slipped area (Mendoza & Hartzell, 1988; Oppenheimer et al., 1990) according to the barrier model (Das & Aki, 1977). The area of the entire estimated aseismic region is around  $30 \text{ km}^2$  which is compatible with an earthquake of  $m_b = 5.3$  (Nuttli, 1983). To avoid confusion the

first hypothesis is called "first alternative" and the second hypothesis is called the "second alternative" in the following discussion.

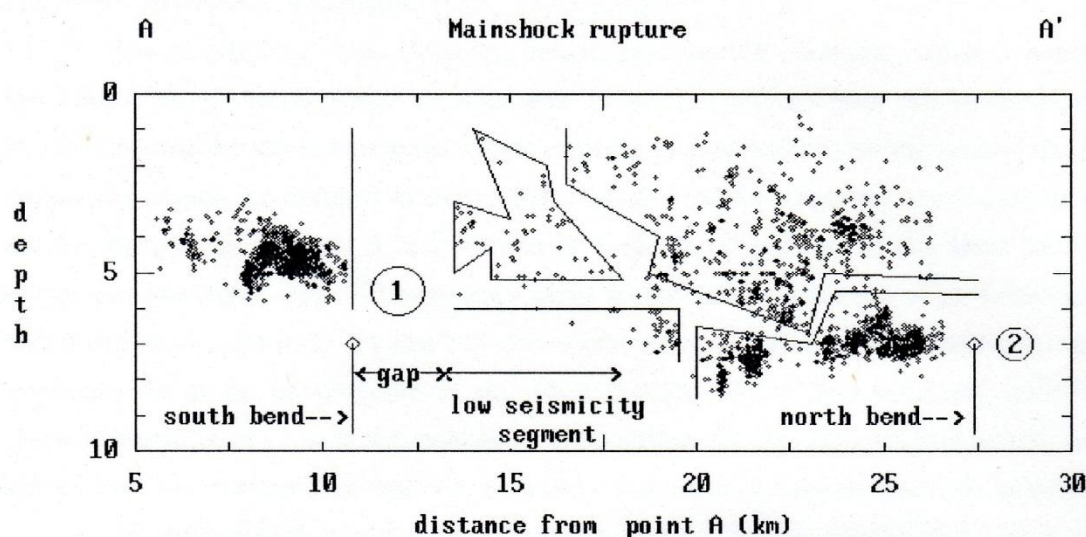


Figure 5.4 Hypocentres of the aftershocks projected onto the vertical plane along the line AA' as defined in figure 4.6. Off-fault events around Poço Branco and J.Câmara towns, and others on bends and secondary faults were excluded in this projection. The sketch shows the hypothetical boundary between the slipped area, inferred by the region with no aftershocks, and the areas with unbroken barriers (Aki, 1979) which correspond to the regions with aftershocks. The ends of the zone of possible main shock fracturing are indicated by arrows which in addition mark the locations of the two fault bends or fault jogs. Circles 1 and 2 indicate possible locations of the magnitude 5.1 and 5.0 earthquakes respectively.

There are different ways to draw the boundaries of the aseismic areas seen in figure 5.4. However, the freedom to do this will be limited if some conditions are imposed. In drawing the boundaries of the aseismic area described in the last paragraph, the following conditions were imposed: a) the rupture extent due to the main shock is limited to the region between the fault bends, which in figure 5.4 is indicated by the arrows; b) the slipped region is the aseismic area; c) major shocks tend to occur at the base of the seismogenic layer; d) the main shock would be located close to a strong barrier, like the fault offset found at the junction between the low seismicity segment and the south segment; e) the aseismic region shown at the north edge of the Samambaia fault would be the region where another strong barrier is located and is the most likely focus of the second major earthquake; f) the base of the seismogenic layer is limited to the depth of 9 km in the north segment, and decreases in the low seismicity region from 9km to 6km, which is the depth of

## Chapter 5

the seismogenic layer for the south segment; g) in the absence of any surface breaking due to the main event, the slipped region is arbitrarily considered to be restricted to below 1 km depth.

It is possible to draw different boundaries for the aseismic region if some of the conditions outlined above are changed. Two other alternatives will be discussed. In the third alternative, the main shock rupture is now limited to the end of the low seismicity region as defined in figure 5.4. The size of the aseismic area towards the north segment is roughly  $6 \text{ km}^2$  which is a small proportion of the total  $30 \text{ km}^2$  estimated aseismic area. If the  $6 \text{ km}^2$  strip in the north segment is excluded from the total, the remaining  $24 \text{ km}^2$  of the aseismic area in the low seismicity region corresponds to an earthquake of  $m_b = 5.2$  (Nuttli, 1983). The difficulty with this third alternative is to find a reasonable explanation for the termination of the main shock rupture because no barrier is evident between the north and low seismicity segments which could stop the rupture propagation. In this alternative, the  $6 \text{ km}^2$  strip can be interpreted as representing a region where the redistribution of stress, after the main-shock, is a minimum due to the effect of the presence of a surface layer in the north segment with lower rigidity than the fault plane according to Ribicki's model. Alternatively, it may represent the pattern of seismicity caused by geometric irregularities in the fault plane. Another possible explanation of the low seismicity strip in the north segment of the main fault is that it represents a region which has slipped in major aftershocks, rather than in the main shock. At least two aftershocks of  $m_b = 4.0$  were located in the north segment (Takeya et al., 1989) and the epicentre of one of them is shown in figure 4.15. The area of this strip is compatible with a magnitude 4.5 event. Thus, in following the barrier model of Das & Aki (1977) it is unlikely that the main event happened in the north segment.

The fourth alternative is to restrict the slipped area to the "gap" shown in figures 4.11a and 5.4. In this particular area, no aftershocks are found and this is the region where the antidilational jog was presumed to be located. The width and depth of the "gap" are about 2.5 km and 6 km respectively, which gives an area of  $15 \text{ km}^2$ , compatible with an earthquake of  $m_b = 5.0$  (Nuttli, 1983). It is possible to locate the main event at a depth of 8 km or 10 km because the depth of 6 km was just inferred by the depth distribution of aftershocks in the south segment. Obviously, this will increase the area of the "gap" in the same proportion. Given the remarkable lack of events in the gap it would be possible to describe the gap as being due to a single plane with no significant irregularities on it, in order to modify the slip function. On the other hand, the same lack of events makes difficult any precise characterization of it. Among other interpretations, this plane could be imagined as a transition between the south segment (section S in figure 4.6) and the

## Chapter 5

low seismicity segment (section C of the same figure). Because a  $5^\circ$  difference in dip was detected between the low seismicity segment and the south segment, the gap can be interpreted as an antidilational jog as shown in figure 4.12. This interpretation has the advantage of explaining the low seismicity region as a consequence of the dilational jog in the junction between the gap and the low seismicity segments. That is, after the occurrence of the main shock in the gap, the rupture stopped or was arrested in the dilational jog in order to leave a slip deficit towards the north.

Considering the 0.22 standard error in the magnitude determination of the main event, it is not possible to make a definitive estimate of the size of the aseismic area. In this case, the second alternative, which estimates an aseismic area of  $30 \text{ km}^2$  will be preferable because the initiation and termination of the earthquake rupture can be associated with the fault bends discussed in sections 4.2 and 4.2.1. In assuming that the scaling relations obtained by Nuttli (1983) are valid for midplate earthquakes, the estimated seismic moment for the  $m_b = 5.1$  J.Câmara earthquake is  $3.16 \times 10^{23}$  dyne.cm, with a stress drop of 8 bars, average slip of 0.04 m and ruptured area of  $20 \text{ km}^2$ .

### 5.4.2 The $m_b = 5.0$ earthquake

In section 4.6.3 it was considered whether the location in depth of the  $m_b = 5.0$  event as given in Table 4.2 was exaggerated. This leads to the question of the depth of the seismogenic layer in the region of segment 2 of figure 4.15 because it is supposed that this shock happened at the base of the seismogenic layer according to the discussion in section 5.2 and according to the hypothesis of Meissner & Strehlau (1982). The delineation of hypocentres in the vertical planes along this segment in figure 4.17 suggests a depth around 4km. But, as can be seen in the same plot, this is a region surrounded by segment 1 with a depth threshold of 9km and by segment 3 in which the depth of the seismogenic layer is around 6km. Thus, it is unlikely that the segment in between has a seismogenic layer of only 4km. Instead, if 7km or 8km is assumed to be the limit of the seismogenic layer in segment 2, this will be considered the probable nucleation depth of the  $m_b = 5.0$  event.

From the arguments in the last paragraph, the aseismic area in segment 2 is roughly limited to the depth between 4km and 7km. It can be seen from figure 5.5 that the aseismic or low seismicity zone extends laterally from the 28km mark to 33km from the point A defined in figure 4.6. This roughly defines the aseismic region as a 3km by 5km rectangle, which gives an area of  $15 \text{ km}^2$ . This, according to

the scaling relations obtained by Nuttli (1983) for mid-plate earthquakes, is compatible with a  $m_b = 5.0$  earthquake.

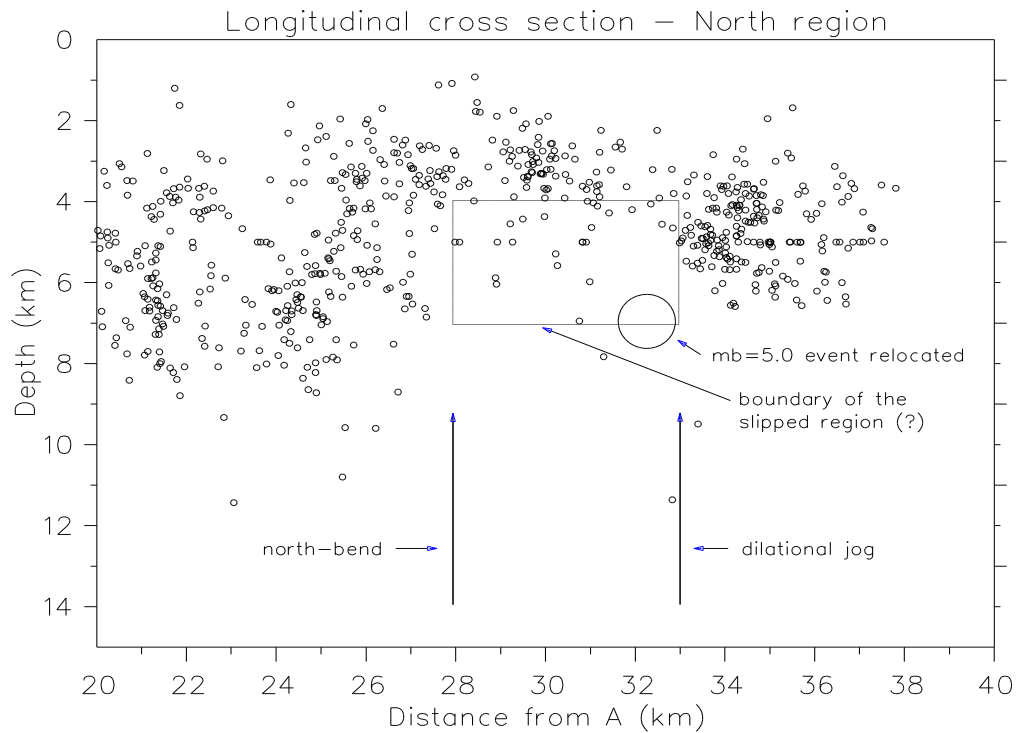


Figure 5.5 Sketch superimposed on the projection of hypocentres onto a vertical plane along the fault strike using data from the drum-recorder network.

The lack of aftershocks around the relocated  $m_b = 5.0$  earthquake is notable in this case because, at the time this event happened, a four station network was working (augmented to ten stations on the day after the occurrence) allowing a continuous coverage of the aftershock activity. So, the low seismicity zone is real and constitutes additional evidence in support of the suggestion of Das & Aki (1977) in which when a barrier is completely broken, there may be no aftershocks within the main-shock fault plane. At the same time, this evidence supports the previous interpretation done in section 4.5 in which the gap between the low seismicity segment (section C of figure 4.6) and the south segment was considered as the probable location of the  $m_b = 5.1$  earthquake.

## 5.5 Off-fault aftershocks

To complete the analysis of the main features of the seismicity of the J.Câmara region, and before the analysis of small clusters, an attempt is made here to interpret some aftershocks which occurred off the main fault plane. In addition to

the activity on the main fault, a significant number of events were found near the town of Poço Branco (PB), and minor events were detected inside or very close to the town of João Câmara. Several similar examples of such off-fault seismicity have been reported by Das & Scholz (1981b) in the case of strike-slip earthquakes. Using a simple crack in a homogeneous half-space, they proposed a model to explain the kind of seismicity that occurs in locations distant from the rupture plane of the mainshock. This model is illustrated in figure 5.6. Similar theoretical results to Das & Scholz (1981b) were found by Segall and Pollard (1980), who additionally point out that changes in the normal stress due to the presence of the crack occur only near the crack tips and are almost zero in the regions off the crack plane where the small increase in the shear stress occurs. It is well-known that after the mainshock, shear stress increases near the crack tips. Also, Das & Scholz (1981b) pointed out

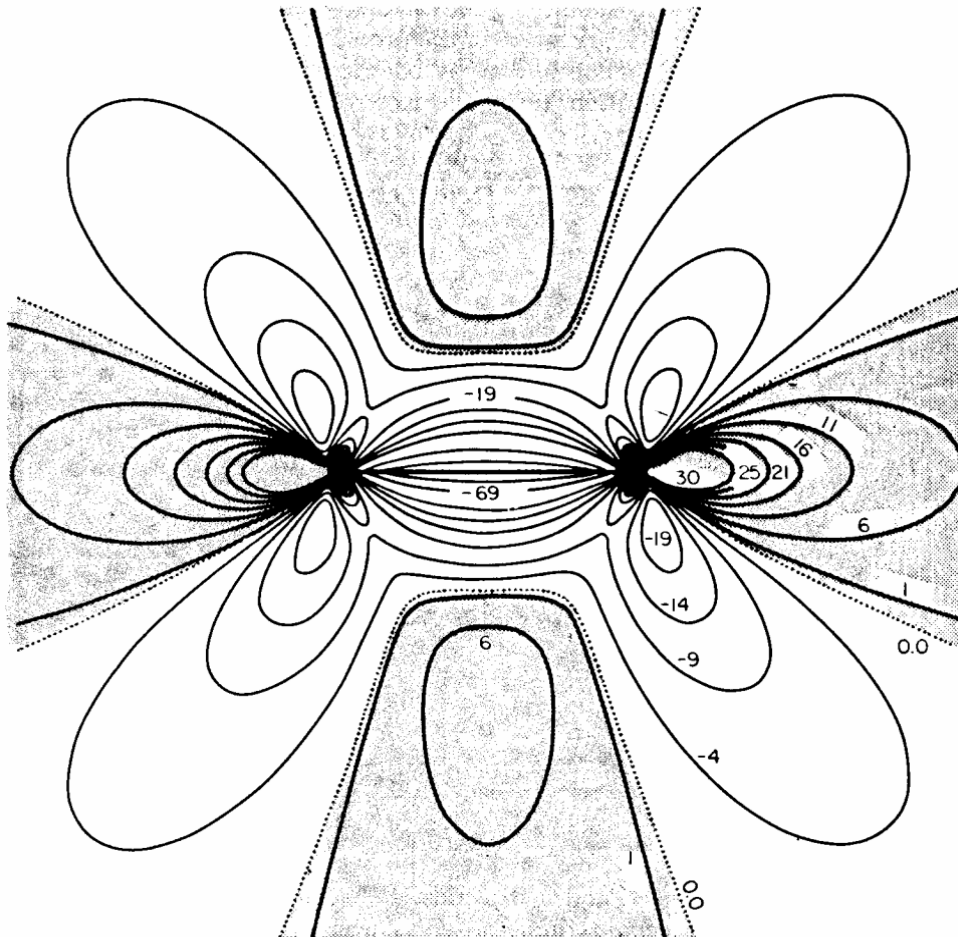


Figure 5.6 Normalized shear stress resulting from slip on a vertical strike-slip fault. The map axes are three times the crack length. Numbers indicate the change in shear stress, as a percentage of the stress drop on the crack. Shaded regions indicate regions where the stress increases due to the presence of the crack; elsewhere the stresses are reduced. (From Das & Scholz, 1981b).

## Chapter 5

that aftershocks can occur at specific locations where the crack model predicts an increase in stress resulting from the main shock rupture. In figure 4.1, starting from the middle point of the hypothetical crack in a direction perpendicular to it, the shear stress has been released in the close proximity of the crack. However, its value increases with distance from the crack line, changing sign at a distance of half the rupture length. The maximum predicted value of the shear stress in this direction is about 10 per cent of the stress drop.

It is interesting to compare the seismicity map of figure 4.1 with the theoretical results of Das & Scholz (1981b). Off-fault epicentres around João Câmara and Poço Branco are not exactly symmetrical in relation to the trend of the Samambaia fault, as predicted by the theoretical model. Epicentres around J.Câmara are compatible with a single crack model located in the region of low seismicity that has an extension of about 5 km. The difficulty is that there is no such symmetry of epicentres on the opposite side of the fault. In fact, the off-fault epicentres close to Poço Branco lie in a region where the theoretical model described above predicts negative values for the shear stress if the location of the crack is assumed to be in the region of low seismicity. On the other hand, off-fault seismicity around Poço Branco could be explained by a single crack located in the north segment of the Samambaia fault, with an length of about 10 km. This would explain the seismicity in the Poço Branco region, but conversely there are no equivalent epicentres on the other side of the fracture, and the locations of epicentres close to J.Câmara do not agree with this model.

It is likely that the single fracture model of Das & Scholz (1981b) as shown in figure 5.6 is too simple to explain accurately the off-fault seismicity of figure 4.1. In chapter 4 it was suggested that *en echelon* distribution of cracks is more capable of explaining the pattern and evolution of the seismicity in the Samambaia fault. In addition, the model of Das & Scholz (1981b) is only valid for a pure strike-slip earthquakes and the effect of the presence of a normal component in the earthquake mechanism has not been calculated. The off-fault epicentres in the J.Câmara region are a secondary effect due to the shear stress increase associated with the mainshock. No case has been found in which this effect has triggered a large earthquake. This appears to be the case for the J.Câmara region. Examining the output of dataset 3 in Appendix C.1, it was found that the largest off-fault aftershock recorded by the telemetric network happened on 16th July 1987 near Poço Branco with a magnitude of only 1.9, and the analysis of the smoked paper data shows that no larger event was detected up to March 1991 by the drum recorder network. Off-fault epicentres were not detected prior to the mainshock of 30th Nov 1986 (Ferreira et al., 1987). A few epicentres close to the town of J.Câmara

were found by Sophia & Assumpção (1989). These events occurred during January 1987, one month after the mainshock. This corroborates the idea that off-fault events typically occur as aftershocks due to the shear stress increase at certain localities after the mainshock.

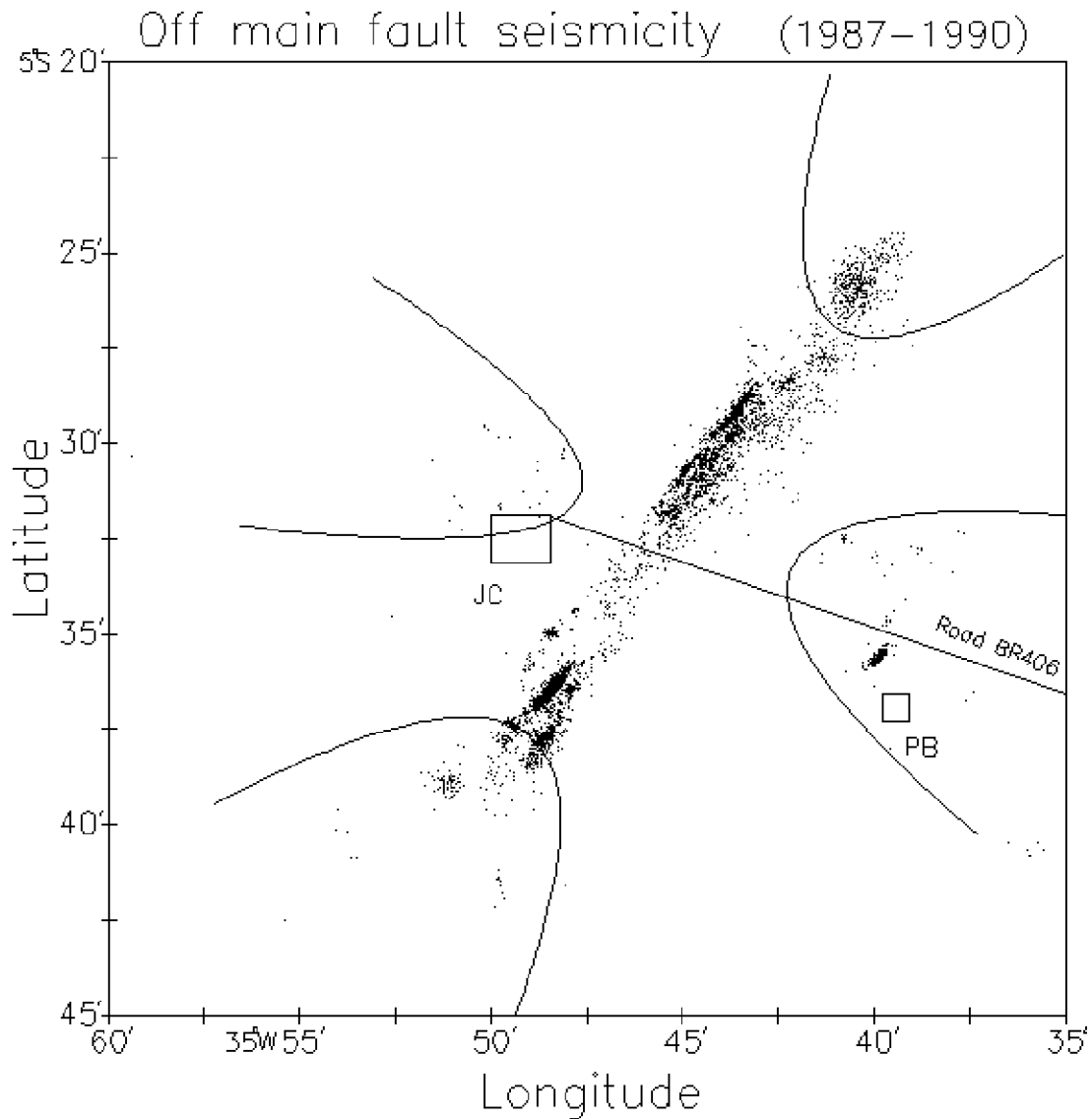


Figure 5.7 Seismicity map of the J. Câmara region during the period 1986-1990. This map is an overplot of events recorded by the telemetered network (dataset 4) and events recorded by the smoked paper drum recorder (used in figure 2.5). The contour lines are arbitrarily drawn just to emphasize the off-fault seismicity and presumed epicentres beyond main the fault ends in order to make a comparison with the model of Das & Scholz (1981b).



## Chapter 5

Considering all the limitations mentioned in the last paragraph, it is surprising how the theoretical results of Das & Scholz (1981b) obtained using a single crack in a homogeneous medium model, can still explain the general features caused by the aftershocks that occurred on either side of the Samambaia fault. Therefore, the J.Câmara sequence of events also constitutes an example of off-fault seismicity.

In addition to those off-fault aftershocks, some cluster of events beyond the ends of the main rupture were observed in the J.Câmara sequence. These zones of activity identified in figure 5.7 can be interpreted in terms of the Das & Scholz (1981b) model. Under this model, the main fault rupture will create excess shear stress both off the end of the ruptured fault segment, and in zones off the ruptured fault segment. In this case, these shear stress increase can be seen to have initiated subsequent activity, both to the north and south of the ruptured fault segment, at the P.Branco fault to the east, and near J.Câmara to the west. Events beyond the ends of the main fault are more evident in examining the epicentres calculated using data recorded after August 1988 by the drum recorder network.

Figure 5.7 is an overplot of epicentres determined using data from the telemetric network (dataset 4) and of epicentres used in figure 2.5 performed with data from the drum recorder networks. Four boundaries were drawn in figure 5.7. One boundary on either side of the Samambaia fault delineates off-fault epicentres which mostly occurred between Jan-Dec 1987. The two other boundaries delineate clusters of events beyond the ends of the Samambaia fault; these events were mainly those recorded by drum recorders between August 1988 and November 1990.

## **CHAPTER 6**

### **CLUSTERING IN TIME AND SPACE**

#### **6.1 Introduction**

Heterogeneities in fault geometry, called barriers by Das & Aki (1977), occur on many length scales. They are responsible for significant local stress concentration and may be important in creating and maintaining heterogeneous stresses on faults (Segall & Pollard, 1980). According to Nur (1978), heterogeneities on many length scales are necessary to explain important aspects of the faulting process. In view of these statements, and because an important aim of the present work is to explain the spatio-temporal distribution of seismicity in the J.Câmara region in terms of the subsurface composition, structural features and stress field, it is important to know how these effects depend upon spatial scale. With this in mind, the analysis of individual clusters or groups of clusters will, wherever possible, be made on the assumption that heterogeneities can be inferred from the clustering of events. In Chapters 4 and 5, the general pattern of seismicity was analysed and in particular, a correlation between fault heterogeneities and faulting process was attempted.

Aftershocks in the epicentral map of figure 4.6 were classified into clusters, or into groups of clusters where the identification of an individual cluster was not clear. In such a classification, events were plotted as circles, with radius equal to the average horizontal Rms error in the case of a plan view, and to the average Rms depth error in case of an elevation. In this way, both the plan and elevations were used to define the clusters. As a general criterion an event was considered to belong to a particular cluster when five or more events overplotted when plotted as circles as above. No strict mathematical definition of a cluster was used. For example, larger clusters can be further subdivided by observing the tendency of clustering in time. This approach is similar to that used by Lovell et al., (1987). It was required that a cluster be planar, so that any offset within the cluster constitutes a new

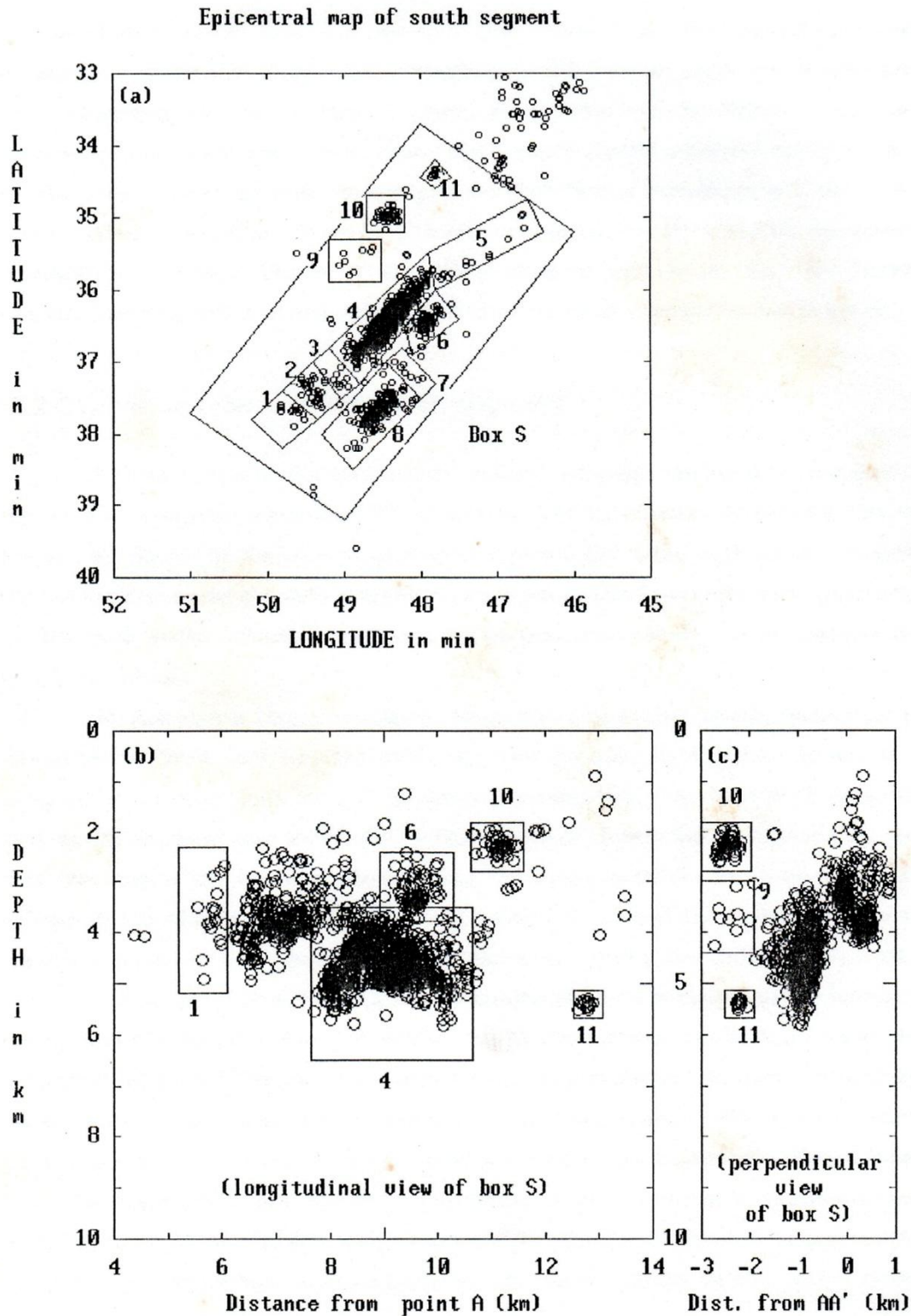


Figure 6.1 (a) Epicentral map showing the delineation of clusters for the aftershocks inside box S in the south segment. Box S was defined in figure 4.6; each cluster of events is identified by a number. (b) Projection of events in box S onto a vertical plane along the line AA' as shown in figure 4.6. (c) Vertical cross section perpendicular to the line AA'. Some of the clusters which do not overplot are identified in the two cross sections.

## Chapter 6

cluster. Other events may not belong to any cluster and were classified as such. Clusters or groups of events were identified by code, for example the largest cluster was identified as C4. In figures showing the clusters the letter C has been suppressed for simplicity. Henderson (1992) made cluster analysis using dataset 3 of the present work in order to analyse the evolution of seismicity and its physical origin based upon the concepts of fracture mechanics. He adopted an objective method for dividing dataset 3 into three clusters and found that the "nearest centroid sorting" method (Anderberg, 1973) is the most suitable for his purpose.

### 6.2 Clustering effects in the south segment

Events in the south region were defined as those enclosed by the box S of figure 4.6. and were examined for clustering. Eleven clusters of varying size were found, as shown in the epicentral map of figure 6.1a. Some of them are illustrated in the vertical cross sections both along (figure 6.1b) and perpendicular (figure 6.1c) to the fault strike. As can be seen in the perpendicular view, not all clusters lie in the same plane.

In examining the evolution in time, clusters in the south segment of the Samambaia fault can be classified into two groups. In the first group is the sequence of events that started the activity recorded by the telemetric network in the south segment and is formed by the events of cluster C4. In the second group are the rest of the clusters which follow the initial activity. The time evolution of cluster C4 is shown in the histogram of figure 6.2. This is the major cluster in the south segment and the peak of activity happened during the 3rd and 4th weeks of June 87. The monthly activity for the remaining clusters is shown in the histograms of figures 6.3 and 6.4. Each cluster's identification above the bars indicates when the peak of activity in that cluster occurred. For example, the peak of activity in cluster C1 happened during September 87. As can be seen, with the exception of cluster C4 no cluster has its main activity during June. In addition, it can be seen that the second (C8) and the third (C6) major clusters had their maximum activity during January 88 and March 88 respectively; that is, at the end of the recording period. However, small clusters had their peaks of activity in the period between July and November 87.

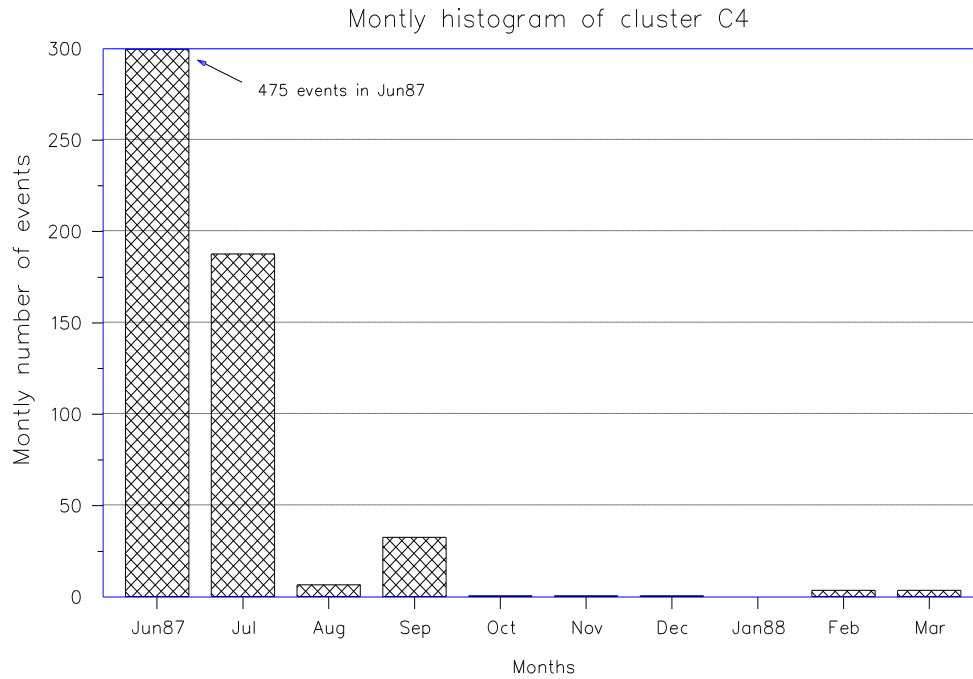


Figure 6.2 Monthly histogram of events in cluster C4 recorded between 1st June 1987 and 31st March 1988. Almost all activity is concentrated during June (475 events) and July (188 events).

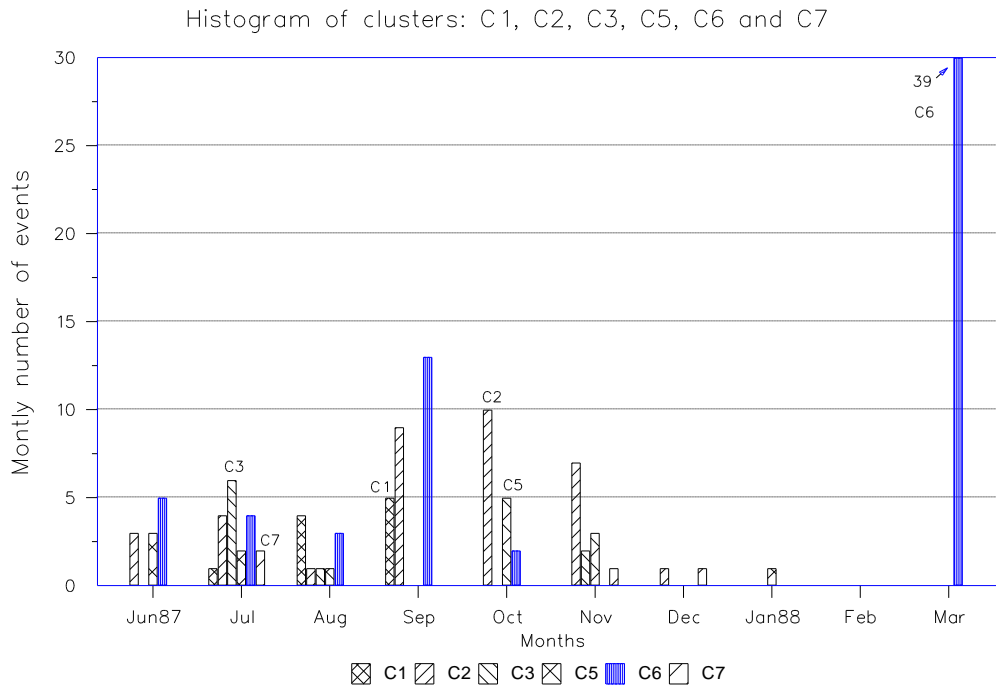


Figure 6.3 Monthly histogram of clusters C1, C2, C3, C5, C6 and C7 found in the south part of the Samambaia fault recorded by the telemetric network. Each cluster is named above the bar corresponding to its month of maximum activity.

## Chapter 6

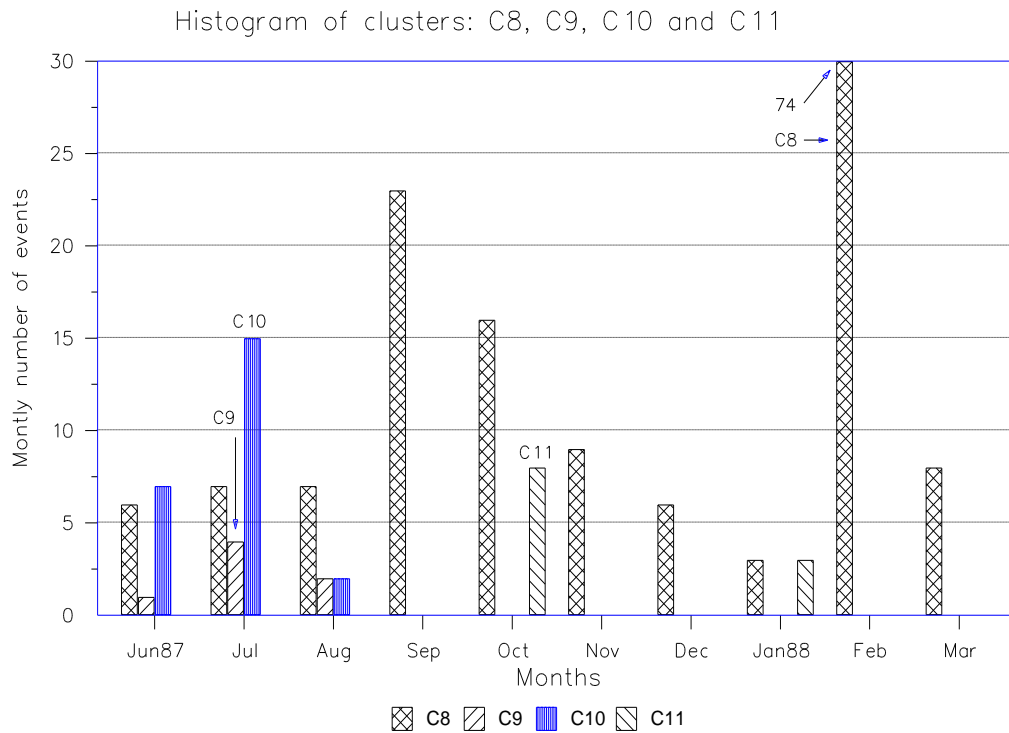


Figure 6.4 Monthly histogram of clusters C8, C9, C10 and C11. See caption to figure 6.3 for details.

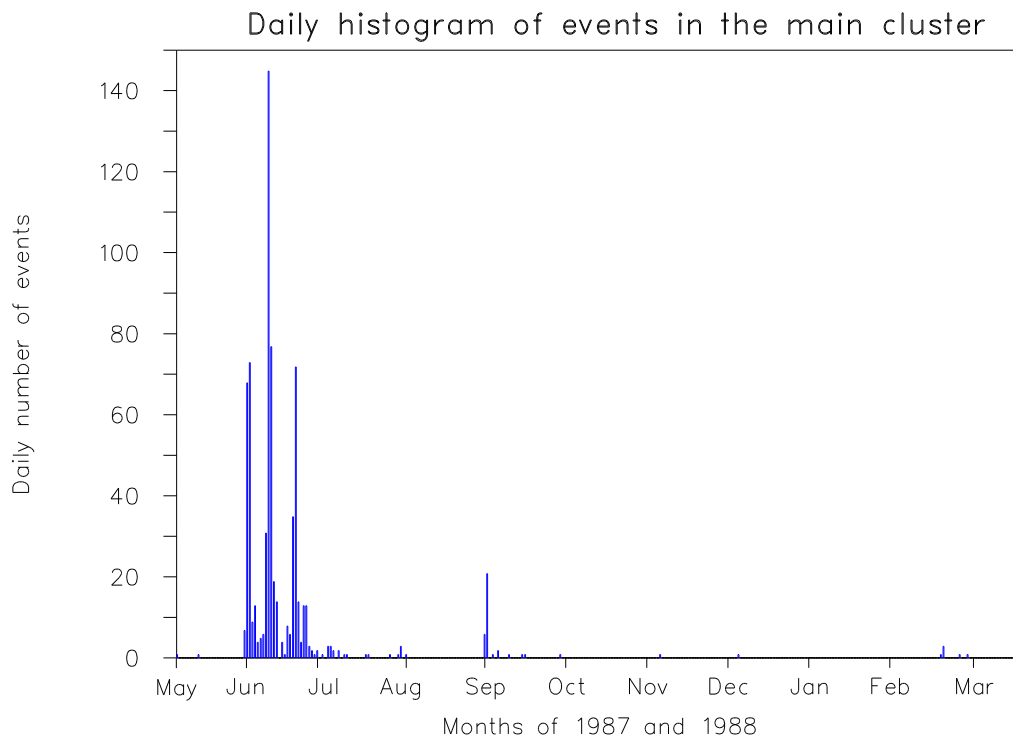


Figure 6.5 Histogram of the best located events in cluster C4 in the whole period recorded by the network. The relative location of this group can be seen in figure 6.1.

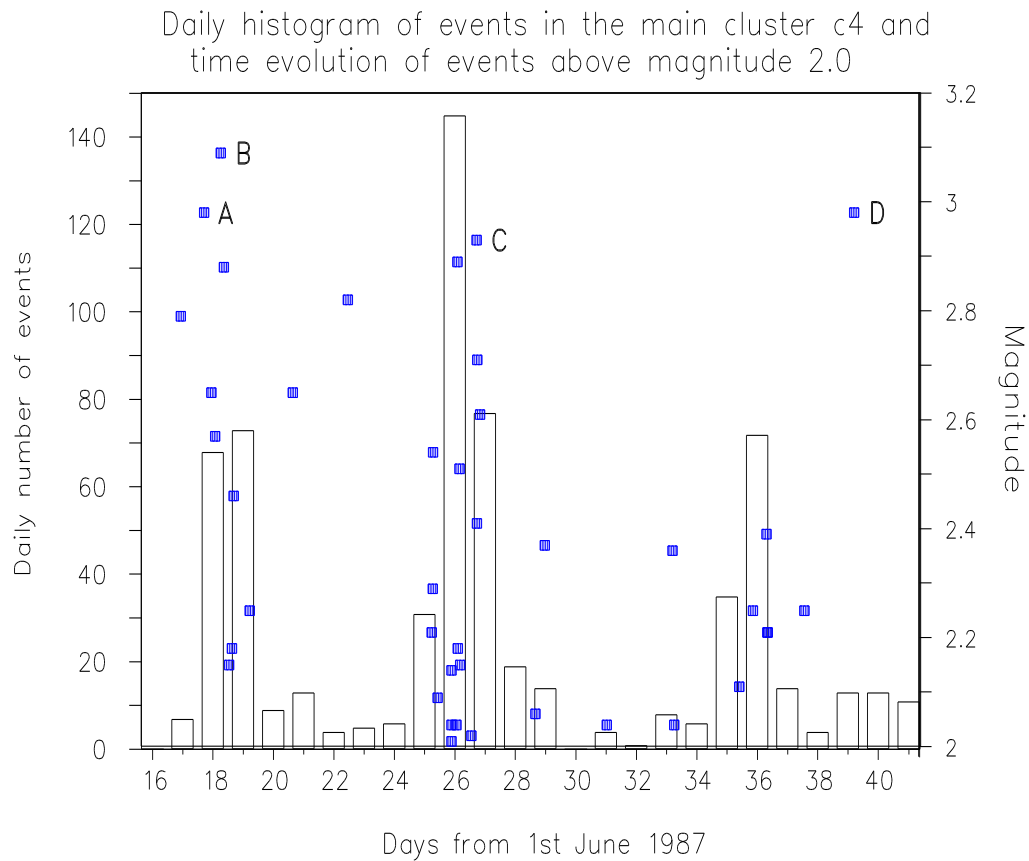


Figure 6.6. Detailed histogram of events in cluster C4 during its most active period (16th June to 17th July) and the time evolution of events above magnitude 2.0 in the same cluster for the same period of time. Events A to D are listed in Table 5. **Erro! Indicador não definido..**

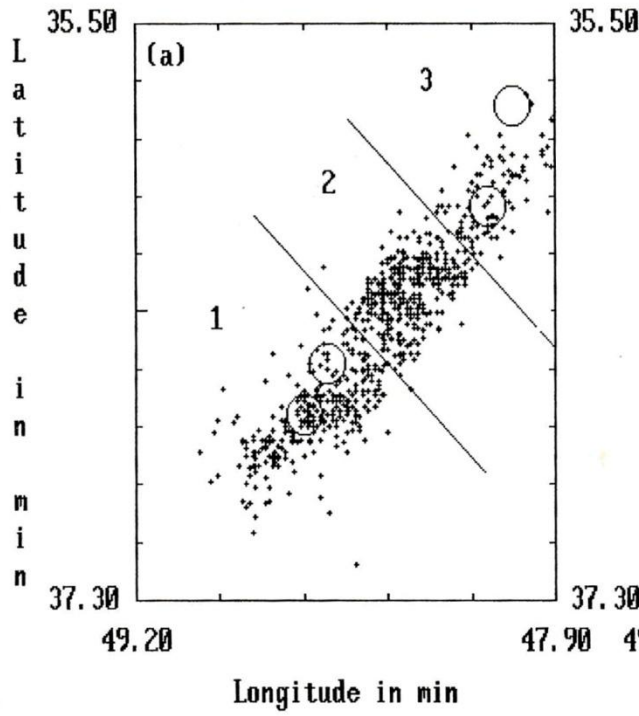
### 6.2.1 Analysis of the main cluster C4

One remarkable characteristic of C4 is that events are not only clustered in space but in a short period of time. Practically all the activity in this cluster happened between 17th June 87 and 17th July 87, that is, within one month. The histogram of figure 6.5 shows the time distribution of these events. Four main peaks appear in the histogram: 18th June, 27th June (the largest), 9th July and 15th September. A first aim is to see what kind of characteristics can be found for each of these periods.

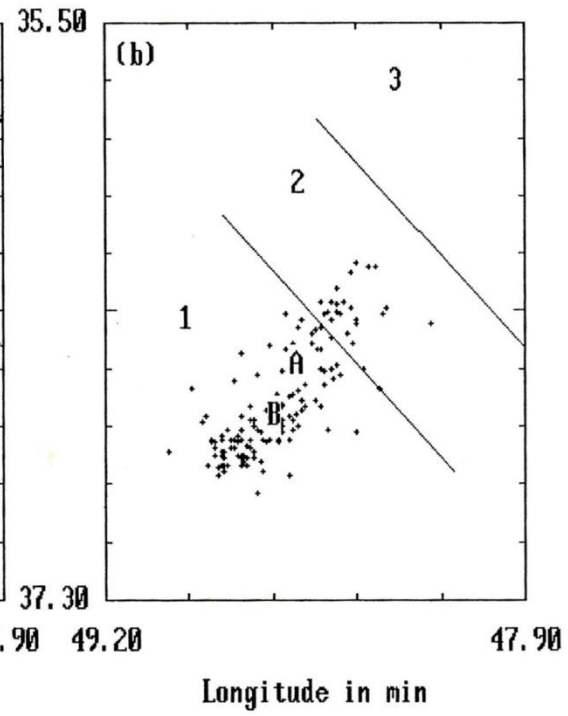
A detailed histogram for the events in cluster C4 for the most active period (between 16th June and 10th July 1987) is shown in figure 6.6. The distribution of

Chapter 6

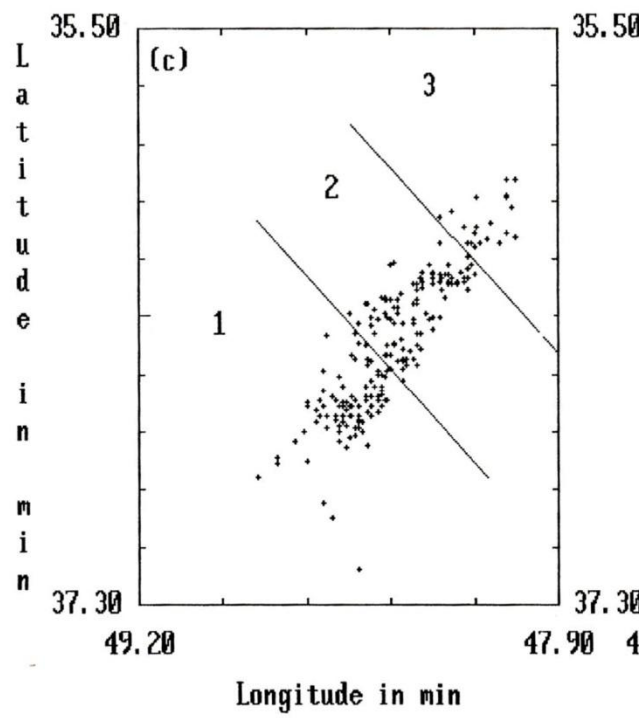
Events from 870523 to 880331



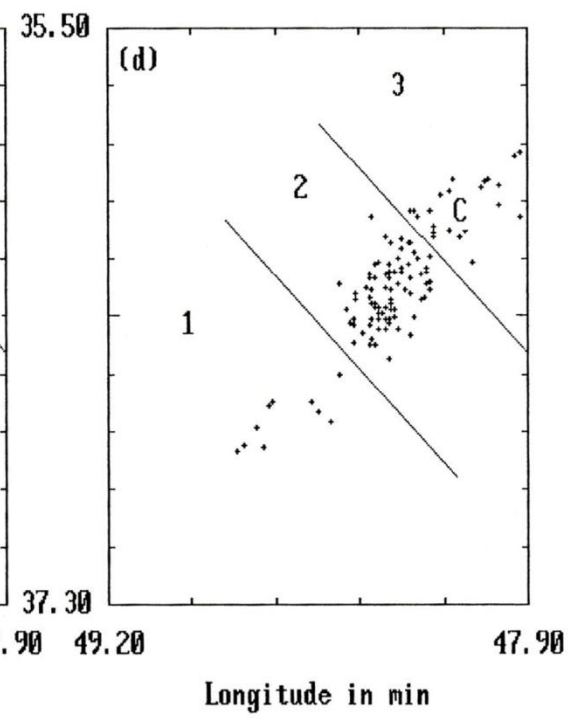
Events from 870523 to 870619



Events from 870620 to 870626



Events from 870627 to 870631





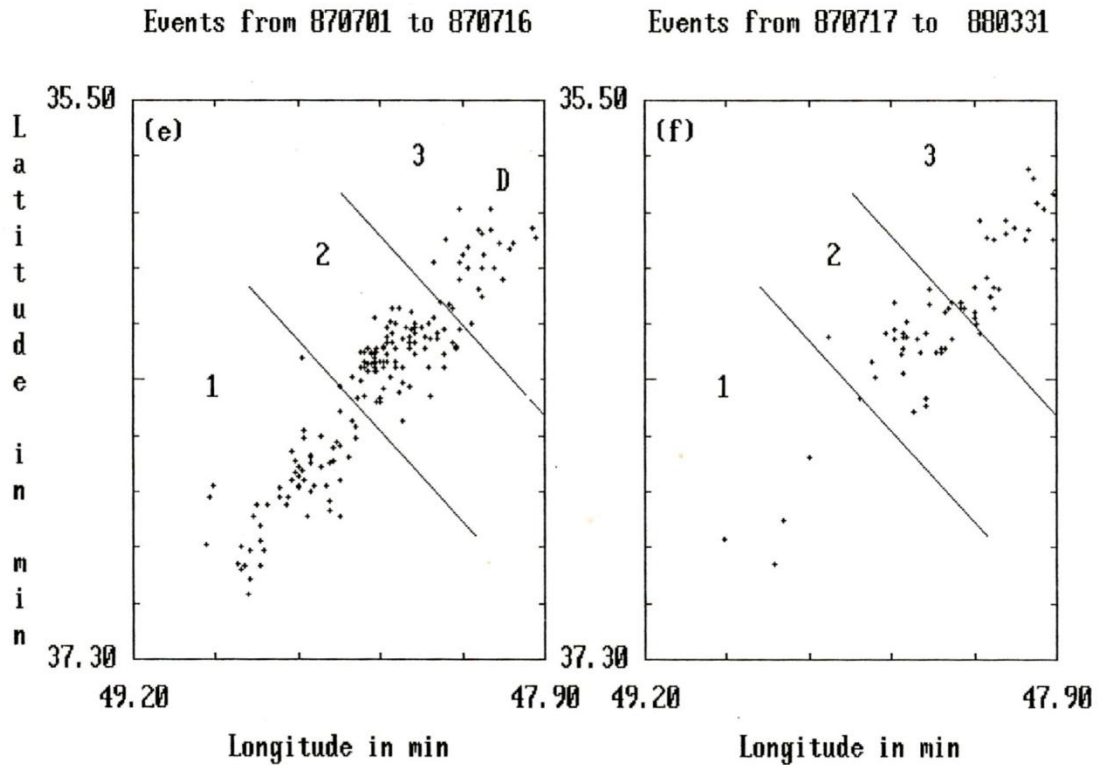


Figure 6.7 Spatio-temporal evolution of epicentres in cluster C4. (a) All events in cluster C4 recorded by the network. Larger circles indicate events between magnitude 2.9 and 3.1. For a better description of the aftershock sequence, auxiliary lines divide the aftershock region into three zones, numbered 1 to 3. (b) The main activity started in zone 1 with the occurrence of events A and B on 19 Jun 87. Foreshocks and aftershocks of these two events are concentrated in this zone. (c) to (f) show the tendency of epicentres to migrate towards the northeast.

these events by magnitude (above magnitude 2.0) for the same period of time is shown in the same figure. Particular attention is paid to the four major events that are listed in Table 5.1. Each one is identified by a letter.

Only two small events had been recorded in this segment of the fault (on 23th and 31st May) before 17th June, when a magnitude 2.8 event began the main sequence in cluster C4. The main shock in this cluster (event B in Table 5.1) occurred on the following day. One week later, another burst of events, with several in the magnitude range between 2.0 and 3.0, took place as can be seen in the histogram of figure 6.6. After that period, there was a relatively calm week. It is interesting to note that the second largest event in this cluster (D in Table 5.1), happened on 9th July. Unlike the other two events (A and B) of similar magnitude which occurred at the beginning, this one was not accompanied by a significant number of aftershocks, as shown in figure 6.6. In particular, after this shock, no event above magnitude 2.0 was recorded until September when a small reactivation took place.

## Chapter 6

Figure 6.7a shows the epicentres of the 721 events in cluster C4 for the entire recording period. The trend of seismicity is very well defined in the direction N40°E; that is, very close to the trend of the Samambaia fault. Separate plots of the space-time evolution of epicentres in cluster C4 are seen in figure 6.7 (b) to (d). To get a better view of the time evolution, the segment was divided into three zones marked 1, 2 and 3. Epicentres migrated from the southwest (zone 1) to the northeast (zone 3), suggesting that this was the direction of the rupture in this segment of the fault. The stress released by the shocks in zone 1 at the beginning of the process probably increased the local stress in the close vicinity and this led to a complicated stress rearrangement along the rest of the segment. Four events with magnitude above 2.9 were found in the outermost zones 1 and 3 and are identified by large circles in the sequence of figure 6.7. Whilst it is possible to correlate the two major events with the initial clustering in zone 1, the same is not clear for the two other major events in zone 3. It seems that zone 2 has been generated as a consequence of all four events because this cluster (C4) contains the largest number of aftershocks and is the most persistent.

### 6.2.2 Fault plane solutions in the south segment

Normally, fault plane solutions are determined for individual earthquakes using the polarity of first P motions at all stations. In the case of sparse polarity data, when due to lack of a sufficiently large number of well-distributed P first motion data it is not possible to derive the source mechanism of single events, readings from a number of earthquakes in the region or from an earthquake sequence are combined to allow a composite solution (Mendiguren, 1980).

Projection of hypocentres in figures 6.1 (a) and (c) show that the two major clusters C4 and C8 form near *en echelon* fault planes with almost the same strike as the Samambaia fault. They constitute a left step or antidilational jog. In their close vicinity small clusters show a complicated pattern of secondary faulting. The trend of hypocentres in clusters C1, C2, C3 and C7 show a tendency to align towards the northwest (figure 6.1a), roughly perpendicular to the strike of the Samambaia fault, but the trend of cluster C6 is nearly parallel to it. Other more distant clusters from the junction of C4 and C8 tend to align parallel (C5 and C11) or in the east-west direction (C9 and C10). This visual examination of the clusters was used as a constraint to decide which nodal plane would be the fault plane in the plot of the fault plane solution for each cluster.

Detailed analysis of the stress distribution near *en echelon* faults for right and left stepping cracks was done by Segall and Pollard (1980). Their results are not entirely appropriate to the conditions presented by the Samambaia fault because

## Chapter 6

their results were based upon a specific model. The inferred T-axis for the Samambaia fault (see table 2.2) lies roughly east-west, making an angle of  $45^\circ$  with the trend of the Samambaia fault. This value is slightly different from the corresponding  $60^\circ$  angle in figure 4.2a and the planes of the clusters C4 and C8, show a small tendency to overplot. This is different from the non-overlapping condition of figure 4.2a. As a consequence, different shear contours would be anticipated in the region between the junction of clusters C4 and C8 and only a qualitative explanation can be made of the understanding of the secondary faulting seen in figure 6.1a.

Shear fracture must occur in a direction  $45^\circ$  relative to the maximum compressive stress in regions where shear failure conditions are satisfied. Clusters C3 and C7 (figure 6.1a) are the most likely to be located in that region and their direction of faulting agrees with the hypothesis of Segall & Pollard (1980). Composite fault plane solutions for the clusters C3 and C7 are shown in figure 6.8. Only ten small events (maximum magnitude  $m_b = 1.87$ ) are found in cluster C3 and all were used in the plot of the polarities, although some of them had emergent P-wave first motions. This means that the fault solutions inferred from the plot are not as reliable as those found for the cluster C4 where only selected impulsive first motions were used.

Because a visual procedure was used to plot the nodal planes, it is difficult to evaluate the precision of the solutions. So, a quality factor was used in the plots of fault mechanism in figure 6.8 which depends on the visual estimation of the error in the determination of the nodal planes. Quality A, B and C was given to the estimated errors in the fault parameters of  $\pm 10^\circ$ ,  $\pm 20^\circ$  and  $\pm 30^\circ$  respectively. These errors roughly indicate the range in which other possible fault plane solutions can be found. For example, quality A was attributed to the fault plane solution of cluster 4 because as a consequence of the large number of events, it was possible to select a sample of them with clear impulsive P first motion. Fault plane solutions with quality A are considered well-constrained, quality C is credited to unreliable fault plane solutions derived from poor quality samples in which the majority of P-wave first motion polarities are emergent. Solutions with quality B lie in between and result from data in which the majority but not all of P-wave first motions are impulsive.

In following the above classification, the composite fault plane solution of events in clusters C3 and C7 (figure 6.8) are qualified as B and C respectively and the fault plane for both clusters was chosen as the northwest trending nodal plane, in accordance with the trend shown in the epicentral map of figure 6.1(a). The fault strikes determined for the clusters C3 and C7 are almost perpendicular to the strike

## Chapter 6

of the Samambaia fault and the mechanisms are right lateral strike slip with a normal component in the case of cluster C3. These results are compatible with secondary fracturing in the region between near *en echelon* discontinuities according to the hypothesis of Segall and Pollard (1980). From the histograms of figures 6.2 and 6.3 it can be seen that activity in the south started in June 87 in cluster C4. It can be presumed that the rearrangement of stress in the surrounding area was responsible for the creation of clusters C3 and C7, but the idea that this stress was originated after the complete destressing of the left stepping cracks C4 and C8 is not correct. In fact, although the peak of activity in cluster C4 happened during June 87 (figure 6.2), activity in cluster C8, which is the second major cluster in the south segment, started at the same time but the peak only occurred in January 88. With the exception of activity in cluster C6 (the third major cluster), the rest of the clusters show their peak in the period between June 87 and January 88 (figures 6.3 and 6.4). As the clusters C3 and C7 lie in the region between C4 and C8, it is possible to interpret the creation of the former clusters as a consequence of stress increase in the region between the left stepping cracks during the slip transfer from cluster C4 to cluster C8. That is, it seems that with time the shear failure condition migrated from cluster C4 in the direction of cluster C8 expanding the aftershock zone.

It can be seen that the scheme for secondary fracturing of Segall & Pollard (1980) in figure 4.2(b), approximately satisfies the condition for the shear failure in cluster C3 and C7, but the same scheme cannot explain the additional C1, C2 and other more distant clusters. This suggests a more complex mode of shear failure than the model presented by those authors, although an apparently more broad zone was previewed by Sibson (1986) for these subsidiary fracturing regions which he called "distributed crushing zones". In choosing the northwest as the direction of the fault plane for clusters C3 and C7, it can be seen from figure 6.8 that predominant left lateral strike slip faults were formed in that region, for cracks striking in the northwest direction, in accordance with Segall & Pollard (1980) (figure 4.2) and Sibson (1986). Although the latter author suggests some minor thrusting component, a small normal, not thrust, component was found in the fault mechanism of events in cluster C3, and the fault mechanism of events in cluster C7 is not reliable enough to verify that hypothesis. Interpreting the fault offset between clusters C4 and C8 as a fault bend, clusters C3 and C7 are consistent with the hypothesis of a third direction of faulting of King & Yielding (1984) discussed in section 4.2.1. In any case, except for clusters C3 and C7, and maybe C2, the remaining clusters cannot be explained as a consequence of shear stress increase due the fault jog formed by clusters C4 and C8.

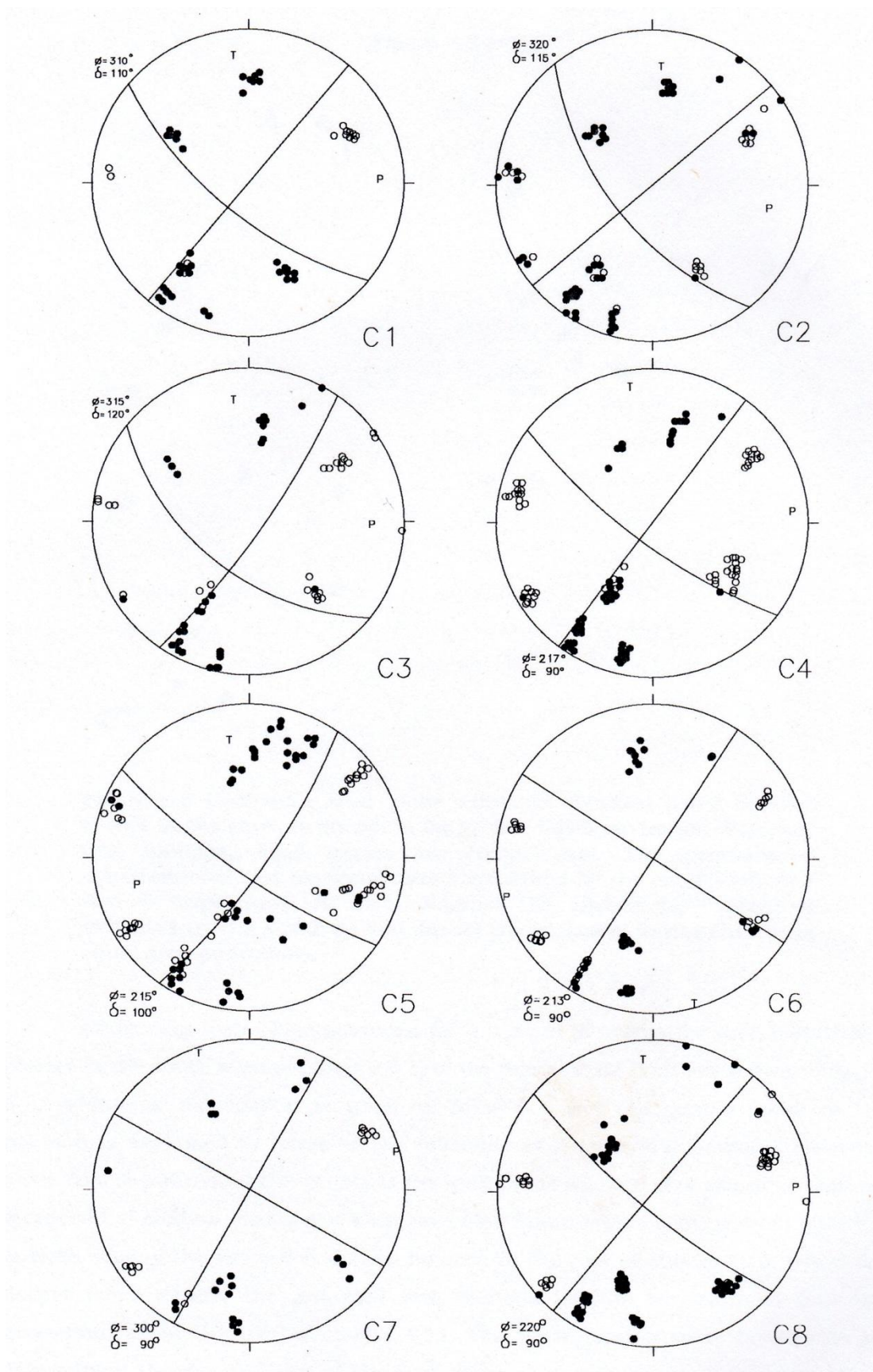


(Figure 6.8 continued on next page)

(Figure 6.8 cont.)

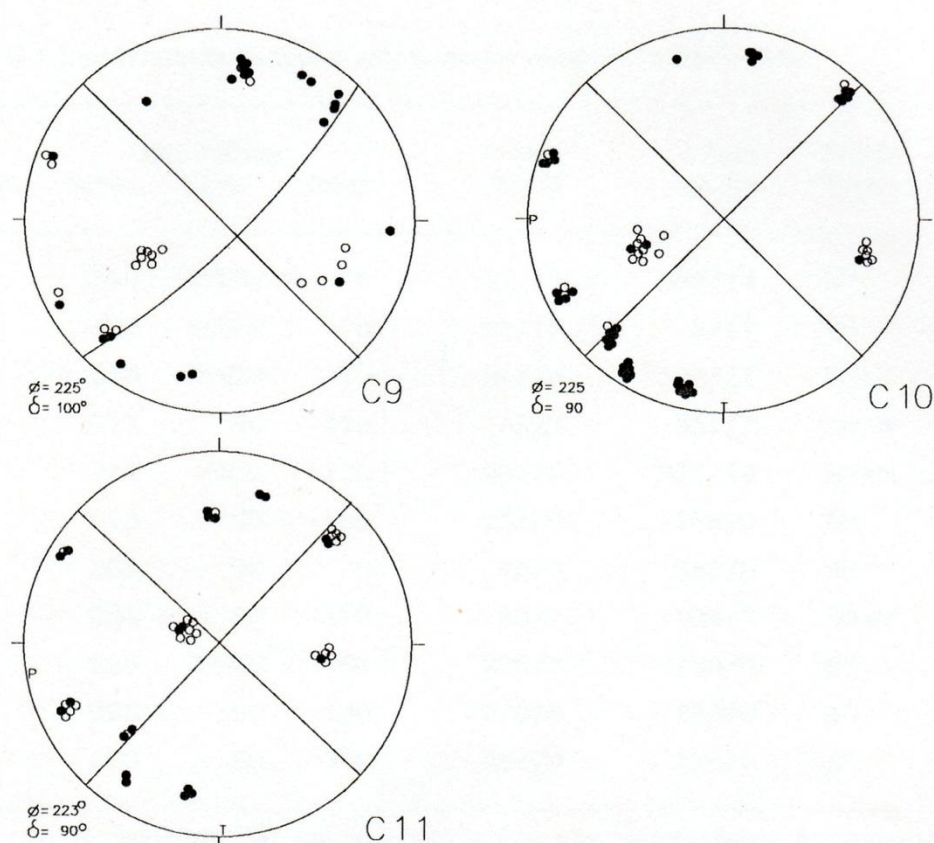


Figure 6.8 Composite fault plane solutions obtained using selected events in the clusters shown in figure 6.1. Open circles are dilational first motions, filled circles are compression. The positions of compressional and tensional axes are marked by the capital letters P and T respectively. In each diagram the chosen fault plane is indicated by the strike ( $\phi$ ) and dip ( $\delta$ ) labels. Lower focal hemisphere equal area projections.

Composite fault plane solutions for a sample of events for each identifiable cluster in the south segment (figure 6.1) of the Samambaia fault are shown in figure 6.8. Additional information is given in Table 6.1 and the quality factor of the solution is explained in terms of the reliability of P-wave first motions. However, other factors influenced the quality of the fault plane solution. For example, clusters composed of shallow events give their projected first motions concentrated near the outside edge of the projection as can be seen in the plot of cluster C10, whilst for deeper focus events, the projected first motions tend to be scattered over the projection, as in the plot of cluster C11. The latter case is more favourable for determining the dip and slip of the fault plane than the former. In the particular example of plot C11, the quality given was the same as that given to C10 because

## Chapter 6

there are more inconsistencies due to ambiguous polarity readings in some poorly defined P-wave first motions.

Table 6.1 Composite fault plane solutions for clusters in figure 6.8.

Cluster	Fault Plane			P Axis Az/Pl	T Axis Az/Pl	Mech. Type	Quality
	Strike	Dip	Rake				
C1	310	70SW	0	87/14	353/14	SS	B
C2	320	65SW	0	98/17	2/17	SS	B
C3	315	60SW	-10	91/14	353/27	SS+N	B
C4	217	90	-170	82/7	351/7	SS+N	A
C5	215	80SE	-170	261/0	351/14	SS+N	B
C6	213	90	-180	258/0	168/0	SS	B
C7	300	90	0	75/0	345/0	SS	C
C8	220	90	-170	85/7	355/7	SS+N	A
C9	225	80SE	-180	270/7	180/0	SS	C
C10	225	90	-180	270/0	180/0	SS	C
C11	223	90	-180	268/0	178/0	SS	C

Az is azimuth; Pl, plunge; SS, strike-slip mechanism; N, normal; SS+N, strike-slip with normal component. All angles in degrees according to the conventions of Aki & Richards (1980).

Reliable composite fault mechanisms with quality A in Table 6.1 show strike-slip with a small normal component as the main faulting mechanism. Although less reliable, the results from other clusters reveal the same basic mechanism. For clusters with epicentres trending in the SW-NE direction, the faulting direction is right lateral, and it is left lateral for clusters in the SE-NW direction.

One of the common features in the diagrams of figure 6.8 is that the direction of the compression axis P is E-W. As this coincides with the compression direction for the entire fault determined by Ferreira et al. (1987), it can be concluded that the local stress rearrangement responsible for the aftershocks in the small clusters of the south segment of the Samambaia fault lies in the same E-W direction or is insignificant if in another direction. If clusters C1, C2, C3 and C7 strike towards the northwest direction, this implies a complex secondary fracturing process in the south segment of the Samambaia fault because the clusters must belong to different fault planes. In this case it is likely that only clusters C9, C10



and C11 belong to a common fault plane as can be seen in the epicentral map of figure 6.1.

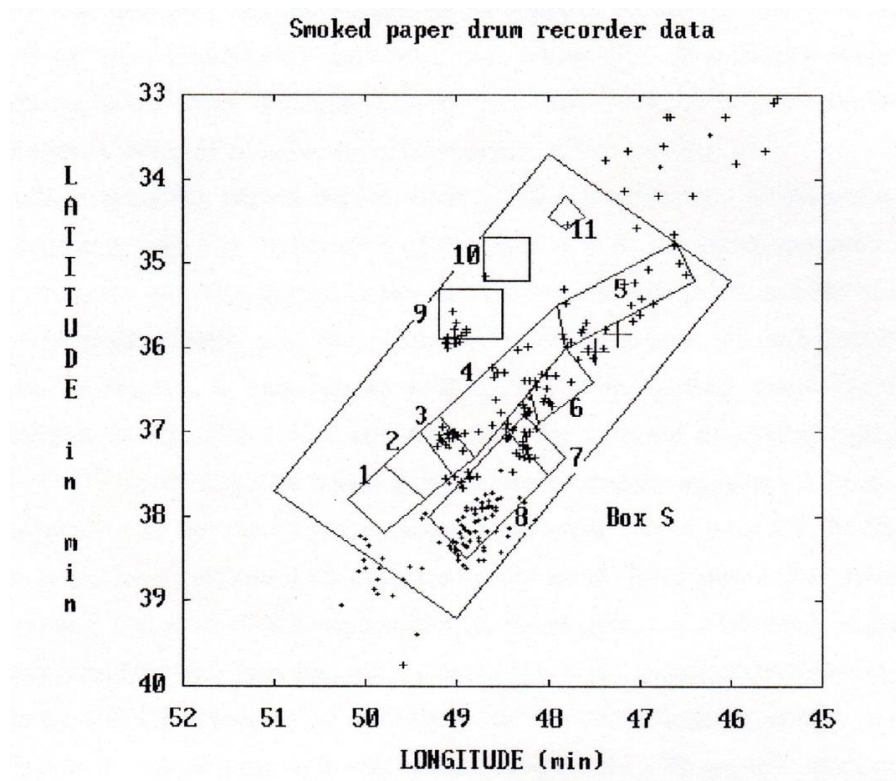


Figure 6.9 Overplot of epicentres in the south segment of the Samambaia fault recorded by the smoked paper drum recorder network for two different periods. Larger crosses are a sample of events recorded during January 87. The two largest crosses represent the two  $m_b = 3.7$  (see Table 2.4) earthquakes which occurred at 7th Jan 87. Small crosses represent epicentres of events recorded after July 88. Numbered boxes are the same as those in figure 6.1 and were drawn to facilitate the comparison between epicentres determined by drum recorder and telemetered networks.

In order to get additional information about the secondary fracturing in the south segment, relocated events recorded by the smoked paper drum recorders from other periods of time were plotted in the epicentral map of figure 6.9. In the figure, box S marks the limits of the activity in the south region recorded by the telemetric network and small boxes numbered 1 to 11 indicate the localities of the clusters identified by the telemetric network data whose epicentres were omitted for clarity.

In the period after April 1988, three small bursts of activity were detected by the drum recorder network. The first burst occurred between August and December 88 and the epicentres were located inside box 8 of figure 6.9, which shows that this burst is a continuation of activity in the cluster C8, whose peak of activity occurred on January 88 as discussed before. The second burst happened on March 1990 around the south boundary of box S in figure 6.9 and the third occurred on September 1990 further to the south in the cluster outside box S of the same figure.



## Chapter 6

Epicentres from this period are represented by small crosses in this figure. As can be seen, the last two bursts happened in regions where no previous activity was detected by the telemetered network, and show that aftershocks were migrating southwards in the form of small clusters probably confined to different fault planes. This confirms the idea of secondary fracturing in the region.

Regarding the period before June 1987, an important activity started in the south segment with the occurrence of two events with the same magnitude  $m_b = 3.7$  on 7th January 87. The period between 7th Jan 87 and 24th Jan 87 was analysed by Takeya et al, (1989) and the period between 25th Jan 87 and 7th Feb 87 was analysed by Sophia & Assumpção (1989). The best located events in that period were plotted in figure 6.9 and are indicated by crosses to distinguish them from events of other periods. The trend of epicentres broadly suggests a fault plane that is an extension to the north of the plane containing the cluster C6. In this case, C5 and C6 must be interpreted as clusters in the same fault plane that have the same strike cluster C6, and is almost parallel to the cluster C4. This fault segment would be responsible for the two  $m_b = 3.7$  events marked by larger crosses in figure 6.9, and the cluster C6 recorded by the telemetric network must be interpreted as a later reactivation in this segment. It seems that this is the only modification necessary to the structure of the south region in order to accommodate all the data. So, if the interpretation of the drum recorder data is correct, the south region of the Samambaia fault is composed of three major, almost parallel, fault segments: the first one encloses cluster C6; the second encloses C4, and the third encloses cluster C8. But as discussed in section 4.5.2 there is a possibility that the first and third segments are not continuous segments but are divided as shown in the sketch of figure 4.14.

Clusters derived from the drum recorder data confined to boxes 3, 9 and 7 indicate that reactivation can take place in some clusters whilst other clusters such as C1, C2 and C10 show that stress is released in a short period of time in a way that is not observed in other periods of reactivation. This seems to be the case for cluster C4 because relatively few events from the drum recorder data are located in this cluster. Another important feature that is preserved is the location of the gap discussed in section 4.5 and shown in figure 5.4.

### 6.3 Clustering effects in the north segment

The north segment of the Samambaia fault is the region where the majority of aftershocks above magnitude  $m_b = 4.0$  occurred as described in section 2.1.1. Unlike in the south segment, hypocentres locations from the north segment show an

apparently well-defined single fault plane. Events are deeper than in any other part of the fault but are limited to a maximum depth of 9 km. Those features can be seen from the epicentral map of figure 6.10 and from the projection of hypocentres onto a vertical plane perpendicular to the strike of the fault as shown in figure 4.10 (section N) in a comparative view with the south segment.

### 6.3.1 Some characteristics of the north segment

Although a single, well defined, fault plane can be inferred for the north segment of the fault, hypocentres projected onto a vertical plane along the fault strike (figure 4.8b) show that events are preferentially located in several patches. As discussed in section 5.3, according to the hypothesis of Eaton et al., (1970) or the barrier model of Das & Aki (1977), clustering of events is a consequence of heterogeneities (barriers) in the fault plane. Barriers can result from changes in the fault geometry or change in rock properties (Aki, 1979). So, it is possible that in a small length scale, the north segment of the fault plane (smooth on a large scale) presents some roughness in the faulting surfaces.

Before identifying and analysing the clusters as for the south segment, epicentres of the north segment were divided into four sections as shown in figure 6.10, and hypocentres of each section were projected onto a vertical plane perpendicular to the fault strike (figure 6.11) in order to verify any small fault offset or variation in the orientation of the fault plane. In general, the projections show a single well defined fault plane dipping  $76^\circ$  NW as indicated by the heavy lines in sections S1 and S2 of figure 6.11. A close examination suggests that the deepest hypocentres in sections S2 and S4 show a tendency to dip more steeply than the intermediate and shallow hypocentres. A small off-fault cluster was located in the sectional projection S2 at a depth of 2 km.

To investigate possible patterns in the time evolution of the clusters, hypocentres were projected onto a cross section along the fault strike according to their time of occurrence, as shown in figure 6.12. No clear pattern in the way events migrate from one cluster to another was detected. However, it was noted that bursts of activity in general initiate in the deepest well-defined clusters and are accompanied by intermediate and shallow aftershocks in more diffuse clusters. The pattern seems to be a consequence of the fact that major aftershocks of the sequence are in general located in the deepest clusters as shown in figure 6.13. In particular, events with magnitude above  $m_b = 2.9$  are found close to the base of the corresponding cluster. This exhibits a similar pattern to the aftershocks of the south

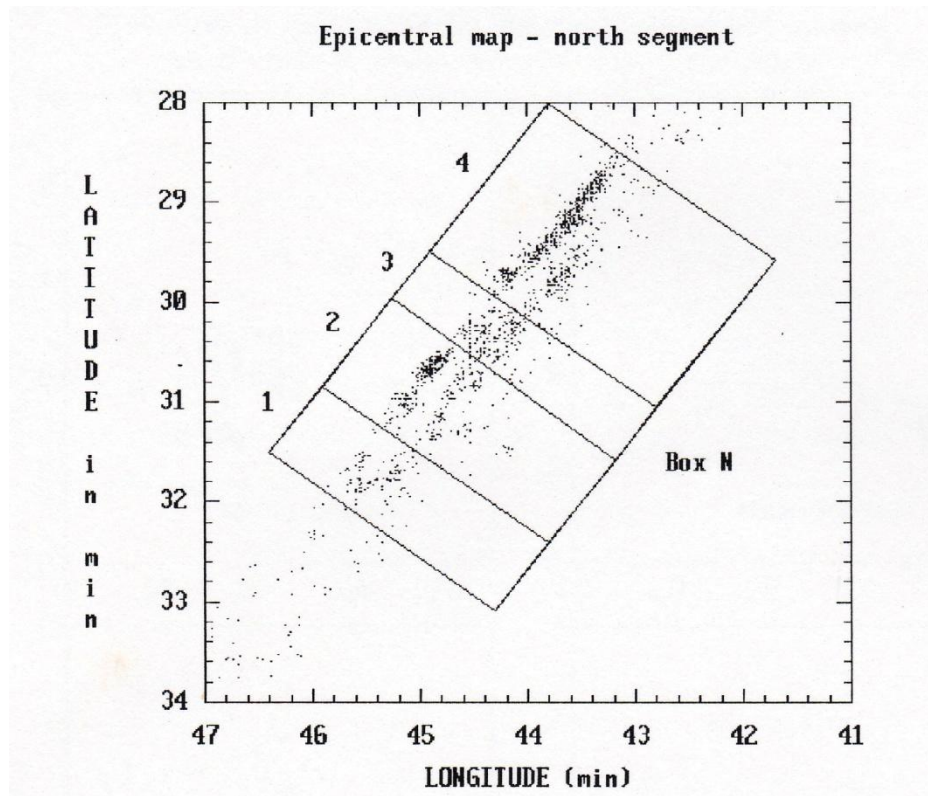


Figure 6.10 Epicentral map of events inside box N (north segment) as defined in fig. 4.6. The region was divided into four sections identified by numbers from 1 to 4. The alignment of some epicentres in this figure is an artifact as explained in section 4.4.

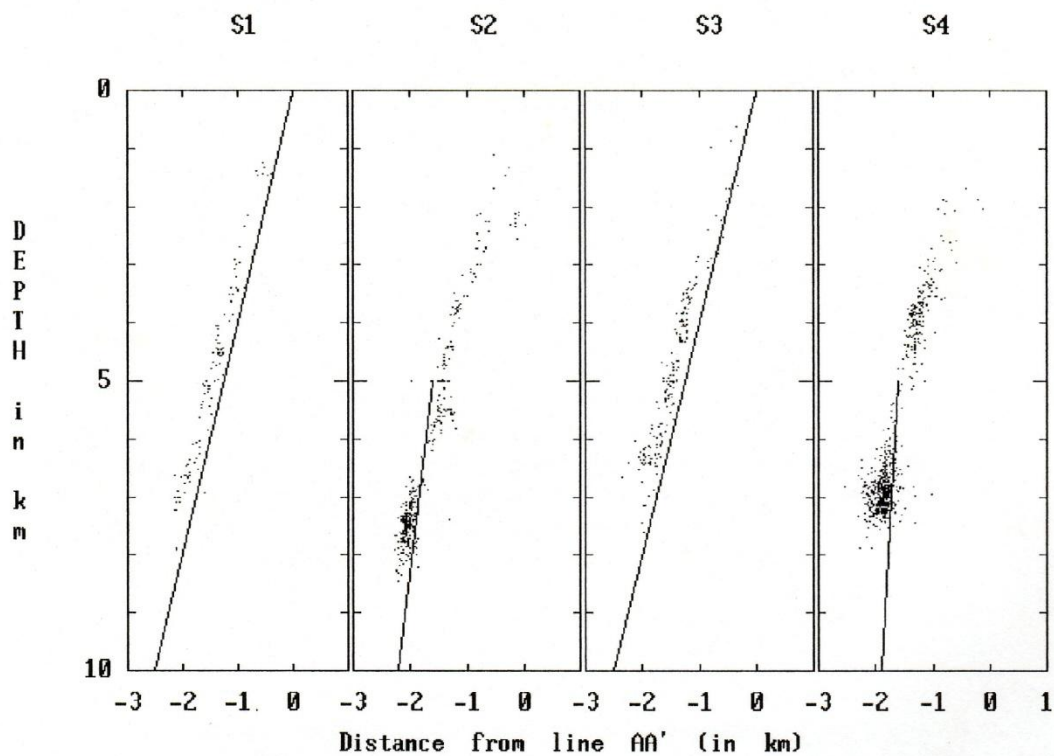


Figure 6.11 Sectional projections of hypocentres of the north segment onto vertical planes perpendicular to the strike AA'.

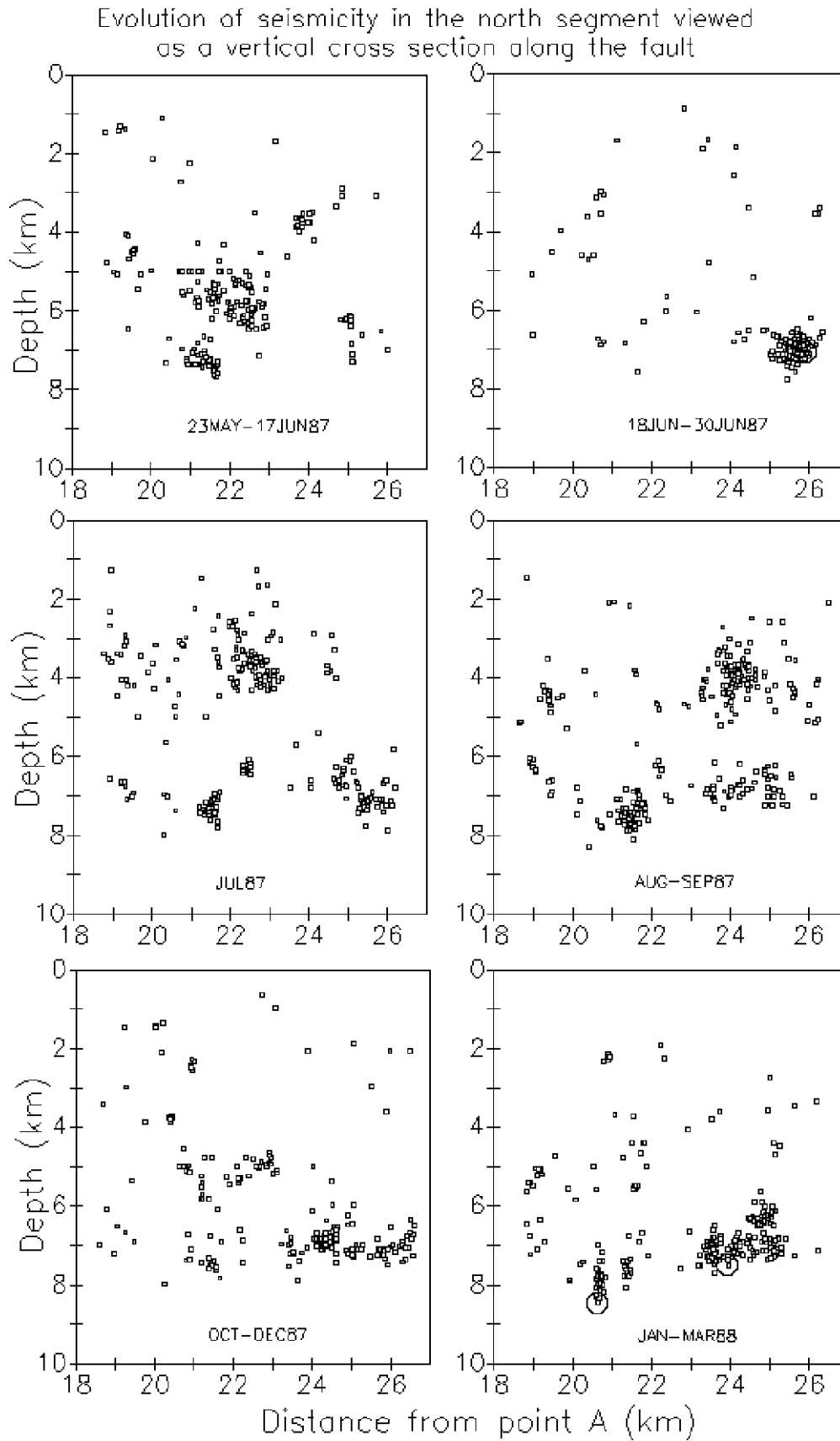


Figure 6.12 Projection of hypocentres onto a vertical section along the strike of the fault. Events were divided into groups according to their time of occurrence. Events in the projection are those shown in the epicentral map of figure 6.10. Larger circles denote events larger than  $m_b = 2.9$ .

## Chapter 6

segment of the Samambaia fault and probably corresponds to the observation of Das & Scholz (1983) about the tendency of larger events to nucleate at the base of the seismogenic layer.

Regarding the events above  $m_b = 2.5$ , the same figure 6.13 shows that those events are not only concentrated at the bottom of the fault plane but also tend to concentrate in the north part of that segment. That is, events above  $m_b = 2.5$  become scarce towards the "gap", which was considered to be a region left with no slip deficit after the event of  $m_b = 5.1$ , while events are more frequent on the opposite side, close to the place where the second major event of  $m_b = 5.0$  probably occurred on 10th March 89.

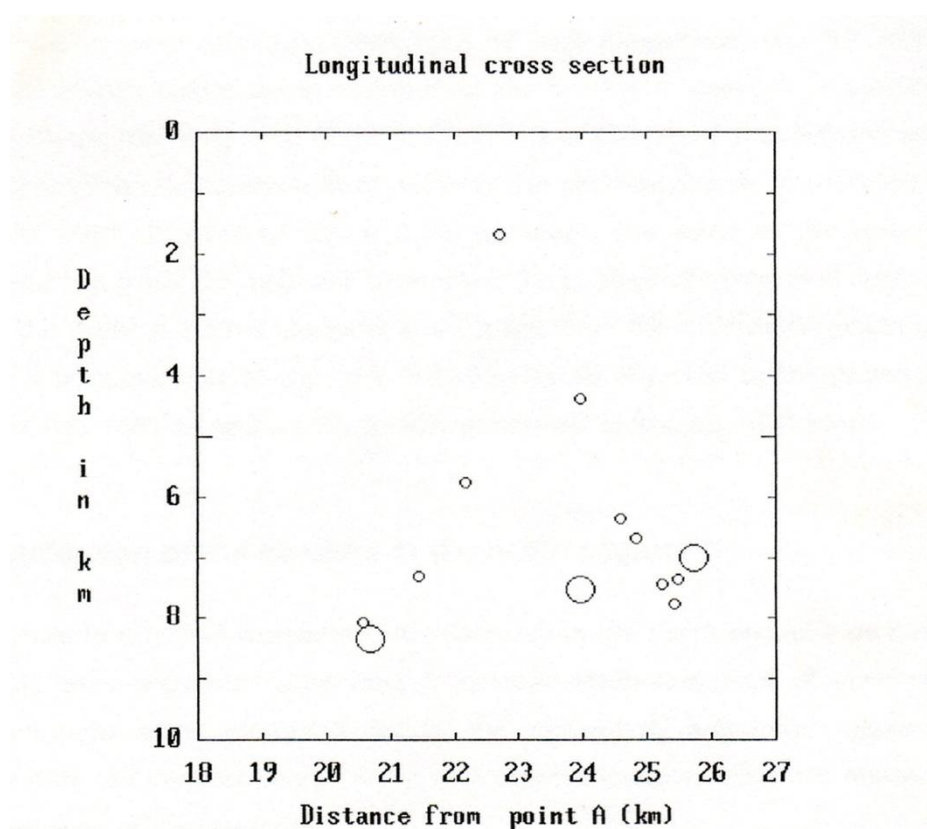


Figure 6.13 Vertical cross section along the fault strike showing the projections of events with magnitude between  $m_b = 2.5$  and  $m_b = 3.1$ . Larger circles denote events above  $m_b = 2.9$ .

It was seen in previous sections that about 450 events, or 45% of the total in the south segment, occurred during the period between 18th and 30th June 1987 which indicates a large concentration of activity in a few days. During the period between 23rd May and 17th June 1987, that is, in the first three recording weeks of the telemetric network, only 50 events were recorded in the same segment. The activity in the north segment is more uniformly distributed in time. This

## Chapter 6

characteristic can be seen in the plots of figure 6.12 although each diagram does not correspond to the same period of time. In particular, in the period of 23rd May to 17th June 1987, when activity in the south was at a minimum, 213 events were recorded in the north segment, which corresponds to the most active period in this segment. The last observation suggests that during June 87 epicentres were showing a tendency to migrate from the north to the south part of the fault.

It is interesting to note that no major event was detected by the telemetric network to correlate with the most active period of the north segment. This happened because the network was only installed on 20th May 1987. Only one earthquake of magnitude above  $m_b = 3.5$  is reported in the bulletin of the Brazilian Geophysical Society for the period between 08th Feb 1987 and 27th Jun 1988 (see table 2.4). This event occurred on 28th April 87 with magnitude  $m_b = 3.6$ , that is, less than one month before the installation of the telemetric network. According to the same bulletin, the epicentre ( $5.53^\circ\text{S}$ ,  $35.75^\circ\text{W}$ ) of the event was located in the north segment of the Samambaia fault, close to the clusters shown in the 23rd May to 17th Jun 1987 diagram of figure 6.12. Although the error in the epicentral location resulting from the regional network is large (typical error is 5 km), it is likely that the event occurred no more than 2 km from the calculated position, in which case it is reasonable to consider the aftershocks observed in the period 23rd May to 17th Jun 1987 as part of the activity generated by the  $m_b = 3.6$  event.

### 6.3.2 Identification of the clusters in the north segment

In order to examine the pattern of seismicity in the north segment on a small scale, events were separated according to their location and time of occurrence. That is, clusters were identified using the epicentral map and hypocentre projections onto the vertical planes along and perpendicular to the fault strike, and the time evolution of those events.

Due to the large scale simplicity of the north segment of the Samambaia fault (see figure 6.11), all the selected clusters can be seen in the vertical cross section along the fault of figure 6.14. Clusters are identified by codes as for the south segment. The small and shallow cluster C13 is the only clear cluster that lies off the main fault plane and it was identified by a combined examination with figure 6.11. Clusters C13 to C16 represent shallow events; cluster C17 represents intermediate depth events and clusters C18 to C23 represent the deepest events.

The number of events per month for each identified cluster is shown in the series of histograms in figure 6.15. As can be seen, June was the most active period in the north segment during the period of study. After comparing the diagrams of

## Chapter 6

23rd May to 17th Jun 1987 in figure 6.12 and figure 6.14 it can be seen that cluster C20 is the most probable locality for the event of  $m_b = 3.6$ , and that its aftershocks migrate upwards forming the cluster C17, which must justify the peak of activity in the histogram of C17. Another significant peak in June is found in cluster C23 which suggests a relationship with the  $m_b = 3.6$  earthquake, but the plot of 17th Jun to 30th Jun 1987 in figure 6.12 shows that activity in C23 started at the end of June and is related to the aftershocks that followed the event of  $m_b = 3.0$  on 22nd Jun 1987 (see Table 5.1).

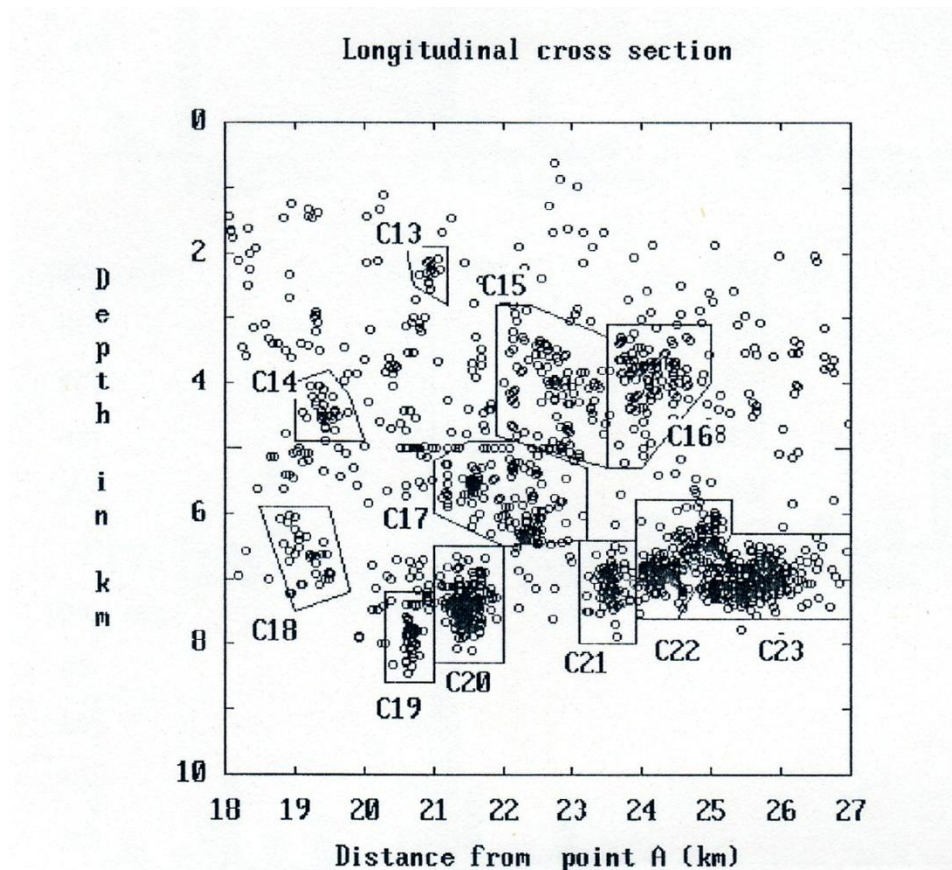


Figure 6.14 Identification of clusters in the north segment of the Samambaia fault shown on a hypocentre projection onto a vertical cross section along the fault. The alignment of some epicentres at 5km depth is an artifact as explained in section 4.4.

## Chapter 6

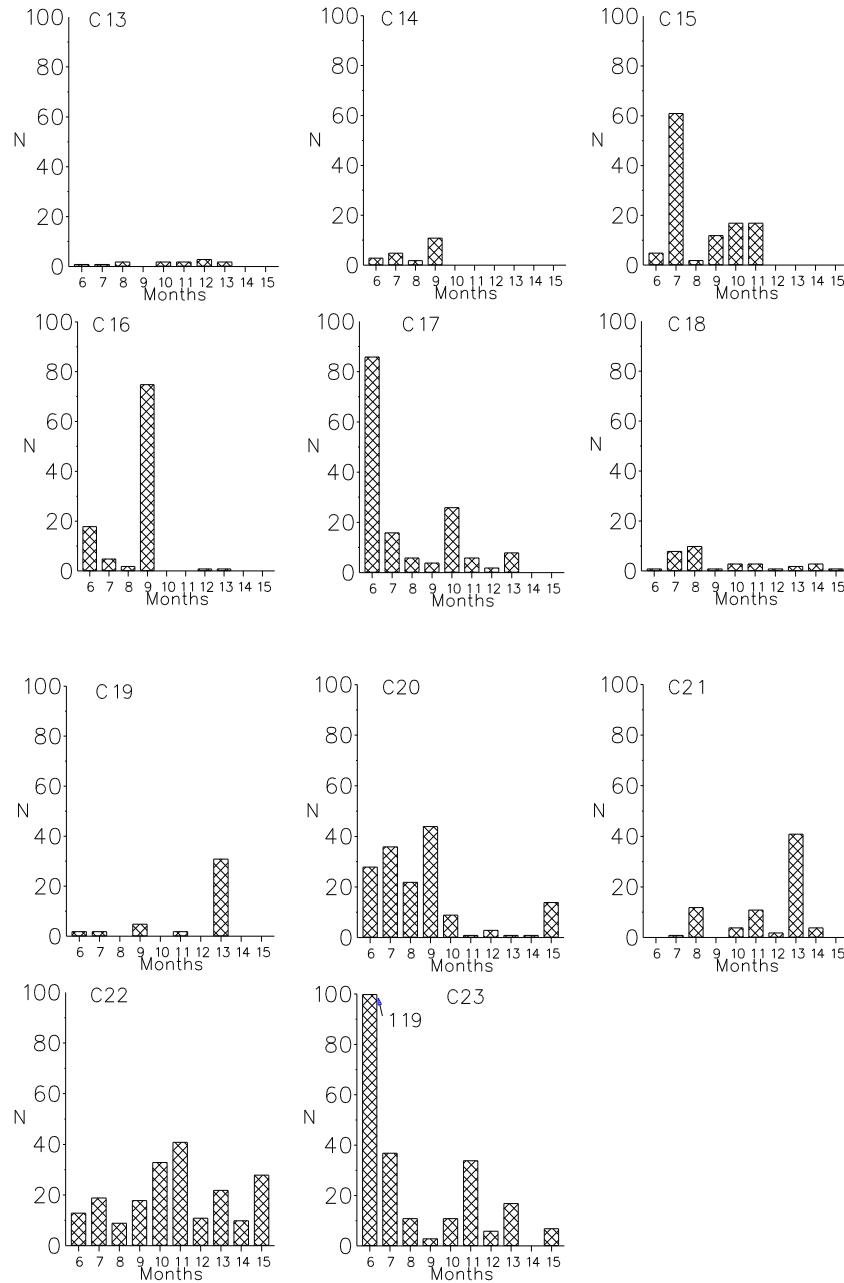


Figure 6.15 Monthly histogram for each cluster in the north segment as defined in figure 6.14.

### 6.3.3 Analysis of the most significant clusters in the north segment

Only clusters which can be linked to a major event ( $m_b$  greater than 2.9) will be analysed.

Cluster C19:

Cluster C19 is one of the most atypical. It is not only sharply defined in space (figure 6.14) but in time (figure 6.15). The majority of the events (31 from the total of 46) in this cluster occurred during January 1988 and of these, 19 occurred



## Chapter 6

before a  $m_b = 2.86$  event on 26th Jan 1988 and five before the event of  $m_b = 2.97$  on 28th Jan 1988. Only seven aftershocks were registered after the main event of this cluster. No events were recorded in February and March. This description of the evolution in time is different from that observed for the clusters in the south segment, where events with similar magnitude were followed by several tens of aftershocks. The  $m_b = 2.97$  event was located at the bottom of the cluster as indicated in the diagram of Jan to Mar 1988 in figure 6.12, which shows a characteristic similar to the major events in the south segment.

Clusters C21 and C22:

The event of  $m_b = 3.07$  that occurred on 9th Jan 1988 was located at the boundary of clusters C21 and C22, at the bottom of these clusters (see figure 6.16). It can be seen from the plot of figure 6.17 that the two clusters under consideration do not share the same fault plane. There is a small but significant fault offset of no more than 300m that can be resolved due to the high resolution of the hypocentre locations. This geometric heterogeneity in the main fault plane confirms the hypothesis of Das & Aki (1977) about the role of geometric barriers as localities of stress concentration responsible for the generation of earthquakes.

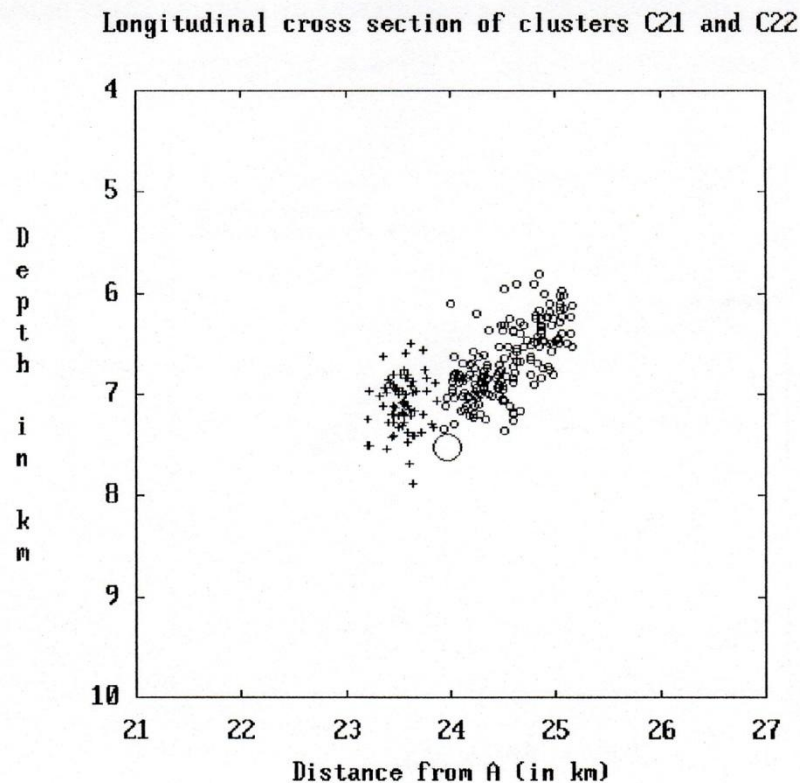


Figure 6.16 Earthquakes of clusters C21 and C22 projected onto the vertical plane along the fault strike. Crosses denote events in cluster C21, circles indicate events in cluster C22, and the large circle represents the  $m_b = 3.07$  event.

## Perpendicular sections of clusters C21, C22 and C23

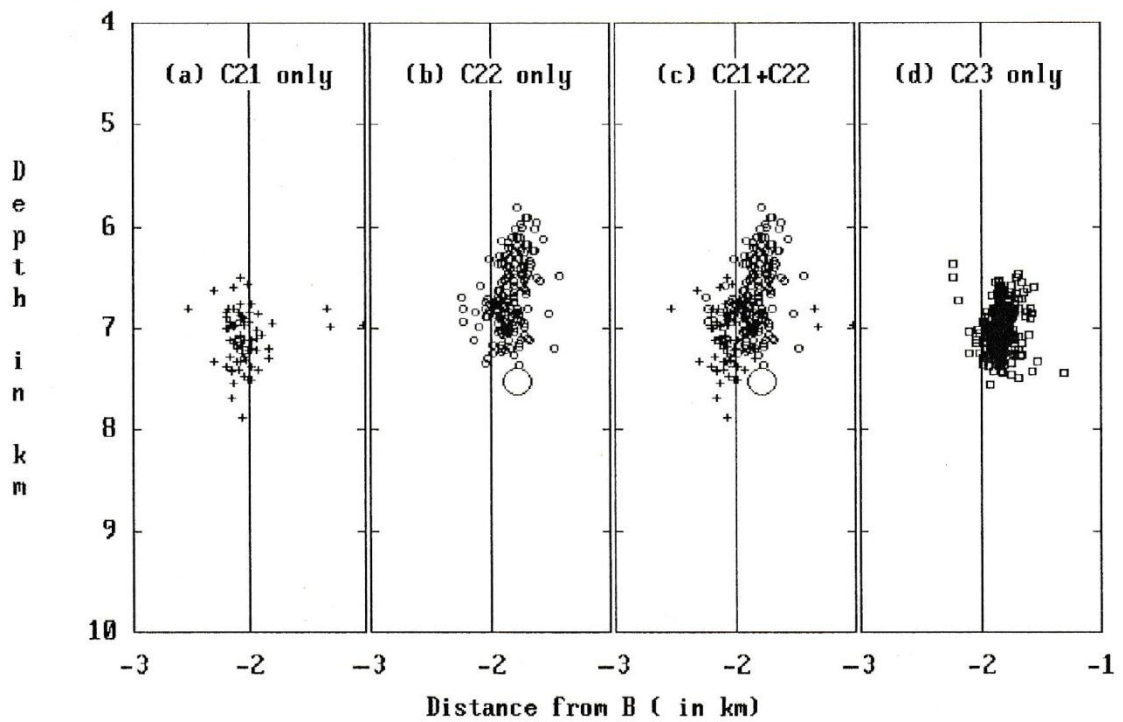


Figure 6.17 Vertical cross sections showing hypocentres of events in clusters C21, C22 and C23 onto planes perpendicular to the fault strike. See fig. 6.16 for further explanation. An auxiliary vertical line was drawn in each plot to facilitate the relative location of the clusters and eventual offset between them.

## Epicentres of events in clusters C21 and C22

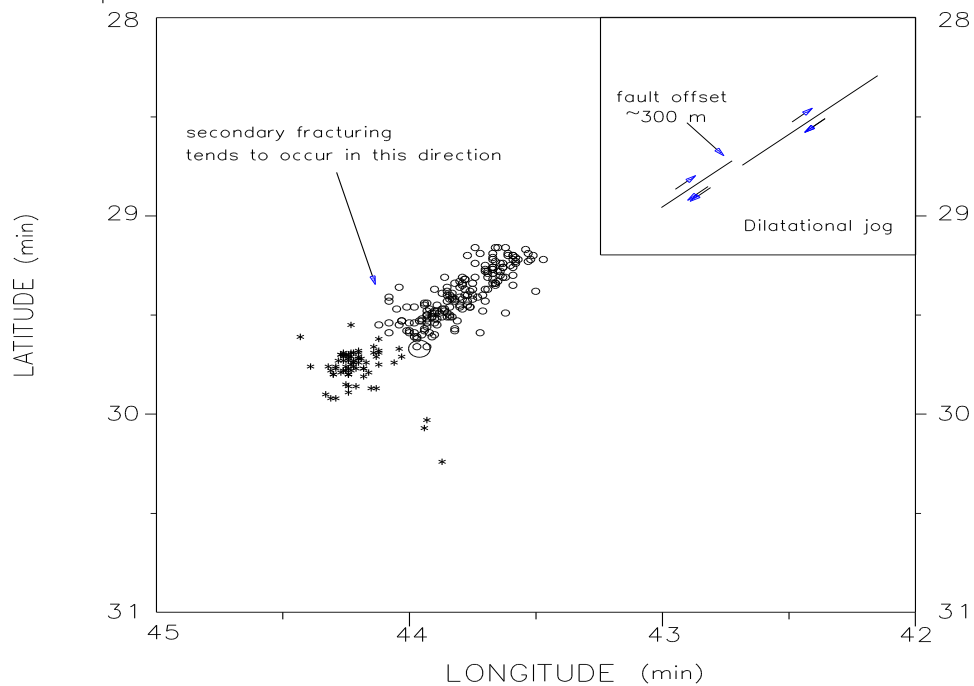


Figure 6.18 Epicentral map of events in figure 6.16. Symbols are the same as in fig. 6.16. The inset shows the interpretation of the clusters as right stepping cracks or dilatational jogs.

## Chapter 6

In considering the high precision (see table Table 5.1) in the location of the  $m_b = 3.07$  event, the close up of the vertical cross sections along and perpendicular to the strike in figures 6.16 and 6.17 show that the  $m_b = 3.07$  event is located in the fault plane of cluster C22, at the boundary with cluster C21. The location of the  $m_b = 3.07$  event in the overlapped region supports the idea that major events tend to occur at fault bends (King & Nabelek, 1985) or, with similar meaning, at fault jogs (Sibson, 1986).

There is an apparent contradiction in the aftershock pattern of clusters C21 and C22 in relation to the  $m_b = 3.07$  event. Although occurring at the boundary of cluster C22, no significant aftershocks were detected in this cluster during January and in the two following months (figure 6.15). On the other hand, the peak of activity during January 88 in the histogram of cluster C21 of figure 6.15 is mostly due to the aftershocks that followed the  $m_b = 3.07$  earthquake. This apparent contradiction can be thought of as a result of the strong mechanical interaction that would be expected to occur at the crack tips due the close proximity between them (Segall & Pollard, 1980). For a dilational jog, with overlapping fault tips, as is the case for the clusters C21 and C22, a tension that reduces the friction will occur at the tip of the inserted crack (C21 in this case). This tension facilitates slip near the end of the inserted crack (Segall & Pollard, 1980). Some of the off-fault hypocentres can be seen in figure 6.17. This idea is consistent with the hypothesis of secondary fracturing due to the state of stress near *en echelon* cracks. As can be seen, the consequences of small irregularities in the main fault plane can be described in terms of fault jogs which are normally used in the analysis of larger fault segments (Sibson, 1986). This supports the statement that fault discontinuities are a fundamental feature of faults and are independent of length scale (Segall & Pollard, 1980).

It can be seen in figure 6.17 that the hypocentres of events in clusters C21 and C22 tend to dip more steeply (almost  $90^\circ$ ) than the events in the overall north fault segment (dipping about  $76^\circ$  in figure 6.11). This constitutes an additional irregularity in the main fault plane which can modify the local stress. The location of the  $m_b = 3.07$  event is consistent with the location of a major event in the south segment; that is, at the bottom of the cluster close to the cluster tip in a region of relatively small number of events (figure 6.16). Considering clusters C21 and C22 as a whole, only forty aftershocks occurred in the period of one month after the  $m_b = 3.07$  event which is one tenth of the number of aftershocks that followed the  $m_b = 3.10$  event of 18th Jun 1987 in the south segment (see histogram of figure 6.2).

## Chapter 6

### Cluster C23:

The major event in this cluster was a magnitude  $m_b = 2.98$  which occurred on 22nd Jun 1987. Activity recorded by the telemetric network started on 10th Jun 1987 and the histogram of figure 6.15 shows that 119 events occurred during June. From this total, 66 happened before the major event in this cluster and 52 after it. During July, 37 more aftershocks were recorded. The number of aftershocks in this cluster is more closely related to the events with similar magnitude in the south segment but the number of foreshocks is higher. The main event hypocentre was located close to but not at the bottom of the cluster and the epicentral map shows it close to the crack tip.

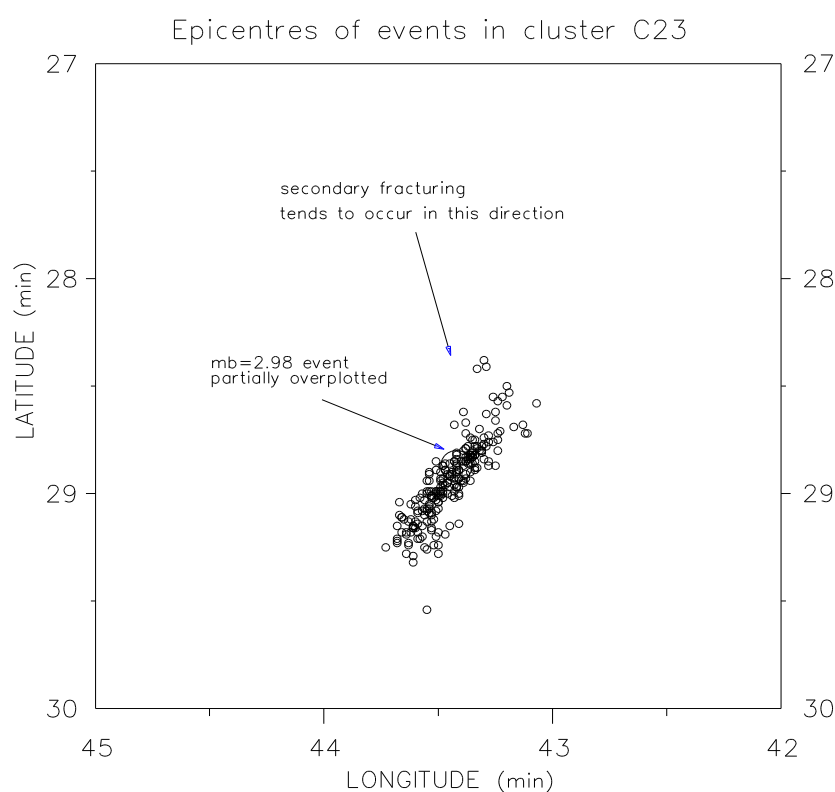


Figure 6.19 Epicentral map of events in cluster C23. The position of this cluster in relation to the north segment is shown in figure 6.14.

Cluster C23 is located at the end of the north segment. In the region to the north of this cluster, a fault bend was found (see figure 4.3) and the region was considered the probable site of the  $m_b = 5.0$  shock of 10th Mar 1989. Therefore, according to the interpretation of King & Nabelek (1985) about the role of fault bends in a fault, the region that encloses the cluster C23 (or fault tip) can be considered a region left with a slip deficit after the occurrence of the  $m_b = 5.1$  shock of 30th Nov 1986. So, major aftershocks such as the two events with  $m_b = 4.0$  and

$m_b = 3.9$  that happened during February 87 (Takeya et al., 1989) are consistent with the hypothesis of those authors, since the events were located in this region (see figure 4.15), probably in the cluster C23. The relatively high number of events prior to the  $m_b = 2.98$  event of 23rd Jun 1987 could be an aftershock sequence that followed a similar magnitude event which occurred in this cluster before the installation of the telemetric network. Indirect evidence of the fault bend can be found in cluster C23 from some off fault activity shown in figure 6.19. Probably these events are associated with other off-fault events in this area found at different depths (see events indicated by line 3 in figure 4.3) or found at different periods in other studies (Sophia & Assumpção, 1989; Ferreira et al., 1987).

### 6.3.4 Clusters and main fault heterogeneities

It can be seen in figure 6.17 that clusters C22 and C23 must be located in the same fault plane, since no geometric irregularity was found to correlate with the two clusters. In this case, it is possible that some irregularity exists that cannot be resolved by the present dataset. Another possibility is to attribute the clustering effect to change in the rock properties (inhomogeneous barrier). In any case, due to the limitations in determining the cause of the clusters by the present methods, it will be stated that clusters C22 and C23 share the same fault plane.

In an attempt to delineate other geometric irregularities in the main fault plane in order to explain the general clustering pattern of the north segment, hypocentres of events in the deepest clusters were projected onto a vertical plane perpendicular to the average fault strike. The analysis of these projections is summarized in figure 6.20, which shows the clusters C19, C20 and C21 in the same plane, forming a dilational jog with the plane containing clusters C22 and C23. The step between these two planes is no more than 300m. Although small, the existence of this transition is supported by the typical third direction of faulting indicated by the line 4 in figure 4.3 using the more complete dataset 4. The projection of events in cluster C18 show that the plane is dipping less steeply (about  $68^\circ$ ) although this tendency cannot be extended downwards because no events below this cluster were recorded. Support for the existence of some fault irregularity in the region between clusters C18 and C19 is given by cluster C13 which is the only clear cluster off the main fault plane that could be identified in figure 6.11; this probably indicates a local stress increase due a geometric irregularity.

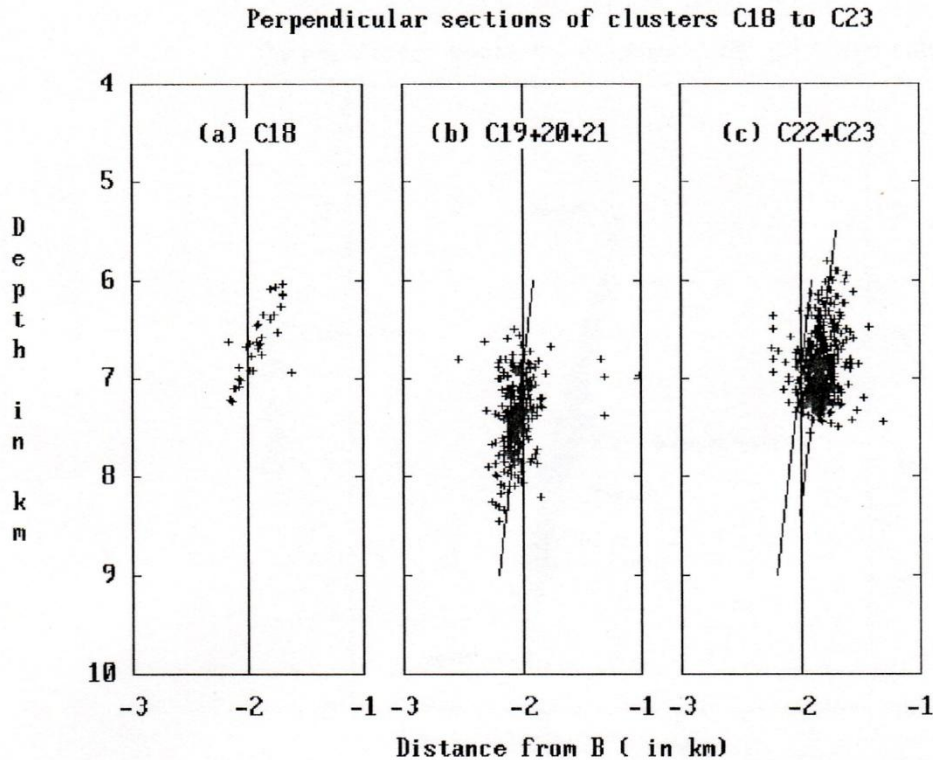


Figure 6.20 Vertical cross sections perpendicular to the strike. Auxiliary vertical lines are drawn to emphasize the identification of a small fault offset. (a) Events in cluster C18. (b) Events in clusters C19, C20 and C21 appear to lie in the same plane. The oblique line represents the dip of the plane. (c) Events in clusters C22 and C23. The two oblique lines show the small offset between the plane containing the clusters C19, C20 and C21 and the plane containing the clusters C22 and C23.

An examination was made of the perpendicular cross sections of the three clusters (C15, C17 and C20) which are located in the same almost vertical plane, forming a continuous sequence of events relative to the depth as can be seen in figure 6.15. The perpendicular cross section of these clusters (figure 6.21) indicates that they are in different planes forming a zigzag-like pattern in depth. The dip of cluster C17 is very similar to that found for cluster C18 and is placed in between the two other more steeply dipping clusters. It is possible to interpret the events in cluster C17 as a consequence of a local stress generated by the interactions of the fault plane containing cluster C15 with the fault plane containing cluster C20, and thought of as a dilational jog with no overlapping tips. This possibility arises from the fact that a small normal component has been systematically detected in the fault mechanism of the events of the north segment (Ferreira et al., 1987; Sophia & Assumpção, 1989). There also appears to be a third direction of faulting close to the transition from the cluster C15 to C17 in figure 6.21 which is a characteristic of bends in a fault according to King & Nabelek (1985). However, this seems to be a local effect because no cluster other than C17 is found at the same depth.

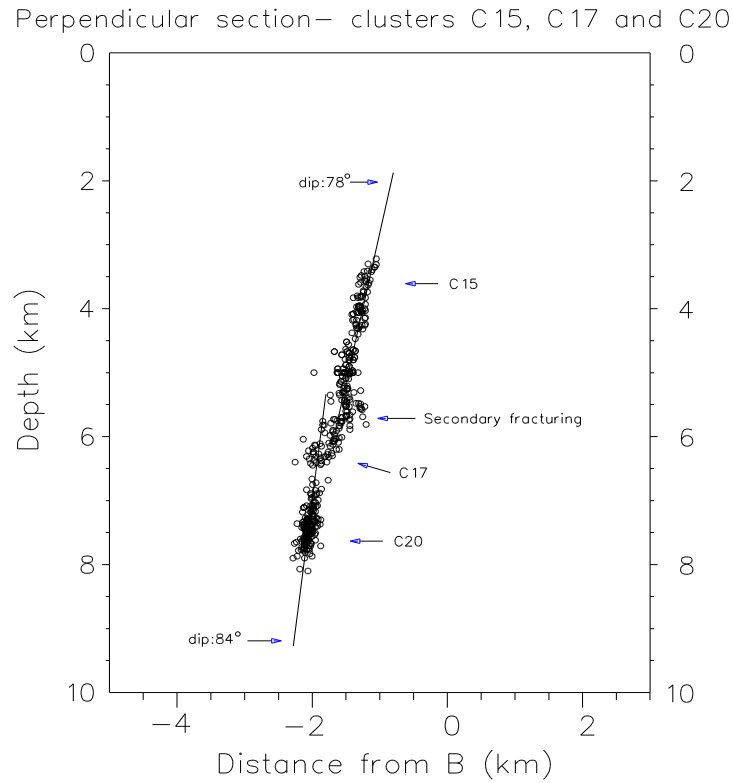


Figure 6.21 Projection of hypocentres in clusters C15, C17 and C20 into a vertical plane perpendicular to the fault strike.

In section 5.3 it was observed that events in the north segment of the Samambaia fault are concentrated at two different depths as can be seen by the two peaks in the family of histograms of figure 5.3(a). The minima in those histograms are centred at 5 km, and separate events belonging to the deepest clusters from events found in the shallow clusters. On the other hand, it was suggested that the deepest clusters are dipping more steeply than the shallow ones in the north segment. This difference in dip characterizes another geometric barrier (see figure 6.22). However, given the predominantly strike-slip nature of the fault movement, this constitutes a conservative barrier which, according to King (1986) can slip without either volume change or the creation of new faulting. This last feature is supported by the relatively low seismicity in the linking region. The small normal component in the slip vector would be sufficient to justify the existence of the cluster C17 and some apparently secondary faulting around the intersection line between the two planes as observed in the previous paragraph.

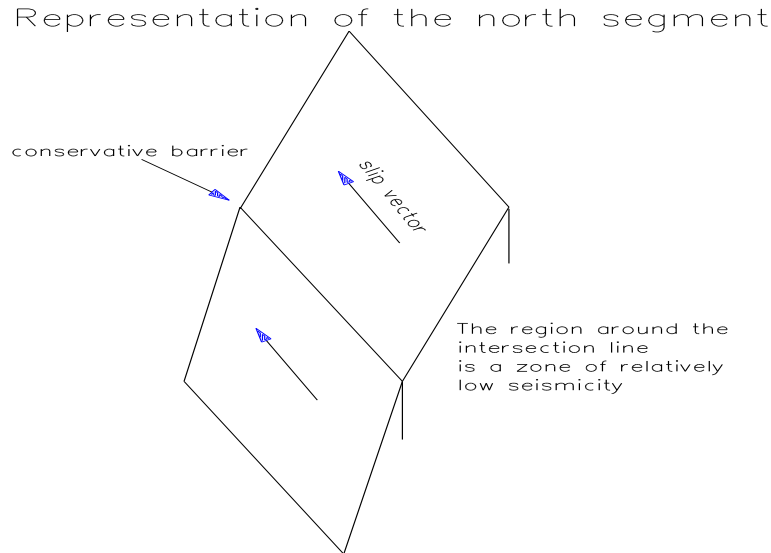


Figure 6.22 Sketch showing the north segment interpreted as consisting of two planes with different dip. The intersection constitutes a conservative barrier.

In comparison with the south segment, the north segment of the Samambaia fault constitutes a well defined and smooth fault plane. However, when examined in detail, it is possible to identify some small but significant irregularities which can be associated with the clustering of events. This correlation between geometric heterogeneities and clusters supports the hypothesis of Das and Aki (1979) in which geometric barriers can be the site of local stress concentration responsible for the clusters of events. Not all clusters in the north segment could be associated with geometric irregularities but in general when this could be done, a small tendency towards a third direction of faulting was found. This secondary fracturing is close to the interface between geometric irregularities, and according to King & Nabelek (1985), arises from the conservation of the slip vectors.

### 6.3.5 Fault plane solutions in the north segment

The large scale simplicity of the north segment of the Samambaia fault is reflected in the composite fault plane solution for each cluster. There is no significant variation in the focal mechanism as can be seen in the plots of figure 6.23. A summary of the fault plane solution parameters for each cluster is given in Table 6.2. The average strike is around N37°E and right lateral strike-slip with a small normal component is the basic fault mechanism. The direction of the maxi-



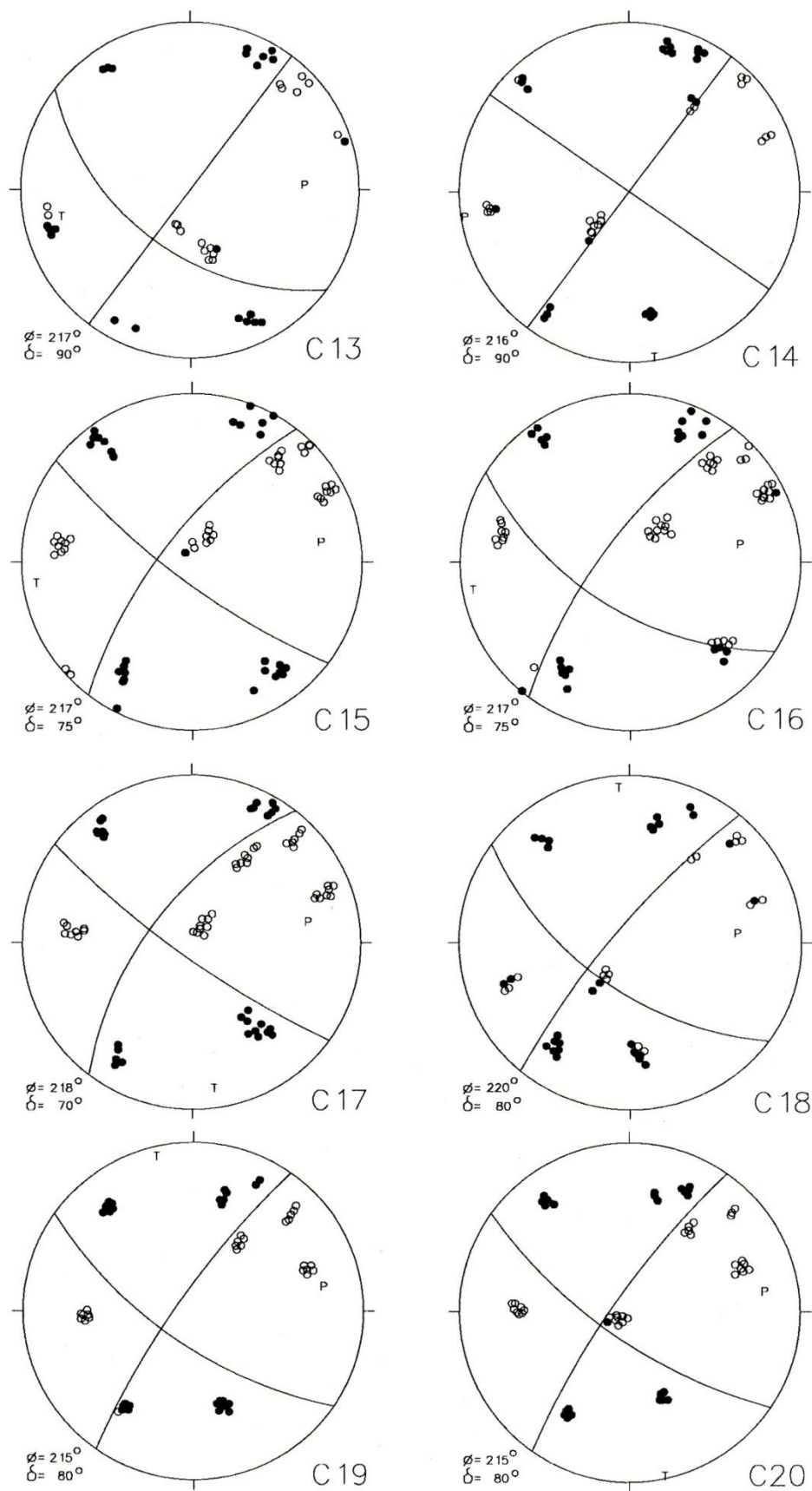


(fig. 6.23 continued on next page)

(fig. 6.23 cont.)

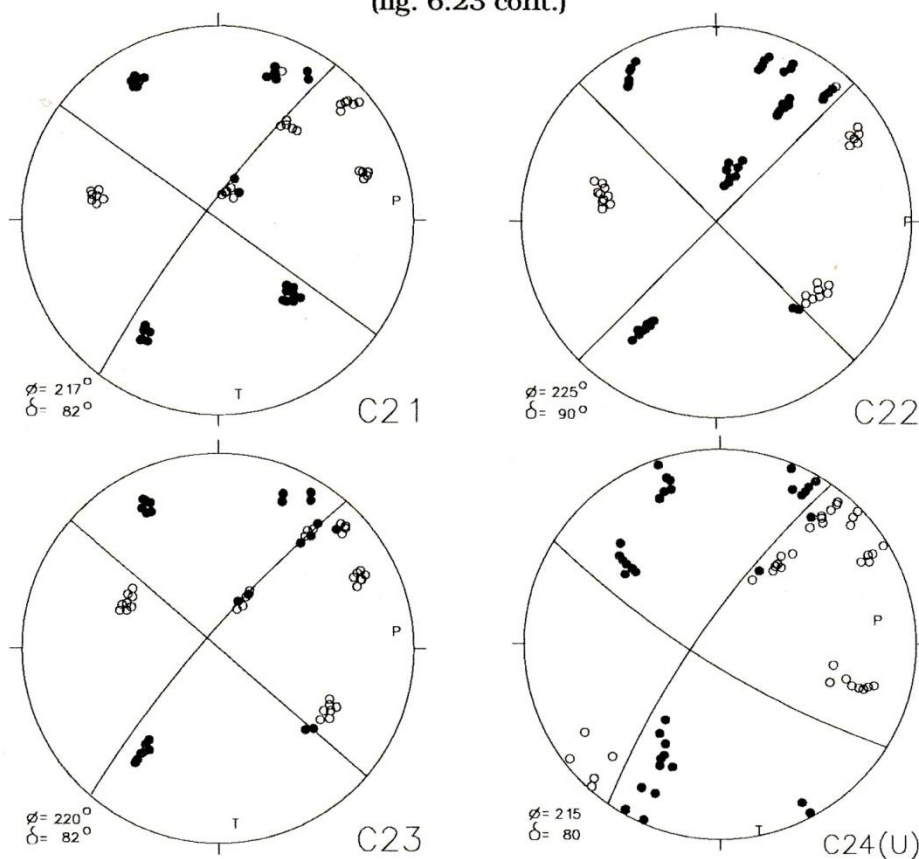


Figure 6.23 Composite fault plane solutions obtained using selected events in the clusters defined in figure 6.14 plus fault plane solution of events in section U as defined in figure 4.6. Open circles are dilatational first motions, filled circles compressional. The positions of compressional and tensional axis are marked by the capital letters P and T respectively. In each diagram the chosen fault plane is indicated by the strike ( $\phi$ ) and dip ( $\delta$ ) values near it. Lower focal hemisphere equal area projections are used.

mum compression approximately is E-W. The quality factor in Table 6.2 follow the definition given in section 6.2.2. The quality of the fault plane solutions for the clusters in the north segment are better than those for the south segment.

Generally, the fault plane solutions for the clusters reveal that deepest clusters (C18 to C23) are dipping more steeply than the shallow clusters (C13 to C16). Although the difference in dip is small and is less than the estimated resolution for a fault mechanism of quality A, this tendency agrees with the discussion in section 6.3.1 (see figure 6.11). This provides additional support for the idea that small geometrical heterogeneities in the fault plane are related to the clustering of events.

A question mark placed aside the strike of the cluster C13 in Table 6.2 indicates that this is one possible solution which was suggested by the other more

## Chapter 6

constrained cluster in the north segment. Cluster C13 was identified as a small off-fault cluster. It was not possible without ambiguity to infer which plane must be the fault plane from the epicentral map. According to Segall & Pollard (1980), secondary shear fracturing which originates as a consequence of the mechanical interaction between *en echelon* segments can be oriented in a direction parallel to the segments or oriented about  $60^\circ$  with lengthened segments (figure 4.2). Thus, given the uncertainties, it is also possible to consider the auxiliary plane as the fault plane in the plot C13 of figure 6.23.

In addition to the fault plane solution for the clusters of the north region, figure 6.23 and Table 6.2 include the results for the cluster in the section U (see figure 4.6). Events in this region, excluding a few events in a third direction of faulting, were classified as belonging to a fault bend following the north segment of the Samambaia fault. No significant difference between the strike of this cluster and the strike of the clusters in the north segment was detected by the fault plane solution method. It is possible that the magnitude of the bend (less than  $10^\circ$ ) is too small to be detected in this way.

Table 6.2 Parameters of the composite fault plane solutions for the clusters in figure 6.14 plus of the events in section U as defined in figure 4.6.

Cluster	Fault Plane			P Axis Az/Pl	T Axis Az/Pl	Mech. Type	Quality
	Strike	Dip	Rake				
C13	217?	90	-150	86/21	348/21	SS+N	B
C14	216	90	-180	261/0	171/0	SS	B
C15	217	75NW	-170	80/18	171/4	SS+N	A
C16	217	75NW	-160	80/25	349/3	SS+N	A
C17	218	70NW	-170	80/21	173/7	SS+N	A
C18	220	80NW	-160	85/21	352/7	SS+N	B
C19	215	80NW	-165	79/18	348/3	SS+N	A
C20	215	80NW	-170	79/14	169/0	SS+N	A
C21	217	82NW	-180	82/6	172/6	SS	B
C22	225	90	-180	90/0	0/0	SS	A
C23	220	82NW	-180	85/6	175/6	SS+N	A
C24	215	80NW	-170	79/14	160/0	SS+N	A

Az is azimuth; Pl, plunge; SS, strike-slip mechanism; N, normal; SS+N, strike-slip with normal component. All angles in degrees according with the conventions of Aki & Richards (1980).

## 6.4 Clustering effects in off-fault segments

Figure 4.6 shows some off-fault events distant from the main fault plane. Those events were interpreted as a consequence of the stress increase due to the mainshock rupture according to the model of Das & Scholz (1981b). The most significant off-fault clusters are those close to Poço Branco and J.Câmara towns in the localities marked by the letters P and J in figure 4.6.

Events close to Poço Branco were grouped into two clusters, C25 and C26, as can be seen in the epicentral map of the region (figure 6.24(a)). The line PP' represents the average strike of  $45^\circ$ . The projections of the hypocentres of these two clusters onto vertical planes along and perpendicular to PP' are shown in figures 6.24 (b) and (c) respectively. Events in cluster C25 are more numerous and restricted to the depth range 3km to 5km, whilst cluster C26 is composed of only nine events which are located at the depth range 5 km to 7km. The plots in figure 6.24 suggest that the planes containing each cluster form a fault offset in which the planes are parallel and dipping almost vertically. The composite fault plane solution for these two clusters (figure 6.26), although not very constrained, confirms the general geometric patterns for these two fault planes. The fault mechanism is compatible with a right lateral strike-slip fault with a small normal component. The axis of maximum compressional stress remains in the E-W direction. This suggests that the fault offset formed by the two segments must constitute an antidilational jog. The main shock in this group of clusters was a  $m_b = 2.7$  event that occurred on 23rd of July 1987. The vertical error ( $\pm 1.1$ km) in the location of this event is relatively poor but it was included in the present analysis due to its importance. The location of the main event is identifiable by the large circle in the plots of figure 6.24. Probably, this was the major off-fault shock since no event greater than that was reported by the authors working with data from smoked paper (for example Sophia & Assumpção, 1989; Costa, 1989; Oliveira, 1989). Although many features found in these two clusters are similar to those found in the clusters of the main fault plane, it seems that the  $m_b = 2.7$  shock did not occur at the base of the seismogenic layer even considering the error in its depth location.

Only twelve events from dataset 5 were considered to belong to the cluster C28 which was located close to J.Câmara. As can be seen in figure 6.25(a) those events are dispersed over a thin but long area and cannot be identified as a cluster in the sense employed for the clusters in the main fault plane. Those events show a strong tendency to align in the SW-NE direction. The line JJ' represents the  $45^\circ$  fault strike which coincides with the strike for the clusters close to Poço Branco. The vertical cross sections along and perpendicular to the strike (figures 6.25(b) and (c)

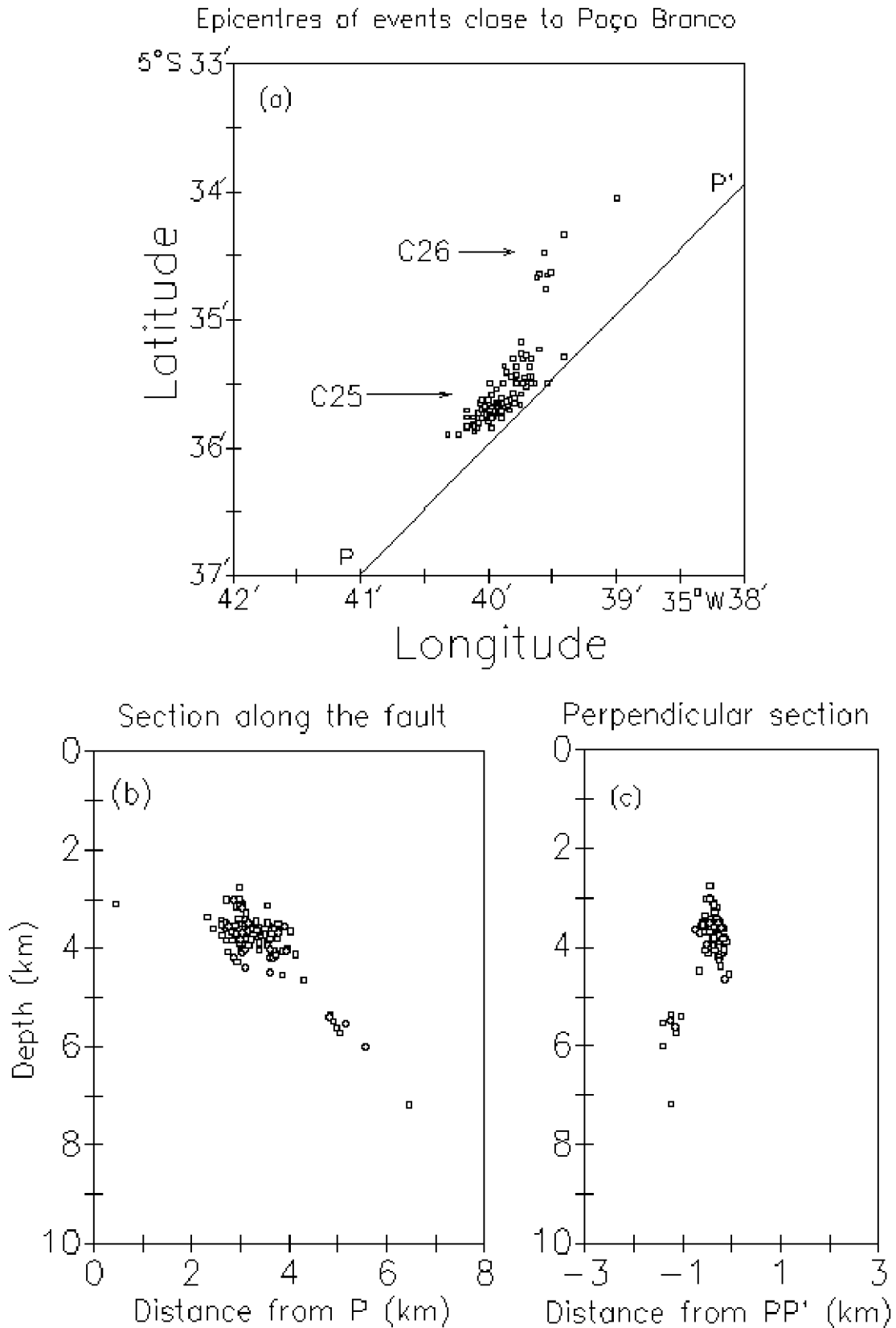


Figure 6.24 (a) Map showing epicentres of events close to Poço Branco. The two clusters are indicated by arrows. Line PP' represents the 45° strike. (b) Projection of events onto a vertical cross section along the line PP'. (c) Projection of events onto a vertical cross section perpendicular to the line PP'.

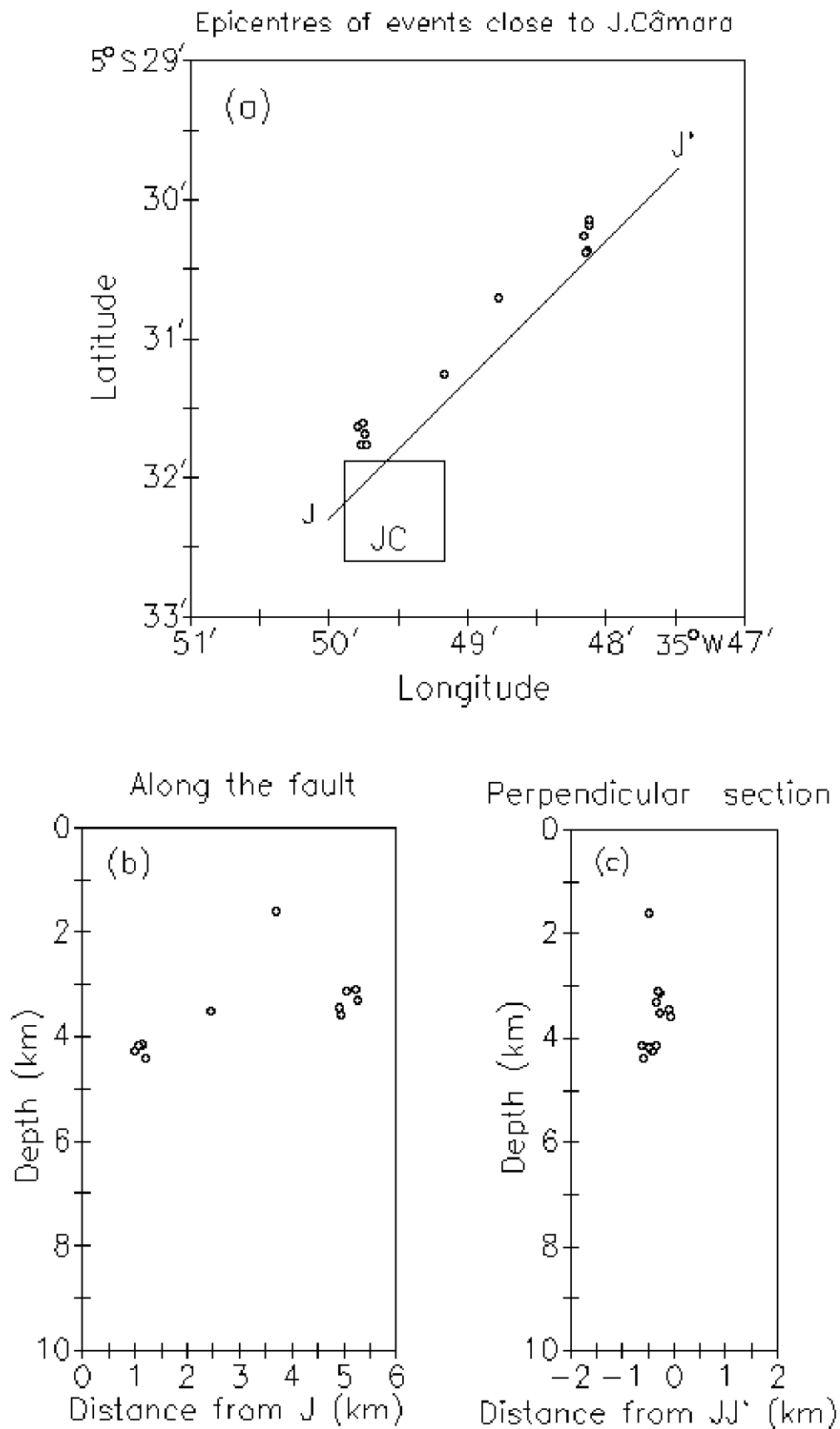


Figure 6.25 (a) Map showing epicentres of events close to João Câmara. Line JJ' represents 45° strike. (b) Projection of events onto a vertical cross section along the line JJ'. (c) Projection of events onto a vertical cross section perpendicular to the line JJ'.

## Chapter 6

respectively), show that events are shallow (maximum depth 4.3 km) and because the number of events is small the fault plane cannot be well determined. The largest event recorded by the telemetered network was a  $m_b = 1.64$  event which occurred on 2nd Oct 87 and there is no indication of any event larger than  $m_b = 2.0$  in the off-fault locality near J.Câmara. Because this cluster is very close to or within a populated area, an event of magnitude  $m_b = 2.5$  or higher would be felt by the population as explained in section 2.1.1. This hypothesis is supported by the analysis of the drum recorder data (Sophia & Assumpção, 1989).

The results for the composite fault plane solution for the events in cluster C28 (see figure 6.26) show an unusual mechanism if compared to the fault mechanism for other clusters analysed in this study. If the nodal plane with strike  $215^\circ$  is chosen as the fault plane as suggested by the trend of seismicity then the probable fault mechanism will be a normal fault with a small right lateral strike-slip component. This can be an indication that in this region the resulting stress rearrangement is influenced by some local heterogeneity. Sophia & Assumpção, (1989) report the same fault mechanism for some events off the main fault located south of J.Câmara in a region that would correspond to the clusters C9 and C10 in figure 6.1a.

The evolution in time of the events in clusters C25 and C26 (figure 6.27) close to P.Branco shows that the number of events before 15th July 1987 is insignificant. On 16th Jul 1987 a  $m_b = 1.91$  event occurred in cluster C25. This event can be considered as a "foreshock" of the major event ( $m_b = 2.71$ ) in this cluster which occurred five days later on 23rd Jul 1987, and which was responsible for the peak of activity seen in figure 6.27. A reactivation happened on 17th August 87 with the occurrence of a  $m_b = 1.85$  event. Activity decreased and after the last week of September the level of the seismicity in this region was similar to that found before 15th of July. During this period no events were detected in cluster C26. Only on the 20th Nov 1987 a small event was located in cluster C26. The maximum magnitude recorded in this cluster was a  $m_b = 1.13$  event. As can be seen in the epicentral map (figure 6.24(a)), very few events were located in this cluster.

A small number of events were also characteristic of the cluster C28 close to J.Câmara. Even considering dataset 3, only 15 events were recorded by the telemetric network. The evolution in time of those events (figure 6.27) shows a uniform distribution, with no significant peaks of activity.

Off-fault aftershocks were analysed in Chapter 5 according to the crack model of Das & Scholz, (1981b). Comparing the vertical cross sections for the clusters close to P.Branco (figures 6.25 (b) and (c)) and for the clusters close to J.Câmara (figures 6.24 (b) and (c)), it can be seen that events close to J.Câmara are

restricted to a maximum depth of 5km, whilst events in cluster C26 close to P.Branco lie between 5km and 7km. This pattern agrees with the suggestion of Das & Scholz (1981b) that for a small deviation of a fault plane from the vertical, the aftershocks on the side towards which the fault dips may be shallower than on the opposite side. This is the case for the Samambaia fault which on average dips about  $76^{\circ}\text{NW}$  and for which the cluster C28 close to J.Câmara is located on the west side. Overall, it is remarkable that for a theoretically small stress increase, the trend of epicentres is close to the trend of seismicity for the main fault events in all of the three clusters off the main fault.

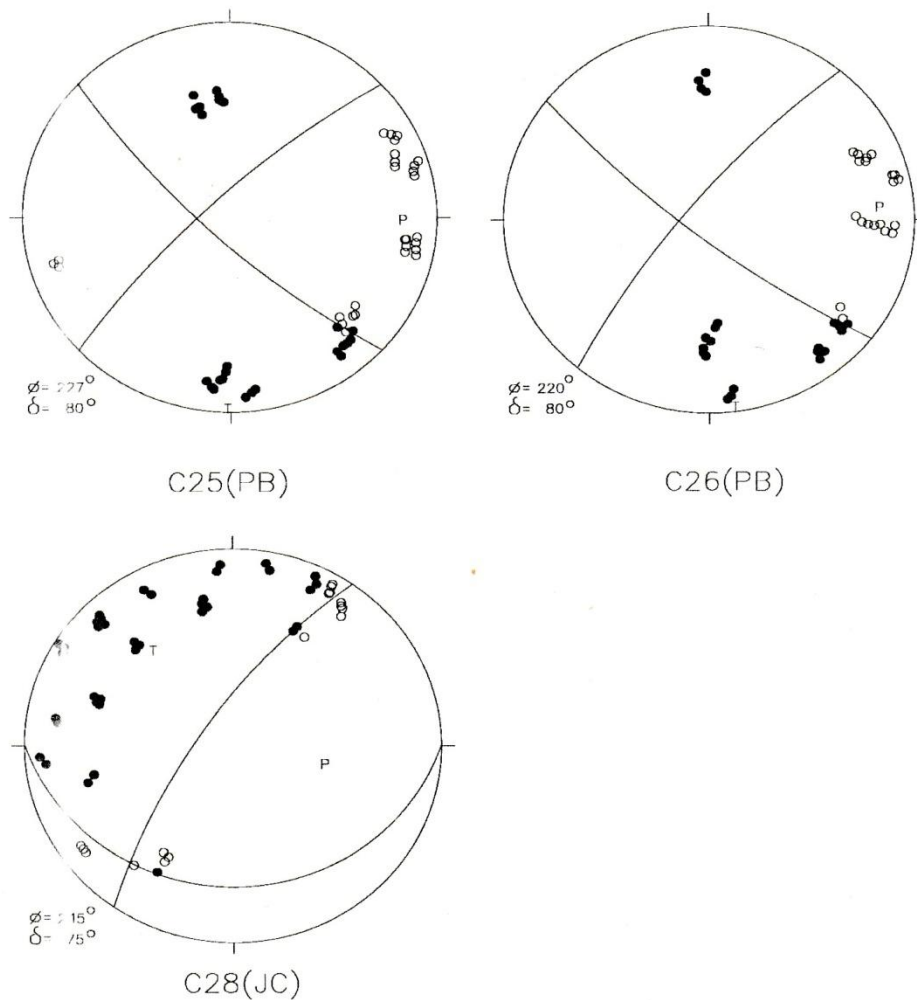


Figure 6.26 Composite fault plane solutions obtained using selected events in the clusters C25 and C26 close to Poço Branco and for the cluster C28 close to J.Câmara.

Regarding the time evolution, it is not certain when events off the main fault first appeared. There is no indication of such events prior to the occurrence of the  $m_b = 5.1$  event as can be seen in the epicentral maps of Ferreira et al. (1987) (see



figure 2.6). Sophia & Assumpção (1989), who analysed the drum recorder data of January 1987, report only three events (see figure 2.10) in the region corresponding to cluster C28, and no events close to Poço Branco. It is almost certain that the peak of activity, as shown in the histogram of figure 6.27, occurred at the end of July 1987, eight months after the  $m_b = 5.1$  earthquake.

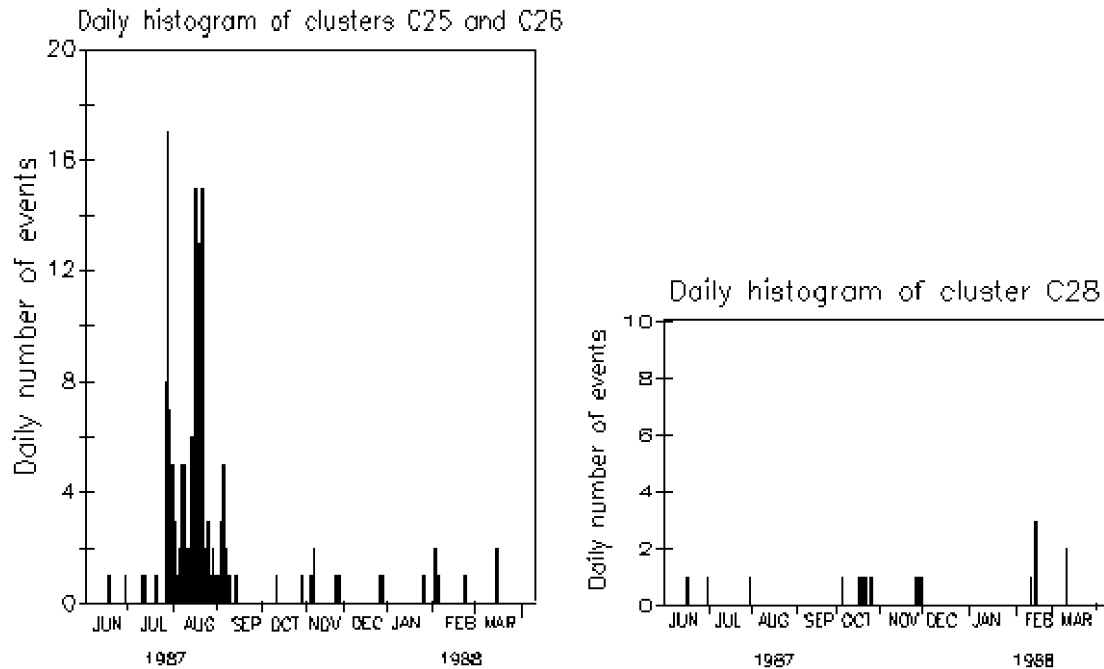


Figure 6.27 Daily histogram for the events recorded by the telemetered network and close to P.Branco (clusters C25 and C26) and for events close to J.Câmara (cluster C28).

## 6.5 Note on analysis of clusters

The detailed analysis of clusters presented in this chapter was prompted by the high quality of the data and the remarkable delineation of the Samambaia fault by the seismicity. Such a detailed analysis would not be possible for a typical interplate aftershock sequence in an area of complex velocity structure and more diffuse seismicity. Although the behaviour of individual clusters has been examined closely, it is not possible to draw firm conclusions relating to the general characteristics of clusters along the Samambaia fault.

## **CHAPTER 7**

### **SHEAR-WAVE ANISOTROPY**

#### **7.1 Introduction**

Shear-waves are transverse waves which potentially carry much more information than P-waves which are longitudinal. One distinct characteristic of shear-waves is that upon entering a region of seismic anisotropy they will generally split, in a phenomenon similar to double refraction or birefringence in optics. This phenomenon, in which a shear-wave polarized in one direction travels faster than another polarized in an orthogonal direction, can be due to any effect which creates directional variations in the elastic properties of the crust, and is usually called "shear wave splitting". The characteristics of the split shear wavetrains are preserved in any subsequent isotropic segments of the path (Crampin, 1981). Figure 7.1 is a illustration of the phenomenon.

There are many kinds of anisotropy such as that caused by high levels of stress responsible for the opening and growth of interconnected dry cracks and their subsequent closure or saturation by water. Scholz et al. (1973) suggested this as the cause of velocity anomalies (Aggarwall et al., 1973) and other precursory phenomena which have been observed before some earthquakes. According to Crampin et al. (1985), stress large enough to cause such conventional dilatancy are only likely to occur at stress concentrations near asperities or extremities of fault planes. Other possible causes of observed seismic anisotropy are: lithology, aligned crystals, periodic thin layers and crack induced anisotropy (Crampin, 1987a).

Since Crampin (1978) suggested that it might be possible to monitor dilatancy and stress through the observations of S-wave splitting, the phenomenon has been detected in widely differing areas of the world in a variety of tectonic regimes (Crampin & Lovell, 1991). These observations indicate that distributions of stress aligned cracks are not confined to the close vicinity of the earthquake focus and, in contrast to conventional dilatancy (caused by high level of stress), they are a low-stress phenomenon (Crampin et al., 1984). In all these observations the

orientation of the first split shear-wave arrival is perpendicular to the direction of minimum compressive stress whenever this has been identified (Peacock, 1988). In order to explain the almost universal presence of S-wave splitting and the alignment of the leading shear-waves, Crampin et al. (1984) suggested the hypothesis that fluid-filled cracks, microcracks and pore spaces are inclusions which are preferentially aligned by stress so that the rocks are effectively anisotropic to seismic waves. They call this phenomenon Extensive Dilatancy Anisotropy or EDA, and the inclusions are known as EDA cracks (Crampin, 1987a). Although they include a wide range of different shaped cracks, microcracks, and preferentially oriented pore-space, in general their seismic effects can be simulated by parallel, penny-shaped cracks (figure 7.1).

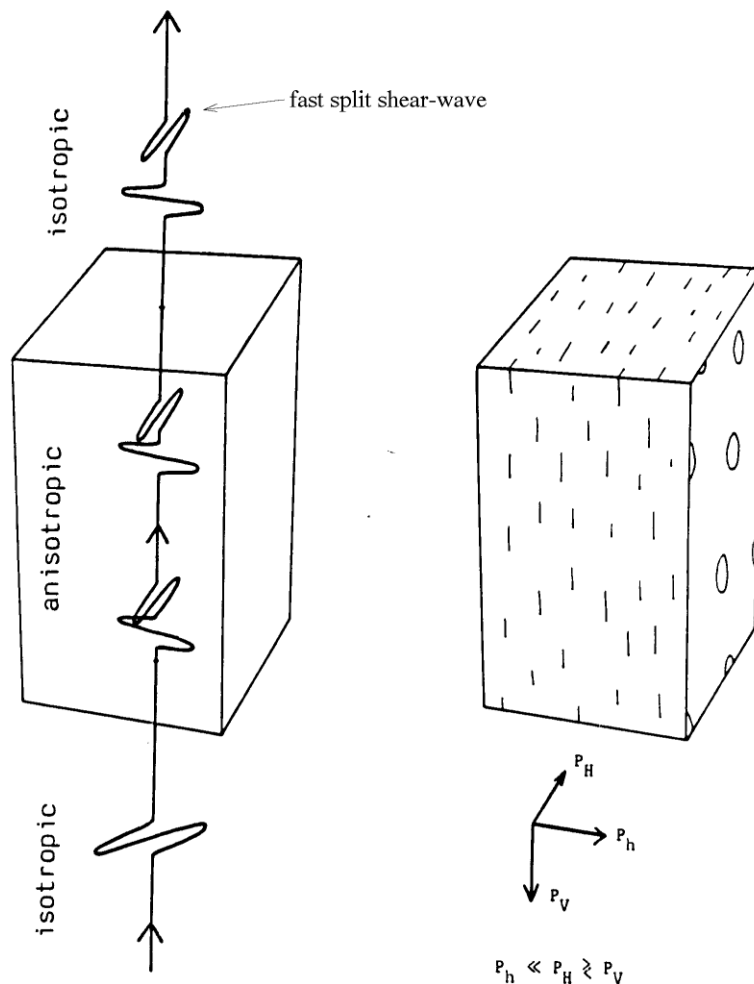


Figure 7.1 The left diagram shows the splitting of an upward travelling shear-wave as it passes through an anisotropic block. The diagram on the right illustrates the arrangement of penny shaped cracks which could cause the anisotropy assumed in the picture on the left. The orientation of the stress field which could lead to such an alignment is shown.  $P_H$ ,  $P_h$ ,  $P_V$  are the principal stress axes;  $P_h$  denotes the smallest compressive stress (in absolute tension),  $P_H$  denotes the other horizontal principal stress and  $P_V$  the vertical principal stress. (From Crampin, 1987b).

Numerical experiments performed by Crampin (1978) demonstrated that S-wave splitting is the most diagnostic phenomenon for the recognition and evaluation of seismic anisotropy. According to Chen et al. (1987), only two parameters characterizing S-wave splitting are quantifiable for local earthquake sources: (1) the polarization direction of the first S-wave, and (2) the time delay between the split S-waves.

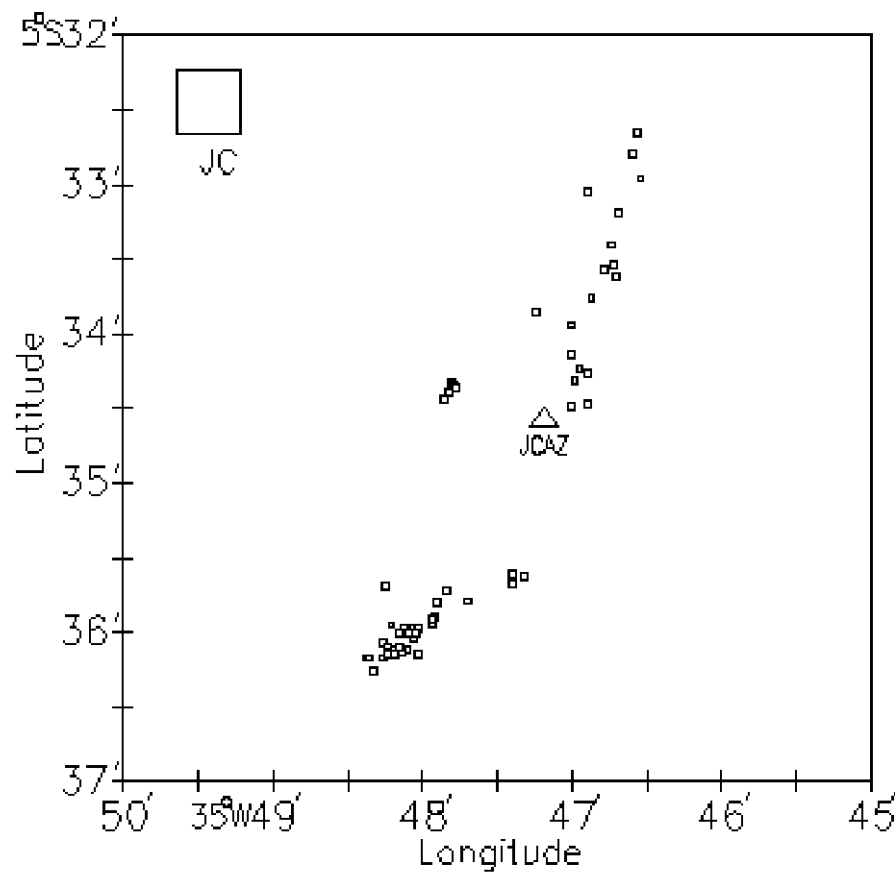
### 7.2 Data selection for the shear-wave splitting study

As stated in section 1.1 the primary objective of the J.Câmara telemetric network was to investigate the spatio-temporal pattern of the seismicity in the Samambaia fault. The network consisted of eight vertical component stations and one three-component station. The three-component station identified by the code JCAZ was located near the centre of the network as indicated in the figure 2.10 and was installed with the intention of identifying possible shear-wave splitting in that area. Since only one three-component station was available, the analysis of the S-wave splitting was considered to be a secondary objective in this study.

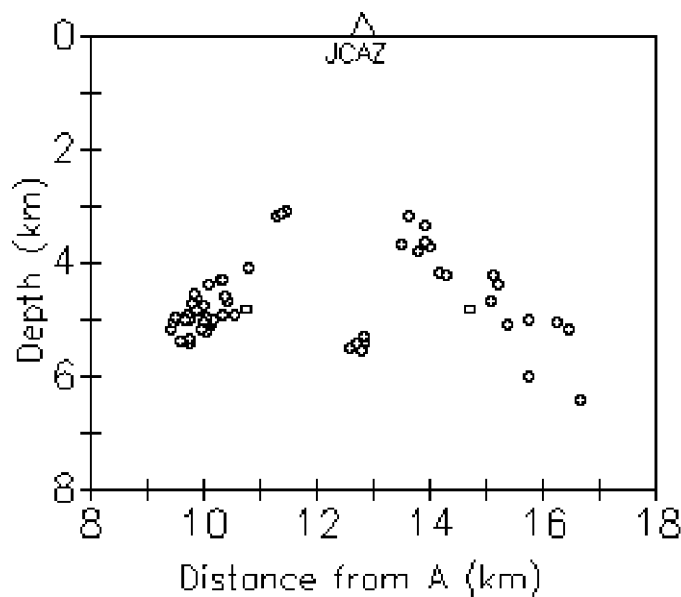
As a rule, only events close to the station JCAZ, having an angle of incidence less than a critical angle of incidence of approximately  $35^\circ$ , should be considered in this kind of study. Evans (1984) and Booth & Crampin (1985) show that, outside the shear-wave window defined by small incidence angles, the waveform of the incident S-wave is severely distorted by phase changes associated with reflected and converted waves at the free surface. The critical angle is calculated for a plane wave incident on the free surface of a homogeneous isotropic half-space with a Poisson's ratio of 0.25. According to Booth & Crampin (1985), for small local earthquakes the shear-wave window can be extended to  $40^\circ$  incidence as a result of the curvature of the wave front and the probable presence of low-velocity surface layers. However, to avoid any complication related to the identification of possible distortion of the incident S-wave at the edge of  $40^\circ$  window, an effective shear-wave window of  $35^\circ$  was assumed for the JCAZ station. It is possible that in a simple area like this, the shear waves are simple even outside the shear-wave window, but this matter needs evidence from additional three-component station.

Because station JCAZ was installed near the centre of the network, the epicentres close to this station were well determined even considering systematic errors in their locations as discussed in section 3.4. This means that even small events with magnitude around  $m_b = 0.4$  that were not recorded by all the stations had a sufficiently good location to be included in this study. On the other hand, a

(a) Epicentres of events for shear-wave splitting



(b) Cross section along the fault



(c) Perpendicular to the fault

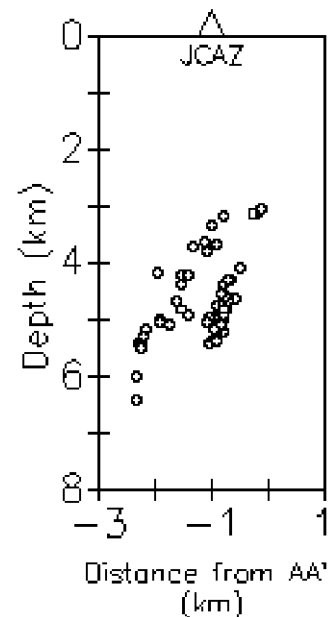


Figure 7.2 (a) Epicentral map showing the selected events for the shear-wave splitting study. Dots represent epicentres; the triangle represents the three component station JCAZ and the square represents J.Câmara town. (b) and (c) Vertical cross sections along, and perpendicular to the fault strike respectively.

limiting factor was that this station was located in the so called "gap" of the Samambaia fault which limited the number of useful events. All events for the S-wave study were selected from dataset 5 with vertical and horizontal errors smaller than 0.5km. About 140 events within the 35° S-window were initially selected. From this total, a number of events were excluded for several reasons. For example, all events above  $m_b = 1.7$  saturated the seismometers of JCAZ, or the P-wave coda amplitude was too large for the interpretation. Sometimes technical problems in one or other channel of the Geostore was the reason; emergent S arrivals and poor signal to noise ratios were other reasons for rejection. In this way, 56 events were selected for the S-wave splitting study. Those events are shown in the epicentral map of figure 7.2 together with the location of the three component station JCAZ.

### 7.3 Data analysis

#### 7.3.1 Procedures for the analysis

The analysis for the S-wave splitting study was performed with the PMPLOT program which is part of the facilities of the BGS in Edinburgh. In general, S-wave splitting is difficult to recognize on recorded time series seismograms because the polarization directions of the split S phases are not usually parallel to the seismometer components. The PMPLOT program rotates the horizontal seismograms into components which are radial and transverse in relation to the line between epicentre and receiver in order to discriminate between shear waves and S to P converted waves. After that, the program displays the data in polarization diagrams to facilitate the determination of the split S-wave polarizations. These diagrams consist of three mutually-orthogonal perpendicular sections (see figure 7.3a) of the particle displacements plotted for a succession of small time intervals along the three component wavetrains. A typical example of such rotated seismograms and particle diagrams for the station JCAZ is shown in figure 7.4. The polarization direction of the first arrival in the horizontal plane is determined from the horizontal section of the polarization diagrams which contain most of the shear wave energy. For shear waves at near-vertical incidence the particle motion following the first S-wave arrival is usually sufficiently linear for the polarization direction to be identified. The arrival of the second split S-wave is in general characterized by an abrupt change of the particle motion to a different direction. When interference by P-wave energy results in slightly elliptical motion of the first S-wave, the average polarization is chosen. Figure 7.3b illustrates the procedure to obtain the

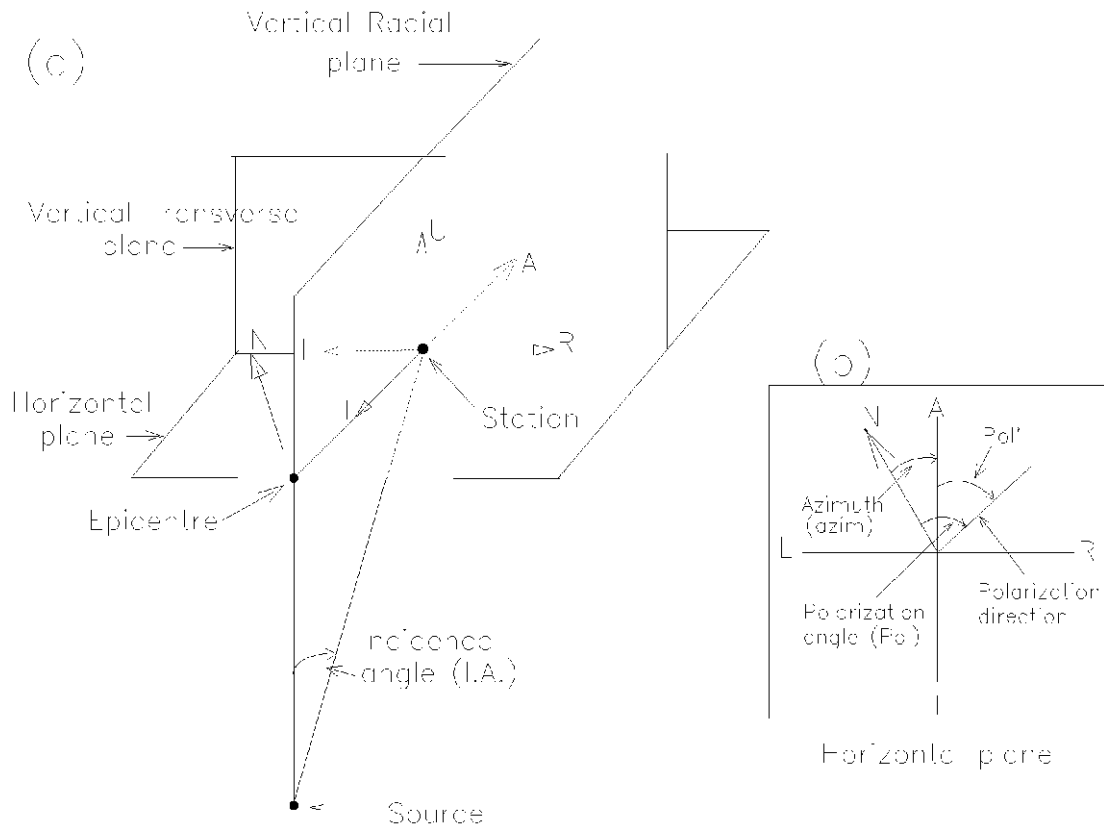


Figure 7.3 Sketch showing (a) conventions and projection planes for the particle motion; (b) determination of the polarization direction.

geographical orientation of the first split S-wave arrival polarization direction ( $Pol$ ). It is obtained by adding the polarization angle ( $Pol'$ ) relative to the radial direction to the azimuth ( $Azim$ ) of the station from the epicentre.

It is more difficult to measure the split S-wave time delay than the first arrival polarization. For the time delay it is necessary to identify the onset of the second split S-wave arrival which often is not very clear. Chen et al., (1987) describes three types of difficulty and gives a procedure for the identification and measurements of split S-wave time delays. In that procedure, they define the onset of the second split S-wave by a change of polarization of the first S-wave, with a significant component of energy (larger than the background noise or P-coda) in the direction perpendicular to the first polarization direction. They observe that the rotation of the horizontal seismograms into components which are parallel and perpendicular to the direction of alignment of the first S-wave polarization aids identification of the second split shear-wave onset. These procedures will be followed in this study.

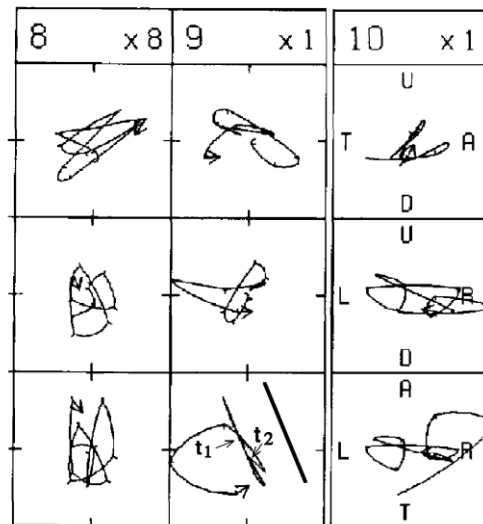
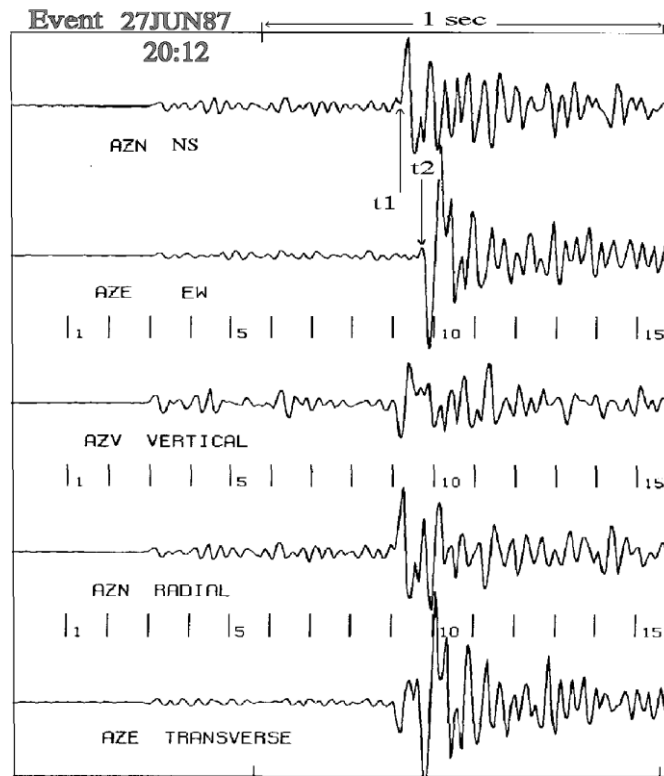


Figure 7.4 Typical example of shear wave splitting at station JCAZ showing the conventional three component seismograms and horizontal seismograms rotated into the radial and transverse directions. The polarization diagrams are shown below and are numbered to correspond with the time intervals marked on the seismograms. S-wave particle motion are shown in three 0.1 sec windows and in three orthogonal planes: vertical radial, vertical transverse and horizontal. Labels: U, up; D, down; T, towards; A, away, L, left, and R, right, all with respect to the radial direction away from the epicentre (see figure 7.3a). Ticks on the particle displacements are every 0.01s and the appropriate relative gain is shown above each set of polarization diagrams. The solid bar indicates the direction of polarization of the leading split S-wave and t1 indicates its arrival time.



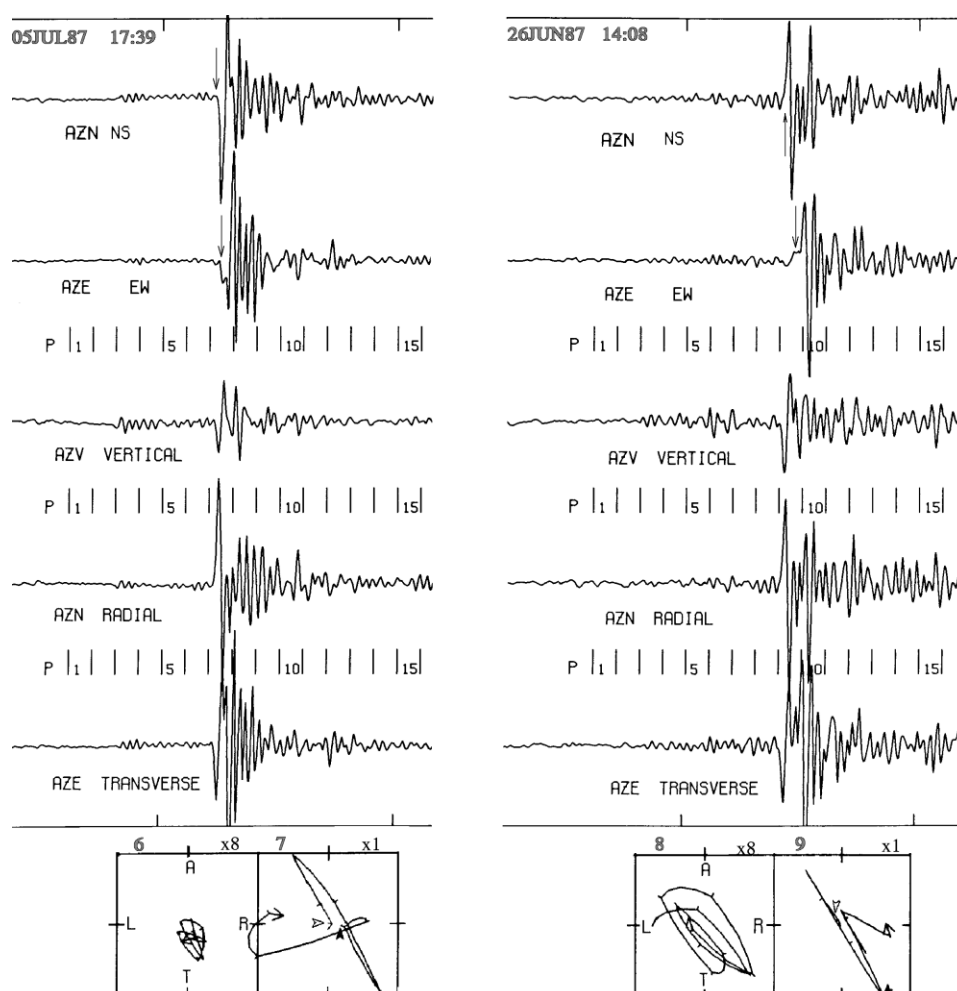


Figure 7.5 Further examples of shear-wave splitting observations. The polarization diagrams shown are for the horizontal component only, where the onsets of the first and second split S-waves are indicated by open and solids arrows respectively. All labelling as for figure 7.4.

### 7.3.2 Shear-wave polarization and time delay measurements

The good quality of the selected seismograms, which show impulsive S arrivals and good signal to noise ratio, allowed the first split S-wave arrival polarization and the split S-wave time delay to be measured for all the selected events. All the measurements consistently show a strong tendency for the first split S-wave arrival to be polarized in the north-south direction as can be seen in Table 7.1. No attempt was made to identify the polarity of the vector; only direction was measured. The average value of the geographical orientation of the polarization direction of the first split S-wave is  $1.32^\circ$  and standard deviation of the mean is  $4.54^\circ$ . The maximum deviation from the average was  $15^\circ$ . The assumed direction of polarization in the NS direction of the first split S-wave is independent of the time in which events were recorded, independent of the depth of the hypocentre and independent of the azimuth. As can be seen in figure 7.6 the observed polarization

directions are remarkably consistent throughout all the events used in the analysis. The non-correlation between the polarization direction and the azimuth provides corroborative evidence that the observations are indeed split shear-waves and not, for example, a consequence of lateral inhomogeneity in the medium.

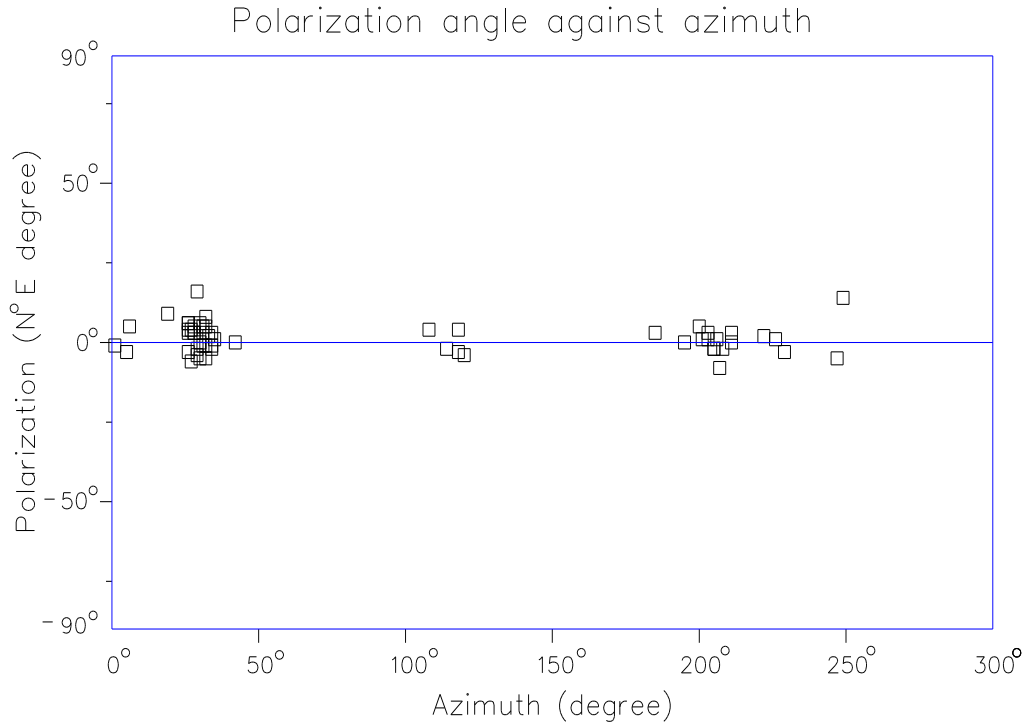


Figure 7.6 Plot of the direction of polarization of the fast split S-wave against epicentre-to-station azimuth. The continuous line represents the average value 1.3° for the polarization direction. These observations are exceptionally consistent and show that the direction of polarization of the fast split S-wave is in the NS direction.

The polarization direction of the split S phases for the events in this study are approximately parallel to the seismometers orientations. That is, the fast split S-wave component coincides with the NS component and the slow split S-wave coincides with the direction of the EW component. Therefore, it was possible to use conventional seismograms (see figure 7.4) to check the time delay between the split S-waves measured from the polarization diagrams. It is known that the magnitude of the time delay depends on the travel path distance in the anisotropic medium. So, the measured time delay between the two split S-waves was normalized to a path length of 1 km. The results of the measurements in time delays are shown in Table 7.1.

## Chapter 7

Table 7.1 Events selected for the Shear-wave splitting study.

Date	HR:MN	Lat. °	Long. °	Mag	Dmin	Depth	Azim °	I.A. °	Pol. N°E	Ndel
870531	22:00	5S34.33'	35W47.81'	.37	1.1	5.42	120.	11.5	-04	5.4
870602	09:10	5S32.65'	35W46.57'	.48	3.9	6.40	200.	31.4	05	4.0
870603	08:13	5S34.47'	35W46.90'	.59	.8	3.17	249.	14.2	14	6.1
870616	12:15	5S35.79'	35W47.70'	.37	2.3	4.08	19.	29.4	09	14.9
870626	14:08	5S36.11'	35W48.11'	.50	3.1	4.85	29.	32.6	-02	6.9
870626	16:30	5S36.03'	35W48.06'	.37	3.0	5.22	28.	29.9	03	10.0
870626	17:29	5S35.97'	35W48.06'	.80	2.9	5.09	29.	29.7	-04	13.7
870626	17:59	5S35.97'	35W48.03'	.50	2.8	4.99	28.	29.3	05	12.2
870626	22:51	5S36.15'	35W48.03'	.97	3.1	4.61	26.	33.9	-03	10.8
870627	05:29	5S36.00'	35W48.04'	.71	2.9	4.35	28.	33.7	03	9.6
870627	06:10	5S35.97'	35W48.13'	.59	2.9	4.97	32.	30.3	08	13.9
870627	06:48	5S35.69'	35W48.25'	.90	2.6	4.90	42.	28.0	00	12.6
870627	08:15	5S36.12'	35W48.19'	.76	3.2	4.99	31.	32.7	05	13.5
870627	10:06	5S36.07'	35W48.26'	.66	3.2	5.40	34.	30.7	-01	11.2
870627	11:24	5S36.09'	35W48.24'	.59	3.2	5.35	33.	30.9	02	11.2
870627	12:33	5S36.26'	35W48.33'	.59	3.6	5.15	32.	35.0	-01	6.4
870627	13:09	5S36.01'	35W48.14'	.84	3.0	4.76	31.	32.2	-01	10.7
870627	18:12	5S36.13'	35W48.14'	1.64	3.2	4.69	29.	34.3	16	1.8
870627	19:45	5S35.89'	35W47.92'	1.45	2.6	4.64	26.	29.3	06	11.3
870627	20:12	5S35.90'	35W47.94'	.87	2.6	4.57	27.	29.6	04	13.3
870628	00:48	5S36.14'	35W48.19'	1.03	3.2	4.91	30.	33.1	-05	13.7
870628	01:23	5S36.17'	35W48.27'	.37	3.4	5.38	32.	32.3	05	9.4
870702	19:46	5S33.57'	35W46.78'	1.08	2.2	4.65	206.	25.3	01	13.6
870705	17:39	5S34.14'	35W47.01'	.37	1.0	3.71	211.	15.1	00	2.6
870705	18:26	5S34.27'	35W46.90'	.76	1.0	3.33	229.	16.7	-03	8.6
870706	00:48	5S34.49'	35W47.00'	.66	.6	3.66	247.	9.3	-05	5.4
870706	03:34	5S35.94'	35W47.93'	.37	2.7	4.27	26.	32.3	06	15.8
870706	03:37	5S35.91'	35W47.94'	.37	2.7	4.30	26.	32.1	03	15.8
870706	08:52	5S36.17'	35W48.38'	.76	3.5	5.05	35.	34.7	01	1.6
870706	21:05	5S36.17'	35W48.36'	.16	3.5	4.95	34.	35.3	03	3.3
870709	18:53	5S36.15'	35W48.23'	.95	3.3	4.98	31.	33.5	03	8.4
870709	19:25	5S36.00'	35W48.09'	1.08	2.9	5.10	30.	29.6	00	13.6
870709	23:53	5S35.95'	35W48.21'	.50	3.0	5.04	34.	30.8	-02	15.3
870710	00:53	5S36.00'	35W48.16'	.97	3.0	5.15	32.	30.2	-05	11.7
870713	15:20	5S33.19'	35W46.69'	.37	2.9	5.01	203.	30.1	01	6.9
870713	22:22	5S33.76'	35W46.87'	1.45	1.8	4.81	207.	20.5	-08	5.8
870714	01:53	5S32.96'	35W46.54'	.50	3.4	5.05	205.	34.0	-02	8.2
870716	00:32	5S33.86'	35W47.24'	.59	1.4	4.15	185.	18.6	03	4.6
870915	10:18	5S36.10'	35W48.16'	1.18	3.2	4.53	30.	35.2	06	5.4
871003	22:28	5S34.23'	35W46.95'	.66	1.0	3.63	222.	15.4	02	5.3
871004	01:39	5S32.80'	35W46.59'	.66	3.6	5.15	201.	35.0	01	1.6
871004	06:44	5S34.35'	35W47.80'	1.08	1.1	5.52	118.	11.3	-03	5.3
871005	07:34	5S34.39'	35W47.82'	.50	1.1	5.40	114.	11.5	-02	7.3
871005	22:42	5S34.36'	35W47.78'	.59	1.0	5.30	118.	10.7	04	3.7
871014	10:02	5S35.67'	35W47.40'	.66	1.9	3.14	5.	31.2	-03	8.2
871014	13:20	5S35.62'	35W47.32'	.37	1.8	3.06	1.	30.5	-01	8.5
871014	13:20	5S35.61'	35W47.40'	.50	1.8	3.12	6.	30.0	05	2.8
871022	05:03	5S34.31'	35W46.98'	.71	.8	3.78	226.	11.9	01	2.6
871023	05:53	5S33.94'	35W47.01'	.59	1.4	4.20	203.	18.4	03	4.5
880126	20:35	5S33.40'	35W46.74'	.76	2.5	5.10	205.	26.1	-02	1.8
880207	08:13	5S34.44'	35W47.86'	1.49	1.1	5.51	108.	11.3	04	1.8
880220	08:14	5S33.62'	35W46.70'	.71	2.2	4.21	211.	27.6	03	2.1
880224	09:14	5S33.54'	35W46.72'	.84	2.3	4.36	208.	27.8	-02	2.0
880227	03:08	5S33.05'	35W46.89'	.84	3.0	5.99	195.	26.6	00	1.5
880302	00:51	5S35.80'	35W47.90'	.50	2.4	4.91	27.	26.0	-06	9.1
880306	21:22	5S35.72'	35W47.84'	.37	2.3	4.81	26.	25.6	04	9.4

HR is hour; MN is minute; Dmin is the epicentral distance to the station JCAZ; Depth in km; Azim is the epicentre to station azimuth in degrees; I.A. is the incidence angle; Pol is the geographical direction of polarization of the first S-wave arrival; Ndel is the time difference between the split S-wave arrivals normalized to a path length of 1 km measured in ms/km.

## Chapter 7

In order to verify possible correlations between the normalized time delay (ndelay) of the split S-waves and other parameters, a test was made using the multiple regression analysis method (Bevington, 1969). The statistical F test shows that the only variable significant in the regression is time. Ndelay correlates negatively with the time within the 95% confidence limit although the correlation coefficient shows that they are weakly correlated (see Table 7.2). This low degree of correlation is a consequence of the small number of data and their irregular distribution. Figure 7.7 shows the plots of ndelay as a function of time. As can be seen, the time variation of ndelay is irregularly sampled. The same statistical F test indicates that the normalized time delay does not correlate with the incident angle or with the depth of the event. Taking the maximum value of 16ms/km in the observed normalized time delay in figure 7.7, this gives 6% as the maximum percentage of anisotropy from S-wave travel time.

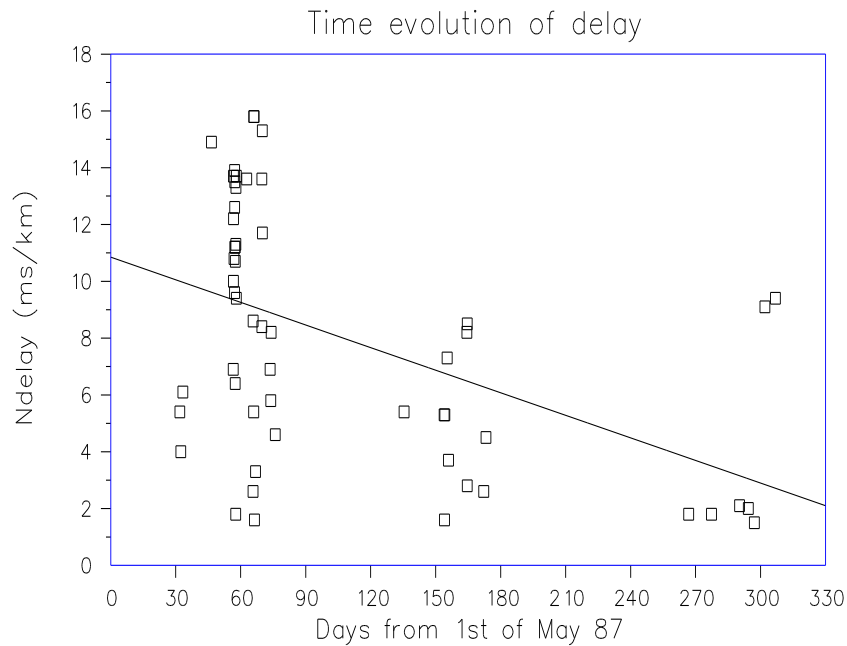


Figure 7.7 Plot of the normalized time delay (ndelay) between the split S-waves against time in days from 1st of May 1987. Solid line indicate the best fit line.

The observed correlation between the normalized time delay and time could be due to event migration in that region. To check this possibility, a new correlation test between ndelay and time was carried using events clustered to the south of station JCAZ (see figure 7.2). This cluster corresponds to the events in the azimuth range  $N0^{\circ}E$  to  $N45^{\circ}E$  in Table 7.1 and the distribution of ndelay with azimuth for those events is shown in figure 7.8. The result of the test for that cluster shows no

## Chapter 7

Table 7.2 Results of the multiple regression analysis for ndelay as a function of time.

ndelay = a0 + a1xtime		
a0 = $10.8 \pm 0.9$	a1 = $-0.026 \pm 0.006$	
r = 0.48	s.d. = 3.9	F = 16

r: correlation coefficient.  
s.d.: standard deviation of the fit.  
F: statistical F test.

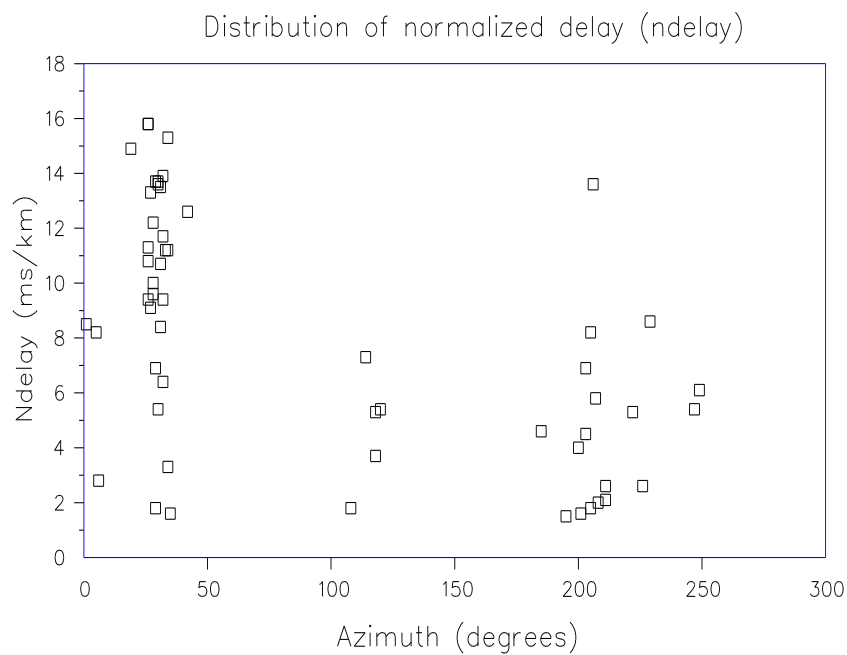


Figure 7.8 Plot of the normalized time delay (ndelay) between the split S-waves against epicentre to station azimuth in degrees.

correlation between ndelay and time (correlation coefficient = -.24) or depth (correlation coefficient = .16) which support the hypothesis that the supposed variation in time of ndelay could be a consequence of the event migration. On the another hand, in excluding this hypothesis, it is difficult to explain the large variation in the observed values of ndelay for the events in this cluster. It can be seen in figure 7.8 that ndelay varies from 2ms/km to 16ms/km. It is unlikely that this scatter is due to errors in the time measurements as the onsets of split shear waves here are in general well defined. The reading error for the S-wave onset for these selected events is estimated to be  $\pm 0.02$  seconds which roughly corresponds to  $\pm 4$ ms/km. So, there is not a direct answer to the question of temporal variation in

the normalized time delay. However, in the absence of further evidence it will be better to assume no correlation between those two variables. Another possibility is that these variations are mainly caused by a localized strong anisotropic layer between source and receiver for example, in which case the assumption of constant anisotropy along the wave path is no longer valid. To test this possibility, delay (not normalized delay) for the events in the same cluster was plotted against depth. This plot is shown in figure 7.9. As can be seen, the correlation between the two variables is too poor (correlation coefficient=0.40) to draw any conclusion about possible variation of anisotropy with depth.

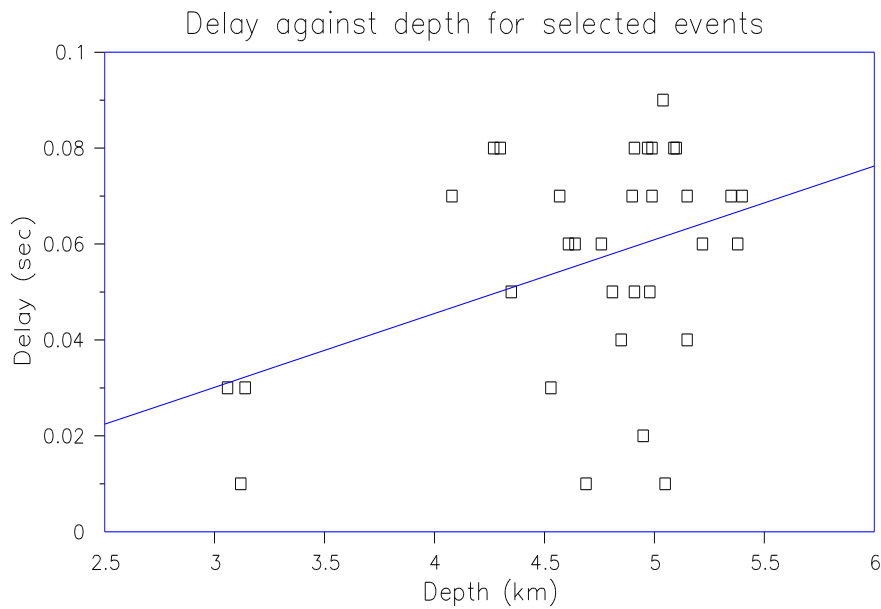


Figure 7.9 Time delay between split shear-wave arrivals and seismic path length.

## 7.4 Results and interpretation

Shear-wave splitting has been observed in the J.Câmara region in all the selected events recorded by the three component station JCAZ. Also, the polarizations of the first split shear-wave arrivals are consistently aligned in the same direction, for a variety of azimuths and incident angles. The splitting indicates that there is anisotropy along the wave path, and the consistent polarization alignments suggest that the anisotropy is of the hexagonal type, with a horizontal symmetry axis, which has been observed in many tectonic regions, and attributed to stress-aligned EDA-cracks (Crampin & Lovell, 1991).

However, the first split shear-wave arrivals are consistently polarized in the NS direction. If the cracks are aligned by the stress field which causes the

earthquakes, this observation cannot be explained by the EDA hypothesis of the anisotropy being caused by stress-aligned EDA-cracks (described in section 8.1) because the possible directions of the principal stress axes from the fault plane solutions are orthogonal to those predicted by the EDA hypothesis. The composite fault plane solution determined by Ferreira et al. (1987) and Sophia & Assumpção (1989), are in close agreement with the right lateral strike-slip fault with a small normal component found in the present study. Therefore, the axis of minimum horizontal compressive stress for the Samambaia fault is in the NS direction. To be consistent with the EDA hypothesis the fast split S-wave arrival would be polarized in a direction perpendicular to the minimum horizontal compressional stress as illustrated in figure 7.1, that is, it would be polarized approximately perpendicular to the NS direction.

There are some alternative interpretations for the origin of the observed anisotropy near João Câmara, but no complete explanation for the characteristics of the observed splitting has yet been found. First, the effect might be attributed to large scale fracture sets whose orientation is due to a "fossil" stress regime existing at the time of their formation as suggested by I.G. Stimpson (pers. commun., 1991). In support of this hypothesis, figure 1.4 shows the trend of the Precambrian shear zones of Bento Fernandes and João Câmara aligned in an almost north-south direction. This seems the most probable cause of the anisotropy in the João Câmara region if temporal variation in the normalized time delay does not exist. Secondly, lithologic anisotropy caused by a fabric such as aligned grains can show little time variation (Crampin, 1987a). Also, it is likely to be confined to particular rock strata and will not change significantly with changes in applied stress. Thirdly, mechanical effects caused by *en echelon* faults (see figure 4.2) as in the case of the south segment of the Samambaia fault could interchange the local compressional and tensional axes, but this tends to be a localized effect and cannot explain the consistency of the observations over a large area as that shown in figure 7.2. Fourthly, local near-surface site stress conditions may significantly affect the polarization of the faster split S-wave arrival (Savage, 1989). It is possible that the EDA phenomenon is present in the region but is obscured by anisotropy in near surface layers. However, it is not possible to draw any firm conclusions using only one station on the fault. It is possible that other locations will exhibit different behaviour. For example, Liu et al. (1992) show shear-wave anisotropy observations from a network in Parkfield, California, where one station located on the fault, gives anomalous polarization directions.

## **CHAPTER 8**

### **CONCLUSIONS AND SUGGESTIONS FOR FURTHER WORK**

#### **8.1 Summary of findings**

The present study is characterized by high precision in the hypocentre locations compared with previous work related to the João Câmara earthquake sequence using data from smoked paper drum-recorders. Such high quality data has made possible an exceptionally detailed study of the seismicity, and this has revealed features which would normally be masked by complexities of velocity structure, high attenuation or scattering. This is possible because the present study is located in a Precambrian shield area.

Data were obtained from the records of the João Câmara telemetric network during a 10 month period, from May 1987 to April 1988. The telemetered network recorded 3,819 local microearthquakes. Epicentres were calculated with the location program HYPO71 using a two-layer velocity model in which a 6.1 km/sec half-space is overlain by a 4 km thick 5.9 km/sec velocity layer with a common  $V_p/V_s = 1.70$ . This velocity model was chosen from among other two-layer models as having the minimum travel-time residual. Events were then selected using a number of criteria. Events in dataset 5 were selected by imposing 0.05 sec as the maximum travel-time residual, and 0.3 km and 0.5 km as the maximum horizontal and vertical allowed error respectively, in the location of each event. This generated a set of 2,746 events which give 0.03 sec, 0.14 km and 0.24 km as averages for the travel-time residual, horizontal and vertical errors respectively. These errors refer to random errors only. Systematic errors introduced by the uncertainty in the velocity model can double the final error in location, and they depend on the position of the located event in relation to the centre of the network where the error function is a minimum.

As a result, the seismicity map obtained from the 1987-88 telemetric network is exceptional both in the high quality of the hypocentral locations, and the sharp delineation of geometric features which it reveals (e.g. figures 4.1 and 4.10). The Samambaia fault has been divided into two main segments with the same



## Chapter 8

N37°E strike. The north segment is dipping 76°NW. The south segment is more nearly vertical, dipping about 82°NW and composed of three or more closely spaced almost parallel faults. It is possible that some additional small faults located in the south segment are striking in a direction almost perpendicular to the main fault. No events deeper than 9 km were found in the entire region studied; this agrees with the previous results found in other parts of northeast Brazil. A small gap and a low seismicity zone were found to separate the north and south segments (see figure 4.11). Because the north and south segments have different dips, the gap can be thought of as a transition zone between those two segments. That is, the gap represents a geometric heterogeneity or barrier liable to accumulate stress.

The two largest shocks occurred outside the period of operation of the telemetered network. In this study, the gap is interpreted as the probable location of the  $m_b = 5.1$  mainshock of 30 November 1986 although no direct evidence was found to support this hypothesis. However, the size of the gap is compatible with the estimated ruptured area due a magnitude  $m_b = 5.1$  intraplate earthquake. The second largest earthquake was the magnitude  $m_b = 5.0$  which occurred on 10th March 1989. It was recorded by the smoked paper drum recorder network and despite significant errors in the epicentre determination, it was located at the northern end of the north segment. Evidence for two small bends in the Samambaia fault was found in the close vicinity of the two largest shock epicentres, which supports the theory that bends or jogs create likely locations for the initiation and termination of major earthquake ruptures.

Examination of the epicentral map and corresponding vertical cross sections also revealed that events are not random but are clustered. It is clear that these clusters of events represent activity on sections of fault which at least in some cases are offset from the main fault and have a slightly different strike and/or dip. Therefore, in these cases it was possible to establish a correlation between geometric irregularities and clustering effects. This is a small scale effect only detectable as a consequence of the high precision in the hypocentre locations. The limit to which such irregularities could be resolved was estimated to be about 300 m. So, this limitation suggests the possibility that other clusters are related to small geometrical heterogeneities not detected by the present network. Additionally it appears that events are also clustered in time, so that it was possible to isolate these discrete clusters for independent analysis.

Within each cluster, the largest events show a tendency to nucleate at the deepest point in the cluster. It is uncertain down to what magnitude this characteristic is present, but an arbitrary selection of events above magnitude 2.9 shows that those events were nucleating at the base of the deepest clusters; that is,

## Chapter 8

at the base of the seismogenic layer. These observations support the hypothesis that major events such as the  $m_b = 5.1$  and  $m_b = 5.0$  earthquakes nucleated at the same depth. Estimation of the area occupied by some of the major clusters has shown that their sizes are larger than the rupture area corresponding to the major event in the cluster. This last result supports the idea that the area enclosed by the aftershocks is not the area which slipped during the main earthquake. In general, clusters in the north segment, where the majority of aftershocks above magnitude  $m_b = 4.0$  were located, persist over a longer time than clusters in the south segment. It was also observed that deeper clusters tend to dip more steeply than the shallow ones.

In general, composite fault plane solutions evaluated for events within the clusters from P wave first motions show remarkable agreement with the fault parameters derived from the seismicity map. Since four stations were located along the Samambaia fault line, resolution of the nodal plane orientation was consequently good although not sufficient to discriminate conclusively between small variations in the strike and/or dip between individual clusters. The average result shows a dextral strike-slip fault with a small normal component as the fault mechanism for the N37°E striking Samambaia fault; the inferred P axis therefore lies approximately east-west.

Off-fault events distant from the Samambaia fault have been observed in the J.Câmara region. One group of events was concentrated around Poço Branco town about 10 km east of the Samambaia fault, and another group was found close to J.Câmara town at a similar distance west of the Samambaia fault. The latter events were first detected one month after the occurrence of the  $m_b = 5.1$  earthquake of 30th November 1986, but the peak of the activity happened eight months later and no event larger than magnitude  $m_b = 2.0$  or deeper than 7km was recorded. A few events were also recorded close to the line of the Samambaia fault beyond the end points of the main activity. In general, active fault has progressively lengthened to the north and to the south. The pattern of seismicity shown by these off-fault aftershocks is a classical example explained by the model of Das & Scholz (1981b) as a consequence of the shear stress increase after the occurrence of the main earthquake. The inferred strike of N45°E for those clusters is slightly different from that of the Samambaia fault. A composite fault plane solution for the events close to Poço Branco is coherent with the main fault mechanism, but the fault plane solution for the events close to J.Câmara town shows an almost normal fault with a small strike-slip component.

Magnitude determinations for the events recorded by the telemetric network have been performed by developing a specific earthquake magnitude scale based on

the duration of the signal of the earthquake on a seismogram. This local scale was calibrated with the regional magnitude scale  $m_R$  (Assumpção, 1985) compatible with the teleseismic body wave magnitude scale  $m_b$ . A correction based upon the instrument response was performed because of an observed non-linearity in the low magnitude region of the inferred duration magnitude. A maximum likelihood estimate of  $b$  in the formula  $\log N = a - bM$  shows no significant variation in the  $b$ -value during the recording period.

Shear wave splitting was observed in the J.Câmara region in all the selected events in the shear-wave window recorded by the three component station JCAZ. The polarization direction of the first split shear-wave arrival for those events lay in the north-south direction which does not agree with the premise of extensive dilatancy anisotropy for a maximum compressive stress in the east-west direction as inferred by the fault plane solutions. Intrinsic anisotropy, due to the ancient deformation of the rock fabric seems to be the likely explanation for the observed polarization direction of the first split shear-wave arrival. On the other hand, small temporal variations in the observed time-delay between split shear-waves cannot be easily explained by other than EDA sources of anisotropy.

### 8.2 Relationship with other geophysical studies

As stated in section 1.6 few geophysical studies have been performed in the J.Câmara region. Most studies were made after the occurrence of the  $m_b = 5.1$  earthquake of 30th Nov 1986. A gravimetric study was made by Moreira et al. (1990) in the J.Câmara area. Their Bouguer anomaly residual map is shown in figure 8.1 and their two-dimensional interpretation of residuals along the profile AB is shown in figure 8.2. In the geophysical model suggested by those authors, hypocentres of selected events concentrate on the west side of a 'mafic intrusive body' responsible for the positive anomaly, and ultimately responsible for the João Câmara earthquake sequence according to the authors. They state that the model is preliminary and more data are necessary, particularly in the region that shows a positive anomaly.

A similar hypothesis was given by Johnston (1982), to explain an earthquake swarm which occurred in Arkansas, Eastern United States - an intraplate area. He reported a small  $m_b = 3.8$  earthquake as the main shock associated with the swarm. In the classification of Mogi (1985), a swarm is characterized by having no large shock which dominates the sequence, (that is, it is characterized by a large  $b$ -value) and that this kind of phenomenon is typical of volcanic regions. Thus, it seems difficult to explain the J.Câmara earthquake sequence by the model of Moreira et al.

(1990), because no abnormal b-values were found in this sequence which was dominated by the  $m_b = 5.1$  shock. However, the analysis of Moreira et al. (1990), reveals a high crustal heterogeneity in the region, which could be useful in the understanding of the spatio-temporal clustering effects observed in the present work.

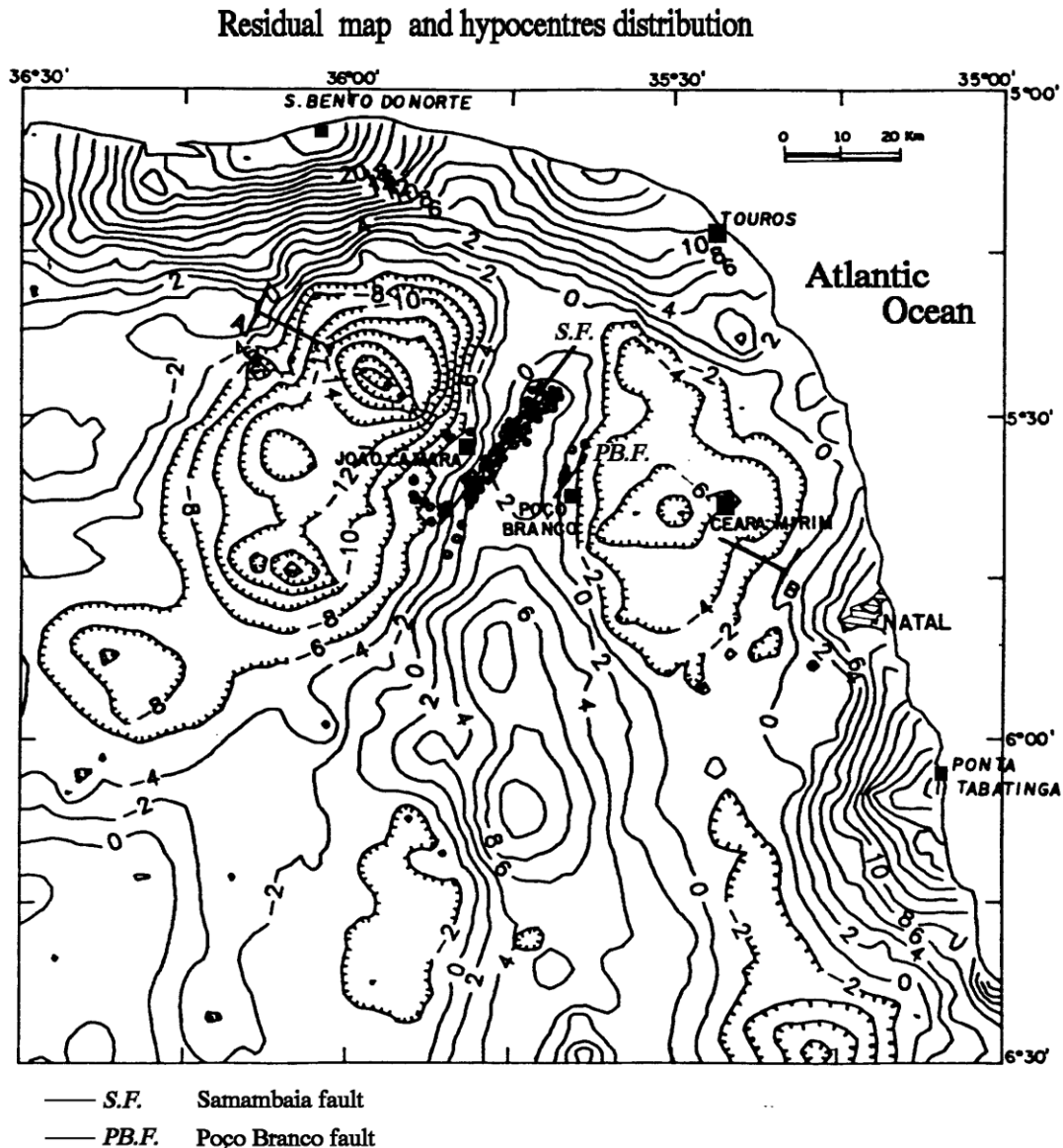


Figure 8.1 Residual map (isolines in mGal) and distribution of epicentres of selected events (after Moreira et al., 1990).

The Samambaia fault is inferred from the seismicity map. No surface trace of the rupture and no geological evidence of the fault were found in the area studied (Gallardo & Perez, 1988). Figure 8.3 shows a reduction of an aeromagnetic map of

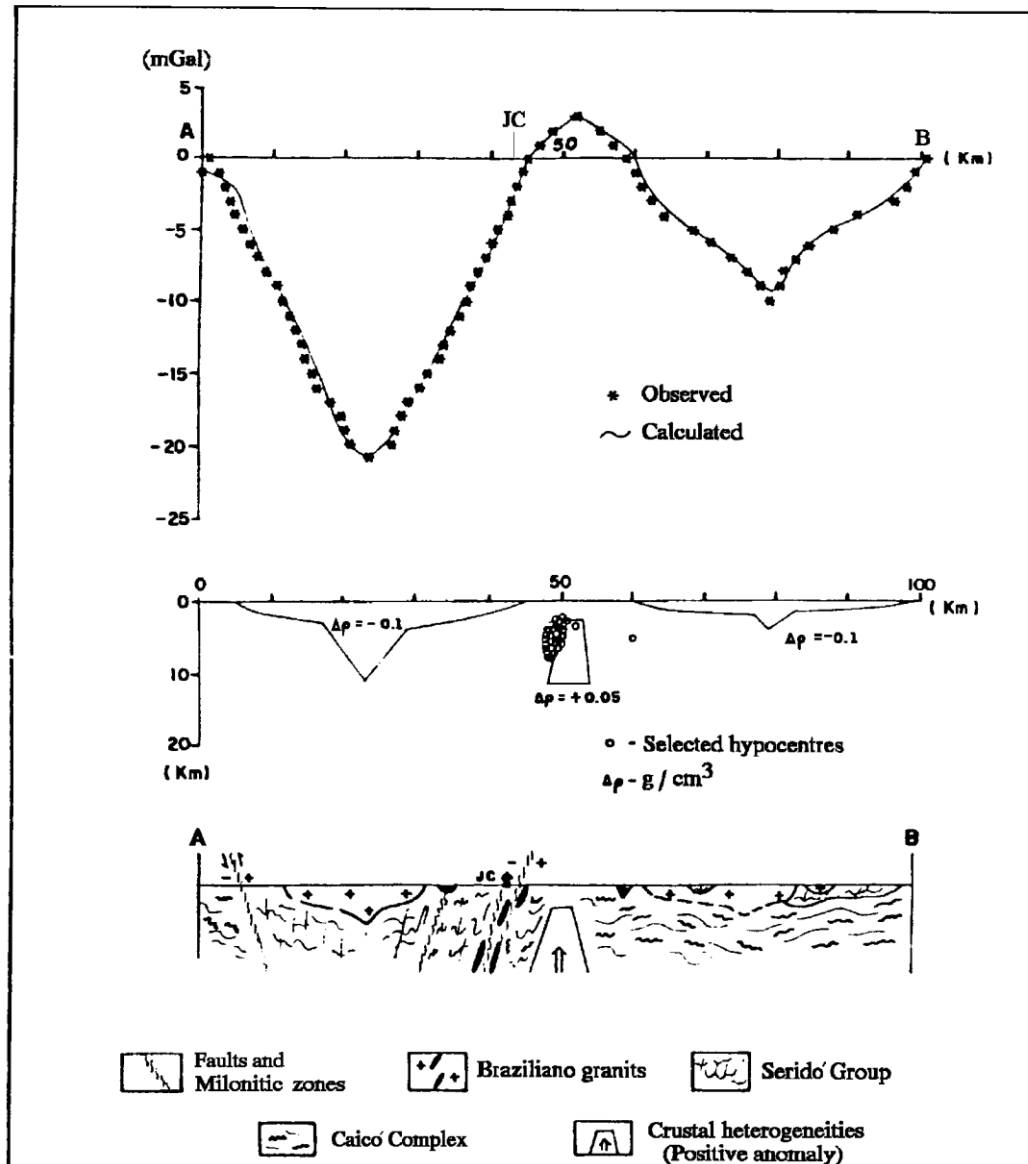


Figure 8.2 Gravimetric profile AB and geophysical model for the João Câmara region. The line AB is parallel to the road BR406 and is indicate in figure 8.1 (after Moreira et al., 1990).

the northeast of Rio Grande do Norte state made by the Brazilian oil company Petrobrás (Petrobrás, 1987). The map shows the contours of the total magnetic intensity in the region. Examination of this map reveals two parallel linear features with strike N40°E indicated in figure 8.3 by thick gray lines numbered 1 and 2, one to the east and one to the west of the Samambaia fault. Each of these features consists of a uniform magnetic gradient dipping NW. It is important to recognise that this gradient persists along the full length of each line despite being masked by other features which distort the contour pattern. Both of these features extend at

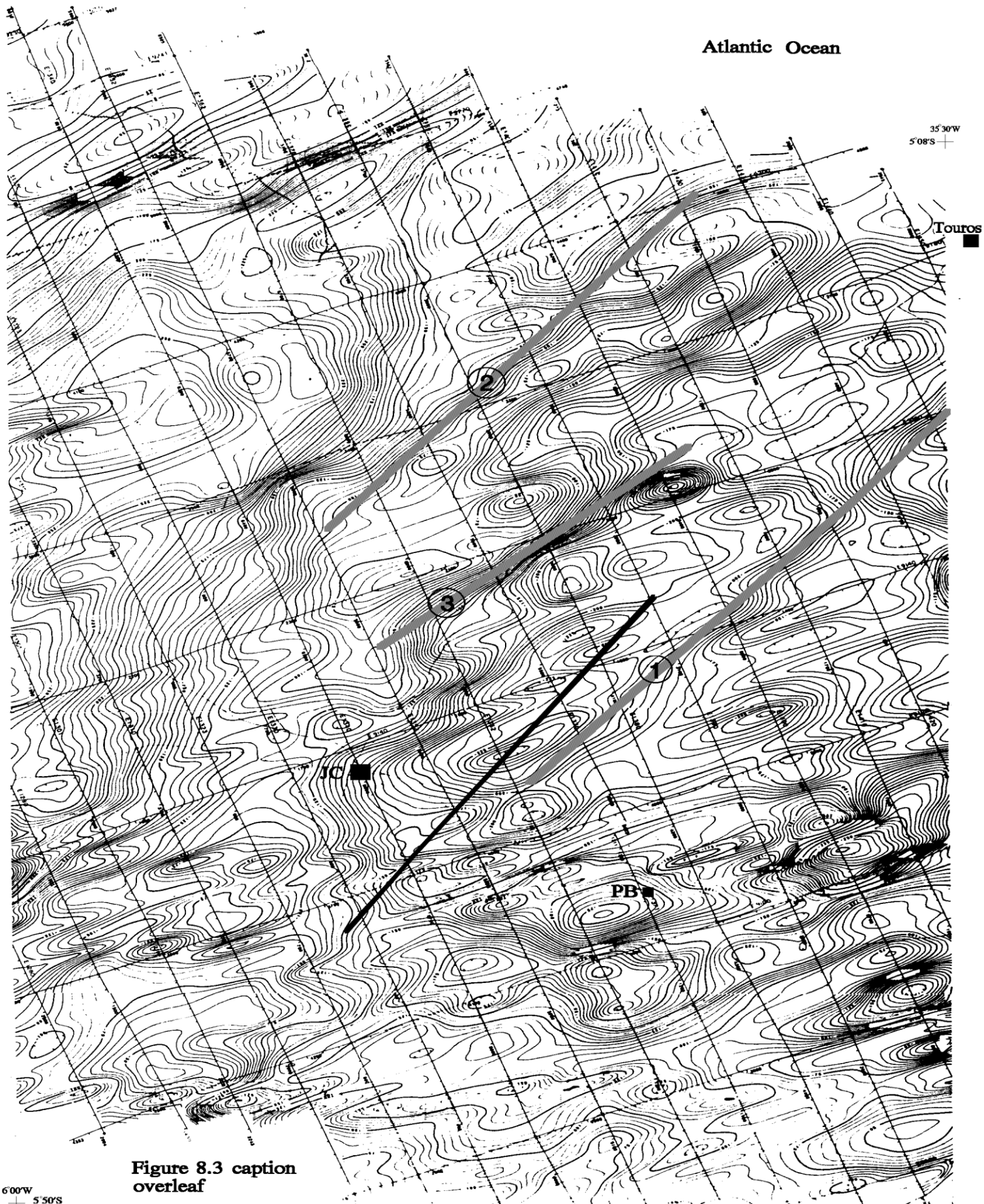


Figure 8.3 caption  
overleaf

Figure 8.3 Total magnetic intensity map (after removing the IGRF) of the eastern part of the Potiguar Basin. Grid lines indicate flight lines (Petrobrás, 1987). Filled squares denote towns and the heavy continuous line represents the Samambaia fault.

least for 40 km parallel to the Samambaia fault, and constitute the only known evidence supporting the existence of a subsurface structure with the strike of the Samambaia fault, as inferred from the seismicity. Indeed, feature 1 shows a remarkable coincidence between the supposed trace of the Samambaia fault on the surface and the positive anomaly alignment close to trace as shown in figure 8.3. A third feature, numbered 3 in figure 8.3, has a larger magnetic gradient than 1 and 2, but it is in the opposite sense.

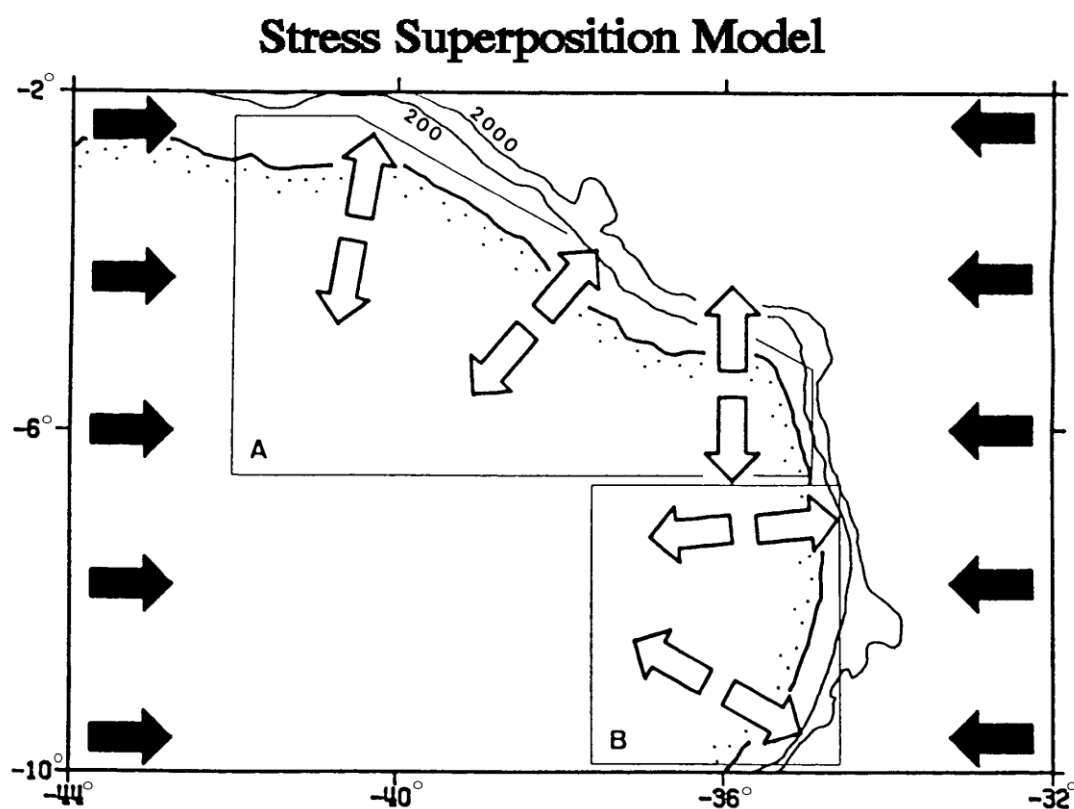


Figure 8.4 Model of superposition of local and regional stresses in the upper crust. White arrows denote local extensional stresses caused by lateral density contrasts and sediment loading at the continental margin. Full arrows denote regional compressional stresses (possibly related to plate driving forces). Area 'A': higher seismic activity with stresses inducing strike-slip faulting; area 'B': lower seismic activity with local and regional stresses balancing each other (after Assumpção, 1992).

## Chapter 8

Gusso & Bagnoli (1989) performed neotectonic studies in a tilted peat deposit in the coastal area close to the town of Touros (see figure 8.3), about 70km northeast of João Câmara. They found evidence of strong deformation in that deposit which they suggest as been caused by an intense Holocene activity. In addition, they observe that the site lies along the line of the Samambaia fault to the northeast as shown in figure 8.3. A map of peat structures observed at this locality (R.G.Pearce, pers. commun., 1988) includes 60cm offset on a left lateral strike-slip fault, with northerly strike, observed at one location, and evidence of a 20 metre synclinal feature with an east-west axis, showing dips up to 50°. It seems that these observations reinforce the supposition that the present day activity of J.Câmara represents reactivation along a zone of weakness during the evolution of the continent. However, this assumption needs additional geological-geophysical investigations to support it.

More recently, Assumpção (1992) proposed a simple model to explain the seismicity pattern of Northeast Brazil. He inferred the  $SH_{max}$  in the Potiguar Basin from the examination of four reliable focal mechanisms and from one onshore borehole breakout measurement. He concluded that is unlikely that the observed strike-slip motion, and particularly the small component of normal motion, could be caused solely by asthenospheric shear stresses and ridge-push. In his model, stresses responsible for the seismicity in the Precambrian Borborema Province would be a superposition of a regional east-west compression with local extensional stresses caused by lateral variations in the density across continental margins and sediment loading at the continental shelf. The model is represented in figure 8.4 and explains why seismicity is relatively high at the border of Potiguar Basin, where the superposition of stresses is coherent with strike-slip motions such as those inferred in the present work, and rare below latitude 6°S, where the E-W compression would be balanced by the local extension, consequently inhibiting seismic activity.

### 8.3 Suggestions for further work

A seismic refraction profile to determine an independent velocity model for the J.Câmara region is recommended in order to verify and/or improve the velocity structure inferred by the present work. Referring to the gravity model of Moreira et al., (1990), more gravimetric data across the Samambaia fault and magnetic susceptibility measurements of local rocks would provide a more reliable geophysical model for the subsurface structure related to the J.Câmara seismicity.

For a fine structure study of the seismicity map in order to obtain the delineation of geometric features on a small scale (better than 300m), and possible



## Chapter 8

correlation with mechanical effects in the stress field caused by such irregularities, a more dense network than that used in the present study is necessary. There is clear evidence that João Câmara, and probably other regions in the Borborema Province with similar geological features, have an unusually simple velocity structure with low attenuation of seismic waves. Therefore, these localities seem ideal for the studies of source parameters involved in an earthquake process. To explore these possibilities, a network with higher dynamic range and higher frequency response will be appropriate. Additionally, three component stations in the João Câmara area will be essential to clarify the nature and extent of the anisotropy found in this study.

At the time of writing, eight three component digital network is been installed by the staff of Geology and Geophysics Department, University of Edinburgh, in the João Câmara region for another one year period, in collaboration with staff of the Department of Physics, UFRN, Natal.

As a practical example, Henderson (1992) made developments in the description of faulting as a fractal process in studying the relationships between the seismic b-value and the fractal dimension of the distribution of earthquake epicentres. Using dataset 3 of the present work, he was able to perform refinements in his model derived from a study of Californian seismicity. He found that such improvements were possible because the seismic data from the J.Câmara seismic network resulted from a process of fracture which is most likely to occur when the velocity structure and the geometry involved in the faulting are simple.

Such additional work in the future promises to provide further evidence showing the value of detailed intraplate seismicity studies in the precise analysis of faulting processes and the evolution of faulting. There is sufficient evidence showing that wavetrains generated by local earthquakes in the J.Câmara region contain very high frequencies. This characteristic combined with the low attenuation and simple velocity structure of the region would provide the necessary requirements for those studies.

## **APPENDIX A**

### **NETWORK STATUS TIMETABLE**

The João Câmara telemetric network was installed during the period 13th to 29th May 1987 with operational recording commencing on 22nd May when stations JCPA, JCAZ, JCSC and JCLR were set up for recording. At the beginning, station JCPA presented some problems, later identified and fixed. These problems were due to a malfunction of the amplifier-modulator unit. Station JCSM was set up on 25th May but it was later verified that its corresponding demodulator unit at the base station was set up incorrectly, receiving signal from station JCPB instead of JCSM. This problem was fixed on 29th August 87. During the period 14th - 21st July station JCSC was out of order due a fire in the site, probably caused by lightning. Other technical problems with the outstations were mainly related to flat batteries.

At the base station, one Geostore tape recorder was used for continuous analogue recording and another Geostore remained in the base station as spare equipment. On 6th June, the first Geostore developed a fault due a capstan servo malfunction and was substituted by the second one. Since then, malfunctions of both Geostores recurred several times, resulting in a total of about 31 days of lost data. The main cause of this was integrated circuit faults on the time encoder board or switch board.

A summary of the network status during the recording period is shown on next page.

## Appendix A

## May 87

[illegible]

## June

	01	02	03	04	05	06	07	08	09	10	11	12	13	14	15	16	17	18	19	20	21	22	23	24	25	26	27	28	29	30
AZ	*****	*****	*****	*****	*****	*****	*****	*****	*****	*****	*****	*****	*****	*****	*****	*****	*****	*****	*****	*****	*****	*****	*****	*****	*****	*****	*****	*****	*****	*****
UM	*****	*****	*****	*****	*****	*****	*****	*****	*****	*****	*****	*****	*****	*****	*****	*****	*****	*****	*****	*****	*****	*****	*****	*****	*****	*****	*****	*****	*****	*****
SC	*****	*****	*****	*****	*****	*****	*****	*****	*****	*****	*****	*****	*****	*****	*****	*****	*****	*****	*****	*****	*****	*****	*****	*****	*****	*****	*****	*****	*****	*****
PA	*****	*****	*****	*****	*****	*****	*****	*****	*****	*****	*****	*****	*****	*****	*****	*****	*****	*****	*****	*****	*****	*****	*****	*****	*****	*****	*****	*****	*****	*****
LR	*****	*****	*****	*****	*****	*****	*****	*****	*****	*****	*****	*****	*****	*****	*****	*****	*****	*****	*****	*****	*****	*****	*****	*****	*****	*****	*****	*****	*****	*****
PB	*****	*****	*****	*****	*****	*****	*****	*****	*****	*****	*****	*****	*****	*****	*****	*****	*****	*****	*****	*****	*****	*****	*****	*****	*****	*****	*****	*****	*****	*****
SP	*****	*****	*****	*****	*****	*****	*****	*****	*****	*****	*****	*****	*****	*****	*****	*****	*****	*****	*****	*****	*****	*****	*****	*****	*****	*****	*****	*****	*****	*****
LU	*****	*****	*****	*****	*****	*****	*****	*****	*****	*****	*****	*****	*****	*****	*****	*****	*****	*****	*****	*****	*****	*****	*****	*****	*****	*****	*****	*****	*****	*****
SM	*****	*****	*****	*****	*****	*****	*****	*****	*****	*****	*****	*****	*****	*****	*****	*****	*****	*****	*****	*****	*****	*****	*****	*****	*****	*****	*****	*****	*****	*****

July

	01	02	03	04	05	06	07	08	09	10	11	12	13	14	15	16	17	18	19	20	21	22	23	24	25	26	27	28	29	30	31
AZ	*****																														
UM	*****																														
SC	*****																														
PC	*****																														
LR	*****																														
PB	*****																														
SP	*****																														
LU	*****																														
SM	*****																														

## August

	01	02	03	04	05	06	07	08	09	10	11	12	13	14	15	16	17	18	19	20	21	22	23	24	25	26	27	28	29	30	31											
AZ	*****											-----																					*****									
UM	*****											*****																					** ** *									
SC	*****											*****																					** ** *									
PA	-----											*****																					** ** *									
LR	*****											*****																					** ** *									
PB	*****											*****																					** ** *									
SP	*****											*****																					** ** *									
LU	*****											*****																					** ** *									
SM	*****											*****																					** ** *									

## September

[illegible]

## October

[illegible]

## November

	01	02	03	04	05	06	07	08	09	10	11	12	13	14	15	16	17	18	19	20	21	22	23	24	25	26	27	28	29	30	
AZ	*****													*****					*****												
UM	-*	*	*	*	*	-*	-*	-*	-*	-*	-*	-*	-*						-*	*	*	*	*	*	*	*	*	*	*	*	*
SC	*****													*****					*****												
PA	*****													*****					*****												
LR	*****													*****					*****												
PB	*****													*****					*****												
SP	-*	*	*	*	-*	-*	-*	-*	-*	-*	-*	-*	-*	-*					-*	-*	-*	-*	-*	-*	-*	-*	-*	-*	-*	-*	-*
LU	*****													*****					*****												
SM	*****													*****					*****												

## Appendix A

[illegible]

```

January88
01 02 03 04 05 06 07 08 09 10 11 12 13 14 15 16 17 18 19 20 21 22 23 24 25 26 27 28 29 30 31
AZ *****
UM *****
SC *****
PA *****
LR *****
PB *****
SP -*-*-
LU *****
SM *****

```

	01	02	03	04	05	06	07	08	09	10	11	12	13	14	15	16	17	18	19	20	21	22	23	24	25	26	27	28
AZ	*****																				*****							
UM	*****																				*****							
SC	*****																				*****							
PA	-----																				-----							
LR	*****																				*****							
PB	*****																				*****							*
SP	*****																				*****							
LU	*****																				*****							
SM	*****																				*****							

	01	02	03	04	05	06	07	08	09	10	11	12	13	14	15	16	17	18	19	20	21	22	23	24	25	26	27	28	29	30	31
AZ	*****.	*****													.....	*****															
UM	*****																														
SC	*****.	*****													.....	*****															
PA	*****.	*****													.....	*****															
LR	*****.	*****													.....	*****															
PB	*****.	*****													.....	*****															
SP	*****.	*****													.....	*****															
LU	*****																														
SM	*****.	*****													.....	*****															

```

      April
01 02 03 04 05 06 07 08 09 10 11
AZ .....
UM -----
SA *****
PC *****
LR *****
PB .....
SP *****
LU *****
SM *****

```

\*\*\*\*\* = WORKING

..... = NOT WORKING

----- = WORKING, BUT WITH TECHNICAL PROBLEMS

Table A.1 Timetable of the João Câmara telemetric network.

**APPENDIX B****STATION LOCATIONS, RESPONSE CURVE OF THE SYSTEM AND  
COMPUTER PROGRAMS****B.1 Station coordinates**

Table B.1.1 Station locations determined with reference to 1:100,000 maps and from compass bearings. These station locations were used for the hypocentre determinations in this thesis.

Station	Latitude	Longitude	Location accuracy*
JCAZ	05°34.62'S	35°47.30'W	±50m
JCUM	05°25.22'S	35°40.86'W	±150m
JCSC	05°39.51'S	35°52.86'W	±50m
JCPA	05°34.27'S	35°51.13'W	±50m
JCLR	05°30.87'S	35°44.43'W	±50m
JCSM	05°38.64'S	35°47.56'W	±50m
JCSP	05°27.34'S	35°46.19'W	±50m
JCLU	05°30.92'S	35°39.78'W	±50m
JCPB	05°38.31'S	35°39.57'W	±50m

\* Assumed station location.

Table B.1.2 Station locations rechecked on July 92 using a hand-held GPS receiver (S.Voss, pers. commun., 1992).

Station	Latitude	Longitude	Location accuracy*
JCAZ	05°34.63'S	35°47.16'W	±20m
JCUM	05°25.10'S	35°41.30'W	±20m
JCSC	05°39.52'S	35°52.83'W	±20m
JCPA	05°34.22'S	35°51.15'W	±20m
JCLR	05°30.98'S	35°44.30'W	±20m
JCSM	05°38.68'S	35°47.43'W	±20m
JCSP	05°27.19'S	35°46.02'W	±20m
JCLU	05°30.95'S	35°39.70'W	±20m
JCPB	05°38.87'S	35°39.93'W	±20m

\* Assumed station location.

## B.2 Response curve

The recording system is composed of the Willmore MKIII-A seismometer, Earth Data amplifier-modulator and the Geostore tape recorder. The Willmore MKII-A is a velocity meter device in which the output signal depends on the frequency of the input signal. The velocity response rises steeply to 1 Hz and flattens towards the higher frequencies. In the high frequency region, the overall response of the the system is severely limited by the recording speed of the Geostore which was set up for 15/160 inches per second. At this speed, the velocity response of the system has a practical upper limit of 32 Hz.

The digitizing sytem comprises a Store 14 tape replay and the BGS digitizer. Events were digitized at a rate of 100 samples per second and each 1 volt input was converted to 2,048 counts by the digitizer. The basic seismic data path for the J.Câmara network is in the sketch of figure B.2.1 and the frequency response curve of the overall system is in figure B.2.2. As an example, a ground motion amplitude of  $10^{-6}$  m/s in a pulse with frequency in the range 1-30 Hz recorded by the seismometer will be finally converted to:

$$(10^{-6} \text{ m/s}) \times (500 \text{ volts/m/s}) \times 400 \times (2048 \text{ counts/volt}) = 409 \text{ counts}$$

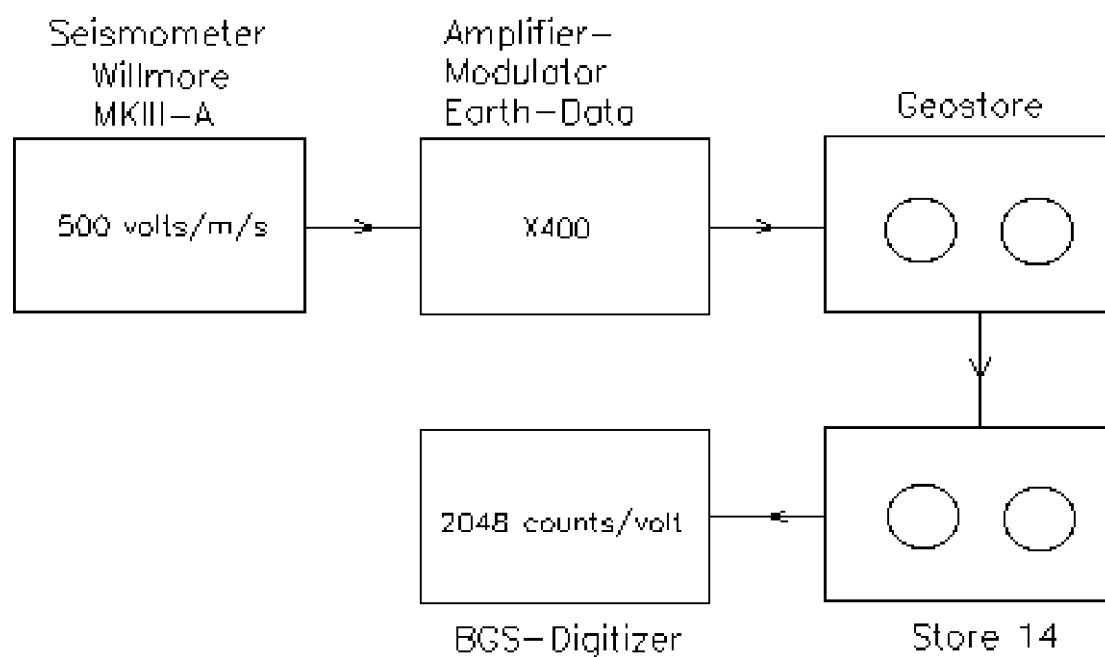


Figure B.2.1 Sketch showing the main stages affecting the seismic signal used in this thesis from the J.Câmara telemetered network. For simplicity, the radio link is not shown. The scheme emphasizea the system amplification of the ground motion.

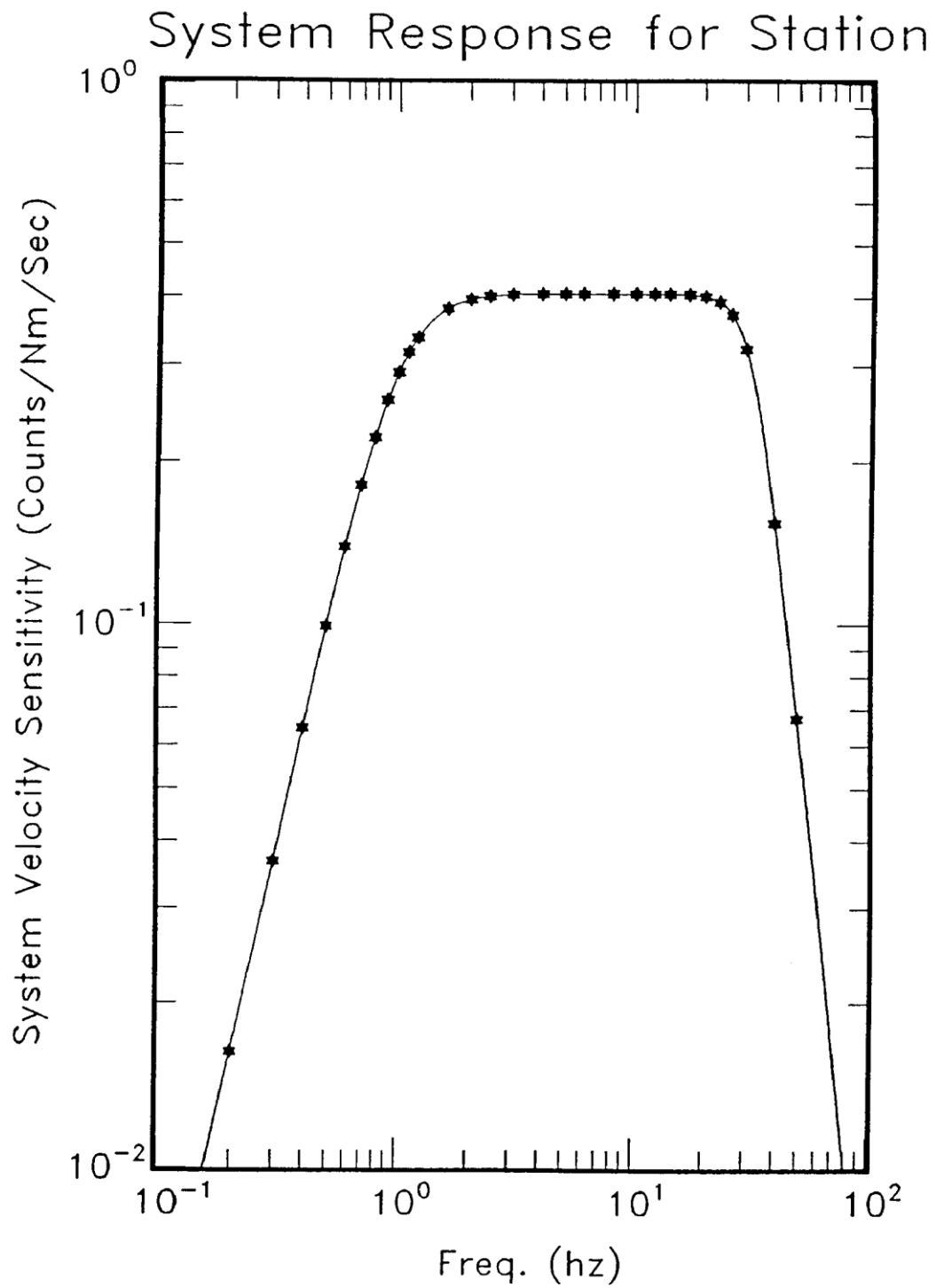


Figure B.2.2 Frequency response curve for the overall J.Câmara seismic network as in the sketch of figure B.2.1. The unit for the vertical axis is in counts per nanometre (Nm) per second.

### B.3 Computer programs

Most software used in this work has been mentioned in the appropriate chapters. Programs to handle the outputs of HYPO71 (Lee & Lahr) were, with minor alteration, performed by several utilities written for the preparation of previous work (Ferreira et al., 1987; Takeya et., 1989 and Assumpção et al., 1990) in which I have participated, or for the work of Assumpção & Sophia, 1989. Graphics were done using commercial software: Lotus 123; Lotus Freelance; Microfax Charisma; Grapher and Surfer programs from Golden Software and the IASPEI Pixplot (Lee & Tottingham, 1990) program.

Below is a listing of the program BGSTOPC.FOR written for this thesis. This program converts the ADC format, used in the seismograms digitized by the BGS digitizer system, to the PCEQ format used by IASPEI software PCEQ (Lee, 1990). This listing is given because some information in the IASPEI manual is conflicting with information displayed by the 'readme' file of the PCEQ program (Valdés, 1989), so this listing will be of value to future users.

#### BGSTOPC.FOR

```
C Program to convert ADC format used by the BGS digitizer
C to PCEQ format used by the seismogram analysis program
C PCEQ (Valdés, 1989).
  CHARACTER*80 HEADER(51)
  CHARACTER*16 PAD
  CHARACTER*25 FILE1
  CHARACTER*4 STAT(12)
  CHARACTER*2 DATE1(6)
  INTEGER*2 DATE(7)
  INTEGER*2 IRATE
  INTEGER*2 PCMAXTRA
  INTEGER*2 GAIN
  INTEGER*2 IBLANK(257)
  INTEGER*2 BLANK
  INTEGER*2 D(257)
  INTEGER*2 NUMSTA
  INTEGER*2 NPCBL
  INTEGER*2 IINPUT(2040)
  INTEGER*2 NADCBL
  INTEGER*2 ADCREC
  INTEGER*2 ADCSAMP
  INTEGER*2 IPAD(8)
  INTEGER*2 nch
  INTEGER*2 MAXTRA
  INTEGER*2 CSAMPL
  REAL TLEN, tsize, TSAMPLE, PCSIZE
  PARAMETER (IRATE=100, GAIN=2048, ADCREC=4096, ADCSAMP=2048)
  DATA NCH/12/NUMSTA/12/BLANK/00/
  PRINT*, 'BGSTOPC V2'
  PRINT*, 'INPUT FILE NAME: '
  READ(*, '(A25)') FILE1
  PRINT*, ' '
  PRINT*, 'OUTPUT FILE WILL BE ALWAYS: EQ.WVM'
  OPEN(1, FILE=FILE1, FORM='BINARY', STATUS='OLD')
```



## Appendix B

```

C  READ ASCII BGSHEADER DATA AND EXCHANGE VARIABLES
  READ (1)HEADER,PAD
    IF (HEADER(17) (13:15).EQ.'Jan')  HEADER(17) (13:15)='01'
    IF (HEADER(17) (13:15).EQ.'Feb')  HEADER(17) (13:15)='02'
    IF (HEADER(17) (13:15).EQ.'Mar')  HEADER(17) (13:15)='03'
    IF (HEADER(17) (13:15).EQ.'Apr')  HEADER(17) (13:15)='04'
    IF (HEADER(17) (13:15).EQ.'May')  HEADER(17) (13:15)='05'
    IF (HEADER(17) (13:15).EQ.'Jun')  HEADER(17) (13:15)='06'
    IF (HEADER(17) (13:15).EQ.'Jul')  HEADER(17) (13:15)='07'
    IF (HEADER(17) (13:15).EQ.'Aug')  HEADER(17) (13:15)='08'
    IF (HEADER(17) (13:15).EQ.'Sep')  HEADER(17) (13:15)='09'
    IF (HEADER(17) (13:15).EQ.'Oct')  HEADER(17) (13:15)='10'
    IF (HEADER(17) (13:15).EQ.'Nov')  HEADER(17) (13:15)='11'
    IF (HEADER(17) (13:15).EQ.'Dec')  HEADER(17) (13:15)='12'
    DATE1(1)=HEADER(17) (17:18)
    DATE1(2)=HEADER(17) (13:15)
    DATE1(3)=HEADER(17) (10:11)
    DATE1(4)=HEADER(17) (20:21)
    DATE1(5)=HEADER(17) (23:24)
    DATE1(6)=HEADER(17) (26:27)
C  WRITE THE BGS  HEADER TO 'TMP'FILE IN 'A' FORMAT AND READ IT IN
C  'I' FORMAT
    OPEN(3,FILE='TMP',STATUS='UNKNOWN')
    WRITE(3,15)DATE1(1),DATE1(2),DATE1(3),DATE1(4),
+DATE1(5),DATE1(6)
    REWIND (3)
    READ(3,17)DATE(1),DATE(2),DATE(3),DATE(4),DATE(5),DATE(6)
    DATE(7)=000
    DO 55 I=1,12
55  STAT(I) (1:4)=HEADER(I+4) (13:16)
C  CALCULATE THE NUMBER OF SAMPLES IN THE LONGEST TRACES (MAXTRA) AND
C  THE NUMBER OF PC BLOCK (NPCBL) FOR EACH CHANNEL
    CSAMPL=(ADCSAMP/NCH)*NCH
    NADCBL=0
58  READ (1,END=59) IINPUT,PAD
    NADCBL=NADCBL+1
    GO TO 58
59  TSAMPL=CSAMPL*NADCBL
    MAXTRA=TSAMPL/NCH
    NPCBL=(MAXTRA/255)
    PCMAXTRA=NPCBL*255
C  WRITE SOME INFORMATION TO THE SCREEN
    TLEN=real(MAXTRA)/real(IRATE)
    TSIZE=real(ADCREC)*real(nadcbl+1)
    PCLEN=real(255)/real(IRATE)
    TPCLN=real(NPCBL)*PCLEN
    PCSIZE=real(516)*real(5+NCH+NPCBL*NCH)
    PRINT*, '*****'
    PRINT*, 'Input File Information:'
    WRITE(*,61) NCH,TLEN,TSIZE,TSAMPLE
61  FORMAT (1x,I2,' channels of data in ADC file, each record length
+','F6.2,' seconds',/,1x,'Input file size ',F7.0,' bytes'
+' (including 4096 bytes header)',/,1x,'Total number of samples:
',
+
+F8.0)
    PRINT*, '*****'
    PRINT*, 'Output File Information'
    WRITE(*,62)NCH,NPCBL,PCLEN,TPCLN,PCSIZE
62  FORMAT (1x,I2,1X,'Channells. Each one has ',I3,
+' blocks. Each block is',1X,F6.2,' seconds long.',/,
+ 1x,'Total time length is',1X,F6.2,' seconds.',1X,
+'Output file size:',F7.0,'bytes')
    PRINT*, '*****'
    PRINT*, 'Writing data blocks'
    PRINT*, 'Station Order:',(STAT(I) (1:4),I=1,12)
C  OPEN OUTPUT FILE AND WRITE DATA RECORDS
    OPEN(2,FILE='EQ.WVM',RECL=516,FORM='UNFORMATTED',
+STATUS='unknown',ACCESS='DIRECT')
C  WRITE FIRST RECORD
    WRITE(2) blank,blank,DATE(1),DATE(2),DATE(3),DATE(4),

```

## Appendix B

```
+DATE (5) , DATE (6) , DATE (7) , IRATE , PCMAXTRA , NUMSTA
C WRITE 4 EMPTY LINES
  WRITE (2,REC=2) IBLANK
  WRITE (2,REC=3) IBLANK
  WRITE (2,REC=4) IBLANK
  WRITE (2,REC=5) IBLANK
  REWIND (1)
C WRITE THE HEADER AND DATA BLOCKS FOR EACH CHANNELL
DO 220 ICH=1,NCH
  INB=1
  READ (1)HEADER,PAD
C HEADER
  WRITE (2) blank,blank,STAT (ICH) (1:4) ,GAIN,DATE (1) ,
+   DATE (2) , DATE (3) , DATE (4) , DATE (5) , DATE (6) , DATE (7) ,
+   NPCBL
C DATA BLOCKS
  J=3
  70 READ (1,END=200) IINPUT,IPAD
    D(1)=BLANK
    D(2)=BLANK
    DO 80 I=ICH,csampl,12
      D(J)=IINPUT(I)
      IF ((J.EQ.257).AND.(INB.NE.NPCBL)) THEN
        WRITE(2) D
        J=2
        INB=INB+1
      ELSE
        IF ((J.EQ.257).AND.(INB.EQ.NPCBL)) THEN
          D(256)=BLANK
          D(257)=BLANK
          WRITE(2) D
          go to 200
        END IF
      END IF
      J=J+1
  80 CONTINUE
  GO TO 70
200 REWIND (1)
220 CONTINUE
15 FORMAT (6A2)
17 FORMAT (6I2)
  CLOSE (1)
  CLOSE (2)
  CLOSE (3)
  STOP
  END
```

## **APPENDIX C**

### **LIST OF EARTHQUAKES**

#### **C.1 Earthquakes recorded by the telemetric network**

The following list of earthquakes is basically the summary output of the location program HYPO71 (Lee & Lahr, 1975). The list contains information on the 3,780 earthquakes recorded by the João Câmara telemetric network, which forms dataset 3 of this work.

DATE	Date of earthquake: year, month and day.
ORIGIN	Origin time: hour, minute and second (Universal time).
LAT S	Latitude of epicentre in degrees and minutes.
LONG W	Longitude of epicentre in degrees and minutes.
DEPTH	Focal depth in km. A '*' may follow the DEPTH to indicate a fixed focal depth solution.
MAG	Duration magnitude of the earthquake. For duration larger than 15.5 seconds, it was calculated from the equation: $MAG = 2.01 \cdot \log(D) - 1.39$ and for earthquakes with duration less than 15.5 seconds, it was calculated from: $MAG = 0.71 \cdot \log(D) + 0.16$ where D is the duration of the earthquake.
NO	Number of station readings used in locating the earthquake. P and S arrivals for the same station are regarded as 2 readings.
GAP	Largest azimuthal separation in degrees between stations.
DMIN	Epicentral distance to the nearest station.
RMS	Root mean square error of time residual in sec. $RMS = (R_i^2 / NO)^{1/2}$ , where $R_i$ is the time residual for the $i$ th station.
ERH	Standard error of the epicentre in km. $ERH = (SDX^2 + SDY^2)^{1/2}$ , where SDX and SDY are the standard errors in latitude and longitude, respectively, of the epicentre. If ERH is blank, this means that ERH cannot be computed because of insufficient data
ERZ	Standard error of the focal depth in km. If ERZ is blank, this means that ERZ cannot be computed either because the focal depth is fixed in the solution or because of insufficient data.

### *Appendix C*

Q      Solution quality of hypocentre. This measure is intended to indicate the general reliability of the solution.

<u>Q</u>	<u>Epicentre</u>	<u>Focal depth</u>
A	excellent	good
B	good	fair
C	fair	poor
D	poor	poor

D      An asterisk (\*) means that the earthquake was selected and used in dataset 4. A plus sign (+) means that the earthquake was used in dataset 5.

# Appendix C

DATE	ORIGIN	LAT S	LONG W	DEPTH	MAG	NO	GAP	DMIN	RMS	ERH	ERZ	Q	D
870523	0306	01.99	5-36.44	35-48.19	3.85	0.57	11	135	3.7	.05	0.2	0.4	B *+
870523	0737	39.84	5-31.86	35-45.47	5.01	0.46	11	127	2.6	.03	0.1	0.2	B *+
870523	0746	07.30	5-31.83	35-45.42	5.08	0.55	12	126	2.5	.02	0.1	0.1	B *+
870523	1532	46.38	5-38.04	35-48.49	2.04	0.54	09	160	6.7	.03	0.2	0.8	B *
870523	1900	03.46	5-31.37	35-44.91	3.24	0.20	07	173	1.3	.02	0.3	0.3	B *
870523	1900	05.78	5-31.34	35-44.72	3.17	0.36	09	133	1.0	.06	0.3	0.4	B *
870523	1945	14.88	5-27.90	35-41.73	0.99	0.74	12	230	6.6	.05	0.3	1.5	C *
870523	2002	21.13	5-32.92	35-45.82	1.72	0.43	10	129	4.2	.02	0.1	0.3	B *+
870523	2053	05.75	5-30.73	35-44.91	6.66	0.52	09	117	0.9	.01	0.1	0.1	B *+
870524	1216	52.59	5-30.00	35-44.53	6.88	0.44	10	133	1.6	.06	0.3	0.4	B *
870525	0612	50.90	5-32.92	35-45.83	1.52	0.31	10	129	4.2	.05	0.2	0.8	B *
870525	0614	14.94	5-32.95	35-45.87	2.00	0.72	12	130	4.1	.03	0.1	0.3	B *+
870525	0948	07.35	5-33.58	35-46.50	3.80	1.25	12	136	2.4	.02	0.1	0.1	B *+
870525	1548	24.48	5-28.26	35-41.77	2.80	0.50	10	221	6.1	.13	0.7	1.8	C
870525	1623	55.55	5-30.41	35-44.86	4.51	0.42	09	161	1.2	.09	0.7	0.7	B *
870525	1624	05.19	5-30.66	35-44.61	5.00	0.41	09	165	0.5	.02	0.1	0.1	B *+
870525	1624	11.28	5-30.57	35-44.53	5.34	0.45	09	175	0.6	.06	0.3	0.4	B *
870525	1921	03.35	5-32.03	35-44.99	1.39	0.65	10	119	2.4	.03	0.1	0.3	B *+
870525	2131	06.42	5-30.72	35-44.94	7.29	0.83	12	118	1.0	.02	0.1	0.1	B *+
870525	2159	02.59	5-37.25	35-48.03	2.69	1.22	11	148	5.0	.02	0.1	0.3	B *+
870525	2320	01.81	5-30.71	35-44.98	7.11	0.54	08	126	1.0	.02	0.1	0.2	B *
870525	2342	41.02	5-37.23	35-47.97	2.91	0.48	10	148	5.0	.03	0.1	0.3	B *+
870526	0217	48.57	5-28.98	35-42.84	2.89	0.51	09	186	4.6	.09	0.4	0.9	C *
870526	0314	02.18	5-31.12	35-45.25	7.34	0.45	08	124	1.6	.03	0.2	0.3	B *+
870526	0322	12.73	5-30.14	35-42.35	3.81	0.51	10	161	4.1	.06	0.3	0.4	B *
870526	0357	07.94	5-30.83	35-44.99	6.05	0.49	07	119	1.0	.04	0.3	0.5	B *
870526	0443	52.66	5-30.86	35-45.00	7.07	0.80	12	119	1.1	.02	0.1	0.1	B *+
870527	0012	57.93	5-34.91	35-48.39	2.75	0.66	09	265	2.1	.08	0.8	0.5	C *
870527	0103	08.67	5-27.17	35-41.43	4.83	0.95	13	140	3.7	.04	0.2	0.3	B *+
870527	0115	21.42	5-28.51	35-42.45	2.49	1.99	10	106	5.7	.03	0.2	0.9	B *
870527	0120	00.19	5-28.59	35-42.43	1.15	0.84	10	106	5.6	.03	0.1	0.8	B *
870527	0233	42.88	5-28.53	35-42.50	2.06	0.93	10	105	5.6	.03	0.1	0.5	B *+
870527	0256	11.17	5-28.52	35-42.37	0.40	0.80	11	108	5.8	.03	0.1	2.4	B *
870527	0317	14.39	5-28.51	35-42.40	0.65	0.59	11	107	5.7	.05	0.2	2.3	B *
870527	0333	55.87	5-28.56	35-42.42	0.88	0.59	10	107	5.6	.03	0.1	1.2	B *
870527	0539	07.59	5-28.48	35-42.41	0.59	0.37	08	107	5.8	.05	0.3	3.4	B *
870527	0652	07.46	5-31.73	35-45.22	4.50	0.76	11	132	2.2	.01	0.1	0.1	B *+
870527	0653	52.24	5-31.73	35-45.17	4.42	1.13	11	130	2.1	.01	0.1	0.1	B *+
870527	0729	49.80	5-31.73	35-45.19	4.45	0.59	10	131	2.1	.01	0.1	0.1	B *+
870527	0818	59.98	5-28.63	35-42.48	1.43	0.66	11	105	5.5	.05	0.2	1.0	B *
870527	0936	58.95	5-29.22	35-42.98	3.07	0.71	11	090	4.0	.03	0.1	0.3	A *+
870527	0953	36.07	5-27.21	35-41.39	4.72	0.50	10	142	3.8	.03	0.1	0.3	B *+
870527	0317	18.98	5-28.53	35-42.39	0.64	1.23	12	108	5.7	.03	0.1	1.3	B *
870527	1058	06.93	5-31.73	35-45.29	4.67	0.80	12	134	2.2	.01	0.0	0.1	B *+
870527	1610	31.04	5-28.43	35-42.38	1.35	1.38	14	108	5.9	.06	0.2	1.6	B *
870527	1641	27.11	5-32.31	35-46.03	4.55	0.59	14	135	4.0	.03	0.1	0.2	B *+
870527	1800	18.97	5-37.66	35-49.20	3.02	0.71	08	149	6.6	.04	0.2	0.6	B *
870527	2333	45.81	5-29.09	35-41.94	2.30	0.50	08	115	5.2	.06	0.3	1.2	B *
870528	1945	06.89	5-29.18	35-43.14	3.06	0.50	11	089	3.9	.07	0.3	0.6	A *
870529	0013	49.03	5-30.97	35-44.99	7.21	0.59	14	119	1.0	.05	0.2	0.3	B *+
870529	0118	14.09	5-31.73	35-42.75	4.10	0.37	08	104	5.6	.01	0.1	0.2	B *+
870529	0121	51.59	5-29.76	35-43.79	3.75	0.71	14	092	2.4	.04	0.1	0.2	B *+
870529	0238	40.91	5-37.57	35-49.15	3.40	0.50	07	148	6.4	.02	0.1	0.3	B *
870529	0326	24.04	5-31.42	35-44.53	2.72	0.50	11	112	1.0	.04	0.2	0.4	B *+
870529	0349	59.73	5-34.96	35-48.52	2.61	1.49	13	153	2.3	.04	0.2	0.5	B *+
870529	0357	48.64	5-34.95	35-48.53	2.48	0.90	14	154	2.3	.04	0.2	0.2	B *+
870529	0457	58.60	5-36.53	35-48.38	5.00	0.37	07	137	9.9	.01	0.1	0.4	B *
870529	0500	53.70	5-34.97	35-48.50	2.58	0.37	06	153	2.3	.03	0.2	0.3	B *
870529	0538	30.54	5-37.93	35-48.52	1.67	0.37	08	158	6.5	.05	0.2	1.3	B *
870529	0547	51.73	5-37.01	35-47.89	2.53	0.50	11	144	4.5	.04	0.2	0.6	B *
870529	0740	32.48	5-34.96	35-48.48	2.47	0.97	14	153	2.3	.05	0.2	0.3	B *+
870529	0928	52.84	5-34.93	35-48.44	2.48	1.52	14	152	2.2	.05	0.2	0.3	B *+
870529	0930	20.63	5-34.91	35-48.51	2.36	0.50	09	154	2.3	.05	0.3	0.4	B *+
870529	1001	51.29	5-28.40	35-42.22	0.38	0.37	09	113	6.1	.04	0.1	2.9	B *
870529	1003	13.70	5-31.62	35-45.25	5.43	0.37	09	132	2.0	.02	0.1	0.1	B *+
870529	1030	16.07	5-35.01	35-48.49	2.44	0.50	11	153	2.3	.05	0.2	0.3	B *+
870529	1033	23.03	5-34.83	35-48.41	2.59	0.37	08	153	2.1	.04	0.2	0.3	B *+
870529	1113	20.02	5-34.88	35-48.61	2.42	1.79	11	155	2.5	.05	0.3	0.7	B *
870529	1115	01.08	5-30.14	35-44.43	7.15	1.66	13	106	1.3	.05	0.2	0.4	B *+
870529	1341	34.88	5-28.59	35-42.44	0.70	0.50	11	106	5.6	.06	0.2	2.7	B *
870529	1354	31.59	5-28.54	35-42.38	0.66	0.59	11	108	5.7	.07	0.2	3.1	B *
870529	1401	56.64	5-34.99	35-48.48	2.29	0.93	12	114	2.3	.03	0.1	0.2	B *+
870529	1504	39.86	5-34.96	35-48.46	2.23	1.13	16	114	2.2	.04	0.1	0.2	B *+
870529	1520	36.90	5-35.00	35-48.47	2.18	0.50	14	114	2.3	.04	0.1	0.2	B *+
870529	1546	28.87	5-32.14	35-44.99	1.44	1.35	15	095	2.6	.03	0.1	0.5	B *+
870529	1547	50.35	5-32.14	35-44.97	1.33	2.38	10	095	2.5	.02	0.1	0.4	B *+
870529	1600	52.10	5-30.45	35-43.65	1.69	1.27	15	078	1.6	.04	0.1	0.5	A *+
870529	1546	49.62	5-32.22	35-44.99	0.12	0.80	14	095	2.7	.04	0.1	6.7	C *
870529	1656	15.00	5-31.73	35-45.20	4.56	0.87	15	100	2.1	.02	0.1	0.1	B *+
870529	1753	59.39	5-31.76	35-49.77	4.26	0.80	12	190	5.3	.02	0.1	0.2	C *+
870529	1825	12.74	5-28.35	35-42.23	0.45	0.59	10	113	6.2	.07	0.3	5.8	C *
870529	1913	02.87	5-28.72	35-42.43	2.00	0.50	11	106	5.4	.05	0.2	0.7	B *

DATE	ORIGIN	LAT S	LONG W	DEPTH	MAG	NO	GAP	DMIN	RMS	ERH	ERZ	Q	D
870529	1932	24.93	5-32.79	35-46.31	4.60	0.37	10	137	3.8	.02	0.1	0.1	B *+
870529	1958	31.42	5-34.98	35-48.48	2.38	0.84	14	114	2.3	.03	0.1	0.2	B *+
870529	2014	11.66	5-36.97	35-47.97	3.05	0.87	14	144	4.5	.06	0.2	0.5	B *
870529	2237	10.22	5-37.06	35-48.15	1.58	0.37	08	144	4.8	.03	0.2	0.8	B *
870530	0811	12.03	5-30.37	35-44.30	5.53	0.37	08	105	0.9	.03	0.1	0.2	B *+
870531	0113	48.75	5-29.26	35-43.63	6.24	0.76	14	088	3.3	.04	0.1	0.2	A *+
870530	1033	12.39	5-30.62	35-44.84	7.51	1.00	14	116	0.9	.04	0.2	0.2	B *+
870530	1034	17.19	5-34.99	35-48.40	2.30	0.76	09	119	2.1	.02	0.1	0.2	B *+
870531	0122	59.54	5-29.20	35-43.61	6.11	0.50	13	089	3.4	.04	0.2	0.2	A *+
870531	0146	53.17	5-29.24	35-43.64	6.19	0.50	14	088	3.3	.04	0.2	0.2	A *+
870531	0212	45.09	5-29.21	35-43.58	6.40	0.59	14	089	3.4	.04	0.1	0.2	A *+
870531	0307	33.38	5-32.78	35-45.97	1.21	0.37	07	132	4.2	.03	0.2	0.7	B *
870531	0619	24.71	5-37.61	35-49.34	4.08	0.50	09	148	6.7	.05	0.3	0.5	B *
870531	1001	14.99	5-30.57	35-44.87	7.44	1.76	14	098	1.0	.04	0.2	0.3	B *
870531	1007	38.01	5-30.68	35-44.83	6.72	0.50	11	115	0.8	.03	0.1	0.3	B *
870531	1009	18.21	5-30.59	35-44.86	7.52	1.42	14	098	1.0	.05	0.2	0.3	B *+
870531	1611	55.97	5-36.42	35-47.88	2.77	0.66	09	135	3.5	.01	0.1	0.1	B *+
870531	1655	21.95	5-30.56	35-44.84	7.42	1.23	15	098	0.9	.05	0.2	0.3	B *
870531	1832	54.62	5-36.64	35-48.35	4.49	0.50	09	137	4.2	.02	0.1	0.2	B *+
870531	1915	28.96	5-36.04	35-47.71	3.93	0.37	06	140	2.7	.01	0.1	0.1	B *
870531	2200	55.54	5-34.33	35-47.81	5.42	0.37	08	149	1.1	.03	0.2	0.2	B *+
870601	0016	32.54	5-29.92	35-42.70	0.41	1.42	14	087	3.6	.06	0.2	3.5	B *
870601	0032	45.39	5-29.55	35-43.31	3.07	0.66	11	084	3.2	.03	0.1	0.2	A *+
870601	0051	20.36	5-30.41	35-44.32	5.40	0.50	12	105	0.9	.04	0.1	0.2	B *+
870601	0116	50.17	5-32.96	35-45.64	3.02	0.37	12	127	4.3	.18	0.7	1.5	B *
870601	0150	13.45	5-30.40	35-44.29	5.39	0.37	08	105	0.9	.03	0.1	0.2	B *+
870601	0032	52.87	5-29.55	35-43.32	2.88	0.66	12	084	3.2	.03	0.1	0.2	A *+
870601	0051	31.07	5-30.72	35-44.32	5.63	0.37	07	125	0.3	.04	0.3	0.4	B *
870602	1347	31.48	5-28.33	35-42.48	3.04	1.79	12	106	5.9	.06	0.3	1.2	B *
870602	1414	43.93	5-34.93	35-48.28	2.57	1.03	16	114	1.9	.04	0.1	0.2	B *+
870602	1911	59.43	5-29.81	35-43.76	3.74	0.59	12	092	2.3	.04	0.1	0.2	B *+
870602	2003	36.74	5-30.58	35-44.81	7.67	0.71	14	097	0.9	.05	0.2	0.3	B *+
870602	2015	50.37	5-30.75	35-44.44	4.33	0.80	14	109	0.2	.05	0.2	0.2	B *+
870602	2027	39.39	5-34.55	35-46.91	3.29	1.58	15	113	0.7	.05	0.2	0.4	B *+
870602	2042	14.37	5-32.32	35-45.05	1.48	0.59	13	120	2.9	.03	0.1	0.4	B *+
870603	0209	49.73	5-29.90	35-43.75	3.53	0.50	10	148	2.2	.02	0.1	0.1	B *+
870603	0221	43.47	5-29.81	35-43.77	4.35	0.71	12	150	2.3	.06	0.3	0.3	B *
870603	0222	29.12	5-29.86	35-43.82	3.88	1.61	13	148	2.2	.03	0.1	0.2	B *+
870603	0224	40.72	5-29.80	35-43.67	3.49	0.66	10	152	2.4	.02	0.1	0.2	B *+
870603	0226	50.42	5-29.90	35-43.83	3.97	0.66	11	147	2.1	.03	0.1	0.2	B *+
870603	0246	34.57	5-29.91	35-43.86	3.82	0.80	12	146	2.1	.03	0.1	0.2	B *+
870603	0252	55.59	5-29.95	35-43.76	3.63	0.66	11	147	2.1	.04	0.2	0.3	B *+
870603	0222	55.46	5-29.86	35-43.83	3.69	0.80	12	148	2.2	.04	0.2	0.2	B *+
870603	0224	57.85	5-29.81	35-43.71	3.52	0.71	12	151	2.4	.03	0.1	0.2	B *+
870603	0252	56.69	5-29.86	35-43.81	3.86	0.59	10	148	2.2	.04	0.2	0.2	B *+
870603	0303	40.94	5-29.97	35-43.81	3.63	0.59	11	145	2.0	.03	0.1	0.2	B *+
870603	0416	01.94	5-29.94	35-43.85	3.87	1.18	16	079	2.0	.04	0.1	0.1	A *+
870603	0420	39.45	5-29.97	35-43.83	3.64	0.59	11	145	2.0	.03	0.1	0.2	B *+
870603	0459	44.25	5-29.94	35-43.71	3.69	0.59	08	148	2.2	.02	0.1	0.2	B *+
870603	0813	47.36	5-34.47	35-46.90	3.17	0.59	09	116	0.8	.04	0.2	0.2	B *+
870603	2145	07.98	5-37.40	35-49.35	4.57	0.76	12	144	6.4	.05	0.2	0.5	B *+
870603	2256	29.07	5-30.41	35-44.75	7.26	1.31	16	096	1.0	.06	0.2	0.3	B *
870604	0052	50.40	5-35.05	35-48.31	2.31	1.00	14	115	2.0	.04	0.1	0.3	B *+
870604	0825	12.30	5-31.17	35-45.11	6.71	0.66	12	121	1.4	.04	0.2	0.3	B *+
870604	1408	36.24	5-32.71	35-46.16	4.62	0.59	12	135	4.1	.02	0.1	0.1	B *+
870604	1806	03.29	5-28.38	35-42.30	2.31	2.24	12	111	6.0	.05	0.2	1.2	B *
870604	1846	57.05	5-28.38	35-42.22	0.95	0.95	14	113	6.1	.05	0.2	1.5	B *
870604	2003	29.55	5-35.00	35-48.53	2.08	0.93	13	114	2.4	.05	0.2	0.4	B *+
870603	0416	49.46	5-29.94	35-43.81	3.82	0.50	09	146	2.1	.02	0.1	0.2	B *+
870604	2011	04.10	5-28.34	35-42.26	2.29	1.23	12	112	6.1	.06	0.2	0.9	B *
870604	2016	02.53	5-28.44	35-42.22	1.25	0.80	15	112	6.1	.06	0.2	1.3	B *
870604	2016	08.69	5-28.27	35-42.18	0.39	0.66	10	114	6.1	.07	0.2	4.7	B *
870604	2032	04.98	5-28.47	35-42.23	0.61	1.31	15	112	6.0	.06	0.2	2.4	B *
870604	2033	49.61	5-28.33	35-42.18	0.79	0.66	13	114	6.2	.05	0.2	1.6	B *
870604	2340	40.30	5-28.36	35-42.21	0.88	0.80	14	113	6.2	.05	0.2	1.4	B *
870605	0127	49.24	5-36.47	35-49.16	3.04	0.90	14	130	4.8	.03	0.1	0.3	B *+
870605	0442	54.77	5-28.24	35-42.17	0.83	0.59	12	216	6.4	.05	0.2	1.7	C *
870605	0936	09.72	5-28.39	35-42.14	2.60	1.23	14	115	6.2	.08	0.3	0.9	B *
870605	0939	54.72	5-28.34	35-42.27	2.20	1.83	12	112	6.1	.06	0.3	1.4	B *
870605	1810	28.37	5-31.88	35-44.68	0.26	0.50	10	115	1.9	.04	0.1	2.6	B *
870526	1213	16.57	5-37.88	35-49.64	4.39	0.70	10	151	6.7	.07	0.4	0.6	B *
870526	1440	48.79	5-35.04	35-48.37	2.08	0.61	08	178	2.1	.03	0.2	0.2	B *+
870526	1632	22.15	5-32.86	35-45.98	1.68	0.46	10	132	4.1	.05	0.2	0.6	B *
870526	1648	21.64	5-30.73	35-45.06	7.36	0.73	13	120	1.2	.02	0.1	0.2	B *+
870526	2104	22.52	5-35.39	35-46.69	0.81	1.09	14	172	1.8	.07	0.3	0.9	B *
870526	2137	53.00	5-34.97	35-48.53	1.96	0.63	06	295	2.4	.01	0.1	0.1	C *
870528	0031	16.47	5-31.59	35-45.50	6.45	0.67	14	128	2.4	.02	0.1	0.1	B *+
870528	0058	18.52	5-28.83	35-41.95	0.43	0.56	11	117	5.6	.08	0.3	4.7	B *
870528	0224	53.11	5-31.71	35-45.78	6.66	0.37	06	147	2.9	.01	0.1	0.1	B *
870528	0227	25.62	5-32.87	35-46.27	3.17	0.42	06	168	3.8	.00	0.0	0.0	B
870528	0253	55.67	5-28.81	35-41.85	0.85	0.42	09	120	5.5	.08	0.3	2.8	B *
870528	1139	18.03	5-27.11	35-41.68	5.00	0.56	10	130	3.8	.17	0.9	1.7	B

# Appendix C

DATE	ORIGIN	LAT S	LONG W	DEPTH	MAG	NO	GAP	DMIN	RMS	ERH	ERZ	Q	D
870528	1227	53.38	5-38.48	35-49.11	2.40	0.87	10	166	7.2	.04	0.2	0.9	B *
870528	1331	08.44	5-36.06	35-47.69	3.16	0.35	05	139	2.7	.01	0.2	0.4	C
870528	1435	29.21	5-34.99	35-48.64	1.65	0.83	11	155	2.6	.06	0.3	0.5	B *
870528	1435	29.21	5-35.07	35-48.58	1.75	0.86	12	153	2.5	.06	0.3	0.5	B *
870528	1938	38.12	5-36.98	35-47.95	2.15	1.34	11	144	4.5	.08	0.4	1.0	B *
870528	2312	19.67	5-28.35	35-42.24	0.78	0.58	12	112	6.2	.07	0.2	2.9	B *
870528	2313	33.52	5-33.76	35-46.68	3.86	0.36	10	137	2.0	.03	0.1	0.1	B *
870530	0100	42.88	5-31.63	35-45.24	4.26	0.38	05	192	2.0	.00	0.0	0.0	C
870530	0101	53.48	5-31.64	35-45.14	3.91	0.50	09	122	1.9	.06	0.3	0.5	B *
870530	0114	08.82	5-31.68	35-45.18	4.04	0.51	12	122	2.0	.08	0.3	0.5	B *
870530	0148	43.58	5-31.80	35-45.28	4.05	0.79	14	124	2.3	.04	0.1	0.2	B *
870530	0149	54.43	5-31.70	35-45.16	3.82	0.44	09	122	2.0	.06	0.3	0.5	B *
870530	0242	54.39	5-27.16	35-41.58	4.10	0.54	12	134	3.8	.08	0.4	0.8	B *
870530	0448	54.79	5-31.76	35-45.30	3.61	0.42	10	124	2.3	.08	0.3	0.6	B *
870530	0525	45.04	5-31.96	35-45.50	4.78	0.48	09	127	2.8	.02	0.1	0.2	B *
870530	0527	10.79	5-32.01	35-45.50	5.69	0.39	08	137	2.9	.09	0.6	0.8	B *
870530	0527	11.18	5-31.88	35-45.28	3.91	0.68	11	124	2.4	.08	0.4	0.6	B *
870530	0527	35.38	5-31.75	35-45.22	4.12	0.39	07	132	2.2	.03	0.2	0.3	B *
870530	0530	34.22	5-37.72	35-49.53	3.23	0.49	08	148	7.0	.02	0.1	0.3	B *
870530	0531	21.17	5-35.01	35-48.46	2.34	0.53	09	152	2.3	.03	0.2	0.2	B *
870530	0531	21.18	5-35.00	35-48.45	2.31	0.55	09	152	2.2	.03	0.1	0.2	B *
870530	1225	42.76	5-27.18	35-41.55	7.06	0.64	13	135	3.8	.05	0.2	0.4	B *
870530	1412	54.54	5-28.44	35-41.79	1.38	0.70	11	125	5.9	.05	0.2	1.3	B *
870530	1542	33.91	5-30.40	35-44.30	5.10	0.45	12	105	0.9	.03	0.1	0.2	B *
870530	2019	19.89	5-37.49	35-49.42	3.89	0.73	10	145	6.6	.04	0.2	0.4	B *
870530	2020	49.61	5-30.97	35-44.73	4.27	0.36	11	114	0.6	.05	0.2	0.4	B *
870530	2020	55.03	5-31.05	35-44.81	5.00	0.67	12	116	0.8	.03	0.1	0.2	B *
870530	2021	17.32	5-31.07	35-44.75	3.73	0.36	08	115	7.4	.04	0.2	0.7	B *
870530	2027	59.05	5-30.46	35-44.30	5.00	0.40	09	127	0.8	.02	0.1	0.2	B *
870530	2311	57.72	5-29.16	35-43.62	6.15	2.25	12	090	3.5	.03	0.1	0.3	A *
870601	0249	16.43	5-28.03	35-42.09	8.18	0.59	14	118	5.7	.03	0.1	0.2	B *
870601	0456	57.96	5-30.03	35-42.67	0.08	0.56	10	086	3.6	.03	0.1	6.1	B *
870601	0610	32.09	5-36.67	35-48.69	5.28	0.61	06	159	4.6	.01	0.1	0.1	B *
870601	0748	20.19	5-34.50	35-46.81	3.44	2.15	11	114	0.9	.04	0.2	0.4	B *
870601	2251	03.60	5-28.41	35-42.32	1.00	0.51	08	110	6.0	.06	0.2	2.7	B *
870602	0001	27.16	5-27.90	35-43.15	4.29	0.49	10	120	5.7	.04	0.2	0.4	B *
870602	0039	18.75	5-27.98	35-43.09	4.16	0.37	06	210	5.8	.01	0.1	0.2	C *
870602	0346	34.70	5-30.58	35-44.86	7.42	0.52	11	116	1.0	.02	0.1	0.2	B *
870602	0418	32.99	5-30.56	35-44.82	7.60	0.46	09	117	0.9	.02	0.1	0.2	B *
870602	0724	03.97	5-37.58	35-49.26	3.93	0.45	09	148	6.6	.06	0.3	0.5	B *
870602	0910	40.49	5-32.65	35-46.57	6.40	0.48	10	142	3.9	.02	0.1	0.1	B *
870602	1113	43.72	5-37.20	35-47.40	3.20	0.41	06	222	4.8	.04	2.1	1.9	C
870601	0753	21.98	5-29.55	35-43.46	3.35	0.58	13	086	3.0	.04	0.1	0.2	A *
870601	0907	02.01	5-34.50	35-46.78	3.10	0.57	06	113	1.0	.01	0.1	0.1	B *
870601	0921	16.22	5-34.48	35-46.83	3.31	0.60	13	112	0.9	.02	0.1	0.1	B *
870601	0942	13.60	5-30.45	35-44.69	6.71	0.51	07	121	6.4	.02	0.1	0.3	B *
870601	1250	34.81	5-32.89	35-45.97	1.93	0.57	12	132	4.0	.03	0.1	0.3	B *
870601	1513	47.59	5-32.18	35-44.97	1.32	1.17	13	119	2.6	.03	0.1	0.6	B *
870601	1737	03.75	5-29.74	35-43.00	0.90	0.44	06	163	3.4	.04	0.2	1.5	B *
870601	1925	59.57	5-29.74	35-43.70	4.19	0.50	09	153	2.5	.04	0.2	0.3	B *
870601	2245	40.99	5-28.41	35-42.37	1.46	0.61	12	109	5.9	.06	0.2	1.2	B *
870606	1729	23.02	5-32.41	35-45.37	2.02	0.71	11	139	3.3	.03	0.1	0.4	B *
870606	1839	32.55	5-32.44	35-45.36	1.63	0.59	11	098	3.4	.03	0.1	0.4	B *
870606	2009	38.12	5-31.57	35-45.24	5.08	0.76	14	123	2.0	.05	0.2	0.3	B *
870606	2054	33.65	5-31.32	35-44.44	2.25	0.59	10	110	0.8	.02	0.1	0.1	B *
870606	1839	40.71	5-32.48	35-45.32	1.22	0.37	07	162	3.4	.01	0.1	0.3	B *
870609	1821	28.75	5-30.12	35-44.36	6.44	0.59	11	133	1.4	.03	0.1	0.2	B *
870609	1822	45.46	5-29.99	35-44.18	5.55	0.37	06	233	1.7	.05	0.7	0.7	C *
870609	2314	48.28	5-30.10	35-44.34	6.15	0.37	11	134	1.4	.02	0.1	0.1	B *
870610	0102	38.86	5-30.87	35-44.53	5.28	0.76	12	116	0.2	.03	0.1	0.2	B *
870610	0103	22.06	5-30.78	35-44.53	5.31	0.50	11	117	0.2	.03	0.1	0.2	B *
870610	0410	53.46	5-32.08	35-45.40	3.47	0.50	11	125	2.9	.09	0.4	0.6	B *
870610	1755	56.82	5-38.56	35-48.90	1.44	0.50	08	168	7.5	.04	0.2	1.3	B *
870610	2052	52.91	5-29.16	35-43.61	7.09	0.59	13	090	3.5	.05	0.2	0.4	A *
870610	2112	00.28	5-29.14	35-43.59	7.31	0.71	12	170	3.5	.05	0.3	0.3	B *
870610	2126	30.26	5-29.11	35-43.66	7.28	0.84	13	091	3.5	.04	0.2	0.3	B *
870611	0128	27.45	5-29.18	35-43.59	6.83	0.37	11	169	3.5	.04	0.2	0.3	B *
870611	0340	33.20	5-30.94	35-44.55	5.00	0.16	09	111	0.3	.08	0.3	0.4	B *
870611	0954	20.41	5-37.93	35-48.52	3.08	1.23	15	158	6.5	.05	0.2	0.6	B *
870611	1254	18.27	5-38.11	35-49.51	5.00	0.50	10	156	6.7	.10	0.5	0.8	B *
870611	1431	19.67	5-38.46	35-48.99	2.66	0.37	07	166	7.4	.01	0.1	0.4	B *
870611	1456	09.30	5-30.80	35-44.95	7.12	1.49	14	100	1.0	.04	0.2	0.3	B *
870611	1517	33.09	5-30.84	35-44.90	6.82	0.50	12	117	0.9	.04	0.2	0.3	B *
870611	1620	47.21	5-28.40	35-42.25	0.10	0.66	10	112	6.1	.03	0.1	0.3	C *
870611	1748	48.95	5-30.58	35-44.87	7.64	1.03	14	098	1.0	.02	0.1	0.1	B *
870611	1807	08.29	5-30.59	35-44.81	7.39	0.50	09	125	0.9	.02	0.1	0.3	B *
870611	1933	36.62	5-37.37	35-49.70	4.86	0.71	13	141	6.3	.09	0.4	0.7	B *
870611	2129	39.31	5-30.97	35-44.99	7.28	0.37	08	123	1.0	.04	0.2	0.4	B *
870611	2310	38.50	5-30.97	35-45.09	6.97	1.61	13	102	1.2	.03	0.1	0.2	B *
870611	2318	31.29	5-30.87	35-45.03	7.37	0.37	10	121	1.1	.04	0.2	0.3	B *
870611	2327	44.51	5-30.88	35-45.07	7.35	0.50	10	120	1.2	.03	0.1	0.3	B *
870612	0002	46.74	5-30.79	35-45.02	7.35	0.37	10	119	1.1	.03	0.2	0.2	B *

DATE	ORIGIN	L S	LONG W	DEPTH MAG	NO	GAP	DMIN	RMS	ERH	ERZ	Q D
870612	0124	21.98	5-34.93	35-48.54	2.49	0.80	12	113	2.4	.05	0.2 0.3 B **
870612	0127	12.53	5-28.23	35-42.17	2.95	1.03	12	216	6.4	.05	0.3 0.8 C *
870612	0131	52.13	5-28.26	35-42.17	1.98	0.84	11	215	6.4	.05	0.3 1.0 C *
870612	0329	55.63	5-30.83	35-44.99	6.97	1.27	12	119	1.0	.03	0.1 0.2 B **
870612	0517	15.41	5-28.51	35-42.04	0.27	0.59	10	211	6.1	.06	0.2 5.6 D *
870612	1353	37.29	5-28.48	35-43.06	3.74	0.50	09	197	5.1	.02	0.1 0.1 C *
870612	1431	18.42	5-36.34	35-47.90	2.84	0.37	10	181	3.4	.02	0.2 0.2 C **
870612	1533	48.71	5-37.39	35-48.22	3.48	0.84	13	149	5.4	.02	0.1 0.2 B *
870612	1702	03.00	5-37.37	35-48.24	3.56	1.08	15	149	5.4	.02	0.1 0.2 B **
870612	1704	35.39	5-37.23	35-48.34	3.37	0.37	08	212	5.2	.02	0.4 0.3 C *
870612	1931	38.16	5-37.34	35-48.23	3.72	1.08	16	149	5.3	.04	0.1 0.2 B *
870612	1941	48.36	5-37.36	35-48.24	3.24	0.37	07	149	5.3	.02	0.1 0.3 B *
870612	1946	44.63	5-33.57	35-46.45	3.91	0.59	12	151	2.5	.02	0.1 0.1 B *
870612	2030	13.97	5-29.96	35-44.50	6.40	1.16	11	134	1.7	.03	0.1 0.2 B *
870612	2153	19.44	5-30.71	35-44.97	1.44	1.03	12	112	1.0	.02	0.1 0.1 B *
870612	2154	54.37	5-28.50	35-42.48	0.08	0.59	08	268	5.7	.03	0.2 6.8 D *
870613	0114	09.68	5-28.26	35-42.16	1.86	0.97	11	215	6.4	.05	0.3 1.0 C *
870606	0112	24.05	5-30.40	35-44.18	3.51	0.69	12	130	1.0	.04	0.1 0.2 B **
870606	0208	44.20	5-31.77	35-45.26	4.10	0.72	11	124	2.3	.04	0.1 0.2 B **
870613	0859	25.90	5-35.84	35-47.63	2.21	1.74	11	128	2.3	.02	0.1 0.2 B **
870613	1021	34.84	5-28.56	35-42.32	2.65	0.84	09	109	5.8	.07	0.3 1.2 B *
870613	1117	19.44	5-30.66	35-44.85	7.21	0.66	13	098	0.9	.03	0.1 0.2 B **
870613	1659	37.35	5-37.67	35-49.38	3.67	0.37	06	152	6.8	.04	0.4 1.0 B *
870613	2216	02.40	5-30.47	35-48.77	2.42	0.95	14	188	7.5	.09	0.3 1.1 C *
870613	2332	18.55	5-29.28	35-43.70	6.22	1.08	14	165	3.2	.04	0.2 0.2 B **
870614	0014	11.60	5-37.54	35-48.03	3.17	0.16	08	197	5.5	.04	0.4 0.5 C *
870614	0235	48.07	5-36.71	35-47.93	3.12	0.84	14	140	4.0	.09	0.3 0.7 B *
870614	0606	29.07	5-27.74	35-41.62	0.41	0.71	12	235	6.8	.08	0.4 5.9 D *
870614	0610	08.72	5-29.58	35-42.84	0.87	0.37	09	170	3.8	.03	0.2 0.7 B *
870614	0633	09.31	5-30.73	35-44.89	7.02	0.66	09	127	0.9	.03	0.2 0.3 B **
870614	0643	15.70	5-35.85	35-47.72	4.10	1.35	13	128	2.4	.03	0.1 0.1 B **
870614	0709	18.21	5-30.71	35-44.91	7.08	0.97	13	113	0.9	.02	0.1 0.2 B **
870614	0840	30.54	5-35.51	35-39.76	3.77	1.23	11	176	5.2	.02	0.1 0.1 B **
870614	0923	00.86	5-28.32	35-42.26	0.30	0.59	08	212	6.2	.02	0.1 2.3 C *
870614	1011	17.09	5-30.63	35-44.88	7.28	0.66	13	116	0.9	.04	0.2 0.3 B **
870614	1040	32.62	5-30.97	35-44.53	6.26	0.50	07	172	0.3	.07	0.7 0.7 B *
870614	1103	53.71	5-30.67	35-44.86	7.24	0.50	08	116	0.9	.02	0.1 0.3 B **
870614	1233	12.65	5-30.62	35-44.75	7.37	1.13	14	096	0.8	.04	0.2 0.2 B **
870614	1358	27.27	5-30.60	35-44.76	7.35	1.42	15	096	0.8	.04	0.2 0.3 B **
870614	1401	03.92	5-30.62	35-44.74	7.30	0.66	13	096	0.7	.04	0.2 0.2 B **
870614	1521	53.24	5-28.39	35-42.22	1.59	1.18	14	113	6.1	.08	0.3 1.4 B *
870614	1527	13.72	5-28.35	35-42.12	0.17	0.66	14	116	6.2	.06	0.2 9.7 C *
870614	1607	07.19	5-30.66	35-44.95	7.18	0.59	10	133	1.0	.03	0.2 0.2 B **
870614	2011	40.87	5-30.18	35-44.19	5.06	0.50	11	102	1.3	.03	0.1 0.2 B **
870614	2038	55.22	5-38.17	35-49.01	3.11	0.37	07	219	7.3	.02	0.5 0.4 C *
870614	2054	39.46	5-30.52	35-44.43	5.21	0.16	12	124	0.6	.02	0.1 0.1 B **
870614	2101	14.07	5-38.42	35-48.98	2.98	0.50	11	165	7.4	.08	0.4 1.2 B *
870614	2218	23.63	5-37.74	35-48.40	1.23	0.50	13	155	6.1	.04	0.2 1.2 B *
870614	2337	57.60	5-37.63	35-49.30	4.17	0.50	09	148	6.7	.04	0.3 0.5 B **
870614	2345	16.91	5-30.75	35-44.53	4.74	0.59	11	118	0.3	.02	0.1 0.1 B **
870614	2356	24.62	5-29.97	35-44.00	4.63	0.59	11	142	1.8	.05	0.2 0.3 B **
870615	0035	43.90	5-30.55	35-44.42	5.26	0.90	12	124	0.6	.02	0.1 0.1 B **
870615	0244	22.47	5-30.47	35-44.53	5.35	0.50	12	123	0.8	.02	0.1 0.1 B **
870615	0305	34.30	5-28.42	35-42.36	1.19	0.71	11	208	5.9	.06	0.3 1.3 C *
870615	0425	04.82	5-31.67	35-44.61	1.11	0.59	11	113	1.5	.03	0.1 0.4 B **
870615	0808	15.26	5-37.85	35-48.50	2.28	0.97	13	156	6.4	.05	0.2 0.9 B *
870615	0833	31.16	5-29.20	35-43.59	6.23	1.03	13	169	3.4	.04	0.2 0.2 B **
870615	0840	43.64	5-31.63	35-44.48	0.88	0.16	07	111	1.4	.03	0.2 0.5 B *
870615	0921	48.16	5-29.64	35-43.41	6.60	0.59	08	173	3.7	.02	0.2 0.2 B **
870614	1409	40.77	5-30.68	35-44.87	7.40	0.37	10	116	0.9	.04	0.2 0.3 B **
870615	1123	22.94	5-31.52	35-43.93	2.45	0.37	06	256	1.5	.03	0.6 0.3 C *
870615	1216	53.07	5-34.99	35-48.57	2.31	0.80	14	113	2.4	.05	0.2 0.3 B **
870615	1448	48.99	5-31.68	35-44.82	2.15	0.87	14	117	1.7	.04	0.1 0.3 B **
870615	1748	49.00	5-38.32	35-48.93	2.94	0.37	11	163	7.5	.07	0.3 0.9 B *
870615	1849	58.57	5-30.27	35-44.22	4.52	0.59	11	132	1.2	.03	0.1 0.2 B **
870615	1901	05.82	5-30.26	35-44.35	5.92	0.37	08	131	1.1	.01	0.1 0.1 B **
870615	1907	36.71	5-30.28	35-44.39	5.98	0.37	14	106	1.1	.03	0.1 0.2 B **
870615	1932	35.86	5-30.41	35-44.47	6.30	0.37	08	126	6.5	.03	0.1 0.3 B **
870615	2038	35.11	5-30.34	35-44.46	6.28	0.80	14	107	1.0	.04	0.2 0.2 B **
870615	2041	09.83	5-30.32	35-44.43	6.32	1.03	16	090	1.0	.03	0.1 0.2 A **
870615	2045	15.39	5-30.39	35-44.53	6.32	0.95	15	092	0.9	.02	0.1 0.1 B **
870615	2115	21.28	5-28.48	35-43.01	5.79	1.27	16	104	5.1	.03	0.1 0.2 B **
870615	2135	27.46	5-37.88	35-48.54	2.30	0.80	13	157	6.4	.05	0.2 0.8 B *
870616	0041	21.02	5-30.50	35-44.53	5.90	1.97	10	123	0.7	.03	0.2 0.3 B **
870616	0045	46.17	5-30.47	35-44.49	5.94	2.59	07	124	0.7	.01	0.1 0.1 B *
870616	0050	28.18	5-30.14	35-44.37	5.89	0.80	12	133	1.3	.02	0.1 0.1 B **
870616	0053	48.42	5-30.31	35-44.37	6.07	0.87	12	129	1.0	.03	0.1 0.2 B **
870616	0054	51.13	5-30.13	35-44.34	6.82	0.59	12	133	1.4	.03	0.1 0.1 B **
870616	0055	58.08	5-30.60	35-44.53	5.76	0.71	12	121	0.5	.02	0.1 0.1 B **
870616	0145	37.84	5-30.27	35-44.48	6.44	0.59	11	128	1.1	.02	0.1 0.2 B **
870615	2041	37.91	5-30.32	35-44.42	6.47	1.87	15	090	1.0	.05	0.2 0.2 A **
870616	0042	06.23	5-30.39	35-44.47	6.15	1.99	12	126	0.9	.03	0.2 0.2 B **

# Appendix C

DATE	ORIGIN	LAT S	LONG W	DEPTH	MAG	NO	GAP	DMIN	RMS	ERH	ERZ	Q	D	DATE	ORIGIN	LAT S	LONG W	DEPTH	MAG	NO	GAP	DMIN	RMS	ERH	ERZ	Q	D		
870616	0050	34.53	5-30.14	35-44.36	5.82	1.13	11	133	1.4	.02	0.1	0.1	B	+	870617	0700	52.82	5-30.16	35-44.28	5.00	0.16	09	134	1.3	.12	0.6	0.9	B	
870616	0053	51.64	5-30.36	35-44.40	5.73	0.95	11	128	0.9	.02	0.1	0.1	B	+	870617	0732	01.72	5-29.00	35-43.55	7.03	0.59	14	175	3.8	.03	0.2	0.2	B	+
870616	0206	05.12	5-30.58	35-44.53	6.02	0.71	12	121	0.6	.04	0.1	0.2	B	+	870617	0743	44.31	5-38.38	35-48.93	2.20	0.97	14	164	7.5	.05	0.2	0.8	B	+
870616	0211	20.95	5-30.33	35-44.53	6.11	0.59	12	126	1.0	.05	0.2	0.3	B	+	870617	0744	46.17	5-38.24	35-49.09	3.07	0.37	07	219	7.3	.03	0.3	0.6	C	*
870616	0214	52.43	5-30.17	35-44.38	5.76	0.50	12	132	1.3	.03	0.1	0.2	B	+	870617	0748	58.76	5-38.18	35-48.85	2.35	0.37	07	161	7.2	.06	0.4	1.6	B	*
870616	0229	12.11	5-30.35	35-44.40	5.96	0.50	12	128	1.0	.02	0.1	0.1	B	+	870617	0819	04.05	5-36.69	35-48.66	5.35	2.79	10	136	4.6	.03	0.2	0.3	B	+
870616	0231	08.71	5-30.54	35-44.45	5.31	0.50	12	123	0.6	.01	0.1	0.1	B	+	870617	0829	46.83	5-36.74	35-48.65	4.90	0.37	13	137	4.6	.04	0.2	0.3	B	+
870616	0243	36.86	5-30.61	35-44.53	5.79	0.37	10	121	0.5	.03	0.2	0.2	B	+	870617	0840	57.21	5-36.80	35-48.71	4.97	0.93	14	138	4.8	.03	0.1	0.2	B	+
870616	0248	25.11	5-30.55	35-44.53	5.91	0.50	11	122	0.6	.03	0.1	0.1	B	+	870617	0855	50.23	5-38.46	35-48.88	2.83	1.97	11	166	7.6	.05	0.3	1.0	B	*
870616	0229	53.79	5-30.36	35-44.44	5.79	0.59	12	127	0.9	.03	0.1	0.2	B	+	870617	0858	01.85	5-38.42	35-48.91	2.67	0.84	14	165	7.6	.07	0.3	1.0	B	*
870616	0249	05.17	5-30.54	35-44.53	6.03	0.59	09	122	0.6	.02	0.1	0.2	B	+	870617	0859	06.44	5-38.19	35-48.97	2.89	0.37	08	161	7.3	.03	0.1	0.5	B	+
870616	0336	46.06	5-30.38	35-44.45	6.26	0.66	12	127	0.9	.02	0.1	0.1	B	+	870617	0900	42.10	5-31.71	35-45.08	3.98	0.71	13	099	2.0	.01	0.1	0.1	B	+
870616	0345	26.80	5-30.58	35-44.58	6.06	0.66	10	121	0.6	.03	0.1	0.2	B	+	870617	0903	49.18	5-38.34	35-48.87	1.82	0.37	11	164	7.4	.03	0.1	0.8	B	+
870616	0402	41.51	5-30.37	35-44.42	5.73	0.66	12	127	0.9	.01	0.1	0.1	B	+	870617	0928	00.49	5-28.89	35-43.51	7.27	0.93	14	178	4.0	.04	0.2	0.3	B	+
870616	0435	22.01	5-28.46	35-43.04	3.63	0.37	11	198	5.1	.02	0.1	0.2	C	+	870617	0940	48.68	5-28.99	35-43.53	6.86	0.59	14	176	3.8	.03	0.1	0.2	B	+
870616	0503	11.29	5-30.45	35-44.43	5.87	0.37	09	125	0.8	.04	0.2	0.3	B	+	870617	0950	40.35	5-28.85	35-43.40	6.66	0.37	12	181	4.2	.02	0.1	0.2	C	+
870616	0526	24.14	5-29.04	35-42.27	1.23	0.66	12	194	5.2	.04	0.2	0.8	C	*	870617	1008	00.20	5-29.47	35-43.67	5.17	0.50	14	160	2.9	.03	0.1	0.2	B	+
870616	0552	24.50	5-30.67	35-44.53	5.49	0.37	09	119	0.4	.02	0.1	0.1	B	+	870617	1046	24.33	5-30.97	35-44.39	3.41	0.50	11	111	0.2	.09	0.3	0.8	B	+
870616	0600	04.42	5-30.28	35-44.41	6.24	0.59	12	129	1.1	.03	0.1	0.2	B	+	870617	1114	43.46	5-29.00	35-43.41	6.77	0.50	11	177	3.9	.02	0.1	0.1	B	+
870616	0606	04.78	5-30.77	35-44.67	5.83	0.50	11	116	0.5	.04	0.2	0.2	B	+	870617	1140	33.90	5-36.43	35-48.86	5.00	0.37	10	131	4.4	.08	0.4	0.8	B	+
870616	0610	36.86	5-30.79	35-44.62	5.60	0.50	10	116	0.4	.02	0.1	0.1	B	+	870617	1156	47.04	5-38.35	35-48.81	0.73	0.59	10	164	7.4	.04	0.2	2.8	C	*
870616	0613	03.05	5-30.79	35-44.61	5.52	0.59	12	116	0.4	.02	0.1	0.1	B	+	870617	1205	59.62	5-38.38	35-48.94	2.51	0.37	10	164	7.5	.07	0.4	1.5	B	*
870616	0616	34.33	5-30.80	35-44.62	5.45	0.50	11	116	0.4	.02	0.1	0.1	B	+	870617	1254	12.45	5-38.35	35-48.96	2.10	0.50	12	164	7.5	.03	0.2	0.7	B	*
870616	0626	01.79	5-30.62	35-44.47	5.00	0.37	09	121	0.5	.03	0.2	0.2	B	+	870617	1302	54.63	5-38.31	35-48.94	2.20	0.50	12	163	7.4	.03	0.1	0.6	B	*
870616	0628	24.61	5-30.80	35-44.66	5.70	0.66	12	115	0.4	.03	0.1	0.2	B	+	870617	0700	55.28	5-29.97	35-44.01	4.79	0.37	13	142	1.8	.05	0.2	0.3	B	+
870616	0644	15.07	5-30.76	35-44.53	5.00	0.37	12	118	0.3	.05	0.2	0.3	B	+	870617	1303	52.06	5-38.40	35-48.80	0.85	0.59	12	165	7.5	.06	0.2	2.7	C	*
870616	0804	40.61	5-31.52	35-45.07	4.97	0.66	12	121	1.7	.03	0.1	0.2	B	+	870617	1312	13.03	5-36.99	35-50.07	3.33	0.37	05	179	6.7	.00	1.0	0.2	C	*
870616	0807	36.04	5-30.80	35-44.61	5.61	0.37	11	116	0.4	.04	0.2	0.3	B	+	870617	1346	27.50	5-37.20	35-48.44	0.50	0.59	10	145	5.2	.05	0.2	3.5	C	*
870616	0858	56.11	5-30.51	35-44.45	5.76	2.49	10	124	0.7	.01	0.1	0.1	B	+	870617	1409	08.64	5-30.97	35-43.59	0.69	0.37	13	125	1.6	.07	0.2	0.9	B	*
870616	0904	09.27	5-30.26	35-44.43	5.94	0.37	10	236	1.1	.02	0.2	0.1	C	+	870617	1558	51.96	5-38.38	35-48.83	1.50	0.59	13	165	7.5	.06	0.2	1.4	B	*
870616	0935	25.36	5-30.44	35-44.71	5.89	0.50	12	114	0.6	.04	0.2	0.3	B	+	870617	1618	42.51	5-29.42	35-43.84	6.52	0.37	12	159	2.9	.04	0.2	0.2	B	+
870616	0937	46.16	5-30.51	35-44.39	5.21	0.16	09	125	0.7	.02	0.1	0.1	B	+	870617	1701	24.87	5-28.85	35-43.43	7.01	0.76	14	181	4.2	.04	0.2	0.3	C	+
870616	0613	56.23	5-30.76	35-44.69	6.20	0.37	11	116	0.5	.05	0.3	0.3	B	+	870617	1712	01.56	5-36.88	35-48.83	5.20	0.50	10	138	5.0	.02	0.1	0.2	B	+
870616	0626	24.93	5-30.58	35-44.53	6.20	0.37	08	121	0.6	.04	0.3	0.4	B	+	870617	1735	17.37	5-30.46	35-44.33	5.66	1.61	11	127	0.8	.04	0.3	0.4	B	+
870616	0628	56.38	5-30.82	35-44.69	5.70	0.66	12	114	0.5	.02	0.1	0.1	B	+	870617	1746	04.56	5-36.79	35-48.73	4.85	0.37	07	201	4.8	.06	0.5	0.8	C	*
870616	0904	37.40	5-30.28	35-44.42	6.40	1.31	14	129	1.1	.03	0.1	0.2	B	+	870617	1756	19.23	5-29.21	35-43.59	7.12	0.50	10	168	3.4	.03	0.1	0.2	B	+
870616	0951	04.14	5-30.79	35-44.61	5.68	0.37	11	116	0.4	.04	0.2	0.3	B	+	870617	1805	29.77	5-29.20	35-43.57	7.22	0.66	14	169	3.5	.03	0.1	0.2	B	+
870616	0953	16.38	5-30.87	35-44.66	5.46	0.66	09	227	0.4	.02	0.2	0.2	C	+	870617	1848	05.69	5-38.43	35-48.96	2.75	0.87	14	165	7.5	.07	0.3	1.1	B	*
870616	0954	33.39	5-30.97	35-44.80	5.77	0.66	12	116	0.7	.04	0.2	0.3	B	+	870617	2023	43.18	5-36.77	35-48.73	5.11	0.93	13	137	4.8	.03	0.2	0.2	B	+
870616	0955	20.10	5-30.69	35-44.63	5.75	0.50	10	118	0.5	.03	0.1	0.2	B	+	870617	2039	46.60	5-36.81	35-48.70	4.91	1.76	14	138	4.8	.04	0.2	0.3	B	+
870616	0957	07.34	5-30.44	35-44.42	5.30	0.16	12	126	0.8	.03	0.1	0.1	B	+	870617	2104	56.86	5-38.33	35-48.93	2.49	0.50	14	163	7.5	.04	0.2	0.6	B	+
870616	0958	17.08	5-30.54	35-44.49	5.17	0.50	11	123	0.6	.02	0.1	0.1	B	+	870617	2108	49.77	5-38.32	35-48.91	2.39	0.50	14	163	7.4	.04	0.2	0.6	B	*
870616	0626	27.14	5-30.50	35-44.53	6.12	0.59	09	123	0.7	.04	0.2	0.3	B	+	870617	2110	54.21	5-38.33	35-48.93	2.60	0.37	10	163	7.5	.06	0.3	1.2	B	+
870616	0905	22.08	5-30.41	35-44.39	5.35	0.37	09	127	0.8	.03	0.2	0.2	B	+	870617	2256	09.21	5-36.76	35-48.65	4.99	1.03	14	137	4.7	.04	0.1	0.3	B	+
870616	0951	27.15	5-30.76	35-44.61	5.43	0.37	12	117	0.4	.03	0.1	0.2	B	+	870618	0159	39.13	5-28.91	35-43.46	6.82	0.59	12	179	4.0	.04	0.2	0.3	B	+
870616	0951	30.94	5-30.77	35-44.61	5.32	0.37	10	117	0.4	.02	0.1	0.2	B	+	870618	0354	26.61	5-28.79	35-43.38	6.80	0.59	14	183	4.3	.04	0.2	0.2	C	+
870616	0951	45.58	5-30.65	35-44.4																									

# Appendix C

DATE	ORIGIN	LAT S	LONGW	DEPTH	MAG	NO	GAP	DMIN	RMS	ERH	ERZ	Q	D	DATE	ORIGIN	LAT S	LONGW	DEPTH	MAG	NO	GAP	DMIN	RMS	ERH	ERZ	Q	D
870618	2355	04.21	5-36.83	35-48.75	5.55	0.37	10	138	4.9	.03	0.1	0.3	B *+	870619	1029	37.63	5-36.43	35-48.42	4.83	0.80	14	133	3.9	.03	0.1	0.2	B *+
870619	0008	56.52	5-36.86	35-48.78	5.39	0.50	11	138	5.0	.04	0.2	0.3	B *+	870619	1538	04.04	5-36.67	35-48.63	4.61	0.50	13	136	4.5	.03	0.1	0.2	B *+
870619	0018	03.26	5-36.86	35-48.74	4.99	0.50	11	138	4.9	.04	0.2	0.3	B *+	870619	1544	02.36	5-36.13	35-49.12	4.40	0.37	05	177	4.4	.04	0.4	0.1	C
870619	0030	17.73	5-36.90	35-48.87	4.94	0.37	08	139	5.1	.05	0.3	0.6	B *	870619	1554	45.67	5-36.53	35-48.78	4.58	0.37	08	196	4.4	.02	0.3	0.2	C *+
870619	0036	00.90	5-36.63	35-48.52	4.52	0.37	08	138	4.3	.05	0.3	0.4	B *+	870619	1621	03.27	5-36.50	35-48.56	4.68	1.38	13	134	4.2	.05	0.2	0.3	B *+
870619	0037	20.16	5-36.70	35-48.75	5.42	0.84	11	136	4.7	.03	0.1	0.2	B *	870619	1626	37.47	5-36.78	35-48.72	5.24	0.50	13	137	4.8	.04	0.2	0.2	B *+
870619	0049	59.65	5-36.77	35-48.82	4.98	0.59	11	136	4.9	.04	0.2	0.3	B *+	870619	1635	15.20	5-29.24	35-43.52	7.06	0.37	09	169	3.4	.02	0.1	0.1	B *
870619	0103	51.56	5-36.99	35-48.86	5.01	0.37	07	140	5.2	.12	0.7	1.6	B	870619	1638	13.09	5-36.39	35-48.33	4.91	0.37	08	200	3.8	.02	0.3	0.2	C *+
870619	0105	40.09	5-36.58	35-48.50	4.89	1.38	13	135	4.2	.04	0.2	0.3	B *+	870619	1639	25.34	5-32.93	35-51.79	1.07	0.16	05	245	8.9	.20	1.4	10.8	D
870619	0117	54.73	5-36.85	35-48.77	5.41	2.18	12	138	4.9	.04	0.2	0.3	B *+	870619	1827	15.80	5-36.69	35-48.50	4.69	0.37	06	153	4.4	.02	0.2	0.3	B *
870619	0119	45.26	5-32.91	35-46.52	4.30	0.37	09	139	3.5	.02	0.1	0.1	B *+	870619	1832	05.06	5-36.41	35-48.43	4.91	0.37	06	157	3.9	.01	0.1	0.2	B *
870619	0137	53.35	5-36.88	35-48.82	5.17	0.93	11	138	5.0	.03	0.2	0.3	B *+	870619	1845	33.84	5-36.68	35-48.59	4.56	1.71	14	136	4.5	.04	0.2	0.3	B *+
870619	0140	50.28	5-36.75	35-48.66	4.64	0.59	10	138	4.7	.02	0.1	0.1	B *+	870619	1916	05.60	5-37.26	35-47.94	0.21	0.37	11	148	5.0	.04	0.1	5.2	C *
870619	0143	59.56	5-36.39	35-48.44	4.80	0.37	08	139	3.9	.02	0.1	0.2	B *+	870619	1928	05.21	5-36.61	35-48.49	4.36	0.59	11	136	4.3	.02	0.1	0.1	B *+
870619	0150	59.82	5-36.86	35-48.83	5.35	0.37	09	139	5.0	.03	0.2	0.3	B *+	870619	1930	17.05	5-36.31	35-48.43	5.02	0.37	05	160	3.8	.03	0.3	0.5	C
870618	2355	50.51	5-36.84	35-48.72	5.06	0.80	13	138	4.9	.06	0.3	0.4	B *	870619	1949	03.40	5-36.74	35-48.74	5.40	0.50	11	136	4.7	.04	0.2	0.3	B *+
870619	0209	18.07	5-36.70	35-48.58	4.74	0.66	09	138	4.5	.01	0.0	0.1	B *+	870619	1537	52.55	5-36.63	35-48.58	4.55	0.71	13	136	4.4	.04	0.1	0.2	B *+
870619	0217	05.02	5-36.82	35-48.58	4.46	0.37	07	139	4.7	.04	0.2	0.4	B *	870619	1952	00.39	5-29.16	35-43.53	6.66	0.50	10	171	3.6	.04	0.2	0.3	B *+
870619	0218	51.91	5-36.88	35-48.76	5.15	1.31	13	139	5.0	.03	0.2	0.2	B *+	870619	2005	55.06	5-36.30	35-48.62	5.23	0.16	06	165	3.9	.07	0.6	0.9	B *
870619	0223	46.03	5-36.86	35-48.76	5.07	0.71	12	138	4.9	.03	0.1	0.2	B *+	870619	2017	30.45	5-36.14	35-48.29	5.00	0.37	06	159	3.4	.03	0.2	0.3	B *
870619	0229	09.23	5-31.43	35-44.86	3.62	0.59	12	117	1.3	.02	0.1	0.2	B *+	870619	2232	13.22	5-36.89	35-48.85	5.00	1.00	13	138	5.1	.04	0.2	0.3	B *+
870619	0241	45.49	5-36.73	35-48.63	4.90	2.46	09	137	4.6	.03	0.2	0.4	B *+	870616	1606	59.01	5-30.14	35-44.28	5.45	0.78	14	103	1.4	.03	0.1	0.2	B *+
870619	0246	37.35	5-36.65	35-48.60	5.07	0.76	12	136	4.5	.02	0.1	0.2	B *+	870616	2056	16.17	5-30.29	35-44.41	6.10	0.82	14	129	1.1	.02	0.1	0.1	B *+
870619	0249	17.91	5-36.83	35-48.86	5.08	0.87	12	137	5.0	.03	0.1	0.2	B *+	870616	2123	56.27	5-28.72	35-43.38	7.00	0.49	11	185	4.4	.04	0.2	0.3	C *+
870619	0302	16.42	5-36.80	35-48.84	5.37	0.59	09	140	4.9	.04	0.2	0.3	B *+	870616	2138	31.70	5-28.83	35-43.38	6.52	0.48	11	182	4.2	.02	0.1	0.2	C *+
870619	0307	15.95	5-36.50	35-48.43	4.72	0.37	08	138	4.1	.02	0.1	0.2	B *+	870616	2142	41.98	5-29.80	35-43.02	1.86	0.92	13	161	3.3	.07	0.3	0.6	B *
870619	0309	37.45	5-36.71	35-48.67	4.75	0.50	10	136	4.6	.02	0.1	0.1	B *+	870616	2158	20.80	5-37.31	35-49.57	4.38	0.35	07	196	6.3	.03	0.2	0.5	C *
870619	0318	05.73	5-36.85	35-48.79	4.91	0.50	09	138	4.9	.03	0.2	0.2	B *+	870616	2248	26.46	5-38.46	35-49.20	2.48	0.49	11	165	7.0	.08	0.4	1.6	B *
870619	0320	59.72	5-36.82	35-48.76	5.43	0.50	14	138	4.9	.04	0.1	0.2	B *+	870618	1329	24.85	5-36.56	35-48.40	4.66	0.45	07	153	4.1	.02	0.1	0.2	B *
870619	0322	00.57	5-36.78	35-48.65	5.48	0.90	14	138	4.7	.04	0.1	0.2	B *+	870618	1333	11.87	5-36.58	35-48.40	4.48	0.50	11	136	4.1	.02	0.1	0.2	B *+
870619	0345	38.98	5-36.85	35-48.84	5.15	1.03	14	138	5.0	.03	0.1	0.2	B *+	870618	1334	37.01	5-29.90	35-43.48	1.87	0.44	09	152	2.5	.02	0.1	0.4	B *+
870619	0349	43.53	5-36.90	35-48.83	5.01	1.08	12	138	5.1	.04	0.2	0.3	B *+	870618	1343	03.23	5-36.81	35-48.81	4.59	0.52	06	158	4.9	.01	0.1	0.2	B *
870619	0413	46.20	5-36.26	35-48.38	5.00	0.37	10	131	3.6	.02	0.1	0.2	B *+	870618	1349	26.64	5-36.33	35-48.48	4.94	0.61	12	140	3.8	.04	0.2	0.3	B *+
870619	0426	35.02	5-36.88	35-48.82	4.93	1.38	14	138	5.0	.04	0.2	0.3	B *+	870618	1408	16.19	5-36.77	35-48.78	4.88	0.58	08	139	4.8	.02	0.1	0.2	B *+
870619	0449	20.72	5-36.86	35-48.72	5.05	0.37	07	138	4.9	.01	0.1	0.1	B *	870618	1418	11.28	5-36.51	35-48.69	4.62	0.87	14	133	4.3	.04	0.2	0.3	B *+
870619	0507	59.81	5-36.57	35-48.48	4.39	0.71	12	135	4.2	.05	0.2	0.3	B *+	870618	1421	05.20	5-36.47	35-48.45	4.88	0.63	11	134	4.0	.03	0.1	0.2	B *+
870619	0526	31.71	5-36.97	35-48.73	5.05	0.37	09	140	5.1	.03	0.2	0.3	B *+	870618	1423	58.09	5-36.35	35-48.44	4.70	0.47	05	159	3.8	.00	0.1	0.1	C
870619	0536	58.43	5-36.75	35-48.60	4.63	0.37	06	154	4.6	.01	0.1	0.2	B *	870618	1520	07.26	5-37.08	35-48.32	4.80	0.53	08	210	4.9	.03	0.6	0.3	C *
870619	0549	09.94	5-36.91	35-48.85	5.06	0.93	14	139	5.1	.03	0.1	0.2	B *+	870618	1621	11.07	5-36.72	35-48.68	4.76	3.09	07	137	4.6	.02	0.2	0.4	B *
870619	0631	00.34	5-35.44	35-49.03	7.25	0.50	06	182	3.5	.18	1.9	2.5	C	870618	1623	24.94	5-36.79	35-48.79	4.58	1.94	13	137	4.9	.03	0.1	0.2	B *+
870619	0653	31.98	5-36.46	35-48.52	4.79	1.83	11	133	4.1	.04	0.2	0.6	B *	870618	1625	25.39	5-36.64	35-48.93	4.91	0.88	11	143	4.8	.05	0.2	0.3	B *+
870619	0656	13.65	5-36.26	35-48.36	5.04	0.66	13	131	3.6	.03	0.1	0.2	B *+	870618	1651	23.20	5-36.83	35-48.81	4.78	0.95	13	137	4.9	.03	0.2	0.3	B *+
870619	0657	03.99	5-36.48	35-48.50	4.83	0.59	09	139	4.1	.02	0.1	0.1	B *+	870618	1718	19.09	5-36.53	35-48.62	4.78	1.30	13	134	4.3	.04	0.2	0.2	B *+
870619	0701	59.65	5-36.60	35-48.47	4.70	0.71	13	136	4.2	.03	0.1	0.2	B *+	870618	1719	45.66	5-36.84	35-48.84	4.73	0.78	11	139	5.0	.03	0.2	0.3	B *+
870619	0702	59.47	5-36.59	35-48.44	4.58	0.50	05	153	4.2	.00	0.0	0.0	C	870618	1725	26.12	5-36.37	35-48.53	4.93	0.74	14	132	3.9	.04	0.2	0.2	B *+
870619	0709	27.61	5-36.41	35-48.52	5.05	0.37	14	132	4.0	.03	0.1	0.2	B *+	870618	1727	10.37	5-36.58	35-48.53	4.43	1.40	13	135	4.3	.03	0.1	0.2	B *+
870619	0735	51.80	5-36.78	35-48.42	4.61	0.37	08	139	4.5	.03	0.2	0.3	B *+	870618	1744	55.26	5-36.88	35-48.78	4.92	1.44	14	138	5.0	.03	0.1	0.2	B *+
870619	0739	48.39	5-36.41	35-48.34	4.91	0.37	08	138	3.8	.02	0.1	0.2	B *+	870618	1806	22.47	5-36.45	3									



# Appendix C

DATE	ORIGIN	LAT S	LONG W	DEPTH	MAG	NO	GAP	DMIN	RMS	ERH	ERZ	Q	D	DATE	ORIGIN	LAT S	LONG W	DEPTH	MAG	NO	GAP	DMIN	RMS	ERH	ERZ	Q	D
870618	2136	06.89	5-36.23	35-49.24	6.92	0.37	06	174	4.7	10	1.0	1.3	B *	870621	0709	02.35	5-28.97	35-43.35	6.87	1.00	07	179	4.0	.03	0.3	0.3	B *
870618	2136	47.24	5-31.83	35-52.90	1.04	0.46	05	264	11.5	.35	0.1	1.2	D	870621	0743	11.32	5-28.83	35-43.36	7.09	0.76	08	182	4.2	.02	0.2	0.2	C *
870618	2139	36.13	5-36.02	35-49.12	7.19	0.42	06	175	4.2	.18	2.0	2.5	C	870621	0824	06.46	5-28.83	35-43.35	6.68	0.66	08	183	4.3	.03	0.2	0.2	C *
870618	2144	33.03	5-36.73	35-48.89	4.72	0.59	11	141	4.9	.02	0.1	0.2	B *	870621	0858	12.68	5-28.86	35-43.36	6.80	0.76	08	182	4.2	.03	0.3	0.3	C *
870618	2149	04.56	5-36.69	35-48.88	5.19	0.49	08	141	4.8	.07	0.3	0.5	B *	870621	0911	14.78	5-36.86	35-48.77	5.00	1.81	09	219	6.5	.02	0.2	0.5	C *
870618	2151	36.83	5-36.83	35-48.80	5.25	0.48	09	139	4.9	.04	0.2	0.3	B *	870621	0948	24.16	5-36.86	35-48.55	4.36	0.50	06	216	6.7	.03	0.4	0.7	C *
870618	2154	59.95	5-36.81	35-48.87	4.74	0.52	10	140	5.0	.02	0.1	0.2	B *	870621	0950	04.69	5-29.35	35-43.59	6.52	0.95	09	165	3.2	.05	0.3	0.3	B *
870618	2156	18.47	5-36.84	35-48.83	4.85	0.61	11	139	5.0	.02	0.1	0.1	B *	870621	1021	29.07	5-36.68	35-48.55	4.27	1.00	09	213	6.5	.02	0.2	0.5	C *
870618	2213	20.24	5-29.62	35-43.57	3.39	0.50	09	158	2.8	.04	0.2	0.4	B *	870621	1106	44.51	5-28.94	35-43.55	6.94	1.66	08	176	3.9	.02	0.1	0.3	B *
870618	2231	07.60	5-36.55	35-48.61	4.63	1.58	13	134	4.3	.04	0.2	0.3	B *	870621	1203	27.88	5-28.80	35-43.35	6.88	0.95	08	183	4.3	.01	0.1	0.1	C *
870618	2231	14.24	5-36.53	35-48.61	4.11	0.78	08	134	4.3	.05	0.3	0.4	B *	870621	1204	11.10	5-28.82	35-43.35	6.91	0.66	08	183	4.3	.01	0.1	0.1	C *
870618	2232	19.80	5-36.43	35-48.59	4.52	0.50	09	176	4.1	.02	0.1	0.1	B *	870621	1222	25.07	5-31.10	35-44.98	6.88	0.50	08	199	1.1	.03	0.2	0.2	C *
870618	2241	22.01	5-33.56	35-46.67	4.12	0.80	13	103	2.3	.03	0.1	0.1	B *	870621	1224	06.05	5-31.10	35-45.04	6.73	0.66	08	200	1.2	.02	0.2	0.2	C *
870618	2249	15.08	5-36.84	35-49.00	5.17	0.66	13	136	5.2	.05	0.2	0.3	B *	870621	1257	35.75	5-28.94	35-43.36	6.49	0.76	08	180	4.1	.03	0.3	0.2	B *
870618	2249	24.52	5-36.47	35-48.56	4.75	0.76	13	133	4.1	.03	0.1	0.2	B *	870621	1322	56.86	5-28.97	35-43.56	7.18	1.85	07	175	3.9	.02	0.2	0.4	B *
870618	2249	35.52	5-36.52	35-48.64	4.53	1.47	12	134	4.3	.02	0.1	0.2	B *	870621	1346	15.76	5-29.02	35-43.52	6.74	1.08	10	175	3.8	.02	0.1	0.1	B *
870618	2252	17.14	5-36.88	35-48.88	5.22	1.35	13	138	5.1	.03	0.1	0.2	B *	870621	1352	50.55	5-38.45	35-49.07	2.36	0.59	09	245	8.6	.05	0.4	1.5	C *
870618	2259	26.61	5-36.79	35-48.79	4.79	0.63	10	137	4.8	.02	0.1	0.2	B *	870621	1406	06.56	5-38.34	35-48.96	2.23	0.66	09	242	8.5	.07	0.6	2.3	C *
870618	2259	39.90	5-36.83	35-48.84	5.29	0.58	07	159	5.0	.03	0.3	0.4	B *	870621	1410	58.34	5-28.85	35-43.39	6.78	0.59	08	181	4.2	.01	0.1	0.1	C *
870618	2306	29.72	5-36.79	35-48.84	5.07	2.15	11	137	4.9	.03	0.1	0.2	B *	870621	1421	05.14	5-36.82	35-48.67	5.00	0.59	10	217	6.5	.07	0.4	1.0	C *
870618	2314	54.78	5-36.83	35-48.87	4.70	0.59	09	137	5.0	.02	0.1	0.2	B *	870621	1356	17.10	5-31.31	35-44.87	4.61	0.87	08	199	1.2	.02	0.2	0.1	C *
870618	0302	56.04	5-36.56	35-48.61	5.33	2.98	07	134	4.3	.02	0.2	0.3	B *	870621	1429	21.95	5-30.97	35-44.83	7.00	0.50	08	195	0.8	.04	0.4	0.3	C *
870620	0309	02.64	5-29.91	35-44.38	6.04	0.50	08	142	1.8	.02	0.2	0.1	B *	870621	1504	12.07	5-36.66	35-48.59	5.00	1.76	10	213	6.4	.04	0.2	0.5	C *
870620	0403	38.55	5-35.14	35-48.46	2.42	0.80	09	178	5.2	.05	0.3	1.0	B *	870621	1507	42.06	5-31.05	35-44.98	6.80	0.37	08	199	1.1	.02	0.1	0.1	C *
870620	0408	51.84	5-32.00	35-45.32	3.24	0.37	07	212	2.7	.02	0.2	0.2	C *	870621	1513	33.37	5-36.52	35-48.54	4.72	0.87	10	210	6.3	.02	0.1	0.3	C *
870620	0435	16.90	5-35.46	35-47.20	8.91	0.59	08	257	9.9	.09	0.2	0.2	C *	870621	1518	39.66	5-36.64	35-48.64	4.59	0.84	10	213	6.4	.04	0.3	0.6	C *
870620	0449	06.34	5-36.35	35-48.40	5.00	1.00	10	205	6.3	.03	0.2	0.5	C *	870621	1603	21.68	5-36.37	35-48.39	5.00	0.80	10	205	6.4	.05	0.3	0.6	C *
870620	0546	44.82	5-36.36	35-48.35	5.00	1.18	08	204	6.4	.02	0.2	0.5	C *	870621	1608	13.07	5-36.44	35-48.40	4.56	2.02	07	206	6.4	.03	0.3	0.9	C *
870620	0549	09.58	5-36.42	35-48.38	5.00	1.23	10	206	6.4	.03	0.2	0.4	C *	870621	1646	28.73	5-36.38	35-48.47	5.00	1.03	09	206	6.3	.01	0.1	0.2	C *
870620	0605	25.67	5-36.24	35-48.30	5.00	0.59	10	201	6.4	.03	0.2	0.5	C *	870621	1651	35.24	5-36.48	35-48.52	5.00	0.87	10	209	6.3	.04	0.2	0.5	C *
870620	0917	59.42	5-36.42	35-48.41	5.00	0.84	09	206	6.4	.03	0.2	0.5	C *	870621	1652	10.60	5-31.04	35-45.00	6.82	0.59	07	199	1.1	.01	0.1	0.2	C *
870620	0934	03.23	5-36.44	35-48.43	5.00	0.59	08	207	6.4	.04	0.3	0.6	C *	870621	1655	39.26	5-36.47	35-48.48	5.00	0.37	07	208	6.4	.06	0.5	1.3	C *
870620	0938	51.21	5-36.33	35-48.39	5.10	0.66	08	204	6.3	.01	0.1	0.2	C *	870621	1656	19.61	5-36.47	35-48.58	5.00	0.80	09	209	6.2	.06	0.4	1.3	C *
870620	1044	45.55	5-36.61	35-48.41	3.69	2.32	08	210	6.6	.03	0.2	0.7	C *	870621	1356	36.48	5-31.41	35-45.01	4.60	1.83	09	103	1.5	.02	0.1	0.2	B *
870620	1147	29.21	5-28.91	35-43.44	6.86	1.49	10	179	4.1	.03	0.2	0.2	B *	870621	1356	39.57	5-31.34	35-44.96	4.71	1.87	09	102	1.3	.02	0.1	0.2	B *
870620	1203	16.13	5-36.35	35-48.44	5.00	0.59	08	205	6.3	.02	0.1	0.3	C *	870621	1700	35.04	5-36.45	35-48.53	5.00	0.71	09	208	6.3	.03	0.2	0.4	C *
870620	1216	02.53	5-36.35	35-48.41	5.00	0.59	07	205	6.3	.01	0.1	0.3	C *	870621	1755	07.03	5-28.86	35-43.42	6.92	0.84	08	181	4.1	.01	0.1	0.1	C *
870620	1228	36.19	5-29.26	35-43.67	6.44	2.65	05	166	3.3	.03	0.3	0.5	C	870621	1804	13.10	5-36.55	35-48.56	5.00	0.87	10	210	6.3	.04	0.3	0.6	C *
870620	1238	52.26	5-28.79	35-43.33	6.85	0.50	08	184	4.3	.02	0.1	0.2	C *	870621	1805	45.80	5-28.74	35-43.30	6.90	0.71	08	186	4.4	.01	0.1	0.1	C *
870620	1250	37.50	5-28.87	35-43.39	6.63	0.80	08	181	4.2	.02	0.2	0.2	C *	870621	1816	54.40	5-38.03	35-48.72	2.97	0.59	09	235	8.2	.03	0.2	0.8	C *
870620	1257	56.33	5-29.26	35-42.92	2.05	0.37	07	177	4.1	.01	0.1	0.2	B *	870621	2107	46.36	5-28.68	35-43.13	6.55	0.37	09	190	4.7	.02	0.2	0.2	C *
870620	1304	04.39	5-36.41	35-48.46	5.00	0.93	10	207	6.3	.03	0.2	0.4	C *	870621	2109	36.90	5-28.78	35-43.27	6.20	0.50	09	185	4.4	.03	0.2	0.2	C *
870620	1317	36.48	5-32.62	35-46.03	4.20	0.59	07	227	4.4	.05	0.4	0.6	C *	870621	2119	38.92	5-28.90	35-43.44	6.96	0.37	08	179	4.1	.01	0.1	0.1	B *
870620	1323	36.47	5-28.95	35-43.46	6.84	2.64	07	178	4.0	.01	0.1	0.2	B *	870621	2159	10.24	5-28.69	35-43.17	6.71	0.37	09	189	4.6	.04	0.3	0.4	C *
870620	1337	46.49	5-28.94	35-43.49	6.86	1.23	10	177	4.0	.02	0.1	0.2	B *	870621	2218	19.77	5-36.32	35-48.50	5.00	0.59	10	205	6.1	.05	0.3	0.8	C *
870620	1407	36.53	5-28.87	35-43.48	6.97	1.23	10	180	4.1	.02	0.1	0.2	B *	870621	2248	06.53	5-36.45	35-48.47	5.00	0.59	10	208	6.4	.03	0.2	0.5	C *
870620	1537	04.93	5-28.94	35-43.35	6.49	0.50	07	180	4.1	.04	0.5	0.4	B *	870621	2326	27.97	5-28.95	35-43.46	6.58	0.59	08	178	4.0	.02	0.2	0.2	B *
870620	1545	55.76	5-29.12	35-43.60	6.78	2.29	07	171	3.6	.01	0.1	0.2	B *	870621	2346	47.01	5-28.93	35-43.41	6.71	0.59	08	179	4.0	.01	0.1		

# Appendix C

DATE	ORIGIN	LAT S	LONG W	DEPTH	MAG	NO	GAP	DMIN	RMS	ERH	ERZ	Q	D	DATE	ORIGIN	LAT S	LONG W	DEPTH	MAG	NO	GAP	DMIN	RMS	ERH	ERZ	Q	D
870622	1108	50.50	5-30.02	35-45.19	7.50	0.37	06	194	2.1	.01	0.1	0.1	C *	870625	1754	32.42	5-36.59	35-48.58	4.19	2.29	12	135	4.3	.03	0.2	0.2	B *+
870622	1125	35.00	5-28.81	35-43.31	6.83	0.50	08	184	4.3	.02	0.1	0.1	C *+	870625	1756	36.48	5-36.68	35-48.48	4.02	0.84	13	137	4.4	.03	0.1	0.2	B *+
870622	1140	49.86	5-28.74	35-43.36	7.18	0.80	10	185	4.4	.03	0.2	0.2	C *+	870625	1757	33.10	5-36.54	35-48.40	4.03	0.50	09	135	4.1	.01	0.1	0.1	B *+
870622	1210	58.34	5-28.90	35-43.54	7.24	2.12	08	178	4.0	.02	0.1	0.2	B *+	870625	1801	44.93	5-36.64	35-48.45	3.80	0.37	11	136	4.3	.02	0.1	0.2	B *+
870622	1434	44.56	5-28.72	35-43.24	6.88	0.50	08	187	4.5	.01	0.1	0.1	C *+	870625	1804	14.95	5-36.75	35-48.52	3.53	1.45	14	138	4.5	.03	0.2	0.3	B *+
870622	1444	46.30	5-36.79	35-48.07	3.09	0.84	10	209	7.3	.04	0.2	0.9	C *	870625	1811	49.71	5-36.71	35-48.55	4.02	1.13	15	137	4.5	.05	0.2	0.3	B *+
870622	1455	05.14	5-28.73	35-43.28	6.89	0.50	08	187	4.5	.02	0.1	0.1	C *+	870625	1814	29.16	5-36.62	35-48.47	4.32	2.54	11	136	4.3	.03	0.2	0.3	B *+
870623	0345	00.76	5-31.39	35-44.69	3.12	0.37	08	196	1.1	.02	0.1	0.1	C *+	870625	1817	02.17	5-36.80	35-48.50	4.10	0.87	14	139	4.6	.06	0.3	0.4	B *
870623	0345	04.53	5-31.30	35-44.56	3.14	0.37	08	193	0.8	.00	0.0	0.0	C	870625	1818	06.60	5-36.70	35-48.63	4.58	0.59	15	136	4.5	.07	0.3	0.5	B *
870623	0153	13.18	5-28.80	35-43.31	7.00	0.76	08	184	4.3	.02	0.2	0.2	C *+	870625	1917	50.17	5-36.54	35-48.38	4.08	0.71	12	135	4.1	.03	0.1	0.2	B *+
870623	0307	48.96	5-36.86	35-48.33	4.27	1.03	09	213	7.0	.04	0.3	0.7	C *	870625	1716	06.12	5-36.46	35-48.62	4.09	0.66	09	197	4.2	.02	0.2	0.1	C *+
870623	0543	16.14	5-36.58	35-48.46	3.90	0.71	10	210	6.5	.02	0.1	0.3	C *+	870625	1757	51.21	5-36.68	35-48.54	3.86	0.93	14	137	4.4	.03	0.1	0.2	B *+
870623	0614	47.35	5-28.80	35-43.32	7.10	0.37	08	184	4.3	.01	0.1	0.1	C *+	870625	1923	48.59	5-36.76	35-48.51	4.20	1.27	14	138	4.5	.03	0.1	0.2	B *+
870623	0737	02.80	5-36.86	35-48.22	3.64	0.50	08	273	13.1	.04	0.6	1.9	C *	870625	1939	23.58	5-36.70	35-48.49	4.18	0.71	13	137	4.4	.03	0.1	0.2	B *+
870623	0805	53.37	5-37.13	35-48.41	1.59	2.40	09	219	7.3	.04	0.3	2.5	C *	870625	1947	20.62	5-36.40	35-48.27	4.52	0.50	09	137	3.7	.02	0.1	0.1	B *+
870623	1113	58.26	5-28.85	35-43.34	6.91	0.37	08	182	4.2	.01	0.1	0.1	C *+	870625	2101	13.55	5-36.66	35-48.50	4.25	0.90	12	137	4.4	.02	0.1	0.1	B *+
870623	1152	55.29	5-29.53	35-43.65	6.72	0.90	10	159	2.9	.07	0.4	0.5	B *	870625	2140	05.02	5-36.39	35-48.55	4.44	0.37	09	161	4.0	.05	0.2	0.2	B *+
870623	1154	29.65	5-36.66	35-48.53	4.17	1.08	10	212	6.5	.02	0.2	0.4	C *+	870625	2142	42.48	5-36.50	35-48.38	4.12	1.31	13	135	4.0	.02	0.1	0.2	B *+
870622	2218	20.19	5-36.98	35-48.53	3.00	0.90	10	218	6.9	.03	0.2	0.6	C *	870625	2143	43.33	5-36.53	35-48.35	4.02	1.45	12	135	4.0	.04	0.2	0.2	B *+
870622	2221	13.88	5-36.41	35-48.42	5.00	0.87	10	206	6.4	.02	0.1	0.3	C *+	870625	2151	19.54	5-36.55	35-48.34	4.12	0.50	12	136	4.0	.03	0.1	0.2	B *+
870622	2312	01.17	5-36.47	35-48.39	4.43	0.87	10	207	6.5	.02	0.1	0.4	C *+	870625	2155	39.15	5-36.62	35-48.47	3.98	2.09	10	136	4.3	.05	0.2	0.4	B *+
870622	2313	44.46	5-37.03	35-48.60	2.96	0.93	09	219	6.9	.02	0.2	0.5	C *+	870625	2156	42.74	5-36.62	35-48.50	4.17	0.50	13	136	4.3	.02	0.1	0.1	B *+
870623	0026	52.99	5-28.42	35-42.30	0.49	1.55	09	209	6.0	.02	0.2	2.2	C *	870625	2252	42.70	5-29.00	35-43.51	7.15	0.50	12	176	3.8	.03	0.2	0.2	B *+
870623	0028	31.23	5-36.63	35-48.45	3.89	1.00	10	211	6.6	.02	0.1	0.3	C *+	870625	2311	53.89	5-36.65	35-48.50	4.39	0.87	13	136	4.4	.02	0.1	0.2	B *+
870623	0033	57.07	5-29.21	35-43.60	6.53	0.59	09	168	3.4	.07	0.3	0.3	B *	870625	2336	42.43	5-36.66	35-48.50	3.81	0.50	13	137	4.4	.03	0.1	0.2	B *+
870622	1902	31.16	5-30.44	35-44.47	6.59	0.50	05	177	0.8	.00	0.7	0.1	C	870625	2339	37.39	5-28.29	35-42.10	1.57	0.71	12	216	6.4	.05	0.3	0.9	C *
870622	2041	28.29	5-28.78	35-43.31	6.98	0.50	08	185	4.4	.02	0.1	0.1	C *+	870625	2357	22.13	5-36.30	35-48.29	4.74	1.08	13	132	3.6	.02	0.1	0.2	B *+
870622	2208	28.50	5-36.97	35-48.58	2.77	1.18	10	218	6.8	.03	0.2	0.6	C *	870625	2359	51.27	5-36.28	35-48.33	4.82	0.84	14	132	3.6	.03	0.1	0.2	B *+
870622	2158	57.93	5-37.19	35-48.52	2.11	2.82	08	221	7.2	.03	0.2	1.6	C *	870626	0000	31.39	5-36.30	35-48.34	4.79	0.66	13	132	3.6	.02	0.1	0.1	B *+
870622	2210	16.84	5-36.99	35-48.54	2.78	0.59	09	218	6.9	.01	0.1	0.3	C *+	870626	0005	36.72	5-36.28	35-48.26	4.84	0.37	11	138	3.5	.02	0.1	0.1	B *+
870622	2212	41.29	5-36.97	35-48.57	3.00	1.18	10	218	6.9	.03	0.2	0.7	C *	870626	0016	53.89	5-36.29	35-48.27	4.78	0.95	13	132	3.6	.02	0.1	0.1	B *+
870622	2319	30.36	5-36.98	35-48.63	3.34	0.59	10	219	6.8	.02	0.1	0.4	C *+	870626	0019	41.57	5-36.73	35-48.57	4.30	0.59	13	137	4.5	.03	0.1	0.2	B *+
870623	1754	11.15	5-36.34	35-48.25	5.00	1.18	09	203	6.5	.02	0.2	0.5	C *+	870626	0020	10.22	5-29.48	35-43.86	6.74	0.50	13	157	2.8	.02	0.1	0.1	B *+
870623	1808	04.24	5-36.67	35-48.51	4.19	0.87	10	211	6.5	.04	0.3	0.7	C *	870626	0021	44.10	5-36.30	35-48.23	4.82	1.38	13	132	3.5	.02	0.1	0.2	B *+
870623	1955	28.41	5-37.90	35-48.57	2.25	0.90	09	232	8.2	.02	0.1	0.6	C *	870626	0025	53.29	5-36.32	35-48.26	4.63	0.50	12	132	3.6	.04	0.2	0.3	B *+
870623	2140	58.48	5-37.78	35-48.53	2.64	0.93	10	230	8.1	.03	0.2	0.8	C *	870626	0026	09.37	5-36.26	35-48.32	4.75	0.16	11	131	3.6	.04	0.2	0.3	B *+
870623	2217	38.56	5-36.41	35-48.30	4.31	0.87	08	205	6.5	.02	0.2	0.5	C *+	870626	0028	35.95	5-36.31	35-48.32	4.93	1.79	12	132	3.6	.04	0.2	0.5	B *+
870624	0011	15.07	5-36.83	35-48.61	5.00	2.36	06	216	6.6	.02	0.5	1.1	C *	870626	0031	10.66	5-36.29	35-48.24	4.66	0.87	12	132	3.5	.02	0.1	0.2	B *+
870624	0014	17.77	5-36.79	35-48.72	4.74	0.80	09	217	6.4	.02	0.1	0.3	C *+	870626	0034	36.63	5-36.25	35-48.18	4.84	0.97	12	132	3.4	.02	0.1	0.2	B *+
870624	0053	38.60	5-28.95	35-43.39	7.12	0.66	08	179	4.0	.02	0.2	0.2	B *+	870626	0041	23.56	5-36.29	35-48.19	4.75	1.31	12	132	3.5	.02	0.1	0.2	B *+
870624	0157	10.08	5-30.57	35-43.80	0.96	0.59	07	131	1.3	.03	0.2	0.6	B *	870626	0000	49.29	5-36.28	35-48.29	4.75	0.50	14	132	3.6	.02	0.1	0.1	B *+
870624	0215	49.65	5-36.67	35-48.47	3.40	1.89	08	212	6.6	.03	0.2	0.9	C *	870626	0017	02.69	5-36.30	35-48.35	4.79	0.84	14	132	3.6	.03	0.1	0.2	B *+
870624	0227	42.57	5-36.68	35-48.52	3.64	0.71	10	212	6.6	.03	0.2	0.5	C *+	870626	0043	16.42	5-36.24	35-48.24	4.80	0.59	14	131	3.5	.03	0.1	0.2	B *+
870624	0228	04.77	5-36.71	35-48.45	3.42	1.27	09	212	6.7	.02	0.1	0.6	C *	870626	0101	14.39	5-36.27	35-48.27	4.68	0.50	14	132	3.5	.02	0.1	0.1	B *+
870624	0246	43.99	5-30.13	35-44.00	1.48	0.37	06	250	1.6	.03	0.4	0.4	C *	870626	0105	20.23	5-36.66	35-48.46	3.91	0.59	13	137	4.3	.02	0.1	0.2	B *+
870624	0256	16.98	5-36.71	35-48.54	3.78	1.69	09	213	6.6	.03	0.2	0.7	C *	870626	0106	35.54	5-36.27	35-48.29	4.73	1.27	14	132	3.5	.03	0.1	0.2	B *+
870624	0327	32.18	5-36.57	35-48.43	3.98	0.84	09	209	6.5	.02	0.1	0.1	C *+	870626	0112	49.70	5-36.40	35-48.48	4.03	0.37	11	133	3.9	.05	0.2	0.3	B *+
870624	0446	35.38	5-36.54	35-48.49	5.00	1.49	09	209	6.4	.04	0.2	0.8	C *	870626	0120	15.28	5-36.27	3									

# Appendix C

DATE	ORIGIN	LAT S	LONG W	DEPTH	MAG	NO	GAP	DMIN	RMS	ERH	ERZ	Q	D
870626	1022	32.77	5-36.52	35-48.43	4.59	1.03	14	135	4.1	.04	0.2	0.2	B *+
870626	1035	04.80	5-36.62	35-48.45	4.31	0.84	13	136	4.3	.03	0.1	0.2	B *+
870626	1040	04.60	5-36.28	35-48.18	4.66	1.69	15	132	3.5	.03	0.1	0.2	B *
870626	1100	39.65	5-36.52	35-48.44	4.58	0.59	13	135	4.1	.03	0.1	0.2	B *+
870626	1020	05.70	5-36.68	35-48.68	4.56	0.50	12	136	4.6	.02	0.1	0.2	B *+
870626	1105	49.96	5-36.67	35-48.56	4.60	0.90	14	136	4.4	.04	0.2	0.3	B *+
870626	1153	54.59	5-36.71	35-48.59	4.20	0.37	13	137	4.5	.03	0.1	0.2	B *+
870626	1156	47.35	5-36.74	35-48.58	4.08	0.66	16	137	4.6	.03	0.1	0.2	B *+
870626	1206	06.23	5-36.74	35-48.56	3.93	0.50	14	137	4.5	.03	0.1	0.2	B *+
870626	1238	23.11	5-36.34	35-48.44	4.79	0.37	12	132	3.8	.05	0.2	0.3	B *+
870626	1255	15.75	5-36.12	35-48.15	4.75	2.04	12	130	3.2	.04	0.2	0.3	B *
870626	1306	41.28	5-36.80	35-48.49	4.22	0.76	12	139	4.6	.02	0.1	0.1	B *+
870626	1310	22.80	5-36.21	35-48.14	4.63	0.50	06	199	3.3	.02	0.2	0.2	C *
870626	1326	40.47	5-36.79	35-48.58	4.26	0.80	14	138	4.6	.04	0.2	0.3	B *+
870626	1329	10.86	5-36.02	35-48.24	4.78	0.37	15	128	3.1	.06	0.2	0.3	B *
870626	1352	02.58	5-36.12	35-48.19	4.87	2.89	10	130	3.2	.02	0.1	0.1	B *+
870626	1354	58.21	5-36.03	35-48.15	4.88	0.37	14	129	3.0	.03	0.1	0.2	B *
870626	1357	34.13	5-36.57	35-48.46	4.37	1.38	14	135	4.2	.04	0.2	0.3	B *+
870626	1402	22.02	5-36.27	35-48.25	4.61	0.76	14	132	3.5	.04	0.2	0.2	B *+
870626	1256	06.61	5-36.14	35-48.06	4.89	0.59	14	131	3.1	.05	0.2	0.3	B *+
870626	1256	20.33	5-36.14	35-48.16	4.90	0.59	13	130	3.2	.03	0.1	0.3	B *+
870626	1256	31.42	5-36.17	35-48.18	4.75	1.81	11	131	3.3	.03	0.2	0.3	B *+
870626	1402	44.85	5-36.09	35-48.27	4.64	0.59	15	129	3.3	.03	0.1	0.2	B *+
870626	1403	18.31	5-36.07	35-48.23	4.91	2.18	10	129	3.2	.04	0.3	0.5	B *+
870626	1405	58.79	5-36.32	35-48.18	4.27	0.16	11	133	3.5	.03	0.1	0.2	B *+
870626	1406	52.56	5-36.14	35-48.27	4.83	2.41	10	130	3.3	.04	0.3	0.6	B *
870626	1408	22.77	5-36.11	35-48.11	4.85	0.50	10	130	3.1	.03	0.2	0.2	B *+
870626	1414	51.89	5-36.30	35-48.34	4.89	0.80	15	132	3.6	.04	0.2	0.3	B *+
870626	1419	10.81	5-36.42	35-48.35	4.07	0.50	11	133	3.8	.03	0.1	0.2	B *+
870626	1408	59.59	5-36.39	35-48.31	4.63	1.27	14	133	3.8	.04	0.2	0.3	B *+
870626	1419	37.25	5-36.35	35-48.43	4.66	1.13	15	132	3.8	.04	0.2	0.2	B *+
870626	1429	51.29	5-36.28	35-48.23	4.58	0.76	15	132	3.5	.02	0.1	0.1	B *+
870626	1459	55.93	5-38.19	35-48.86	2.80	0.16	09	161	7.2	.03	0.2	0.5	B *+
870626	1503	19.49	5-36.18	35-48.16	4.91	0.84	14	131	3.3	.03	0.1	0.2	B *+
870626	1518	40.07	5-36.17	35-48.14	4.88	0.50	14	131	3.2	.02	0.1	0.1	B *+
870626	1523	50.35	5-36.16	35-48.12	4.58	0.16	13	131	3.2	.04	0.2	0.2	B *+
870626	1527	02.41	5-36.53	35-48.49	4.55	1.31	13	134	4.2	.04	0.2	0.3	B *+
870626	1530	16.08	5-36.65	35-48.46	4.26	2.51	10	137	4.3	.02	0.1	0.2	B *+
870626	1533	35.81	5-36.74	35-48.56	4.18	1.31	12	137	4.5	.03	0.2	0.4	B *+
870626	1535	23.34	5-36.06	35-48.04	4.83	1.27	13	130	3.0	.03	0.2	0.3	B *+
870626	1537	01.11	5-36.66	35-48.55	4.91	1.45	14	136	4.4	.06	0.3	0.4	B *
870626	1539	48.50	5-36.66	35-48.43	4.30	0.93	14	137	4.3	.03	0.1	0.2	B *+
870626	1543	08.90	5-36.68	35-48.48	3.40	0.50	13	137	4.4	.06	0.2	0.5	B *
870626	1543	21.60	5-36.68	35-48.52	3.49	0.50	14	137	4.4	.04	0.1	0.3	B *+
870626	1543	42.70	5-36.66	35-48.64	4.29	0.37	13	136	4.5	.03	0.1	0.2	B *+
870626	1545	04.65	5-36.69	35-48.46	3.44	0.37	10	137	4.4	.07	0.3	0.6	B *
870626	1553	34.22	5-36.57	35-48.63	4.54	0.37	08	134	4.4	.02	0.2	0.3	B *+
870626	1558	58.69	5-36.52	35-48.44	4.65	2.15	11	135	4.1	.04	0.2	0.3	B *+
870626	1601	41.45	5-36.27	35-48.16	4.61	0.59	10	132	3.4	.03	0.1	0.2	B *+
870626	1605	04.43	5-36.71	35-48.48	4.61	0.59	11	137	4.4	.02	0.1	0.2	B *+
870626	1616	43.40	5-36.54	35-48.48	4.31	0.37	08	135	4.2	.02	0.1	0.2	B *+
870626	1616	45.54	5-36.45	35-48.34	5.08	0.50	11	134	3.9	.05	0.2	0.4	B *+
870626	1626	17.79	5-36.59	35-48.42	3.84	0.37	07	153	4.2	.03	0.2	0.4	B *
870626	1627	39.82	5-36.53	35-48.43	3.55	1.00	15	135	4.1	.06	0.2	0.4	B *
870626	1630	25.48	5-36.03	35-48.06	5.22	0.37	09	138	3.0	.02	0.1	0.2	B *+
870626	1650	05.92	5-36.71	35-48.52	3.88	0.95	13	137	4.5	.03	0.1	0.2	B *+
870626	1652	15.35	5-36.02	35-48.06	5.00	0.16	08	155	2.9	.04	0.3	0.4	B *+
870626	1700	58.94	5-36.66	35-48.49	3.58	0.37	11	137	4.4	.07	0.3	0.5	B *
870626	1701	18.93	5-36.28	35-48.19	4.59	1.42	15	132	3.5	.04	0.1	0.2	B *+
870626	1703	51.74	5-36.21	35-48.18	4.61	0.37	11	131	3.3	.03	0.1	0.2	B *+
870626	1706	27.30	5-36.52	35-48.21	4.49	1.13	15	132	3.5	.02	0.1	0.1	B *+
870626	1708	08.64	5-36.30	35-48.24	4.55	0.50	12	132	3.6	.04	0.2	0.3	B *+
870626	1711	40.82	5-36.26	35-48.20	4.57	0.37	12	132	3.5	.03	0.1	0.2	B *+
870626	1712	41.59	5-36.49	35-48.50	3.87	0.95	14	134	4.1	.03	0.1	0.1	B *+
870626	1708	16.07	5-36.17	35-48.27	4.70	0.71	12	130	3.4	.03	0.1	0.2	B *+
870626	1712	57.31	5-36.36	35-48.50	3.91	0.37	08	198	3.9	.02	0.1	0.2	C *+
870626	1714	05.08	5-36.32	35-48.34	4.66	0.37	09	132	3.7	.04	0.2	0.3	B *+
870626	1719	47.09	5-36.60	35-48.38	3.70	0.95	13	136	4.2	.03	0.1	0.3	B *+
870626	1726	44.09	5-36.71	35-48.54	4.25	0.76	15	137	4.5	.03	0.1	0.2	B *+
870626	1727	08.95	5-36.23	35-48.41	4.23	1.42	14	130	3.6	.04	0.2	0.2	B *+
870626	1729	19.03	5-36.57	35-48.06	5.09	0.80	13	128	2.9	.02	0.1	0.1	B *+
870626	1747	28.55	5-36.56	35-48.38	4.49	1.27	13	136	4.1	.03	0.1	0.2	B *+
870626	1748	18.93	5-36.24	35-48.42	4.29	0.66	15	131	3.6	.03	0.2	0.2	B *+
870626	1750	15.16	5-36.49	35-48.34	4.04	0.71	12	135	4.0	.03	0.1	0.2	B *+
870626	1759	04.86	5-35.97	35-48.03	4.99	0.50	12	128	2.8	.02	0.1	0.1	B *+
870626	1806	51.87	5-36.29	35-48.32	5.05	0.37	08	132	3.6	.03	0.2	0.5	B *+
870626	1808	45.98	5-36.68	35-48.63	4.20	0.66	14	136	4.5	.04	0.2	0.2	B *+
870626	1818	40.42	5-36.39	35-48.40	4.77	0.37	10	133	3.8	.02	0.1	0.1	B *+
870626	1820	21.38	5-36.40	35-48.43	4.79	1.13	14	133	3.9	.04	0.2	0.3	B *+
870626	1714	44.92	5-36.20	35-48.48	5.78	0.37	05	164	3.6	.06	1.3	1.6	C
870626	1729	36.94	5-36.75	35-48.62	4.14	0.50	12	137	4.6	.02	0.1	0.2	B *+
870626	1840	56.49	5-36.71	35-48.62	4.26	0.50	10	137	4.6	.03	0.2	0.2	B *+

DATE	ORIGIN	LAT S	LONG W	DEPTH	MAG	NO	GAP	DMIN	RMS	ERH	ERZ	Q	D
870626	1857	13.88	5-36.17	35-48.17	4.87	0.50	11	131	3.3	.02	0.1	0.2	B *+
870626	1914	47.05	5-36.44	35-48.29	4.11	0.71	12	134	3.8	.02	0.1	0.1	B *+
870626	1921	05.78	5-36.50	35-48.07	4.35	0.37	06	205	3.7	.01	0.3	0.2	C *
870626	1943	19.52	5-29.00	35-43.48	7.36	2.63	08	093	3.9	.01	0.1	0.2	B *+
870626	2016	45.45	5-38.19	35-48.81	2.68	0.71	13	161	7.1	.03	0.1	0.4	B *+
870626	2031	02.47	5-28.94	35-43.40	6.99	0.71	12	179	4.0	.03	0.2	0.2	B *+
870626	2041	23.07	5-36.36	35-48.34	4.79	0.37	09	138	3.7	.02	0.1	0.1	B *+
870626	2044	17.45	5-28.89	35-43.47	7.56	1.42	13	179	4.1	.03	0.1	0.2	B *+
870626	2031	30.35	5-28.97	35-43.42	7.06	0.87	13	178	4.0	.03	0.1	0.2	B *+
870626	2041	38.93	5-36.37	35-48.40	4.81	1.58	11	132	3.8	.03	0.2	0.2	B *+
870626	2050	07.64	5-36.26	35-48.29	4.63	1.79	12	131	3.5	.03	0.1	0.2	B *+
870626	2123	54.20	5-36.24	35-48.17	5.05	0.87	13	132	3.4	.03	0.1	0.2	B *+
870626	2137	52.89	5-36.46	35-48.28	4.14	0.71	10	134	6.6	.05	0.2	0.7	B *
870626	2138	10.59	5-37.46	35-48.43	2.66	1.13	11	150	7.7	.04	0.2	0.8	B *
870626	2144	30.14	5-36.78	35-48.60	5.00	0.95	11	138	6.6	.03	0.1	0.6	B *
870626	2154	29.48	5-36.27	35-48.13	4.53	1.27	10	132	6.7	.03	0.2	0.6	B *
870626	2207	51.21	5-37.70	35-49.54	3.35	0.59	12	148	7.0	.04	0.2	0.6	B *
870626	2209	01.90	5-36.40	35-48.29	3.98	0.66	08	133	6.5	.01	0.1	0.3	B *+
870626	2224	58.84	5-36.85	35-48.42	3.84	1.58	11	140	6.9	.03	0.1	0.7	B *
870626	2241	16.64	5-29.08	35-43.57	7.26	0.50	09	172	3.7	.04	0.2	0.3	B *+
870626	2245	55.65	5-36.59	35-48.37	4.43	0.97	11	136	6.7	.04	0.2	0.8	B *
870626	2253	02.41	5-36.49	35-48.41	4.17	0.76	11	134	6.5	.04	0.2	0.5	B *+
870626	2357	35.53	5-36.63	35-48.34	3.32	1.31	11	137	6.7	.03	0.1	0.8	B *
870627	0050	39.10	5-36.49	35-48.39	4.63	0.02	11	134	4.0	.03	0.1	0.4	B *+
870626	1825	00.47	5-36.35	35-48.34	4.57	0.37	09	138	3.7	.02	0.1	0.2	B *+
870626	1845	44.33	5-36.43	35-48.48	3.91	0.59	09	199	4.0	.01	0.1	0.1	C *+
870626	1910	52.63	5-36.66	35-48.44	4.30	1.13	13	137	4.3	.02	0.1	0.2	B *+
870626	1940	27.72	5-36.53	35-48.38	4.63	1.31	14	135	4.0	.03	0.1	0.2	B *+
870626	1949	30.09	5-36.36	35-48.49	4.56	0.50	11	132	3.9	.05	0.2	0.3	B *+
870626	1953	43.77	5-28.82	35-43.36	6.79	0.37	13	097	4.3	.03	0.1	0.2	B *+
870626	1955	02.64	5-28.99	35-43.55	7.12	0.16	10	175	3.8	.03	0.2	0.2	B *+
870626	2006	13.54	5-29.00	35-43.46	6.96	0.50	12	093	3.9	.02	0.1	0.2	B *+
870626	2012	59.58	5-36.51	35-48.36	3.97	0.50	12	135	4.0	.02	0.1	0.1	B *+
870626	2019	17.94	5-36.71	35-48.59	4.15	0.37	13	137	4.5	.02	0.1	0.2	B *+
870626	2037	43.23	5-36.34	35-48.45	5.14	0.50	10	132	3.8	.04	0.2	0.3	B *+
870626	2039	28.99	5-36.41	35-48.35	4.98	1.38	12	133	3.8	.02	0.1	0.1	B *+
870626	2040	05.28	5-36.37	35-48.41	4.88	0.59	14	132	3.8	.03	0.1	0.2	B *+
870626	2040	08.97	5-36.35	35-48.42	4.97	0.76	11	132	3.8	.02	0.1	0.2	B *+
870626	2043	16.40	5-36.39	35-48.44	4.85	0.66	10	133	3.9	.02	0.1	0.1	B *+
870626	2043	29.76	5-36.02	35-47.97	4.76	0.16	07	151	2.9	.02	0.2	0.2	B *
870626	2045	06.53	5-28.90	35-43.36	6.91	0.37	09	181	4.1	.02	0.1	0.2	C *+
870626	2109	43.65	5-28.96	35-43.43	7.15	1.13	14	178	4.0	.03	0.1	0.2	B *+
870626	2116	59.65	5-36.32	35-48.39	4.23	0.50	11	132	3.7	.07	0.3	0.4	B *
870626	2134	25.39	5-28.97	35-43.45	7.20	0.50	11	177	3.9	.04	0.2	0.3	B *+
870626	2142	53.21	5-36.17	35-48.08	4.62	1.27	10	131	6.6	.02	0.1	0.4	B *+
870626	2151	01.97	5-36.74	35-48.62	5.00	1.18	11	137	6.5	.03	0.2	0.6	B *
870626	2200	25.22	5-36.78	35-48.55	4.24	0.87	12	138	6.6	.02	0.1	0.4	B *+
870626	2208	25.50	5-29.22	35-43.67	6.50	0.87	08	167	3.3	.05	0.3	0.5	B *+
870626	2134	53.03	5-36.50	35-48.33	4.13	1.08	12	135	4.0	.02	0.1	0.1	B *+
870626	2215	29.98	5-36.73	35-48.65	4.25	0.50	13	137	4.6	.03	0.1	0.2	B *+
870626	2237	25.57	5-28.76	35-43.26	6.82	0.93	13	186	4.5	.04	0.2	0.2	C *+
870626	2239	24.22	5-29.04	35-43.67	7.12	1.03	12	172	3.7	.03	0.2	0.2	B *+
870626	2247	30.19	5-28.78	35-43.16	7.25	0.50	07	187	4.5	.03	0.4	0.7	C *
870626	2251	48.12	5-36.15	35-48.03	4.61	0.97	13	131	3.1	.03	0.1	0.2	B *+
870627	0026	43.34	5-36.34	35-48.23	4.33	1.31	13	133	3.6	.06	0.3	0.4	B *
870627	0045	42.29	5-36.39	35-48.35	4.68	1.27	12	133	3.8	.02	0.1	0.1	B *
870627	0103	56.64	5-36.38	35-48.31	4.56	0.90	12	133	3.7	.03	0.1	0.2	B *+
870627	0108	50.51	5-36.32	35-48.20	4.51	0.76	13	133	3.6	.03	0.1	0.2	B *+
870627	0158	43.41	5-36.48	35-48.44	4.54	0.93	14	134	4.0	.03	0.1	0.2	B *+
870627	0206	59.29	5-28.97	35-43.49	7.20	0.50	10	176	3.9	.02	0.1	0.2	B *+
870627	0225	36.47	5-36.22	35-48.24	4.66	0.50	13	131	3.4	.02	0.1	0.1	B *+
870627	0232	24.29	5-37.46	35-49.33	4.27	0.90	13	145	6.4	.04	0.2	0.3	B *+
870627	0251	54.33	5-28.93	35-43.48	7.27	0.93	12	178	4.0	.05	0.2	0.3	B *+
870627	0325	58.81	5-29.05	35-43.62	6.89	0.50	11	172	3.7	.03	0.2	0.2	B *+
870627	0343	33.96	5-36.38	35-48.32	4.50	0.90	13	133	3.8	.04	0.1	0.3	B *+
870627	0410	29.20	5-36.41	35-48.38	4.48	1.18	13	133	3.8	.03	0.1	0.2	B *+
870627	0500	49.97	5-36.41	35-48.33	4.51	0.84	13	133	3.8	.01	0.1	0.1	B *+
870627	0509	04.21	5-36.07	35-48.11	4.87	2.93	08	129	3.1	.02	0.1	0.2	B *+
870627	0513	35.14	5-36.16	35-48.30	5.59	1.03	14	130	3.4	.08	0.3	0.4	B *
870627	0515	25.98	5-36.30	35-48.26	4.43	1.31	14	132	3.6	.06	0.2	0.3	B *
870627	0521	31.15	5-36.06	35-48.11	4.82	2.41	09	129	3.1	.02	0.1	0.2	B *+
870627	0529	23.72	5-36.00	35-48.04	4.35	0.71	13	129	2.9	.03	0.1	0.2	B *+
870627	0534	58.57	5-36.73	35-48.51	4.32	1.66	12	137	4.5	.03	0.1	0.4	B *+
870627	0542	03.70	5-36.25	35-48.21	4.96	2.71	10	132	3.5	.02	0.1	0.3	B *+
870627	0551	42.96	5-36.36	35-48.37	4.38	1.00	14	133	3.8	.02	0.1	0.1	B *+
870627	0610	26.06	5-35.97	35-48.13	4.97	0.59	13	128	2.9	.05	0.2	0.3	B *+
870627	0612	23.27	5-36.19	35-48.29	4.91	0.59	14	130	3.4	.03	0.1	0.2	B *+
870627	0619	04.83	5-36.47	35-48.38	4.01	1.45	13	134	3.9	.04	0.1	0.2	B *+
870627	0633	58.18	5-36.20	35-48.25	4.92	0.59	11	131	3.4	.01	0.1	0.1	B *+
870627	0612	46.63	5-36.30	35-48.48	4.24	0.76	13	131	3.8	.05	0.2	0.3	B *+
870627	0648	18.16	5-36.13	35-48.14	4.47	0.66	13	130	3.2	.03	0.1	0.2	B *+
870627	0648	25.32	5-35.69	35-48.25	4.90	0.90	12	124	2.6	.05	0.2	0.3	B *+

# Appendix C

DATE	ORIGIN	LAT S	LONG W	DEPTH	MAG	NO	GAP	DMIN	RMS	ERH	ERZ	Q	D
870627	0648	48.85	5-28.91	35-43.42	7.22	1.49	13	179	4.1	.05	0.2	0.3	B *+
870627	0653	40.20	5-36.44	35-48.34	4.81	1.38	14	134	3.9	.03	0.1	0.2	B *+
870627	0656	24.86	5-36.44	35-48.30	4.44	0.66	13	134	3.8	.03	0.1	0.2	B *+
870627	0707	48.60	5-29.01	35-43.50	7.42	1.35	14	175	3.8	.04	0.2	0.2	B *+
870627	0723	26.63	5-36.43	35-48.44	4.38	0.84	14	133	3.9	.05	0.2	0.3	B *+
870627	0731	51.76	5-36.29	35-48.20	4.45	0.87	13	132	3.5	.02	0.1	0.1	B *+
870627	0737	47.40	5-36.27	35-48.34	5.02	0.80	14	131	3.6	.05	0.2	0.3	B *+
870627	1505	55.47	5-28.93	35-43.38	7.06	0.59	14	095	4.1	.04	0.2	0.2	B *+
870627	1513	29.80	5-36.24	35-48.37	4.49	1.89	15	131	3.6	.04	0.1	0.2	B *+
870627	1539	46.95	5-28.97	35-43.41	7.07	1.38	16	094	4.0	.04	0.2	0.2	B *+
870627	1541	21.77	5-35.99	35-47.99	4.33	0.50	12	129	2.8	.03	0.1	0.2	B *+
870627	1554	50.56	5-36.31	35-48.40	4.86	0.50	11	132	3.7	.03	0.1	0.2	B *+
870627	1626	47.22	5-28.95	35-42.86	3.54	0.71	13	094	4.6	.03	0.1	0.2	B *+
870627	1506	05.04	5-28.95	35-43.48	7.19	1.52	15	094	3.9	.04	0.2	0.2	B *+
870627	1722	54.63	5-36.41	35-48.28	4.81	1.13	14	134	3.8	.08	0.3	0.4	B *
870627	1812	30.32	5-36.13	35-48.14	4.69	1.64	15	130	3.2	.04	0.1	0.2	B *+
870627	1840	14.27	5-36.16	35-48.29	4.44	0.84	12	130	3.4	.04	0.2	0.3	B *+
870627	1945	55.87	5-35.89	35-47.92	4.64	1.45	16	128	2.6	.05	0.2	0.3	B *+
870627	2012	48.82	5-35.90	35-47.94	4.57	0.87	13	128	2.6	.04	0.1	0.2	B *+
870627	2133	07.10	5-36.46	35-48.26	4.02	0.71	14	135	3.8	.04	0.2	0.2	B *+
870627	2137	38.17	5-36.17	35-48.26	4.83	0.95	14	130	3.4	.04	0.1	0.2	B *+
870627	2213	17.19	5-34.98	35-48.33	2.32	0.90	14	114	2.0	.05	0.2	0.3	B *+
870627	2216	53.50	5-36.13	35-48.09	4.53	1.00	13	130	3.1	.02	0.1	0.2	B *+
870627	2259	13.41	5-36.68	35-48.70	4.34	1.03	14	136	4.6	.04	0.2	0.3	B *+
870627	2303	26.73	5-36.27	35-48.39	4.89	0.95	14	131	3.6	.03	0.1	0.2	B *+
870627	2342	31.68	5-32.40	35-45.01	1.54	0.71	11	119	3.0	.05	0.2	0.9	B *
870628	0025	07.33	5-36.35	35-48.32	4.40	1.64	13	133	3.7	.03	0.1	0.2	B *+
870628	0048	13.44	5-36.14	35-48.19	4.91	1.03	14	130	3.2	.04	0.2	0.2	B *+
870628	0110	04.56	5-31.91	35-45.48	5.09	1.58	13	104	2.7	.02	0.1	0.1	B *+
870628	0112	23.49	5-36.82	35-48.80	4.80	0.93	14	137	4.9	.04	0.2	0.3	B *+
870628	0116	25.44	5-36.40	35-48.25	4.31	1.76	12	134	3.7	.04	0.2	0.3	B *+
870628	0123	20.51	5-36.17	35-48.27	5.38	0.37	12	139	3.4	.03	0.1	0.2	B *+
870628	0248	57.80	5-36.80	35-48.78	4.78	1.31	13	137	4.9	.03	0.1	0.2	B *+
870628	0313	08.43	5-36.36	35-48.38	4.65	0.50	10	133	3.8	.02	0.1	0.1	B *+
870628	0331	24.77	5-36.15	35-48.11	4.15	0.59	14	131	3.2	.04	0.1	0.2	B *+
870628	0346	25.75	5-36.75	35-48.74	4.80	0.50	13	137	4.7	.02	0.1	0.1	B *+
870628	0350	55.33	5-36.67	35-48.69	4.64	0.76	14	136	4.6	.03	0.1	0.2	B *+
870628	0354	11.74	5-36.15	35-48.19	4.95	1.35	13	130	3.3	.04	0.2	0.3	B *+
870628	0413	54.97	5-36.45	35-48.41	4.63	1.38	13	134	3.9	.02	0.1	0.2	B *+
870628	0608	40.93	5-36.53	35-48.33	4.29	0.50	12	135	4.0	.03	0.1	0.2	B *+
870628	0636	10.31	5-36.32	35-48.38	4.76	0.59	13	132	3.7	.03	0.1	0.2	B *+
870628	0713	35.49	5-36.70	35-48.55	4.39	0.59	13	137	4.5	.02	0.1	0.2	B *+
870628	0715	48.65	5-28.82	35-43.36	6.99	0.50	10	183	4.3	.03	0.2	0.2	C *+
870628	0723	40.40	5-28.82	35-43.34	6.99	0.59	11	183	4.3	.02	0.1	0.1	C *+
870628	1517	59.51	5-29.46	35-44.01	6.58	0.59	13	093	2.7	.05	0.2	0.3	B *+
870628	1523	49.63	5-36.37	35-48.36	4.62	0.66	14	133	3.8	.03	0.1	0.2	B *+
870628	1614	46.81	5-30.59	35-44.67	6.31	0.76	13	094	0.7	.03	0.1	0.2	B *+
870628	1615	52.57	5-29.04	35-43.50	7.15	1.35	16	093	3.8	.04	0.1	0.2	B *+
870628	1616	50.39	5-29.01	35-43.44	6.81	0.84	15	093	3.9	.04	0.2	0.3	B *+
870628	1631	13.55	5-36.79	35-48.68	5.34	0.84	12	138	4.7	.06	0.3	0.5	B *
870628	1717	07.88	5-36.81	35-48.72	4.79	0.50	14	138	4.8	.05	0.2	0.3	B *+
870628	1720	47.04	5-28.99	35-43.43	7.46	2.02	13	094	3.9	.04	0.2	0.4	B *+
870628	1722	43.20	5-28.93	35-43.43	7.01	0.95	15	095	4.0	.03	0.1	0.2	B *+
870628	1723	04.37	5-28.82	35-43.45	7.06	0.50	13	095	4.0	.03	0.1	0.2	B *+
870628	1757	00.57	5-31.30	35-44.34	1.69	0.66	12	109	0.8	.05	0.2	0.5	B *+
870628	1845	51.29	5-36.28	35-48.37	5.08	0.66	14	131	3.6	.04	0.1	0.2	B *+
870628	1937	43.96	5-36.38	35-48.46	4.41	0.66	14	132	3.9	.04	0.1	0.2	B *+
870627	0739	12.72	5-36.37	35-48.34	4.60	0.50	11	133	3.8	.02	0.1	0.1	B *+
870627	0740	16.85	5-36.27	35-48.23	4.41	0.95	13	132	3.5	.03	0.1	0.2	B *+
870627	0758	48.87	5-36.09	35-48.38	5.02	0.62	12	129	3.4	.04	0.2	0.3	B *+
870627	0811	15.52	5-36.30	35-48.30	4.91	1.79	12	132	3.6	.01	0.1	0.2	B *+
870627	0815	28.32	5-36.12	35-48.19	4.99	0.76	14	130	3.2	.03	0.1	0.2	B *+
870627	0816	04.72	5-36.24	35-48.33	4.84	1.38	14	131	3.5	.03	0.1	0.2	B *+
870627	0818	49.28	5-36.41	35-48.44	4.68	1.97	12	133	3.9	.03	0.1	0.3	B *+
870627	0820	40.27	5-36.32	35-48.28	4.90	0.59	12	132	3.6	.02	0.1	0.2	B *+
870627	0830	15.63	5-36.21	35-48.20	5.04	1.27	14	131	3.4	.03	0.1	0.2	B *+
870627	0839	47.06	5-36.36	35-48.29	4.51	0.66	14	131	3.5	.04	0.1	0.2	B *+
870627	0842	46.32	5-36.30	35-48.21	4.26	0.59	13	132	3.5	.02	0.1	0.1	B *+
870627	0915	58.62	5-36.31	35-48.34	5.06	0.50	12	132	3.7	.02	0.1	0.1	B *+
870627	0921	47.55	5-36.24	35-48.27	4.94	0.84	09	131	3.5	.02	0.1	0.2	B *+
870627	0933	02.30	5-36.28	35-48.26	4.47	1.35	13	132	3.5	.02	0.1	0.1	B *+
870627	0941	26.65	5-36.23	35-48.07	4.08	0.50	11	132	3.3	.02	0.1	0.1	B *+
870627	0942	19.80	5-36.41	35-48.34	4.48	1.08	14	133	3.8	.03	0.1	0.2	B *+
870627	0948	51.66	5-36.32	35-48.32	4.48	1.99	13	132	3.6	.03	0.1	0.2	B *+
870627	0950	44.21	5-36.34	35-48.22	3.63	0.50	10	133	3.6	.04	0.2	0.4	B *+
870627	0956	54.16	5-36.26	35-48.21	4.51	0.71	13	132	3.5	.02	0.1	0.1	B *+
870627	1002	27.40	5-36.42	35-48.45	4.61	1.27	14	133	3.9	.03	0.1	0.2	B *+
870627	1006	42.16	5-36.07	35-48.26	5.40	0.66	13	129	3.2	.02	0.1	0.1	B *+
870627	1009	09.17	5-36.33	35-48.26	4.42	0.59	12	133	3.6	.01	0.1	0.1	B *+
870627	0816	48.67	5-36.28	35-48.33	4.82	0.50	14	132	3.6	.02	0.1	0.1	B *+
870627	0942	20.80	5-36.43	35-48.39	4.21	0.90	13	133	3.9	.03	0.1	0.2	B *+
870627	1025	49.73	5-36.23	35-48.36	4.44	0.50	15	131	3.6	.05	0.2	0.3	B *+

DATE	ORIGIN	LAT S	LONG W	DEPTH	MAG	NO	GAP	DMIN	RMS	ERH	ERZ	Q	D
870627	1035	26.81	5-36.25	35-48.29	4.59	1.64	15	131	3.5	.03	0.1	0.2	B *+
870627	1044	30.91	5-36.17	35-48.32	5.29	0.87	16	130	3.4	.05	0.2	0.3	B *+
870627	1059	55.40	5-36.15	35-48.34	4.40	1.18	13	175	3.4	.04	0.2	0.2	B *+
870627	1109	43.31	5-36.26	35-48.31	4.52	1.38	16	131	3.6	.04	0.2	0.2	B *+
870627	1124	18.03	5-36.09	35-48.24	5.35	0.59	15	129	3.2	.04	0.1	0.2	B *+
870627	1130	05.00	5-36.07	35-48.25	5.36	0.59	14	129	3.2	.04	0.1	0.2	B *+
870627	1142	36.20	5-36.35	35-48.43	4.79	0.87	16	132	3.8	.04	0.2	0.3	B *+
870627	1151	24.51	5-36.58	35-48.48	4.40	0.37	10	138	4.2	.01	0.0	0.1	B *+
870627	1212	56.61	5-36.67	35-48.57	3.94	0.66	14	136	4.4	.03	0.1	0.1	B *+
870627	1233	22.85	5-36.26	35-48.33	5.15	0.59	11	131	3.6	.01	0.1	0.1	B *+
870627	1259	09.28	5-36.36	35-48.32	4.38	0.90	16	133	3.7	.04	0.1	0.2	B *+

# Appendix C

DATE	ORIGIN	LAT S	LONG W	DEPTH	MAG	NO	GAP	DMIN	RMS	ERH	ERZ	Q	D	DATE	ORIGIN	LAT S	LONG W	DEPTH	MAG	NO	GAP	DMIN	RMS	ERH	ERZ	Q	D
870701	0205	05.06	5-36.27	35-47.74	3.27	0.80	13	134	3.1	.03	0.1	0.2	B	870705	2340	58.28	5-36.34	35-48.40	4.59	0.50	11	132	3.8	.03	0.1	0.2	B
870701	0315	46.42	5-36.27	35-47.78	3.32	0.71	13	134	3.2	.03	0.1	0.2	B	870705	2353	30.49	5-36.56	35-48.66	4.74	0.50	10	134	4.4	.03	0.2	0.3	B
870701	0444	38.28	5-30.59	35-43.66	1.64	0.59	11	133	1.5	.02	0.1	0.2	B	870705	2353	30.97	5-36.67	35-48.58	4.53	0.50	09	180	4.5	.04	0.3	0.3	B
870701	0458	15.92	5-29.01	35-43.53	7.19	0.76	14	175	3.8	.04	0.2	0.2	B	870705	2355	11.50	5-36.34	35-48.44	4.68	0.93	11	132	3.8	.02	0.1	0.1	B
870701	0509	51.14	5-28.99	35-43.51	7.29	0.59	13	176	3.9	.03	0.1	0.2	B	870705	2356	28.60	5-36.39	35-48.51	4.95	0.37	10	132	4.0	.02	0.1	0.2	B
870701	0532	57.39	5-36.42	35-48.33	4.30	1.13	12	134	3.8	.03	0.1	0.2	B	870705	2357	31.35	5-36.32	35-48.44	4.66	0.66	16	132	3.8	.03	0.1	0.2	B
870701	0540	36.09	5-36.44	35-48.36	4.28	1.42	13	134	3.9	.03	0.1	0.2	B	870705	2359	53.56	5-36.33	35-48.67	4.79	0.37	08	174	4.0	.03	0.2	0.2	B
870701	0613	07.15	5-34.60	35-47.27	4.06	0.71	14	113	0.1	.02	0.1	0.1	B	870706	0000	16.01	5-36.48	35-48.64	5.00	0.37	07	133	4.2	.03	0.2	0.3	B
870701	0813	26.68	5-28.84	35-43.36	7.13	0.71	14	182	4.2	.02	0.1	0.1	C	870706	0003	32.20	5-36.34	35-48.47	4.90	0.59	15	132	3.8	.02	0.1	0.1	B
870701	1217	09.09	5-36.11	35-48.11	4.67	0.37	09	130	3.1	.03	0.2	0.3	B	870706	0005	22.72	5-36.56	35-48.50	4.72	0.37	07	135	4.2	.02	0.1	0.2	B
870701	1325	37.22	5-36.02	35-48.17	5.04	2.04	09	129	3.0	.02	0.2	0.3	B	870706	0011	08.59	5-36.45	35-48.47	4.79	1.31	15	133	4.0	.03	0.1	0.2	B
870701	1647	12.54	5-29.04	35-43.50	7.28	0.59	12	175	3.8	.03	0.2	0.2	B	870706	0012	25.42	5-36.30	35-48.37	4.72	0.97	16	132	3.7	.04	0.1	0.2	B
870701	1750	48.28	5-28.86	35-43.37	7.11	1.45	12	096	4.2	.03	0.2	0.3	B	870706	0024	08.82	5-36.60	35-48.56	4.35	0.37	12	135	4.3	.02	0.1	0.1	B
870701	2009	55.33	5-29.10	35-43.56	7.44	2.42	08	091	3.6	.01	0.1	0.2	B	870706	0026	21.84	5-36.62	35-48.57	5.02	1.74	16	135	4.4	.04	0.2	0.3	B
870701	2239	56.34	5-29.08	35-43.55	7.33	0.76	15	092	3.7	.03	0.1	0.2	B	870706	0037	37.27	5-36.34	35-48.37	4.71	0.37	10	132	3.7	.02	0.1	0.2	B
870701	2256	56.71	5-28.90	35-43.42	7.11	2.08	13	095	4.1	.02	0.1	0.1	B	870706	0031	41.85	5-36.99	35-48.87	3.76	0.76	14	140	5.2	.03	0.1	0.2	B
870701	2259	03.87	5-28.80	35-43.39	7.10	0.80	16	098	4.3	.03	0.1	0.2	B	870706	0036	38.94	5-36.27	35-48.35	5.02	0.93	15	131	3.6	.03	0.1	0.2	B
870704	0301	18.64	5-37.34	35-48.95	4.39	1.87	14	145	5.9	.03	0.1	0.4	B	870706	0038	32.61	5-36.29	35-48.41	5.02	0.71	15	131	3.7	.03	0.1	0.2	B
870704	0317	18.52	5-37.23	35-48.96	4.15	0.50	11	143	5.7	.03	0.2	0.3	B	870705	2355	12.88	5-36.33	35-48.44	4.84	0.97	16	132	3.8	.04	0.2	0.3	B
870704	0355	32.98	5-36.70	35-48.73	4.74	0.37	08	136	4.7	.04	0.3	0.6	B	870706	0037	02.21	5-36.63	35-48.70	4.83	0.87	15	135	4.5	.03	0.1	0.2	B
870704	0430	01.51	5-37.28	35-49.00	3.92	0.37	14	144	5.8	.05	0.2	0.3	B	870706	0038	45.82	5-36.29	35-48.38	5.00	0.37	07	131	3.7	.02	0.1	0.3	B
870704	0638	00.24	5-38.21	35-49.43	5.00	0.37	05	159	6.8	.08	1.0	3.0	C	870706	0046	42.12	5-28.67	35-43.38	7.14	0.37	10	175	4.5	.03	0.2	0.2	B
870704	0831	36.89	5-36.74	35-48.95	5.72	0.37	09	135	5.0	.03	0.2	0.3	B	870706	0048	24.33	5-34.49	35-47.00	3.66	0.66	12	112	0.6	.04	0.1	0.2	B
870704	1232	47.21	5-31.09	35-45.10	7.38	0.50	11	189	1.3	.05	0.3	0.3	C	870706	0055	07.59	5-36.58	35-48.61	4.75	0.16	08	135	4.3	.02	0.1	0.2	B
870704	1510	12.25	5-29.31	35-43.79	6.28	1.23	16	086	3.1	.04	0.1	0.2	A	870706	0105	46.03	5-36.47	35-48.58	4.56	0.37	07	133	4.2	.03	0.2	0.4	B
870704	1524	29.70	5-37.24	35-49.14	4.09	0.37	14	142	5.9	.04	0.2	0.4	B	870706	0112	20.75	5-36.78	35-48.71	4.60	1.45	16	137	4.8	.03	0.1	0.2	B
870704	1743	20.80	5-37.29	35-49.06	4.03	0.37	11	144	5.9	.04	0.2	0.3	B	870706	0126	30.63	5-36.28	35-48.33	5.00	0.50	15	132	3.6	.03	0.1	0.2	B
870704	1932	21.66	5-36.74	35-48.63	4.25	1.38	14	137	4.6	.03	0.2	0.2	B	870706	0134	36.06	5-36.54	35-48.70	5.11	0.37	07	134	4.4	.02	0.2	0.4	B
870704	1953	06.07	5-36.60	35-48.77	4.33	0.80	15	134	4.6	.06	0.2	0.3	B	870706	0136	23.26	5-36.95	35-48.79	3.10	0.50	14	139	5.1	.04	0.1	0.4	B
870704	2016	00.05	5-27.77	35-42.44	2.82	0.66	15	115	5.5	.04	0.1	0.4	B	870706	0148	13.60	5-36.36	35-48.41	4.97	1.00	16	132	3.8	.03	0.1	0.2	B
870704	2108	07.07	5-29.53	35-42.51	0.50	0.71	14	098	4.5	.08	0.2	0.4	B	870706	0153	01.46	5-36.28	35-48.40	5.03	1.00	16	131	3.7	.02	0.1	0.1	B
870704	2141	54.63	5-37.09	35-48.84	3.47	1.00	16	142	5.4	.04	0.1	0.3	B	870706	0154	31.14	5-36.18	35-48.36	5.05	0.37	07	130	3.5	.03	0.2	0.4	B
870704	2154	25.16	5-37.34	35-49.06	4.09	1.08	15	145	6.0	.04	0.2	0.3	B	870706	0155	14.38	5-36.37	35-48.43	4.75	0.59	09	132	3.8	.02	0.1	0.2	B
870705	0315	02.06	5-35.10	35-48.48	2.42	0.16	08	116	2.4	.05	0.4	0.5	B	870706	0158	50.58	5-30.11	35-44.03	4.08	0.37	14	082	1.6	.05	0.2	0.3	A
870705	0415	57.76	5-41.26	35-53.89	3.69	0.37	08	303	3.8	.13	1.6	1.1	C	870706	0200	47.64	5-31.06	35-44.99	6.70	0.37	10	100	1.1	.07	0.3	0.5	B
870705	0607	58.91	5-36.68	35-48.66	4.27	0.37	07	136	4.5	.03	0.2	0.4	B	870706	0153	36.99	5-36.31	35-48.44	4.83	0.59	13	132	3.8	.03	0.1	0.2	B
870705	1212	30.82	5-37.01	35-48.86	3.89	1.00	16	140	5.3	.04	0.1	0.2	B	870706	0153	37.68	5-36.26	35-48.40	5.00	0.59	13	131	3.7	.04	0.2	0.3	B
870705	1527	37.83	5-36.26	35-48.28	4.32	0.87	15	131	3.5	.03	0.1	0.2	B	870706	0202	19.39	5-36.34	35-48.44	4.92	1.89	15	132	3.8	.04	0.2	0.3	B
870705	1642	22.35	5-36.82	35-48.82	3.83	0.16	09	137	4.9	.05	0.2	0.6	B	870706	0204	36.47	5-36.53	35-48.46	4.64	0.16	09	135	4.1	.06	0.4	0.6	B
870705	1654	59.82	5-31.67	35-45.56	6.69	0.59	16	107	2.6	.03	0.1	0.2	B	870706	0205	15.86	5-36.70	35-48.65	4.42	0.37	07	136	4.6	.01	0.1	0.2	B
870705	1725	47.20	5-36.61	35-48.65	4.86	0.37	09	135	4.4	.06	0.3	0.5	B	870706	0207	49.85	5-36.75	35-48.68	4.48	0.66	16	137	4.7	.02	0.1	0.1	B
870705	1726	45.41	5-36.76	35-48.64	4.45	0.59	15	137	4.7	.04	0.1	0.2	B	870706	0213	36.20	5-36.20	35-48.41	5.10	0.37	07	130	3.6	.02	0.1	0.2	B
870705	1739	57.15	5-34.14	35-47.01	3.71	0.37	08	139	1.0	.04	0.2	0.3	B	870706	0223	34.29	5-36.33	35-48.47	4.81	0.37	06	132	3.8	.02	0.2	0.3	B
870705	1806	25.50	5-36.95	35-48.83	3.56	0.80	16	139	5.1	.03	0.1	0.2	B	870706	0233	11.61	5-36.50	35-48.55	4.91	0.37	10	134	4.2	.03	0.1	0.3	B
870705	1826	21.46	5-34.27	35-46.90	3.33	0.76	15	110	1.0	.05	0.2	0.2	B	870706	0237	44.92	5-36.42	35-48.47	4.62	0.16	05	133	4.0	.03	0.4	0.8	C
870705	1832	29.63	5-37.04	35-48.83	3.39	0.50	14	141	5.3	.03	0.1	0.3	B	870706	0243	27.32	5-36.31	35-48.47	4.76	0.50	14	131	3.8	.02	0.1	0.1	B
870705	1837	51.56	5-37.00	35-48.85	3.26	1.13	15	140	5.2	.04	0.2	0.4	B	870706	0245	27.44	5-36.30	35-48.46	4.65	0.37	08	131	3.8	.03	0.2	0.3	B
870705	1847	17.28	5-37.00	35-48.80	3.22	0.37	12	140	5.2	.03	0.1	0.4	B	870706	0246	26.03	5-36.36	35-48.47	4.72	0.50	12	132	3.9	.04	0.2	0	

# Appendix C

DATE	ORIGIN	LAT S	LONG W	DEPTH	MAG	NO	GAP	DMIN	RMS	ERH	ERZ	Q	D
870706	1319	53.47	5-36.80	35-48.78	5.24	0.50	14	137	4.9	.04	0.1	0.2	B *+
870706	1320	56.31	5-36.34	35-48.41	5.02	0.37	08	132	3.8	.02	0.2	0.3	B *+
870706	1351	12.38	5-36.33	35-48.52	4.43	2.04	12	131	3.9	.07	0.4	0.8	B *
870706	1355	34.59	5-36.33	35-48.39	4.65	0.37	10	133	3.8	.02	0.1	0.2	B *+
870706	1403	59.93	5-36.34	35-48.44	4.98	0.50	12	132	3.8	.03	0.2	0.4	B *+
870706	1513	36.71	5-36.85	35-48.85	5.00	0.50	07	138	5.0	.03	0.2	0.4	B *
870706	1515	29.02	5-36.84	35-48.82	4.97	0.50	14	138	5.0	.03	0.1	0.2	B *+
870706	1629	05.35	5-29.01	35-43.53	7.09	0.76	16	093	3.8	.04	0.1	0.2	B *+
870706	0952	17.74	5-36.46	35-48.42	4.63	1.31	13	134	4.0	.04	0.2	0.3	B *+
870706	1515	37.21	5-36.87	35-48.80	5.02	0.66	13	138	5.0	.03	0.1	0.2	B *+
870706	1719	34.84	5-38.32	35-49.26	3.56	0.50	12	162	7.0	.05	0.2	0.6	B *
870706	2008	53.60	5-38.39	35-48.93	1.55	0.50	12	165	7.5	.05	0.2	1.5	B *
870706	2046	30.97	5-29.07	35-43.54	7.02	0.59	15	092	3.7	.04	0.2	0.2	B *+
870706	2101	38.01	5-36.19	35-48.31	4.37	0.84	15	130	3.4	.06	0.2	0.3	B *
870706	2102	24.46	5-36.32	35-48.40	4.84	2.39	12	132	3.7	.04	0.2	0.4	B *+
870706	2103	43.18	5-36.36	35-48.37	4.43	0.59	14	132	3.8	.03	0.1	0.2	B *+
870706	2105	45.27	5-36.17	35-48.36	4.95	0.16	11	130	3.5	.05	0.2	0.3	B *+
870706	2106	48.60	5-36.20	35-48.25	4.60	0.37	08	131	3.4	.02	0.1	0.2	B *+
870706	2140	28.72	5-36.36	35-48.35	4.36	0.76	14	133	3.7	.02	0.1	0.1	B *
870706	2148	08.95	5-36.23	35-48.29	4.74	0.80	16	131	3.5	.04	0.1	0.2	B *+
870706	2156	29.56	5-36.27	35-48.24	4.18	0.59	10	132	3.5	.02	0.1	0.2	B *+
870706	2204	31.84	5-36.28	35-48.31	4.74	2.21	15	132	3.6	.05	0.2	0.3	B *+
870706	2156	43.55	5-36.43	35-48.46	4.54	0.50	08	133	4.0	.05	0.3	0.6	B *
870706	2205	04.75	5-36.28	35-48.38	4.64	2.21	15	131	3.7	.04	0.2	0.4	B *+
870706	2205	50.74	5-36.23	35-48.31	4.79	0.50	12	131	3.5	.02	0.1	0.2	B *+
870706	2206	46.19	5-36.30	35-48.41	4.73	0.76	15	131	3.7	.03	0.1	0.2	B *+
870706	2217	57.38	5-36.25	35-48.24	4.61	1.83	16	132	3.5	.02	0.1	0.1	B *+
870706	2226	03.99	5-36.25	35-48.31	4.65	0.76	15	131	3.5	.05	0.2	0.3	B *+
870706	2259	34.20	5-36.30	35-48.33	4.76	1.55	16	132	3.6	.03	0.1	0.2	B *+
870706	2305	47.86	5-35.67	35-48.51	7.10	0.37	10	122	3.0	.16	0.8	1.1	B
870706	2313	40.28	5-36.53	35-48.35	3.70	0.59	16	135	4.0	.03	0.1	0.1	B *+
870706	2349	58.27	5-33.62	35-46.36	3.40	0.37	14	099	2.5	.03	0.1	0.2	B *+
870707	0022	21.11	5-36.36	35-48.22	4.25	0.37	10	133	3.6	.03	0.1	0.2	B *+
870707	0036	56.46	5-36.34	35-48.49	5.00	0.37	07	132	3.8	.02	0.2	0.3	B *
870707	0119	41.27	5-36.17	35-48.19	4.13	0.37	15	131	3.3	.04	0.2	0.2	B *+
870707	0138	01.16	5-35.85	35-48.17	5.63	0.50	10	126	2.8	.03	0.2	0.2	B *+
870707	0149	00.82	5-36.30	35-48.18	4.23	0.50	11	132	3.5	.02	0.1	0.1	B *+
870707	0150	11.19	5-36.30	35-48.33	4.83	1.64	16	132	3.6	.02	0.1	0.1	B *+
870707	0206	27.88	5-36.24	35-48.22	4.42	0.59	15	131	3.4	.02	0.1	0.1	B *+
870707	0224	13.32	5-36.30	35-48.28	4.21	0.37	11	132	3.6	.02	0.1	0.1	B *+
870707	0235	32.19	5-36.28	35-48.19	4.38	0.76	16	132	3.5	.02	0.1	0.1	B *+
870707	0236	16.46	5-36.27	35-48.26	4.41	0.37	10	132	3.5	.02	0.1	0.1	B *+
870706	2205	51.90	5-36.26	35-48.33	4.67	0.50	11	131	3.6	.02	0.1	0.2	B *+
870706	2206	03.21	5-36.21	35-48.33	5.44	0.37	10	130	3.5	.07	0.3	0.4	B *
870706	2218	01.05	5-36.22	35-48.27	4.70	1.52	16	131	3.5	.03	0.1	0.2	B *+
870707	0236	20.53	5-36.18	35-48.32	4.54	0.16	09	130	3.4	.02	0.1	0.2	B *+
870707	0245	28.71	5-36.24	35-48.32	4.80	0.50	10	131	3.5	.02	0.1	0.1	B *+
870707	0253	23.32	5-37.51	35-48.07	3.15	0.59	15	152	5.5	.05	0.2	0.5	B *+
870707	0257	49.18	5-36.22	35-48.31	4.82	0.16	09	131	3.5	.02	0.1	0.2	B *+
870707	0314	08.43	5-30.24	35-44.08	4.06	1.74	14	084	1.3	.04	0.1	0.3	A *+
870707	0316	58.71	5-30.27	35-44.16	4.18	0.50	15	085	1.2	.04	0.1	0.2	A *+
870707	0317	42.20	5-30.21	35-44.10	4.17	0.71	14	084	1.4	.03	0.1	0.1	A *+
870707	0326	42.99	5-30.11	35-43.96	4.00	0.37	09	098	1.6	.04	0.2	0.2	B *+
870707	0329	21.55	5-30.33	35-44.17	4.26	0.59	14	085	1.1	.03	0.1	0.1	A *+
870707	0332	12.31	5-30.42	35-44.23	4.30	0.59	16	087	0.9	.05	0.2	0.2	A *+
870707	0336	14.50	5-30.31	35-44.06	3.93	0.37	15	084	1.2	.03	0.1	0.1	A *+
870707	0337	39.96	5-30.16	35-44.00	3.82	0.37	15	082	1.5	.03	0.1	0.1	A *+
870707	0344	57.25	5-36.32	35-48.31	4.59	0.37	11	132	3.6	.04	0.2	0.3	B *+
870707	0314	08.97	5-30.20	35-44.04	4.28	1.55	13	083	1.4	.04	0.2	0.4	A *+
870707	0314	13.33	5-30.16	35-44.07	3.83	1.81	14	083	1.5	.05	0.2	0.3	A *+
870707	0314	16.06	5-30.10	35-44.17	4.48	1.35	12	137	1.5	.08	0.4	0.5	B *
870707	0314	30.94	5-30.20	35-44.01	3.73	0.59	10	112	1.5	.08	0.3	0.5	B *
870707	0314	39.01	5-30.25	35-44.08	4.31	1.83	16	084	1.3	.03	0.1	0.1	A *+
870707	0315	00.67	5-30.31	35-44.05	3.57	1.71	15	083	1.3	.03	0.1	0.3	A *+
870707	0317	25.63	5-30.33	35-44.14	3.96	0.16	09	132	1.1	.02	0.1	0.1	B *+
870707	0317	45.79	5-30.28	35-44.10	4.15	0.90	16	084	1.2	.07	0.2	0.3	A *
870707	0326	54.24	5-30.06	35-43.96	3.98	0.16	05	141	1.7	.01	0.2	0.3	C
870707	0329	23.58	5-30.35	35-44.14	4.14	0.37	07	132	1.1	.02	0.1	0.1	B *
870707	0336	33.49	5-30.36	35-44.23	4.04	0.37	11	111	1.0	.06	0.2	0.3	B *
870707	0347	28.05	5-30.26	35-44.10	4.31	0.50	14	084	1.3	.04	0.1	0.3	A *+
870707	0350	48.94	5-30.19	35-44.04	3.96	0.37	12	099	1.4	.05	0.2	0.2	B *+
870707	0352	34.74	5-30.16	35-44.17	4.13	0.50	12	085	1.4	.06	0.2	0.3	A *
870707	0353	32.06	5-30.27	35-44.12	3.97	0.59	16	084	1.2	.04	0.1	0.2	A *+
870707	0354	52.04	5-30.30	35-44.05	3.83	0.50	14	083	1.3	.03	0.1	0.1	A *+
870707	0357	48.35	5-30.36	35-44.09	3.66	0.50	12	101	1.1	.03	0.1	0.2	B *+
870707	0400	53.15	5-30.39	35-44.17	4.03	0.71	15	086	1.0	.03	0.1	0.2	A *+
870707	0401	34.78	5-30.36	35-44.15	3.97	0.59	15	085	1.1	.03	0.1	0.1	A *+
870707	0418	30.78	5-36.32	35-48.37	4.29	0.37	07	132	6.3	.01	0.1	0.2	B *
870707	0434	51.68	5-30.44	35-44.20	3.82	0.37	15	086	0.9	.03	0.1	0.1	A *+
870707	0427	36.76	5-30.15	35-43.94	3.04	0.50	09	098	1.6	.04	0.2	0.3	B *+
870707	0439	50.87	5-30.42	35-44.16	3.74	0.50	14	085	1.0	.03	0.1	0.1	A *+
870707	0453	36.24	5-30.45	35-44.13	3.73	0.16	10	130	1.0	.06	0.2	0.4	B *

DATE	ORIGIN	L S	LONG W	DEPTH MAG	NO	GAP	DMIN	RMS	ERH	ERZ	Q D	
870707	0619	00.36	5-30.39	35-44.19	3.98	0.59	15	086	1.0	.03	0.1	0.1 A *+
870707	0745	39.32	5-36.80	35-48.81	3.94	0.37	08	137	4.9	.02	0.1	0.3 B B *+
870707	0754	38.62	5-30.47	35-44.20	3.72	0.37	10	128	0.8	.05	0.2	0.3 B B *+
870707	1053	40.52	5-30.56	35-44.32	3.83	0.50	08	125	0.6	.04	0.2	0.3 B B *+
870707	1054	00.76	5-30.69	35-44.35	4.00	0.50	14	122	0.4	.04	0.1	0.2 B B *+
870707	1055	27.02	5-30.33	35-44.14	3.62	0.37	12	132	1.1	.03	0.1	0.2 B B *+
870707	1111	18.15	5-30.66	35-44.35	4.23	0.66	13	122	0.4	.06	0.2	0.3 B B *+
870707	1209	31.52	5-30.56	35-44.38	4.09	1.23	13	124	0.6	.05	0.2	0.2 B B *+
870707	1250	46.63	5-29.96	35-42.98	1.18	0.37	09	146	3.2	.05	0.2	0.8 B B *+
870707	0400	54.04	5-30.33	35-44.17	4.24	0.66	14	085	1.1	.05	0.2	0.2 A *+
870707	0401	10.02	5-30.35	35-44.15	3.95	0.50	15	085	1.1	.03	0.1	0.1 A *+
870707	0401	12.80	5-30.38	35-44.11	4.03	0.37	08	132	1.1	.02	0.1	0.1 B B *+
870707	0401	19.68	5-30.35	35-44.13	4.05	0.16	08	132	1.1	.02	0.1	0.1 B B *+
870707	0427	47.56	5-29.92	35-43.94	4.12	0.50	09	145	2.0	.08	0.3	0.5 B B *+
870707	0439	51.36	5-30.37	35-44.19	4.18	0.37	09	152	1.0	.04	0.2	0.3 B B *+
870707	1053	42.43	5-30.97	35-44.53	4.19	0.37	04	259	0.3	.03	0.0	0.0 C
870707	1054	08.40	5-30.64	35-44.31	4.24	0.59	14	123	0.5	.05	0.2	0.2 B B *+
870707	1209	32.22	5-30.67	35-44.32	3.53	1.03	12	123	0.4	.05	0.2	0.5 B B *+
870707	1412	46.48	5-30.56	35-44.29	3.80	0.50	11	125	0.6	.03	0.1	0.2 B B *+
870707	1414	41.64	5-30.63	35-44.28	3.74	0.50	12	124	0.5	.05	0.2	0.3 B B *+
870707	1807	38.04	5-30.45	35-44.21	3.42	0.37	13	104	0.8	.04	0.1	0.2 B B *+
870707	1911	23.27	5-34.95	35-48.42	2.27	0.37	10	114	2.2	.01	0.1	0.1 B B *+
870707	2341	30.45	5-35.29	35-39.67	4.39	0.37	07	180	5.6	.02	0.2	0.3 B B *+
870708	0019	38.21	5-35.29	35-39.54	4.31	0.37	08	184	5.6	.04	0.3	0.6 C
870708	0325	00.10	5-36.41	35-48.35	4.37	2.25	11	133	3.8	.02	0.1	0.2 B B *+
870708	0346	03.26	5-36.43	35-48.41	4.12	0.50	09	133	3.9	.01	0.1	0.1 B B *+
870708	0527	48.47	5-30.39	35-44.17	3.59	0.59	16	085	1.0	.04	0.1	0.2 A *+
870708	0550	34.99	5-30.48	35-44.17	3.41	1.08	15	086	0.9	.02	0.1	0.1 A *+
870708	0558	26.57	5-30.48	35-44.14	3.55	0.50	14	085	0.9	.03	0.1	0.1 A *+
870708	0612	29.72	5-30.52	35-44.12	3.35	0.50	11	123	0.9	.02	0.1	0.1 B B *+
870708	0628	32.99	5-30.46	35-44.11	3.42	0.50	15	085	1.0	.04	0.1	0.2 A *+
870708	0654	18.94	5-30.63	35-44.31	3.49	0.50	12	124	0.5	.05	0.2	0.5 B B *+
870708	0720	29.49	5-30.69	35-44.24	3.22	0.59	14	087	0.5	.04	0.1	0.2 A *+
870708	0850	12.17	5-30.61	35-44.20	3.35	0.37	09	125	0.6	.03	0.1	0.2 B B *+
870708	0882	08.04	5-31.55	35-45.61	7.09	0.37	09	108	2.5	.03	0.2	0.2 B B *+
870708	0550	41.04	5-30.47	35-44.11	3.39	1.00	14	085	0.9	.03	0.1	0.2 A *+
870708	0903	08.40	5-37.14	35-48.20	2.09	0.37	08	145	4.9	.02	0.1	0.4 B B *+
870708	0915	13.43	5-31.31	35-45.04	5.65	1.31	14	100	1.4	.03	0.1	0.2 B B *+
870708	1042	25.38	5-30.35	35-44.13	3.48	0.59	16	085	1.1	.04	0.1	0.2 A *+
870708	1317	51.25	5-29.00	35-43.49	7.16	0.50	12	093	3.9	.03	0.1	0.2 B B *+
870708	1756	20.98	5-36.56	35-47.95	0.69	0.37	06	207	3.8	.06	0.4	3.0 C
870708	1758	29.24	5-28.63	35-43.51	7.88	0.37	09	102	4.5	.04	0.3	0.4 B B *+
870708	1759	11.60	5-36.36	35-48.27	4.22	0.37	11	133	3.7	.02	0.1	0.1 B B *+
870708	1900	01.13	5-34.37	35-51.23	7.43	0.37	06	207	0.3	.36	0.9	0.8 D
870708	2154	43.33	5-36.47	35-48.43	4.90	0.37	08	134	4.0	.03	0.2	0.3 B B *+
870708	2157	14.14	5-30.56	35-44.22	3.63	0.50	15	087	0.7	.03	0.1	0.2 A *+
870708	2158	56.05	5-30.59	35-44.24	3.30	0.50	15	087	0.6	.03	0.1	0.2 A *+
870708	2209	42.35	5-30.49	35-44.20	3.56	0.37	13	128	0.8	.03	0.1	0.2 B B *+
870708	2345	21.72	5-37.94	35-49.20	4.04	0.50	10	155	7.1	.15	0.8	1.7 C
870709	0155	50.27	5-28.91	35-43.54	7.05	0.50	12	161	4.0	.04	0.2	0.3 B B *+
870709	0303	51.77	5-37.58	35-48.31	2.97	0.76	15	152	5.8	.02	0.1	0.2 B B *+
870709	0315	34.08	5-36.28	35-48.26	4.26	0.37	07	132	3.5	.01	0.1	0.1 B B *+
870709	0317	46.54	5-36.24	35-48.29	4.39	0.50	10	131	3.5	.07	0.3	0.5 B B *+
870709	0602	25.72	5-36.53	35-48.31	3.74	0.50	11	135	4.0	.08	0.4	0.5 B B *+
870709	0626	37.31	5-30.84	35-44.46	4.39	0.59	14	091	0.1	.02	0.1	0.1 B B *+
870709	0626	38.54	5-30.84	35-44.45	3.61	0.50	10	091	0.1	.03	0.1	0.2 B B *+
870709	0901	51.92	5-28.90	35-43.49	6.91	0.50	12	161	4.0	.04	0.2	0.3 B B *+
870709	1257	48.49	5-33.29	35-45.46	1.08	0.80	16	100	4.2	.06	0.2	1.1 B B *+
870709	1342	09.12	5-36.36	35-47.98	3.34	0.50	08	134	3.5	.03	0.2	0.3 B B *+
870709	1420	48.65	5-30.26	35-44.61	6.31	0.59	16	093	1.7	.04	0.1	0.2 B B *+
870709	1443	32.32	5-32.74	35-45.42	2.06	1.97	13	097	3.9	.03	0.1	0.5 B B *+
870709	1445	18.81	5-32.67	35-45.50	3.31	1.85	14	098	3.9	.07	0.3	0.6 B B *+
870709	1658	26.54	5-30.69	35-44.24	3.31	0.50	08	125	0.5	.02	0.1	0.3 B B *+
870709	1758	50.96	5-25.69	35-39.37	3.42	0.71	10	257	2.9	.07	0.6	0.6 C
870709	1811	58.43	5-31.02	35-42.74	0.18	0.50	06	144	3.1	.04	0.3	9.3 C
870709	1813	09.82	5-30.84	35-43.86	1.26	0.37	14	125	1.1	.06	0.2	0.4 B B *+
870709	1830	52.22	5-37.46	35-48.69	0.67	0.37	08	211	5.8	.03	0.2	2.1 C
870709	1835	01.74	5-30.63	35-44.23	3.37	0.37	07	125	0.6	.02	0.1	0.2 B B *+
870710	0145	29.98	5-36.95	35-48.88	4.05	0.50	14	139	5.2	.08	0.4	0.6 B B *+
870710	0537	49.39	5-36.02	35-48.25	5.12	1.00	16	128	3.1	.03	0.1	0.2 B B *+
870710	1415	34.86	5-27.51	35-41.35	2.62	0.59	08	143	4.3	.03	0.2	0.7 B B *+
870710	1450	39.61	5-31.33	35-44.58	3.20	0.90	14	092	0.9	.02	0.1	0.2 B B *+
870710	1527	56.98	5-31.34	35-44.53	2.98	0.50	13	091	0.9	.02	0.1	0.1 B B *+
870710	1632	16.93	5-30.97	35-43.91	3.37	0.37	12	134	1.0	.09	0.4	0.5 B B *+
870710	1649	28.34	5-30.97	35-44.53	3.48	0.50	13	092	0.3	.12	0.4	0.6 B
870710	1709	19.60	5-36.74	35-48.68	4.40	0.76	14	137	4.7	.03	0.1	0.2 B B *+
870710	1715	04.32	5-36.04	35-48.06	5.06	1.13	15	129	3.0	.03	0.1	0.2 B B *+
870710	1919	46.49	5-35.81	35-48.26	3.38	0.66	10	171	2.8	.02	0.1	0.1 B B *+
870710	1941	18.97	5-31.49	35-45.06	4.29	0.50	13	099	1.6	.02	0.1	0.1 B B *+
870710	2044	51.60	5-36.68	35-48.68	4.57	0.37	08	136	4.6	.02	0.1	0.3 B B *+
870710	2045	21.74	5-36.65	35-48.64	4.59	0.37	11	136	4.5	.04	0.2	0.3 B B *+
870710	2142	10.22	5-36.66	35-48.71	4.57	0.37	13	135	4.6	.06	0.2	0.4 B B *+

# Appendix C

DATE	ORIGIN	LAT S	LONG W	DEPTH	MAG	NO	GAP	DMIN	RMS	ERH	ERZ	Q	D	DATE	ORIGIN	LAT S	LONG W	DEPTH	MAG	NO	GAP	DMIN	RMS	ERH	ERZ	Q	D
870710	2158	47.38	5-36.78	35-48.74	4.37	0.66	14	137	4.8	.05	0.2	0.3	B *	870713	1803	16.35	5-29.67	35-42.46	1.43	0.50	13	095	4.2	.07	0.2	1.1	B *
870710	2231	42.40	5-31.06	35-44.27	2.78	0.50	12	116	0.5	.03	0.1	0.3	B *	870713	1848	29.34	5-35.30	35-46.85	1.83	1.13	14	123	1.5	.04	0.1	0.5	B *
870709	1853	29.94	5-36.15	35-48.23	4.98	0.95	13	130	3.3	.02	0.1	0.1	B *	870713	1954	59.62	5-29.01	35-43.49	7.10	0.80	16	093	3.8	.04	0.1	0.2	B *
870709	1915	30.85	5-35.76	35-48.03	5.00	2.98	09	126	2.5	.05	0.4	0.6	B *	870713	1959	48.77	5-28.99	35-43.50	7.10	0.90	16	094	3.9	.05	0.2	0.3	B *
870710	1528	11.82	5-31.37	35-44.66	3.08	0.37	08	134	1.0	.01	0.1	0.1	B *	870713	2016	14.24	5-29.05	35-43.43	6.85	0.50	09	176	3.8	.07	0.5	0.6	B *
870710	1649	38.68	5-27.56	35-41.35	2.42	0.37	08	143	4.4	.02	0.1	0.4	B *	870713	2222	07.55	5-33.76	35-46.87	4.81	1.45	13	103	1.8	.02	0.1	0.1	B *
870709	1919	33.41	5-36.00	35-48.10	4.93	0.37	07	129	3.0	.02	0.1	0.2	B *	870713	2242	15.65	5-36.29	35-48.18	4.04	0.37	08	132	3.5	.01	0.1	0.1	B *
870709	1920	54.79	5-36.08	35-48.03	4.80	0.50	12	130	3.0	.04	0.2	0.3	B *	870713	2326	15.76	5-30.85	35-44.03	2.59	0.87	13	072	0.7	.09	0.3	0.8	A *
870709	1921	40.62	5-35.92	35-48.11	5.29	0.71	12	127	2.8	.01	0.1	0.1	B *	870713	2328	28.17	5-30.84	35-44.19	2.71	0.50	14	071	0.4	.04	0.1	0.3	A *
870709	1925	53.25	5-36.00	35-48.09	5.10	1.08	16	128	2.9	.04	0.2	0.2	B *	870713	2329	04.68	5-30.87	35-44.10	2.69	0.37	09	130	0.6	.03	0.1	0.2	B *
870709	1938	06.05	5-36.08	35-48.17	4.82	0.16	12	129	3.1	.02	0.1	0.1	B *	870713	2331	41.99	5-30.82	35-44.06	2.79	0.37	09	129	0.7	.04	0.2	0.3	B *
870709	1939	51.16	5-35.92	35-48.07	5.02	0.95	16	128	2.8	.05	0.2	0.3	B *	870713	2333	49.76	5-30.94	35-44.13	2.87	0.50	07	131	0.6	.01	0.1	0.1	B *
870709	1943	08.86	5-35.85	35-48.07	5.10	0.50	12	127	2.7	.01	0.1	0.1	B *	870713	2335	09.40	5-30.86	35-44.18	2.58	2.33	13	072	0.5	.03	0.1	0.3	A *
870709	1946	29.02	5-35.96	35-48.04	4.93	1.42	15	128	2.8	.04	0.2	0.2	B *	870713	2343	55.68	5-30.74	35-44.14	2.93	0.59	15	082	0.6	.04	0.1	0.3	A *
870709	2007	31.59	5-36.24	35-48.17	4.19	0.37	09	132	3.4	.01	0.1	0.1	B *	870714	0028	05.57	5-30.69	35-44.05	2.87	0.50	15	083	0.8	.05	0.2	0.3	A *
870709	2021	11.91	5-36.11	35-48.11	4.55	0.59	10	130	3.1	.02	0.1	0.1	B *	870714	0104	55.52	5-31.82	35-45.65	6.58	0.59	11	150	2.9	.04	0.2	0.2	B *
870709	2026	38.62	5-35.85	35-48.06	5.27	0.37	07	127	2.7	.01	0.0	0.1	B *	870714	0127	54.37	5-30.73	35-44.13	3.03	0.80	16	083	0.6	.05	0.2	0.3	A *
870709	2048	57.46	5-36.02	35-48.30	5.69	0.50	13	128	3.2	.08	0.3	0.4	B *	870714	0153	18.22	5-32.96	35-46.54	5.05	0.50	14	110	3.4	.03	0.1	0.1	B *
870709	2102	47.99	5-36.30	35-48.37	4.80	0.37	09	132	3.7	.02	0.1	0.2	B *	870714	0208	06.79	5-36.22	35-48.13	4.28	0.37	08	132	3.3	.02	0.1	0.2	B *
870709	2232	18.91	5-31.11	35-45.34	8.00	1.95	12	106	1.7	.02	0.1	0.2	B *	870714	0236	22.12	5-29.57	35-43.84	5.42	0.59	14	091	2.6	.05	0.2	0.2	B *
870709	2302	00.10	5-32.56	35-45.39	1.77	0.59	14	098	3.6	.02	0.1	0.2	B *	870714	0247	01.43	5-36.13	35-48.10	4.25	0.87	13	130	3.1	.02	0.1	0.1	B *
870709	2353	18.90	5-35.95	35-48.21	5.04	0.50	13	127	3.0	.05	0.2	0.3	B *	870714	0303	36.74	5-37.51	35-49.33	4.09	0.50	08	146	6.5	.04	0.2	0.5	B *
870709	1919	39.17	5-35.99	35-48.10	5.00	0.37	06	128	2.9	.02	0.1	0.2	B *	870714	0325	49.87	5-29.32	35-43.78	6.68	0.95	16	086	3.1	.03	0.1	0.2	A *
870709	1922	05.31	5-36.00	35-48.16	4.95	0.59	10	128	3.0	.01	0.1	0.1	B *	870714	0537	40.01	5-34.93	35-48.32	2.26	0.66	13	114	2.0	.02	0.1	0.1	B *
870710	0002	39.27	5-36.04	35-48.14	5.06	0.37	09	129	3.0	.01	0.1	0.1	B *	870714	0827	15.09	5-28.99	35-43.48	7.14	0.59	13	094	3.9	.03	0.1	0.2	B *
870710	0031	49.12	5-32.58	35-45.39	1.69	1.18	14	098	3.6	.02	0.1	0.3	B *	870713	2326	17.83	5-30.80	35-44.17	2.71	1.87	15	075	0.5	.04	0.1	0.3	A *
870710	0036	05.96	5-35.91	35-48.11	5.36	0.16	06	127	2.8	.01	0.1	0.2	B *	870714	0835	05.15	5-29.94	35-42.86	0.94	0.50	06	144	3.4	.01	0.0	0.2	B *
870710	0053	57.61	5-36.00	35-48.16	5.15	0.97	16	128	3.0	.03	0.1	0.1	B *	870714	1147	05.54	5-28.71	35-43.23	6.79	0.59	15	099	4.6	.03	0.1	0.2	B *
870710	0602	42.69	5-30.32	35-44.60	6.76	0.37	06	125	1.1	.02	0.2	0.4	B *	870714	1155	28.62	5-30.44	35-43.84	3.03	0.93	14	081	1.3	.05	0.2	0.4	A *
870710	0908	25.81	5-36.16	35-48.20	5.04	1.52	15	130	3.3	.04	0.2	0.2	B *	870714	1302	10.49	5-30.86	35-44.04	2.54	1.18	15	072	0.7	.04	0.1	0.3	A *
870710	1504	25.53	5-32.24	35-45.07	1.26	0.66	13	096	2.8	.03	0.1	0.4	B *	870716	0032	40.67	5-33.86	35-47.24	4.15	0.59	11	105	1.4	.02	0.2	0.2	B *
870710	1530	43.82	5-31.34	35-44.61	3.15	0.37	11	093	0.9	.04	0.1	0.2	B *	870716	0110	54.87	5-30.63	35-44.88	7.29	0.90	15	098	0.9	.03	0.1	0.2	B *
870710	1643	28.40	5-27.57	35-41.35	3.27	0.50	11	143	4.4	.03	0.1	0.4	B *	870716	0223	19.19	5-31.38	35-44.89	4.06	0.59	15	097	1.3	.03	0.1	0.1	B *
870710	1704	46.63	5-30.71	35-44.35	3.28	0.16	10	130	0.2	.05	0.2	0.3	B *	870716	0521	34.60	5-30.65	35-44.89	7.22	1.45	13	099	0.9	.03	0.1	0.2	B *
870710	1706	59.83	5-36.84	35-48.65	4.43	1.35	14	138	4.8	.02	0.1	0.1	B *	870716	0617	51.85	5-30.65	35-44.92	7.40	0.76	12	099	1.0	.02	0.1	0.1	B *
870710	1804	39.29	5-31.03	35-44.41	3.62	0.50	07	130	0.3	.01	0.1	0.2	B *	870716	0848	12.99	5-35.39	35-39.75	3.80	1.91	10	177	5.4	.03	0.2	0.5	B *
870710	1805	01.82	5-36.69	35-48.77	4.41	0.84	15	136	4.7	.07	0.2	0.4	B *	870716	1434	41.19	5-36.10	35-48.18	4.97	0.71	12	130	3.2	.02	0.1	0.1	B *
870710	2032	37.94	5-36.67	35-48.68	4.29	2.17	12	136	4.6	.06	0.3	0.8	B *	870716	2044	34.10	5-30.31	35-43.94	2.94	0.50	11	136	1.4	.02	0.1	0.1	B *
870710	2206	08.30	5-36.75	35-48.74	4.63	0.50	09	137	4.7	.01	0.1	0.1	B *	870716	2051	30.15	5-30.30	35-43.91	2.86	0.50	11	136	1.4	.03	0.1	0.2	B *
870710	2207	58.32	5-36.72	35-48.70	4.47	0.37	10	136	4.6	.02	0.1	0.2	B *	870716	2059	14.60	5-30.70	35-44.87	7.32	0.59	09	098	0.9	.02	0.1	0.2	B *
870710	2236	56.91	5-30.28	35-44.53	6.41	0.37	09	118	1.1	.04	0.2	0.4	B *	870716	2106	09.32	5-30.65	35-44.85	7.14	0.80	15	098	0.9	.05	0.2	0.3	B *
870710	2335	28.91	5-30.58	35-44.02	2.38	0.37	10	125	0.9	.04	0.2	0.3	B *	870716	2108	00.72	5-30.65	35-44.92	7.27	0.50	11	114	1.0	.02	0.1	0.2	B *
870710	2342	32.74	5-31.03	35-44.20	2.43	0.37	10	132	0.5	.03	0.1	0.2	B *	870716	2109	02.11	5-31.15	35-45.22	7.01	0.66	15	104	1.6	.03	0.1	0.2	B *
870710	1805	23.04	5-36.71	35-48.68	4.30	0.66	14	136	4.6	.01	0.0	0.1	B *	870716	2128	09.28	5-30.73	35-44.88	7.17	2.20	13	098	0.9	.04	0.2	0.3	B *
870711	0352	26.54	5-31.81	35-45.30	4.04	0.59	12	101	2.4	.05	0.2	0.3	B *	870716	2134	21.23	5-30.68	35-44.82	7.08	1.71	15	097	0.8	.04	0.1	0.2	B *
870711	0351	42.76	5-31.84	35-45.34	4.04	0.50	11	102	2.5	.04	0.2	0.3	B *	870716	2138	04.65	5-30.65	35-44.83	7.08	0.66	16	097	0.8	.04	0.1	0.2	B *
870711	0414	44.42	5-30.82	35-44.47	3.73	0.37	10	118	0.1	.03	0.1	0.2	B *	870716	2159	58.66	5-30.64	35-44.80	7.09	1.38	14	097	0.8	.04	0.1	0.3	B *
870711	0950	15.78	5-36.04	35-48.10	4.82	0.37	08	129	3.0	.02	0.1	0.2	B *	870716	2210	03.02	5-30.59	35-44.81	7.67	0.93	15	097	0.9	.04	0.1	0	

# Appendix C

DATE	ORIGIN	LAT S	LONG W	DEPTH	MAG	NO	GAP	DMIN	RMS	ERH	ERZ	Q	D	DATE	ORIGIN	LAT S	LONG W	DEPTH	MAG	NO	GAP	DMIN	RMS	ERH	ERZ	Q	D
870719	0409	52.52	5-33.28	35-46.22	3.23	0.50	09	138	3.2	.01	0.1	0.1	B *+	870723	0559	00.72	5-30.77	35-44.98	7.28	1.52	13	100	1.0	.02	0.1	0.2	B *+
870719	0814	47.67	5-31.68	35-45.55	6.64	0.50	13	106	2.5	.03	0.1	0.2	B *+	870723	0608	55.62	5-29.13	35-43.65	6.18	0.37	05	261	3.5	.03	0.6	0.8	C
870719	1350	12.33	5-35.89	35-48.14	5.30	0.37	09	127	2.8	.03	0.2	0.3	B *+	870723	0609	49.40	5-29.12	35-43.52	6.80	0.66	11	091	3.6	.03	0.2	0.2	B *+
870719	1527	05.97	5-35.81	35-47.76	2.44	0.37	08	127	2.4	.01	0.0	0.1	B *+	870723	0648	27.93	5-35.16	35-48.45	2.23	1.31	14	179	2.4	.04	0.2	0.3	B *+
870719	1643	51.24	5-36.32	35-48.39	4.77	0.71	13	132	3.7	.05	0.2	0.3	B *+	870723	0750	31.26	5-29.67	35-43.42	2.93	0.59	11	090	2.9	.02	0.1	0.2	B *+
870719	2020	29.34	5-36.55	35-48.37	3.94	0.37	11	135	4.1	.10	0.4	0.8	B *	870723	0904	18.88	5-29.46	35-43.27	6.59	0.50	07	170	3.4	.09	0.8	1.1	B *
870719	2150	16.09	5-36.26	35-48.38	4.86	0.76	13	131	3.6	.04	0.2	0.3	B *+	870723	0955	47.44	5-29.34	35-43.66	6.66	1.18	15	086	3.2	.02	0.1	0.1	A *+
870719	2228	51.36	5-28.18	35-42.84	6.03	1.97	14	110	5.8	.04	0.2	0.3	B *+	870723	1110	38.83	5-29.35	35-43.66	6.81	0.71	16	086	3.1	.04	0.1	0.2	A *+
870719	2300	31.27	5-29.59	35-44.00	6.62	0.37	09	174	2.5	.05	0.3	0.4	B *+	870723	1122	05.04	5-29.34	35-43.66	6.62	0.59	15	086	3.2	.04	0.1	0.2	A *+
870720	0225	38.11	5-30.58	35-44.81	7.12	0.50	13	097	6.5	.04	0.1	0.3	B *+	870723	1157	28.42	5-35.49	35-39.87	3.37	0.80	13	173	5.2	.04	0.2	0.5	B *+
870720	0247	53.78	5-38.24	35-49.03	2.07	0.50	09	161	7.4	.03	0.1	0.7	B *	870723	1355	09.32	5-35.63	35-39.77	3.68	2.71	09	176	5.0	.04	0.4	1.1	B *
870720	0246	37.25	5-30.61	35-44.84	7.49	1.71	15	098	0.9	.02	0.1	0.2	B *+	870723	1428	48.07	5-35.45	35-39.69	3.71	0.50	08	179	5.3	.04	0.2	0.3	B *+
870720	0255	07.02	5-30.58	35-44.84	7.36	0.71	15	098	0.9	.02	0.1	0.2	B *+	870723	1611	45.87	5-30.82	35-44.46	4.47	0.76	13	091	0.1	.03	0.1	0.1	B *+
870720	0348	14.67	5-36.25	35-48.14	4.02	0.50	11	132	3.4	.04	0.2	0.3	B *+	870723	1617	46.18	5-30.97	35-44.27	4.08	0.37	08	147	0.3	.05	0.8	0.4	B *
870720	0356	53.64	5-28.31	35-42.74	5.00	0.59	12	106	5.7	.03	0.1	0.2	B *+	870723	1701	46.04	5-35.60	35-40.01	2.85	0.90	12	168	5.1	.07	0.3	1.0	B *
870720	1527	18.56	5-37.69	35-49.59	3.52	0.59	09	147	6.9	.03	0.2	0.5	B *+	870723	1707	31.23	5-30.83	35-44.40	4.48	0.59	13	109	0.1	.06	0.2	0.3	B *
870720	1919	43.92	5-35.78	35-47.89	4.69	0.37	11	126	2.4	.02	0.1	0.2	B *+	870723	1749	51.56	5-35.44	35-39.76	4.14	0.50	10	177	5.3	.01	0.1	0.1	B *+
870720	2357	41.24	5-37.95	35-48.61	3.06	0.84	16	158	6.6	.04	0.2	0.5	B *+	870723	1850	15.46	5-35.57	35-39.99	2.81	0.59	13	169	5.1	.07	0.3	1.0	B *
870721	0021	28.64	5-28.42	35-43.09	3.84	0.59	16	106	5.2	.03	0.1	0.1	B *+	870723	1917	22.75	5-30.66	35-44.33	4.15	0.50	08	123	0.4	.04	0.2	0.3	B *+
870721	0458	18.14	5-37.36	35-49.30	4.22	0.80	10	234	6.3	.05	0.4	0.5	C *	870723	1954	10.69	5-35.53	35-39.96	2.93	0.76	13	170	5.2	.06	0.2	0.8	B *
870718	0347	10.99	5-30.67	35-44.88	7.31	0.80	14	098	0.9	.04	0.1	0.2	B *+	870723	2051	32.17	5-35.55	35-39.70	4.37	0.66	11	178	5.1	.04	0.2	0.4	B *+
870718	0444	28.70	5-30.62	35-44.88	7.39	0.66	13	098	0.9	.03	0.1	0.3	B *+	870723	2101	34.00	5-30.32	35-44.58	6.37	0.80	15	093	1.0	.03	0.1	0.1	B *+
870718	0548	21.10	5-35.95	35-48.10	5.71	1.42	13	194	2.9	.04	0.2	0.3	C *+	870723	2247	41.01	5-30.61	35-44.31	4.32	0.37	11	124	0.5	.04	0.2	0.2	B *+
870718	0622	18.69	5-34.87	35-48.52	3.90	0.50	11	172	4.9	.07	0.3	0.5	B *	870724	0155	07.36	5-35.32	35-39.71	3.65	0.71	14	178	5.5	.04	0.2	0.4	B *+
870718	0717	00.50	5-35.94	35-48.12	5.82	0.37	10	194	2.9	.04	0.2	0.3	C *+	870724	0205	07.95	5-30.56	35-44.31	4.19	0.37	11	125	0.6	.07	0.3	0.4	B *
870718	0941	28.30	5-29.37	35-43.75	6.58	0.37	15	085	3.0	.05	0.2	0.3	A *+	870724	0215	56.70	5-30.65	35-44.32	4.26	1.00	15	088	0.5	.03	0.1	0.2	A *+
870718	1113	43.06	5-29.20	35-43.77	6.32	0.37	09	238	3.3	.03	0.3	0.3	C *+	870724	0219	50.86	5-30.63	35-44.30	4.14	0.37	16	088	0.5	.05	0.1	0.2	A *+
870718	1114	36.38	5-35.89	35-48.06	5.72	0.50	12	127	2.7	.05	0.2	0.3	B *+	870724	0401	59.53	5-35.54	35-39.80	4.07	0.50	07	175	5.1	.02	0.2	0.4	B *
870718	1208	21.98	5-29.44	35-43.82	5.37	0.37	11	090	2.9	.07	0.3	0.4	A *	870724	0436	39.73	5-35.31	35-39.67	4.04	0.50	08	180	5.5	.01	0.1	0.2	B *+
870718	1417	43.16	5-30.70	35-44.98	7.34	0.66	15	100	1.1	.02	0.1	0.1	B *+	870724	0618	15.39	5-36.48	35-48.31	3.86	0.50	08	206	3.9	.04	0.3	0.4	C *+
870718	1521	54.59	5-27.74	35-43.30	5.00	0.50	16	126	5.4	.05	0.2	0.3	B *+	870724	0654	09.62	5-35.53	35-39.47	5.00	0.50	08	186	5.1	.05	0.4	0.7	C *
870718	2003	38.59	5-33.25	35-46.13	3.67	0.50	11	101	3.3	.02	0.1	0.2	B *+	870724	0703	19.19	5-35.49	35-40.01	3.66	0.37	05	168	5.3	.01	0.1	0.2	C
870718	2050	55.88	5-33.64	35-46.99	4.45	0.37	06	142	1.9	.02	0.1	0.2	B *	870724	0746	20.74	5-35.48	35-39.86	2.54	2.21	10	173	5.3	.05	0.3	1.7	B *
870718	2221	13.87	5-34.94	35-48.34	2.34	0.50	08	179	2.0	.01	0.1	0.1	B *+	870724	0839	45.86	5-35.48	35-39.87	2.88	0.59	09	173	5.2	.04	0.2	0.7	B *+
870722	2122	14.52	5-30.33	35-44.53	6.39	0.37	07	126	1.0	.02	0.1	0.2	B *	870724	0854	43.88	5-35.58	35-39.80	3.98	0.59	08	175	5.0	.04	0.3	0.6	B *
870722	2132	05.63	5-28.62	35-43.39	7.24	0.50	08	183	4.6	.02	0.1	0.2	C *+	870724	0846	58.97	5-35.54	35-39.89	3.17	0.59	08	172	5.1	.04	0.3	0.9	B *
870722	2137	02.67	5-28.80	35-43.31	7.24	0.50	10	097	4.3	.04	0.2	0.3	B *+	870724	0924	28.36	5-35.58	35-39.82	3.84	0.50	07	174	5.1	.02	0.1	0.3	B *
870722	2153	19.54	5-30.71	35-43.74	1.28	0.50	12	071	1.3	.03	0.1	0.4	A *+	870724	0931	48.95	5-35.55	35-39.91	3.20	0.66	10	171	5.1	.04	0.2	0.6	B *
870722	2211	42.91	5-28.92	35-43.11	6.55	0.50	12	094	4.3	.07	0.3	0.5	B *	870724	1040	00.61	5-35.76	35-48.88	3.09	0.50	08	121	3.6	.03	0.2	0.3	B *+
870722	2219	23.84	5-28.87	35-43.25	6.61	0.50	12	096	4.3	.05	0.2	0.4	B *+	870724	1419	22.85	5-37.50	35-49.33	4.33	0.50	12	146	6.5	.04	0.2	0.3	B *+
870722	2223	57.71	5-30.24	35-44.53	6.27	0.76	14	092	1.2	.03	0.1	0.2	B *+	870724	1447	17.68	5-35.45	35-39.67	3.82	0.50	11	179	5.3	.03	0.1	0.2	B *+
870722	2227	53.05	5-30.24	35-44.53	6.83	0.50	06	118	1.2	.02	0.2	0.4	B *	870724	1500	28.91	5-35.59	35-39.74	3.87	0.50	10	177	5.0	.04	0.2	0.3	B *+
870722	2235	16.42	5-29.19	35-43.53	6.40	0.50	09	170	3.5	.04	0.4	0.3	A *+	870724	1520	06.60	5-35.52	35-39.67	3.93	0.50	09	179	5.1	.04	0.2	0.3	B *+
870722	2309	00.67	5-30.16	35-44.53	6.76	0.37	06	118	1.3	.04	0.4	1.0	B *	870724	1606	31.76	5-30.97	35-43.74	5.00	0.37	07	171	1.3	.09	1.0	0.8	C *
870722	2323	48.45	5-33.40	35-46.52	3.83	0.50	11	169	2.7	.05	0.2	0.3	B *+	870724	1643	03.25	5-35.64	35-39.96	3.21	0.90	14	169	5.0	.05	0.2	0.5	B *+
870722	2352	07.07	5-29.06	35-43.43	7.33	0.37	07	175	3.8	.05	0.4	0.5	B *	870724	1857	35.11	5-35.52	35-39.73	3.64	0.50	11	177	5.2	.05	0.2	0.6	B *
870723	0007	24.99	5-29.16	35-43.50	6.64	0.50	10	089	3.6	.03	0.1	0.2	A *+	870724	1936	47.85	5-31.32	35-44.20	1.48	0.37	08	111	0.9	.04	0.2	0.3	B *+
870723	0349	51.62	5-30.28	35-44.49	6.27	0.66	14	091	1.1	.03	0.1	0.2	B *+	870724	2234	48.77	5-35.60	35-39									



# Appendix C

DATE	ORIGIN	LAT S	LONG W	DEPTH	MAG	NO	GAP	DMIN	RMS	ERH	ERZ	Q	D
870727	1951	54.17	5-27.82	35-41.66	2.89	0.71	12	153	5.0	.07	0.3	0.9	B *
870727	2143	34.58	5-35.45	35-39.73	4.00	0.50	11	177	5.3	.03	0.2	0.4	B *
870727	2244	53.91	5-35.00	35-48.35	2.25	0.76	12	114	2.1	.03	0.1	0.2	B *
870727	2305	07.06	5-30.13	35-44.53	6.11	0.50	11	108	1.4	.08	0.3	0.5	B *
870728	0050	19.87	5-32.05	35-45.31	3.61	0.50	09	132	2.7	.02	0.1	0.2	B *
870728	0051	39.19	5-32.10	35-45.32	3.51	0.37	10	124	2.8	.05	0.2	0.4	B *
870728	0137	00.43	5-35.04	35-48.29	2.39	0.50	13	115	2.0	.05	0.2	0.3	B *
870728	0137	44.32	5-29.14	35-42.96	2.97	0.37	06	180	4.2	.01	0.1	0.1	C *
870728	0155	11.66	5-29.16	35-43.66	6.13	0.37	08	174	3.5	.04	0.3	0.4	B *
870728	0229	26.88	5-29.27	35-43.67	6.37	0.76	12	087	3.3	.04	0.2	0.3	A *
870728	0303	10.55	5-32.18	35-45.33	3.31	0.37	07	176	2.9	.02	0.1	0.2	B *
870728	0417	49.22	5-32.16	35-45.33	3.39	0.50	14	124	2.9	.04	0.1	0.2	B *
870728	0522	13.76	5-31.98	35-45.18	3.42	0.37	10	129	2.5	.01	0.0	0.1	B *
870728	0542	27.98	5-36.26	35-48.12	3.96	0.50	07	132	3.4	.02	0.1	0.2	B *
870728	0602	49.52	5-29.27	35-43.70	6.48	0.95	14	087	3.2	.05	0.2	0.3	A *
870728	0603	17.54	5-29.19	35-43.61	6.02	0.50	10	180	3.5	.03	0.2	0.2	C *
870728	0622	33.00	5-29.23	35-43.66	6.10	0.71	11	093	3.3	.03	0.2	0.3	B *
870728	0827	46.61	5-31.76	35-45.01	3.44	0.66	11	126	2.0	.01	0.0	0.0	B *
870727	1952	24.09	5-27.81	35-41.58	2.05	0.59	07	134	5.0	.02	0.2	0.7	B *
870727	1952	27.52	5-27.83	35-41.60	1.58	0.59	10	134	5.0	.04	0.2	0.9	B *
870728	0522	24.85	5-31.99	35-45.27	3.39	0.59	12	123	2.6	.04	0.2	0.3	B *
870728	0937	57.62	5-31.61	35-45.05	3.85	0.50	08	128	1.8	.01	0.1	0.1	B *
870728	0944	27.58	5-28.99	35-42.91	3.19	0.37	06	185	4.5	.01	0.1	0.1	C *
870728	1455	09.47	5-35.58	35-39.96	3.13	0.50	10	170	5.1	.07	0.3	0.9	B *
870728	1648	54.34	5-31.91	35-45.17	2.91	0.37	11	122	2.4	.03	0.1	0.3	B *
870728	1652	02.54	5-31.93	35-45.16	3.20	0.50	10	122	2.4	.02	0.1	0.2	B *
870728	1909	19.89	5-37.88	35-48.41	1.64	1.23	15	157	6.3	.05	0.2	1.0	B *
870728	1913	00.88	5-31.77	35-45.69	6.27	0.50	14	108	2.8	.09	0.3	0.5	B *
870728	1936	24.11	5-31.59	35-44.97	3.64	1.27	14	097	1.7	.02	0.1	0.2	B *
870728	2002	25.21	5-35.27	35-39.67	3.77	1.03	13	180	5.6	.05	0.2	0.3	B *
870729	0125	43.17	5-35.02	35-48.40	2.10	0.76	15	115	2.2	.04	0.1	0.2	B *
870729	0127	17.12	5-35.54	35-39.86	2.97	0.93	13	173	5.1	.05	0.2	0.6	B *
870729	0317	00.56	5-35.66	35-39.96	3.38	0.59	13	170	4.9	.07	0.3	0.8	B *
870729	0544	47.17	5-31.62	35-45.56	6.77	0.71	15	107	2.5	.03	0.1	0.2	B *
870729	0646	50.89	5-31.72	35-45.22	4.20	0.71	13	123	2.1	.05	0.2	0.3	B *
870729	0827	17.39	5-40.89	35-53.51	3.41	1.23	13	300	2.8	.07	0.5	0.5	C *
870729	0953	47.17	5-35.48	35-48.65	3.64	0.95	16	119	3.0	.05	0.2	0.3	B *
870729	1102	20.35	5-29.59	35-43.98	6.79	0.37	10	102	2.5	.05	0.3	0.4	B *
870729	1118	31.86	5-34.03	35-46.18	1.24	0.37	13	118	2.3	.06	0.2	0.7	B *
870729	1422	16.31	5-35.71	35-40.00	3.92	0.76	12	168	4.9	.04	0.2	0.2	B *
870729	1500	01.97	5-30.64	35-45.16	8.18	0.50	07	245	1.4	.03	0.3	0.3	C *
870730	0011	02.05	5-30.45	35-44.48	5.96	0.50	05	125	0.8	.01	0.1	0.1	C *
870730	0346	23.95	5-31.65	35-45.54	6.65	0.90	16	106	2.5	.04	0.1	0.2	B *
870730	0610	18.81	5-35.42	35-48.63	3.98	0.95	15	118	2.9	.05	0.2	0.2	B *
870730	0901	57.35	5-37.65	35-48.21	3.21	0.50	11	154	5.8	.02	0.1	0.3	B *
870730	0939	51.44	5-37.68	35-48.17	2.93	0.50	10	155	5.9	.01	0.1	0.3	B *
870730	1436	44.53	5-31.61	35-44.89	3.12	0.59	14	096	1.6	.06	0.2	0.3	B *
870730	1629	46.93	5-31.05	35-48.41	1.97	1.27	16	115	2.2	.04	0.1	0.2	B *
870730	1802	02.45	5-37.56	35-48.10	3.23	0.50	11	153	5.6	.03	0.1	0.3	B *
870730	1936	41.43	5-30.70	35-44.95	7.49	1.64	15	100	1.0	.02	0.1	0.1	B *
870730	2028	46.16	5-37.46	35-43.30	6.79	0.50	10	097	4.3	.06	0.3	0.6	B *
870730	2152	00.15	5-29.31	35-43.72	7.02	0.37	11	095	3.1	.07	0.3	0.4	B *
870730	2244	12.32	5-30.70	35-44.89	7.93	0.59	10	117	0.9	.06	0.3	0.5	B *
870730	2338	44.21	5-28.78	35-43.34	6.60	0.50	12	098	4.3	.03	0.1	0.2	B *
870731	0615	19.42	5-29.24	35-43.60	5.52	0.50	11	172	3.4	.03	0.2	0.2	B *
870731	0648	41.79	5-29.35	35-43.64	5.68	1.66	15	086	3.2	.04	0.1	0.3	A *
870731	0702	04.63	5-29.29	35-43.67	5.81	1.71	14	087	3.2	.03	0.1	0.3	A *
870731	0832	39.47	5-29.39	35-43.59	5.47	0.76	14	086	3.1	.04	0.2	0.2	A *
870731	0916	37.33	5-32.23	35-44.97	1.28	1.83	13	094	2.7	.03	0.1	0.7	B *
870731	1114	20.22	5-33.22	35-45.95	1.76	0.50	14	130	3.6	.04	0.1	0.4	B *
870731	1529	36.22	5-27.96	35-41.58	0.73	0.50	09	134	5.2	.03	0.2	0.3	B *
870731	1903	18.79	5-37.92	35-48.46	1.11	1.35	16	158	6.4	.06	0.2	1.7	B *
870731	2054	44.43	5-35.76	35-39.90	3.97	0.71	12	171	4.7	.04	0.2	0.2	B *
870801	0127	14.81	5-35.95	35-47.91	4.69	0.59	09	129	2.7	.03	0.1	0.2	B *
870728	1609	45.26	5-35.71	35-39.88	4.06	0.37	10	172	4.8	.03	0.2	0.4	B *
870728	1644	57.47	5-31.90	35-45.16	3.07	0.50	11	122	2.3	.03	0.1	0.2	B *
870728	1640	42.03	5-31.66	35-45.21	5.00	1.42	15	101	2.0	.03	0.1	0.2	B *
870801	0734	16.69	5-30.64	35-44.86	7.18	1.03	16	098	0.9	.03	0.1	0.2	B *
870801	0905	28.94	5-30.63	35-44.76	6.88	0.93	14	114	0.8	.03	0.1	0.2	B *
870801	1028	15.36	5-30.59	35-44.81	7.19	1.03	16	097	0.9	.03	0.1	0.2	B *
870801	1123	42.88	5-29.39	35-48.39	1.72	1.31	15	156	6.3	.05	0.2	1.0	B *
870801	1150	58.14	5-30.62	35-44.78	6.89	0.59	12	114	0.8	.02	0.1	0.1	B *
870801	2030	49.23	5-31.52	35-44.24	2.11	0.59	09	108	1.3	.03	0.1	0.2	B *
870801	2223	15.47	5-29.92	35-43.73	6.45	0.37	09	148	2.2	.09	0.4	0.7	B *
870802	0139	26.35	5-36.84	35-49.36	2.66	0.37	06	190	5.6	.11	5.7	1.7	D
870802	0415	41.63	5-35.66	35-39.87	3.98	0.50	09	172	4.9	.02	0.1	0.1	B *
870802	0527	47.82	5-37.95	35-48.50	1.50	1.42	12	158	6.5	.05	0.2	1.3	B *
870802	0531	40.67	5-36.11	35-48.30	5.09	0.93	13	129	3.3	.04	0.2	0.2	B *
870802	0539	13.36	5-35.76	35-39.97	3.88	0.50	11	169	4.8	.01	0.1	0.1	B *
870802	0841	30.08	5-30.32	35-44.53	6.99	0.76	12	126	1.0	.03	0.1	0.2	B *
870802	0920	01.03	5-30.62	35-44.90	7.60	1.45	12	115	1.0	.02	0.1	0.1	B *
870802	0933	32.99	5-30.59	35-44.87	7.68	0.97	13	116	1.0	.02	0.1	0.2	B *

DATE	ORIGIN	LAT S	LONG W	DEPTH	MAG	NO	GAP	DMIN	RMS	ERH	ERZ	Q	D
870802	1447	05.45	5-34.19	35-46.92	3.57	0.50	10	138	1.1	.02	0.1	0.1	B *
870802	1504	18.88	5-37.86	35-49.59	2.42	0.37	07	151	6.8	.03	0.2	1.2	B *
870802	1732	24.95	5-36.62	35-47.40	2.97	0.37	08	140	3.7	.04	0.3	0.5	B *
870802	1920	52.06	5-28.75	35-43.24	7.02	0.90	16	098	4.5	.04	0.1	0.2	B *
870803	0222	04.57	5-35.66	35-39.90	3.74	0.37	08	171	4.9	.01	0.1	0.2	B *
870803	0223	53.43	5-35.68	35-40.02	2.90	0.66	13	167	4.9	.04	0.2	0.5	B *
870803	0536	59.87	5-32.12	35-45.59	5.34	0.37	10	128	3.1	.08	0.3	0.5	B *
870803	0538	47.49	5-32.05	35-45.57	5.14	0.37	09	180	3.0	.01	0.1	0.1	B *
870803	0643	31.32	5-35.63	35-40.08	3.28	0.76	12	166	5.0	.08	0.4	1.0	B *
870803	1040	45.60	5-35.51	35-39.99	3.50	1.64	13	169	5.2	.04	0.2	0.7	B *
870803	1745	06.25	5-35.50	35-39.76	3.98	0.50	11	176	5.2	.03	0.2	0.2	B *
870803	2040	27.73	5-36.22	35-47.79	3.90	0.50	09	133	3.1	.04	0.2	0.3	B *
870804	0246	19.59	5-35.42	35-39.75	3.16	0.50	11	177	5.3	.05	0.2	0.6	B *
870807	0722	59.15	5-37.79	35-49.52	3.50	0.50	09	150	6.9	.03	0.2	0.5	B *
870807	1202	31.40	5-35.05	35-48.48	2.22	0.87	12	114	2.3	.04	0.1	0.2	B *
870807	1204	03.73	5-29.84	35-43.37	2.43	0.66	11	127	2.7	.06	0.2	0.8	B *
870807	1808	06.61	5-35.89	35-48.65	1.89	0.37	06	147	3.4	.01	0.1	0.2	B *
870807	1917	17.43	5-36.29	35-48.44	5.32	0.37	06	160	3.7	.03	0.3	0.4	B *
870807	2123	22.86	5-29.82	35-43.14	1.77	0.80	10	131	3.1	.08	0.4	0.9	B *
870807	2128	05.66	5-30.41	35-44.71	6.15	0.50	07	173	1.0	.02	0.1	0.2	B *
870807	2302	55.78	5-35.77	35-40.12	2.42	0.59	09	172	4.8	.07	0.4	1.5	B *
870807	2306	06.45	5-28.54	35-43.25	6.14	0.50	07	175	4.8	.03	0.2	0.3	B *
870808	0247	58.89	5-33.27	35-42.92	2.13	0.50	06	224	5.2	.17	3.6	6.7	D
870808	0328	14.43	5-35.07	35-48.27	2.22	0.50	07	177	2.0	.02	0.2	0.2	B *
870804	1830	19.19	5-30.56	35-44.85	7.46	0.95	13	098	1.0	.02	0.1	0.1	B *
870805	0300	49.30	5-35.75	35-39.98	3.34	0.84	12	168	4.8	.05	0.2	0.5	B *
870805	1335	31.82	5-37.97	35-49.64	3.99	1.89	13	152	6.6	.06	0.3	0.3	B *
870805	1605	56.44	5-37.30	35-47.90	0.30	0.66	11	149	5.1	.03	0.1	3.3	C *
870805	1651	36.36	5-37.87	35-49.68	3.46	0.90	13	150	6.6	.06	0.2	0.6	B *
870805	1844	48.32	5-35.75	35-40.00	3.79	0.37	10	168	4.8	.01	0.0	0.1	B *
870805	1846	23.70	5-35.72	35-40.00	3.70	0.37	09	168	4.8	.01	0.1	0.2	B *
870805	2245	00.16	5-35.76	35-40.03	3.60	0.71	11	167	4.8	.02	0.1	0.2	B *
870805	2310	15.10	5-37.82	35-49.78	3.76	0.59	11	148	6.5	.05	0.3	0.7	B *
870805	2348	40.83	5-35.78	35-40.11	3.14	0.97	12	164	4.8	.03	0.2	0.4	B *
870806	0041	19.46	5-29.15	35-43.61	7.02	0.71	13	090	3.5	.05	0.2	0.3	B *
870806	0315	07.83	5-29.58	35-43.16	2.60	0.50	09	163	3.3	.02	0.1	0.2	B *
870806	0345	59.81	5-34.98	35-48.38	2.20	0.66	11	114	2.1	.03	0.1	0.2	B *
870806	0346	40.22	5-31.53	35-45.57	7.00	0.76	14	108	2.4	.04	0.2	0.2	B *
870806	0519	39.82	5-35.46	35-39.84	3.38	1.49	14	178	5.3	.09	0.4	1.1	B *
870806	0658	53.13	5-35.78	35-40.01	3.86	0.59	11	167	4.7	.01	0.1	0.1	B *
870806	0731	29.23	5-30.63	35-44.81	7.31	0.59	13	115	0.8	.03	0.1	0.2	B *
870806	0740	28.48	5-32.74	35-38.77	8.39	0.50	07	217	3.8	.01	0.1	0.1	C *
870806	0816	19.13	5-32.76	35-38.83	8.04	0.37	07	215	3.8	.01	0.1	0.1	C *
870806	1119	24.85	5-38.08	35-49.59	3.91	1.27	15	155	6.6	.06	0.3	0.3	B *
870806	1235	57.12	5-37.88	35-49.65	3.50	1.03	14	151	6.7	.05	0.2	0.4	B *
870806	2041	40.18	5-34.24	35-50.64	2.26	0.37	06	219	6.2	.02	1.3	3.1	C
870806	0731	56.53	5-30.52	35-44.75	7.48	1.23	16	096	0.9	.03	0.1	0.2	B *
870806	2152	34.85	5-35.51	35-47.10	2.80	1.00	14	125	1.7	.03	0.1	0.2	B *
870807	0412	20.30	5-37.66	35-49.68	3.60	0.59	08	146	6.8	.03	0.2	0.5	B *
870807	0608	38.80	5-35.80	35-40.04	3.08	0.71	11	174	4.7	.05	0.2	0.6	B *
870808	1434	01.63	5-30.38	35-44.68	6.22	0.37	09	174	1.0	.02	0.1	0.2	B *
870808	1610	23.53	5-37.58	35-49.06	3.52	0.50	11	149	6.3	.05	0.2	0.5	B *
870808	2019	27.12	5-31.56	35-45.49	6.62	0.59	10	128	2.3	.04	0.2	0.3	B *
870809	0022	09.05	5-30.28	35-44.21	4.18	0.37	05	234	1.2	.01	0.3	0.2	C
870809	0112	33.43	5-35.69	35-39.85	3.06	1.85	12	179	4.9	.06	0.3	1.1	B *
870809	0115	46.77	5-36.84	35-40.32	7.09	0.50	09	155	3.0	.20	1.5	1.8	C
870809	0425	32.99	5-30.19	35-44.28	4.67	0.37	10	115	1.3	.04	0.2	0.2	B *
870809	0448	23.60	5-30.40	35-44.11	5.00	0.50	07	182	1.0	.04	0.3	0.3	C *
870809	0508	40.45	5-30.18	35-44.20	4.72	0.50	10	116	1.3	.04	0.2	0.2	B *
870809	0653	09.11	5-37.07	35-49.08	5.51	1.58	13	140	5.6	.06	0.2	0.4	B *
870809	1120	59.34	5-31.63	35-44.09	1.25	0.59	07	170	1.5	.06	0.4	1.0	B *
870809	1129	24.86	5-32.72	35-39.05	6.66	0.66	08	199	10.3	.05	0.4	0.8	C *
870809	1310	14.10	5-35.89	35-40.30	3.38	0.59	10	166	4.7	.03	0.2	0.4	B *
870809	1354	28.65	5-36.78	35-47.98	1.86	0.59	12	141	4.2	.03	0.1	0.3	B *
870809	1520	10.26	5-37.58	35-49.07	3.66	0.50	10	149	6.4	.05	0.3	0.7	B *
870809	1559	27.81	5-35.55	35-39.94	3.24	1.27	12	177	5.1	.07	0.3	0.9	B *
870809	1716	04.28	5-34.01	35-47.50	5.59	0.90	12	147	1.2	.03	0.1	0.2	B *
870809	2201	25.00	5-35.54	35-39.92	3.86	1.13	11	178	5.2	.04	0.2	0.3	B *
870810	0139	13.19	5-28.68	35-43.43	7.15	0.66	10	122	4.4	.07	0.3	0.5	B *
870810	0400	02.08	5-35.80	35-40.13	3.64	0.97	10	171	4.7	.02	0.1	0.3	B *
870810	0409	53.07	5-35.92	35-40.23	3.40	0.87	10	168	4.6	.03	0.1	0.3	B *
870810	0421	24.64	5-29.52	35-43.95	6.71	1.64	14	118	2.6	.03	0.1	0.2	B *
870810	0428	05.57	5-29.51	35-43.91	7.03	1.81	14	118	2.7	.04	0.2	0.2	B *
870810	0519	07.32	5-31.44	35-44.90	3.82	0.59	08	168	1.4	.04	0.3	0.2	B *
870810	0635	35.68	5-35.69	35-39.96	3.15	1.08	11	177	4.9	.08	0.4	1.1	B *
870810	0636	36.30	5-35.70	35-40.16	2.65	1.13	11	171	4.9	.08	0.4	1.3	B *
870810	0749	36.84	5-30.78	35-45.03	7.11	0.76	12	101	1.1	.02	0.1	0.1	B *
870810	0920	41.33	5-29.60	35-43.95	6.83	0.59	12	118	2.5	.05	0.2	0.3	B *
870810	1107	06.08	5-36.07	35-48.12	4.41	0.84	12	129	3.1	.03	0.1	0.2	B *
870810	1159	12.95	5-35.61	35-39.90	3.18	0.93	10	178	5.0	.04	0.2	0.5	B *
870810	1233	22.60	5-35.61	35-39.77	3.39	0.76	10	182	5.0	.04	0.2	0.6	C *
870810	1305	14.53	5-29.52	35-43.89	6.20	0.59	09	119	2.7	.04	0.2	0.3	B *

## Appendix C

DATE	ORIGIN	LAT S	LONG W	DEPTH	MAG	NO	GAP	DMIN	RMS	ERH	ERZ	Q	D	DATE	ORIGIN	LAT S	LONG W	DEPTH	MAG	NO	GAP	DMIN	RMS	ERH	ERZ	Q	D
870810	1812	24.96	5-32.23	35-45.15	1.41	0.59	07	126	2.8	.02	0.1	0.3	B *	870817	1937	04.23	5-29.23	35-43.63	7.02	0.90	14	088	3.4	.05	0.2	0.3	A +*
870811	0159	32.12	5-37.79	35-48.42	0.68	1.23	06	286	6.2	.03	0.3	2.0	C *	870817	2001	37.71	5-29.28	35-43.64	7.26	1.23	15	087	3.3	.03	0.1	0.2	A +*
870811	0403	30.12	5-38.19	35-49.80	2.66	1.38	08	251	7.6	.03	0.3	1.0	C *	870817	2009	08.49	5-29.20	35-43.51	6.23	0.50	08	170	3.5	.05	0.3	0.5	B +*
870813	1100	24.10	5-35.78	35-39.98	3.17	1.89	13	168	4.7	.04	0.2	0.7	B *	870817	2121	37.92	5-35.57	35-39.67	2.92	0.50	11	179	5.1	.07	0.4	1.1	B *
870813	1123	33.84	5-35.77	35-40.10	3.09	1.27	13	164	4.8	.04	0.2	0.4	B +*	870817	2203	02.15	5-35.49	35-39.67	3.41	0.50	08	179	5.2	.05	0.4	1.0	B *
870813	1224	16.75	5-35.74	35-40.06	2.67	1.58	12	166	4.8	.05	0.2	1.0	B *	870817	2308	20.23	5-35.53	35-39.80	2.77	0.71	11	175	5.1	.04	0.2	0.7	B *
870813	1225	22.11	5-35.74	35-39.95	3.99	0.50	11	170	4.8	.02	0.1	0.1	B +*	870818	0209	47.99	5-35.52	35-39.75	3.18	0.50	07	177	5.2	.01	0.1	0.3	B *
870813	1241	45.86	5-35.68	35-39.87	3.80	0.59	12	172	4.9	.02	0.1	0.2	B +*	870818	0218	39.44	5-40.86	35-53.68	4.09	1.64	14	301	2.9	.05	0.4	0.5	C *
870813	1348	58.87	5-35.69	35-40.01	3.01	0.90	13	168	4.9	.03	0.2	0.4	B +*	870818	0243	42.26	5-37.99	35-49.70	3.39	1.18	14	153	6.5	.05	0.2	0.6	B *
870813	1449	11.32	5-35.73	35-39.95	3.97	0.71	11	170	4.8	.01	0.1	0.1	B +*	870818	0247	11.36	5-30.34	35-44.66	6.52	0.50	12	111	1.1	.04	0.2	0.2	B +*
870813	1942	26.81	5-36.85	35-48.76	5.36	1.49	15	138	4.9	.04	0.2	0.2	B +*	870818	0300	56.94	5-35.69	35-39.87	3.41	0.50	09	172	4.9	.06	0.4	0.9	B *
870813	1949	14.63	5-35.66	35-39.75	3.93	0.59	10	177	4.9	.02	0.1	0.2	B +*	870818	0515	23.39	5-29.01	35-43.41	6.47	0.50	13	093	3.9	.02	0.1	0.1	B +*
870813	2016	14.02	5-35.80	35-40.12	3.09	0.71	13	163	4.7	.04	0.2	0.5	B +*	870818	0630	15.39	5-29.10	35-43.53	6.86	0.66	10	172	3.7	.03	0.2	0.3	B +*
870813	2103	06.24	5-35.67	35-40.02	2.78	1.08	11	167	4.9	.04	0.2	0.7	B *	870818	0631	39.49	5-29.24	35-43.48	5.78	0.50	06	171	3.5	.04	0.4	0.7	B *
870813	2309	12.09	5-30.36	35-44.59	6.31	0.66	14	110	1.0	.04	0.1	0.2	B +*	870818	0633	36.58	5-29.18	35-43.41	6.39	0.50	11	089	3.6	.06	0.3	0.4	A *
870814	0020	39.42	5-35.74	35-40.07	2.88	0.80	13	165	4.8	.07	0.3	0.9	B *	870818	0835	48.60	5-38.12	35-49.71	3.85	1.76	15	155	6.4	.07	0.3	0.4	B *
870814	0222	25.46	5-35.69	35-39.98	3.06	0.87	12	169	4.9	.04	0.2	0.5	B +*	870818	1213	01.64	5-31.72	35-44.53	1.19	0.66	09	112	1.6	.06	0.3	0.7	B *
870814	0235	18.26	5-35.76	35-39.94	3.24	0.66	11	170	4.7	.04	0.2	0.5	B +*	870815	0348	39.33	5-35.48	35-39.67	3.24	0.59	12	179	5.2	.04	0.2	0.5	B +*
870814	0407	04.11	5-35.78	35-39.94	3.04	0.37	09	170	4.7	.04	0.2	0.8	B *	870815	0351	36.53	5-35.52	35-39.67	3.60	0.50	08	179	5.2	.03	0.2	0.5	B +*
870814	0422	24.60	5-35.69	35-39.98	3.03	0.66	13	169	4.9	.04	0.2	0.5	B +*	870815	0900	11.96	5-35.77	35-40.02	2.72	1.45	14	167	4.8	.07	0.3	1.0	B *
870814	0235	51.56	5-35.61	35-39.84	3.38	0.59	09	174	5.0	.01	0.1	0.2	B +*	870815	0903	38.64	5-35.53	35-39.67	3.94	0.37	08	179	5.1	.01	0.1	0.2	B +*
870814	0407	04.98	5-35.75	35-39.96	3.21	0.71	10	169	4.8	.04	0.2	0.6	B *	870818	0835	11.72	5-29.03	35-43.56	7.23	0.50	14	093	3.8	.04	0.2	0.2	B +*
870814	0640	20.26	5-35.74	35-40.02	2.87	0.90	11	167	4.8	.04	0.2	0.6	B *	870815	0907	43.31	5-35.68	35-39.81	3.79	0.50	09	174	4.9	.03	0.2	0.2	B +*
870814	0901	33.78	5-35.66	35-40.03	2.79	0.76	14	167	4.9	.04	0.2	0.5	B +*	870815	1146	01.09	5-35.68	35-39.88	3.25	0.59	12	172	4.9	.07	0.3	0.9	B *
870814	0919	08.41	5-35.63	35-39.85	3.49	0.59	11	173	5.0	.01	0.1	0.2	B +*	870815	1226	27.66	5-37.72	35-48.48	2.07	1.61	14	154	6.1	.05	0.2	1.0	B *
870814	1046	10.84	5-35.67	35-40.04	2.85	1.00	12	167	4.9	.04	0.2	0.5	B +*	870815	1938	32.35	5-29.18	35-43.66	7.23	1.38	14	089	3.4	.04	0.2	0.3	A +*
870814	1404	03.25	5-35.92	35-47.99	5.25	0.71	12	128	2.7	.03	0.1	0.2	B +*	870815	2239	29.00	5-37.08	35-49.04	5.35	1.45	14	140	5.6	.05	0.2	0.3	B +*
870814	1407	51.15	5-35.93	35-48.06	5.24	1.35	14	128	2.8	.04	0.1	0.2	B +*	870815	2325	42.88	5-35.74	35-39.84	4.14	0.50	07	173	4.8	.01	0.1	0.2	B *
870814	1421	03.51	5-35.91	35-48.03	5.17	0.59	14	128	2.7	.04	0.1	0.2	B +*	870815	2330	18.73	5-35.53	35-39.73	4.08	0.50	11	177	5.1	.03	0.2	0.4	B +*
870814	1741	51.16	5-35.82	35-40.11	3.24	0.59	13	164	4.7	.05	0.2	0.5	B +*	870816	0422	51.95	5-35.72	35-39.95	3.65	0.50	10	170	4.8	.02	0.1	0.3	B +*
870814	2046	00.76	5-37.28	35-48.73	2.60	0.71	09	145	5.6	.02	0.1	0.3	B +*	870816	0424	11.19	5-35.73	35-40.02	3.04	0.76	13	167	4.8	.02	0.2	0.5	B +*
870814	2107	22.09	5-35.63	35-40.05	2.82	1.71	14	167	5.0	.08	0.4	1.2	B *	870816	0542	31.04	5-35.62	35-39.92	3.05	1.79	15	171	5.0	.09	0.4	1.1	B *
870815	0115	43.85	5-35.57	35-39.95	2.16	1.71	15	170	5.1	.08	0.3	1.3	B *	870816	0544	56.56	5-35.58	35-39.98	2.78	1.55	13	169	5.1	.08	0.4	1.2	B *
870815	0117	13.29	5-35.66	35-40.01	2.71	0.90	13	168	4.9	.06	0.3	0.8	B *	870816	0546	20.42	5-35.56	35-39.67	4.32	0.50	07	179	5.1	.02	0.2	0.5	B +*
870815	0125	25.28	5-38.06	35-48.54	1.99	0.71	12	160	6.7	.04	0.2	0.9	B *	870816	0550	03.40	5-35.57	35-39.99	2.74	0.84	13	169	5.1	.08	0.3	1.0	B *
870815	0140	44.23	5-35.67	35-40.04	2.86	1.52	13	167	4.9	.06	0.3	0.9	B *	870816	0555	57.49	5-35.62	35-40.00	2.77	0.97	13	168	5.0	.07	0.3	1.0	B *
870812	0347	25.02	5-35.79	35-40.01	3.12	0.84	10	167	4.7	.05	0.3	0.9	B *	870816	0559	09.43	5-36.39	35-48.47	5.63	1.91	15	133	3.9	.04	0.2	0.3	B +*
870812	0802	16.54	5-35.68	35-39.91	3.43	0.66	08	171	4.9	.01	0.1	0.2	B +*	870816	1428	22.94	5-29.06	35-43.54	7.01	1.52	15	092	3.7	.04	0.2	0.3	B +*
870812	0808	48.80	5-35.83	35-40.28	2.53	0.66	08	158	4.8	.08	0.6	1.8	B *	870816	1659	35.62	5-29.39	35-43.57	6.69	1.31	16	085	3.2	.06	0.2	0.3	A *
870812	1024	00.20	5-35.61	35-39.84	3.82	0.50	07	173	5.0	.01	0.1	0.2	B *	870816	2237	57.09	5-37.93	35-48.59	3.08	1.18	16	157	6.5	.04	0.2	0.4	B +*
870812	1047	55.30	5-35.69	35-39.91	3.53	0.80	09	171	4.9	.01	0.1	0.2	B +*	870817	0142	03.81	5-31.94	35-44.80	1.33	0.16	07	156	2.1	.02	0.2	0.4	B *
870812	1142	41.17	5-32.91	35-38.84	7.59	1.00	12	202	4.1	.04	0.2	0.3	C +*	870817	0506	22.95	5-35.73	35-40.02	2.76	0.76	12	167	4.8	.07	0.3	1.0	B *
870812	1403	50.59	5-35.77	35-39.99	3.71	1.35	11	168	4.8	.06	0.4	1.0	B *	870817	0558	30.52	5-29.17	35-43.54	6.53	0.50	10	090	3.5	.03	0.2	0.2	A +*
870812	1414	19.67	5-35.75	35-40.05	3.24	0.80	10	166	4.8	.07	0.4	1.2	B *	870816	0543	02.91	5-35.58	35-39.85	3.01	1.64	15	173	5.1	.07	0.3	0.9	B *
870812	1605	02.63	5-37.58	35-49.31	3.93	1.03	14	147	6.6	.05	0.2	0.3	B +*	870818	1618	29.96	5-31.51	35-45.55	6.89	0.50	13	108	2.4	.04	0.2	0.2	B +*
870812	1853	12.71	5-35.59	35-39.78	3.84	0.66	11	175	5.0	.01	0.1	0.1	B +*	870818	1751	24.44	5-30.58	35-44.79	7.08	0.50	10	117	0.9	.02	0.1	0.3	B +*
870812	2056	10.59	5-35.76	35-40.08	3.19	0.76	12	165	4.8	.03	0.2	0.4	B +*	870818	1827	38.72	5-30.38	35-44.70	6.23	0.37	08	122	1.0	.09	0.5	0.7	B *
870812	2110	40.93	5-35.63	35-39.83	3.63	0.59	11	174	5.0	.02	0.1	0.2	B +*	870819	0115	15.41	5-29.26	35-43.59	6.81								

# Appendix C

DATE	ORIGIN	LAT S	LONG W	DEPTH	MAG	NO	GAP	DMIN	RMS	ERH	ERZ	Q	D
870821	2152	03.61	5-29.64	35-44.13	6.97	0.50	08	148	2.3	.08	0.5	0.7	B *
870821	2153	33.51	5-29.68	35-44.20	6.80	0.37	09	146	2.2	.06	0.4	0.5	B *
870821	2114	13.37	5-29.60	35-43.96	6.19	0.50	07	152	2.5	.04	0.3	0.4	B *
870821	2117	55.56	5-29.74	35-44.22	6.75	0.76	13	099	2.1	.03	0.1	0.2	B **
870821	2150	55.99	5-29.80	35-44.03	6.61	0.59	09	146	2.1	.09	0.4	0.7	B *
870821	2158	35.32	5-29.75	35-44.17	6.17	0.50	12	098	2.1	.05	0.2	0.3	B **
870821	2236	05.86	5-29.73	35-44.22	6.83	0.84	14	099	2.1	.05	0.2	0.2	B *
870821	2328	20.99	5-29.71	35-44.23	7.14	0.76	15	084	2.2	.04	0.2	0.2	A *
870821	2341	33.51	5-35.72	35-39.90	4.03	0.50	10	171	4.8	.02	0.1	0.2	B **
870822	0034	55.75	5-35.61	35-39.99	3.49	1.03	12	169	5.0	.04	0.2	0.4	B *
870822	2021	14.71	5-35.60	35-48.98	3.71	0.50	10	119	3.6	.03	0.1	0.2	B *
870822	2123	45.94	5-37.60	35-49.63	4.24	0.37	09	145	6.7	.03	0.2	0.4	B **
870823	0038	10.35	5-30.32	35-44.63	6.35	0.50	09	125	1.1	.02	0.1	0.2	B *
870824	0011	28.25	5-35.56	35-39.75	3.41	0.50	11	176	5.1	.02	0.1	0.3	B **
870824	0212	55.96	5-35.70	35-40.03	3.69	0.37	11	167	4.9	.04	0.2	0.5	B *
870824	0244	02.74	5-29.43	35-43.85	6.84	0.50	13	090	2.9	.03	0.1	0.2	A **
870824	0506	48.80	5-27.26	35-40.96	1.50	0.50	07	159	3.8	.09	0.7	3.3	C *
870824	1119	27.29	5-35.50	35-49.00	4.27	0.37	09	117	3.5	.05	0.3	0.4	B *
870825	0302	57.30	5-34.22	35-46.93	3.58	0.37	08	169	1.0	.01	0.1	0.1	B **
870825	0359	41.38	5-38.28	35-48.70	2.26	0.50	10	163	7.2	.04	0.2	0.9	B *
870825	0435	26.56	5-36.17	35-48.18	4.87	0.50	09	155	3.3	.08	0.5	0.6	B *
870825	0749	11.75	5-31.08	35-44.36	2.16	0.76	13	106	0.4	.04	0.2	0.4	B **
870825	1111	28.58	5-37.06	35-48.48	2.24	1.35	13	143	5.0	.03	0.1	0.4	B **
870825	1601	35.47	5-35.81	35-40.14	3.35	0.90	14	163	4.7	.07	0.3	0.7	B *
870826	0457	09.94	5-35.30	35-39.67	4.23	0.90	11	180	5.6	.02	0.1	0.2	B **
870826	1259	34.35	5-29.35	35-43.32	4.19	0.50	10	169	3.5	.04	0.2	0.3	B *
870826	1326	38.81	5-31.48	35-44.17	2.08	0.59	11	107	1.2	.05	0.2	0.5	B *
870826	1559	54.55	5-28.92	35-43.10	3.18	0.50	12	094	4.4	.06	0.2	0.6	B *
870826	1824	54.80	5-32.96	35-46.19	3.55	0.50	13	134	3.7	.04	0.1	0.3	B *
870827	0437	32.26	5-36.48	35-47.86	2.49	0.71	12	136	3.6	.05	0.2	0.5	B *
870827	0537	47.34	5-37.78	35-49.64	3.66	0.50	08	149	6.7	.04	0.3	0.7	B *
870827	1819	33.78	5-38.25	35-49.16	2.64	0.59	11	161	7.2	.05	0.3	0.9	B *
870828	0416	31.73	5-38.29	35-49.16	3.32	0.66	13	162	7.2	.05	0.2	0.7	B *
870829	0017	54.07	5-32.23	35-41.20	11.17	0.50	10	118	3.6	.19	1.3	1.5	B *
870826	1559	57.49	5-28.75	35-42.97	2.19	0.66	08	190	4.7	.03	0.1	0.6	C *
870829	0533	15.32	5-37.67	35-48.50	2.87	0.59	11	134	2.5	.06	0.3	0.4	B *
870829	1152	44.61	5-35.30	35-39.43	4.44	0.84	13	187	5.6	.04	0.2	0.4	C **
870830	0130	33.58	5-40.20	35-53.78	3.90	1.08	11	302	2.1	.07	0.6	0.4	C *
870830	0141	03.11	5-37.80	35-49.80	4.47	0.59	12	130	4.4	.06	0.2	0.4	B *
870830	0406	21.43	5-38.11	35-48.87	3.84	0.66	13	139	2.6	.05	0.2	0.3	B *
870830	1917	15.88	5-35.80	35-40.07	3.28	1.03	16	165	4.7	.06	0.2	0.6	B *
870830	1932	12.99	5-35.81	35-40.07	3.44	1.13	16	165	4.7	.06	0.2	0.6	B *
870830	2141	44.00	5-35.79	35-40.07	3.46	0.59	15	165	4.7	.06	0.2	0.6	B *
870831	0005	11.55	5-35.78	35-39.96	4.14	0.50	14	169	4.7	.04	0.2	0.4	B **
870831	0354	24.89	5-37.49	35-48.69	2.65	0.66	11	142	3.0	.06	0.3	0.5	B *
870831	0418	11.70	5-35.71	35-39.97	3.88	0.50	12	169	4.8	.02	0.1	0.2	B *
870831	0657	49.22	5-35.67	35-49.07	3.53	0.76	14	094	3.8	.04	0.2	0.3	B **
870831	0918	57.83	5-37.67	35-49.83	4.91	0.50	11	126	4.6	.05	0.2	0.4	B **
870831	0924	30.31	5-31.88	35-45.35	4.55	0.50	14	125	2.5	.02	0.1	0.1	B **
870831	2153	10.84	5-34.72	35-48.14	2.00	0.66	12	150	1.6	.04	0.2	0.3	B *
870831	2200	36.00	5-31.83	35-45.57	6.07	0.50	12	129	2.8	.03	0.1	0.2	B *
870831	2230	16.47	5-31.89	35-45.58	6.15	0.71	18	106	2.8	.03	0.1	0.1	B **
870831	2233	47.98	5-31.89	35-45.58	6.14	0.90	18	106	2.8	.03	0.1	0.2	B **
870901	0138	12.13	5-31.79	35-45.57	6.40	0.84	18	106	2.7	.04	0.1	0.2	B *
870901	0212	20.60	5-31.84	35-45.55	6.26	0.76	18	105	2.7	.04	0.1	0.2	B **
870901	0704	53.37	5-37.82	35-49.83	4.19	1.00	17	131	4.4	.07	0.3	0.4	B *
870831	2234	25.65	5-31.88	35-45.57	6.04	0.66	18	105	2.8	.03	0.1	0.2	B **
870901	0212	58.13	5-31.79	35-45.55	6.34	0.66	18	106	2.7	.04	0.1	0.2	B **
870901	1431	54.85	5-37.58	35-49.05	3.24	1.55	17	118	3.4	.07	0.3	0.6	B *
870901	1606	36.82	5-35.77	35-40.27	2.80	0.97	16	159	4.9	.08	0.3	1.0	B *
870901	1727	19.41	5-35.79	35-40.08	3.63	1.18	16	165	4.7	.08	0.3	0.8	B *
870901	1732	03.77	5-35.69	35-39.89	4.30	0.37	12	172	4.9	.05	0.3	0.6	B *
870901	1830	09.31	5-37.59	35-49.11	3.40	1.31	17	119	3.4	.08	0.3	0.6	B *
870901	1951	29.37	5-35.79	35-40.12	3.64	0.50	15	164	4.8	.06	0.3	0.6	B *
870901	1606	51.52	5-35.73	35-40.02	3.59	1.00	17	167	4.8	.10	0.4	0.9	B *
870901	2241	09.20	5-32.14	35-45.17	2.04	0.59	15	122	2.7	.08	0.3	0.7	B *
870902	0428	50.40	5-29.46	35-43.00	2.58	0.71	16	088	3.7	.03	0.1	0.3	A **
870902	1226	49.77	5-34.88	35-47.89	2.77	0.59	16	092	1.2	.07	0.2	0.3	B *
870902	1819	01.63	5-35.70	35-39.89	4.40	0.50	14	172	4.8	.04	0.2	0.4	B **
870902	2037	38.01	5-35.75	35-40.02	3.52	0.84	16	167	4.8	.09	0.4	0.9	B *
870903	0719	29.01	5-35.76	35-40.07	3.63	1.18	17	165	4.8	.08	0.3	0.7	B *
870903	0722	50.42	5-35.75	35-39.96	4.17	0.50	13	169	4.8	.04	0.2	0.4	B **
870903	1157	36.76	5-30.01	35-42.56	0.27	0.59	13	088	3.8	.05	0.2	3.3	B *
870903	1312	23.35	5-29.31	35-43.62	6.33	0.59	18	087	3.2	.04	0.2	0.2	A **
870903	1352	42.31	5-29.28	35-43.65	6.40	0.66	17	087	3.3	.04	0.1	0.2	A **
870903	1401	59.03	5-29.26	35-43.67	6.46	0.66	16	088	3.3	.04	0.1	0.2	A **
870903	1412	15.43	5-29.21	35-43.67	6.58	0.59	16	089	3.4	.03	0.1	0.2	A **
870903	1639	17.63	5-29.19	35-43.67	6.51	0.50	15	089	3.4	.04	0.1	0.2	A **
870903	1655	12.42	5-29.62	35-43.97	6.95	1.03	17	080	2.5	.04	0.1	0.2	A **
870903	1739	51.18	5-29.66	35-43.97	7.03	1.69	17	079	2.4	.04	0.1	0.2	A **
870903	2125	21.88	5-31.33	35-45.22	6.80	0.66	18	103	1.7	.03	0.1	0.1	B **
870904	0317	11.38	5-31.58	35-45.54	6.64	0.66	15	128	2.4	.03	0.1	0.2	B **

DATE	ORIGIN	LAT S	LONG W	DEPTH	MAG	NO	GAP	DMIN	RMS	ERH	ERZ	Q	D
870904	0743	02.67	5-29.23	35-43.58	6.50	1.00	16	088	3.4	.05	0.2	0.3	A **
870904	0809	37.18	5-29.25	35-43.60	6.25	1.38	17	088	3.4	.03	0.1	0.2	A **
870904	2204	39.06	5-29.32	35-43.36	4.84	0.71	16	087	3.5	.04	0.1	0.2	A **
870905	2109	06.99	5-37.76	35-48.52	2.88	0.66	16	116	2.4	.05	0.2	0.3	B **
870905	2110	53.81	5-35.76	35-40.12	3.59	0.93	15	164	4.8	.04	0.2	0.4	B **
870905	2320	15.02	5-29.46	35-43.98	6.74	0.50	15	092	2.7	.04	0.2	0.2	B **
870905	2338	16.82	5-29.69	35-43.86	4.79	0.66	17	079	2.4	.05	0.2	0.3	A **
870906	0535	49.50	5-29.56	35-43.81	4.74	1.76	15	081	2.7	.07	0.3	0.5	A *
870906	0542	02.91	5-29.57	35-43.66	4.53	0.76	16	089	2.8	.04	0.1	0.2	A **
870906	1552	43.13	5-36.45	35-48.08	3.50	0.76	18	071	3.7	.04	0.1	0.2	A **
870906	2229	06.46	5-29.58	35-44.01	6.80	0.66	15	094	2.5	.05	0.2	0.3	B **
870906	2252	20.70	5-30.12	35-43.99	4.40	0.37	15	098	1.6	.05	0.2	0.2	B **
870906	2255	03.81	5-30.20	35-43.89	4.41	0.66	16	097	1.6	.06	0.2	0.3	B *
870906	2312	38.42	5-30.12	35-43.95	4.26	0.50	16	098	1.6	.05	0.2	0.2	B *
870906	2338	13.93	5-30.14	35-43.98	4.08	1.35	17	081	1.7	.04	0.1	0.3	A *
870906	2345	21.16	5-30.09	35-43.98	4.05	0.66	16	098	1.7	.05	0.2	0.2	B **
870907	0205	01.47	5-30.60	35-44.38	4.66	0.71	14	123	0.5	.02	0.1	0.1	B **
870907	0300	31.99	5-31.07	35-45.30	8.31	0.71	13	125	1.6	.04	0.2	0.2	B **
870907	0418	37.93	5-30.55	35-44.42	4.67	0.59	15	108	0.6	.03	0.1	0.2	B **
870906	2252	24.39	5-30.04	35-43.94	3.80	0.50	10	142	1.8	.04	0.2	0.2	B **
870906	2252	42.58	5-30.09	35-44.03	4.38	0.59	17	082	1.6	.04	0.1	0.2	A **
870906	2255	05.29	5-30.06	35-44.04	4.56	0.66	15	099	1.7	.05	0.2	0.2	B **
870907	0439	22.79	5-30.56	35-44.37	4.80	0.59	15	107	0.6	.02	0.1	0.1	B **
870907	0753	55.10	5-37.61	35-49.34	4.69	1.61	14	121	3.8	.06	0.3	0.5	B *
870907	0755	29.01	5-37.27	35-49.46	4.51	0.50	12	111	4.3	.06	0.2	0.4	B *
870907	0938	25.00	5-37.53	35-49.36	4.52	1.52	15	119	3.9	.05	0.2	0.4	B **
870907	0953	16.61	5-37.36	35-49.43	4.84	0.59	12	114	4.2	.06	0.2	0.4	B *
870907	1156	55.39	5-30.08	35-42.66	1.07	0.50	13	158	3.6	.09	0.3	1.4	B *
870907	1236	51.07	5-30.10	35-43.93	4.03	0.80	18	081	1.7	.05	0.2	0.2	A **
870907	1451	40.33	5-29.56	35-43.84	1.57	0.50	12	091	2.6	.07	0.2	0.6	B *
870907	1716	15.73	5-30.80	35-45.02	7.08	0.59	14	110	1.1	.02	0.1	0.1	B **
870907	2308	28.95	5-29.61	35-43.98	6.87	0.84	17	080	2.5	.04	0.2	0.2	A **
870908	1639	38.59	5-37.62	35-48.50	2.58	0.87	17	109	2.6	.05	0.2	0.3	B **
870908	2105	24.62	5-29.66	35-43.58	3.67	0.76	16	088	2.7	.05	0.2	0.3	A **
870909	0010	09.75	5-37.66	35-48.59	3.82	0.97	18	113	2.6	.04	0.1	0.2	B **
870909	0317	08.04	5-29.51	35-43.85	6.61	0.76	17	082	2.7	.04	0.1	0.2	A **
870909	0812	31.72	5-35.56	35-39.92	4.07	0.50	10	171	5.1	.02	0.1	0.2	B **
870909	0920	55.27	5-31.65	35-45.12	4.47	0.66	13	169	1.9	.03	0.1	0.2	B **
870909	1629	17.88	5-37.98	35-48.58	3.51	0.50	10	127	2.2	.06	0.3	0.4	B *
870909	2226	17.55	5-29.72	35-42.98	2.26	1.27	16	085	3.4	.06	0.2	0.5	A *
870828	1525	05.98	5-33.34	35-45.43	0.27	0.60	13	117	4.2	.08	0.3	5.6	C *
870828	1546	31.51	5-35.85	35-39.96	4.11	1.07	14	169	4.6	.09	0.4	0.7	B *
870828	1910	41.28	5-30.38	35-44.62	6.13	0.47	10	124	1.0	.04	0.2	0.3	B **
870828	2100	45.92	5-33.45	35-46.19	2.28	0.43	12	132	3.0	.04	0.2	0.4	B **
870914	2158	18.60	5-25.90	35-41.75	0.93	0.50	11	160	2.1	.03	0.2	0.8	B *
870915	0243	31.05	5-37.74	35-48.63	3.83	0.84	14	117	2.6	.06	0.2	0.4	B *
870915	0001	06.68	5-30.85	35-44.49	5.69	0.59	17	091	0.1	.03	0.1	0.1	B **
870914	0945	04.60	5-36.50	35-48.35	4.70	2.56	12	077	4.0	.06	0.3	0.6	A *
870915	0377	56.97	5-36.30	35-48.38	4.72	1.03	18	074	3.7	.04	0.1	0.2	A **
870914	1104	51.72	5-36.27	35-48.34	4.47	1.45	18	073	3.6	.04	0.1	0.2	A **
870914	1106	15.38	5-36.25	35-48.31	4.40	0.66	12	072	3.5	.03	0.1	0.2	A **
870914	1414	53.92	5-36.26	35-48.37	4.47	0.90	16	073	3.6	.05	0.2	0.3	A **
870915	0748	54.50	5-36.15	35-48.23	4.81	0.66	12	089	3.3	.03	0.1	0.2	A **
870915	0756	47.16	5-37.24	35-49.55	4.35	0.76	10	111	4.5	.05	0.2	0.5	B **
870915	0837	52.28	5-36.43	35-48.28	4.83	0.90	18	074	3.8	.08	0.2	0.3	A *
870915	0840	35.49	5-36.31	35-48.26	4.28	0.59	14	084	3.6	.05	0.2	0.2	A *
870915	0839	46.29	5-36.38	35-48.28	4.23	0.87	18	074	3.7	.07	0.2	0.3	A *
870915	0916	21.06	5-37.29	35-49.45	4.63	0.87	16	111	4.3	.06	0.2	0.3	B *
870915	0851	48.28	5-36.25	35-48.38	4.10	0.71	12	103	3.6	.02	0.1	0.1	B **
870915	0920	57.06	5-37.42	35-49.39	4.84	0.95	18	115	4.1	.06	0.2	0.3	B *
870915	0923	31.02	5-36.15	35-48.20	4.53	0.93	17	070	3.3	.05	0.2	0.3	A **
870915	1004	44.68	5-36.27	35-48.41	4.70	0.76	12	074	3.7	.04	0.1	0.2	A **
870915	1018	23.07	5-36.10	35-48.16	4.53	1.18	18	071	3.2	.05	0.2	0.2	A **
870915	1043	42.86	5-36.46	35-48.52	4.42	0.50	12	079	4.1	.04	0.1	0.3	A *
870915	1056	08.62	5-37.27	35-49.67	4.46	0.50	11	142	4.7	.04	0.2	0.4	B **
870915	1106	30.88	5-36.21	35-48.37	4.20	0.50	10	125	3.5	.03	0.2	0.3	B **
870915	1120	59.07	5-36.10	35-48.10	4.85	1.66	14	071	3.1	.05	0.2	0.4	A **
870915	1129	38.30	5-37.62	35-49.82	3.82	0.76	10	124	4.6	.04	0.2	0.4	B **
870915	1302	38.09	5-36.34	35-48.48	5.02	0.93	18	076	3.9	.05	0.2	0.3	A **
870915	1316	28.38	5-36.20	35-48.16	4.57	0.84	14	070	3.3	.04	0.1	0.2	A **
870915	1318	13.46	5-36.30	35-48.25	4.34	0.37	14	072	3.6	.03	0.1	0.2	A **
870915	1330	35.13	5-31.02	35-45.17	7.61	0.50	16	103	3.4	.02	0.1	0.1	B **
870915	1400	23.31	5-30.89	35-45.06	7.47	1.00	18	101	1.2	.04	0.1	0.2	B **
870915	0721	08.83	5-36.31	35-48.28	4.55	2.71	10	072	3.6	.03	0.2	0.4	A **
870915	1302	48.32	5-36.26	35-48.62	4.75	0.71	11	117	3.9	.05	0.2	0.4	B **
870915	0738	46.71	5-36.25	35-48.44	4.44	0.50	10	123	3.7	.03	0.1	0.2	B **
870915	0804	36.54	5-36.17	35-48.19	4.46	0.93	17	070	3.3	.05	0.2	0.2	A **
870915	0715	57.64	5-37.37	35-49.42	4.18	1.35	16	114	4.2	.07	0.3	0.4	B *
870915	0740	12.50	5-36.18	35-48.25	4.79	1.81	13	070	3.4	.04	0.2	0.3	A **
870915	0744	40.06	5-36.13	35-48.13	4.71	1.23	18	071	3.2	.06	0.2	0.3	A *
870912	1630	18.61	5-31.23	35-44.86	5.00	0.37	15	117	1.0	.07	0.2	0.3	B *
870912	1633	26.81	5-31.27	35-44.88	4.42	0.37	13	117	1.1	.02	0.1	0.1	B **

# Appendix C

DATE	ORIGIN	LAT S	LONG W	DEPTH	MAG	NO	GAP	DMIN	RMS	ERH	ERZ	Q	D
870913	0745	27.20	5-29.25	35-43.10	4.15	0.59	14	088	3.9	.03	0.1	0.2	A *+
870913	0747	53.21	5-29.15	35-43.13	4.44	0.95	16	090	4.0	.05	0.2	0.3	A *+
870913	0802	17.76	5-29.12	35-43.17	4.34	0.76	16	090	4.0	.04	0.1	0.2	B *+
870913	0803	48.33	5-29.17	35-43.15	4.28	0.59	16	089	3.9	.04	0.1	0.2	A *+
870913	0809	52.18	5-28.94	35-43.12	5.09	0.50	16	094	4.3	.05	0.2	0.3	B *+
870913	0934	51.09	5-29.12	35-43.23	4.50	0.59	14	090	3.9	.04	0.1	0.2	B *+
870913	1258	17.29	5-29.70	35-43.86	5.12	0.66	17	079	2.4	.04	0.1	0.2	A *+
870913	1438	56.25	5-33.75	35-46.37	2.80	0.59	15	133	2.3	.02	0.1	0.1	B *+
870913	1448	33.53	5-37.37	35-49.34	4.50	1.35	15	113	4.0	.06	0.3	0.4	B *
870913	1950	26.71	5-28.92	35-43.15	5.54	2.21	13	094	4.3	.06	0.3	0.4	B *
870913	2002	44.61	5-27.94	35-41.63	3.24	0.66	16	132	5.2	.04	0.1	0.3	B *+
870913	2034	07.87	5-27.90	35-41.71	2.11	1.49	15	130	5.2	.04	0.2	0.7	B *
870913	2105	47.16	5-37.31	35-49.59	3.92	0.59	12	113	4.5	.06	0.2	0.5	B *
870913	2145	45.89	5-27.93	35-41.64	2.66	0.59	13	132	5.2	.03	0.1	0.4	B *+
870914	0016	38.61	5-27.89	35-41.58	2.72	0.50	07	151	5.1	.01	0.1	0.2	B *
870914	0023	46.81	5-37.57	35-48.65	3.79	0.76	14	111	2.8	.05	0.2	0.2	B *+
870914	0217	02.47	5-27.84	35-41.65	2.94	0.59	14	132	5.1	.03	0.1	0.4	B *+
870914	0237	54.73	5-28.97	35-43.03	4.69	0.76	16	093	4.4	.04	0.2	0.2	B *+
870914	0514	59.73	5-28.85	35-43.06	5.14	0.59	16	096	4.5	.04	0.1	0.2	B *+
870914	0528	15.19	5-28.76	35-43.12	5.05	1.42	18	098	4.6	.04	0.1	0.2	B *+
870914	0538	00.85	5-29.39	35-43.44	4.31	0.66	18	085	3.3	.05	0.2	0.3	A *+
870914	0620	46.68	5-29.24	35-43.18	3.82	0.59	11	089	3.8	.06	0.3	0.3	A *
870914	0645	59.12	5-29.44	35-43.45	3.98	0.84	17	084	3.2	.03	0.1	0.1	A *+
870914	0940	02.85	5-36.16	35-48.30	4.48	1.64	16	070	3.4	.05	0.2	0.3	A *+
870914	0943	03.37	5-36.30	35-48.26	4.43	1.66	16	072	3.6	.04	0.1	0.3	A *+
870914	0947	17.26	5-36.15	35-48.41	4.41	0.37	10	124	3.5	.03	0.1	0.2	B *+
870913	0803	53.43	5-29.31	35-42.96	4.43	0.37	09	176	4.0	.07	0.4	0.6	A *
870916	2051	44.03	5-29.38	35-43.08	3.48	0.37	15	087	3.7	.06	0.2	0.4	A *
870916	2245	05.06	5-29.40	35-43.48	3.86	0.50	18	085	3.2	.04	0.1	0.2	A *+
870917	0128	37.69	5-37.78	35-49.68	4.20	0.95	18	130	4.2	.07	0.3	0.4	B *
870917	0129	03.36	5-37.59	35-49.82	3.92	0.37	10	123	4.6	.04	0.2	0.4	B *+
870917	0142	19.46	5-37.76	35-49.79	4.27	1.23	18	129	4.4	.09	0.3	0.5	B *
870917	0225	15.14	5-31.54	35-45.18	5.29	0.84	17	101	1.9	.05	0.2	0.3	B *+
870917	0402	36.60	5-29.92	35-43.71	3.66	0.37	12	112	2.2	.04	0.2	0.3	B *+
870917	0605	32.77	5-37.66	35-48.54	4.05	0.71	13	112	2.6	.05	0.2	0.3	B *+
870917	0949	56.88	5-30.10	35-44.00	4.47	0.37	15	082	1.6	.04	0.1	0.2	A *+
870917	1321	28.88	5-29.82	35-43.60	3.79	0.16	10	152	2.5	.03	0.1	0.2	B *+
870917	1528	37.66	5-37.58	35-48.56	4.04	0.37	15	109	2.7	.05	0.2	0.2	B *+
870917	1649	41.80	5-36.17	35-48.20	4.38	0.37	10	087	3.3	.03	0.1	0.3	A *+
870917	0402	52.11	5-29.92	35-43.72	3.70	0.37	10	148	2.2	.07	0.2	0.4	B *
870917	0403	03.67	5-29.92	35-43.75	3.82	0.16	14	077	2.2	.05	0.2	0.2	A *+
870917	1321	36.98	5-29.78	35-43.72	3.95	0.37	11	152	2.4	.04	0.2	0.4	B *+
870917	1711	28.66	5-29.36	35-43.11	3.11	0.37	16	086	3.7	.04	0.1	0.3	A *+
870917	1743	52.91	5-29.72	35-43.36	2.49	0.59	17	079	2.9	.03	0.1	0.2	A *+
870917	1834	59.14	5-29.62	35-43.28	2.97	0.37	11	081	3.1	.06	0.2	0.5	A *
870918	0121	21.38	5-30.69	35-44.92	7.65	1.13	17	099	1.0	.02	0.1	0.1	B *+
870918	1408	04.95	5-30.74	35-44.92	7.56	0.76	15	099	0.9	.02	0.1	0.1	B *+
870918	1541	47.46	5-28.47	35-42.60	3.62	0.59	17	103	5.6	.04	0.1	0.2	B *+
870918	1540	41.74	5-28.44	35-42.66	4.22	1.27	17	102	5.5	.04	0.1	0.3	B *+
870918	1604	49.21	5-28.36	35-42.55	3.96	0.50	15	104	5.8	.04	0.2	0.2	B *+
870918	1605	41.35	5-28.41	35-42.64	4.05	1.27	15	103	5.6	.03	0.2	0.4	B *+
870918	1616	03.03	5-37.74	35-49.68	3.74	1.08	13	128	4.3	.07	0.3	0.5	B *
870918	1626	10.61	5-37.79	35-49.62	4.00	0.87	14	130	4.1	.07	0.3	0.4	B *
870918	1650	14.89	5-28.33	35-42.54	4.08	0.37	14	105	5.8	.04	0.2	0.3	B *+
870918	1744	02.77	5-28.44	35-42.61	3.90	1.00	17	103	5.6	.04	0.1	0.2	B *+
870918	1751	00.18	5-28.42	35-42.61	4.18	0.93	17	103	5.6	.05	0.2	0.3	B *+
870918	1851	05.41	5-37.80	35-49.62	4.05	0.50	12	130	4.1	.08	0.3	0.5	B *
870918	1939	23.03	5-28.39	35-42.64	3.97	1.13	17	103	5.6	.04	0.1	0.1	B *+
870918	2022	40.81	5-37.43	35-49.49	4.58	0.50	17	116	4.2	.06	0.2	0.3	B *
870918	2047	18.93	5-29.95	35-43.66	3.23	0.37	17	076	2.2	.04	0.1	0.2	A *+
870918	2244	04.66	5-30.68	35-44.84	7.62	0.71	18	098	0.8	.04	0.1	0.2	B *+
870919	0207	37.66	5-32.37	35-45.42	2.25	0.66	14	141	3.3	.02	0.1	0.2	B *+
870916	0719	44.43	5-29.72	35-43.67	4.09	0.50	17	079	2.6	.03	0.1	0.1	A *+
870916	0720	29.03	5-30.04	35-43.70	3.28	0.50	18	077	2.0	.03	0.1	0.2	A *+
870916	0736	49.00	5-29.61	35-43.59	4.01	0.59	18	081	2.8	.04	0.1	0.2	A *+
870916	1227	03.79	5-29.89	35-43.65	3.02	0.50	15	150	2.3	.03	0.1	0.2	B *+
870916	1243	53.76	5-29.84	35-43.77	4.43	0.87	16	077	2.3	.02	0.1	0.2	A *+
870916	1248	01.91	5-30.70	35-48.77	1.59	0.37	16	184	7.7	.02	0.1	0.3	C *+
870916	1320	27.46	5-29.83	35-43.75	4.19	0.37	14	150	2.3	.03	0.1	0.1	B *+
870916	1328	50.16	5-29.73	35-43.81	4.38	0.71	18	078	2.4	.04	0.1	0.2	A *+
870916	1329	14.44	5-29.72	35-43.80	4.12	1.03	16	078	2.4	.04	0.1	0.3	A *+
870916	1332	33.71	5-29.76	35-43.83	4.38	2.54	11	078	2.3	.05	0.3	0.5	A *+
870916	1334	29.03	5-29.70	35-43.61	3.96	0.37	12	155	2.6	.03	0.1	0.2	B *+
870916	1334	36.73	5-29.49	35-43.55	4.23	0.37	14	083	3.0	.03	0.1	0.2	A *+
870916	1344	37.15	5-29.07	35-42.96	3.36	0.37	06	182	4.3	.00	0.0	0.1	C *
870916	1337	45.44	5-29.74	35-43.70	4.26	0.71	17	078	2.5	.04	0.1	0.2	A *+
870916	1342	47.90	5-29.72	35-43.65	4.18	2.18	13	079	2.6	.03	0.1	0.2	A *+
870916	1354	04.68	5-29.57	35-43.59	4.22	0.50	17	082	2.9	.04	0.1	0.2	A *+
870916	1400	52.42	5-29.71	35-43.74	4.93	0.66	18	079	2.5	.05	0.2	0.3	A *+
870916	1401	19.41	5-29.64	35-43.56	4.15	0.50	15	080	2.8	.04	0.1	0.2	A *+
870916	1406	16.17	5-29.77	35-43.73	4.46	0.71	18	078	2.4	.03	0.1	0.2	A *+
870916	1505	08.55	5-29.63	35-43.57	4.32	0.59	15	124	2.8	.03	0.1	0.2	B *+

DATE	ORIGIN	L S	LONG W	DEPTH	MAG	NO	GAP	DMIN	RMS	ERH	ERZ	Q D
870916	1506	42.36	5-29.75	35-43.65	3.91	0.50	12	153	2.5	.07	0.4	0.3 B *
870916	1558	23.67	5-29.86	35-43.83	4.39	0.37	15	078	2.2	.03	0.1	0.2 A *+
870916	1631	28.01	5-29.76	35-43.79	4.60	0.59	18	078	2.4	.04	0.1	0.2 A *+
870916	1556	19.83	5-29.88	35-43.80	4.38	2.17	15	078	2.2	.03	0.1	0.2 A *+
870916	1635	02.32	5-29.85	35-43.83	4.21	0.37	16	078	2.2	.05	0.2	0.3 A *+
870916	1804	23.02	5-29.26	35-42.98	3.55	0.37	13	176	4.0	.04	0.1	0.3 B *+
870916	1810	56.85	5-37.30	35-49.58	4.27	0.71	13	113	4.5	.05	0.2	0.3 B *+
870916	1813	36.85	5-29.80	35-43.67	4.05	0.16	14	152	2.4	.04	0.2	0.3 B *+
870916	1812	48.14	5-30.69	35-44.86	7.44	1.76	16	098	0.9	.06	0.2	0.5 B *
870916	1838	52.24	5-30.71	35-44.95	7.45	0.59	15	113	1.0	.02	0.1	0.2 B *+
870916	1930	50.28	5-29.36	35-43.85	6.82	0.76	17	085	3.0	.04	0.1	0.2 A *+
870916	1931	20.35	5-31.24	35-45.34	7.46	0.37	12	105	1.8	.03	0.1	0.3 B *+
870916	1936	29.30	5-29.24	35-43.17	3.53	0.37	15	088	3.8	.05	0.2	0.3 A *+
870916	2034	30.21	5-29.43	35-43.58	3.95	0.76	17	083	3.0	.05	0.1	0.3 A *+
870916	2040	51.64	5-29.52	35-43.54	4.04	0.59	16	083	3.0	.04	0.2	0.3 A *+
870915	1428	37.31	5-30.97	35-45.11	7.81	0.71	17	102	1.3	.03	0.1	0.2 B *+
870915	1502	37.94	5-30.97	35-45.15	7.78	0.50	16	103	1.3	.03	0.1	0.2 B *+
870915	1533	20.08	5-36.31	35-48.33	4.49	0.50	13	073	3.6	.03	0.1	0.2 A *+
870915	1554	22.82	5-36.22	35-48.15	4.33	0.71	13	069	3.3	.04	0.1	0.2 A *+
870915	1555	34.38	5-29.34	35-43.79	6.67	0.71	18	086	3.1	.04	0.2	0.2 A *+
870915	1557	40.43	5-36.18	35-48.16	4.34	0.59	12	086	3.3	.03	0.1	0.2 A *+
870915	1956	05.77	5-30.77	35-44.95	7.52	0.95	17	099	1.0	.04	0.1	0.2 B *+
870915	2021	15.25	5-29.74	35-43.63	3.74	0.59	17	078	2.5	.04	0.1	0.2 A *+
870915	2128	48.77	5-29.80	35-43.62	3.96	0.59	18	077	2.5	.04	0.1	0.2 A *+
870915	2128	18.24	5-29.84	35-43.75	3.82	2.38	14	076	2.3	.02	0.1	0.1 A *+
870915	2129	42.19	5-29.73	35-43.67	4.10	0.50	17	079	2.5	.04	0.1	0.2 A *+
870916	1931	28.69	5-31.21	35-45.32	7.14	0.50	13	105	1.8	.02	0.1	0.2 B *+
870916	2040	57.63	5-29.38	35-43.42	4.59	1.03	16	085	3.3	.05	0.2	0.3 A *+
870915	2021	21.99	5-29.76	35-43.63	3.69	1.00	15	078	2.5	.02	0.1	0.2 A *+
870915	2130	42.05	5-29.79	35-43.66	4.05	0.80	18	078	2.5	.04	0.1	0.2 A *+
870915	2134	52.52	5-29.89	35-43.74	3.63	0.71	17	077	2.2	.04	0.1	0.3 A *+
870915	2131	55.95	5-29.62	35-43.65	4.05	0.59	16	081	2.7	.05	0.1	0.3 A *+
870915	2141	26.55	5-29.80	35-43.75	3.81	0.66	16	077	2.3	.04	0.1	0.2 A *+
870915	2140	26.08	5-29.73	35-43.70	3.71	1.58	17	078	2.5	.03	0.1	0.3 A *+
870915	2143	59.50	5-29.82	35-43.77	3.82	0.95	18	077	2.3	.03	0.1	0.2 A *+
870915	2146	07.87	5-29.83	35-43.70	3.78	0.71	17	077	2.4	.03	0.1	0.2 A *+
870915	2145	22.91	5-29.67	35-43.71	3.85	1.89	17	080	2.6	.03	0.1	0.2 A *+
870915	2149	50.76	5-29.74	35-43.71	3.68	0.59	17	078	2.5	.04	0.1	0.3 A *+
870915	2147	25.78	5-29.74	35-43.64	3.89	0.66	18	078	2.5	.04	0.1	0.2 A *+
870915	2154	00.00	5-29.83	35-43.78	3.95	0.87	17	077	2.3	.04	0.1	0.2 A *+
870915	2159	39.95	5-29.98	35-43.80	3.65	0.93	17	078	2.0	.03	0.1	0.2 A *+
870915	2203	17.33	5-29.81	35-43.83	4.25	0.76	18	078	2.2	.04	0.1	0.2 A *+
870915	2206	53.04	5-29.51	35-43.56	3.78	0.37	12	161	3.0	.05	0.2	0.3 B *+
870915	2210	28.86	5-29.70	35-43.69	3.66	0.59	18	079	2.6	.05	0.1	0.3 A *+
870915	2317	44.30	5-29.92	35-43.63	4.55	0.50	12	149	2.3	.02	0.1	0.1 B *+
870915	2327	43.36	5-37.43	35-49.41	4.42	1.31	17	116	4.1	.06	0.2	0.4 B *
870916	0004	20.96	5-29.73	35-43.64	4.14	0.37	15	154	2.6	.04	0.4	0.7 B *
870916	0007	57.00	5-30.75	35-44.92	7.46	1.61	18	099	0.9	.04	0.1	0.2 B *+
870916	0029	56.52	5-29.71	35-43.49	3.35	0.66	18	079	2.8	.03	0.1	0.2 A *+
870915	2146	07.87	5-29.85	35-43.67	3.71	0.66	17	077	2.3	.03	0.1	0.2 A *+
870915	2150	01.59	5-29.83	35-43.71	4.45	0.50	16	077	2.3	.03	0.1	0.2 A *+
870915	2207	01.43	5-29.80	35-43.84	4.21	0.50	15	078	2.3	.05	0.2	0.3 A *+
870916	0208	10.60	5-30.02	35-43.74	3.37	1.13	18	077	2.0	.03	0.1	0.2 A *+
870916	0215	54.66	5-30.02	35-43.70	3.33	0.50	16	077	2.1	.04	0.1	0.2 A *+
870916	0247	07.46	5-29.61	35-43.59	3.83	0.93	17	081	2.8	.03	0.1	0.1 A *+
870916	0248	56.06	5-29.55	35-43.59	4.00	0.76	18	082	2.9	.03	0.1	0.1 A *+
870916	0254	34.23	5-29.61	35-43.63	3.76	0.66	18	081	2.8	.04	0.1	0.2 A *+
870916	0315	24.68	5-29.38	35-43.09	3.89	0.59	14	091	3.7	.06	0.2	0.3 B *+
870916	0337	48.71	5-30.03	35-43.74	3.40	0.50	11	101	2.0	.03	0.1	0.2 B *+
870916	0422	41.95	5-29.79	35-43.57	3.15	0.66	18	078	2.5	.05	0.1	0.3 A *+
870916	0434	41.36	5-29.72	35-43.57	3.55	1.18	18	079	2.7	.04	0.1	0.2 A *+
870916	0609	58.99	5-29.74	35-43.52	3.52	0.95	17	079	2.7	.03	0.1	0.2 A *+
870916	0548	40.70	5-29.66	35-43.49	3.67	0.50	13	096	2.8	.03	0.1	0.2 B *+
870916	0624	48.83	5-29.34	35-43.75	6.40	1.03	18	086	3.1	.04	0.1	0.2 A *+
870915	2328	26.67	5-29.65	35-43.50	3.11	0.16	09	158	2.8	.03	0.2	0.3 B *+
870916	0247	19.90	5-29.60	35-43.58	3.72	0.66	18	081	2.8	.03	0.1	0.1 A *+
870919	0323	35.78	5-30.63	35-43.77	0.90	0.59	17	073	1.3	.05	0.1	0.6 A *
870919	0418	10.56	5-32.02	35-45.58	1.53	1.66	16	105	3.0	.02	0.1	0.1 B *+
870919	0842	44.15	5-36.13	35-48.11	4.47	0.50	11	087	3.2	.03	0.1	0.2 A *+
870919	0909	19.73	5-36.30	35-48.33	4.19	1.08	18	073	3.6	.06	0.2	0.3 A *+
870919	0928	14.06	5-36.24	35-48.41	3.90	0.37	11	102	3.6	.02	0.1	0.2 B *+
870919	0958	34.14	5-30.70	35-44.90	7.48	0.71	17	099	0.9	.03	0.1	0.2 B *+
870919	1215	59.65	5-28.80	35-42.56	2.93	0.50	17	102	5.1	.06	0.2	0.5 B *+
870919	1511	05.85	5-37.67	35-49.69	3.80	0.50	11	125	4.3	.04	0.2	0.3 B *+
870919	1600	45.56	5-37.91	35-49.63	4.23	0.50	13	134	4.0	.09	0.4	0.6 B *+
870919	2055	42.84	5-30.91	35-44.47	3.81	0.76	17	091	0.1	.02	0.0	0.1 B *+
870919	1812	59.02	5-37.29	35-49.52	4.30	0.66	13	112	4.4	.04	0.1	0.2 B *+
870919	1838	49.20	5-37.86	35-49.67	3.12	1.27	14	132	4.2	.09	0.4	0.9 B *+
870919	1857	05.92	5-38.01	35-49.62	4.06	1.08	15	138	4.0	.09	0.4	0.5 B *
870919	2053	21.33	5-30.90	35-44.45	3.92	1.83	13	091	0.1	.02	0.1	0.1 B *+
870919	2149	52.44	5-37.66	35-49.64	3.77	0.50	11	125	4.2	.03	0.1	0.3 B *+
870919	2226	43.40	5-30.68	35-44.93	7.59	1.31	17	099	1.0	.03	0.1	0.2 B *+

# Appendix C

DATE	ORIGIN	LAT S	LONG W	DEPTH	MAG	NO	GAP	DMIN	RMS	ERH	ERZ	Q	D	DATE	ORIGIN	LAT S	LONG W	DEPTH	MAG	NO	GAP	DMIN	RMS	ERH	ERZ	Q	D
870919	2233	17.55	5-37.81	35-49.56	4.31	0.50	11	130	4.0	.06	0.3	0.5	B *	870929	1025	35.53	5-32.39	35-45.99	6.07	0.50	15	108	4.0	.03	0.1	0.2	B *
870919	2254	48.64	5-30.66	35-44.90	7.45	1.03	16	099	0.9	.04	0.1	0.3	B *	870929	1130	46.26	5-37.62	35-48.49	3.93	0.87	17	109	2.5	.05	0.2	0.2	B *
870919	2348	14.00	5-28.13	35-42.56	4.76	0.66	18	108	6.1	.04	0.2	0.3	B *	870929	1132	21.81	5-37.58	35-48.46	4.07	0.50	11	107	2.6	.05	0.2	0.3	B *
870919	2254	53.62	5-30.73	35-44.96	7.32	1.35	14	100	1.0	.02	0.1	0.2	B *	870926	2201	48.38	5-37.64	35-48.53	3.90	1.00	17	111	2.6	.05	0.2	0.2	B *
870920	0111	57.25	5-30.66	35-44.93	7.58	1.27	16	099	1.0	.04	0.2	0.3	B *	870926	2301	00.18	5-30.63	35-44.90	7.55	1.35	17	099	1.0	.03	0.1	0.2	B *
870920	0156	58.49	5-30.61	35-44.90	7.75	2.02	16	099	1.0	.03	0.1	0.3	B *	870926	2315	01.06	5-29.54	35-44.08	6.98	0.90	16	081	2.5	.04	0.1	0.3	A *
870920	0205	26.41	5-30.75	35-44.90	7.53	1.38	16	099	0.9	.03	0.1	0.2	B *	870929	1025	39.41	5-32.35	35-45.98	6.02	0.50	16	108	4.0	.02	0.1	0.1	B *
870920	0226	15.25	5-30.66	35-44.93	7.69	0.71	15	099	1.0	.02	0.1	0.2	B *	870927	0127	23.28	5-29.21	35-43.58	7.24	0.76	18	089	3.4	.05	0.2	0.3	A *
870920	0540	59.36	5-30.65	35-44.89	7.59	1.42	17	098	0.9	.04	0.1	0.3	B *	870927	0135	51.67	5-30.64	35-44.96	7.60	1.18	17	100	1.1	.03	0.1	0.2	B *
870920	0727	51.32	5-33.26	35-46.93	5.40	1.00	16	111	2.6	.04	0.2	0.2	B *	870927	0139	19.13	5-30.67	35-44.97	7.73	1.49	16	100	1.1	.02	0.1	0.1	B *
870920	0910	21.78	5-37.56	35-49.45	4.08	0.50	11	121	4.0	.05	0.2	0.4	B *	870927	0143	10.15	5-30.71	35-44.97	7.74	0.84	18	100	1.0	.03	0.1	0.2	B *
870920	1145	08.52	5-30.60	35-44.84	7.33	0.59	15	116	0.9	.02	0.1	0.1	B *	870927	0150	23.17	5-30.68	35-44.95	7.90	0.71	18	100	1.0	.04	0.1	0.2	B *
870920	1712	12.03	5-30.71	35-44.91	7.67	2.33	11	099	0.9	.02	0.1	0.2	B *	870927	0252	18.50	5-30.67	35-44.86	7.50	0.71	17	098	0.9	.05	0.2	0.3	B *
870920	1713	23.47	5-30.62	35-44.86	7.75	0.37	13	115	0.9	.03	0.1	0.3	B *	870927	0711	22.04	5-36.40	35-47.90	3.44	0.71	13	075	3.5	.04	0.1	0.2	A *
870920	1722	29.93	5-30.72	35-44.92	7.41	0.66	16	099	0.9	.02	0.1	0.2	B *	870927	1519	13.76	5-36.38	35-47.93	3.51	0.50	15	068	3.4	.03	0.1	0.2	A *
870920	1723	18.93	5-30.64	35-44.87	7.71	1.87	16	098	0.9	.04	0.1	0.3	B *	870927	1541	14.20	5-33.23	35-45.80	1.06	0.59	16	097	3.8	.05	0.1	0.7	B *
870920	1743	06.54	5-30.61	35-44.93	7.77	0.66	15	099	1.0	.03	0.1	0.2	B *	870927	1549	37.11	5-33.25	35-45.85	1.48	0.59	18	098	3.7	.04	0.1	0.4	B *
870920	1754	41.07	5-30.59	35-44.94	7.78	1.35	16	100	1.1	.02	0.1	0.2	B *	870927	1920	56.52	5-37.42	35-49.38	4.11	0.90	17	115	4.0	.05	0.2	0.3	B *
870920	1713	23.44	5-30.62	35-44.83	7.87	0.50	14	097	0.9	.03	0.1	0.3	B *	870928	0200	59.47	5-36.27	35-48.23	4.38	0.50	11	085	3.5	.03	0.1	0.2	A *
870920	1849	17.12	5-30.69	35-44.96	7.33	0.87	17	100	1.0	.03	0.1	0.2	B *	870928	0815	28.89	5-30.48	35-44.89	7.65	0.71	14	159	1.1	.06	0.3	0.4	B *
870920	2047	52.99	5-37.48	35-49.43	4.63	0.97	16	118	4.1	.06	0.2	0.3	B *	870926	0611	54.72	5-36.33	35-47.96	3.19	0.80	14	078	3.4	.03	0.1	0.2	A *
870920	2104	52.06	5-37.54	35-49.39	4.45	0.93	18	120	3.9	.07	0.2	0.3	B *	870926	0648	28.82	5-36.39	35-47.86	3.33	1.08	17	069	3.4	.05	0.1	0.3	A *
870920	2125	53.97	5-37.42	35-49.47	4.18	0.59	15	116	4.2	.05	0.2	0.3	B *	870926	0656	21.61	5-36.41	35-47.89	3.43	1.35	17	069	3.5	.05	0.2	0.3	A *
870920	2217	08.44	5-30.66	35-44.94	7.73	1.27	17	100	1.0	.02	0.1	0.1	B *	870926	0657	47.72	5-36.43	35-47.88	3.28	0.66	14	069	3.5	.05	0.2	0.3	A *
870920	2336	10.95	5-32.63	35-46.54	2.12	0.50	16	113	3.9	.02	0.1	0.2	B *	870926	0658	06.03	5-36.35	35-47.96	3.17	0.66	14	114	3.4	.04	0.2	0.2	B *
870921	0308	22.90	5-30.54	35-44.84	7.69	0.87	17	098	1.0	.04	0.1	0.2	B *	870926	0700	49.47	5-36.39	35-47.88	3.28	0.50	14	069	3.4	.05	0.2	0.3	A *
870921	0510	01.86	5-37.37	35-49.41	4.20	0.71	14	114	4.1	.06	0.2	0.4	B *	870926	1507	29.25	5-36.40	35-47.91	3.41	0.59	17	068	3.5	.04	0.1	0.2	A *
870922	0124	47.85	5-37.63	35-48.50	3.71	0.90	16	110	2.5	.04	0.1	0.2	B *	870926	1509	08.15	5-29.24	35-43.50	6.85	0.93	16	088	3.5	.03	0.1	0.1	A *
870922	0212	13.90	5-28.42	35-42.42	3.44	1.23	18	107	5.8	.03	0.1	0.2	B *	870926	1516	07.27	5-30.59	35-44.88	7.76	0.71	18	099	1.0	.04	0.1	0.2	B *
870922	0225	27.46	5-31.79	35-45.26	4.51	1.42	18	101	2.3	.03	0.1	0.2	B *	870926	1639	19.22	5-36.46	35-47.87	3.60	0.90	17	069	3.6	.06	0.2	0.4	A *
870922	0245	27.57	5-31.80	35-45.22	4.53	1.76	16	100	2.3	.02	0.1	0.2	B *	870926	1758	13.41	5-34.18	35-46.91	3.57	0.37	15	097	1.1	.03	0.1	0.1	B *
870922	0309	03.97	5-31.79	35-45.21	4.88	0.37	09	100	2.2	.01	0.1	0.1	B *	870926	1951	03.60	5-36.50	35-47.96	3.41	0.50	15	069	3.7	.04	0.1	0.3	A *
870922	0402	01.96	5-31.80	35-45.25	4.57	0.66	15	101	2.3	.01	0.0	0.1	B *	870926	2032	06.57	5-34.48	35-46.26	0.51	0.37	14	088	1.9	.04	0.1	0.8	A *
870922	0402	02.29	5-31.87	35-45.19	3.51	0.59	08	168	6.4	.03	0.3	0.5	B *	870926	2208	49.98	5-37.67	35-48.49	4.06	0.66	12	111	2.5	.03	0.1	0.2	B *
870922	0402	04.84	5-31.79	35-45.25	4.34	0.93	17	101	2.3	.03	0.1	0.2	B *	870923	0316	14.03	5-30.74	35-45.00	7.11	0.61	16	101	1.1	.02	0.1	0.1	B *
870922	0402	05.58	5-31.81	35-45.31	4.30	0.90	12	102	6.3	.03	0.1	0.3	B *	870925	0038	01.09	5-29.85	35-43.78	4.70	0.48	11	171	2.2	.05	0.3	0.3	B *
870922	0309	04.24	5-31.78	35-45.28	4.44	1.76	16	101	2.3	.03	0.1	0.2	B *	870925	0120	10.28	5-37.35	35-49.49	3.96	0.43	09	114	4.3	.03	0.1	0.3	B *
870922	0309	19.72	5-31.77	35-45.23	4.71	2.14	16	101	2.2	.01	0.0	0.1	B *	870925	1142	33.63	5-28.88	35-42.96	4.05	1.44	16	094	4.6	.04	0.2	0.3	B *
870922	0245	42.39	5-31.71	35-45.15	4.52	1.00	16	100	2.0	.04	0.1	0.2	B *	870925	1154	57.23	5-29.16	35-42.18	6.65	0.52	09	192	5.2	.23	1.5	1.8	C
870922	0449	11.58	5-28.40	35-42.45	3.55	0.76	18	107	5.8	.04	0.1	0.2	B *	870925	1324	37.91	5-37.45	35-49.56	4.17	0.80	14	117	4.3	.04	0.1	0.2	B *
870922	0707	03.82	5-30.62	35-45.03	7.38	0.95	16	101	1.1	.03	0.1	0.2	B *	870925	1426	30.30	5-28.87	35-43.02	4.16	0.87	18	095	4.5	.04	0.1	0.3	B *
870922	1750	28.05	5-32.10	35-45.70	5.63	2.14	13	106	5.5	.02	0.1	0.2	B *	870925	1430	14.22	5-28.87	35-42.98	4.03	0.46	11	175	4.6	.05	0.3	0.3	B *
870922	2301	19.17	5-30.62	35-44.87	8.10	0.95	17	098	0.9	.04	0.1	0.2	B *	870929	1659	39.45	5-37.31	35-49.52	4.94	0.71	17	113	4.4	.05	0.2	0.3	B *
870923	0036	25.97	5-30.67	35-45.02	7.65	1.35	16	101	1.1	.01	0.1	0.1	B *	870930	0459	33.81	5-37.47	35-49.38	4.54	1.35	18	117	4.0	.07	0.2	0.4	B *
870923	0044	35.37	5-30.72	35-45.08	7.67	0.80	14	102	1.2	.02	0.1	0.1	B *	870930	1120	35.41	5-32.37	35-45.45	2.49	0.37	15	100	3.3	.05	0.2	0.4	B *
870923	0246	22.77	5-37.53	35-49.35	3.76	0.95	14	119	3.9	.05	0.2	0.3	B *	870930	1251	23.25	5-37.57	35-49.38	4.43	1.31	14	121	3.9	.06	0.3	0.4	B *
870923	0251	57.71	5-36.17	35-48.10	4.27	0.50	11	085	3.2	.02	0.1	0.1	A *	870930	1417	56.28	5-29.87	35-49.79	4.22	0.71	16	217	8.1	.08	0.4	0.6	C *
870923	1423	59.29	5-28.89	35-42.70	2.11	0.71	15	098	4.8	.04	0.1	0.4	B *	870930	1422	59.76	5-32.08	35-45.96	6.97	0.37	13	110	3.6	.03	0.1	0	

# Appendix C

DATE	ORIGIN	LAT S	LONG W	DEPTH	MAG	NO	GAP	DMIN	RMS	ERH	ERZ	Q	D	DATE	ORIGIN	LAT S	LONG W	DEPTH	MAG	NO	GAP	DMIN	RMS	ERH	ERZ	Q	D
871005	1404	30.71	5-30.58	35-44.82	7.83	1.97	16	097	0.9	.04	0.1	0.3	B *+	871017	0455	30.64	5-34.01	35-46.53	1.91	0.50	13	127	1.8	.03	0.1	0.2	B *+
871005	1455	58.40	5-30.60	35-44.88	7.54	1.18	16	098	1.0	.03	0.1	0.2	B *+	871017	1015	22.31	5-29.48	35-43.93	6.63	0.66	16	083	2.7	.04	0.2	0.2	A *+
871005	1658	34.51	5-30.69	35-44.85	7.51	1.23	16	098	0.8	.03	0.1	0.2	B *+	871017	1020	32.79	5-29.47	35-43.87	6.70	1.31	17	083	2.8	.04	0.2	0.2	A *+
871005	1704	31.17	5-30.68	35-44.82	7.40	0.50	16	097	0.8	.04	0.1	0.3	B *+	871017	1027	36.84	5-30.30	35-44.25	4.88	0.59	16	131	1.1	.02	0.1	0.1	B *+
871005	1746	12.48	5-30.66	35-44.91	7.51	0.59	17	099	1.0	.04	0.1	0.2	B *+	871017	2223	41.01	5-30.53	35-44.46	5.43	1.52	17	091	0.6	.02	0.1	0.1	B *+
871005	2242	53.68	5-34.36	35-47.78	5.30	0.59	14	126	1.0	.05	0.2	0.3	B *+	871017	2335	26.89	5-30.97	35-44.28	5.00	0.16	12	145	0.3	.06	0.3	0.4	B *+
871006	0025	48.67	5-30.88	35-44.60	4.77	0.59	15	093	0.3	.02	0.1	0.2	B *+	871018	0520	53.31	5-29.76	35-44.04	6.58	2.50	11	081	2.2	.08	0.5	0.5	A *
871006	1431	07.96	5-36.20	35-47.59	3.79	1.55	14	075	3.0	.05	0.2	0.3	A *+	871018	0525	13.17	5-29.59	35-43.92	6.69	1.03	16	080	2.5	.04	0.2	0.2	A *+
871006	1514	58.52	5-34.40	35-47.85	5.38	1.27	16	101	1.1	.05	0.2	0.3	B *+	871018	0529	56.52	5-29.44	35-43.94	6.82	0.71	14	233	2.8	.02	0.2	0.1	C *+
871007	0453	05.39	5-35.75	35-39.98	3.68	0.95	17	168	4.8	.09	0.3	0.8	B *	871018	0551	49.32	5-29.39	35-43.87	6.77	0.66	13	234	2.9	.04	0.2	0.2	C *+
871007	0656	05.78	5-31.90	35-45.66	6.09	2.04	16	107	3.0	.04	0.1	0.3	B *+	871018	0556	27.57	5-29.57	35-43.82	7.09	0.59	11	231	2.7	.01	0.1	0.1	C *+
871007	0827	23.51	5-37.51	35-48.51	3.62	0.50	11	105	2.7	.02	0.1	0.2	B *+	871018	0615	46.67	5-29.33	35-43.80	6.55	0.59	13	235	3.1	.04	0.3	0.2	C *+
871007	1530	58.88	5-30.68	35-44.93	7.59	0.93	17	099	1.0	.04	0.1	0.2	B *+	871018	0559	35.00	5-29.31	35-43.86	6.88	0.59	09	236	3.1	.03	0.3	0.2	C *+
871010	1627	12.87	5-37.37	35-49.17	3.31	0.50	12	112	3.8	.06	0.3	0.6	B *	871018	0804	36.32	5-29.27	35-43.73	6.50	0.76	09	237	3.2	.04	0.4	0.5	C *
871011	0310	35.08	5-37.60	35-48.49	4.08	0.76	14	108	2.6	.04	0.2	0.2	B *+	871018	0946	07.74	5-29.41	35-43.83	6.87	1.42	16	084	2.9	.04	0.2	0.2	A *+
871011	0716	33.74	5-37.34	35-49.32	3.03	0.66	12	112	4.0	.06	0.2	0.5	B *	871018	1001	46.59	5-29.46	35-43.80	6.80	0.59	16	083	2.8	.04	0.1	0.2	A *+
871011	0805	00.16	5-37.24	35-49.25	3.46	0.50	10	108	4.1	.04	0.2	0.4	B *+	871018	1006	51.16	5-29.36	35-43.80	6.84	0.76	17	085	3.0	.03	0.1	0.2	A *+
871011	0806	51.64	5-32.17	35-44.89	1.46	0.84	14	094	2.5	.02	0.1	0.4	B *+	871018	2317	34.57	5-29.21	35-43.50	5.94	0.76	14	089	3.5	.06	0.3	0.6	A *
871011	1201	35.02	5-31.24	35-44.88	5.00	1.49	16	097	1.1	.02	0.1	0.2	B *+	871018	1439	59.19	5-30.32	35-44.07	4.01	0.50	12	134	1.2	.06	0.2	0.3	B *
871011	1358	34.06	5-31.12	35-44.82	4.98	0.37	12	097	0.9	.02	0.1	0.1	B *+	871019	0022	54.65	5-32.68	35-45.58	1.81	2.06	08	125	4.0	.01	0.1	0.3	B *+
871011	1400	12.64	5-31.17	35-44.86	5.00	0.50	13	097	1.0	.02	0.1	0.1	B *+	871019	0053	01.92	5-32.74	35-45.59	1.81	0.66	14	126	4.1	.02	0.1	0.3	B *+
871011	1424	29.84	5-29.58	35-44.00	6.84	0.59	17	080	2.5	.05	0.2	0.2	A *+	871017	2224	13.41	5-30.54	35-44.45	5.29	0.50	17	091	0.6	.04	0.1	0.2	B *+
871011	1449	10.62	5-37.78	35-48.53	3.99	1.00	15	117	2.4	.05	0.2	0.2	B *+	871017	2335	28.79	5-30.69	35-44.53	5.25	0.50	13	119	0.4	.05	0.2	0.3	B *+
871012	0055	11.32	5-31.19	35-44.84	4.54	0.76	15	097	1.0	.02	0.1	0.2	B *+	871017	2335	29.58	5-30.66	35-44.51	5.46	0.59	17	092	0.4	.05	0.1	0.2	B *+
871012	0407	03.35	5-37.56	35-48.35	3.96	0.66	13	103	2.5	.03	0.1	0.1	B *+	871019	0106	27.54	5-32.65	35-45.65	1.29	1.27	16	101	4.0	.05	0.2	0.7	B *
871012	1155	08.81	5-36.65	35-48.68	5.78	1.76	14	085	4.2	.04	0.2	0.4	A *+	871019	0335	56.46	5-29.32	35-43.40	7.73	1.83	12	090	3.4	.05	0.4	0.6	B *
871006	1444	57.42	5-30.38	35-48.15	3.44	0.59	11	175	6.7	.04	0.2	0.5	B *+	871019	0624	33.79	5-30.24	35-43.83	7.26	0.93	12	218	1.6	.04	0.4	0.3	C *
871013	1835	08.77	5-34.96	35-46.66	1.38	0.80	15	079	1.3	.04	0.1	0.3	A *+	871019	0737	27.45	5-30.07	35-43.94	6.98	1.18	14	141	1.7	.05	0.2	0.3	B *+
871013	2146	47.84	5-29.44	35-43.70	5.24	0.66	17	084	3.0	.06	0.2	0.3	A *	871019	0812	14.78	5-37.63	35-48.57	2.49	1.27	12	111	2.6	.02	0.1	0.2	B *+
871014	1002	17.57	5-35.67	35-47.40	3.14	0.66	14	075	1.9	.04	0.1	0.2	A *+	871019	1338	27.65	5-29.42	35-43.79	6.64	0.59	18	084	2.9	.05	0.2	0.2	A *+
871014	1153	03.38	5-28.23	35-42.43	3.89	0.76	17	108	6.1	.04	0.1	0.2	B *+	871019	1850	19.20	5-30.03	35-43.93	6.81	0.90	18	080	1.8	.04	0.2	0.2	A *+
871014	1156	16.85	5-35.90	35-47.40	3.87	1.89	14	076	2.4	.04	0.1	0.2	A *+	871020	1546	02.95	5-29.47	35-43.92	6.95	0.66	18	083	2.7	.03	0.1	0.2	A *+
871014	1320	23.55	5-35.62	35-47.32	3.06	0.37	12	075	1.8	.03	0.1	0.2	A *+	871020	1613	19.78	5-29.48	35-43.90	6.87	0.59	18	082	2.7	.04	0.1	0.2	A *+
871014	1320	24.53	5-35.61	35-47.40	3.12	0.50	16	076	1.8	.04	0.1	0.2	A *+	871020	1628	02.05	5-29.02	35-43.32	6.48	0.37	07	178	4.0	.03	0.2	0.4	B *+
871013	1352	21.83	5-36.56	35-47.92	3.48	0.66	13	069	3.8	.05	0.2	0.4	A *+	871020	1712	05.96	5-29.43	35-43.82	7.02	0.95	18	084	2.9	.04	0.1	0.2	A *+
871013	1537	45.98	5-31.68	35-45.38	5.35	0.76	16	104	2.3	.02	0.1	0.1	B *+	871020	1747	26.40	5-29.18	35-43.64	7.10	0.71	18	089	3.4	.03	0.1	0.2	A *+
871013	1829	46.41	5-34.97	35-46.68	1.57	1.35	17	078	1.3	.05	0.1	0.5	A *+	871020	1900	52.76	5-29.19	35-43.64	7.25	0.76	18	089	3.4	.05	0.2	0.2	A *+
871019	1853	40.61	5-31.46	35-44.25	2.32	0.37	13	100	1.1	.04	0.1	0.4	B *+	871020	2102	53.08	5-29.55	35-43.89	7.00	0.80	16	094	2.6	.04	0.2	0.2	B *+
871019	2326	15.16	5-28.27	35-42.30	3.81	0.50	11	149	6.2	.04	0.2	0.3	B *+	871020	2109	08.76	5-29.46	35-43.76	7.07	0.59	14	158	2.9	.03	0.2	0.2	B *+
871020	0425	11.58	5-29.18	35-43.62	7.28	1.27	15	089	3.5	.02	0.1	0.1	A *+	871020	2115	05.91	5-29.49	35-43.90	7.00	1.18	16	092	2.7	.03	0.1	0.2	B *+
871020	0433	40.37	5-29.54	35-43.55	7.44	0.76	09	232	2.9	.02	0.2	0.3	C *+	871020	2128	07.82	5-29.46	35-43.76	6.95	0.59	15	092	2.9	.04	0.2	0.2	B *+
871020	0644	00.28	5-29.59	35-43.72	6.85	0.84	12	231	2.7	.02	0.2	0.2	C *+	871020	2348	34.24	5-29.25	35-43.56	7.26	0.90	16	089	3.4	.02	0.1	0.1	A *+
871020	0656	01.01	5-30.24	35-43.87	6.97	1.08	12	218	1.6	.03	0.3	0.2	C *+	871021	0048	08.52	5-36.31	35-48.03	3.18	0.59	12	112	3.4	.02	0.1	0.2	B *+
871020	0703	23.19	5-29.32	35-43.61	7.14	1.52	12	165	3.2	.01	0.1	0.1	B *+	871021	0301	05.95	5-29.29	35-43.61	7.21	1.13	15	090	3.3	.02	0.1	0.1	A *+
871020	0941	28.09	5-34.43	35-47.03	4.20	1.93	14	094	0.6	.03	0.1	0.2	B *+	871021	0429	44.51	5-37.72	35-48.56	2.47	1.81	12	115	2.5	.05	0.2	0.6	B *
871020	1043	09.05	5-29.12	35-43.65	6.98	0.59	16	091	3.5	.04	0.2	0.2	B *+	871021	1048	27.76	5-32.52	35-45.62	2.30	1.76	14	101	3.8	.02	0.1	0.2	B *+
871020	1103	38.65	5-29.15	35-43.57	7.09	0.50	13	090	3.5	.03	0.1	0.2	B *+	871021	2354	07.46	5-32.62	35-45.59	2.59	0.59	14	125	3.9	.03	0.2	0.3	B *+
871020	1209	52.66	5-29.09	35-43.53	6.98	0.59	15	091	3.7	.02	0.1	0.1	B *+	871021	2108	36.90											

# Appendix C

DATE	ORIGIN	LAT S	LONG W	DEPTH	MAG	NO	GAP	DMIN	RMS	ERH	ERZ	Q	D
871031	0205	39.24	5-35.84	35-40.03	3.59	0.66	14	167	4.6	.05	0.2	0.6	B *
871031	0610	22.35	5-37.59	35-48.46	3.93	1.38	14	107	2.6	.05	0.2	0.2	B *+
871031	0637	20.62	5-37.44	35-48.54	3.37	0.50	12	104	2.9	.03	0.1	0.3	B *
871031	0818	10.98	5-32.63	35-40.60	3.66	0.37	10	204	3.5	.03	0.2	0.3	C *+
871031	0639	57.48	5-37.25	35-49.43	4.48	0.50	08	110	4.3	.04	0.2	0.5	B *+
871031	0956	55.47	5-37.58	35-48.51	3.83	0.59	14	108	2.6	.04	0.1	0.2	B *+
871101	1535	11.80	5-35.83	35-40.05	4.12	0.50	12	166	4.6	.04	0.2	0.5	B *+
871102	0040	59.58	5-29.51	35-43.87	6.89	1.31	18	082	2.7	.03	0.1	0.2	A *+
871102	0055	50.81	5-37.66	35-48.42	2.81	2.36	14	109	2.4	.04	0.2	0.3	B *+
871102	0209	18.86	5-37.48	35-48.36	3.08	1.45	14	101	2.6	.05	0.2	0.5	B *+
871102	1639	30.01	5-35.84	35-40.15	3.60	1.23	16	162	4.7	.02	0.1	0.2	B *+
871102	1732	09.43	5-35.85	35-40.05	3.62	0.97	16	166	4.6	.08	0.3	0.8	B *
871102	2130	33.13	5-30.08	35-43.48	2.06	0.50	15	074	2.3	.03	0.1	0.2	A *+
871103	0230	49.70	5-31.80	35-45.54	6.52	0.66	12	164	2.7	.02	0.1	0.1	B *+
871102	2139	14.81	5-30.89	35-44.09	2.10	1.38	17	061	0.6	.06	0.2	0.4	A *
871103	1831	51.72	5-37.61	35-48.45	3.67	0.50	16	107	2.5	.04	0.1	0.2	B *+
871103	1958	10.58	5-37.63	35-48.46	3.85	0.93	16	108	2.5	.05	0.2	0.3	B *+
871103	2125	50.17	5-37.64	35-48.51	3.68	1.27	16	110	2.5	.06	0.2	0.4	B *
871103	2225	44.69	5-37.62	35-48.48	3.69	1.27	16	109	2.5	.06	0.2	0.3	B *
871103	2322	05.94	5-37.51	35-48.52	3.68	0.50	11	106	2.7	.02	0.1	0.2	B *+
871104	2119	59.42	5-29.49	35-43.62	7.20	0.59	11	161	3.0	.03	0.2	0.2	B *+
871105	0148	25.11	5-31.86	35-45.87	7.00	0.84	15	110	3.2	.01	0.1	0.1	B *+
871105	0313	27.40	5-35.14	35-46.64	0.89	0.66	12	081	1.5	.02	0.1	0.2	A *+
871105	1427	57.83	5-30.93	35-44.15	2.07	0.50	18	060	0.5	.06	0.2	0.3	A *
871106	0118	07.48	5-37.32	35-49.45	4.37	0.59	12	112	4.3	.05	0.2	0.3	B *+
871106	0252	03.72	5-37.29	35-49.50	4.18	0.90	13	112	4.4	.05	0.2	0.3	B *+
871106	0836	14.34	5-29.81	35-44.18	7.22	1.03	15	143	2.0	.03	0.1	0.2	B *+
871106	0859	42.04	5-37.48	35-49.34	3.53	0.87	11	145	6.5	.04	0.2	0.5	B *+
871103	1958	12.73	5-37.59	35-48.51	3.76	1.00	11	109	2.6	.05	0.2	0.4	B *+
871103	2227	17.42	5-37.68	35-48.43	3.84	1.45	16	110	2.4	.04	0.2	0.2	B *+
871103	2236	17.20	5-37.62	35-48.49	3.67	1.27	17	109	2.5	.07	0.2	0.4	B *+
871104	0130	27.72	5-37.52	35-48.46	3.48	0.66	13	104	2.7	.04	0.2	0.3	B *+
871104	0916	45.07	5-29.40	35-43.78	6.52	0.97	17	085	3.0	.04	0.1	0.2	A *+
871104	1817	14.09	5-30.40	35-42.99	1.22	0.80	18	082	3.1	.06	0.2	0.8	A *
871107	0749	02.28	5-27.73	35-42.37	4.24	0.66	12	268	6.9	.04	0.3	0.4	C *+
871107	1322	38.39	5-37.65	35-48.51	3.70	0.90	17	111	2.5	.05	0.2	0.2	B *+
871107	1411	26.18	5-30.18	35-48.12	3.10	0.76	18	178	6.3	.04	0.1	0.4	B *+
871107	1608	12.66	5-29.45	35-43.80	6.91	0.50	17	083	2.9	.04	0.1	0.2	A *+
871107	1827	52.71	5-29.45	35-43.89	6.37	1.38	18	083	2.8	.04	0.1	0.2	A *+
871107	1919	06.74	5-37.17	35-49.10	3.30	0.50	10	105	3.9	.02	0.1	0.2	B *+
871107	1921	03.41	5-29.46	35-43.84	7.01	0.59	17	083	2.8	.03	0.1	0.2	A *+
871108	0047	20.19	5-29.72	35-44.19	7.88	0.71	16	145	2.2	.04	0.2	0.2	B *+
871108	0744	10.35	5-29.47	35-43.86	7.00	0.95	14	233	2.8	.03	0.2	0.2	C *+
871108	0821	18.06	5-29.80	35-44.30	7.53	1.93	13	142	2.0	.02	0.1	0.2	B *+
871108	0910	19.27	5-29.75	35-44.12	7.40	0.66	12	146	2.1	.05	0.2	0.3	B *+
871108	1249	35.93	5-29.53	35-43.81	6.99	0.37	12	156	2.7	.02	0.1	0.1	B *+
871108	1251	44.34	5-29.51	35-43.83	6.86	0.59	15	082	2.7	.04	0.2	0.2	A *+
871108	1347	40.66	5-29.50	35-43.84	6.83	2.15	17	082	2.8	.03	0.1	0.2	A *+
871108	1353	26.44	5-28.59	35-42.54	2.67	0.76	17	104	5.5	.06	0.2	0.8	B *
871108	1533	52.55	5-30.78	35-44.99	7.44	0.80	16	100	1.1	.02	0.1	0.2	B *+
871108	2249	05.70	5-28.77	35-43.50	7.44	1.00	18	099	4.2	.06	0.2	0.3	B *
871108	2316	29.06	5-28.99	35-43.49	7.30	1.27	17	094	3.9	.04	0.2	0.3	B *+
871109	0035	34.15	5-28.86	35-43.47	7.10	1.27	16	096	4.1	.02	0.1	0.2	B *+
871109	0043	10.35	5-28.86	35-43.45	7.11	0.95	17	096	4.1	.03	0.1	0.2	B *+
871109	0238	52.15	5-28.68	35-43.43	7.04	0.84	13	247	4.4	.03	0.2	0.2	C *+
871109	0350	05.39	5-37.47	35-48.50	2.55	0.87	10	104	2.8	.03	0.1	0.4	B *+
871108	2249	07.85	5-28.81	35-43.42	7.10	0.97	14	098	4.2	.05	0.2	0.3	B *+
871109	1626	12.55	5-30.88	35-44.12	2.05	0.37	16	061	0.6	.06	0.2	0.5	A *
871109	2053	37.36	5-28.84	35-43.30	7.09	0.87	16	097	4.3	.03	0.1	0.2	B *+
871109	1843	33.84	5-31.02	35-44.98	6.71	1.45	14	100	1.1	.02	0.1	0.2	B *+
871109	2101	12.83	5-28.83	35-43.37	7.34	1.76	17	097	4.2	.03	0.1	0.2	B *+
871109	2307	37.24	5-28.63	35-43.29	7.02	0.76	17	102	4.6	.04	0.1	0.2	B *+
871110	1557	32.46	5-31.26	35-49.17	3.52	0.50	16	184	6.6	.04	0.1	0.3	C *+
871110	2153	39.06	5-28.93	35-43.41	6.83	0.50	11	095	4.0	.01	0.1	0.1	B *+
871110	2220	13.04	5-28.97	35-43.26	7.24	0.37	07	243	4.1	.01	0.2	0.1	C *
871111	0229	42.84	5-28.88	35-43.33	7.14	0.37	09	181	4.2	.01	0.1	0.1	C *+
871116	0120	23.61	5-31.39	35-44.84	3.71	1.13	13	103	7.5	.01	0.1	0.2	B *+
871116	0319	34.79	5-28.58	35-43.07	7.27	1.23	14	194	6.2	.04	0.2	0.3	C *+
871116	0559	56.90	5-28.72	35-43.20	7.09	0.71	09	188	6.1	.06	0.4	0.6	C *
871116	0726	18.34	5-35.78	35-47.69	3.79	0.50	08	159	2.3	.02	0.1	0.2	B *+
871116	0803	04.53	5-33.34	35-45.94	0.66	0.66	11	169	3.4	.02	0.1	0.7	B *
871114	0458	37.35	5-31.71	35-45.03	3.87	1.93	11	098	1.9	.01	0.0	0.1	B *+
871115	0524	04.56	5-28.94	35-43.39	7.24	0.66	13	243	4.0	.03	0.3	0.2	C *+
871115	0540	39.67	5-28.41	35-43.29	6.73	0.59	13	252	5.0	.04	0.3	0.3	C *+
871115	0557	54.48	5-28.85	35-43.28	7.49	0.50	12	245	7.5	.04	0.3	0.4	C *+
871115	0625	20.68	5-29.16	35-43.08	7.96	0.50	08	255	6.9	.03	0.6	0.5	C *
871115	1002	20.81	5-35.77	35-47.60	3.99	0.71	14	077	2.2	.05	0.2	0.2	A *+
871115	1040	19.80	5-29.14	35-42.93	3.59	0.90	16	091	6.7	.04	0.1	0.4	B *+
871115	1331	35.11	5-30.90	35-45.05	7.10	0.50	14	108	6.9	.04	0.2	0.3	B *+
871115	1414	12.75	5-30.93	35-45.05	7.35	1.45	16	101	6.9	.02	0.1	0.1	B *+
871115	1422	19.83	5-31.39	35-44.88	3.86	1.00	14	097	7.4	.02	0.1	0.2	B *+
871115	1607	36.11	5-31.42	35-44.89	3.75	1.71	12	097	7.4	.02	0.1	0.4	B *+

DATE	ORIGIN	LAT S	LONG W	DEPTH	MAG	NO	GAP	DMIN	RMS	ERH	ERZ	Q	D
871115	1805	18.49	5-31.50	35-44.90	4.13	1.13	14	097	7.3	.06	0.2	0.6	B *
871115	2116	58.62	5-31.37	35-44.90	3.86	0.50	14	103	7.5	.01	0.0	0.2	B **
871115	2328	10.20	5-31.40	35-44.81	3.76	0.37	13	103	7.5	.03	0.1	0.3	B **
871116	0016	05.38	5-31.41	35-44.85	3.78	0.50	13	103	7.4	.02	0.1	0.2	B **
871116	0425	20.31	5-28.38	35-43.30	6.49	0.66	12	253	8.0	.03	0.2	0.3	C **
871116	0712	31.57	5-28.42	35-43.33	6.36	0.50	08	264	8.0	.02	0.2	0.4	C **
871117	1644	35.53	5-36.52	35-48.04	2.27	0.37	06	146	3.8	.01	0.1	0.2	B *
871117	1945	11.53	5-28.50	35-43.20	6.84	0.59	16	104	4.9	.04	0.2	0.2	B **
871118	0105	55.24	5-35.39	35-39.85	4.58	0.50	10	174	5.4	.02	0.1	0.2	B **
871118	0343	40.43	5-28.72	35-43.12	6.90	0.50	14	189	4.6	.03	0.2	0.2	C **
871118	0801	20.07	5-28.53	35-43.19	6.67	0.59	12	264	4.9	.03	0.2	0.2	C **
871118	1733	02.40	5-36.99	35-48.79	4.41	0.50	10	095	3.8	.03	0.1	0.2	B **
871119	0235	15.02	5-28.75	35-43.34	6.54	0.59	14	247	4.4	.03	0.2	0.2	C **
871120	0749	33.86	5-27.85	35-43.26	4.83	0.76	14	211	5.5	.02	0.1	0.1	C **
871120	1644	24.28	5-34.12	35-39.19	6.61	0.59	16	196	6.0	.05	0.2	0.3	C **
871120	1952	57.53	5-32.57	35-44.88	1.37	0.59	14	091	3.2	.09	0.3	1.6	B *
871120	2324	54.33	5-34.61	35-48.19	1.97	0.59	10	129	1.6	.03	0.2	0.2	B **
871121	0255	37.65	5-37.60	35-48.53	3.72	0.59	14	109	2.6	.05	0.2	0.3	B **
871121	0751	46.85	5-28.40	35-43.11	6.95	1.00	12	266	5.2	.02	0.2	0.2	C **
871121	1747	37.74	5-28.62	35-43.25	7.00	0.59	18	102	4.7	.04	0.1	0.2	B **
871125	1436	16.12	5-30.34	35-44.62	7.45	1.13	18	093	1.0	.03	0.1	0.2	B **
871125	1656	53.68	5-37.60	35-48.72	3.22	0.50	10	113	2.9	.04	0.2	0.4	B **
871125	1835	37.27	5-31.55	35-45.50	6.92	0.59	15	152	2.3	.03	0.1	0.2	B **
871125	2242	17.48	5-28.46	35-43.08	7.43	0.93	15	105	5.1	.04	0.2	0.2	B **
871125	2245	12.88	5-30.75	35-44.66	6.09	0.59	10	116	0.5	.05	0.3	0.3	B **
871126	0126	43.75	5-31.16	35-44.48	6.28	0.66	09	125	0.5	.07	0.6	0.5	B *
871126	0157	54.45	5-30.93	35-44.78	5.83	0.37	18	096	0.6	.03	0.1	0.1	B **
871126	0159	51.91	5-30.97	35-44.71	5.83	0.37	11	114	0.5	.03	0.2	0.2	B **
871126	0200	11.57	5-30.97	35-44.53	5.00	0.37	06	181	0.3	.07	1.0	0.8	C *
871126	0202	53.36	5-31.24	35-44.53	5.38	0.37	07	150	0.7	.05	0.6	0.6	B *
871126	0418	14.19	5-28.52	35-42.99	6.85	0.37	09	171	5.1	.03	0.2	0.3	B **
871126	0423	07.36	5-29.87	35-44.15	7.19	0.66	10	173	1.9	.03	0.2	0.4	B **
871126	0424	16.39	5-30.18	35-44.03	6.69	0.50	07	243	1.5	.02	0.2	0.2	C *
871126	0517	47.82	5-29.79	35-44.27	7.20	0.66	14	175	2.0	.05	0.2	0.3	B **
871126	0613	33.47	5-29.59	35-44.40	7.68	0.59	09	179	2.4	.06	0.4	0.6	B *
871126	0642	39.22	5-29.76	35-44.22	7.18	0.50	10	175	2.1	.05	0.3	0.5	B **
871126	0126	44.09	5-30.97	35-44.67	6.04	0.66	12	184	0.5	.07	0.4	0.4	C *
871126	0126	51.73	5-30.97	35-44.55	5.81	0.59	14	112	0.3	.05	0.2	0.3	B **
871126	0157	57.58	5-30.97	35-44.71	5.72	0.71	16	095	0.6	.04	0.1	0.2	B **
871126	0158	05.96	5-30.97	35-44.72	5.53	0.50	11	114	0.6	.05	0.2	0.3	B **
871126	0159	54.61	5-31.18	35-44.53	5.44	0.50	07	153	0.6	.04	0.4	0.4	B *
871126	0640	56.35	5-29.77	35-44.19	7.20	0.50	08	174	2.1	.05	0.4	0.5	B *
871126	0645	42.32	5-31.19	35-44.79	7.38	0.50	08	184	0.9	.02	0.3	0.2	C **
871126	0646	15.13	5-29.88	35-44.17	7.50	0.37	07	182	1.9	.05	0.4	0.5	C *
871126	0650	36.33	5-30.44	35-43.81	6.82	0.37	08	222	1.4	.03	0.4	0.3	C *
871126	0652	15.00	5-30.39	35-43.92	6.40	0.37	06	231	1.3	.05	1.0	0.6	C *
871126	0653	44.72	5-29.76	35-44.29	6.94	0.59	16	100	2.1	.05	0.2	0.3	B **
871126	0655	28.76	5-29.62	35-43.89	7.09	0.50	07	172	8.0	.04	0.4	0.8	B *
871126	1134	33.62	5-28.42	35-43.03	7.06	0.66	18	105	5.2	.04	0.2	0.2	B **
871126	0829	52.60	5-30.97	35-44.53	5.98	0.50	07	181	0.3	.04	0.5	0.4	C *
871127	0311	02.16	5-41.59	35-49.74	3.84	0.59	08	261	6.8	.02	0.3	0.2	C **
871127	0323	54.67	5-41.50	35-49.75	3.92	0.37	06	259	6.6	.01	0.1	0.1	C *
871127	0326	35.77	5-41.40	35-49.79	3.97	0.37	06	258	6.5	.01	0.1	0.1	C *
871127	0327	33.98	5-41.45	35-49.78	4.01	0.59	09	259	6.6	.02	0.2	0.2	C **
871127	0332	19.06	5-41.79	35-49.69	3.69	0.71	14	263	7.0	.05	0.4	0.3	C *
871128	0356	18.20	5-30.02	35-43.30	2.16	1.45	13	102	2.6	.06	0.2	0.7	B *
871128	0506	23.62	5-37.22	35-49.38	4.07	0.50	12	141	4.3	.04	0.2	0.3	B **
871128	0636	04.45	5-28.77	35-42.94	7.30	0.50	13	097	4.7	.06	0.3	0.4	B *
871128	2131	55.27	5-37.91	35-48.67	3.26	0.59	15	126	2.5	.05	0.2	0.3	B **
871128	2236	01.44	5-28.59	35-43.20	6.75	0.59	15	102	4.8	.04	0.2	0.2	B **
871201	1818	49.39	5-29.21	35-43.50	6.34	0.87	18	089	3.5	.06	0.2	0.3	A *
871202	0001	43.30	5-29.17	35-43.59	6.30	0.59	13	090	3.5	.07	0.3	0.4	A *
871203	0422	16.84	5-37.08	35-48.26	2.58	0.50	13	130	3.2	.04	0.2	0.3	B **
871202	1550	46.54	5-28.70	35-43.22	7.17	0.76	17	100	4.6	.06	0.2	0.3	B *
871203	0449	15.36	5-28.55	35-43.22	7.07	0.95	13	192	4.8	.04	0.2	0.3	B **
871203	1152	09.28	5-37.13	35-49.28	4.68	0.50	12	105	4.2	.03	0.1	0.2	B **
871203	0449	16.30	5-28.72	35-43.12	6.91	1.00	14	189	4.6	.06	0.3	0.4	C *
871205	0622	56.81	5-31.78	35-44.53	1.34	0.50	13	112	1.7	.04	0.1	0.3	B **
871205	0656	04.33	5-28.57	35-43.24	7.07	1.74	12	191	4.8	.03	0.2	0.2	C **
871205	0908	39.11	5-37.04	35-48.23	2.95	0.59	11	139	3.2	.05	0.2	0.4	B **
871205	1508	24.38	5-28.55	35-43.26	7.36	1.66	16	103	4.8	.05	0.2	0.4	B **
871206	1637	57.85	5-31.83	35-44.64	1.43	1.83	14	091	1.8	.03	0.1	0.5	B **
871206	0734	57.00	5-33.14	35-39.88	3.44	0.50	08	174	4.1	.03	0.2	0.5	B **
871206	1100	43.13	5-31.82	35-44.64	1.45	1.81	14	092	1.8	.03	0.1	0.5	B **
871207	0556	55.14	5-32.87	35-39.97	3.61	0.50	09	170	3.6	.05	0.3	0.5	B **
871208	1630	48.00	5-29.85	35-43.66	4.99	0.37	16	077	2.4	.04	0.1	0.2	A **
871208	2139	12.04	5-28.70	35-43.32	7.18	0.93	15	187	4.5	.03	0.2	0.2	C **
871209	0809	18.93	5-37.85	35-48.76	2.92	0.71	12	126	2.7	.04	0.2	0.3	B **
871209	0811	58.00	5-37.55	35-49.23	5.02	0.87	14	135	3.7	.07	0.3	0.4	B *
871210	0815	06.54	5-31.51	35-44.22	2.55	0.80	10	123	1.2	.03	0.2	0.3	B **
871210	1844	56.11	5-32.48	35-45.06	1.45	0.37	10	128	3.2	.04	0.2	0.6	B *

# Appendix C

DATE	ORIGIN	LAT S	LONG W	DEPTH	MAG	NO	GAP	DMIN	RMS	ERH	ERZ	Q	D	DATE	ORIGIN	LAT S	LONG W	DEPTH	MAG	NO	GAP	DMIN	RMS	ERH	ERZ	Q	D
871210	1952	16.81	5-28.76	35-43.28	6.98	2.21	13	186	4.4	.04	0.2	0.3	C *	880106	1242	45.99	5-34.06	35-46.63	3.21	0.50	09	214	1.6	.06	0.4	0.4	C *
871210	2036	19.15	5-37.58	35-48.50	2.80	0.59	16	108	2.6	.06	0.2	0.4	B *	880106	1500	28.90	5-31.04	35-45.17	7.85	0.37	15	103	1.4	.03	0.1	0.2	B *
871210	2105	12.62	5-28.72	35-43.11	7.42	1.52	11	189	4.7	.01	0.1	0.1	C *	880106	1500	29.17	5-31.15	35-45.22	8.09	0.37	12	103	7.2	.06	0.3	0.4	B *
871210	2332	45.35	5-31.63	35-45.60	6.67	0.71	11	129	2.6	.01	0.1	0.1	B *	880106	1500	29.53	5-31.06	35-45.09	6.98	0.37	09	105	7.1	.03	0.1	0.4	B *
871211	0104	54.97	5-29.74	35-44.06	7.19	0.59	10	147	2.2	.05	0.3	0.5	B *	880106	1500	34.73	5-31.07	35-45.09	7.77	0.80	16	101	1.3	.03	0.1	0.1	B *
871211	2000	42.20	5-29.66	35-43.93	6.11	0.71	16	151	2.4	.03	0.1	0.2	B *	880106	1500	41.91	5-31.05	35-45.05	8.21	0.50	09	131	1.2	.04	0.2	0.4	B *
871212	0010	19.89	5-29.48	35-43.71	5.96	0.59	12	159	2.9	.03	0.1	0.2	B *	880106	1533	58.56	5-30.97	35-45.18	7.74	0.95	18	103	1.4	.04	0.1	0.2	B *
871212	0450	34.62	5-30.71	35-44.89	7.33	0.59	11	117	0.9	.03	0.2	0.3	B *	880106	1702	56.76	5-28.57	35-43.03	3.15	0.37	17	102	5.0	.02	0.1	0.2	B *
871212	0800	59.33	5-33.17	35-46.76	5.20	1.71	11	142	2.9	.01	0.0	0.1	B *	880107	0815	36.18	5-29.41	35-43.40	3.57	0.50	14	168	3.3	.04	0.2	0.2	B *
871212	2151	00.49	5-29.08	35-42.93	2.05	0.66	08	260	4.3	.02	0.3	0.3	C *	880109	0051	58.08	5-29.67	35-43.96	7.52	3.07	11	079	2.4	.01	0.1	0.2	A *
871215	1638	01.67	5-32.05	35-45.08	2.78	0.37	06	163	2.5	.05	1.0	0.8	C *	880109	0056	49.89	5-29.87	35-44.07	7.83	0.59	16	082	2.0	.06	0.2	0.3	A *
871215	1807	17.54	5-33.35	35-46.93	5.09	1.38	12	143	2.4	.01	0.1	0.1	B *	880109	0057	24.58	5-29.77	35-44.18	7.19	0.93	18	083	2.1	.03	0.1	0.2	A *
871215	2223	52.06	5-37.69	35-48.98	3.33	0.50	08	144	3.1	.03	0.2	0.4	B *	880109	0106	31.68	5-29.89	35-44.24	7.01	0.95	17	085	1.8	.03	0.1	0.2	A *
871216	0135	53.34	5-30.52	35-43.71	1.96	0.59	13	110	1.5	.06	0.2	0.4	B *	880109	0100	49.54	5-29.40	35-43.85	6.76	1.27	16	084	2.9	.03	0.1	0.2	A *
871216	2212	44.60	5-37.61	35-48.70	2.99	0.59	11	128	2.8	.04	0.3	0.4	B *	880109	0109	22.55	5-29.39	35-43.83	7.07	0.71	17	085	2.9	.04	0.2	0.2	A *
871217	0715	38.03	5-36.91	35-48.95	4.09	0.66	11	140	4.1	.03	0.2	0.2	B *	880109	0113	27.43	5-29.69	35-44.26	7.38	0.71	17	084	2.2	.05	0.2	0.4	A *
871217	0818	52.41	5-36.90	35-48.85	4.36	0.37	06	139	4.0	.01	0.1	0.2	B *	880109	0117	04.52	5-29.69	35-44.20	7.17	0.71	15	083	2.2	.04	0.2	0.3	A *
871217	2316	02.08	5-37.44	35-48.46	3.81	0.76	12	128	2.8	.02	0.1	0.1	B *	880109	0136	07.54	5-29.15	35-43.61	6.96	0.59	17	090	3.5	.03	0.1	0.1	B *
871218	0124	31.21	5-31.63	35-44.75	2.11	0.37	11	120	1.5	.05	0.2	0.4	B *	880109	0122	48.05	5-29.35	35-43.79	6.79	0.66	15	159	3.0	.04	0.2	0.2	B *
871218	0355	27.72	5-37.46	35-48.46	3.83	0.50	10	128	2.7	.02	0.1	0.2	B *	880109	0135	05.25	5-29.77	35-44.18	7.22	1.52	15	083	2.1	.04	0.2	0.3	A *
871218	1140	07.64	5-35.66	35-39.97	3.05	0.80	13	246	8.7	.03	0.2	0.7	C *	880109	0056	50.22	5-29.70	35-44.23	7.26	0.37	13	084	2.2	.06	0.3	0.5	A *
871218	1143	40.46	5-41.47	35-49.83	3.89	0.37	06	264	6.7	.01	0.2	0.2	C *	880109	0113	28.50	5-29.95	35-44.04	6.84	0.71	13	082	6.2	.09	0.4	0.8	A *
871219	0201	00.90	5-37.60	35-48.46	3.98	0.87	13	126	2.5	.03	0.2	0.2	B *	880109	0139	40.74	5-29.76	35-44.25	7.33	0.80	15	084	2.1	.05	0.2	0.3	A *
871219	0406	43.29	5-35.71	35-39.88	2.86	0.71	13	248	8.8	.05	0.3	1.1	C *	880109	0142	41.15	5-29.72	35-44.20	6.92	0.50	14	083	2.2	.04	0.1	0.3	A *
871219	0906	43.43	5-37.59	35-48.46	3.91	0.50	12	126	2.5	.03	0.2	0.2	B *	880109	0154	39.76	5-29.69	35-44.22	6.99	0.50	14	083	2.2	.04	0.1	0.3	A *
871219	0901	17.21	5-37.53	35-48.42	4.03	0.37	06	135	2.6	.01	0.1	0.2	B *	880109	0202	26.74	5-29.59	35-44.08	7.35	0.97	17	080	2.4	.04	0.1	0.2	A *
871220	0303	49.97	5-29.76	35-44.39	6.63	0.59	13	102	2.1	.04	0.2	0.3	B *	880109	0209	08.34	5-29.70	35-44.27	6.83	0.71	17	084	2.2	.05	0.2	0.3	A *
871224	0753	42.77	5-33.48	35-39.69	2.01	0.59	12	239	4.7	.08	0.6	1.5	C *	880109	0257	32.87	5-29.75	35-44.23	7.08	0.80	17	084	2.1	.04	0.1	0.3	A *
871224	2239	03.08	5-29.53	35-43.95	7.01	0.97	14	093	2.6	.03	0.2	0.2	B *	880109	0259	29.83	5-29.74	35-44.20	7.47	0.71	18	083	2.1	.05	0.2	0.3	A *
871225	0823	43.33	5-32.24	35-45.29	3.41	0.66	12	166	3.0	.04	0.3	0.3	B *	880109	0301	29.27	5-29.72	35-44.15	7.52	0.66	13	082	2.2	.06	0.3	0.4	A *
871225	1544	27.02	5-32.22	35-44.98	2.38	2.28	11	094	2.7	.05	0.3	0.7	B *	880109	0304	35.03	5-29.60	35-43.90	7.14	0.71	17	080	2.5	.04	0.2	0.2	A *
871225	1731	55.98	5-31.29	35-44.53	2.45	0.66	17	091	0.8	.04	0.1	0.2	B *	880109	0308	28.35	5-29.52	35-43.93	7.23	0.66	18	082	2.7	.04	0.1	0.2	A *
871225	1755	38.11	5-31.30	35-44.53	2.46	0.59	17	091	0.8	.04	0.1	0.2	B *	880109	0314	00.86	5-29.69	35-44.12	6.76	0.80	17	082	2.2	.04	0.1	0.3	A *
871226	2042	49.66	5-31.24	35-43.75	5.37	0.50	12	093	2.9	.03	0.1	0.2	B *	880109	0323	24.83	5-29.68	35-44.12	6.84	0.80	17	082	2.3	.04	0.1	0.3	A *
871225	1756	52.96	5-31.45	35-44.65	1.76	0.16	12	093	1.1	.07	0.3	0.5	B *	880109	0327	55.04	5-29.77	35-44.24	7.33	0.76	18	084	2.1	.04	0.1	0.2	A *
871226	2206	16.32	5-32.76	35-45.15	1.41	0.59	12	131	3.7	.07	0.4	1.0	B *	880109	0326	44.85	5-29.54	35-43.90	7.20	0.76	18	081	2.6	.04	0.1	0.2	A *
871227	0347	05.69	5-29.41	35-43.73	6.61	0.50	12	172	3.0	.04	0.2	0.2	B *	880109	0345	32.62	5-29.80	35-44.24	7.11	1.55	17	084	2.0	.04	0.1	0.2	A *
871227	0430	53.22	5-33.59	35-46.25	2.89	0.37	11	165	2.7	.05	0.4	0.4	B *	880109	0356	06.77	5-29.80	35-44.24	6.90	0.84	18	084	2.0	.04	0.1	0.2	A *
871227	0506	52.20	5-29.38	35-43.50	6.48	1.91	13	091	3.2	.04	0.2	0.3	B *	880109	0358	39.07	5-29.64	35-44.32	7.15	0.37	11	162	2.3	.07	0.4	0.5	B *
871227	0507	41.07	5-29.20	35-43.59	5.97	0.59	11	172	3.5	.03	0.2	0.2	B *	880109	0359	49.52	5-29.73	35-44.28	7.00	0.66	16	085	2.1	.04	0.2	0.2	A *
871227	0508	48.58	5-29.24	35-43.58	6.46	0.50	10	179	3.4	.03	0.2	0.2	B *	880109	0401	37.97	5-29.77	35-44.29	7.42	0.95	17	085	2.0	.05	0.2	0.3	A *
871227	0516	04.97	5-29.30	35-43.59	6.23	0.66	12	172	3.3	.03	0.2	0.2	B *	880109	0402	17.42	5-29.78	35-44.31	7.28	0.71	18	086	2.0	.05	0.2	0.3	A *
871227	0935	32.90	5-32.62	35-40.56	3.61	0.50	07	205	3.4	.02	0.2	0.4	C *	880109	0403	56.08	5-29.79	35-44.16	7.10	0.87	17	083	2.1	.03	0.1	0.2	A *
871227	0950	45.02	5-31.24	35-45.22	7.98	0.71	11	173	1.6	.03	0.2	0.3	B *	880109	0415	36.88	5-29.80	35-44.24	7.28	0.71	17	084	2.0	.04	0.2	0.3	A *
871227	1939	12.49	5-32.93	35-39.88	1.89	0.50	12	231	3.7	.05	0.3	0.7	C *	880109	0301	29.71	5-29.71	35-44.26	7.27	0.59	16	084	2.2	.05	0.2	0.3	A *
871228	0101	40.03	5-29.40	35-42.94	2.97	0.71	13	091	3.9	.04	0.2	0.3	B *	880109	0358	42.79	5-29.78	35-44.25	7.13	0.71	17	085	2.0	.04	0.1	0.2	A *
871228	0342	19.34	5-29.58	35-43.94	7.02	1.00	11	173	2.5	.03	0.2	0.2	B *	880109	0421	53.33	5-29.74	35-44.17	7.22	1.42	18	083	2.1	.03	0.1	0.2	A *
871228	1310	26.07	5-37.60	35-48.39	3.95	0.71	16	105	2.4	.04	0.1	0.2	B *	880109	0506	32.70	5-29.68	35-44.20	6.96	0.80	18	083	2.2	.04	0.2	0	



# Appendix C

DATE	ORIGIN	LAT S	LONG W	DEPTH	MAG	NO	GAP	DMIN	RMS	ERH	ERZ	Q	D	DATE	ORIGIN	LAT S	LONG W	DEPTH	MAG	NO	GAP	DMIN	RMS	ERH	ERZ	Q	D
880115	0934	51.46	5-34.40	35-47.72	5.47	2.32	16	100	0.9	.05	0.2	0.4	B *+	880129	0142	30.60	5-31.85	35-45.50	5.05	0.59	14	104	2.7	.04	0.1	0.2	B *+
880115	1053	15.44	5-34.40	35-47.80	5.33	1.31	17	101	1.0	.02	0.1	0.1	B *+	880129	0144	16.08	5-31.82	35-45.40	5.08	0.50	14	103	2.5	.03	0.1	0.2	B *+
880116	0446	10.82	5-37.69	35-48.38	4.04	1.13	15	109	2.3	.05	0.2	0.3	B *+	880129	0151	31.90	5-31.80	35-45.42	5.20	0.71	18	104	2.5	.02	0.1	0.1	B *+
880116	1715	35.00	5-38.39	35-49.09	2.48	0.37	10	154	2.9	.07	0.3	0.7	B *	880129	0156	09.11	5-31.82	35-45.47	5.22	1.00	18	104	2.6	.03	0.1	0.2	B *+
880117	0724	10.35	5-32.02	35-51.11	3.05	1.18	14	213	4.1	.04	0.2	0.5	C *+	880129	0247	55.49	5-31.81	35-45.46	5.08	0.76	18	104	2.6	.03	0.1	0.2	B *+
880117	1058	05.34	5-31.79	35-45.51	5.10	0.66	16	105	2.6	.06	0.2	0.3	B *	880129	0359	43.99	5-31.71	35-45.56	6.35	0.16	10	129	2.6	.04	0.2	0.3	B *+
880117	1232	47.46	5-31.22	35-45.30	7.46	0.66	16	105	1.7	.03	0.1	0.2	B *	880129	0432	07.52	5-31.30	35-45.43	7.90	1.13	18	107	2.0	.03	0.1	0.2	B *+
880117	1240	36.26	5-34.05	35-46.55	5.13	0.37	10	096	1.7	.03	0.1	0.2	B *+	880129	0738	21.81	5-31.86	35-45.54	5.47	0.50	18	105	2.8	.03	0.1	0.1	B *+
880117	1058	06.23	5-31.80	35-45.49	5.00	0.66	14	105	2.6	.07	0.3	0.5	B *	880129	0748	36.37	5-31.89	35-45.55	5.40	0.66	18	105	2.8	.03	0.1	0.1	B *+
880117	1801	10.88	5-34.64	35-39.67	5.00	0.71	18	180	6.8	.03	0.1	0.3	C *+	880129	1305	04.27	5-30.97	35-45.23	8.45	0.71	14	104	1.5	.03	0.1	0.2	B *+
880118	0735	17.64	5-32.80	35-45.25	0.56	0.59	14	094	3.9	.06	0.2	2.2	B *	880129	1535	22.38	5-34.43	35-46.37	1.27	0.50	15	090	1.8	.03	0.1	0.3	A *+
880119	0146	33.43	5-38.08	35-48.73	3.92	0.97	16	135	2.4	.05	0.2	0.2	B *+	880129	0748	52.85	5-31.90	35-45.57	5.42	0.71	18	105	2.8	.03	0.1	0.2	B *+
880119	0452	13.25	5-37.56	35-49.50	3.80	0.59	14	121	4.1	.06	0.2	0.5	B *	880130	0426	03.98	5-31.63	35-49.80	4.15	0.37	12	193	5.5	.03	0.2	0.2	C *+
880119	2153	33.79	5-31.91	35-45.59	5.63	0.50	16	106	2.9	.03	0.1	0.1	B *+	880130	0427	14.40	5-31.61	35-49.76	4.40	0.90	15	193	5.5	.05	0.2	0.4	C *+
880120	0154	14.19	5-29.70	35-43.87	6.84	0.50	07	151	2.4	.02	0.1	0.2	B *	880130	0516	57.26	5-31.76	35-49.73	4.16	0.37	10	190	5.3	.04	0.2	0.3	C *+
880120	0431	48.70	5-30.35	35-59.41	3.83	1.27	14	293	16.9	.04	0.3	0.4	C *+	880130	0726	06.15	5-36.40	35-49.18	3.78	0.50	11	088	4.8	.02	0.1	0.2	A *+
880120	0936	41.14	5-37.88	35-48.71	2.99	0.50	13	125	2.5	.07	0.3	0.5	B *	880130	0839	12.49	5-33.57	35-46.79	4.58	1.42	18	105	2.2	.03	0.1	0.1	B *+
880120	1334	37.66	5-30.86	35-44.53	5.56	0.71	17	092	0.2	.03	0.1	0.1	B *+	880130	0842	05.07	5-30.97	35-45.14	7.77	0.59	12	103	1.3	.03	0.1	0.3	B *+
880120	1335	31.12	5-30.89	35-44.53	5.58	0.37	14	196	0.2	.02	0.1	0.1	C *+	880201	0958	09.65	5-37.99	35-48.69	3.37	0.80	16	130	2.4	.05	0.2	0.3	B *+
880120	1343	48.62	5-30.87	35-44.53	5.49	0.37	14	092	0.2	.02	0.1	0.1	B *+	880201	1345	32.58	5-31.28	35-44.93	5.00	0.66	15	098	1.2	.03	0.1	0.3	B *+
880120	2104	24.48	5-29.12	35-43.62	7.24	0.90	16	091	3.5	.03	0.1	0.2	B *	880203	0304	57.70	5-40.12	35-54.04	3.82	0.37	11	309	2.5	.05	0.5	0.3	C *
880121	0416	36.03	5-29.13	35-43.63	7.13	0.71	13	170	3.5	.04	0.2	0.2	B *+	880203	1158	50.82	5-30.15	35-48.12	3.31	0.66	16	178	6.3	.05	0.2	0.5	B *+
880121	1100	41.72	5-29.21	35-43.68	7.35	0.90	18	089	3.4	.05	0.2	0.2	A *+	880203	1404	06.98	5-29.34	35-43.67	5.62	0.50	15	086	3.1	.05	0.2	0.3	A *+
880121	1113	23.89	5-29.08	35-43.59	7.23	0.80	17	092	3.6	.04	0.1	0.2	B *+	880203	2341	01.78	5-37.79	35-48.53	4.07	0.95	18	117	2.4	.09	0.3	0.4	A *+
880121	1346	53.31	5-38.41	35-39.67	5.00	1.08	11	220	0.3	.87	3.6	2.9	D	880204	0603	43.73	5-37.52	35-48.39	3.70	0.87	17	102	2.6	.06	0.2	0.3	B *
880121	2252	36.79	5-29.53	35-43.96	7.03	0.66	13	154	2.6	.02	0.1	0.1	B *+	880204	0835	22.75	5-37.69	35-48.53	3.46	0.59	15	113	2.5	.06	0.2	0.4	B *
880121	2348	35.53	5-32.38	35-46.01	4.91	0.76	13	108	4.0	.05	0.2	0.3	B *+	880205	1241	41.86	5-31.59	35-44.18	2.30	0.66	17	086	1.4	.05	0.1	0.4	A *+
880122	0117	01.75	5-31.82	35-45.65	6.75	0.50	14	107	2.9	.02	0.1	0.1	B *+	880205	1246	17.52	5-31.52	35-44.13	2.42	0.59	17	085	1.3	.06	0.2	0.5	A *
880122	0937	17.74	5-29.32	35-43.78	7.16	1.27	16	086	3.1	.04	0.2	0.2	A *+	880205	1249	09.91	5-31.55	35-44.24	2.07	0.59	17	087	1.3	.07	0.2	0.4	A *
880122	2122	04.93	5-29.25	35-43.73	7.15	1.79	14	088	3.3	.02	0.1	0.1	A *+	880205	1249	21.23	5-31.55	35-44.22	2.14	0.37	10	100	1.3	.03	0.1	0.2	B *+
880122	2124	34.92	5-29.31	35-43.69	6.90	0.50	11	158	3.2	.02	0.1	0.1	B *+	880205	1627	28.25	5-35.41	35-47.06	1.99	0.66	17	078	1.5	.07	0.2	0.4	A *
880122	2202	19.08	5-29.10	35-43.67	7.30	1.00	13	091	3.6	.03	0.2	0.3	B *+	880205	1752	33.15	5-37.59	35-48.55	3.98	0.59	12	109	2.7	.04	0.2	0.2	B *+
880122	2225	01.58	5-29.23	35-43.68	7.13	0.80	16	088	3.3	.03	0.1	0.2	A *+	880205	2037	06.35	5-40.80	35-35.96	1.98	1.42	15	292	8.1	.03	0.3	0.8	C *
880122	2202	19.19	5-29.28	35-43.50	7.32	1.00	13	087	3.4	.03	0.2	0.2	A *+	880206	0121	29.56	5-29.57	35-43.14	2.75	0.50	11	084	3.4	.04	0.2	0.4	A *+
880122	2225	25.40	5-29.22	35-43.68	6.91	0.80	16	088	3.3	.03	0.1	0.2	A *+	880206	0124	13.17	5-29.32	35-43.08	2.61	0.37	09	090	3.8	.07	0.3	0.8	A *
880106	1724	28.86	5-29.15	35-43.18	4.30	0.49	10	177	3.9	.09	0.6	0.6	B *	880206	1230	37.16	5-30.97	35-44.88	7.26	0.37	13	098	0.9	.07	0.3	0.4	B *
880106	1724	33.86	5-29.15	35-43.15	3.44	0.77	17	090	3.9	.05	0.1	0.3	A *+	880206	1936	41.41	5-38.38	35-49.62	3.21	1.03	18	154	3.8	.08	0.3	0.5	B *
880107	1710	34.43	5-30.85	35-44.53	5.48	0.56	15	116	0.2	.03	0.1	0.2	B *+	880207	0813	44.80	5-34.44	35-47.86	5.51	1.49	17	100	1.1	.03	0.1	0.1	B *+
880109	1330	06.11	5-29.73	35-44.26	6.97	0.55	15	144	2.1	.05	0.2	0.3	B *+	880207	1248	23.92	5-29.29	35-43.43	4.41	0.50	10	169	3.4	.04	0.2	0.3	B *+
880109	1332	04.35	5-29.72	35-44.20	6.49	0.55	14	145	2.2	.05	0.2	0.3	B *+	880207	1252	58.42	5-29.30	35-43.38	4.71	0.59	17	087	3.5	.03	0.1	0.2	A *+
880109	1337	21.30	5-29.71	35-44.24	6.80	0.53	15	084	2.2	.04	0.2	0.2	B *+	880207	1254	45.67	5-29.26	35-43.33	4.47	0.59	15	088	3.6	.05	0.2	0.3	A *+
880110	1553	26.49	5-29.54	35-44.00	7.16	0.63	16	081	2.6	.04	0.2	0.3	A *+	880213	0618	00.06	5-29.90	35-44.33	7.25	0.71	14	087	1.8	.04	0.1	0.2	A *+
880124	0443	36.39	5-30.97	35-45.12	7.82	0.50	10	102	1.3	.02	0.1	0.2	B *+	880213	0631	12.08	5-29.92	35-44.29	7.50	0.87	14	086	1.8	.05	0.2	0.3	A *+
880124	0550	16.11	5-37.83	35-49.03	1.88	0.16	07	153	6.7	.02	0.2	1.0	B *	880213	0631	38.65	5-29.92	35-44.31	7.50	0.76	14	086	1.8	.04	0.2	0.2	A *+
880125	0435	51.38	5-26.21	35-39.99	3.53	0.37	06	219	2.4	.01	0.1	0.1	C *	880213	0655	52.32	5-32.64	35-45.59	1.79	0.50	12	100	3.9	.03	0.1	0.4	B *+
880125	1304	49.69	5-34.67	35-39.55	5.43	0.93	17	184	6.7	.04	0.2	0.3	C *+	880213	0941	51.30	5-29.38	35-43.76	7.26	0.66	14	085	3.0	.03	0.1	0.2	A *+
880123	0203	05.89	5-34.99	35-43.46	0.55	0.59	05	298	7.8	.02	0.7	8.1	D	880213	1123	35.80	5-29.51	35-43.84	6.92	0.87	14	082	2.7	.04	0.1	0.2	A *+
880123	0207	32.54	5-29.03	35-43.60	7.21	1.38	15	093	3.7	.02	0.1	0.2	B *+	880214	0224	05.00	5-34.77										

# Appendix C

DATE	ORIGIN	LAT S	LONG W	DEPTH	MAG	NO	GAP	DMIN	RMS	ERH	ERZ	Q	D	DATE	ORIGIN	LAT S	LONG W	DEPTH	MAG	NO	GAP	DMIN	RMS	ERH	ERZ	Q	D
880225	0302	50.13	5-32.35	35-37.65	4.24	1.38	18	222	4.7	.07	0.3	0.5	C *	880308	1758	10.60	5-35.79	35-47.90	5.07	0.37	12	092	2.4	.04	0.2	0.3	B *+
880225	0508	41.86	5-32.39	35-45.15	1.10	1.23	18	096	3.1	.04	0.1	0.6	B *	880308	2002	56.04	5-29.40	35-43.77	6.25	0.87	18	085	3.0	.03	0.1	0.1	A *+
880225	1916	32.19	5-31.68	35-45.67	7.08	1.31	17	109	2.7	.03	0.1	0.2	B *	880308	2051	53.88	5-29.40	35-43.71	5.90	0.50	10	161	3.0	.02	0.1	0.1	B *
880226	0326	46.08	5-29.45	35-43.77	6.92	0.66	18	084	2.9	.03	0.1	0.2	A *+	880309	0021	36.95	5-37.40	35-48.46	4.78	1.08	17	100	2.8	.06	0.1	0.2	B *
880226	0633	21.71	5-37.43	35-48.40	3.78	0.37	11	100	2.7	.05	0.2	0.4	B *+	880309	0310	30.12	5-37.64	35-48.61	4.09	0.76	17	113	2.7	.04	0.1	0.2	B *+
880226	1311	59.37	5-31.67	35-45.69	7.09	0.71	18	109	2.7	.04	0.1	0.2	B *+	880309	0359	48.21	5-37.92	35-48.65	3.11	0.37	15	157	6.6	.04	0.2	0.4	B *+
880226	0954	44.28	5-37.51	35-48.34	3.85	1.93	17	101	2.5	.06	0.2	0.3	B *	880309	0426	51.08	5-37.65	35-48.83	3.50	0.37	10	117	3.0	.05	0.2	0.4	B *
880201	1659	50.01	5-30.97	35-45.24	7.98	0.99	14	104	1.5	.03	0.1	0.2	B *+	880309	0605	39.63	5-36.84	35-48.14	3.31	0.37	12	078	3.5	.03	0.1	0.2	A *+
880223	1706	22.25	5-37.76	35-48.61	3.84	0.74	15	118	2.5	.06	0.2	0.3	B *	880309	0702	14.88	5-37.77	35-48.69	4.86	1.89	18	120	2.6	.09	0.3	0.4	B *
880227	0259	31.37	5-31.52	35-45.16	5.56	0.50	17	101	1.8	.04	0.1	0.2	B *	880309	0723	22.54	5-37.69	35-48.59	4.50	0.50	15	114	2.6	.08	0.3	0.4	B *
880227	0308	30.89	5-33.05	35-46.89	5.99	0.84	16	113	3.0	.04	0.2	0.2	B *+	880309	0744	56.20	5-37.59	35-48.56	4.14	0.50	13	110	2.7	.03	0.1	0.2	B *+
880227	0403	33.97	5-37.52	35-48.33	3.73	1.00	17	101	2.5	.05	0.1	0.2	B *+	880309	0821	20.80	5-30.02	35-43.91	3.91	0.50	14	143	1.8	.06	0.2	0.3	B *
880227	0445	09.06	5-29.43	35-43.77	7.36	0.87	18	084	2.9	.02	0.1	0.1	A *+	880309	1009	42.42	5-34.22	35-47.15	4.11	0.37	10	119	0.8	.02	0.1	0.1	B *
880227	0801	21.72	5-27.81	35-43.21	4.82	0.71	16	123	5.6	.03	0.1	0.2	B *+	880309	1021	57.63	5-37.57	35-48.61	3.78	0.59	14	110	2.8	.05	0.2	0.3	B *+
880227	1352	54.77	5-29.60	35-44.04	6.86	0.59	14	159	2.5	.06	0.3	0.4	B *	880309	1147	26.27	5-30.04	35-43.84	3.80	0.59	18	079	1.9	.04	0.1	0.2	A *+
880227	1636	11.40	5-37.63	35-48.49	3.60	0.59	14	110	2.5	.04	0.2	0.3	B *	880309	1150	09.69	5-29.96	35-43.77	3.59	0.59	12	094	2.1	.04	0.1	0.2	B *+
880227	1638	32.63	5-30.27	35-44.10	4.06	0.59	17	084	1.3	.04	0.1	0.2	A *+	880309	1241	22.90	5-31.73	35-45.75	7.23	0.50	13	110	2.9	.02	0.1	0.2	B *+
880227	1638	45.17	5-30.29	35-44.08	4.06	0.87	18	084	1.2	.04	0.1	0.2	A *+	880309	1523	33.75	5-40.51	35-36.47	1.16	0.87	14	290	7.0	.10	0.9	5.6	D *
880227	2308	46.27	5-37.33	35-48.23	3.58	2.63	13	092	2.7	.06	0.3	0.6	B *	880309	2048	25.68	5-32.42	35-40.80	4.04	0.50	12	134	3.4	.03	0.1	0.3	B *+
880227	2319	12.18	5-32.51	35-40.81	4.00	0.59	16	135	3.5	.05	0.2	0.2	B *+	880309	2057	55.95	5-32.59	35-40.78	3.67	0.71	17	137	3.6	.05	0.2	0.3	B *
880227	2335	30.44	5-37.28	35-48.37	3.62	0.59	09	094	2.9	.03	0.1	0.2	B *+	880309	2237	39.08	5-30.97	35-44.53	6.16	0.50	06	246	0.3	.11	0.7	0.5	C
880228	0109	45.70	5-37.41	35-48.31	3.18	1.38	17	097	2.7	.06	0.2	0.4	B *	880309	2244	06.92	5-32.51	35-40.77	3.78	0.50	15	136	3.5	.04	0.1	0.3	B *+
880301	1533	42.08	5-37.45	35-48.38	3.82	0.93	16	100	2.7	.03	0.1	0.2	B *+	880309	2255	00.57	5-37.77	35-48.81	3.45	0.50	14	122	2.8	.04	0.2	0.3	B *+
880302	0051	34.77	5-35.80	35-47.90	4.91	0.50	16	076	2.4	.04	0.1	0.2	A *+	880310	0206	35.10	5-31.58	35-44.28	2.33	0.50	10	123	1.3	.03	0.1	0.2	B *
880302	0323	26.55	5-37.80	35-48.68	3.97	0.87	18	121	2.6	.06	0.2	0.2	B *	880310	0436	39.34	5-31.51	35-44.23	2.21	0.59	11	100	1.2	.04	0.2	0.3	B *+
880302	0712	17.98	5-35.80	35-47.88	4.72	1.49	18	076	2.4	.04	0.1	0.2	A *+	880311	0123	05.63	5-35.72	35-47.99	4.87	0.37	09	135	2.4	.04	0.2	0.3	B *+
880302	0730	23.17	5-35.81	35-47.90	4.81	1.00	18	076	2.5	.04	0.1	0.2	A *+	880310	1654	28.58	5-36.35	35-48.03	4.85	0.37	14	079	3.5	.08	0.3	0.4	A *
880302	1716	10.72	5-37.81	35-48.71	4.03	0.87	16	122	2.6	.06	0.2	0.3	B *	880310	2000	51.70	5-37.46	35-48.41	3.90	0.71	15	101	2.7	.04	0.1	0.2	B *+
880302	1718	45.37	5-32.33	35-45.40	1.93	0.50	13	100	3.2	.05	0.1	0.5	B *+	880311	0321	38.18	5-37.43	35-48.43	3.94	0.37	13	100	2.8	.05	0.2	0.3	B *+
880302	1734	23.49	5-37.86	35-48.80	4.09	0.71	14	126	2.7	.07	0.3	0.4	B *	880311	0523	10.43	5-37.72	35-48.70	3.65	0.50	14	118	2.7	.05	0.2	0.4	B *+
880302	1845	49.06	5-37.66	35-48.85	3.45	0.50	12	118	3.0	.05	0.2	0.4	B *+	880311	0552	00.29	5-31.62	35-45.57	6.92	1.03	18	107	2.5	.04	0.1	0.2	B *+
880302	1950	24.66	5-37.86	35-48.73	4.26	1.42	17	124	2.6	.06	0.2	0.3	B *	880311	0740	26.81	5-37.58	35-48.82	3.93	0.37	09	114	3.0	.07	0.3	0.6	B *
880303	0354	33.30	5-37.86	35-48.68	4.27	1.87	14	124	2.5	.07	0.3	0.5	B *	880311	0834	11.96	5-37.84	35-48.65	3.82	1.38	18	122	2.5	.06	0.2	0.3	B *
880303	0501	57.15	5-37.72	35-48.78	5.00	1.00	18	119	2.8	.10	0.3	0.5	B *	880311	0834	44.28	5-37.80	35-48.67	3.94	0.50	15	121	2.6	.06	0.2	0.2	B *
880303	0400	01.39	5-37.86	35-48.69	3.32	0.50	13	156	6.5	.06	0.2	0.7	B *	880311	0901	39.93	5-37.80	35-48.63	3.94	1.27	18	120	2.5	.05	0.2	0.2	B *+
880303	0402	17.24	5-37.77	35-48.71	4.11	1.35	17	120	2.7	.05	0.2	0.3	B *+	880311	0925	24.16	5-37.83	35-48.65	3.77	1.13	18	121	2.5	.05	0.2	0.2	B *
880303	0511	03.43	5-37.78	35-48.53	3.27	1.08	17	117	2.4	.07	0.2	0.6	B *	880311	0925	43.04	5-37.86	35-48.70	3.98	0.50	13	124	2.5	.05	0.2	0.2	B *+
880305	0533	57.87	5-37.85	35-48.71	4.06	0.59	16	124	2.6	.07	0.3	0.4	B *	880311	0929	22.85	5-37.78	35-48.72	3.84	0.50	13	121	2.7	.06	0.2	0.4	B *
880305	0605	04.34	5-37.84	35-48.75	4.11	0.59	16	124	2.6	.07	0.2	0.3	B *	880311	1004	53.90	5-37.86	35-48.58	4.09	1.03	17	121	2.4	.05	0.2	0.2	B *+
880305	0641	12.69	5-32.22	35-45.10	1.77	0.37	08	160	2.8	.03	0.3	0.6	B *	880311	1200	30.86	5-37.87	35-48.62	4.04	1.42	17	123	2.4	.04	0.2	0.2	B *+
880305	2119	18.75	5-37.72	35-48.70	3.38	0.50	10	116	2.8	.04	0.2	0.4	B *+	880311	1336	37.03	5-30.13	35-43.81	1.22	0.50	10	142	1.8	.06	0.2	0.6	B *
880305	2145	14.78	5-37.78	35-48.62	3.86	1.08	17	119	2.5	.05	0.2	0.2	B *+	880311	1336	37.66	5-30.10	35-43.86	1.11	0.66	12	102	1.8	.07	0.2	0.7	B *
880305	2145	31.61	5-37.74	35-48.58	3.77	0.93	17	116	2.5	.05	0.2	0.3	B *+	880311	1338	06.77	5-37.48	35-48.40	3.75	0.80	16	102	2.6	.06	0.2	0.3	B *
880305	2204	35.26	5-37.74	35-48.61	3.70	1.13	17	117	2.6	.05	0.2	0.3	B *+	880311	1607	52.45	5-37.77	35-48.69	3.61	0.59	17	120	2.6	.05	0.2	0.3	B *+
880305	2310	58.47	5-37.76	35-48.64	3.88	0.93	17	118	2.6	.05	0.2	0.2	B *+	880311	1726	17.27	5-37.82	35-48.71	3.74	0.59	17	122	2.6	.05	0.2	0.3	B *+
880306	0220	45.19	5-37.81	35-48.67	3.82	0.90	18	121	2.6	.06	0.2	0.3	B *	880311	1905	35.51	5-37.75	35-48.61	4.10	0.66	17	117	2.5	.08	0.3	0.4	B *
880306	0414	52.55	5-37.98	35-48.70	4.12	0.71	18	130	2.4	.08	0.3	0.4	B *	880311	2101	44.85	5-37.78	35-48.68	3.72	0.50	15	120	2.6	.04	0.2	0.3	B *+
880306	1120	50.30	5-29.65	35-43.09	1.65	0.66	17	084	3.3	.06	0.2	0.6	A *	880311	2349	34.02	5-37.48	35-48.35	3.59								

# Appendix C

DATE	ORIGIN	LAT S	LONG W	DEPTH	MAG	NO	GAP	DMIN	RMS	ERH	ERZ	Q	D	DATE	ORIGIN	LAT S	LONG W	DEPTH	MAG	NO	GAP	DMIN	RMS	ERH	ERZ	Q	D
880317	0612	44.68	5-37.73	35-48.70	3.98	0.53	13	118	2.7	.04	0.2	0.2	B +*	880322	0717	32.50	5-30.68	35-44.95	7.70	1.03	14	100	1.0	.02	0.1	0.2	B +*
880317	0613	51.64	5-37.85	35-48.67	3.71	0.77	18	123	2.5	.05	0.2	0.2	B +*	880322	0818	54.99	5-30.65	35-44.94	7.78	0.93	16	100	1.0	.02	0.1	0.1	B +*
880317	0908	57.58	5-37.57	35-48.49	3.99	0.76	18	107	2.6	.04	0.1	0.2	B +*	880322	1649	26.05	5-29.20	35-43.51	6.88	0.87	17	089	3.5	.02	0.1	0.1	A +*
880317	1439	23.27	5-36.48	35-48.03	3.63	0.55	15	070	3.7	.07	0.2	0.4	A *	880322	1957	23.29	5-31.02	35-45.05	7.17	0.50	10	109	7.1	.03	0.1	0.3	B +*
880317	2342	12.11	5-37.57	35-48.51	4.18	0.95	18	107	2.6	.07	0.2	0.4	B *	880322	2006	30.99	5-37.51	35-48.43	3.61	0.66	13	103	2.6	.04	0.2	0.3	B +*
880317	2358	19.74	5-37.42	35-48.56	3.85	0.70	16	103	2.9	.08	0.2	0.3	B *	880322	2114	20.53	5-29.15	35-43.45	7.07	0.97	12	090	3.7	.01	0.1	0.1	B +*
880319	0059	52.34	5-41.95	35-49.66	1.50	0.67	13	237	7.4	.04	0.2	1.4	C *	880322	2131	00.28	5-37.34	35-48.48	3.48	0.87	14	099	2.9	.02	0.1	0.2	B +*
880319	0257	39.68	5-37.66	35-48.63	4.12	0.68	18	114	2.7	.08	0.3	0.4	B *	880322	2150	15.41	5-30.97	35-45.13	7.41	1.83	14	102	1.3	.02	0.1	0.2	B +*
880319	0918	02.59	5-37.43	35-48.33	3.77	0.66	09	171	2.6	.04	0.3	0.3	B +*	880322	2150	43.13	5-29.03	35-43.51	6.85	1.71	13	093	3.8	.02	0.1	0.3	B +*
880319	1813	01.44	5-28.91	35-42.95	3.33	0.53	14	094	4.5	.05	0.1	0.3	B +*	880322	2200	22.22	5-31.03	35-45.11	7.39	1.74	12	102	1.3	.02	0.1	0.2	B +*
880320	0046	27.13	5-36.50	35-47.97	3.77	0.67	16	069	3.7	.05	0.1	0.3	A +*	880322	2315	16.21	5-31.18	35-45.28	7.42	2.14	13	105	1.7	.01	0.1	0.1	B +*
880320	0054	60.00	5-36.45	35-47.95	3.43	0.48	12	068	3.6	.04	0.1	0.3	A +*	880322	2325	43.57	5-30.65	35-44.90	7.63	0.87	14	099	1.0	.02	0.1	0.1	B +*
880320	0133	22.60	5-37.55	35-48.37	3.86	0.69	17	103	2.5	.04	0.1	0.2	B +*	880322	2330	51.23	5-30.71	35-44.81	7.71	1.61	16	097	0.8	.03	0.1	0.2	B +*
880320	0225	42.86	5-36.44	35-47.96	3.58	0.60	16	068	3.6	.06	0.2	0.4	A *	880323	0020	19.99	5-29.22	35-43.52	6.50	0.71	12	089	3.5	.03	0.2	0.3	A +*
880320	0147	50.30	5-36.51	35-47.98	3.84	0.58	16	070	3.7	.04	0.1	0.2	A +*	880323	0138	27.42	5-29.11	35-43.66	7.13	1.61	13	091	3.6	.02	0.1	0.2	B +*
880320	0308	15.50	5-36.17	35-48.26	3.63	0.43	11	128	3.4	.18	0.8	1.4	B	880323	0551	10.86	5-37.59	35-48.40	3.96	0.95	16	106	2.5	.05	0.2	0.2	B +*
880320	0648	16.05	5-29.47	35-43.79	6.94	0.51	16	083	2.8	.04	0.1	0.2	A +*	880323	0315	00.88	5-37.56	35-48.40	3.70	0.95	17	104	2.5	.05	0.2	0.2	B +*
880320	1208	16.68	5-31.43	35-45.13	5.84	0.57	18	101	1.7	.02	0.1	0.1	B +*	880323	0739	36.93	5-37.86	35-48.82	3.59	0.80	16	126	2.7	.05	0.2	0.3	B +*
880320	1635	11.06	5-36.47	35-48.00	3.33	0.61	14	070	3.7	.05	0.2	0.3	A +*	880323	0835	16.06	5-37.46	35-48.35	3.25	0.87	18	099	2.6	.06	0.2	0.4	B *
880320	1639	30.60	5-36.43	35-47.98	3.26	0.66	15	069	3.6	.04	0.1	0.3	A +*	880323	1237	19.49	5-37.63	35-48.41	3.96	0.97	16	107	2.4	.06	0.2	0.2	B *
880320	1647	35.75	5-30.75	35-44.47	4.41	0.54	14	119	0.2	.03	0.1	0.2	B +*	880323	1559	15.31	5-32.34	35-37.80	3.15	0.93	16	220	4.5	.08	0.4	0.7	C *
880320	1650	24.64	5-30.76	35-44.44	4.40	0.64	17	090	0.2	.03	0.1	0.1	B +*	880323	2308	34.05	5-38.01	35-48.83	4.06	0.59	16	133	2.6	.09	0.3	0.4	B *
880320	2326	38.93	5-36.12	35-47.20	0.60	0.63	08	133	4.7	.13	0.6	7.6	C	880323	2341	13.35	5-30.72	35-44.98	7.41	0.68	18	100	1.1	.02	0.1	0.1	B +*
880320	2328	43.05	5-36.50	35-48.62	4.25	0.66	16	115	2.6	.06	0.2	0.3	B *	880324	0022	42.58	5-29.23	35-43.53	6.02	1.47	16	088	3.4	.03	0.1	0.3	A +*
880320	2335	24.02	5-36.43	35-47.91	3.06	0.68	16	068	3.5	.04	0.1	0.2	A +*	880324	2049	20.93	5-36.64	35-48.01	2.70	0.84	14	072	3.8	.05	0.2	0.4	A +*
880320	2338	59.62	5-36.49	35-47.89	3.33	0.61	15	069	3.6	.05	0.2	0.3	A +*	880324	2141	27.15	5-37.55	35-48.36	3.52	0.68	16	103	2.5	.04	0.1	0.2	B +*
880320	2342	55.67	5-36.43	35-47.78	3.07	0.71	17	071	3.4	.06	0.2	0.4	A *	880324	2313	04.87	5-37.59	35-48.51	4.34	1.49	17	108	2.6	.09	0.3	0.4	B *
880321	0030	30.01	5-38.01	35-48.86	4.06	0.53	16	134	2.7	.07	0.3	0.4	A *	880324	2356	36.00	5-36.48	35-47.85	3.36	2.01	12	070	3.6	.03	0.1	0.4	A +*
880321	0110	25.86	5-36.41	35-48.00	3.52	0.62	16	069	3.5	.03	0.1	0.2	A +*	880325	0004	00.57	5-36.43	35-47.88	3.25	2.44	10	069	3.5	.02	0.1	0.3	A +*
880321	0153	35.83	5-36.30	35-47.74	3.17	0.60	15	072	3.2	.04	0.1	0.3	A +*	880325	0014	26.29	5-36.50	35-47.93	2.90	1.44	15	069	3.7	.03	0.1	0.3	A +*
880321	0200	13.58	5-36.34	35-47.71	2.69	0.63	14	135	3.3	.03	0.1	0.3	B +*	880325	0154	56.04	5-36.37	35-47.83	2.93	0.60	16	070	3.4	.05	0.1	0.3	A +*
880321	0230	45.99	5-36.31	35-47.79	3.21	0.66	18	071	3.2	.04	0.1	0.2	A +*	880325	0400	59.84	5-36.32	35-47.75	3.09	0.86	15	072	3.2	.05	0.2	0.3	A +*
880321	0639	39.21	5-30.76	35-44.53	4.66	0.66	17	092	0.3	.03	0.1	0.1	B +*	880325	0406	41.54	5-36.44	35-47.69	4.19	0.86	17	074	3.4	.08	0.2	0.3	A +*
880321	0913	13.18	5-36.50	35-48.01	3.38	0.79	17	070	3.7	.04	0.1	0.3	A +*	880325	0411	06.68	5-36.34	35-47.70	2.96	1.42	16	073	3.3	.04	0.1	0.3	A +*
880321	0929	02.45	5-36.52	35-48.00	3.04	0.66	10	074	3.7	.03	0.1	0.3	A +*	880325	0539	38.16	5-36.48	35-47.74	3.03	1.43	18	073	3.5	.06	0.2	0.4	A *
880321	1021	49.89	5-36.40	35-47.94	3.28	0.43	12	070	3.5	.04	0.1	0.3	A +*	880325	0541	43.98	5-36.37	35-47.92	2.44	0.40	13	115	3.4	.07	0.2	0.5	B *
880321	1717	49.90	5-37.73	35-48.76	4.32	0.51	13	120	2.8	.09	0.4	0.5	B *	880325	0559	14.27	5-36.38	35-47.82	2.84	0.39	15	070	3.4	.05	0.2	0.3	A +*
880321	2312	23.18	5-30.71	35-44.95	7.77	0.63	17	100	1.0	.05	0.2	0.2	B +*	880325	0843	45.26	5-37.60	35-48.46	3.92	0.55	16	108	2.5	.05	0.2	0.2	B +*
880321	2324	44.46	5-37.57	35-48.51	4.01	0.57	16	108	2.6	.05	0.2	0.3	B +*	880325	0903	31.40	5-36.53	35-47.91	3.11	0.70	14	073	3.7	.04	0.1	0.2	A +*
880321	2354	10.08	5-36.55	35-47.95	3.06	0.64	15	070	3.8	.03	0.1	0.2	A +*	880325	1729	57.83	5-32.49	35-40.74	3.97	0.57	13	137	3.4	.02	0.1	0.2	B +*
880322	0101	03.52	5-36.59	35-47.95	3.35	0.81	18	070	3.8	.05	0.1	0.3	A +*	880325	2046	11.62	5-36.49	35-48.04	2.84	0.47	13	111	3.7	.03	0.1	0.2	B +*
880322	0107	01.69	5-30.69	35-44.91	7.77	0.69	18	099	1.0	.05	0.2	0.3	B +*	880326	0740	07.37	5-37.59	35-48.57	3.33	0.50	12	110	2.7	.04	0.2	0.4	B +*
880322	0130	54.47	5-37.41	35-48.41	3.11	0.51	12	099	2.8	.02	0.1	0.2	B +*	880326	1049	34.56	5-38.86	35-49.41	4.05	0.50	12	176	3.4	.02	0.1	0.1	B +*
880322	0247	45.00	5-30.71	35-44.94	7.56	0.80	18	099	1.0	.02	0.1	0.1	B +*	880326	1150	38.92	5-29.55	35-44.12	7.11	0.50	14	161	2.5	.04	0.2	0.2	B +*
880322	0225	56.52	5-30.68	35-44.96	7.59	0.60	16	100	1.0	.04	0.2	0.3	B +*	880326	1212	35.54	5-29.67	35-43.99	7.48	0.80	18	079	2.4	.06	0.2	0.3	A *
880322	0322	30.71	5-34.39	35-39.46	5.88	0.69	16	187	6.4	.03	0.1	0.2	C +*	880326	1331	02.36	5-31.30	35-44.83	5.58	0.50	15	096	1.1	.04	0.1	0.2	B +*
880322	0352	43.68	5-30.74	35-44.92	7.42	0.66	16	099	0.9	.02	0.1	0.2	B +*	880326	1435	58.96	5-38.74	35-49.40	4.07	0.50	08	171	3.4	.03	0.2	0.4	B +*
880322	0428	47.57	5-28.66	35-43.25	7.15	0.71	18	101	4.6	.04	0.1	0.2	B +*	880327	0213	55.61	5-42.18										

## Appendix C

DATE	ORIGIN	LAT S	LONG W	DEPTH	MAG	NO	GAP	DMIN	RMS	ERH	ERZ	Q	D	DATE	ORIGIN	LAT S	LONG W	DEPTH	MAG	NO	GAP	DMIN	RMS	ERH	ERZ	Q	D
880404	1448	03.15	5-30.13	35-44.45	7.60	1.55	09	106	1.4	.02	0.1	0.2	B*+	880407	0904	58.66	5-35.49	35-49.62	2.92	0.50	14	100	3.6	.04	0.2	0.3	B*+
880404	2124	41.10	5-38.74	35-47.66	5.90	0.59	07	216	0.3	.11	0.2	0.2	C	880407	1250	04.99	5-37.46	35-48.54	3.60	0.50	09	108	2.8	.02	0.1	0.2	B*+
880407	0243	46.68	5-37.59	35-48.61	3.94	1.03	16	111	2.7	.06	0.2	0.3	B*	880407	2102	27.29	5-29.91	35-44.53	6.65	0.37	09	207	1.8	.03	0.2	0.2	C*+
880407	0423	03.14	5-28.80	35-43.19	6.63	0.59	13	186	4.4	.08	0.4	0.5	C*	880407	2336	48.82	5-33.54	35-46.32	3.43	0.50	13	100	2.7	.02	0.1	0.1	B*+

### C.2 Earthquakes recorded by the drum-recorder network

The following is a list of the best located earthquakes recorded by the smoked paper drum recorder network during the period 11th - 21st March 1989 after the occurrence of the  $m_b = 5.0$  on 10th March 1989. No magnitude was calculated for these events. All labelling as for list C.2, except that there is no data subsets in this list.

DATE	ORIGIN	LAT S	LONG W	DEPTH	MAG	NO	GAP	DMIN	RMS	ERH	ERZ	Q
89 311	1654	42.58	5 29.86	35 43.11	3.53	.00	8 165	9.6	.03	.2	1.0	B
89 313	1147	31.57	5 31.08	35 44.52	6.08	.00	8 163	13.1	.02	.1	.5	B
89 313	1433	29.98	5 27.59	35 41.52	3.08	.00	8 183	4.7	.02	.2	.5	C
89 314	2 3	29.63	5 27.30	35 41.17	3.49	.00	8 186	3.9	.04	.3	.5	C
89 314	3 6	27.28	5 31.38	35 44.87	5.00	.00	8 162	12.7	.02	.1	.5	B
89 314	542	.49	5 26.94	35 41.89	5.58	.00	8 203	4.9	.04	.3	.6	C
89 314	650	10.48	5 39.10	35 50.16	.60	.00	5 180	4.2	.02	.0	.3	C
89 314	754	56.38	5 27.08	35 40.93	3.27	.00	7 188	3.3	.03	.3	.9	C
89 314	1335	54.38	5 33.15	35 45.68	5.00	.00	8 144	10.3	.02	.1	.5	B
89 314	1534	46.67	5 26.95	35 41.44	6.95	.00	8 199	4.1	.05	.4	.6	C
89 314	1934	39.80	5 30.08	35 43.85	6.54	.00	12 170	5.9	.07	.4	.6	B
89 314	2010	34.21	5 28.15	35 42.15	3.46	.00	14 180	5.8	.06	.3	.5	C
89 315	020	4.15	5 31.23	35 44.78	7.10	.00	7 163	13.0	.03	.3	.5	B
89 315	050	21.02	5 26.70	35 40.21	2.24	.00	12 188	1.8	.06	.4	1.0	C
89 315	146	3.03	5 29.61	35 42.84	2.88	.00	14 166	3.7	.07	.3	.5	B
89 315	310	5.32	5 27.18	35 41.28	2.62	.00	15 190	4.0	.06	.3	.6	C
89 315	320	31.47	5 29.31	35 42.45	2.25	.00	14 165	4.4	.04	.2	.4	B
89 315	327	41.99	5 29.17	35 42.45	1.70	.00	14 167	4.6	.07	.3	.8	B
89 315	4 4	20.66	5 27.88	35 40.87	3.71	.00	10 165	4.1	.04	.4	.5	B
89 315	510	29.15	5 29.78	35 42.98	7.98	.00	14 165	3.3	.04	.2	.2	B
89 315	555	49.97	5 29.20	35 42.18	2.79	.00	14 164	4.2	.07	.3	.6	B
89 315	6 8	4.17	5 26.36	35 40.37	3.20	.00	12 198	1.9	.07	.4	.5	C
89 315	615	5.94	5 28.47	35 42.78	5.30	.00	14 182	5.4	.06	.3	.5	C
89 315	729	25.36	5 26.91	35 40.77	2.65	.00	11 191	2.9	.06	.4	1.0	C
89 315	732	6.73	5 27.00	35 40.97	2.78	.00	15 191	3.3	.05	.2	.5	C
89 315	733	4.15	5 27.04	35 40.89	2.24	.00	12 189	3.2	.05	.3	1.0	C
89 315	836	25.04	5 28.77	35 43.12	5.68	.00	14 181	4.7	.06	.3	.4	C
89 315	930	35.79	5 28.89	35 42.30	4.22	.00	12 170	4.8	.07	.5	.6	B
89 315	1120	16.20	5 29.73	35 42.55	1.96	.00	13 171	3.9	.07	.3	.9	B
89 315	1410	27.19	5 29.50	35 43.57	5.26	.00	10 175	3.1	.04	.3	.5	B
89 315	1719	56.39	5 27.42	35 42.13	3.88	.00	14 194	5.6	.07	.3	.5	C
89 315	1831	38.92	5 27.16	35 40.92	4.64	.00	13 188	7.1	.06	.3	.5	C
89 315	2023	34.34	5 30.24	35 42.92	2.31	.00	12 87	2.8	.06	.2	.8	A
89 315	2127	26.59	5 29.06	35 42.01	3.18	.00	12 105	4.3	.05	.2	.8	B
89 315	2158	2.88	5 27.23	35 40.79	4.03	.00	13 139	3.2	.04	.2	.5	B
89 315	2332	37.98	5 29.95	35 43.66	5.05	.00	16 96	2.3	.05	.2	.2	B
89 316	022	15.93	5 29.11	35 41.91	3.18	.00	14 103	4.1	.05	.2	.7	B
89 316	252	3.28	5 30.08	35 42.77	3.02	.00	14 89	3.2	.04	.1	.4	A
89 316	3 9	28.00	5 28.39	35 42.63	6.64	.00	16 122	5.7	.06	.2	.3	B
89 316	6 4	29.05	5 28.18	35 41.64	3.14	.00	14 173	5.5	.07	.3	.8	B
89 316	9 4	33.73	5 28.42	35 42.84	6.53	.00	13 205	5.5	.05	.3	.4	C
89 316	1431	21.36	5 29.98	35 43.21	1.60	.00	11 91	2.7	.05	.2	1.0	B
89 316	15 2	20.74	5 25.83	35 39.65	2.70	.00	13 173	1.0	.06	.4	.6	B
89 317	028	31.78	5 30.67	35 44.90	7.95	.00	17 100	1.4	.05	.2	.3	B
89 317	223	43.28	5 28.64	35 42.93	7.52	.00	17 123	5.0	.06	.3	.3	B
89 317	231	9.56	5 26.86	35 41.42	5.00	.00	13 164	4.0	.07	.4	.9	B
89 317	339	27.85	5 28.49	35 41.80	3.63	.00	14 122	5.0	.06	.3	.4	B
89 317	436	6.55	5 25.85	35 39.71	5.00	.00	15 240	1.0	.06	.4	.4	C
89 317	458	2.21	5 28.13	35 42.37	5.00	.00	11 135	6.1	.06	.4	.8	B
89 317	1215	24.19	5 28.62	35 42.10	2.68	.00	12 121	5.0	.05	.3	1.0	B

# Appendix C

DATE	ORIGIN	LAT S	LONG W	DEPTH	MAG	NO	GAP	DMIN	RMS	ERH	ERZ	Q
89 317	1248 28.07	5 35.23	35 46.45	1.08	.00	8	122	1.9	.03	.2	.8	B
89 317	1424 59.12	5 28.17	35 42.23	5.00	.00	9	134	5.9	.06	.4	.9	B
89 317	1850 14.50	5 28.47	35 43.22	6.13	.00	14	128	5.1	.07	.3	.7	B
89 317	1911 16.19	5 26.80	35 41.29	3.75	.00	11	202	3.7	.06	.4	.5	C
89 317	1939 31.06	5 29.29	35 42.95	4.17	.00	17	108	4.0	.06	.2	.4	B
89 317	2010 16.19	5 28.92	35 43.10	6.02	.00	12	194	4.4	.05	.3	.3	C
89 317	2050 58.45	5 29.58	35 43.72	6.70	.00	18	99	2.9	.06	.2	.3	B
89 317	22 4 39.89	5 29.64	35 42.12	1.97	.00	16	99	3.5	.07	.2	.7	B
89 317	2225 18.03	5 27.55	35 41.35	4.37	.00	13	144	4.4	.07	.4	.6	B
89 317	2344 26.45	5 30.59	35 44.69	8.39	.00	10	96	1.2	.06	.4	.8	B
89 318	023 52.71	5 30.69	35 44.69	8.11	.00	18	96	1.1	.06	.2	.3	B
89 318	8 3 18.81	5 28.69	35 43.35	5.73	.00	17	122	4.6	.07	.3	.5	B
89 318	8 5 39.78	5 27.12	35 41.15	5.00	.00	13	156	3.7	.07	.5	.9	B
89 318	8 9 40.54	5 27.37	35 41.18	3.91	.00	14	148	4.0	.07	.4	.4	B
89 318	1020 13.38	5 28.57	35 43.35	5.43	.00	16	125	4.8	.07	.3	.7	B
89 318	1029 12.91	5 27.35	35 41.39	5.29	.00	13	151	4.3	.06	.4	.8	B
89 318	1138 .15	5 34.87	35 46.74	1.41	.00	11	106	1.1	.05	.2	.5	B
89 318	1247 33.01	5 36.60	35 48.76	3.32	.00	11	85	4.4	.05	.3	.7	A
89 318	14 5 54.28	5 28.10	35 41.57	1.89	.00	15	173	5.3	.05	.2	.7	B
89 318	1432 .59	5 28.43	35 43.48	5.73	.00	15	190	5.0	.05	.3	.4	C
89 318	2147 34.86	5 30.77	35 44.80	7.71	.00	10	98	1.2	.06	.4	.8	B
89 318	2150 43.36	5 30.82	35 44.82	7.28	.00	17	98	1.2	.06	.2	.3	B
89 319	054 15.00	5 30.55	35 44.59	8.08	.00	17	94	1.1	.06	.2	.3	B
89 319	3 6 55.16	5 28.94	35 41.54	3.36	.00	17	121	4.1	.06	.2	.4	B
89 319	3 8 19.69	5 28.96	35 41.63	3.38	.00	16	118	4.1	.06	.2	.4	B
89 319	440 32.36	5 36.26	35 47.56	1.81	.00	17	74	3.1	.04	.1	.5	A
89 319	440 32.39	5 36.25	35 47.61	.84	.00	17	73	3.1	.05	.1	.8	A
89 319	819 35.01	5 33.83	35 46.39	3.08	.00	10	156	2.2	.04	.2	.5	B
89 319	831 34.81	5 30.23	35 42.34	2.47	.00	17	89	3.2	.06	.2	.4	A
89 319	924 41.59	5 29.16	35 41.80	3.45	.00	13	159	3.9	.05	.3	.4	B
89 319	1110 47.91	5 31.13	35 44.92	5.65	.00	14	166	7.6	.04	.1	.3	B
89 319	1338 .52	5 27.69	35 40.94	2.93	.00	14	133	4.0	.05	.3	.9	B
89 319	14 3 24.73	5 27.73	35 42.05	5.00	.00	14	145	5.7	.07	.3	.7	B
89 319	1439 43.33	5 28.75	35 41.80	3.83	.00	17	112	4.6	.06	.2	.4	B
89 319	1440 34.52	5 28.49	35 41.62	3.55	.00	14	117	4.9	.06	.3	.8	B
89 319	1535 54.49	5 29.26	35 43.52	6.89	.00	20	70	3.5	.04	.1	.2	A
89 319	1836 46.04	5 27.46	35 40.70	5.00	.00	15	125	3.3	.06	.3	.5	B
89 319	1942 25.78	5 27.32	35 40.81	3.70	.00	15	119	3.4	.07	.4	.6	B
89 319	2211 17.59	5 28.92	35 41.65	3.26	.00	17	118	4.2	.06	.2	.5	B
89 319	2214 45.82	5 28.81	35 41.97	3.23	.00	18	107	4.6	.05	.2	.4	B
89 319	2315 6.98	5 31.31	35 43.78	1.20	.00	16	64	1.0	.05	.2	.5	A
89 319	2316 12.00	5 31.28	35 43.71	2.91	.00	14	64	1.1	.07	.2	.9	A
89 320	0 5 56.38	5 27.56	35 42.09	5.00	.00	18	114	5.6	.05	.2	.4	B
89 320	031 38.96	5 27.34	35 40.45	5.00	.00	16	140	2.9	.05	.2	.3	B
89 320	035 41.98	5 27.57	35 41.56	4.71	.00	17	108	4.8	.06	.2	.5	B
89 320	351 18.09	5 26.15	35 39.65	6.50	.00	15	151	.6	.04	.3	.4	B
89 320	515 46.87	5 31.14	35 43.91	1.62	.00	10	61	.6	.04	.2	.4	A
89 320	559 23.99	5 29.77	35 44.12	7.68	.00	20	83	2.4	.07	.2	.3	A
89 320	840 40.07	5 25.06	35 39.00	4.41	.00	15	310	2.3	.06	.5	.3	C
89 320	1155 13.48	5 26.66	35 40.92	3.52	.00	15	103	3.0	.07	.4	.5	B
89 320	1157 56.70	5 26.83	35 40.74	3.70	.00	15	202	7.7	.05	.3	.3	C
89 320	1540 20.43	5 27.64	35 42.00	5.63	.00	13	105	5.5	.05	.3	.6	B
89 320	1619 46.19	5 26.81	35 40.06	3.02	.00	18	125	1.7	.06	.3	.6	B
89 320	1659 18.15	5 27.64	35 41.89	5.97	.00	13	101	5.3	.04	.3	.5	B
89 320	1710 52.49	5 31.14	35 43.72	1.81	.00	17	62	1.0	.07	.2	.5	A
89 320	1810 35.55	5 27.93	35 41.94	5.27	.00	19	103	5.7	.07	.2	.4	B
89 320	1949 45.53	5 27.74	35 41.57	6.07	.00	18	111	4.9	.07	.3	.4	B
89 320	20 5 14.77	5 29.31	35 43.60	6.79	.00	19	72	3.4	.07	.2	.3	A
89 320	2023 16.49	5 27.61	35 41.91	5.00	.00	9	100	5.4	.06	.5	1.0	B
89 320	2218 52.65	5 27.33	35 41.17	3.70	.00	10	112	3.9	.05	.3	.6	B
89 320	2227 23.53	5 27.34	35 40.99	3.52	.00	14	116	3.7	.06	.3	.5	B
89 320	2248 41.57	5 27.61	35 41.83	5.00	.00	18	102	5.2	.07	.3	.4	B
89 320	2339 3.11	5 28.25	35 41.48	3.23	.00	16	120	5.3	.04	.2	.4	B
89 321	252 43.75	5 29.91	35 42.75	3.37	.00	18	77	3.5	.07	.2	.7	A
89 321	414 38.11	5 27.39	35 40.80	5.00	.00	17	141	3.4	.07	.3	.4	B
89 321	610 41.11	5 29.90	35 42.93	3.28	.00	18	74	3.2	.07	.2	.5	A
89 321	728 3.09	5 27.53	35 41.90	5.00	.00	17	150	5.3	.07	.3	.5	B
89 321	811 35.80	5 27.03	35 40.48	4.36	.00	19	119	2.5	.06	.3	.4	B
89 321	1340 17.42	5 30.56	35 44.25	2.82	.00	18	88	.9	.06	.2	.5	A
89 321	1341 25.49	5 34.83	35 46.55	1.19	.00	13	78	1.4	.07	.3	1.0	A
89 321	1415 .26	5 27.58	35 41.95	5.00	.00	14	99	5.4	.04	.2	.5	B

## References

### References

- Adams, R.D., 1977. Survey of practice in determining magnitudes of near earthquakes. Part 2: Europe, Asia, Africa, Australasia, the Pacific. *World Data Center A*, rep. SE-8, 67pp.
- Aggarwal Y.P., Sykes, L.R., Armbruster, J. Sbar, M.L. 1973. Premonitory changes in seismic velocities and the prediction of earthquakes. *Nature*, **241**, 101-104.
- Aki, K., 1965. Maximum likelihood estimate of b in the formula  $\log N = a - bM$  and its confidence limits. *Bull. Earth. Res. Inst.*, **43**, 237-239.
- Aki, K., 1969. Scaling law of seismic spectrum. *J. Geophys. Res.*, **72**, 1217-1231.
- Aki, K. & Chouet, B., 1975. Origin of coda waves: source, attenuation, and scattering effects. *J. Geophys. Res.*, **80**, 3322-3342.
- Aki, K., 1979. Characterization of barriers on an earthquake fault. *J. Geophys. Res.*, **84**, 6140-6148.
- Aki, K. and Richards, P., 1980. Quantitative Seismology: Theory and Methods. Volume 1 and 2. W. H. Freeman & Co., San Francisco.
- Aki, K., 1984. Asperities, barriers, characteristic earthquakes and strong motion prediction. *J. Geophys. Res.*, **89**, 5867-5872.
- Almeida, F.F.M., 1971. Mapa geológico do Brasil (Geological map of Brazil), scale 1:5,000,000. Min. das Minas e Energ., *Dep. Nac. da Prod. Miner.*, Brasilia, Brazil.
- Almeida, F.F.M., Amaral, G., Cordani, U.G. & Kawashita, K., 1973. The Precambrian evolution of the South American cratonic margin south of the Amazon River, in *The Ocean Basins and Margins*, vol. 1, The South Atlantic, edited by A.E.M. Nairn & F.G. Stehli, pp. 411-446, Plenum, New York.
- Almeida, F.F.M., Hasui. Y., Neves, B.B. de B. and Fuck, R.A., 1981. Brazilian structural provinces: an introduction. *Earth Sci. Rev.*, **17**, 1-29.
- Anderberg, M.R., 1973. Cluster analysis for applications. Academic Press, New York.
- Anderson, J.G., 1986. Seismic strain rates in the Central and Eastern United States. *Bull. Seism. Soc. Am.*, **76**, 273-290.
- Ansell, J., Aspinall, W., King, G. & Westaway, R., 1986. The 1984 July 19 North Wales earthquake - a lower crustal continental event indicating brittle behaviour at an unusual depth. *Geophys. J. R. astr. Soc.*, **84**, 201-206.
- Asmus, H.E. & Ponte, F.C., 1973. The Brazilian marginal basins, in *The Ocean Basis and Margins*, vol.1, The South Atlantic, edited by A.E.M. Nairn & F.G. Stehli, pp. 87-133, Plenum, New York.
- Assumpção, M. and Bamford, D., 1978. LISPB-V. Studies of crustal shear waves. *Geophys. J. R. astr. Soc.*, **54**, 61-73.

- Assumpção, M., Dias Neto, C.M., Berrocal, J., Antezana, R., França, H. and Ortega, R., 1980. Sismicidade do sudeste do Brasil (Seismicity of southeast Brazil). *An. 31º Congr. Bras. Geol.*, **2**, 1093-1098.
- Assumpção, M., 1983. A regional magnitude scale for Brazil. *Bull. Seism. Soc. Am.*, **73**, 237-246.
- Assumpção, M., Suarez, G. and Veloso, J.A.V., 1985. Fault plane solutions of intraplate earthquakes in Brazil: some constraints on the regional stress field. *Tectonophys.*, **113**, 238-293.
- Assumpção, M., 1986. Esforços litosféricos no Brasil e estudo de mecanismo focal em João Câmara (Lithospheric stresses in Brazil and the study of focal mechanism in João Câmara). In: Sismicidade na regi\_o de João Câmara, RN. Proceedings of the Rio de Janeiro Symposium, 10-11 November 1986. Dep. Geophys., Nat.Obs., Rio de Janeiro, pp. 13-16.
- Assumpção, M. & Suarez, G., 1988. Source mechanism of moderate-size earthquakes and stress orientation in mid-plate South America. *Geophys. J. R. astr. Soc.*, **92**, 253-267
- Assumpção, Ferreira, J.M., Carvalho, J.M., Blum, M.L., Menezes, E.A., Fontenele, D., Aires, A., 1989a. Seismic activity in Palhano, CE, October, 1988 - Preliminary results. *Rev. Bras. Geofis.*, **7**, 11-17.
- Assumpção, M., Takeya, M.K., Ferreira, J.M., Costa, J.M. and Sophia, C.M., 1989b. Cálculo de magnitudes e relaç\_o de freqüência-magnitudes dos sismos de João Câmara, RN (Magnitude calculation and magnitude-frequency relation of João Câmara earthquakes). *Rev. Bras. Geofis.*, **7**, 107-116.
- Assumpção, M., 1992. The regional intraplate stress field in South America. *J. Geophys. Res.*, **97**, 11889-11903.
- Baker, P.E., 1973. Islands of the South Atlantic, in *The Ocean Basins and Margins*, vol. 1, The South Atlantic, edited by A.E.M. Nairn & F.G.Stehli, pp. 493-553, Plenum, New York.
- Bakun, W.H. & Lindh, A.G., 1977. Local magnitudes, seismic moments, and coda durations for earthquake near Oroville, California. *Bull. Seism. Soc. Am.*, **67**, 615-629.
- Barka, A. & Kadinsky-Cade, K., 1988. Strike-slip fault geomety in Turkey and its influence on earthquake activity. *Tectonics*, **7**, 663-684.
- Båth, M., 1981. Earthquake magnitude - Recent research and current trends. *Earth Sci. Rev.*, **17**, 315-398.
- Bergman, E.A. & Solomon, S.C., 1980. Oceanic intraplate earthquakes: implications for local and regional intraplate stress. *J. Geophys. Res.*, **85**, 5389-5410.
- Berrocal, J., Assumpção, M., Antezana, R., Dias Neto, C.M., Ortega, R., França, H. & Veloso, J.A.V., 1984, Sismicidade do Brasil (Seismicity of Brazil). IAG-USP/CNEN, 320pp.

## References

- Berrocal, J., Fernandes, C., França, H. & Barbosa, J.R., 1987. A atividade sísmica de João Câmara-RN registrada pelas redes sismográficas supervisionadas pelo IAG/USP, entre agosto de 1986 e abril de 1987 (The seismic activity of João Câmara-RN recorded by the networks supervised by the IAG/USP, between August 1986 and April 1987). II Regional Meeting of Geophys., SBGF, Salvador, BA.
- Bevington, P.R., 1969. Data reduction and error analysis for the physical sciences. McGraw-Hill, New York, 335pp.
- Bisztricsany, E., 1958. A new method for the determination of the magnitude of earthquake. *Geofiz. Kozlement.*, **7**, 69-96.
- Booth, D.C., & Crampin, S., 1985. Shear-wave polarizations on a curved wavefront at an isotropic free surface. *Geophys. J. R. astr. Soc.*, **83**, 31-45.
- Bouchon, M., 1979. Predictability of ground displacement and velocity near an earthquake fault: An example: The Parkfield earthquake of 1966. *J. Geophys. Res.*, **84**, 6149-6156.
- Brace, W.F. & Byerlee, J.D., 1966. Stick-slip as a mechanism for earthquakes. *Science*, **153**, 990-992.
- Brace, W.F. & Byerlee, J.D., 1970. California earthquakes - why only shallow focus?. *Science*, **168**, 1573-1575.
- Branner, J.C., 1912. Earthquakes in Brazil. *Bull. Seism. Soc. Am.*, **2**, 105-117.
- Branner, J.C., 1920. Recent earthquakes in Brazil. *Bull. Seism. Soc. Am.*, **10**, 90-104.
- Brune, J.N., 1968. Seismic moment, seismicity and rate of slip along major fault zones. *J. Geophys. Res.*, **73**, 777-784.
- Brazilian Geophysical Society. 1984. Boletim sísmico Brasileiro No.3. *Rev. Bras. Geofis.*, **2**, 127-130.
- Brazilian Geophysical Society. 1985. Boletim sísmico Brasileiro No.4. *Rev. Bras. Geofis.*, **3**, 69-73.
- Brazilian Geophysical Society. 1987. Boletim sísmico Brasileiro No.9. *Rev. Bras. Geofis.*, **5**, 351-355.
- Buland, R., 1976. The mechanics of locating earthquakes. *Bull. Seism. Soc. Am.*, **66**, 173-187.
- Bullen, K.E. & Bolt, A.B., 1985. An introduction to the theory of seismology. Cambridge University Press.
- Chen, W.P. & Molnar, P., 1983. Focal depths of intracontinental and intraplate earthquakes and their implications for the thermal and mechanical properties of the lithosphere. *J. Geophys. Res.*, **88**, 4183-4214.
- Chen, T.-C., Booth, D.C. & Crampin, S., 1987. Shear-wave polarizations near the North Anatolian fault - III, Observations of temporal changes, *Geophys. J. R. astr. Soc.*, **91**, 287-311.



- Chiu, J., Johnston, A., Metzger, A., Haar, L. and Fletcher, J., 1984. Analysis of analog and digital records of the 1982 Arkansas earthquake swarm. *Bull. Seism. Soc. Am.*, **74**, 1721-1742
- Choy, G.L. & Bowman, J.R., 1990. Rupture process of a multiple main shock sequence: analysis of teleseismic, local, and field observation of the Tennant Creek, Australia, earthquakes of January 22, 1988. *J. Geophys. Res.*, **95**, 6867-6882.
- Costa, J.M., Ferreira, J.M., Oliveira, R.T., Assumpção, M., Anjos, C.A., Menezes, E. & Aires, A., 1989. O sismo de João Câmara de marco de 1989 ( $m_b=4.9$ ) (The João Câmara earthquake of March 1989 ( $m_b=4.9$ )). 1st Congress of the Brazilian Geophys. Soc., 20-24 Nov. 1989. Rio de Janeiro.
- Crampin, S., 1978. Seismic wave propagation through a cracked solid: polarization as a possible dilatancy diagnostic. *Geophys. J. R. astr. Soc.*, **53**, 467-496.
- Crampin, S., 1981. A review of wave motion in anisotropic and cracked elastic-media. *Wave Motion*, **3**, 342-391.
- Crampin, S., Evans, R. & Atkinson, B.K., 1984. Earthquake prediction: A new physical basis. *Geophys. J. R. astr. Soc.*, **76**, 147-156.
- Crampin, S., Evans, R. & Üçer, S.B., 1985. Analysis of records of local earthquakes: the Turkish Dilatancy Projects (TDP1 and TDP2). *Geophys. J. R. astr. Soc.*, **83**, 1-16.
- Crampin, S., 1987a. The geological and industrial implications of extensive-dilatancy anisotropy. *Nature*, **328**, 491-496.
- Crampin, S., 1987b. The basis for earthquake prediction. *Geophys. J. R. astr. Soc.*, **91**, 331-347.
- Crampin, S., Booth, D.C., Evans, R., Peacock, S. & Fletcher, J.B., 1990. Changes in shear wave splitting at Anza near the time of the North Palm Springs earthquake, *J. Geophys. Res.*, **95**, 11197-11212.
- Crampin, S. & Lovell, J.H., 1992. A decade of shear-wave splitting in the Earth's crust: what does it mean? what use can we make of it? and what should we do next? *Geophys. J.*, **107**, 387-407.
- Das, S. & Aki, K., 1977. Fault planes with barriers: A versatile earthquake model. *J. Geophys. Res.*, **82**, 5658-5670.
- Das, S. & Scholz, C.H., 1981a. Theory of time-dependent rupture in the Earth. *J. Geophys. Res.*, **86**, 6039-6051.
- Das, S. & Scholz, C.H., 1981b. Off fault aftershock clusters caused by shear stress increase? *Bull. Seism. Soc. Am.*, **71**, 1669-1675.
- Das, S. & Scholz, C.H., 1983. Why large earthquakes do not nucleate at shallow depths. *Nature*, **305**, 621-623.
- DNPM (Department of Mineral Production), 1975. Project Radambrasil. Radar imagery at 1:250,000. Minist. Mines Energy Braz., Sheet SB.25.V.C

## References

- Doser, D. & Kanamori, H., 1986. Depth of seismicity in the Imperial Valley region (1977-1983) and its relation to heat flow, crustal structure, and the October 15, 1979 earthquake. *J. Geophys. Res.*, **91**, 675-688.
- Doyle, M., McGonigle, R. and Crampin, S., 1982. The effects of crack anisotropy on the hypocentral locations of local earthquakes. *Geophys. J. R. astr. Soc.*, **69**, 137-157.
- Eaton, J.P., O'Neill, M.E. & Murdock, J.N., 1970. Aftershocks of the 1966 Parkfield-Cholame, California, earthquake: a detailed study, *Bull. Seism. Soc. Am.*, **60**, 1151-1197.
- Evans, R., 1984. Effects of the free surface on shear wavetrains. *Geophys. J. R. astr. Soc.*, **76**, 165-172.
- Evans, R., Beamish, D., Crampin, S. & Üçer, S.B., 1987. The Turkish dilatancy project (TDP3): multidisciplinary studies of a potential earthquake source region. *Geophys. J. R. astr. Soc.*, **91**, 265-286.
- Evernden, J.F., 1975. Seismic intensities, "size" of earthquakes and related parameters, *Bull. Seism. Soc. Am.*, **65**, 1287-1313.
- Ferreira, J.M. & Assumpção, M., 1983. Sismicidade do Nordeste do Brasil (Seismicity of Northeast Brazil). *Rev. Bras. Geofis.*, **1**, 67-88.
- Ferreira, J.M., Takeya, M.K., Costa, J.M., Moreira, J.A., Assumpção, M., Veloso, J.A. & Pearce, R.G., 1987. A continuing intraplate earthquake sequence near João Câmara, northeastern Brazil - preliminary results. *Geophys. Res. Letts.*, **14**, 1042-1045.
- Fletcher, J.B., Sbar, M.L. & Sykes, L.R., 1978. Seismic trends and travel-time residuals in eastern North America and their tectonic implications. *Geol. Soc. Amer. Bull.*, **89**, 1656-1676.
- Francheteau, J. & Le Pichon, X., 1972. Marginal fracture zones as structural framework of continental margins in South Atlantic Ocean, *Amer. Ass. Petrol. Geol. Bull.*, **56**, 991-1007.
- Gallardo, C., 1988. Ejemplos de la deformacion intraplaca reciente en el borde Atlantico de Sudamerica: la depression de Taubate (SP) y la actividad sismica confinada de João Câmara (RN) Brasil (Examples of recent intraplate deformation in the South America Atlantic coast: The Taubate (SP) through and the confined seismic activity in João Câmara (RN) Brazil). In: Congresso Geol. Chileno, 5, Actas 1, 433-451, Universidad de Chile.
- Gallardo, C & Perez, A.A.B., 1988. Estado dos esforços inferido a partir de feições morfológicas de origem tectônica na região de João Câmara (RN) (The state of stresses in the João Câmara (RN) region inferred from morphological features of tectonic origin). Observatório Nacional, Rio de Janeiro, Relat. interno.
- Gorini, M.A. & Brian, G.M., 1976. The tectonic fabric of the equatorial Atlantic and adjoining continental margins: Gulf of Guinea to northeastern Brazil, *An. Acad. Brasil. Cienc.*, **48**, 101-119.
- Gusso, G.L.N. & Bagnoli, E., 1989. Evidências de intensa deformação tectônica em sedimentos costeiros holocênicos do Rio Grande do Norte. 1st Congress of the Brazilian Geophys. Soc., 20-24 Nov. 1989. Rio de Janeiro.

- Gutenberg, B., 1945. Amplitudes of surface waves and magnitudes of shallow earthquakes. *Bull. Seism. Soc. Am.*, **35**, 3-12.
- Gutenberg, B. & Richter, C.F., 1954. Seismicity of the Earth, 2nd ed., 310 pp., Princeton University Press, Princeton, N.Y.
- Gutenberg, B. & Richter, C.F., 1956. Magnitude and energy of earthquakes. *Ann. Geofis.*, **9**, 1-15.
- Hartzell, S., 1980, Faulting process of the May 17, 1976 Gazli, USSR earthquake. *Bull. Seism. Soc. Am.*, **70**, 1715,1736.
- Hartzell, S.H. & Heaton, T.H., 1986. Rupture history of the 1984 Morgan Hill, California, earthquake from the inversion of strong motion records. *Bull. Seism. Soc. Am.*, **76**, 649-674.
- Henderson, J., 1992. Fracture mechanics and the evolution of seismicity in an intra-plate setting. PhD thesis. University of Edinburgh.
- Herrmann, R.B., 1975. The use of duration as a measure of seismic moment and magnitude. *Bull. Seism. Soc. Am.*, **65**, 899-913.
- Herrmann, R.B., Cheng, S.H., Nuttli, O.W., 1978. Archeoseismology applied to the New Madrid earthquakes of 1811 to 1812. *Bull. Seism. Soc. Am.*, **68**, 1751-1759.
- Hinze, W.J., Braile, L.W., Keller, G.R., Lidiak, E.G., 1988. Models for midcontinent tectonism: an update. *Rev. Geophys.*, **26**, 699-717.
- Hurley, P.M. & Rand, J.R., 1973. Outline of Precambrian chronology in lands bordering the South Atlantic, exclusive of Brazil, in *The Ocean Basin and Margins*, vol.1, The South Atlantic, edited by A.E.M. Nairn & F.G. Stehli, pp. 391-410, Plenum, New York.
- Kanamori, H. & Anderson, D.L., 1975. Theoretical basis of some empirical relations to seismology. *Bull. Seism. Soc. Am.*, **65**, 1073-1095.
- King, G.C.P. & Yielding, G., 1984. The evolution of a thrust fault system: processes of rupture initiation, propagation and termination in the 1980 El Asnam (Algeria) earthquake. *Geophys. J. R. astr. Soc.*, **77**, 915-933.
- King, G.C.P., Ouyang, Z.X., Papadimitriou, P., Deschamps, A., Gagnepain, J., Houseman, G., Jackson, J.A., Soufleris, C. & Virieux, J., 1985. The evolution of the Gulf of Corinth (Greece): an aftershock study of the 1981 earthquakes, *Geophys. J. R. astr. Soc.*, **80**, 677-693.
- King, G.C.P. & Nabelek, J., 1985. Role of fault bends in the initiation and termination of earthquake rupture. *Science*, **228**, 984-987.
- King, G.C.P., 1986. Speculations on the geometry of the initiation and termination processes of earthquake rupture and its relation to morphology and geological structure. *Pageoph*, **124**, 567-586.
- Kisslinger, C. & Engdahl, E.R., 1973. The interpretation of the Wadati diagram with relaxed assumptions. *Bull. Seism. Soc. Am.*, **63**, 1723-1736.
- Kristy, M.J., Burdock, L.J. & Simpson, D.W., 1980, The focal mechanism of the Gazli, USSR, earthquakes. *Bull. Seism. Soc. Am.*, **70**, 1737-1750.

## References

- Kumar, N., Bryan, G., Gorini, M. & Carvalho, J., 1977. Evolution of the continental margin of northern Brazil: Sediment distribution and carbon potential. *An. Acad. Brasil. Cienc.*, **48**, 131-143.
- Langer, C.J., Bonilla, M.G. & Bollinger, G.A., 1987. Aftershock and surface faulting associated with the intraplate Guinea, West Africa earthquake of 22 December 1983. *Bull. Seism. Soc. Am.*, **77**, 1579-1601.
- Lee, W.H.K., Eaton, M.S. & Brabb, E.E., 1971. The earthquake sequence near Danville, California, 1970. *Bull. Seism. Soc. Am.*, **61**, 1771-1794.
- Lee, W.H.K., Bennett, R.E. & Meagher, K.L., 1972. A method of estimating magnitude of local earthquakes from the signal duration. *U.S. Geol. Surv. Open File Rep.*, 28pp.
- Lee, W.H.K. & Lahr, J.C., 1975. HYPO71 (revised): A computer program for determining hypocentre, magnitude and first motion pattern of local earthquakes. *U.S. Geol. Surv., Open-File Rep.*, 75-311.
- Lee, E.C.W. & Tottingham, D.M., 1990. User manual for pixplot. IASPEI Software Library Volume 2. Edited by W.H.K. Lee. International Association of Seismology and Physics of the Earth's Interior.
- Liu, H.L. & Kanamori, H., 1980. Determination of source parameters of mid-plate earthquakes from the waveforms of body waves. *Bull. Seism. Soc. Am.*, **70**, 1989-2004.
- Liu, H.L., 1983. Interpretation of near-source ground motion and implications. PhD thesis, California Institute of Technology, Pasadena, California.
- Liu, Y., Booth, D.C., Crampin, S., Evans, R. & Larry, P., 1992. Shear-wave polarizations and possible temporal variations in shear-wave splitting at Parkfield. (in press).
- Loczy, L., 1970. role of transcurrent faulting in South American tectonic framework, *Amer. Ass. Petrol. Geol. Bull.*, **54**, 2111-2119.
- Lomnitz, C., 1986. Sismicidade Intraplaca (Intraplate seismicity). In: Sismicidade na regio de João Câmara, RN. Proceedings of the Rio de Janeiro Symposium, 10-11 November 1986. Dep. Geophys., Nat. Obs., Rio de Janeiro, pp. 30-31.
- Lovell, J.H., Crampin, S., Evans, R. & Üçer, S.B., 1987. Microearthquakes in the TDP swarm, Turkey: clustering in space and time. *Geophys. J. R. astr. Soc.*, **91**, 313-330.
- Marsh, J.S., 1973. Relationships between transform directions and alkaline igneous rocks lineaments in Africa and South America. *Earth Planet. Sci. Lett.*, **18** 317-323.
- McEvelly, T.V. & Johnson, L.R., 1974. Stability of P and S velocities from central California quarry blasts. *Bull. Seism. Soc. Am.*, **64**, 343-353.
- Meissner, R. & Strehlau, J., 1982. Limits of stresses in continental crusts and their relation to the depth-frequency distribution of shallow earthquakes. *Tectonics*, **1**, 73-89.

- Mendiguren, J.A., 1971. Focal Mechanism of a shock in the middle of the Nazca Plate. *J. Geophys. Res.*, **76**, 3861-3879.
- Mendiguren, J.A. & Richter, F.M., 1978. On the origin of compressional intraplate stresses in South America. *Phys. Earth Planet. Int.*, **16**, 318-326.
- Mendiguren, J.A., 1980. A procedure to resolve areas of different source mechanisms when using the method of composite nodal plane solutions. *Bull. Seism. Soc. Am.*, **70**, 985-998.
- Mendoza, C. & Hartzell, S.H., 1988. Aftershock patterns and main shock faulting. *Bull. Seism. Soc. Am.*, **78**, 1438-1449.
- Mogi, K., 1985. Earthquake Prediction. Tokyo. Academic Press.
- Moreira, J.A.M., Baraud, R., Lins, F.A.P.L., Macedo, J.W.P., 1990. Contribuição da gravimetria para o entendimento da sismicidade de João Câmara (Contribution of the gravity to the understanding of João Câmara seismicity). Proceedings of the 36th Brazilian Geological Congress, Natal, RN.
- Neill, W.M., 1973. Possible continental rifting in Brazil and Angola related to the opening of the South Atlantic. *Nature Phys. Sci.*, **245**, 104-107.
- Nicholson, C., Simpson, D.W., Singh, S. & Zollweg, J.E., 1984. Crustal studies, velocity inversions and tectonics: results from a microearthquake survey in the New Madrid Seismic Zone. *J. Geophys. Res.*, **89**, 4545-4558.
- Nur, A., 1978. Nonuniform friction as a physical basis for earthquake mechanics. *Pure Appl. Geophys.*, **116**, 964-991.
- Nuttli, O.W., 1973. Seismic wave attenuation and magnitude relations for eastern North America. *J. Geophys. Res.*, **78**, 876-885.
- Nuttli, O.W., 1983. Average seismic source-parameter relations for mid-plate earthquakes. *Bull. Seism. Soc. Am.*, **73**, 519-535.
- Oliveira, R.T., Ferreira, J.M., Costa, J.M., Assumpção, M., Anjos, C.A., Menezes, E.A., E. & Aires, A., 1989. O crescimento da falha de Samambaia e o sismo de 01/10/1988 ( $m_b=3.9$ ) (The increase of the Samambaia fault and the earthquake of 1st October 1988 ( $m_b=3.9$ )). 1st Congress of the Brazilian Geophys. Soc., 20-24 Nov. 1989. Rio de Janeiro. Brazil.
- Oppenheimer, D.H., Bakun, W.H. & Lindh, A.G., 1990. Slip partitioning of Calaveras Fault, California, and prospects for future earthquakes. *J. Geophys. Res.*, **95**, 8483-8498.
- O'Reilly S.H., 1955. Seismicité et morphologie en Amazonie Brésilienne (Seismicity and morphology in Brazilian Amazon). *Ann. Geogr.*, **64**, 97-107.
- Padilha, A.L., Vitorello, I., Costa, J.M. & Trivedi, N.B., 1990. Levantamento magnetotélúrico na região de João Câmara, RN (Magnetotelluric survey in the João Câmara (RN) region). Proceedings of the 36th Brazilian Geological Congress, Natal, RN.
- Peacock, S., Crampin, S., Fletcher, J.B. & Booth, D.C., 1988. Shear-wave polarizations in the Anza seismic gap, Southern California: temporal changes as possible precursors. *J. Geophys. Res.*, **93**, 3339-3356.

## References

- Pearce, R.G., Bainbridge, H., Young, J.B. & Key, P.F., 1980. The 1976 earthquake sequence in Uzbekistan: focal mechanism determined using the relative amplitude method. AWRE Report No.026/80, HMSO.
- Pearce, R.G., 1987. The relative amplitude method applied to 19th March 1984 Uzbekistan earthquake and its aftershocks. *Phys. Earth Planet. Int.*, **47**, 137-149
- Petrobrás (Brazilian Petroleum Company), (1987). Aeromagnetometric Project of the Potiguar Basin. Maps at 1:100,000. Internal report. Sheets SB.25-V-C-I and SB.25-V-C-IV.
- Phillips, W.S., Aki, K., 1986. Site amplification of coda waves from local earthquakes in Central California. *Bull. Seism. Soc. Am.*, **76**, 627-648.
- Real, C.R. & Teng, T.L., 1973. Local Richter magnitude and total signal duration in southern California. *Bull. Seism. Soc. Am.*, **63**, 1809-1827.
- Reasenber, P. & Ellsworth, W.L., 1982. Aftershocks of the Coyote Lake, California, earthquake of August 6, 1979: a detailed study. *J. Geophys. Res.*, **87**, 10637-10655.
- Ribicki, K., 1973. Analysis of aftershocks on the basis of dislocation theory. *Phys. Earth Planet. Int.*, **7**, 409-422.
- Richardson, R.M., Solomon, S.C. & Sleep, N.H., 1976. Intraplate stresses as an indicator of plate tectonic driving forces. *J. Geophys. Res.*, **81**, 1847-1856.
- Richardson, R.M., 1978. Finite element modeling of stress in the Nazca plate: driving forces and plate boundary earthquakes. *Tectonophysics*, **50**, 223-248.
- Richter, C.F., 1958. Elementary seismology. W.H. Freeman and Company, San Francisco, 786pp.
- Rothé, J.P., 1969. The Seismicity of the Earth, 1953-1965. UNESCO, Paris, 336 pp.
- Savage, M.K., Shih, X.R., Meyer, R.P. & Aster, R.C., 1989. Shear-wave anisotropy of active tectonic regions via automated S-wave polarization analysis. *Tectonophysics*, **165**, 279-292.
- Savage, M.K., Peppin, W.A. & Vetter, U.R., 1990. Shear wave anisotropy and stress direction in and near Long Valley Caldera, California, 1979-1988. *J. Geophys. Res.*, **95**, 11165-11177.
- Schwartz, S.Y., Dewey, J.W. & Lay, T., 1989. Influence of fault plane heterogeneity on the seismic behavior in the southern Kurile Islands Arc. *J. Geophys. Res.*, **94**, 5637-5649.
- Segall, P. & Pollard, D.D., 1980. Mechanics of discontinuous faults, *J. Geophys. Res.*, **85**, 4337-4350.
- Scholz, C.H., Sykes, L.R. & Aggarwal, Y.P., 1973. Earthquake prediction: A physical basis. *Science*, **181**, 803-810.
- Scholz, C.H., Aviles, C.A. & Wesnousky, S.G., 1986. Scaling differences between large interplate and intraplate earthquakes. *Bull. Seism. Soc. Am.*, **76**, 65-70.
- Scholz, C.H., 1990. The mechanics of earthquakes and faulting. Cambridge University Press.

- Sibson, R.H., 1982. Fault zones models, heat flow, and the depth distribution of earthquakes in the continental crust of the United States. *Bull. Seism. Soc. Am.*, **72**, 151-163.
- Sibson, R.H., 1984. Roughness at the base of the seismogenic zone; Contributing factors. *J. Geophys. Res.*, **89**, 5791-5799.
- Sibson, R.H., 1985. Stopping of earthquake ruptures at dilational jogs. *Nature*, **316**, 248-251.
- Sibson, R.H., 1986. Brecciation processes in fault zones: Inferences from earthquake rupturing. *Pageoph*, **124**, 159-176.
- Sommerville, P.G., McLaren, J.P., LeFevre, Burger, R.W. & Helmberger, D.V., 1987. Comparison of source scalling relations of eastern and western North American earthquakes. *Bull. Seism. Soc. Am.*, **77**, 322-346.
- Sophia, C.M. & Assumpção, M., 1989. Padrão de ruptura da Falha de Samambaia, RN, na reativação de Fevereiro de 1987 (The rupturing pattern of Samambaia fault, RN, during the reactivation of February 1987). 1st Congress of the Brazilian Geophys. Soc., 20-24 Nov. 1989. Rio de Janeiro. Brazil.
- Sophia, C.M., 1990. A reativação sísmica de João Câmara, RN, de Janeiro-Fevereiro de 1987 (The reactivation in the seismicity of João Câmara (RN), of January-February 1987). MSc thesis, Universidade de São Paulo. São Paulo. Brazil.
- Sutheau, A.M. & Whitcomb, J.H., 1979. A local earthquake coda magnitude and its relation to duration, moment  $M_0$ , and local Richter magnitude  $M_L$ . *Bull. Seism. Soc. Am.*, **69**, 353-368.
- Sykes, L.R. & Sbar, M.L., 1973. Intraplate earthquakes, lithospheric stresses and the driving mechanism of plate tectonics. *Nature*, **245**, 298-302.
- Sykes, L.R., 1978. Intraplate seismicity, reactivation of preexisting zones of weakness, alkaline magmatism and other tectonism postdating continental fragmentation, *Rev. Geophys. Space Physics.*, **16**, 621-688.
- Takeya, M., Ferreira, J.M., Pearce, R.G., Assumpção, M., Costa, J.M. & Sophia, C.M., 1989. The 1986-1988 intraplate earthquake sequence near João Câmara, northeast Brazil - evolution of seismicity. *Tectonophys.*, **167**, 117-131.
- Teague, A.G., Bollinger, G.A. & Johnston, A.C., 1986. Focal mechanism analyses for eastern Tennessee earthquakes (1981-1983). *Bull. Seism. Soc. Am.*, **76**, 95-109.
- Torquato, J.R. & Cordani, U.G., 1981. Brazil-Africa geological links. *Earth Sci. Rev.*, **17**, 155-176.
- Tsumura, K., 1967. Determination of earthquake magnitude from total duration of oscillation. *Bull. Earthq. Res. Inst.*, **15**, 7-18.
- Valdés, C.M., 1989. User manual for PCEQ. IASPEI Software Library Volume 1. Edited by W.H.K. Lee. International Association of Seismology and Physics of the Earth's Interior.
- Veloso, J.A.V., 1986. O caso atual de sismicidade em João Câmara, RN (The recent seismicity in João Câmara (RN)). In: Sismicidade na região de João Câmara, RN. Proceedings of the Rio de Janeiro Symposium, 10-11 November 1986. Dep. Geophys., Nat. Obs., Rio de Janeiro, pp. 7-12.

## References

- Xie, J., Liu, Z., Herrmann, R.B. & Cranswick, E., 1991. Source processes of three aftershocks of the 1983 Goodnow, New York, earthquake: high -resolution images of small, symmetric ruptures. *Bull. Seism. Soc. Am.*, **81**, 818-843.
- Young, P.A.V., Maguire, P.K.H., Laffoley, N.d'A. & Evans, J.R., 1991. Implications of the distribution of seismicity near Lake Bogoria in the Kenya Rift. *Geophys. J.*, **105**, 665-674.